NASA Contractor Report 189085

High Strain Rate Properties of Angle-Ply Composite Laminates

Part III—Final Report

I.M. Daniel
IIT Research Institute
Chicago, Illinois

December 1991

Prepared for
Lewis Research Center
Under Contract NAS3-21016

National Aeronautics and
Space A

(NASA-CR-189085) HIGH STRAIN RATE PROPERTIES OF ANGLE-PLY COMPOSITE LAMINATES, PART 3 Final Report (IIT Research Inst.) 383 p CSCL 11D

N92-20880

Unclas
G3/24 0078286

FOREWORD

This is the Final Report on IIT Research Institute Project No. K06013 (formerly M06026), "High Strain Rate Properties of Angle-Ply Composite Laminates," prepared by IITRI for NASA-Lewis Research Center, under Contract No. NAS3-21016. The work described in this report was conducted in the period July 11, 1977 to April 11, 1981. Dr. C. C. Chamis was the NASA-Lewis Project Manager. Dr. I. M. Daniel formerly of IITRI was the Principal Investigator. Additional contributions to the work reported herein were made by Messrs. W. G. Hamilton, G. M. Koller, T. Niiro, and S. W. Schramm of IITRI, Dr. T. Liber of Travenol Laboratories, and Mr. R. H. LaBedz of Broutman and Associates.

Respectfully submitted,
IIT RESEARCH INSTITUTE

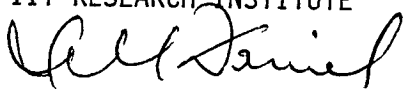

I. M. Daniel
Professor and Director
Experimental Stress
Analysis Laboratory
Illinois Institute of Technology

APPROVED:

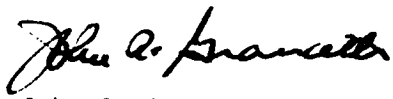

John A. Granath, Director
Engineering Division

HIGH STRAIN RATE PROPERTIES OF ANGLE-PLY COMPOSITE LAMINATES

ABSTRACT

Angle-ply graphite/epoxy and graphite/S-glass/epoxy laminates were characterized in uniaxial tension at strain rates ranging from quasi-static to over $500s^{-1}$. Laminate ring specimens of $[\pm 15]_{2s}$, $[\pm 22.5]_{2s}$, $[\pm 30]_{2s}$, $[\pm 45]_{2s}$, $[\pm 60]_{2s}$, $[\pm 67.5]_{2s}$ and $[\pm 75]_{2s}$ layups were loaded under internal pressure. Results were presented in the form of stress-strain curves to failure. Properties determined included moduli, Poisson's ratios, strength, and ultimate strain. In all seven laminates for the two materials tested the modulus and strength increase with strain rate. The effect of strain rate varies with layup, being lowest for the fiber dominated $[\pm 15]_{2s}$ laminates and highest for the matrix dominated $[\pm 75]_{2s}$ laminates. The highest increments over the static values are 10% to 25% for the $[\pm 15]_{2s}$ layup and 200% to 275% for the $[\pm 75]_{2s}$ layup. Ultimate strains do not show any significant trends with strain rate. In almost all cases the ultimate strain values are within ±20% of the mean value and in half of the cases the deviations from the mean are less than 10%.

TABLE OF CONTENTS

LIST OF TABLES

LIST OF TABLES (Cont.)

LIST OF TABLES (Concluded)

LIST OF FIGURES

LIST OF FIGURES (Cont.)

LIST OF FIGURES (Cont.)

LIST OF FIGURES (Cont.)

LIST OF FIGURES (Cont.)

LIST OF FIGURES (Cont.)

LIST OF FIGURES (Cont.)

LIST OF FIGURES (Cont.)

LIST OF FIGURES (Cont.)

LIST OF FIGURES (Cont.)

LIST OF FIGURES (Cont.)

LIST OF FIGURES (Cont.)

LIST OF FIGURES (Cont.)

LIST OF FIGURES (Cont.)

LIST OF FIGURES (Cont.)

LIST OF FIGURES (Concluded)

HIGH STRAIN RATE PROPERTIES OF ANGLE-PLY COMPOSITE LAMINATES

1. INTRODUCTION

In Part I of this report methods were described for testing and characterization of composite materials at strain rates ranging from quasi-static to over $500s^{-1}$. Three unidirectional materials were characterized: SP288/T300 graphite/epoxy, SP288/AS graphite/epoxy, and 80AS/20S/PR288 graphite/S-glass/epoxy.

It was found that the longitudinal modulus increases moderately with strain rate by up to 20%, but the longitudinal strength and ultimate strain did not vary much. Transverse modulus and strength increase sharply with strain rate, reaching values up to three times the static value. The in-plane shear modulus and shear strength increase noticeably with strain rate by up to approximately 65%. In all cases, it was found that ultimate strains did not vary with strain rate in any significant manner.

In Part II of this report the same experimental methods were used to characterize unidirectional off-axis laminates in the same range of strain rates. Rings of $[22.5_8]$, $[30_8]$, and $[45_8]$ layups were tested. Two materials were characterized: SP288/AS graphite/epoxy and 80AS/20S/PR288 graphite/S-glass/epoxy. It was found that in all three laminates of both materials the modulus and strength increase sharply with strain rate, reaching values roughly 100%, 150%, and 200% higher than corresponding static values for the $[22.5_8]$, $[30_8]$, and $[45_8]$ laminates, respectively. In the case of ultimate strain no definite trends were established, but the maximum deviation from the average was less than 18%.

The objective of the task descrived in this Part III of the report is to characterize angle-ply composite laminates in uniaxial tension at three strain rates. The same material systems were characterized as in the case of the off-axis laminates. The three strain rates selected are quasi-static, intermediate, and high rates ranging from $10^{-4}s^{-1}$ to over $500s^{-1}$. All characterization tests were conducted by testing thin rings 10.16 cm (4 in.) in diameter, 2.54 cm (1 in.) wide, and 8-plies thick under internal pressure. Rings of

$[\pm 15]_{2s}$, $[\pm 22.5]_{2s}$, $[\pm 30]_{2s}$, $[\pm 45]_{2s}$, $[\pm 60]_{2s}$, $[\pm 67.5]_{2s}$, and $[\pm 75]_{2s}$ layups were tested. Three replications per test were used. The data were analyzed according to procedures described in Part I of this report. Results were presented in the form of stress-strain curves to failure. Properties determined included initial, secant, and terminal strain rates; initial, secant, and terminal modulus and Poisson's ratio; and strengh and ultimate strain. The effects of strain rate on the various properties are discussed below.

2. QUASI-STATIC TENSILE PROPERTIES OF ANGLE-PLY LAMINATES

Quasi-static tensile properties of $[\pm\theta]_{2s}$ laminates were obtained by testing rings instrumented with strain gages under internal pressure. Three rings were tested for each of the two material systems, the SP288/AS graphite/epoxy and the 80AS/20S/PR288 graphite/S-glass/epoxy, and for each of the values of θ = 15°, 22.5°, 30°, 45°, 60°, 67.5°, and 75°. Each ring was instrumented with a 2-gage rosette with elements in the axial and circumferential directions.

Stress-strain curves for all specimens tested are shown in Figures 2-1 through 2-41. Values for the modulus, Poisson's ratio, strength, and ultimate strain computed from these curves are shown in these figures and summarized in Tables 2-1 and 2-2. All but the $[\pm15]_{2s}$ specimens show nonlinear strain response to failure. Difficulties were encountered with the $[\pm45]_{2s}$ specimens due to excessive deformation of the rings. These specimens deformed into a conical shape and allowed the bladder to extrude through the opening between the sides of the ring specimen and the steel plates in contact with them. For these reasons only lower bounds are given in Tables 2-1 and 2-2 for the strength and ultimate strain values of these specimens.

Tables 2-1 and 2-2 include also results for the modulus and Poisson's ratio calculated using measured unidirectional properties. The agreement between experimental and predicted values is satisfactory. The calculated properties were obtained by using a computer program called SQ5. This program is a point stress analysis of a laminate under in-plane loads, moments, and temperature effects. The formulation uses the usual lamination theory whereby the laminate constitutive relations are derived from those of each ply of the laminate.

The modulus of the hybrid laminates is lower than that of the graphite/epoxy laminates for $0°\leq\theta<45°$, but the relationship is reversed for $45°\leq\theta\leq90°$. The strength of the hybrid laminates is consistently lower than that of the graphite/epoxy laminates for all layups. Poisson's ratios for the hybrid

laminates are lower than those for the graphite/epoxy for $0° \leq \theta \leq 22.5°$, but no significant differences exist for $\theta \geq 30°$. The ultimate strain in the hybrid material is not significantly different from that of the graphite/epoxy for $0° \leq \theta \leq 30°$, but it becomes smaller than that of the graphite/epoxy material for $\theta \geq 45°$.

TABLE 2-1. STATIC TENSILE PROPERTIES OF $[\pm\theta]_{2s}$ ANGLE-PLY SP288/AS GRAPHITE/EPOXY LAMINATES

Laminate	Measured				Calculated	
	Modulus, $E_{\theta\theta}$ GPa (10^6 psi)	Poisson's Ratio, $\nu_{\theta x}$	Strength, $S_{\theta\theta T}$ MPa (ksi)	Ultimate Strain, $\epsilon^u_{\theta\theta T}$	Modulus, $E_{\theta\theta}$ GPa (10^6 psi)	Poisson's Ratio, $\nu_{\theta x}$
$[0_8]$	135 (19.5)	0.36	1458 (211)	0.0106	-	-
$[\pm15]_{2s}$	104.5 (15.2)	0.86	823 (119.3)	0.0078	112.8 (16.3)	0.91
$[\pm22.5]_{2s}$	81.4 (11.8)	1.18	773 (112.0)	0.0103	82.8 (12.0)	1.23
$[\pm30]_{2s}$	58.6 (8.50)	1.25	566 (82.0)	0.0132	53.3 (7.72)	1.23
$[\pm45]_{2s}$	20.4 (2.95)	0.69	>224 (32.5)	>0.0305	21.6 (3.13)	0.72
$[\pm60]_{2s}$	14.0 (2.03)	0.32	105 (15.2)	0.0116	13.0 (1.88)	0.30
$[\pm67.5]_{2s}$	12.0 (1.74)	0.17	85.1 (12.3)	0.0081	11.5 (1.67)	0.17
$[\pm75]_{2s}$	12.1 (1.75)	0.09	74.8 (10.8)	0.0075	10.8 (1.57)	0.09
$[90_8]$	10.3 (1.49)	0.03	52 (7.6)	0.0052	-	-

TABLE 2-2. STATIC TENSILE PROPERTIES OF $[\pm\theta]_{2s}$ ANGLE-PLY 80AS/20S/PR288 GRAPHITE/S-GLASS/EPOXY LAMINATES

	Measured				Calculated	
Laminate	Modulus, $E_{\theta\theta}$ GPa (10^6 psi)	Poisson's Ratio, $\nu_{\theta x}$	Strength, $S_{\theta\theta T}$ MPa (ksi)	Ultimate Strain, $\varepsilon^u_{\theta\theta T}$	Modulus, $E_{\theta\theta}$ GPa (10^6 psi)	Poisson's Ratio, $\nu_{\theta x}$
$[0_8]$	107 (15.6)	0.18	1240 (180)	0.0114	-	-
$[\pm15]_{2s}$	94.5 (13.7)	0.68	806 (116.8)	0.0084	89.7 (13.0)	0.71
$[\pm22.5]_{2s}$	68.5 (9.93)	0.83	653 (94.6)	0.0104	68.7 (9.96)	0.98
$[\pm30]_{2s}$	44.9 (6.51)	1.26	503 (73.0)	0.0139	46.8 (6.78)	1.04
$[\pm45]_{2s}$	21.5 (3.12)	0.74	>191 (27.7)	>0.0265	20.8 (3.01)	0.67
$[\pm60]_{2s}$	18.2 (2.64)	0.30	94.8 (13.7)	0.0085	13.4 (1.94)	0.30
$[\pm67.5]_{2s}$	14.4 (2.08)	0.16	76.1 (11.0)	0.0062	12.3 (1.78)	0.17
$[\pm75]_{2s}$	15.5 (2.25)	0.10	61.4 (8.9)	0.0047	11.8 (1.71)	0.09
$[90_8]$	11.8 (1.71)	0.02	49.0 (7.1)	0.0045	-	-

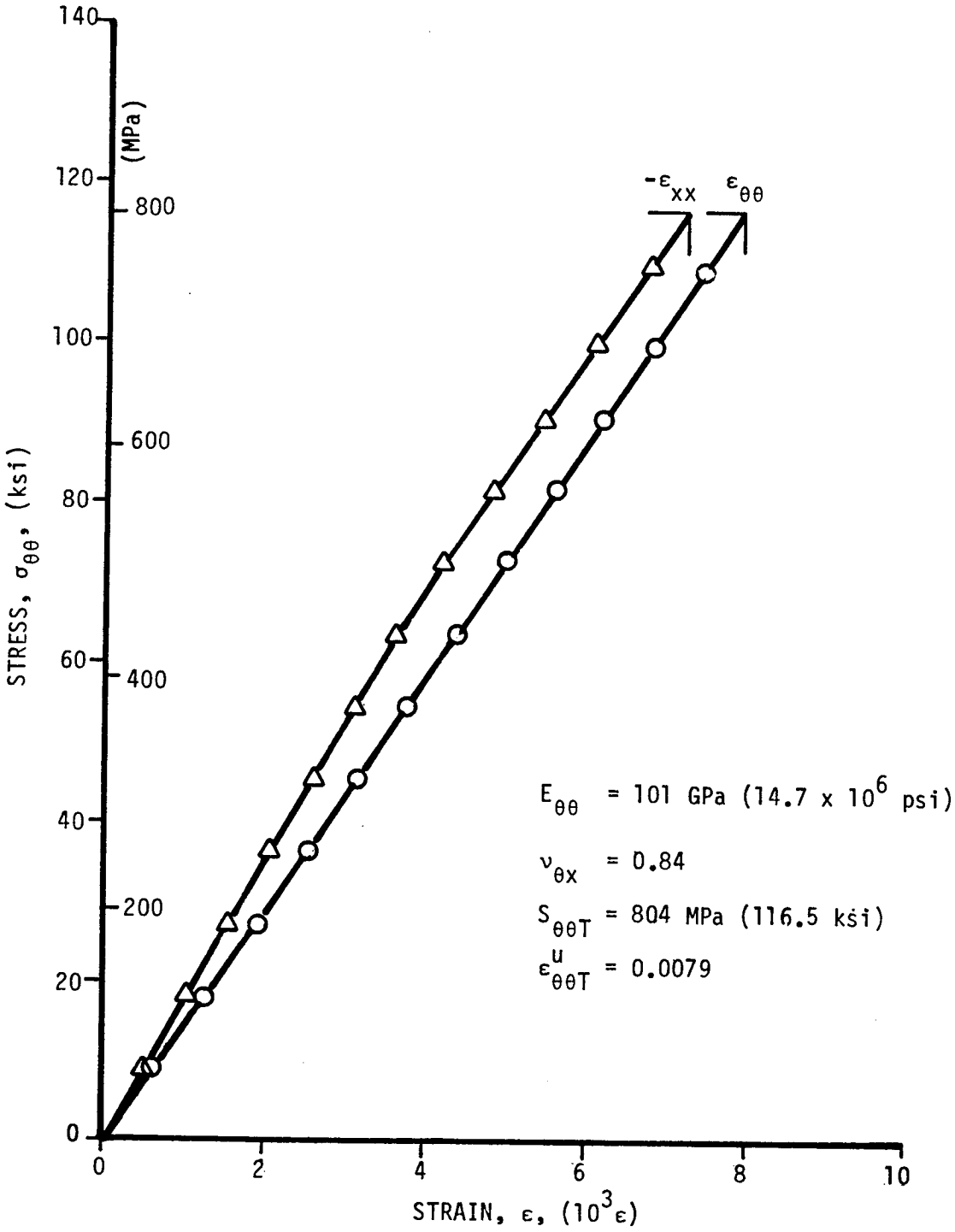

Figure 2-1. Strains in $[\pm 15]_{2S}$ SP288/AS ring specimen under static tensile loading (Specimen No. 35-1).

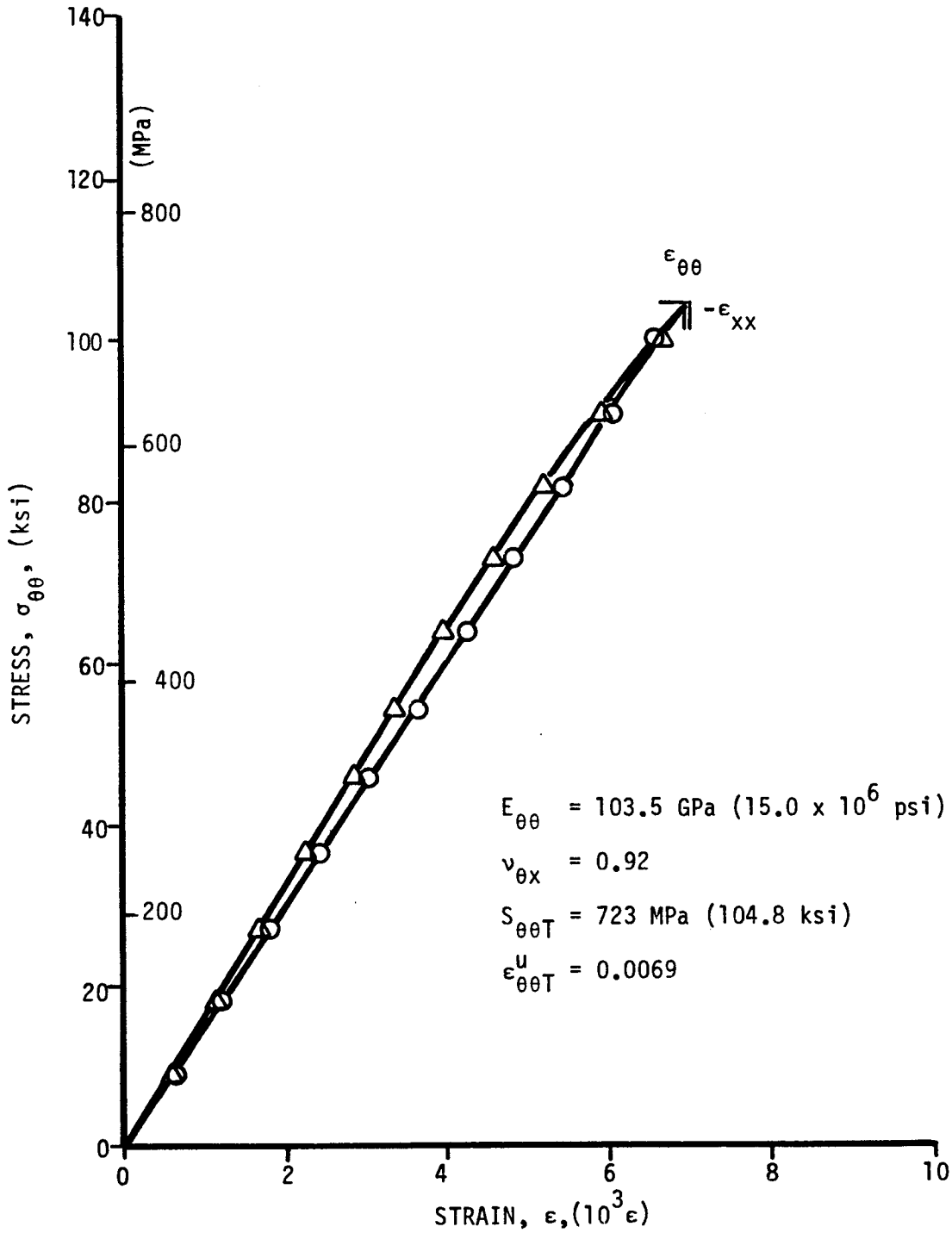

Figure 2-2. Strains in $[\pm 15]_{2S}$ SP288/AS ring specimen under static tensile loading (Specimen No. 35-3).

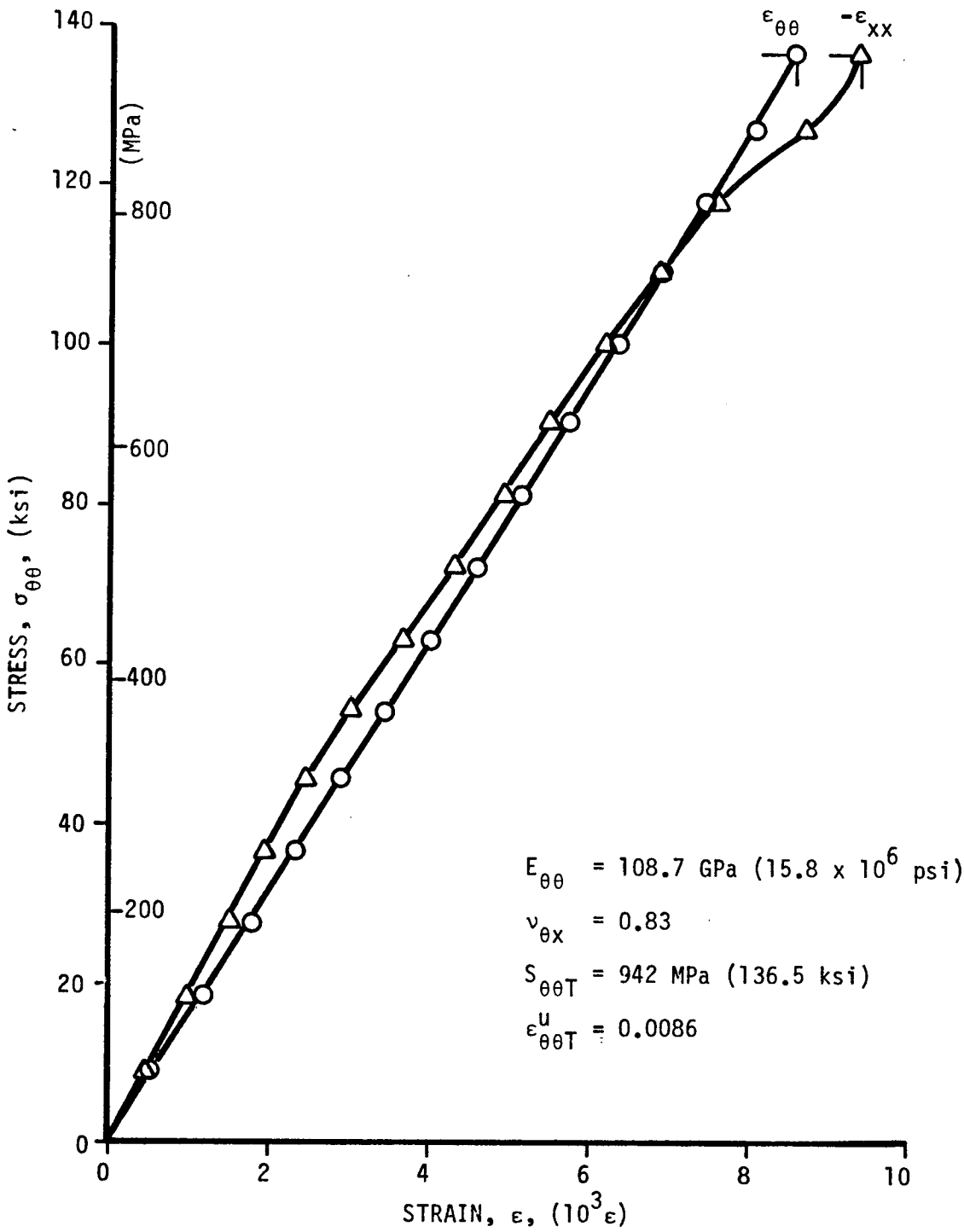

Figure 2-3. Strains in $[\pm 15]_{2S}$ SP288/AS ring specimen under static tensile loading (Specimen No. 35-5).

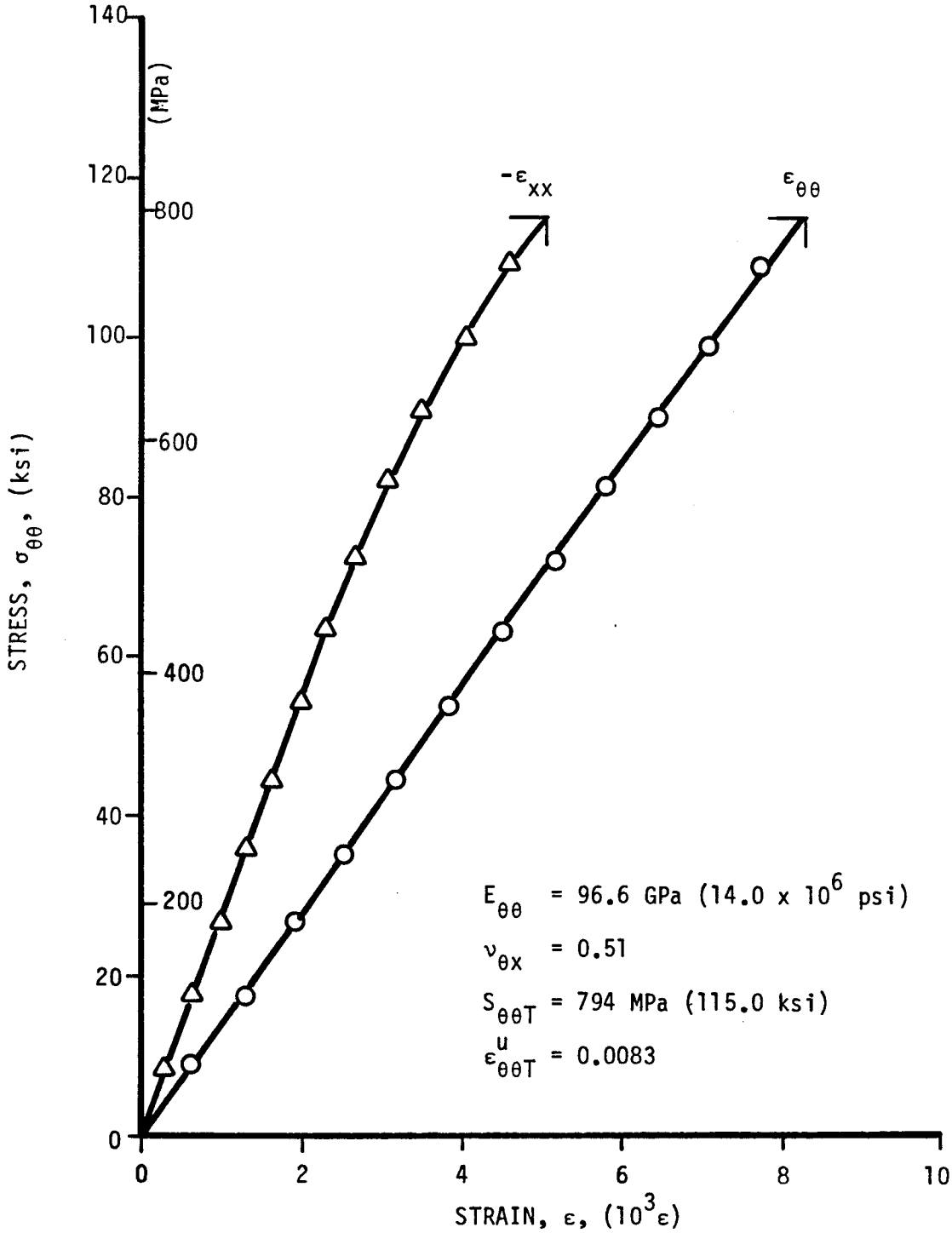

Figure 2-4. Strains in $[\pm 15]_{2S}$ 80AS/20S/PR288 ring specimen under static tensile loading (Specimen No. 36-1).

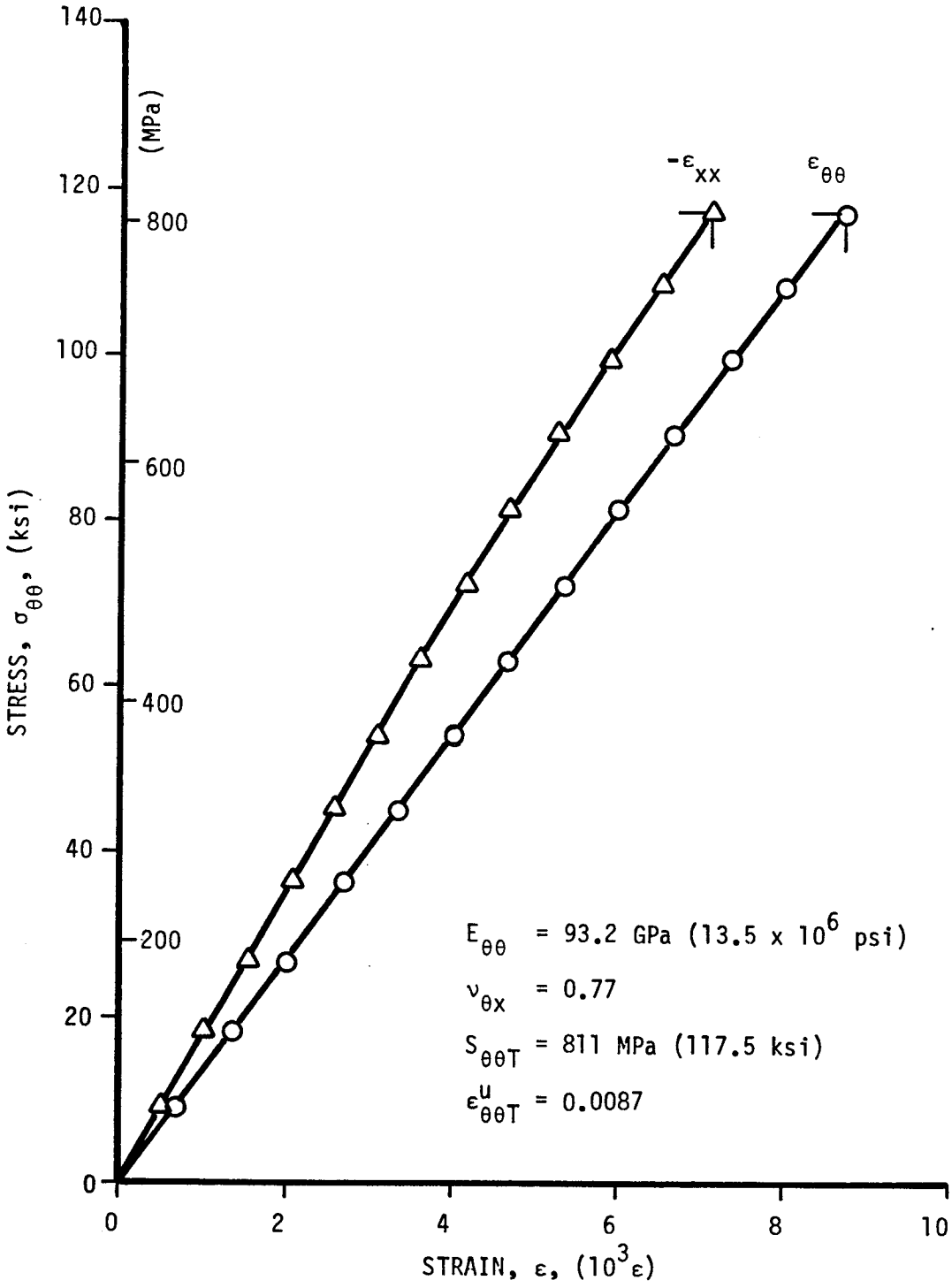

Figure 2-5. Strains in $[\pm 15]_{2S}$ 80AS/20S/PR288 ring specimen under static tensile loading (Specimen No. 36-3).

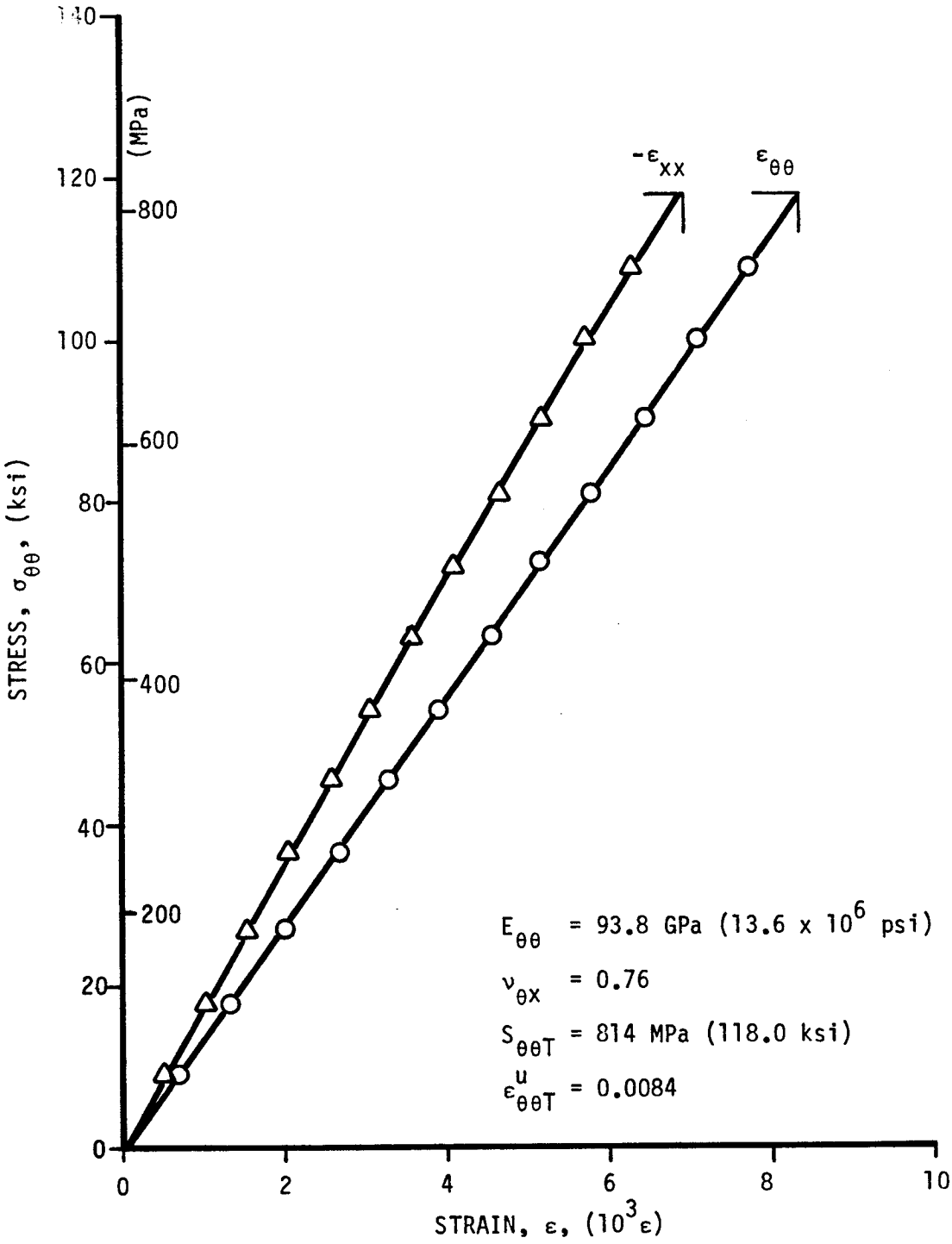

Figure 2-6. Strains in $[\pm 15]_{2S}$ 80AS/20S/PR288 ring specimen under static tensile loading (Specimen No. 36-5).

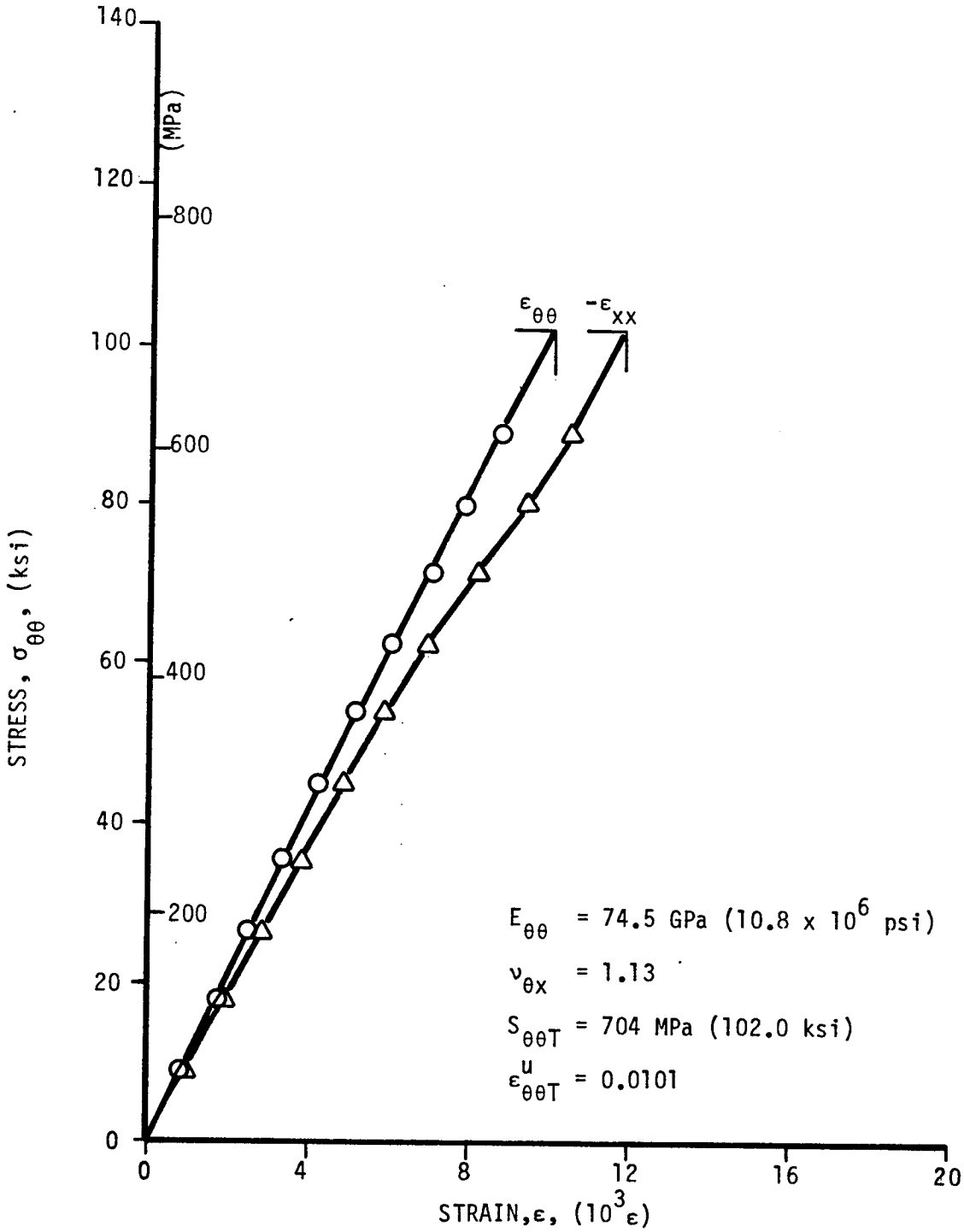

Figure 2-7. Strains in $[\pm 22.5]_{2s}$ SP288/AS ring specimen under static tensile loading (Specimen No. 33-1).

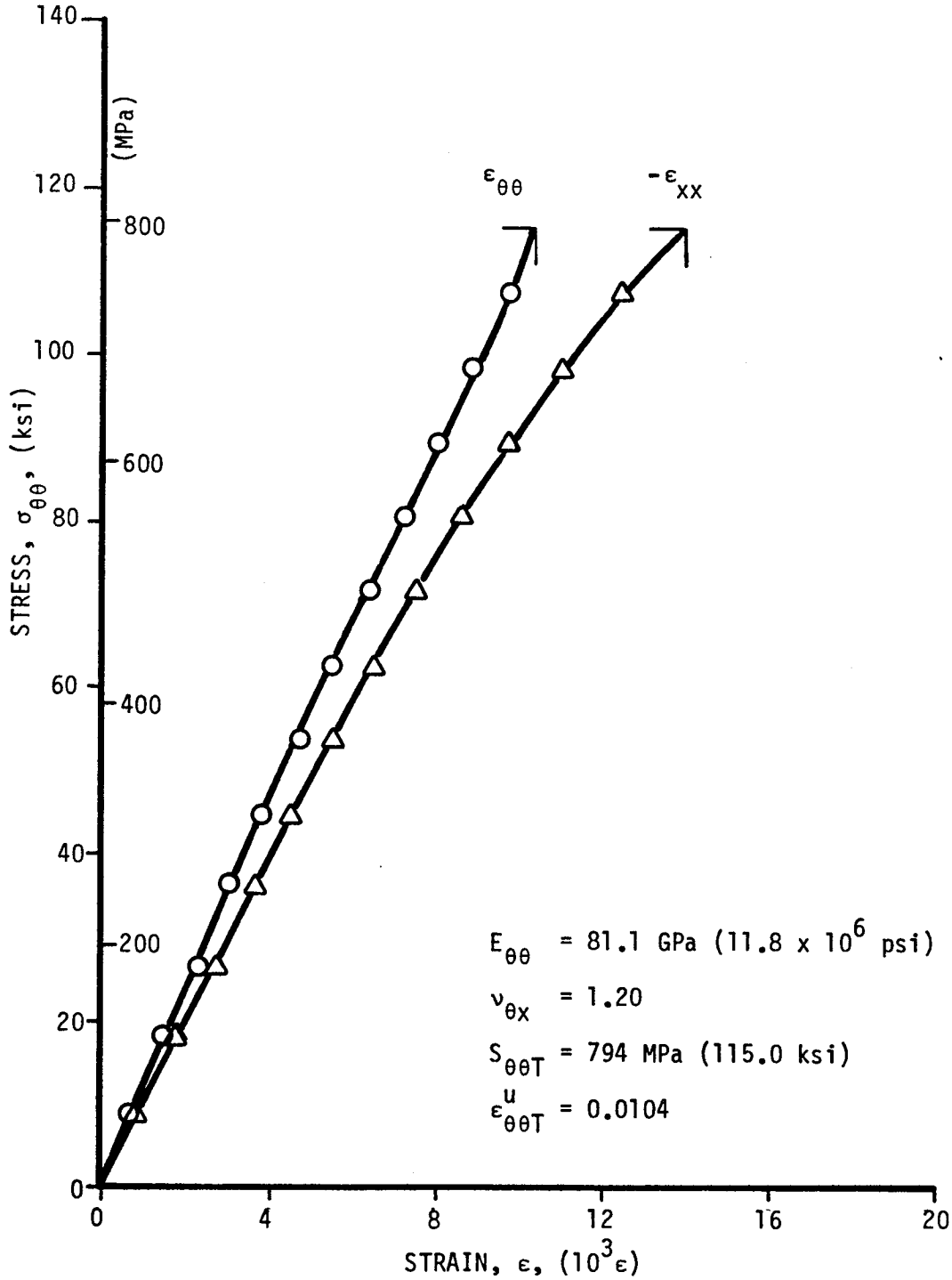

Figure 2-8. Strains in $[\pm 22.5]_{2S}$ SP288/AS ring specimen under static tensile loading (Specimen No. 33-3).

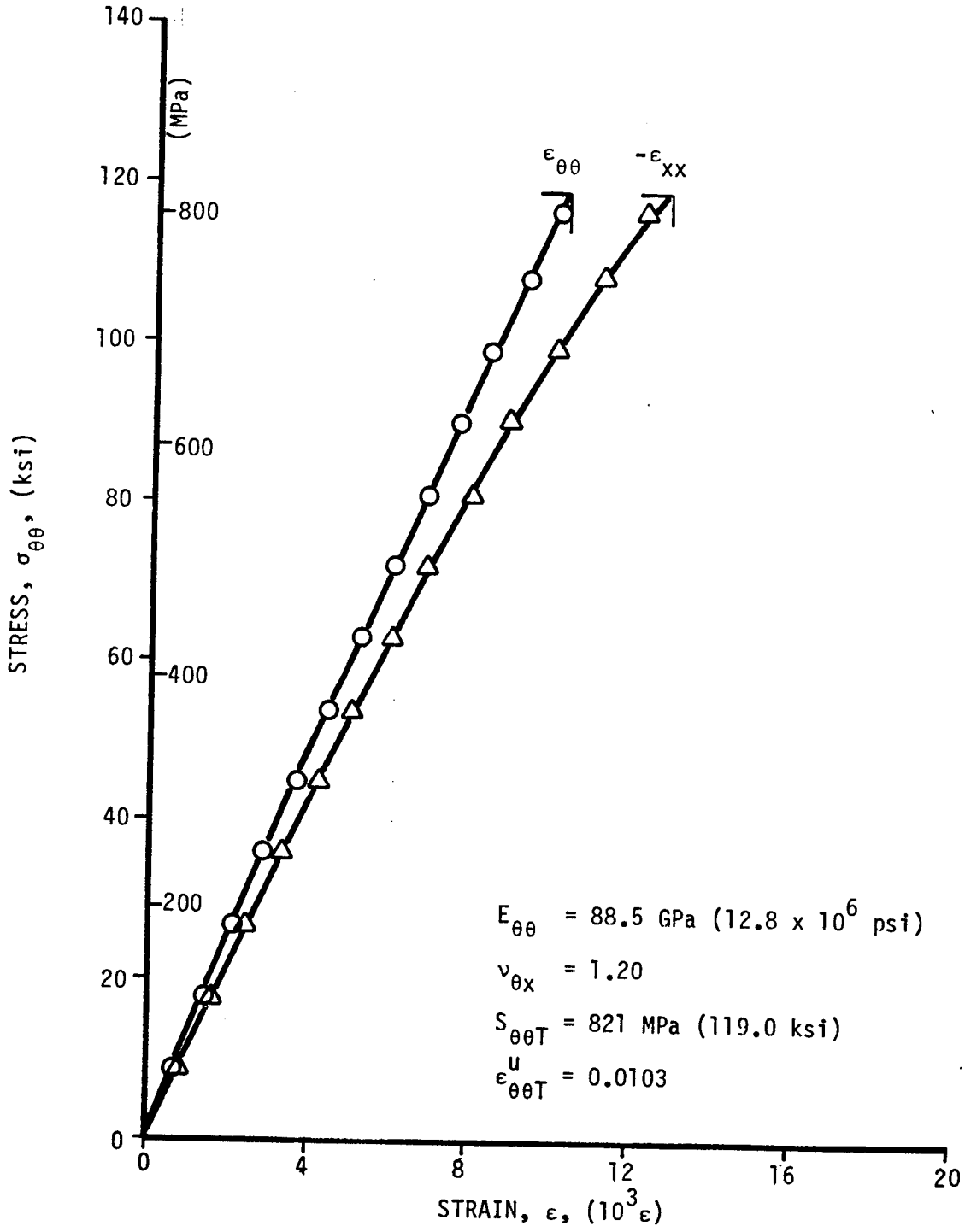

Figure 2-9. Strains in $[\pm 22.5]_{2s}$ SP288/AS ring specimen under static tensile loading (Specimen No. 33-5).

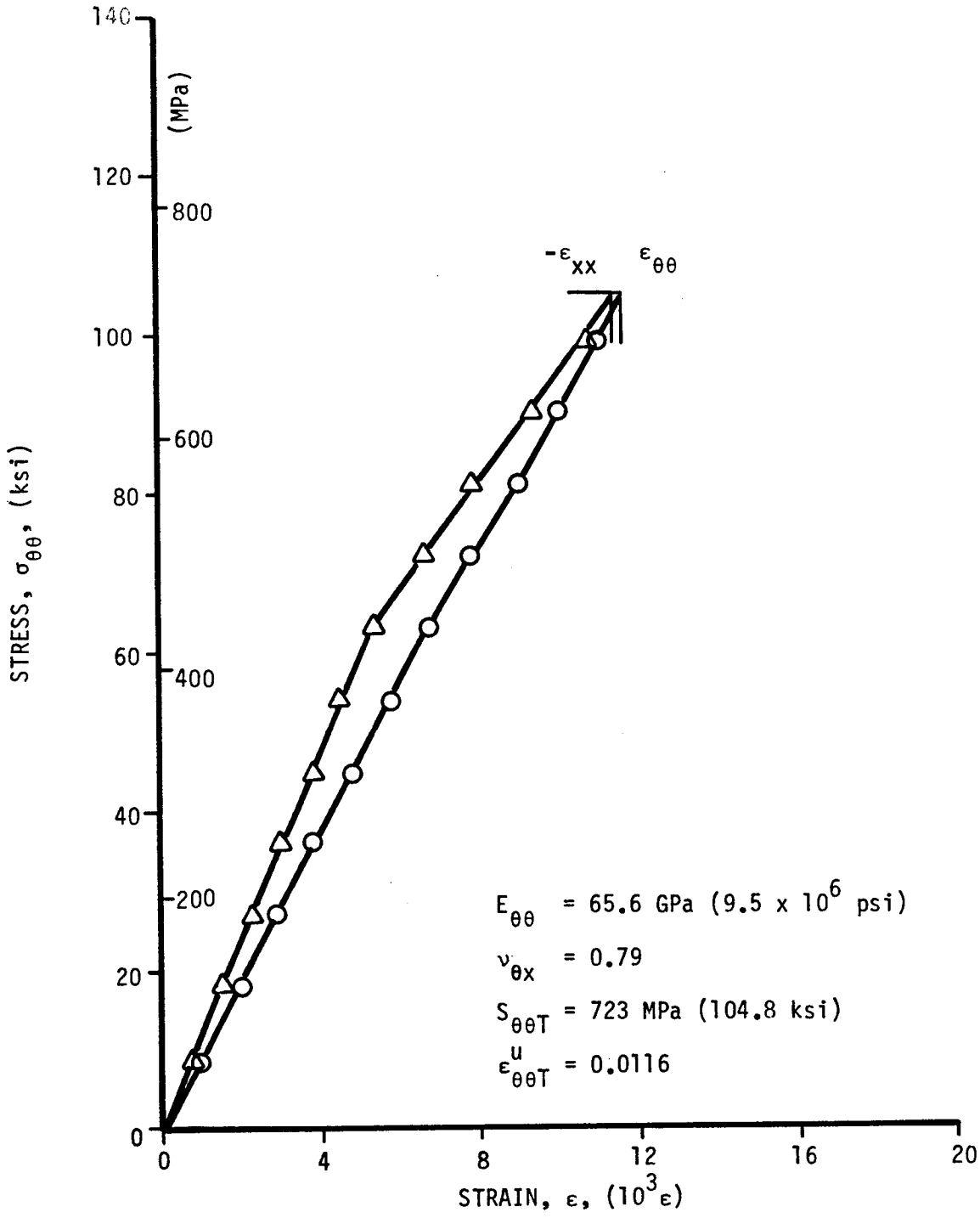

Figure 2-10. Strains in $[\pm 22.5]_{2S}$ 80AS/20S/PR288 ring specimen under static tensile loading (Specimen No. 34-1).

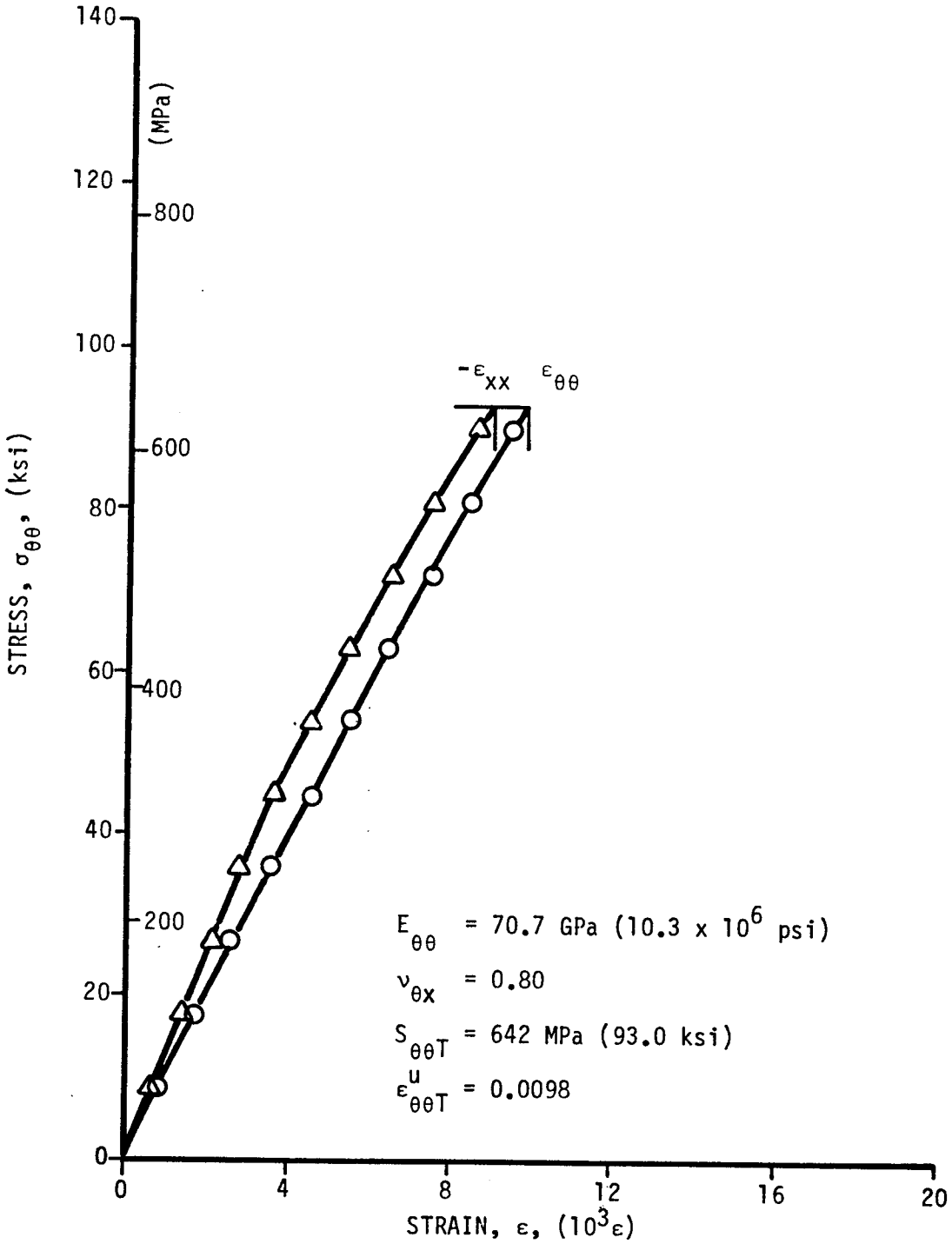

Figure 2-11. Strains in $[\pm 22.5]_{2S}$ 80AS/20S/PR288 ring specimen under static tensile loading (Specimen No. 34-3).

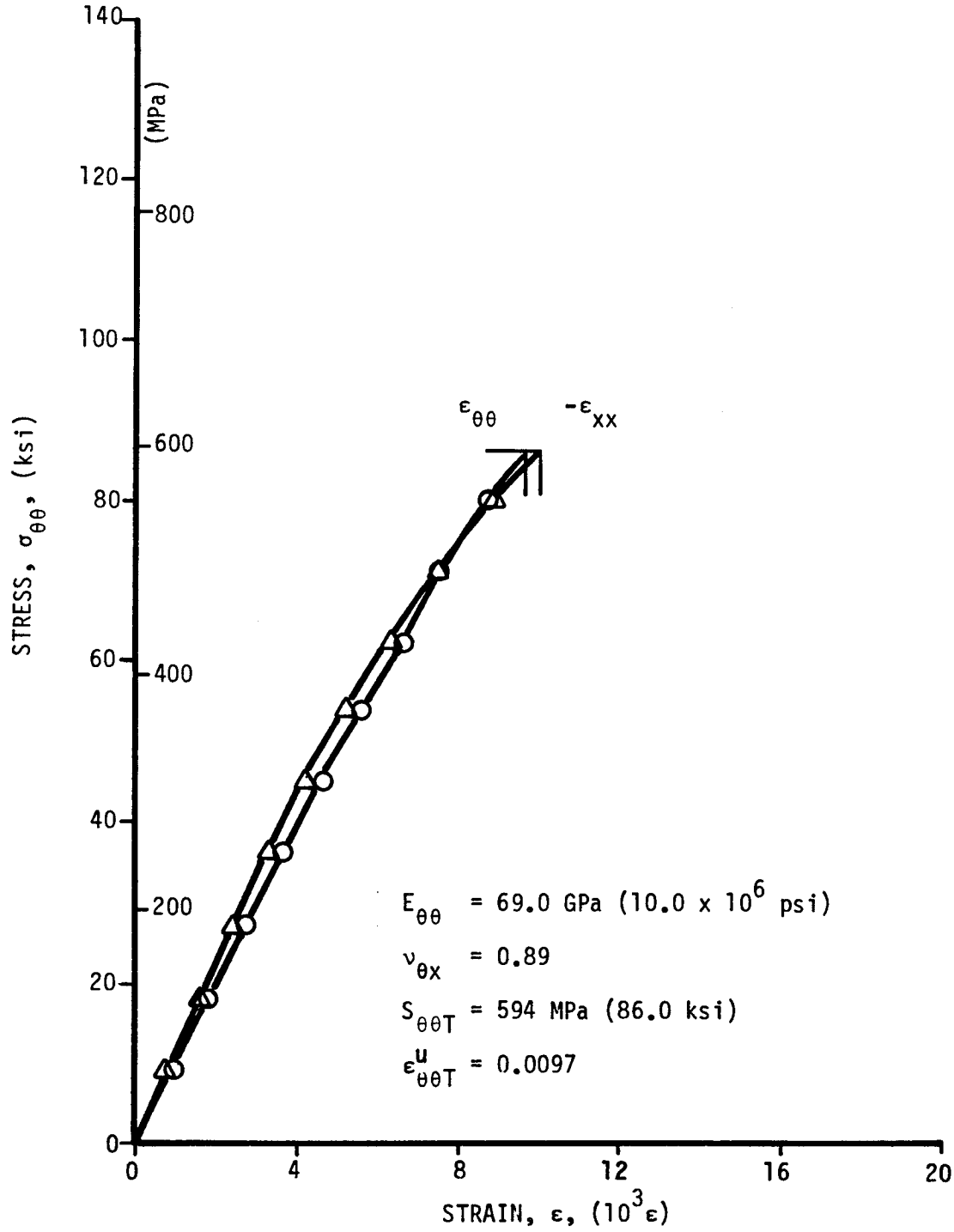

Figure 2-12. Strains in $[\pm 22.5]_{2S}$ 80AS/20S/PR288 ring specimen under static tensile loading (Specimen No. 34-5).

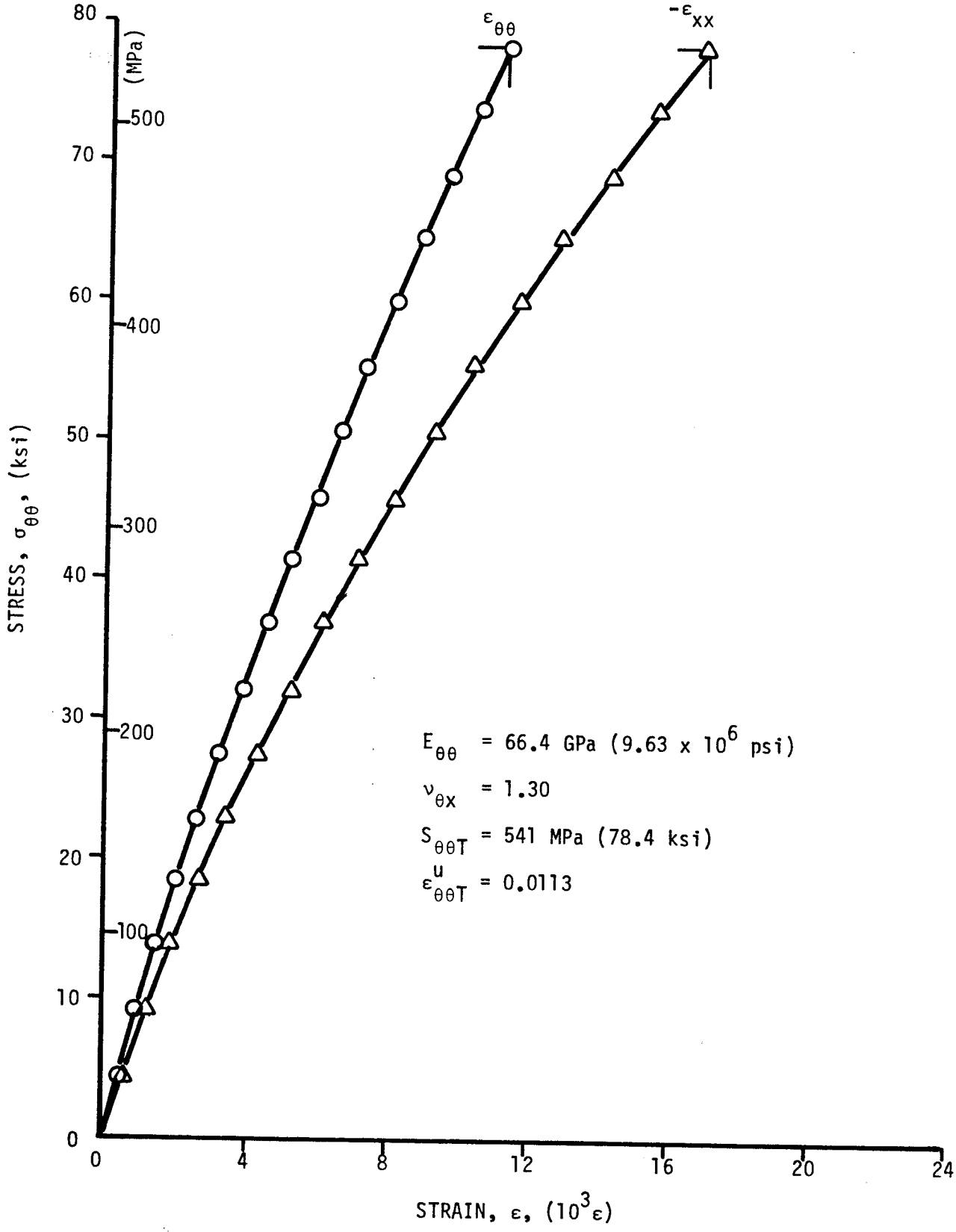

Figure 2-13. Strains in $[\pm 30]_{2S}$ SP288/AS ring specimen under static tensile loading (Specimen No. 28-1).

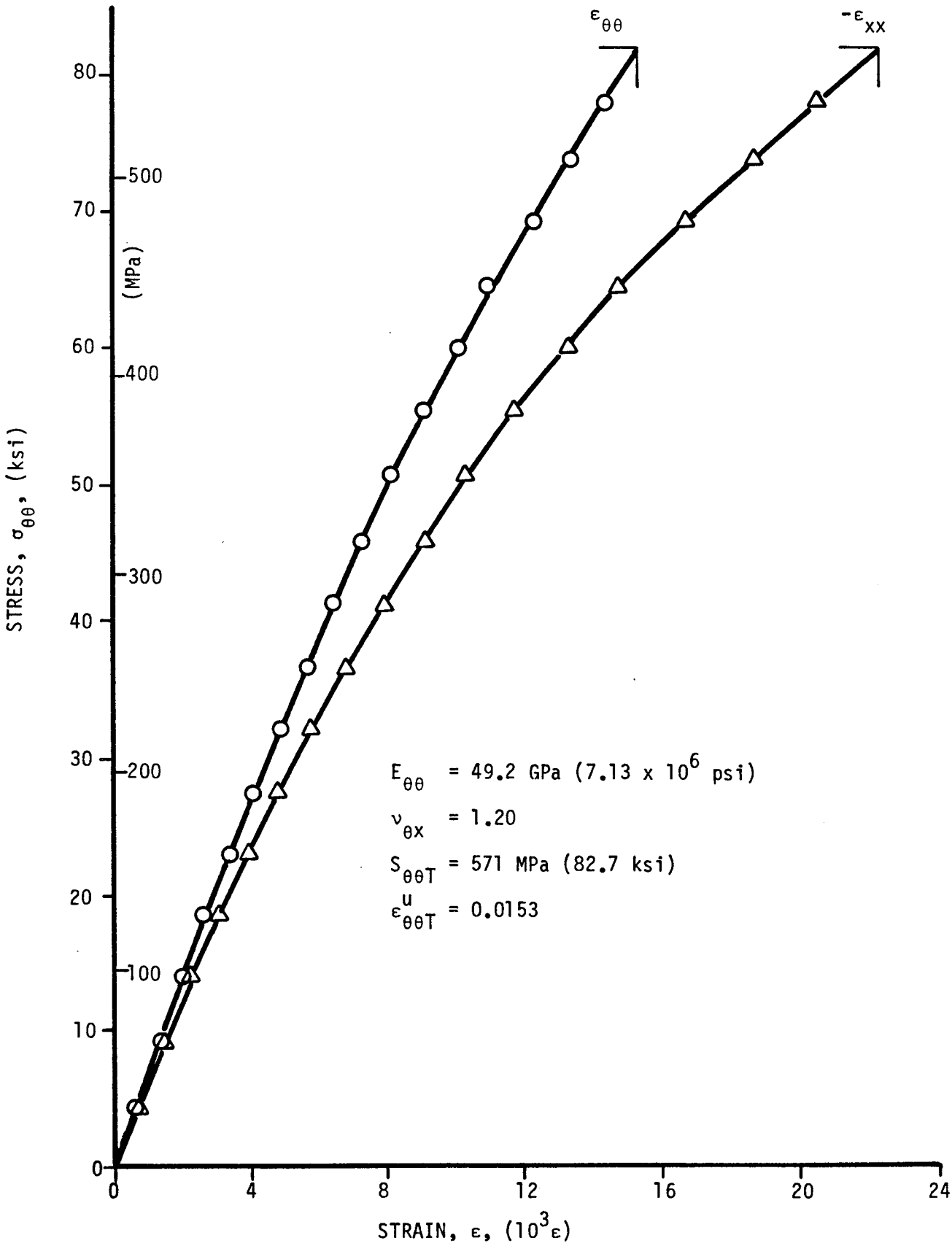

Figure 2-14. Strains in $[\pm 30]_{2S}$ SP288/AS ring specimen under static tensile loading (Specimen No. 28-3).

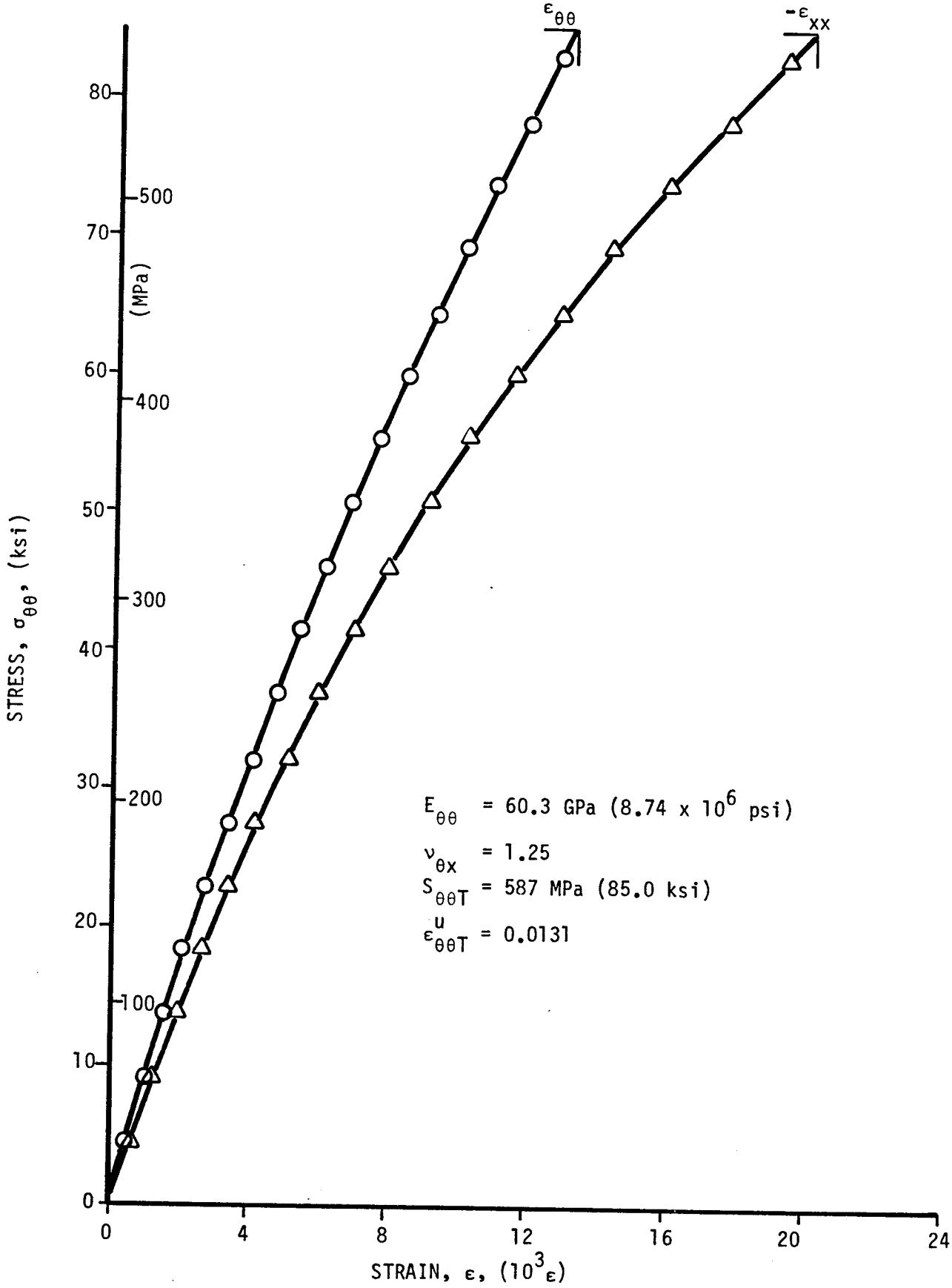

Figure 2-15. Strains in $[\pm 30]_{2s}$ SP288/AS specimen under static tensile loading (Specimen No. 28-5).

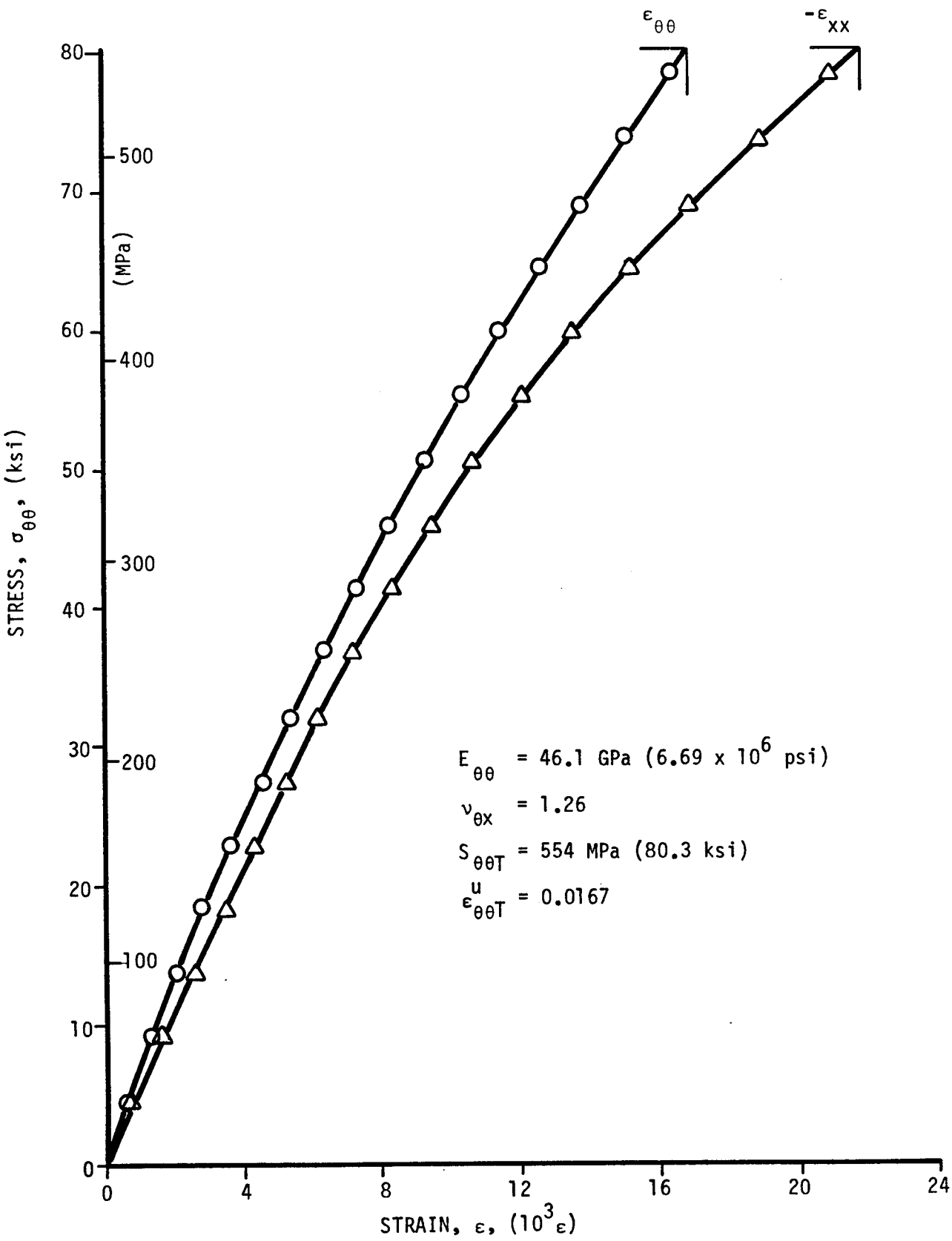

Figure 2-16. Strains in $[\pm 30]_{2S}$ 80AS/20S/PR288 ring specimen under static tensile loading (Specimen No. 29-1).

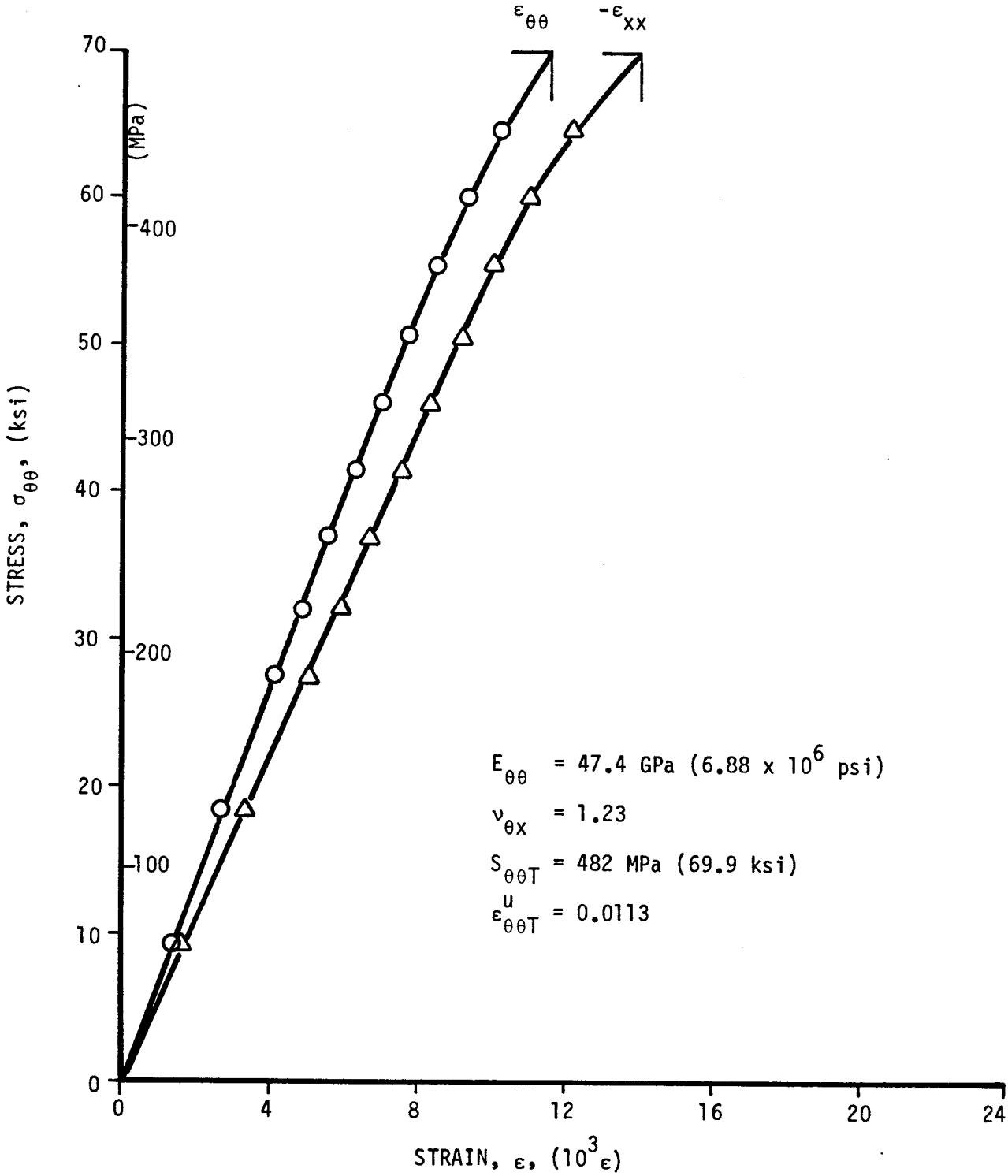

Figure 2-17. Strains in $[\pm 30]_{2S}$ 80AS/20S/PR288 ring specimen under static tensile loading (Specimen No. 29-3).

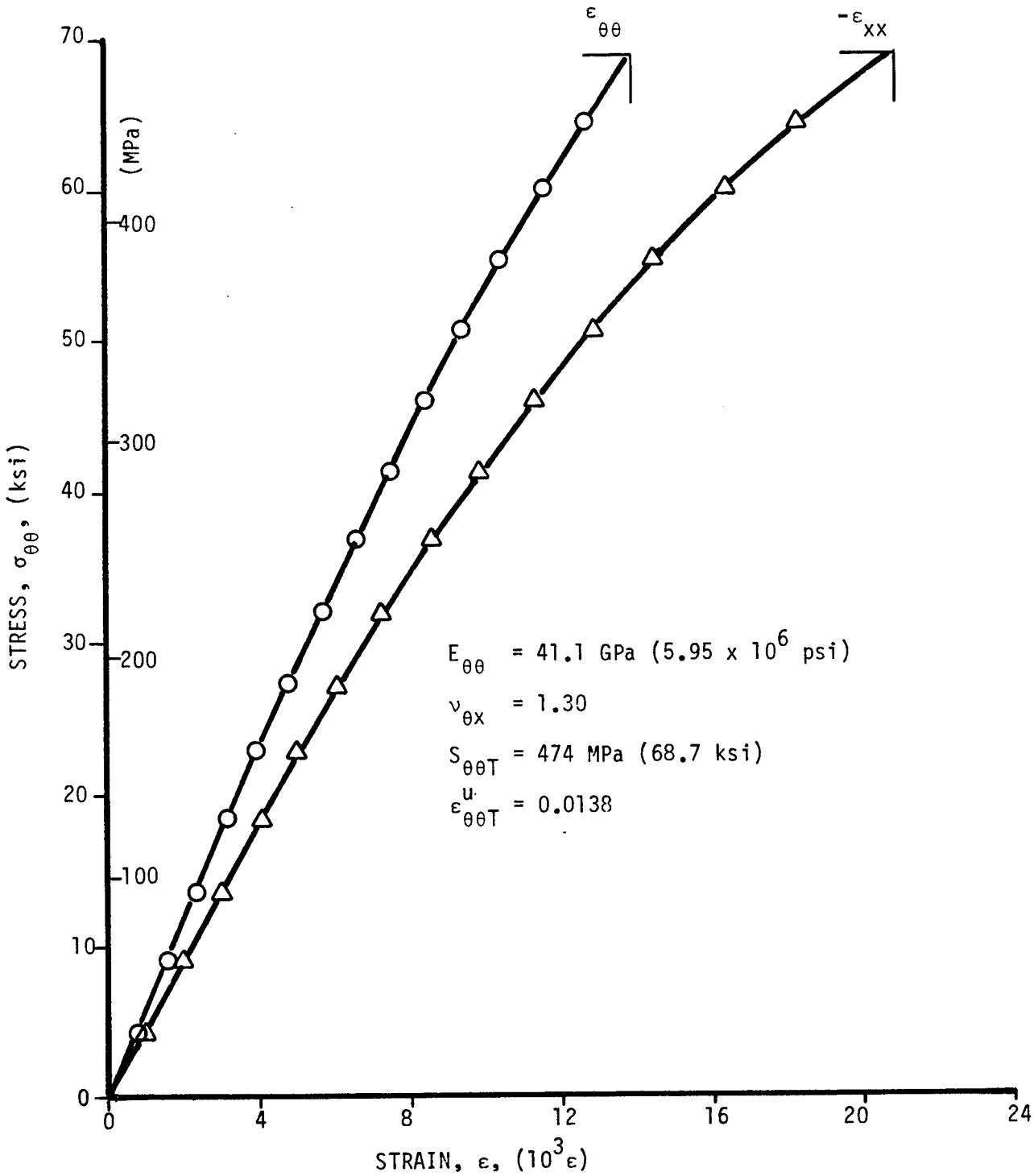

Figure 2-18. Strains in $[\pm 30]_{2S}$ 80AS/20S/PR288 ring specimen under static tensile loading (Specimen No. 29-5).

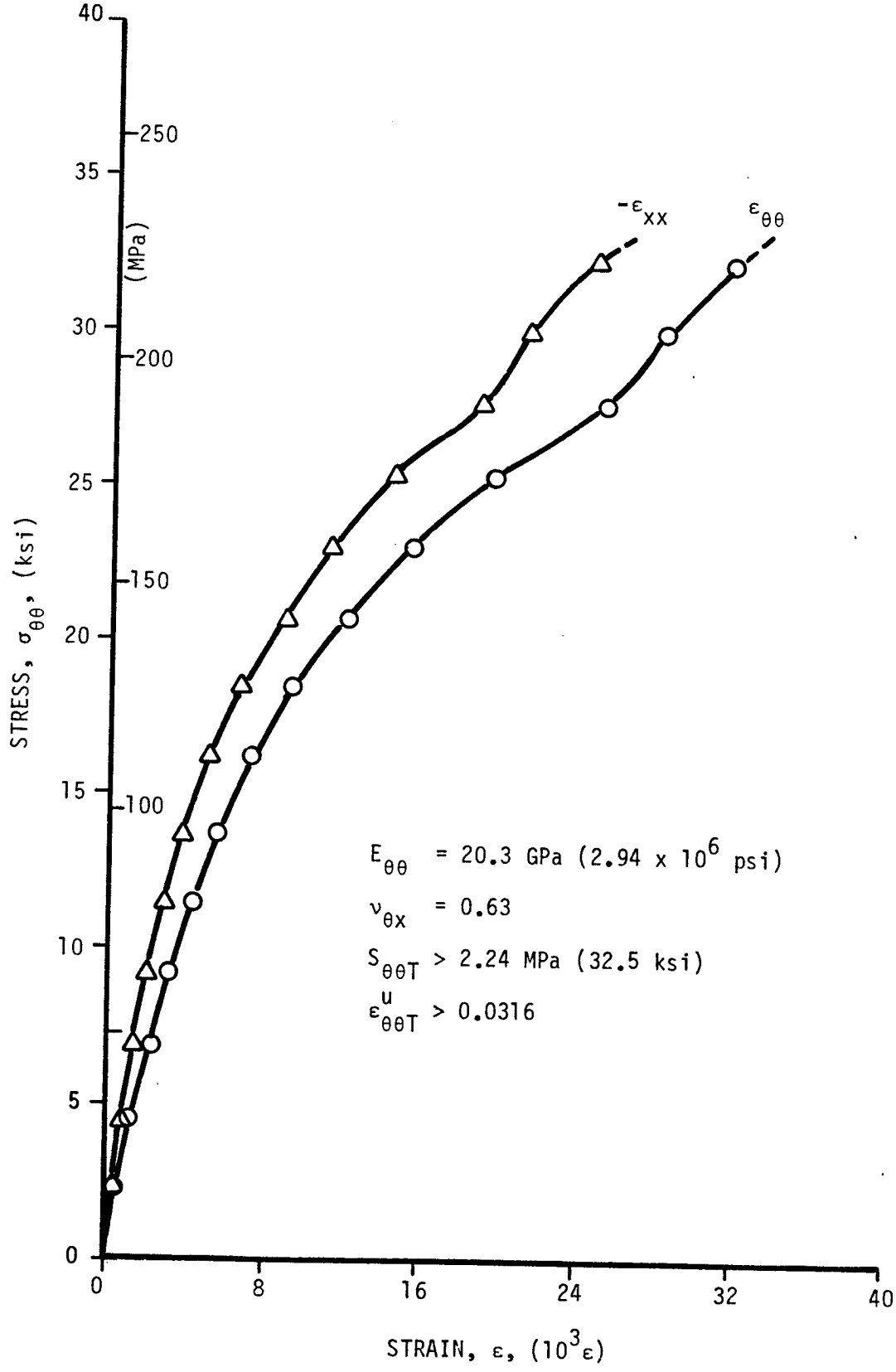

Figure 2-19. Strains in $[\pm 45]_{2S}$ SP288/AS ring specimen under static tensile loading (Specimen No. 24-1).

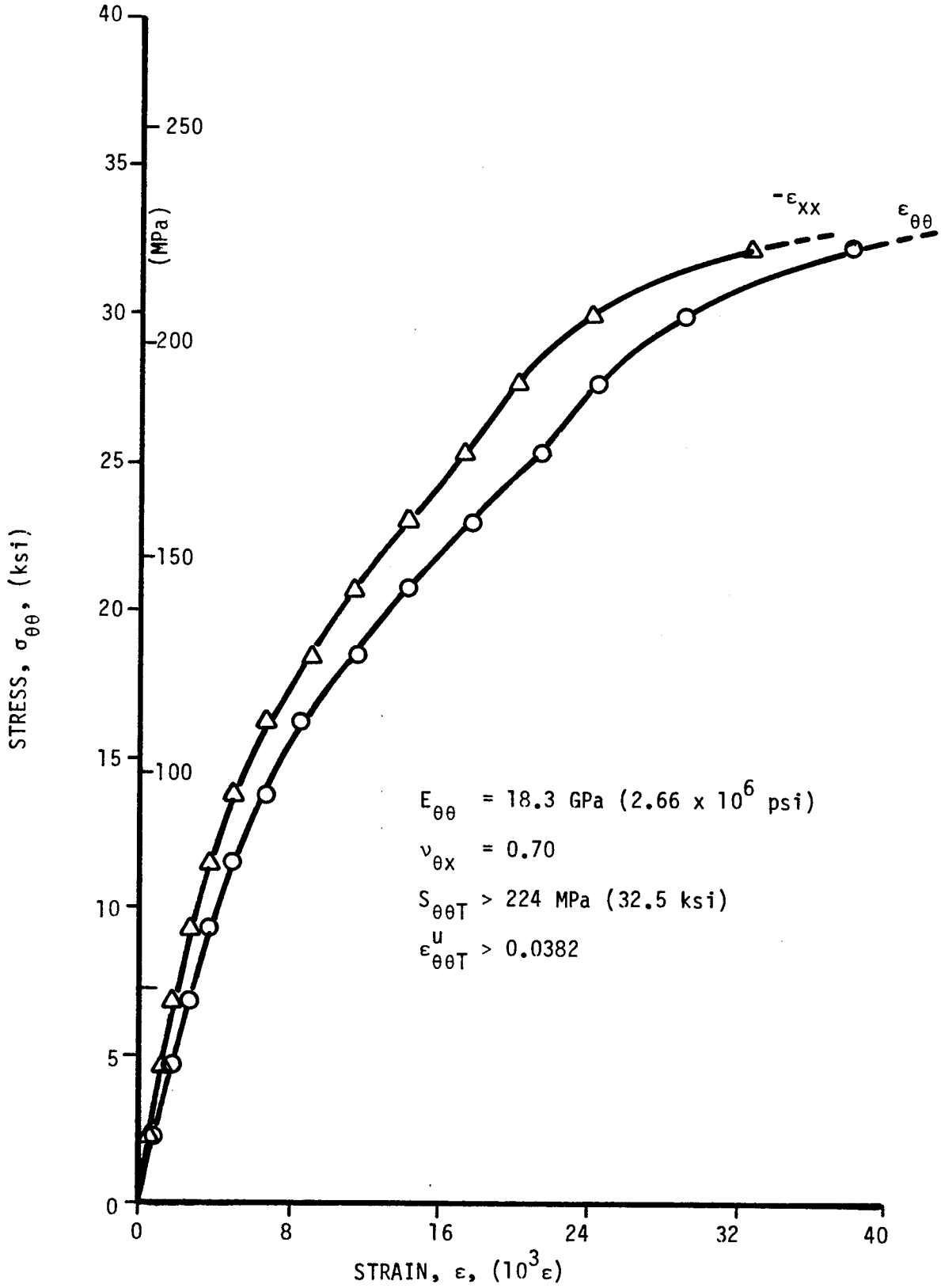

Figure 2-20. Strains in $[\pm 45]_{2S}$ SP288/AS ring specimen under static tensile loading (Specimen No. 24-3).

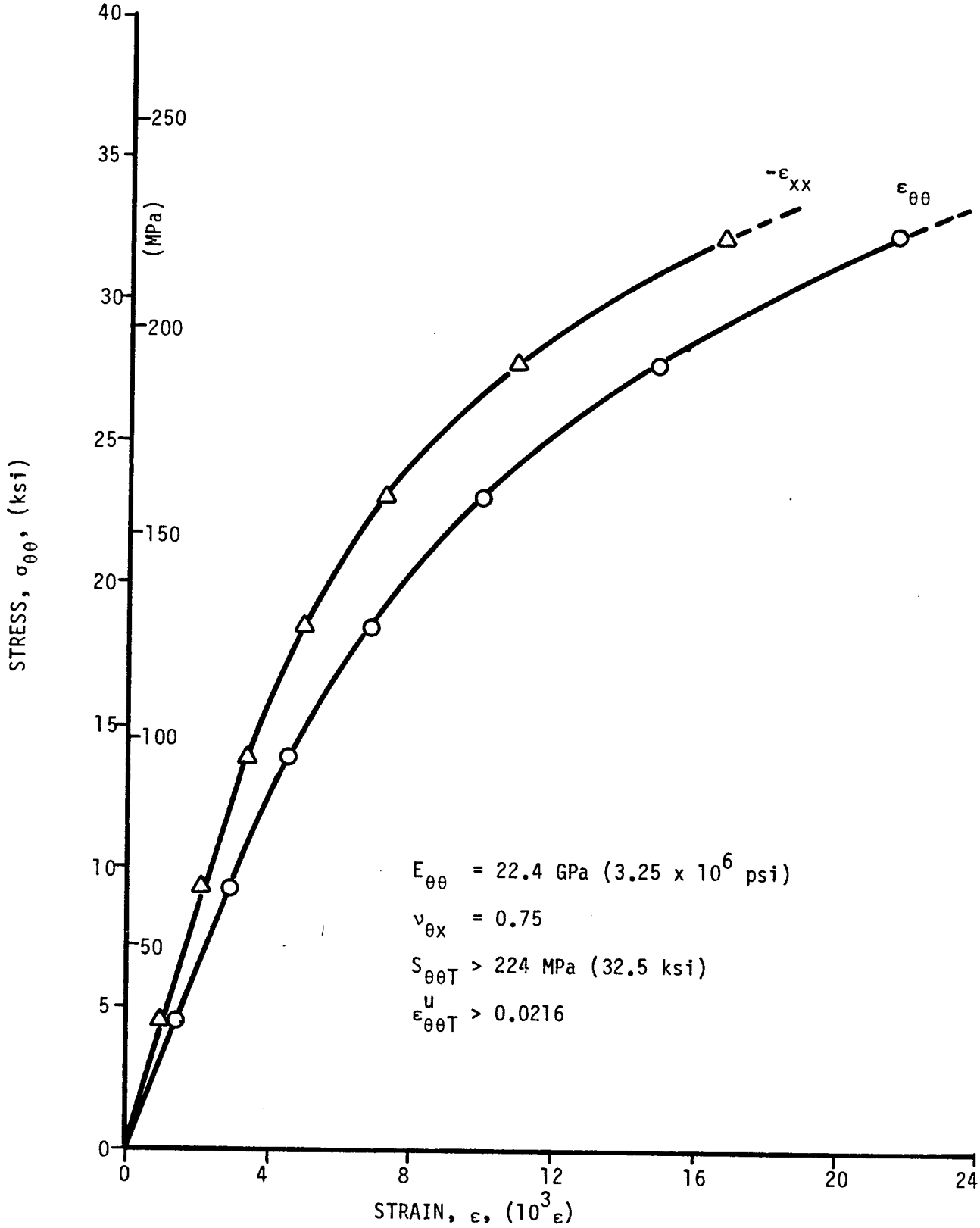

Figure 2-21. Strains in $[\pm 45]_{2S}$ SP288/AS ring specimen under static tensile loading (Specimen No. 24-5).

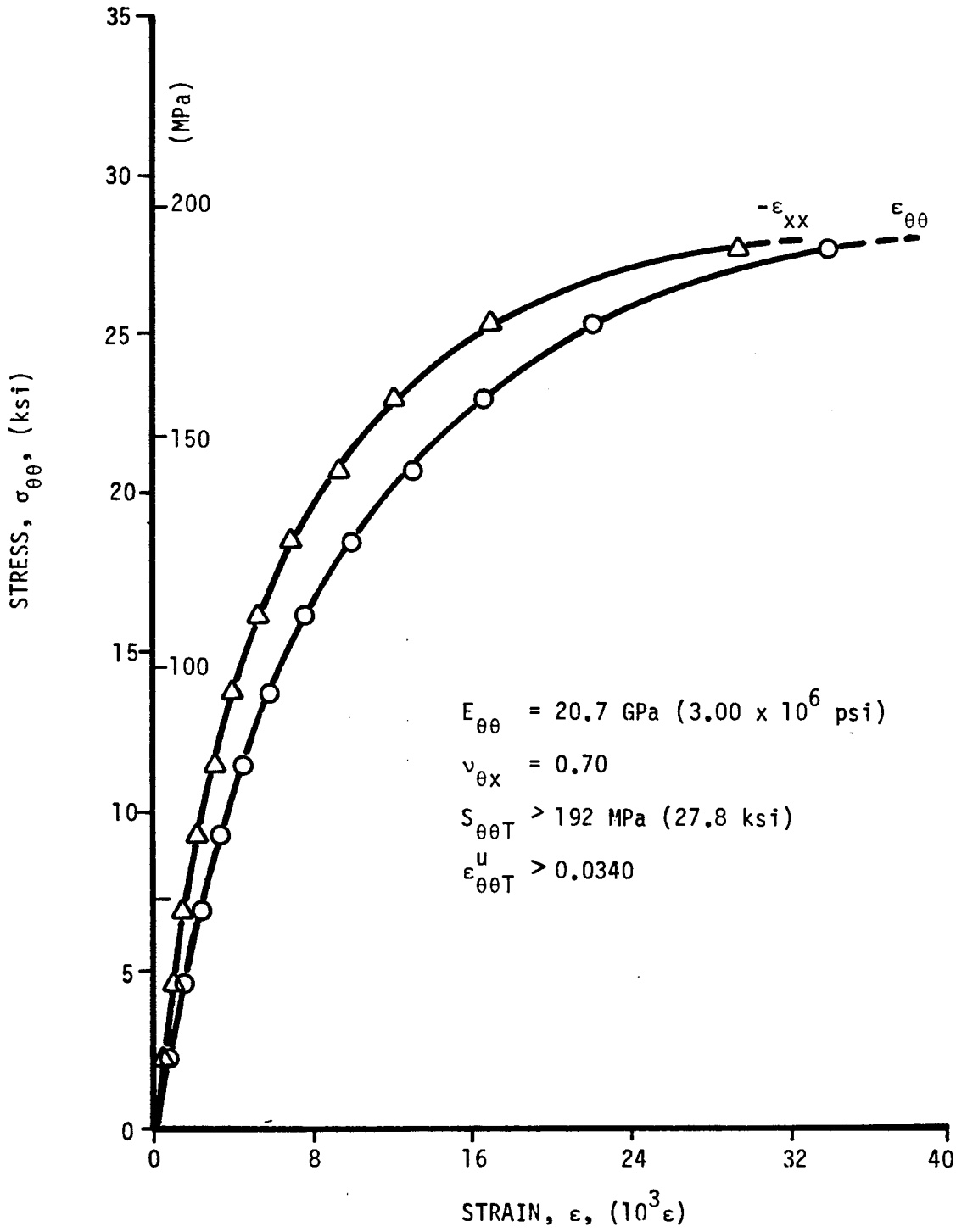

Figure 2-22. Strains in $[\pm 45]_{2S}$ 80AS/20S/PR288 ring specimen under static tensile loading (Specimen No. 25-1).

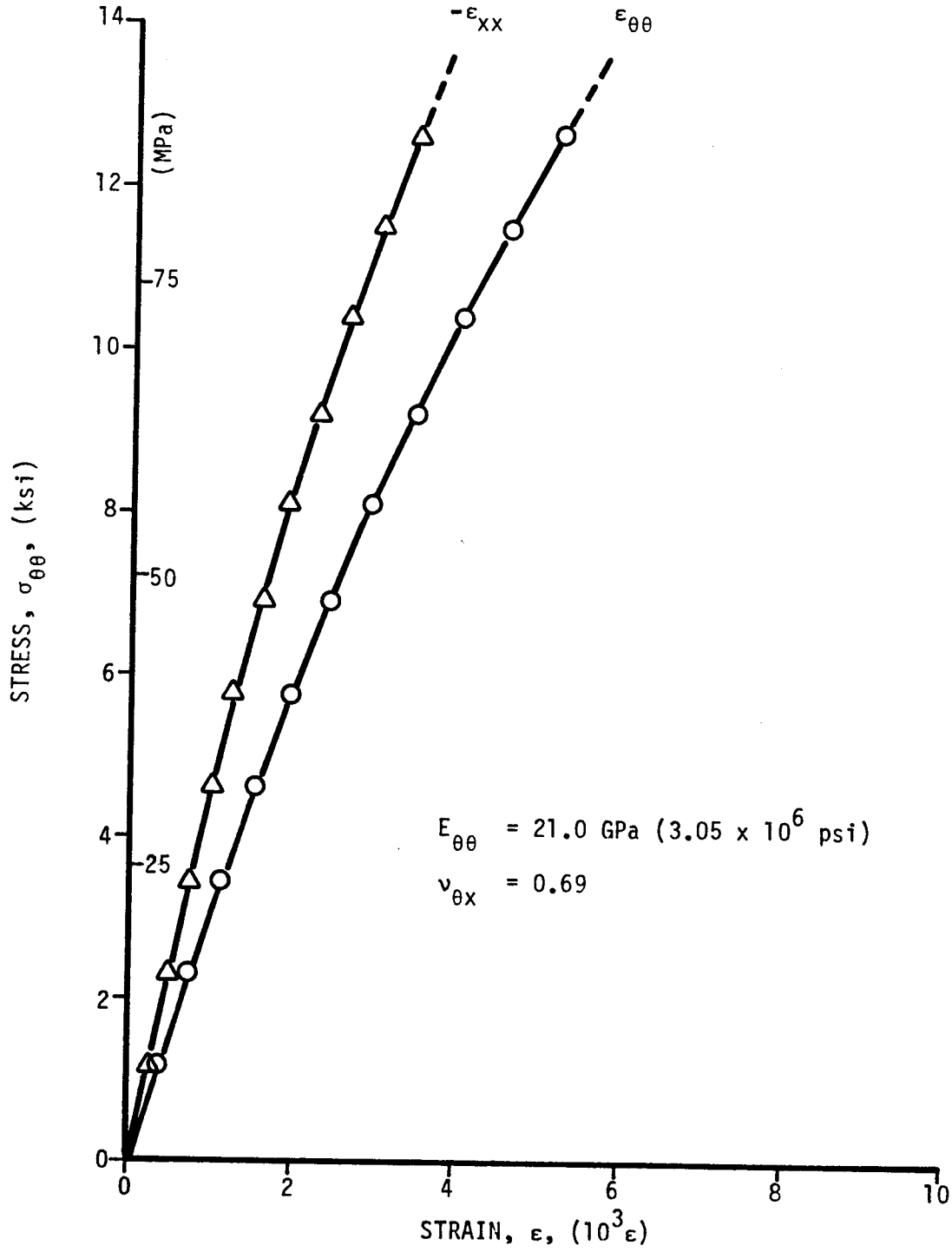

Figure 2-23. Strains in $[\pm 45]_{2S}$ 80AS/20S/PR288 ring specimen under static tensile loading (Specimen No. 25-3).

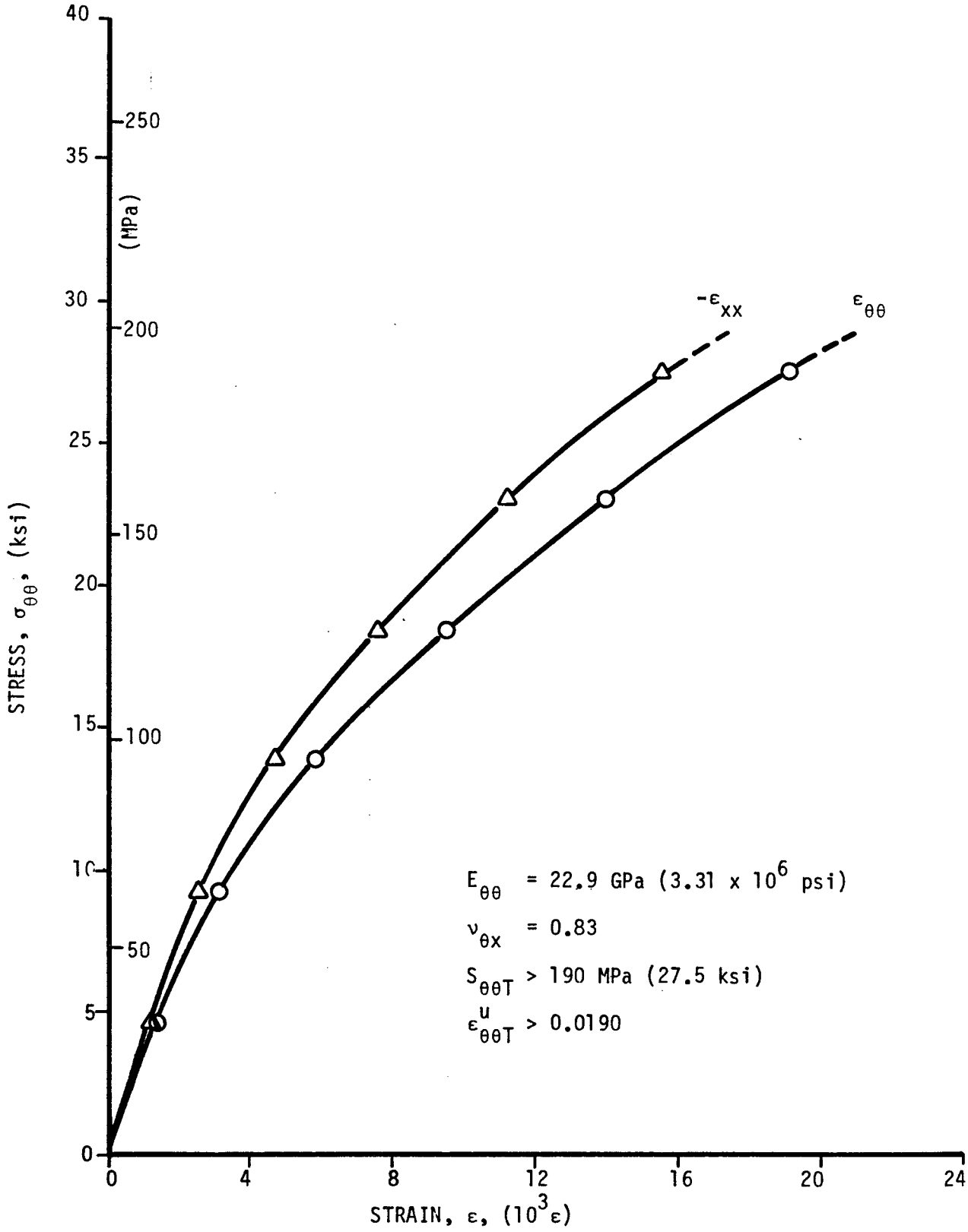

Figure 2-24. Strains in $[\pm 45]_{2S}$ 80AS/20S/PR288 ring specimen under static tensile loading (Specimen No. 25-5).

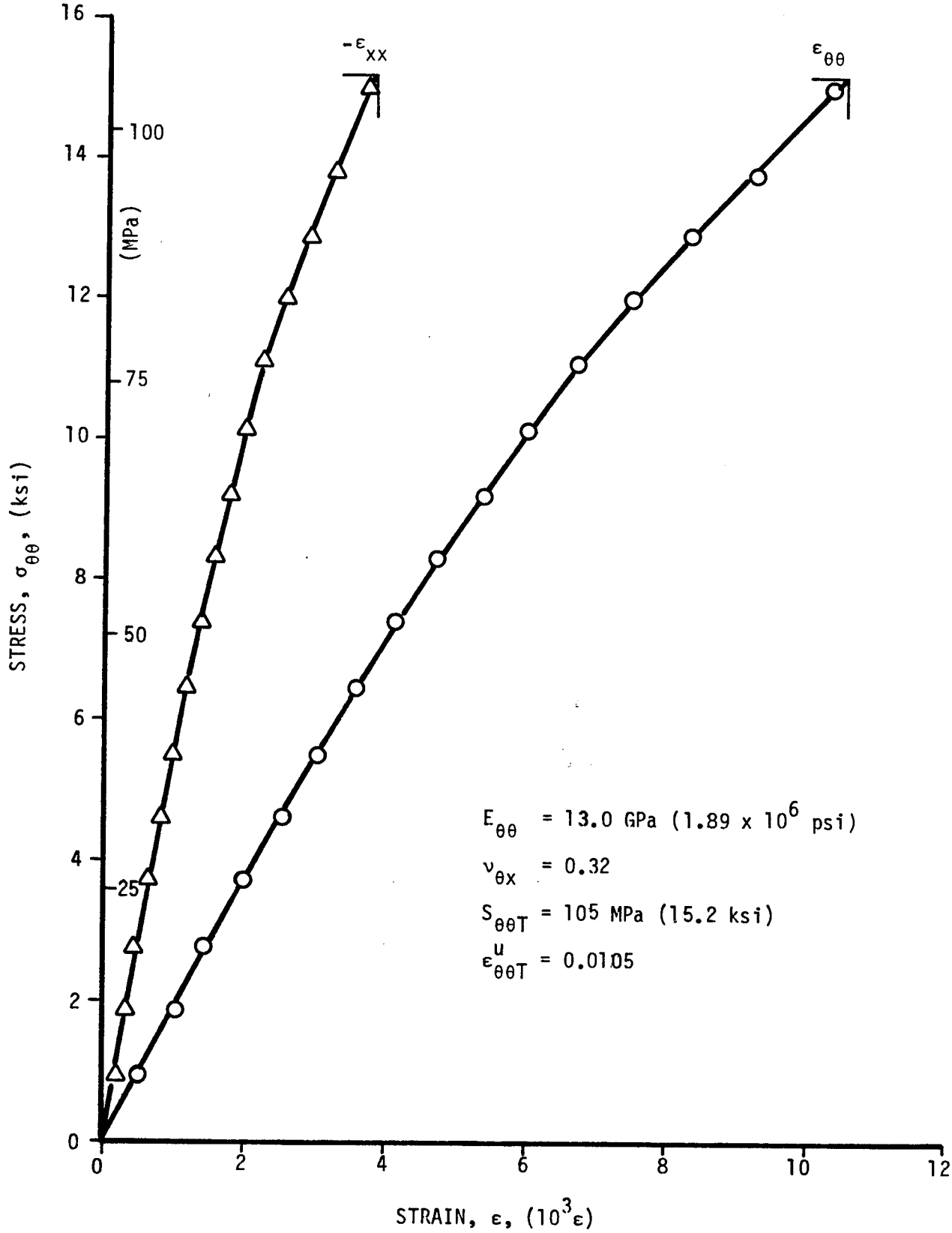

Figure 2-25. Strains in $[\pm 60]_{2S}$ SP288/AS ring specimen under static tensile loading (Specimen No. 22-1).

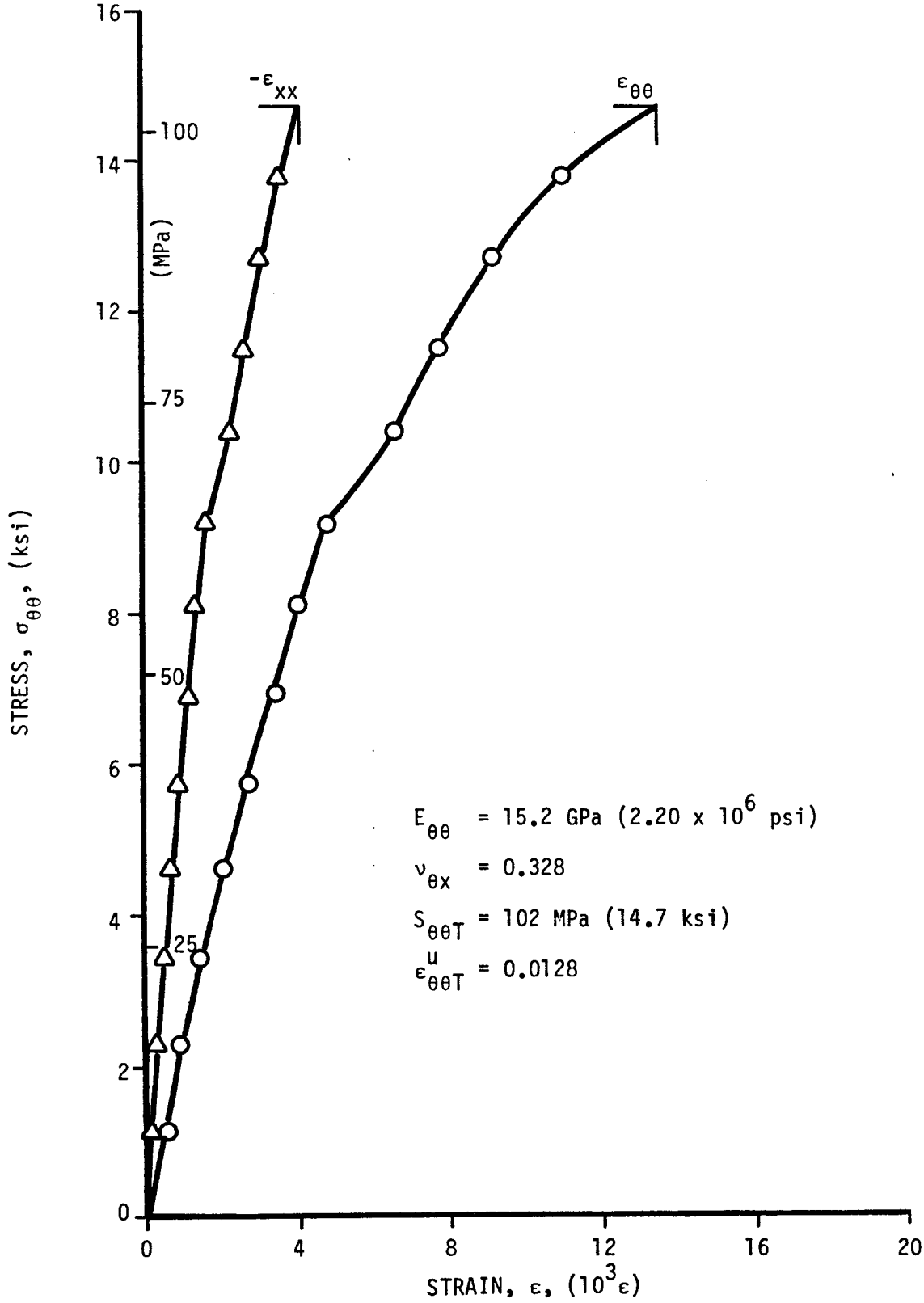

Figure 2-26. Strains in $[\pm 60]_{2s}$ SP288/AS ring specimen under static tensile loading (Specimen No. 22-3).

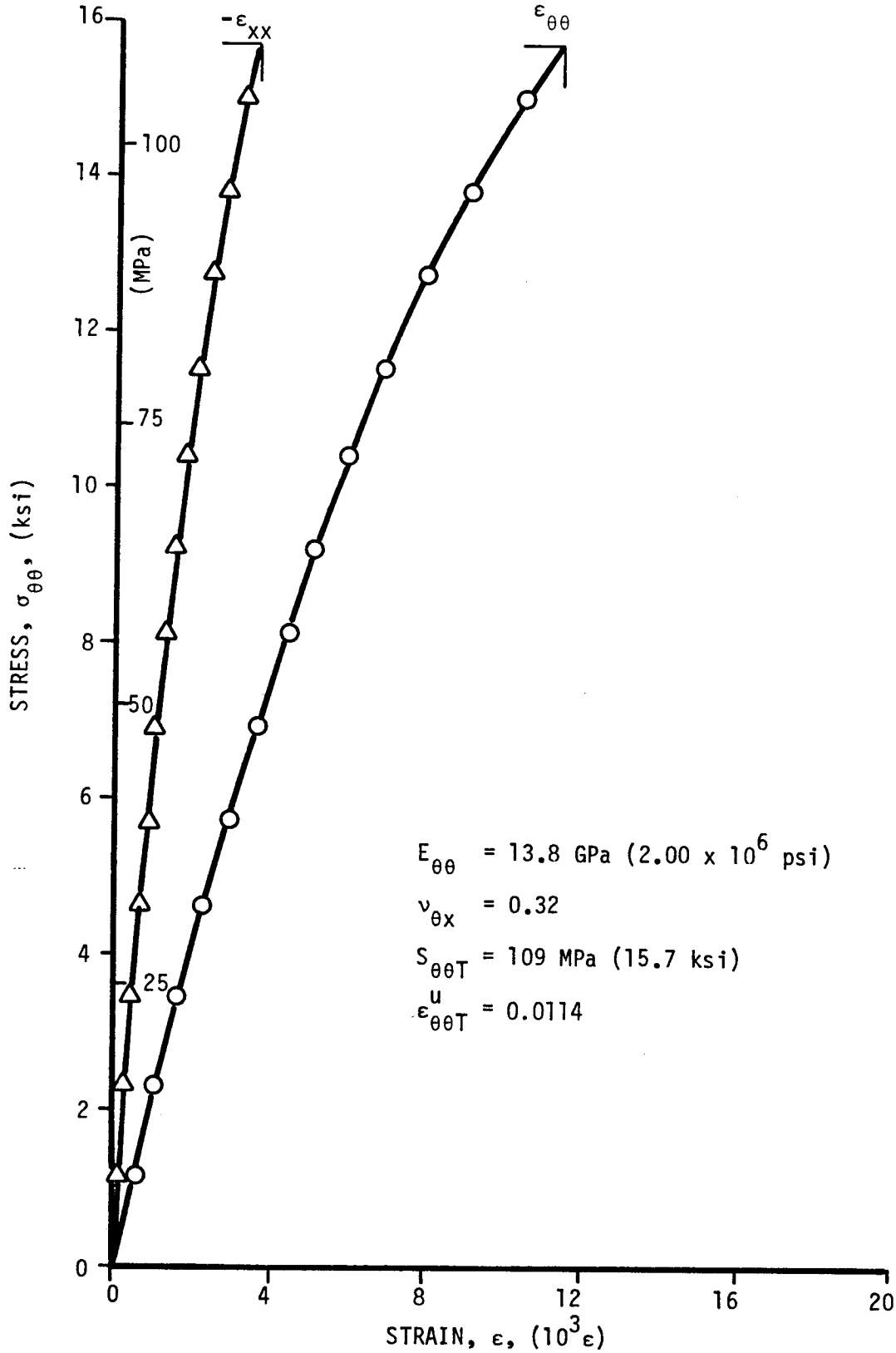

Figure 2-27. Strains in $[\pm 60]_{2S}$ SP288/AS ring specimen under static tensile loading (Specimen No. 22-5).

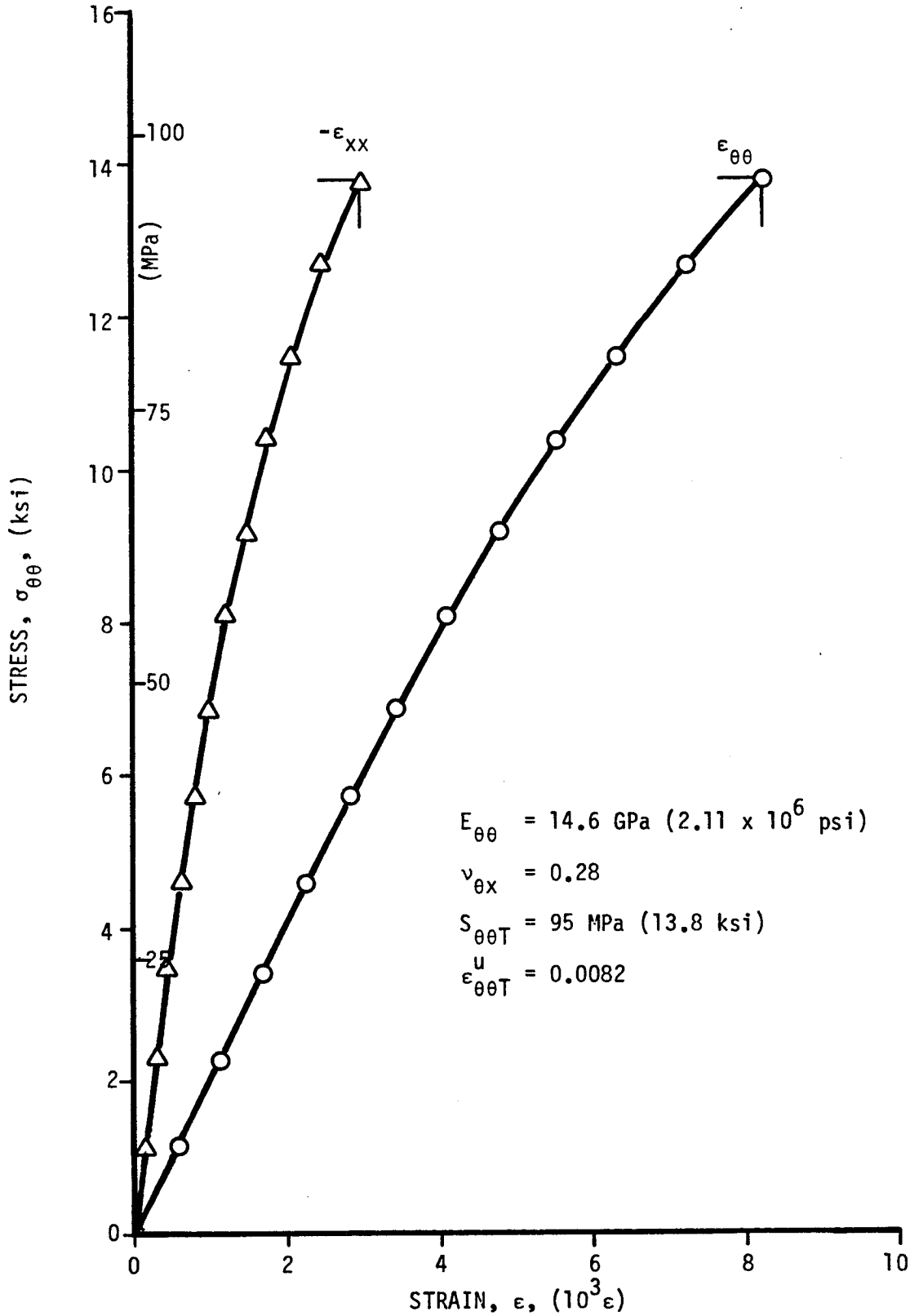

Figure 2-28. Strains in $[\pm 60]_{2S}$ 80AS/20S/PR288 ring specimen under static tensile loading (Specimen No. 23-1).

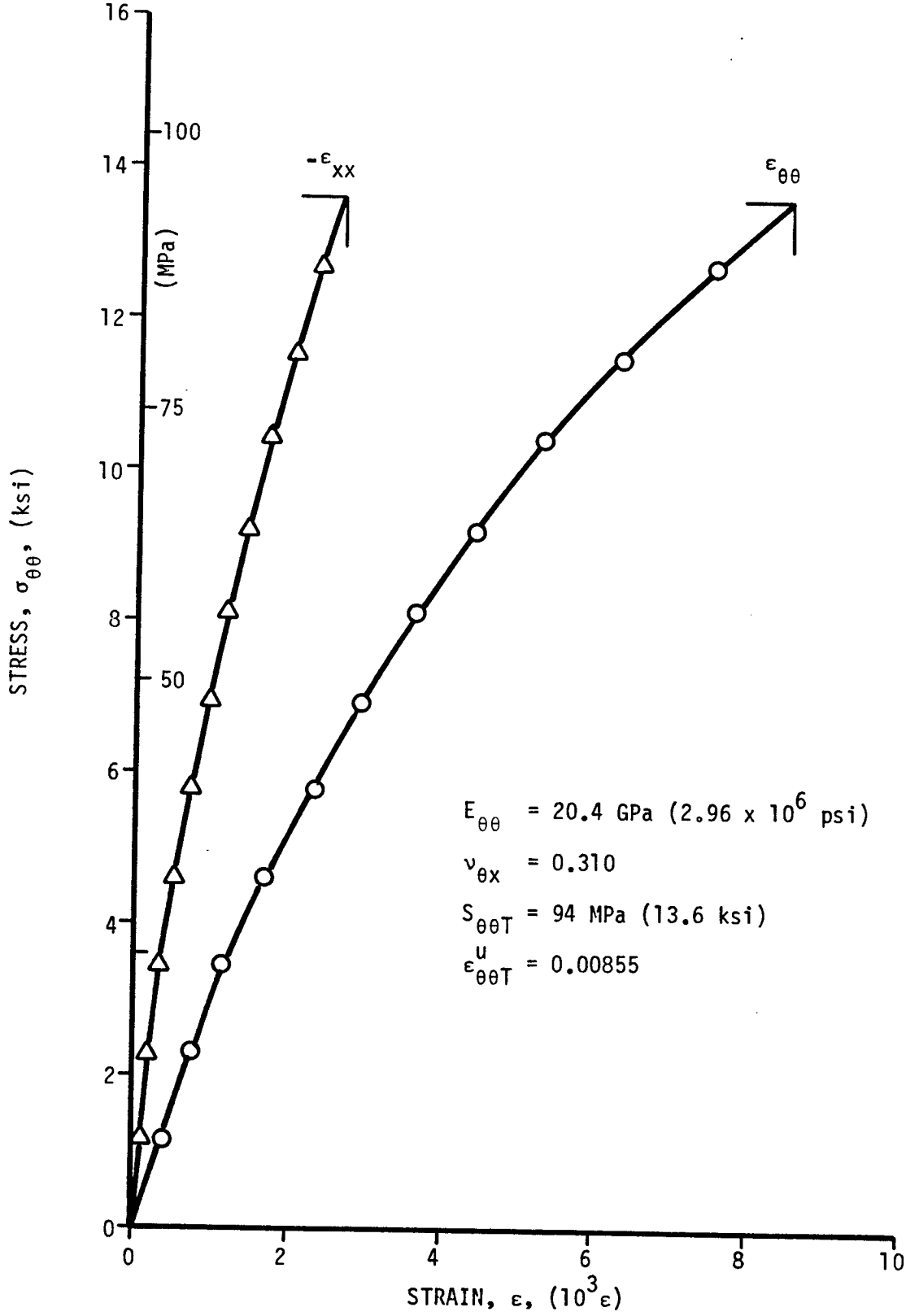

Figure 2-29. Strains in $[\pm 60]_{2S}$ 80AS/20S/PR288 ring specimen under stactic tensile loading (Specimen No. 23-3).

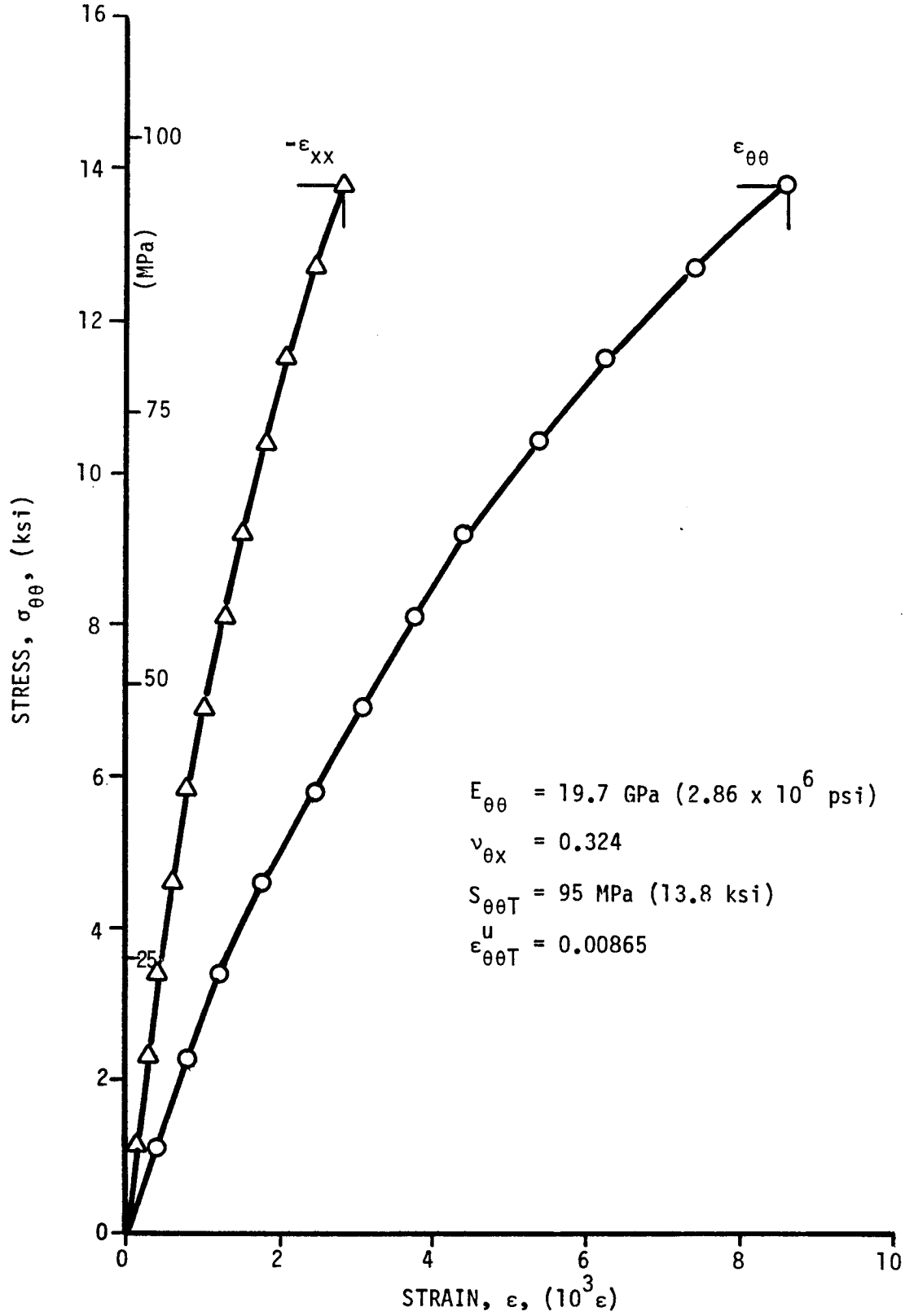

Figure 2-30. Strains in $[\pm 60]_{2S}$ 80AS/20S/PR288 ring specimen under static tensile loading (Specimen No. 23-5).

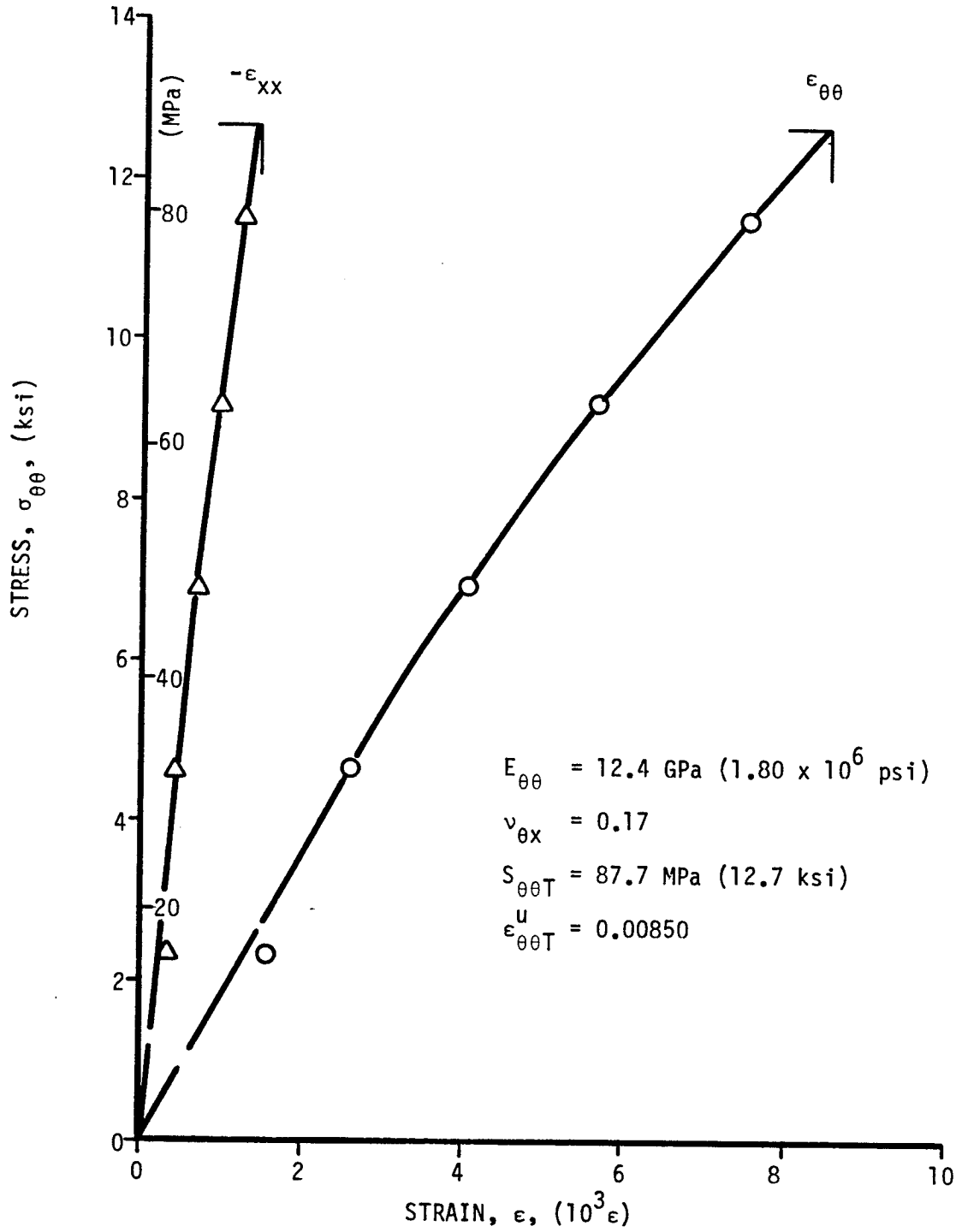

Figure 2-31. Strains in $[\pm 67.5]_{2S}$ SP288/AS ring specimen under static tensile loading (Specimen No. 26-1).

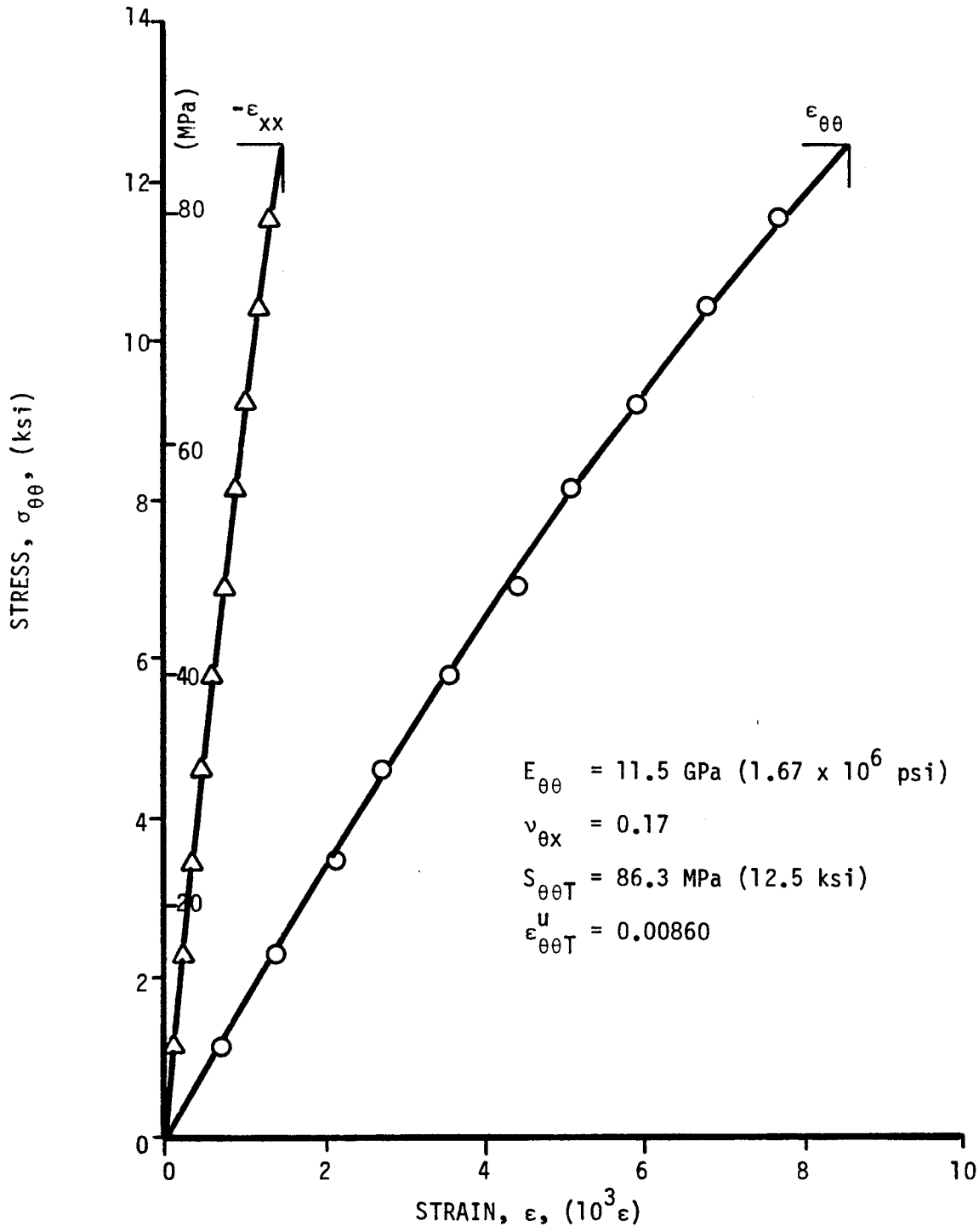

Figure 2-32. Strains in $[\pm 67.5]_{2S}$ SP288/AS ring specimen under static tensile loading (Specimen No. 26-3).

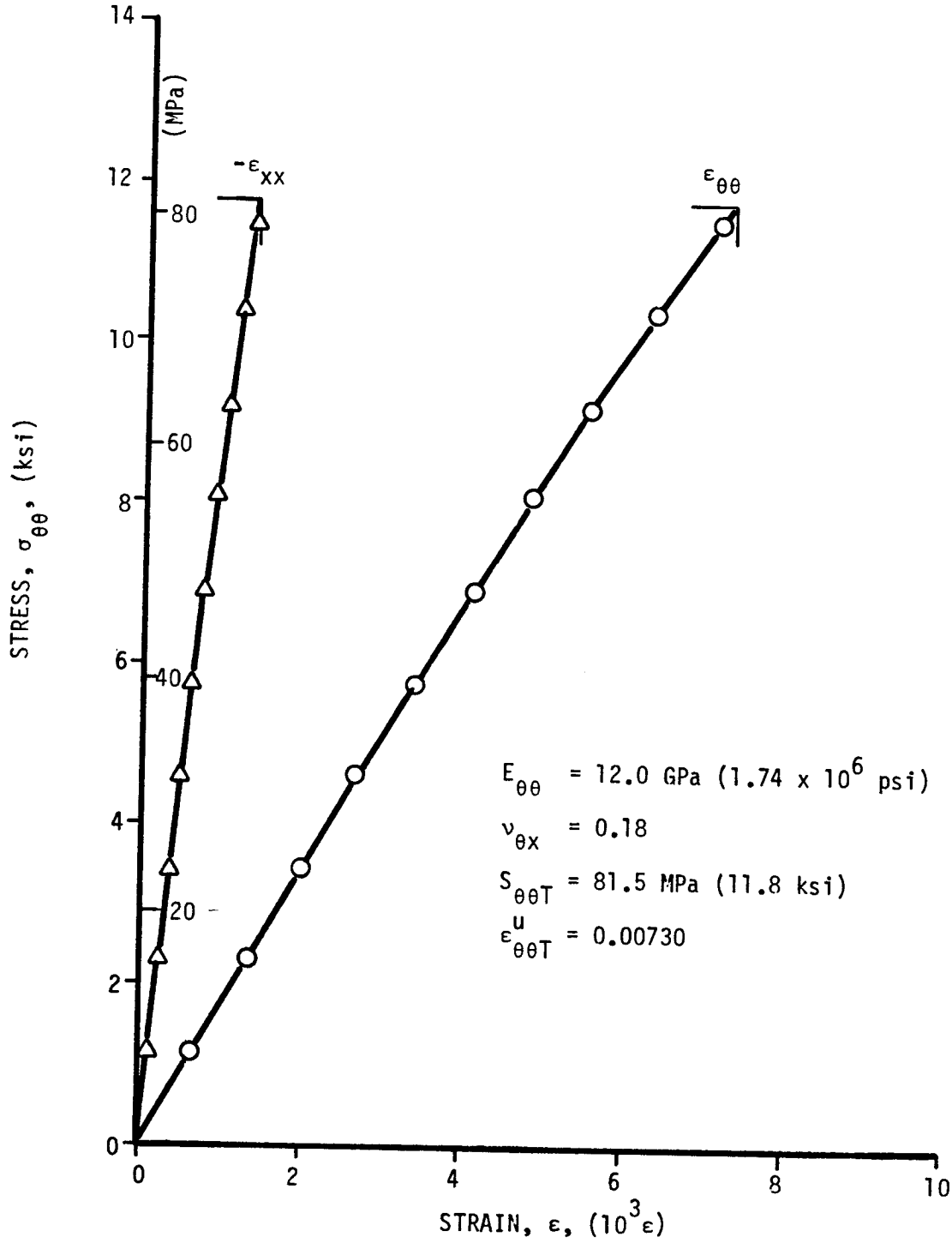

Figure 2-33. Strains in $[\pm 67.5]_{2s}$ SP288/AS ring specimen under static tensile loading (Specimen No. 26-5).

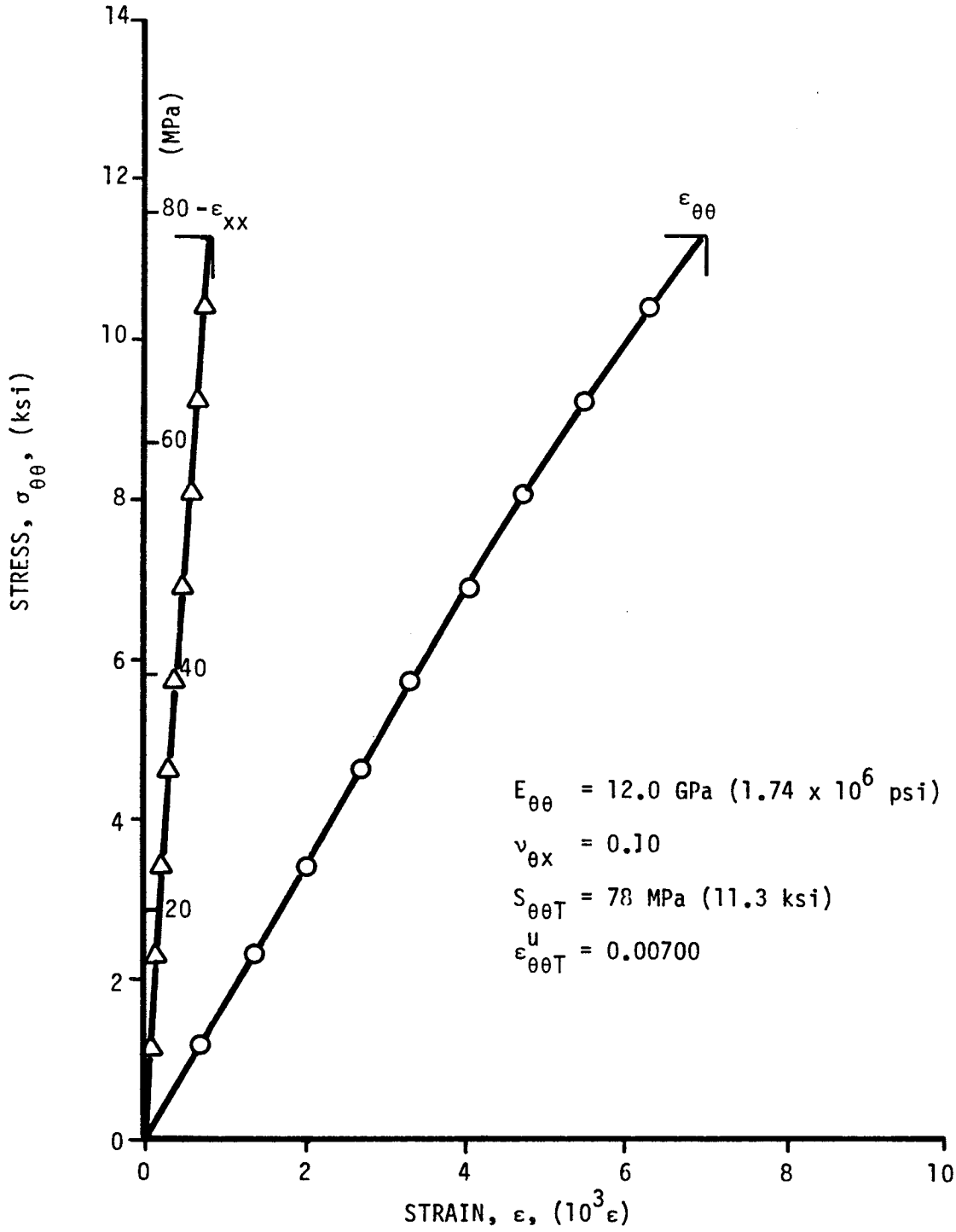

Figure 2-34. Strains in $[\pm 67.5]_{2S}$ 80AS/20S/PR288 ring specimen under static tensile loading (Specimen No. 27-1).

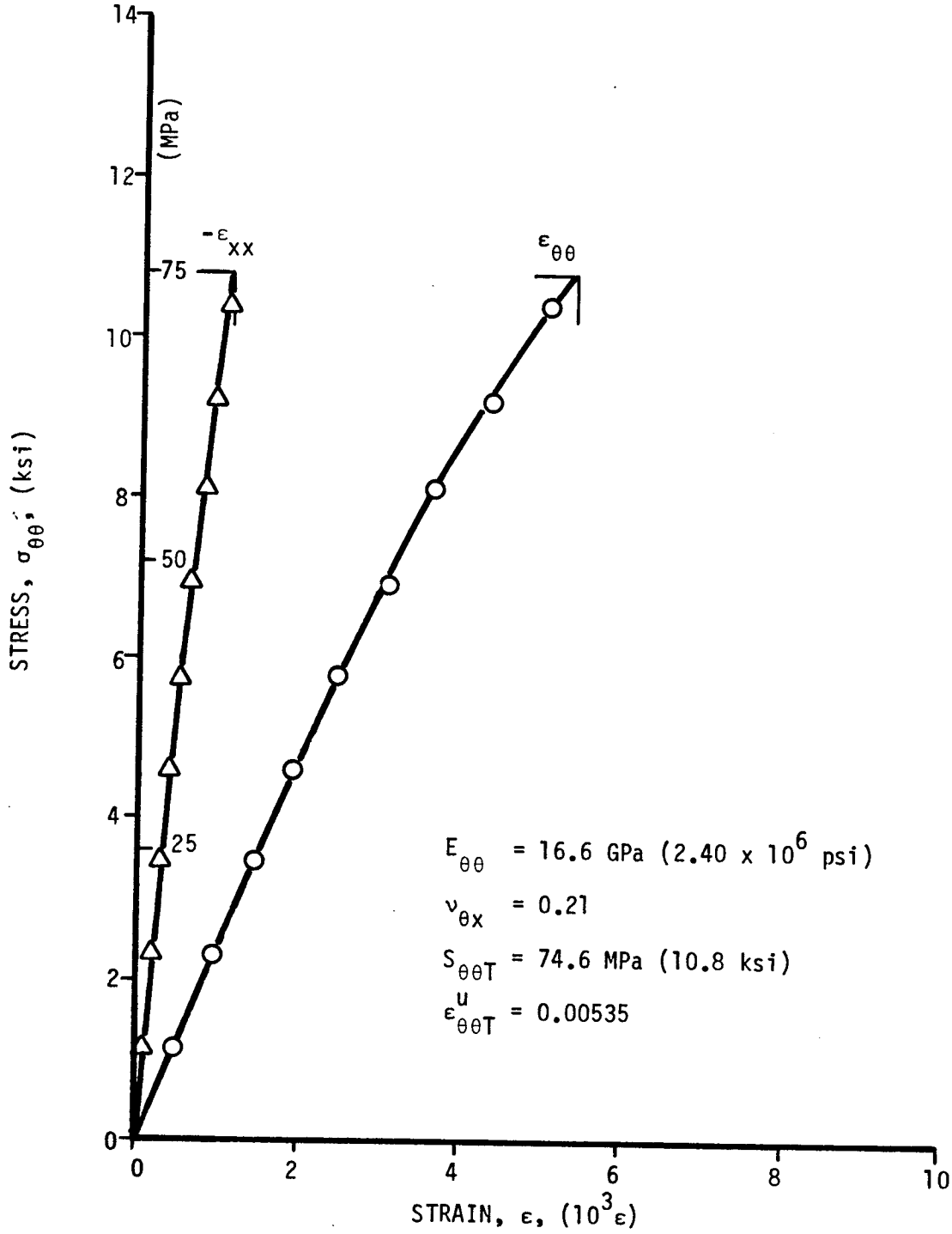

Figure 2-35. Strains in $[\pm 67.5]_{2s}$ 80AS/20S/PR288 ring specimen under static tensile loading (Specimen No. 27-3).

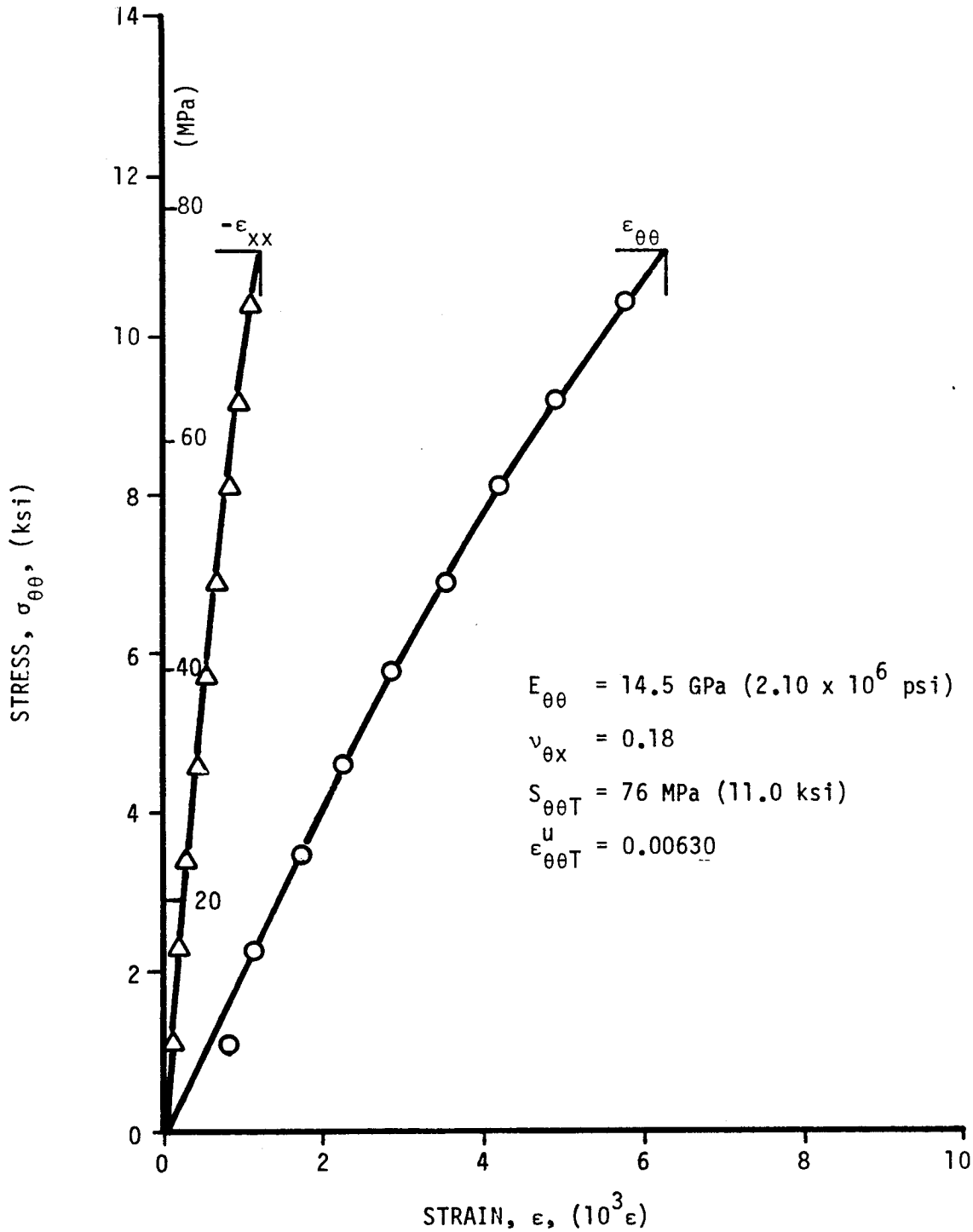

Figure 2-36. Strains in $[\pm 67.5]_{2S}$ 80AS/20S/PR288 ring specimen under static tensile loading (Specimen No. 27-5).

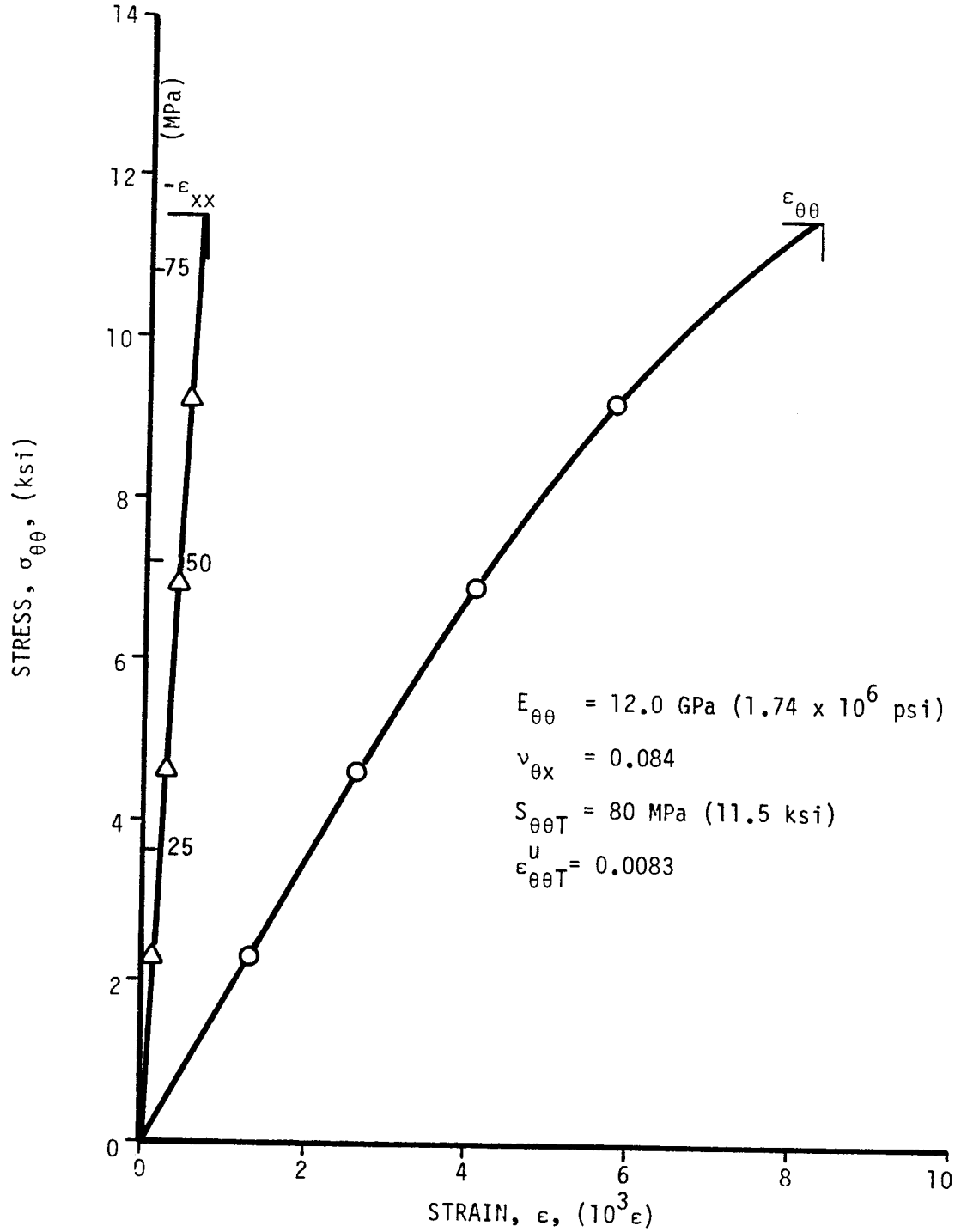

Figure 2-37. Strains in $[\pm 75]_{2S}$ SP288/AS ring specimen under static tensile loading (Specimen No. 20-1).

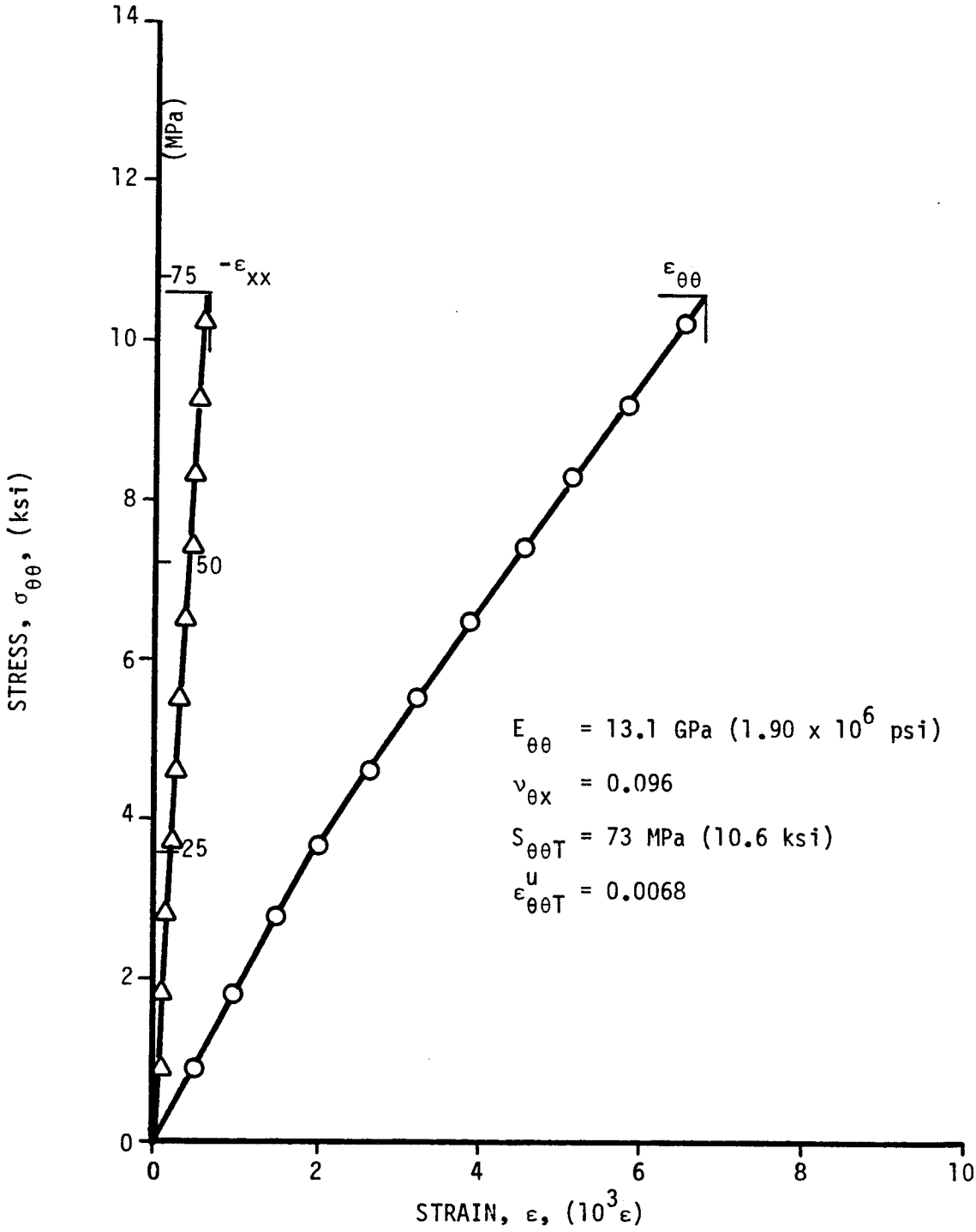

Figure 2-38. Strains in $[\pm 75]_{2S}$ SP288/AS ring specimen under static tensile loading (Specimen No. 20-3).

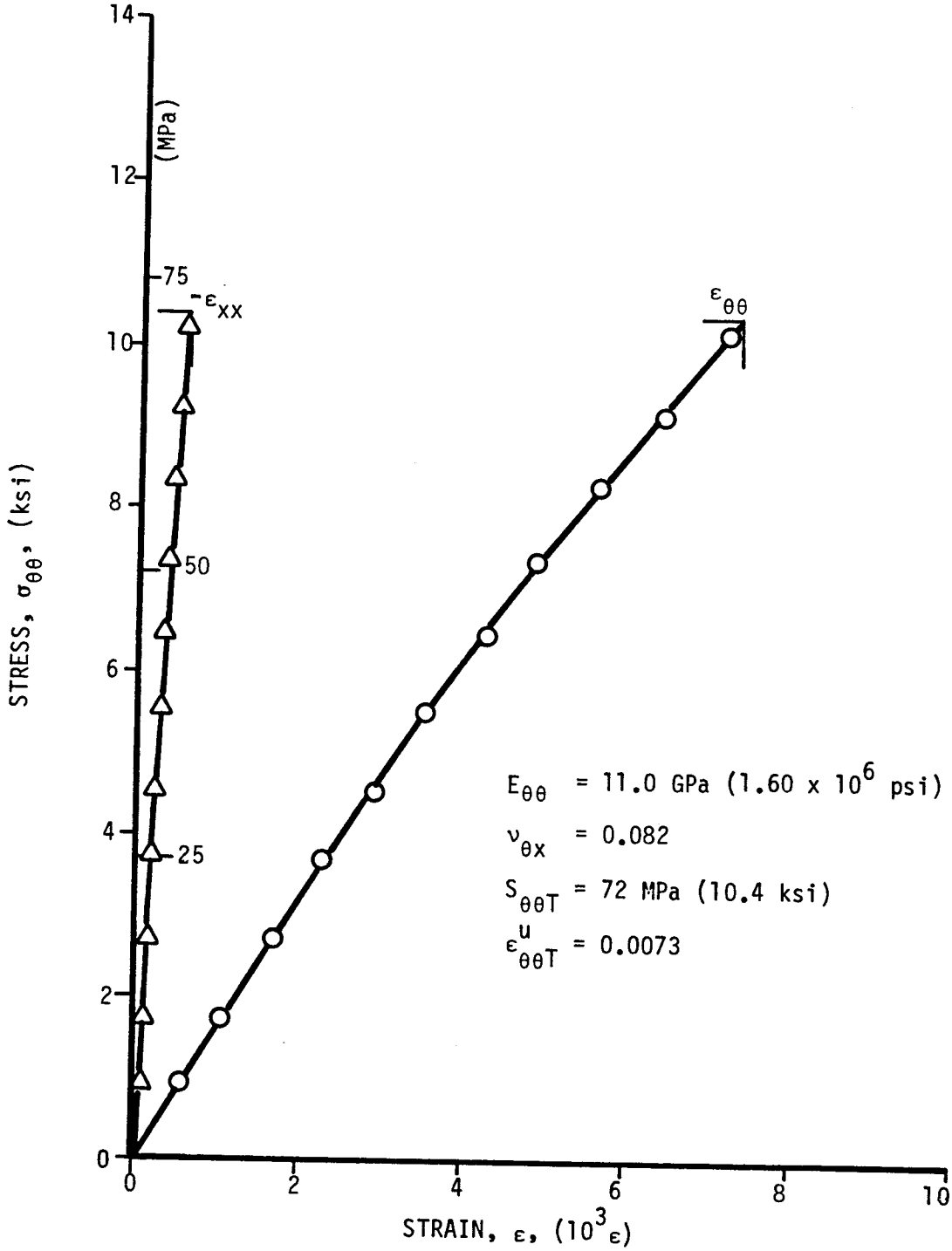

Figure 2-39. Strains in $[\pm 75]_{2s}$ SP288/AS ring specimen under static tensile loading (Specimen No. 20-5).

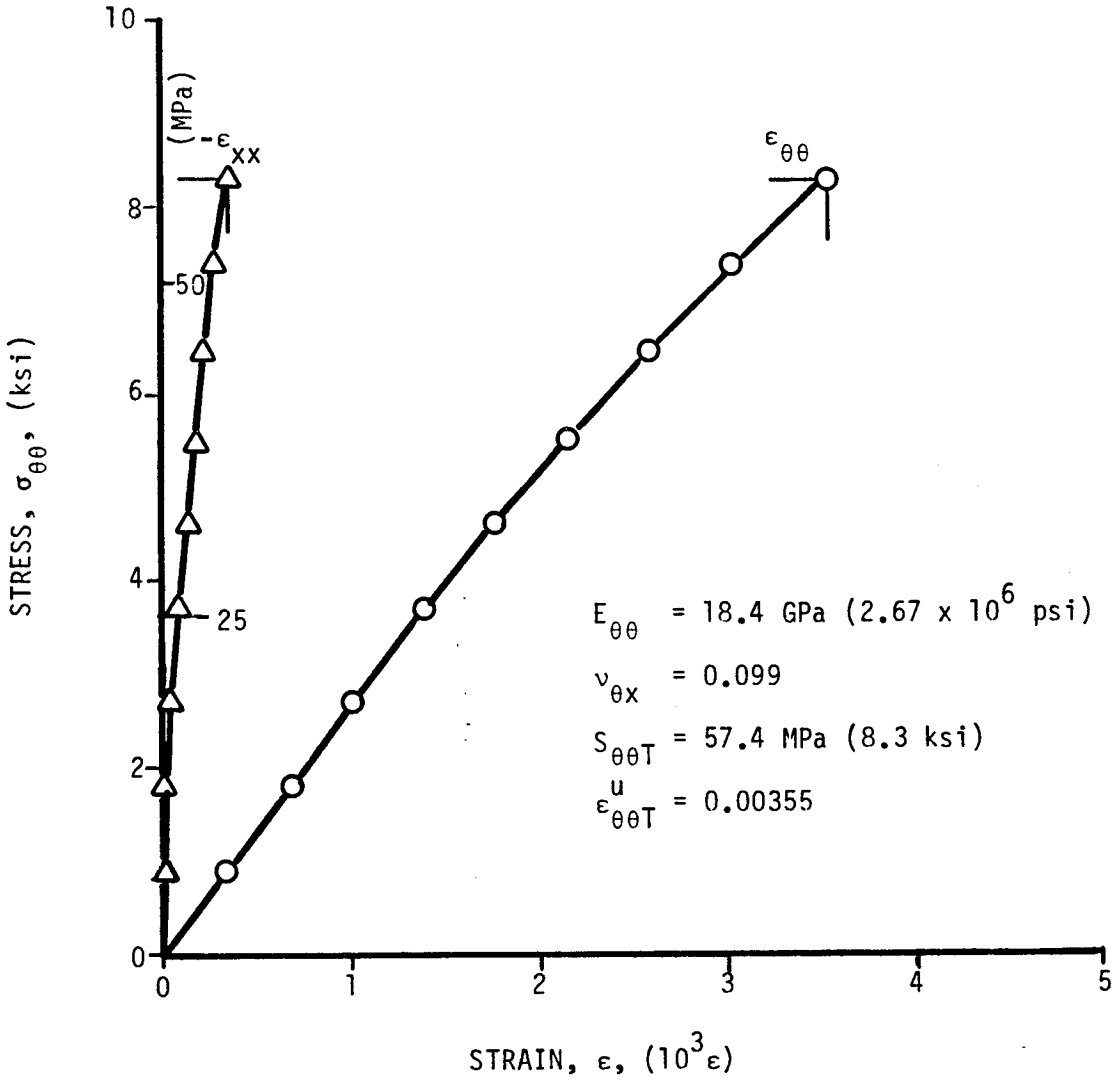

Figure 2-40. Strains in $[\pm 75]_{2S}$ 80AS/20S/PR288 ring specimen under static tensile loading (Specimen No. 21-1).

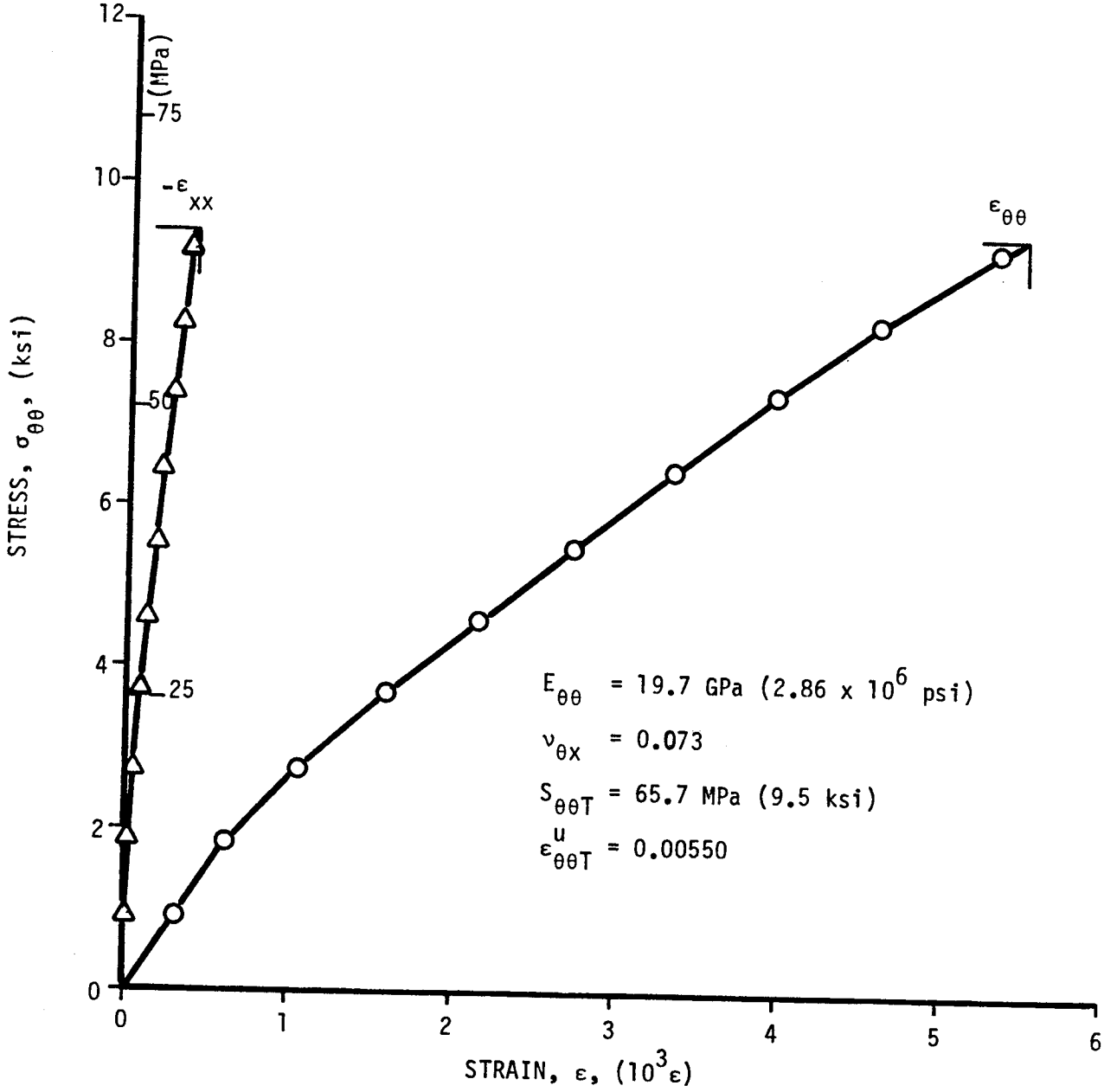

Figure 2-41. Strains in $[\pm 75]_{2S}$ 80AS/20S/PR288 ring specimen under static tensile loading (Specimen No. 21-5).

3. INTERMEDIATE STRAIN RATE TENSILE PROPERTIES OF ANGLE-PLY LAMINATES

3.1 $[\pm 15]_{2s}$ LAMINATES

Intermediate rate tensile properties of $[\pm 15]_{2s}$ SP288/AS graphite/epoxy and 80AS/20S/PR288 graphite/S-glass/epoxy were obtained by testing rings under dynamic internal pressure. Three rings of each material were loaded dynamically using 650 mg of slow burning pistol powder (red dot) in the pressure chamber of the fixture. The circumferential and axial strains in the composite rings and the circumferential strain in the steel calibration ring were recorded in every case.

Strain records for the three graphite/epoxy rings are shown in Figures 3-1, 3-2, and 3-3 (Specimen Nos. 35-7, 35-10, and 35-11). These data were analyzed following the procedures described in Part I of this report (Section 3.3.2). Results in the form of dynamic stress-strain curves are shown in Figures 3-4, 3-5, and 3-6. Results for the three rings tested are tabulated in Table 3-1. The initial strain rates range between $9s^{-1}$ and $20s^{-1}$, and the average (secant) rates between $36s^{-1}$ and $52s^{-1}$. The times to failure range between 184 μs and 213 μs. The initial and secant moduli of 121 GPa (17.5×10^6 psi) and 123 GPa (17.8×10^6 psi), respectively, are higher than the static modulus of 105 GPa (15.2×10^6 psi) by 15% and 17%, respectively. The average initial and secant Poisson's ratios of 0.80 and 0.81 are a little lower than the static value of 0.86. The average dynamic strength of 1049 MPa (152 ksi) is much higher than the static strength of 823 MPa (119 ksi). The increase in dynamic strength is higher than the increase in dynamic modulus. The average dynamic ultimate strain of 0.0086 is higher than the static value of 0.0078.

Strain records for the three hybrid rings are shown in Figures 3-7, 3-8, and 3-9 (Specimen Nos. 36-6, 36-10, and 36-11). The corresponding dynamic stress-strain curves are shown in Figures 3-10, 3-11, and 3-12. Results are tabulated in Table 3-2. The initial strain rates range between $16s^{-1}$ and $18s^{-1}$, and the average (secant) rates between $41s^{-1}$ and $45s^{-1}$. The time to failure ranges between 222 μs and 270 μs. The initial and secant moduli of

TABLE 3-1. INTERMEDIATE STRAIN RATE TENSILE PROPERTIES OF $[\pm 15]_{2s}$ SP288/AS GRAPHITE/EPOXY

Specimen Number	Strain Rate ($\dot{\varepsilon}_{\theta\theta}$), s^{-1}	Modulus ($E_{\theta\theta}$), GPa (10^6 psi)	Poisson's Ratio ($\nu_{\theta x}$)
	Initial Properties		
35-7	20	124 (17.9)	0.73
35-10	20	124 (17.9)	0.80
35-11	9	115 (16.6)	0.88
	Secant Properties		
35-7	52	119 (17.3)	0.78
35-10	43	128 (18.6)	0.82
35-11	36	120 (17.4)	0.84
	Terminal Properties		
35-7	134	135 (19.6)	0.52
35-10	80	175 (25.3)	0.68
35-11	88	131 (19.0)	0.80
	Ultimate Properties		
	Time to Failure (t_f), μs	Strength ($S_{\theta\theta T}$), MPa (ksi)	Strain ($\varepsilon^u_{\theta\theta T}$)
35-7	184	1129 (164)	0.0095
35-10	200	1107 (160)	0.0086
35-11	213	911 (132)	0.0076

TABLE 3-2. INTERMEDIATE STRAIN RATE TENSILE PROPERTIES OF $[\pm 15]_{2s}$ 80AS/20S/PR288 GRAPHITE/S-GLASS/EPOXY

Specimen Number	Strain Rate ($\dot{\varepsilon}_{\theta\theta}$), s^{-1}	Modulus ($E_{\theta\theta}$), GPa (10^6 psi)	Poisson's Ratio ($\nu_{\theta x}$)
		Initial Properties	
36-6	16	104 (15.0)	0.56
36-10	18	112 (16.3)	0.50
36-11	16	97 (14.0)	0.25
		Secant Properties	
36-6	43	97 (14.1)	0.55
36-10	45	99 (14.3)	0.65
36-11	41	88 (12.7)	0.30
		Terminal Properties	
36-6	124	106 (15.3)	0.58
36-10	244	86 (12.5)	0.49
36-11	268	81 (11.8)	0.45
		Ultimate Properties	
	Time to Failure (t_f), μs	Strength ($S_{\theta\theta T}$), MPa (ksi)	Strain ($\varepsilon^u_{\theta\theta T}$)
36-6	222	932 (135)	0.0096
36-10	228	997 (145)	0.0101
36-11	270	973 (141)	0.0111

104 GPa (15.1 x 10^6 psi) and 95 GPa (13.7 x 10^6 psi), respectively, are higher than and equal to, respectively, the initial static modulus of 95 GPa (13.7 x 10^6 psi). The average initial and secant Poisson's ratios of 0.44 and 0.50 are lower than the static value of 0.68. The average dynamic strength of 968 MPa (140 ksi) is higher than the static strength of 806 MPa (11.7 ksi). The average dynamic ultimate strain of 0.0103 is higher than the static value of 0.0084.

3.2 $[\pm 22.5]_{2s}$ LAMINATES

Intermediate rate tensile properties of $[\pm 22.5]_{2s}$ SP288/AS graphite/epoxy and 80AS/20S/PR288 graphite/S-glass/epoxy were obtained by testing rings under dynamic internal pressure. Three rings of each material were loaded dynamically using 650 mg pistol powder in the pressure chamber of the fixture.

Strain records for the three graphite/epoxy rings tested are shown in Figures 3-13, 3-14, and 3-15 (Specimen Nos. 33-10, 33-11, and 33-13). The corresponding dynamic stress-strain curves are shown in Figures 3-16, 3-17, and 3-18. Results are tabulated in Table 3-3. The initial strain rates range between $8s^{-1}$ and $30s^{-1}$ and the average (secant) between $40s^{-1}$ and $48s^{-1}$. The times to failure range between 187 μs and 221 μs. The initial and secant moduli of 78.4 GPa (11.4 x 10^6 psi) and 84.0 GPa (12.2 x 10^6 psi), respectively, are close to the static initial modulus of 81.4 GPa (11.8 x 10^6 psi). The average dynamic strength of 770 MPa (112 ksi) is exactly equal to the static strength. The dynamic ultimate strain of 0.0093 is lower than the static value of 0.0103.

Strain records for the three hybrid rings are shown in Figures 3-19, 3-20, and 3-21 (Specimen Nos. 34-2, 34-10, and 34-11). The corresponding dynamic stress-strain curves are shown in Figures 3-22, 3-23, and 3-24. Results are tabulated in Table 3-4. The initial strain rates range between $9s^{-1}$ and $31s^{-1}$ and the average (secant) rates between $35s^{-1}$ and $57s^{-1}$. The times to failure range between 181 μs and 275 μs. The initial and secant moduli of 75.7 GPa (11.0 x 10^6 psi) and 72.5 GPa (10.5 x 10^6 psi), respectively, are a little higher than the static initial modulus of 68.5 GPa

TABLE 3-3. INTERMEDIATE STRAIN RATE TENSILE PROPERTIES OF $[\pm 22.5]_{2s}$ SP288/AS GRAPHITE/EPOXY

Specimen Number	Strain Rate ($\dot{\varepsilon}_{\theta\theta}$), s^{-1}	Modulus ($E_{\theta\theta}$), GPa (10^6 psi)	Poisson's Ratio ($\nu_{\theta x}$)
		Initial Properties	
33-10	8	64.9 (9.4)	1.25
33-11	13	69.7 (10.1)	1.30
33-13	30	100.7 (14.6)	1.07
		Secant Properties	
33-10	40	81.5 (11.8)	1.18
33-11	47	67.6 (9.8)	1.16
33-13	48	102.8 (14.9)	1.33
		Terminal Properties	
33-10	112	56.6 (8.2)	1.25
33-11	195	40.0 (5.8)	1.06
33-13	104	106.3 (15.4)	1.37
		Ultimate Properties	
	Time to Failure (t_f), μs	Strength ($S_{\theta\theta T}$), MPa (ksi)	Strain ($\varepsilon^u_{\theta\theta T}$)
33-10	221	718 (104)	0.0088
33-11	215	674 (98)	0.0100
33-13	187	920 (133)	0.0090

TABLE 3-4. INTERMEDIATE STRAIN RATE TENSILE PROPERTIES OF $[\pm 22.5]_{2s}$ 80AS/20S/PR288 GRAPHITE/S-GLASS/EPOXY

Specimen Number	Strain Rate ($\dot{\varepsilon}_{\theta\theta}$), s^{-1}	Modulus ($E_{\theta\theta}$), GPa (10^6 psi)	Poisson's Ratio ($\nu_{\theta x}$)
	Initial Properties		
34-2	9	71.1 (10.3)	1.33
34-10	31	82.8 (12.0)	1.00
34-11	11	73.3 (10.6)	0.99
	Secant Properties		
34-2	50	73.6 (10.7)	0.83
34-10	57	77.0 (11.2)	1.16
34-11	35	66.2 (9.6)	1.08
	Terminal Properties		
34-2	160	62.1 (9.0)	1.17
34-10	120	78.7 (11.4)	1.42
34-11	337	69.7 (10.1)	1.25
	Ultimate Properties		
	Time to Failure (t_f), μs	Strength ($S_{\theta\theta T}$), MPa (ksi)	Strain ($\varepsilon^u_{\theta\theta T}$)
34-2	224	818 (118)	0.0111
34-10	181	800 (116)	0.0104
34-11	275	641 (93)	0.0097

(9.9 x 10^6 psi). The average dynamic strength of 752 MPa (109 ksi) is higher than the static strength of 653 MPa (94.6 ksi). The dynamic strain of 0.0104 is exactly equal to the static value.

3.3 $[\pm 30]_{2s}$ LAMINATES

Intermediate rate tensile properties of $[\pm 30]_{2s}$ SP288/AS graphite/epoxy and 80AS/20S/PR288 graphite/S-glass/epoxy were obtained by testing three rings of each material under dynamic internal pressure. The pressure was produced by detonating 650 mg pistol powder in the pressure chamber of the fixture.

Strain records for the three graphite/epoxy rings tested are shown in Figures 3-25, 3-26, and 3-27 (Specimen Nos. 28-2, 28-12, and 28-13). The corresponding dynamic stress-strain curves are shown in Figures 3-28, 3-29, and 3-30. Results are tabulated in Table 3-5. The initial strain rates range between $10s^{-1}$ and $17s^{-1}$, and the average (secant) rates between $49s^{-1}$ and $73s^{-1}$. The times to failure range between 195 μs and 237 μs. The initial and secant moduli of 48.4 GPa (7.02 x 10^6 psi) and 44.7 GPa (6.48 x 10^6 psi), respectively, are noticeably lower than the static initial modulus of 58.6 GPa (8.50 x 10^6 psi). The average dynamic strength of 571 MPa (83 x 10^6 psi) is almost equal to the static strength of 566 MPa (82 ksi). The dynamic ultimate strain of 0.0128 is almost equal to the static value of 0.0132.

Strain records for the three hybrid rings are shown in Figures 3-31, 3-32, and 3-33 (Specimen Nos. 54-2, 54-3, and 54-5). The corresponding dynamic stress-strain curves are shown in Figures 3-34, 3-35, and 3-36. Results are tabulated in Table 3-6. The initial strain rates range between $12s^{-1}$ and $22s^{-1}$, and the average (secant) rates between $56s^{-1}$ and $85s^{-1}$. The times to failure range between 179 μs and 224 μs. The initial and secant moduli of 43.5 GPa (6.31 x 10^6 psi) and 41.9 GPa (6.07 x 10^6 psi), respectively, are a little lower than the static value of 44.9 GPa (6.51 x 10^6 psi). The dynamic initial and secant Poisson's ratios of 1.11 and 1.23 are lower than the static value of 1.26. The average dynamic strength of 611 MPa (89 ksi) is higher than the static strength of 503 MPa (73 ksi). The dynamic ultimate strain of 0.0144 is very close to the static value of 0.0139 as in the case mentioned before.

TABLE 3-5. INTERMEDIATE STRAIN RATE TENSILE PROPERTIES OF $[\pm 30]_{2s}$ SP288/AS GRAPHITE/EPOXY

Specimen Number	Strain Rate ($\dot{\varepsilon}_{\theta\theta}$), s^{-1}	Modulus ($E_{\theta\theta}$), GPa (10^6 psi)	Poisson's Ratio ($\nu_{\theta x}$)
	Initial Properties		
28-2	17	43.8 (6.35)	1.09
28-12	10	46.6 (6.75)	1.10
28-13	10	54.9 (7.95)	0.83
	Secant Properties		
28-2	73	41.1 (5.96)	1.04
28-12	49	42.9 (6.22)	1.27
28-13	53	50.1 (7.26)	1.19
	Terminal Properties		
28-2	281	44.2 (6.40)	1.14
28-12	252	27.6 (4.00)	1.41
28-13	270	42.1 (6.10)	1.44
	Ultimate Properties		
	Time to Failure (t_f), μs	Strength ($S_{\theta\theta T}$), MPa (ksi)	Strain ($\varepsilon^u_{\theta\theta T}$)
28-2	195	588 (85)	0.0143
28-12	237	504 (73)	0.0117
28-13	236	621 (90)	0.0124

TABLE 3-6. INTERMEDIATE STRAIN RATE TENSILE PROPERTIES OF $[\pm 30]_{2S}$ 80AS/20S/PR288 GRAPHITE/S-GLASS/EPOXY

Specimen Number	Strain Rate ($\dot{\varepsilon}_{\theta\theta}$), s^{-1}	Modulus ($E_{\theta\theta}$), GPa (10^6 psi)	Poisson's Ratio ($\nu_{\theta x}$)
	Initial Properties		
54-2	17	40.0 (5.80)	1.11
54-3	22	44.9 (6.50)	1.11
54-5	12	45.7 (6.63)	1.12
	Secant Properties		
54-2	56	38.9 (5.63)	1.16
54-3	76	38.9 (5.63)	1.39
54-5	85	47.9 (6.94)	1.14
	Terminal Properties		
54-2	251	30.4 (4.40)	1.36
54-3	229	34.6 (5.02)	1.53
54-5	397	60.0 (8.70)	1.40
	Ultimate Properties		
	Time to Failure (t_f), μs	Strength ($S_{\theta\theta T}$), MPa (ksi)	Strain ($\varepsilon^u_{\theta\theta T}$)
54-2	224	490 (71)	0.0126
54-3	179	528 (77)	0.0136
54-5	200	814 (118)	0.0170

3.4 $[\pm 45]_{2s}$ LAMINATES

Intermediate strain rate tensile properties of $[\pm 45]_{2s}$ SP288/AS graphite/epoxy and 80AS/20S/PR288 graphite/S-glass/epoxy were obtained by testing rings under dynamic internal pressure. Four rings of each material were loaded dynamically using 650 mg pistol powder in the pressure chamber of the fixture.

Strain records for the four graphite/epoxy rings tested are shown in Figures 3-37 through 3-40 (Specimen Nos. 24-11, 52-2, 52-3, and 52-4). The corresponding dynamic stress-strain curves are shown in Figures 3-41 through 3-44. Results are tabulated in Table 3-7. The initial strain rates range between $10s^{-1}$ and $17s^{-1}$ and the average (secant) rates between $66s^{-1}$ and $101s^{-1}$. The times to failure range between 300 μs and 348 μs. The initial and secant moduli of 19.1 GPa (2.77×10^6 psi) and 17.6 GPa (2.55×10^6 psi), respectively, are both lower than the static modulus of 20.4 GPa (2.95×10^6 psi). This difference may be due in part to the fact that three of the specimens were taken from a different tube (No. 52) which was fabricated much later than tube No. 24 from which the static specimens came. The moduli for Specimen No. 24-11 are much closer to the static modulus. The average dynamic Poisson's ratio of 0.85 is higher than the static value of 0.69. The average dynamic strength of 494 MPa (72 ksi) is much higher than the low bound of 224 MPa (32.5 ksi) established by static testing. On the other hand, the dynamic ultimate strain of 0.0279 is lower than the lower bound established by static testing. Again, the value of 0.0348 for Specimen No. 24-11 is more in line with the static results.

Strain records for the four hybrid rings are shown in Figure 3-45 through 3-48 (Specimen Nos. 25-9, 53-1, 53-4, and 53-5). The corresponding dynamic stress-strain curves are shown in Figures 3-49 through 3-52. Results are tabulated in Table 3-8. The initial strain rates range between $7s^{-1}$ and $30s^{-1}$ and the average (secant) rates between $81s^{-1}$ and $163s^{-1}$. The times to failure range between 171 μs and 344 μs. The initial modulus of 21.1 GPa (3.06×10^6 psi) is only slightly lower than the static modulus of 21.5 GPa (3.12×10^6 psi). The overall average Poisson's ratio of 0.71 is a little lower than the static value of 0.74. The average dynamic strength of 371 MPa (54 ksi) is much higher than the lower bound of 191 MPa (27.7 ksi) established by static testing. The dynamic ultimate strain of 0.0270 is very close to the lower bound of 0.0265 established by static testing.

TABLE 3-7. INTERMEDIATE STRAIN RATE TENSILE PROPERTIES OF $[\pm 45]_{2s}$ SP288/AS GRAPHITE/EPOXY

Specimen Number	Strain Rate ($\dot{\varepsilon}_{\theta\theta}$), s^{-1}	Modulus ($E_{\theta\theta}$), GPa (10^6 psi)	Poisson's Ratio ($\nu_{\theta x}$)
	Initial Properties		
24-11	10	20.0 (2.90)	0.83
52-2	15	17.3 (2.50)	0.95
52-3	12	20.3 (2.94)	0.89
52-4	17	18.8 (2.73)	0.92
	Secant Properties		
24-11	101	19.8 (2.87)	0.94
52-2	96	15.7 (2.28)	0.65
52-3	66	16.0 (2.32)	0.77
52-4	75	18.8 (2.73)	0.84
	Terminal Properties		
24-11	483	10.6 (1.53)	0.95
52-2	421	10.5 (1.52)	0.62
52-3	250	9.2 (1.33)	0.95
52-4	280	15.7 (2.27)	0.86
	Ultimate Properties		
	Time to Failure (t_f), μs	Strength ($S_{\theta\theta T}$), MPa (ksi)	Strain ($\varepsilon^u_{\theta\theta T}$)
24-11	344	690 (100)	0.0348
52-2	325	490 (71)	0.0312
52-3	348	366 (53)	0.0228
52-4	300	428 (62)	0.0227

TABLE 3-8. INTERMEDIATE STRAIN RATE TENSILE PROPERTIES OF $[\pm 45]_{2s}$ 80AS/20S/PR288 GRAPHITE/S-GLASS/EPOXY

Specimen Number	Strain Rate ($\dot{\varepsilon}_{\theta\theta}$), s^{-1}	Modulus ($E_{\theta\theta}$), GPa (10^6 psi)	Poisson's Ratio ($\nu_{\theta x}$)
	Initial Properties		
25-9	13	15.4 (2.24)	0.91
53-1	7	24.7 (3.58)	0.87
53-4	17	17.8 (2.58)	0.76
53-5	30	26.4 (3.83)	0.56
	Secant Properties		
25-9	103	13.6 (1.98)	-
53-1	163	14.8 (2.15)	0.60
53-4	96	12.2 (1.77)	0.53
53-5	81	14.2 (2.06)	0.90
	Terminal Properties		
25-9	333	13.2 (1.92)	-
53-1	427	9.6 (1.39)	0.53
53-4	395	10.4 (1.50)	0.54
53-5	395	11.6 (1.68)	0.95
	Ultimate Properties		
	Time to Failure (t_f), μs	Strength ($S_{\theta\theta T}$), MPa (ksi)	Strain ($\varepsilon^u_{\theta\theta T}$)
25-9	344	483 (70)	0.0354
53-1	171	414 (60)	0.0279
53-4	260	304 (44)	0.0249
53-5	244	283 (41)	0.0199

3.5 $[\pm 60]_{2s}$ LAMINATES

Intermediate strain rate tensile properties of $[\pm 60]_{2s}$ SP288/AS graphite/epoxy and 80AS/20S/PR288 graphite/S-glass/epoxy were obtained by testing rings under dynamic internal pressure. Three rings of each material were loaded dynamically using 650 mg pistol powder in the pressure chamber of the fixture.

Strain records for the three graphite/epoxy rings tested are shown in Figures 3-53, 3-54, and 3-55 (Specimen Nos. 22-9, 22-10, and 22-11). The corresponding dynamic stress-strain curves are shown in Figures 3-56, 3-57, and 3-58. Results are tabulated in Table 3-9. The initial strain rates range between $16s^{-1}$ and $27s^{-1}$, and the average (secant) rates between $44s^{-1}$ and $84s^{-1}$. The times to failure range between 196 μs and 281 μs. The initial and secant moduli of 23.0 GPa (3.34×10^6 psi) and 13.9 GPa (2.01×10^6 psi), respectively, are higher than the initial static modulus of 13.4 GPa (1.95×10^6 psi) by 71% and 3%, respectively. The average Poisson's ratio of 0.32 is identical to the static value. The average dynamic strength of 182 MPa (26.4 ksi) is appreciably higher than the static strength of 105 MPa (15.2 ksi), by approximately the same percentage (73%) as the initial modulus. The average dynamic ultimate strain of 0.0134 is slightly higher than the static value of 0.0120.

Strain records for the three hybrid rings tested are shown in Figures 3-59, 3-60, and 3-61 (Specimen Nos. 23-7, 23-10, and 23-11). The corresponding dynamic stress-strain curves are shown in Figures 3-62, 3-63, and 3-64. Results are tabulated in Table 3-10. The initial strain rates range between $20s^{-1}$ and $35s^{-1}$, and the average (secant) rates between $51s^{-1}$ and $75s^{-1}$. The times to failure range between 155 μs and 219 μs. The initial modulus of 24.7 GPa (3.58×10^6 psi) is much higher than the static modulus of 15.2 GPa (2.20×10^6 psi). The average initial and secant Poisson's ratio of 0.31 is only slightly higher than the static value of 0.29. The average dynamic strength of 155.5 MPa (22.5 ksi) is much higher than the static strength of 94.8 MPa (13.7 ksi). The increase in dynamic strength outpaces the increase in dynamic modulus. The average dynamic ultimate strain of 0.0112 is higher than the static value of 0.0087.

TABLE 3-9. INTERMEDIATE STRAIN RATE TENSILE PROPERTIES OF $[\pm 60]_{2s}$ SP288/AS GRAPHITE/EPOXY

Specimen Number	Strain Rate ($\dot{\varepsilon}_{\theta\theta}$), s^{-1}	Modulus ($E_{\theta\theta}$), GPa (10^6 psi)	Poisson's Ratio ($\nu_{\theta x}$)
	Initial Properties		
22-9	27	22.5 (3.26)	0.15
22-10	23	23.6 (3.42)	0.28
22-11	16	23.0 (3.33)	0.33
	Secant Properties		
22-9	44	15.0 (2.17)	0.47
22-10	84	12.5 (1.82)	0.31
22-11	52	14.1 (2.04)	0.38
	Terminal Properties		
22-9	138	9.3 (1.35)	0.43
22-10	205	8.5 (1.23)	0.34
22-11	156	18.5 (2.68)	0.35
	Ultimate Properties		
	Time to Failure (t_f), μs	Strength ($S_{\theta\theta T}$), MPa (ksi)	Strain ($\varepsilon^u_{\theta\theta T}$)
22-9	196	129 (18.7)	0.0086
22-10	200	210 (30.5)	0.0168
22-11	281	207 (30.0)	0.0147

TABLE 3-10. INTERMEDIATE STRAIN RATE TENSILE PROPERTIES OF $[\pm 60]_{2S}$ 80AS/20S/PR288 GRAPHITE/S-GLASS/EPOXY

Specimen Number	Strain Rate ($\dot{\varepsilon}_{\theta\theta}$), s^{-1}	Modulus ($E_{\theta\theta}$), GPa (10^6 psi)	Poisson's Ratio ($\nu_{\theta x}$)
	Initial Properties		
23-7	35	17.6 (2.55)	0.25
23-10	23	25.4 (3.67)	0.26
23-11	20	31.1 (4.51)	0.22
	Secant Properties		
23-7	75	15.7 (2.28)	0.39
23-10	51	12.7 (1.84)	0.34
23-11	51	13.2 (1.91)	0.41
	Terminal Properties		
23-7	163	12.9 (1.88)	0.41
23-10	153	9.0 (1.30)	0.34
23-11	180	7.8 (1.13)	0.30
	Ultimate Properties		
	Time to Failure (t_f), μs	Strength ($S_{\theta\theta T}$), MPa (ksi)	Strain ($\varepsilon^u_{\theta\theta T}$)
23-7	155	182.2 (26.4)	0.0116
23-10	219	142.1 (20.6)	0.0112
23-11	210	142.1 (20.6)	0.0108

3.6 $[\pm 67.5]_{2s}$ LAMINATES

Intermediate strain rate tensile properties of $[\pm 67.5]_{2s}$ SP288/AS graphite/epoxy and 80AS/20S/PR288 graphite/S-glass/epoxy were obtained by testing rings under dynamic internal pressure. Three rings of each material were loaded dynamically using 650 mg pistol powder in the pressure chamber of the fixture.

Strain records for the three graphite/epoxy rings tested are shown in Figures 3-65, 3-66, and 3-67 (Specimen Nos. 26-10, 26-11, and 26-13). The corresponding dynamic stress-strain curves are shown in Figure 3-68, 3-69, and 3-70. Results are tabulated in Table 3-11. The initial strain rates range between $19s^{-1}$ and $35s^{-1}$ and the average (secant) rates between $58s^{-1}$ and $89s^{-1}$. The times to failure vary between 123 μs and 158 μs. The initial and secant moduli of 17.3 GPa (2.51×10^6 psi) and 12.8 GPa (1.86×10^6 psi), respectively, are higher than the initial static modulus of 12.0 GPa (1.74×10^6 psi). The average initial and secant Poisson's ratio is equal to the static value of 0.17. The average dynamic strength of 132.2 MPa (19.2 ksi) is higher than the static strength of 85.1 MPa (12.3 ksi) by 56%. The average dynamic ultimate strain of 0.0103 is higher than the static value of 0.0081.

Strain records for the three hybrid rings tested are shown in Figures 3-71, 3-72, and 3-73 (Specimen Nos. 27-10, 27-11, and 27-13). The corresponding dynamic stress-strain curves are shown in Figures 3-74, 3-75, and 3-76. Results are tabulated in Table 3-12. The initial strain rates range between $23s^{-1}$ and $49s^{-1}$ and the average (secant) rates between $56s^{-1}$ and $71s^{-1}$. The times to failure vary between 130 μs and 151 μs. The initial and secant moduli of 20.3 GPa (2.94×10^6 psi) and 15.7 GPa (2.28×10^6 psi), respectively, are higher than the initial static modulus of 14.4 GPa (2.08×10^6 psi) by 41% and 10%, respectively. The average initial and secant Poisson's ratio of 0.14 is slightly lower than the static value of 0.16. The average dynamic strength of 136.6 MPa (19.8 ksi) is much higher than the static strength of 76.1 MPa (11.0 ksi) by a higher percentage than the dynamic modulus. The average dynamic ultimate strain of 0.0087 is higher than the static value of 0.0062.

TABLE 3-11. INTERMEDIATE STRAIN RATE TENSILE PROPERTIES OF $[\pm 67.5]_{2s}$ SP288/AS GRAPHITE/EPOXY

Specimen Number	Strain Rate ($\dot{\varepsilon}_{\theta\theta}$), s^{-1}	Modulus ($E_{\theta\theta}$), GPa (10^6 psi)	Poisson's Ratio ($\nu_{\theta x}$)
	Initial Properties		
26-10	23	15.0 (2.18)	0.21
26-11	35	13.3 (1.93)	0.14
26-13	19	23.6 (3.41)	0.11
	Secant Properties		
26-10	73	12.7 (1.85)	0.17
26-11	89	13.8 (2.00)	0.20
26-13	58	11.9 (1.73)	0.16
	Terminal Properties		
26-10	169	8.0 (1.16)	0.21
26-11	182	14.0 (2.04)	0.15
26-13	150	3.3 (0.48)	0.25
	Ultimate Properties		
	Time to Failure (t_f), μs	Strength ($S_{\theta\theta T}$), MPa (ksi)	Strain ($\varepsilon^u_{\theta\theta T}$)
26-10	146	136.3 (19.8)	0.0107
26-11	123	150.1 (21.8)	0.0109
26-13	158	109.7 (15.9)	0.0092

TABLE 3-12. INTERMEDIATE STRAIN RATE TENSILE PROPERTIES OF $[\pm 67.5]_{2S}$ 80AS/20S/PR288 GRAPHITE/S-GLASS/EPOXY

Specimen Number	Strain Rate ($\dot{\varepsilon}_{\theta\theta}$), s^{-1}	Modulus ($E_{\theta\theta}$), GPa (10^6 psi)	Poisson's Ratio ($\nu_{\theta x}$)
		Initial Properties	
27-10	24	16.8 (2.43)	0.09
27-11	49	20.7 (3.00)	0.13
27-13	23	23.5 (3.40)	0.16
		Secant Properties	
27-10	56	13.8 (1.99)	0.10
27-11	71	16.4 (2.38)	0.17
27-13	56	17.0 (2.47)	0.14
		Terminal Properties	
27-10	119	7.2 (1.05)	0.16
27-11	148	25.2 (3.66)	0.26
27-13	136	9.3 (1.35)	0.19
		Ultimate Properties	
	Time to Failure (t_f), μs	Strength ($S_{\theta\theta T}$), MPa (ksi)	Strain ($\varepsilon^u_{\theta\theta T}$)
27-10	151	115.6 (16.8)	0.0084
27-11	130	151.1 (21.9)	0.0092
27-13	150	143.2 (20.8)	0.0084

3.7 $[\pm 75]_{2s}$ LAMINATES

Intermediate strain rate tensile properties of $[\pm 75]_{2s}$ SP288/AS graphite/epoxy and 80AS/20S/PR288 graphite/S-glass/epoxy were obtained by testing rings under dynamic internal pressure. Three rings of each material were loaded dynamically using 650 mg pistol powder in the pressure chamber of the fixture.

Valid data were obtained only for one of the three graphite/epoxy rings tested, Specimen No. 20-12. Strain records and the corresponding dynamic stress-strain curve for this specimen are shown in Figures 3-77 and 3-78, respectively. Results are tabulated in Table 3-13. The initial and secant strain rates are $19s^{-1}$ and $45s^{-1}$, respectively, and the time to failure is 201 μs. The initial modulus of 19.7 GPa (2.86×10^6 psi) is much higher than the static modulus of 11.2 GPa (1.63×10^6 psi). The average Poisson's ratio of 0.06 is lower than the static value of 0.09. The dynamic strength of 98.3 MPa (14.2 ksi) is higher than the static strength of 74.8 MPa (10.8 ksi) by 31%. The dynamic ultimate strain of 0.0090 is also higher than the static value of 0.0076 by 18%.

Strain records for the three hybrid rings tested are shown in Figures 3-79, 3-80, and 3-81 (Specimen Nos. 21-10, 21-11, and 21-12). The corresponding dynamic stress-strain curves are shown in Figures 3-82, 3-83, and 3-84. Results are tabulated in Table 3-14. The initial strain rates range between $28s^{-1}$ and $37s^{-1}$ and the average (secant) rates between $62s^{-1}$ and $68s^{-1}$. The times to failure range between 107 μs and 111 μs. The initial modulus of 16.9 GPa (2.45×10^6 psi) is a little higher than the static modulus of 15.5 GPa (2.25×10^6 psi). The overall average Poisson's ratio of 0.08 is slightly lower than the static value of 0.10. The average dynamic strength of 94.9 MPa (13.8 ksi) is higher than the static strength of 61.4 MPa (8.9 ksi) by 55%. The dynamic ultimate strain of 0.0070 is also higher than the static value of 0.0047 by 49%.

TABLE 3-13. INTERMEDIATE STRAIN RATE TENSILE PROPERTIES OF $[\pm 75]_{2s}$ SP288/AS GRAPHITE/EPOXY

Specimen Number	Strain Rate ($\dot{\varepsilon}_{\theta\theta}$), s^{-1}	Modulus ($E_{\theta\theta}$), GPa (10^6 psi)	Poisson's Ratio ($\nu_{\theta x}$)
		Initial Properties	
20-12	19	19.7 (2.86)	-
		Secant Properties	
20-12	45	10.9 (1.58)	0.04
		Terminal Properties	
20-12	132	6.0 (0.87)	0.08
		Ultimate Properties	
	Time to Failure (t_f), μs	Strength ($S_{\theta\theta T}$), MPa (ksi)	Strain ($\varepsilon^u_{\theta\theta T}$)
20-12	201	98.3 (14.2)	0.0090

TABLE 3-14. INTERMEDIATE STRAIN RATE TENSILE PROPERTIES OF $[\pm 75]_{2s}$ 80AS/20S/PR288 GRAPHITE/S-GLASS/EPOXY

Specimen Number	Strain Rate ($\dot{\varepsilon}_{\theta\theta}$), s^{-1}	Modulus ($E_{\theta\theta}$), GPa (10^6 psi)	Poisson's Ratio ($\nu_{\theta x}$)
		Initial Properties	
21-10	36	15.4 (2.22)	-
21-11	28	16.9 (2.45)	-
21-12	37	18.5 (2.68)	-
		Secant Properties	
21-10	68	13.4 (1.94)	0.04
21-11	62	8.4 (1.21)	0.04
21-12	62	18.5 (2.68)	0.05
		Terminal Properties	
21-10	128	11.5 (1.66)	0.07
21-11	108	7.7 (1.11)	0.11
21-12	113	15.9 (2.30)	0.14
		Ultimate Properties	
	Time to Failure (t_f), μs	Strength ($S_{\theta\theta T}$), MPa (ksi)	Strain ($\varepsilon^u_{\theta\theta T}$)
21-10	111	101.8 (14.8)	0.0076
21-11	107	55.2 (8.0)	0.0066
21-12	111	127.7 (18.5)	0.0069

C-2

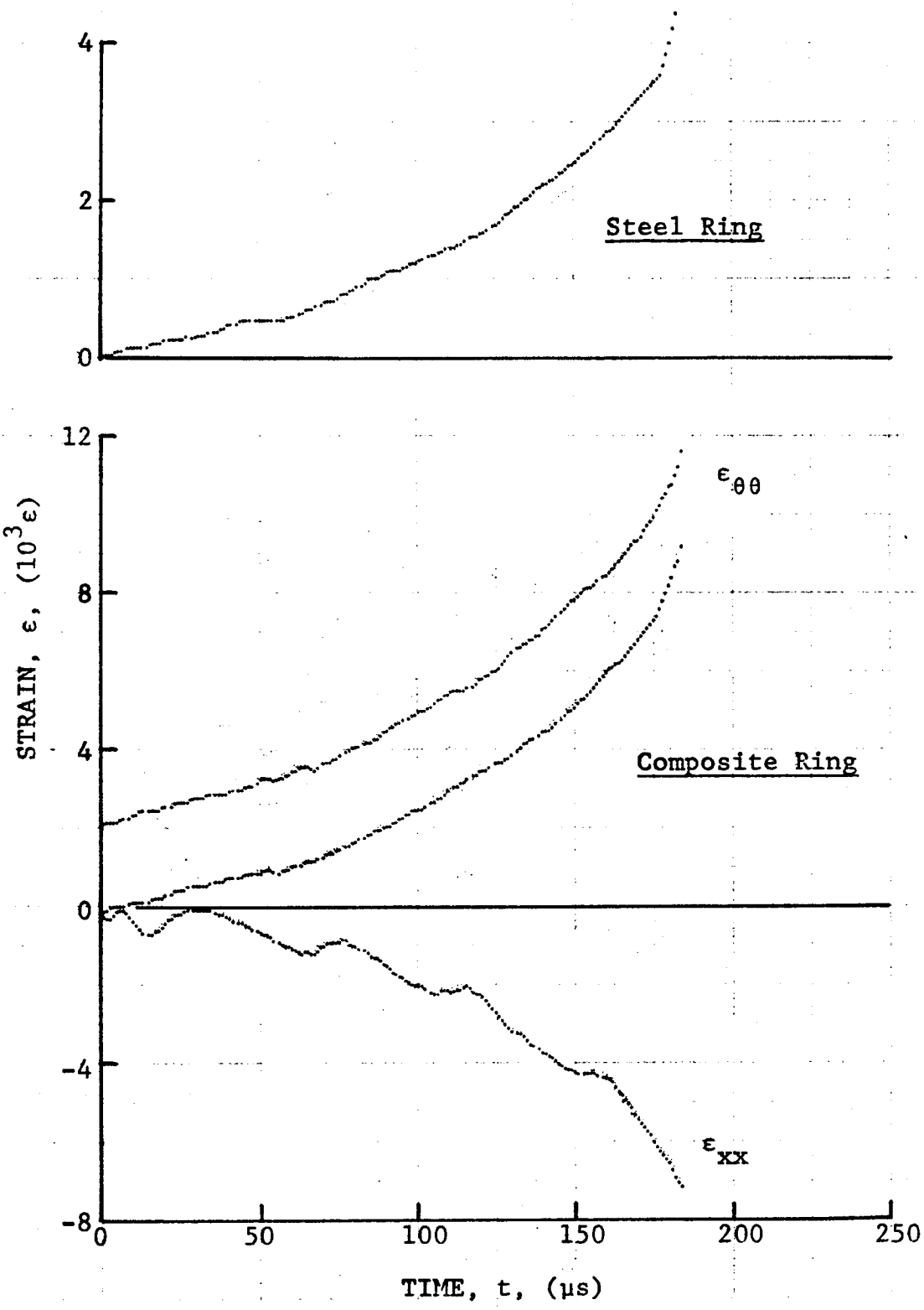

Figure 3-1. Strain records in steel ring and $[\pm 15]_{2S}$ SP288/AS graphite/epoxy ring under dynamic loading for Specimen No. 35-7 (0.65 g shotgun powder).

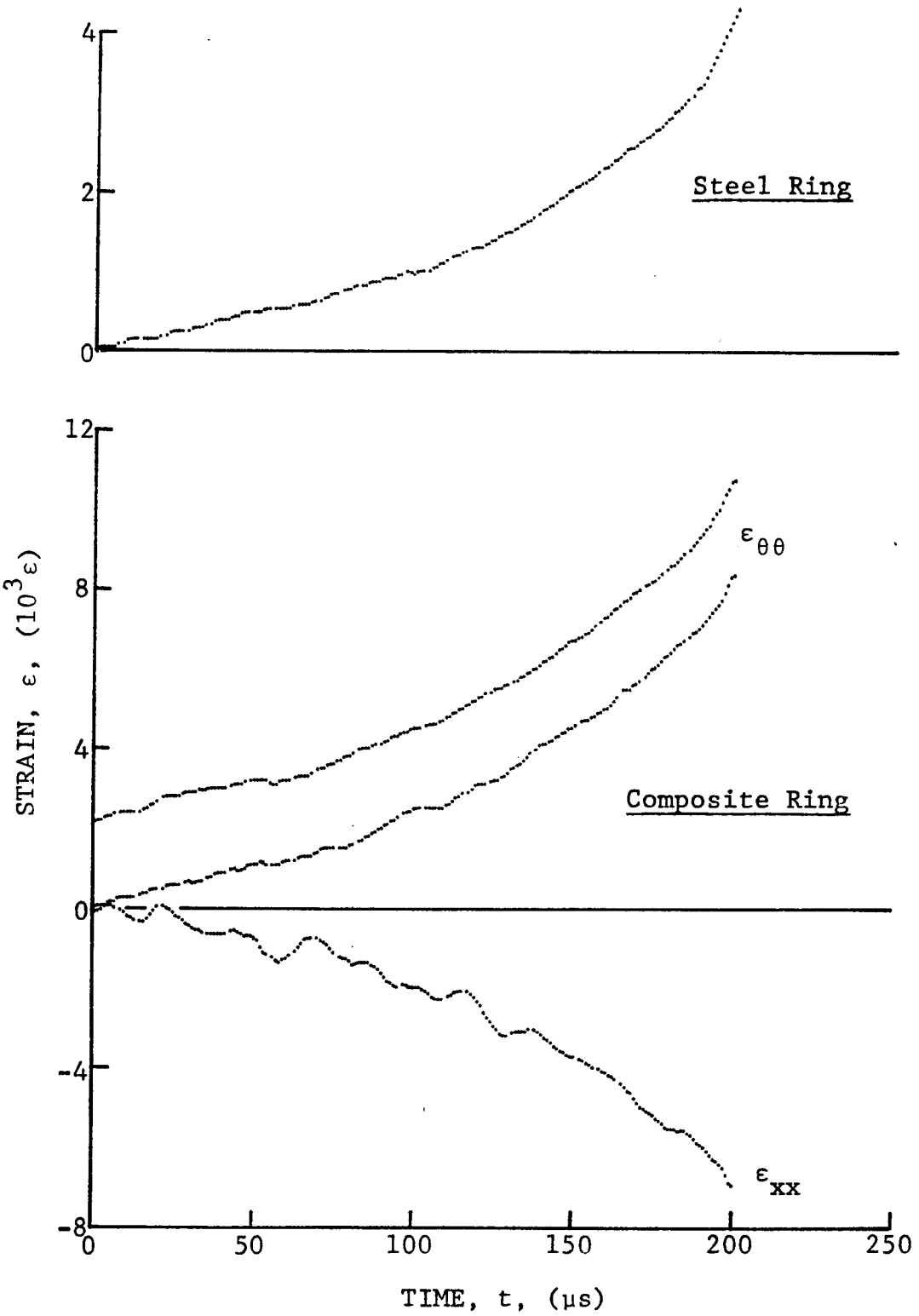

Figure 3-2. Strain records in steel ring and $[\pm 15]_{2S}$ SP288/AS graphite/epoxy ring under dynamic loading for Specimen No. 35-10 (0.65 g shotgun powder).

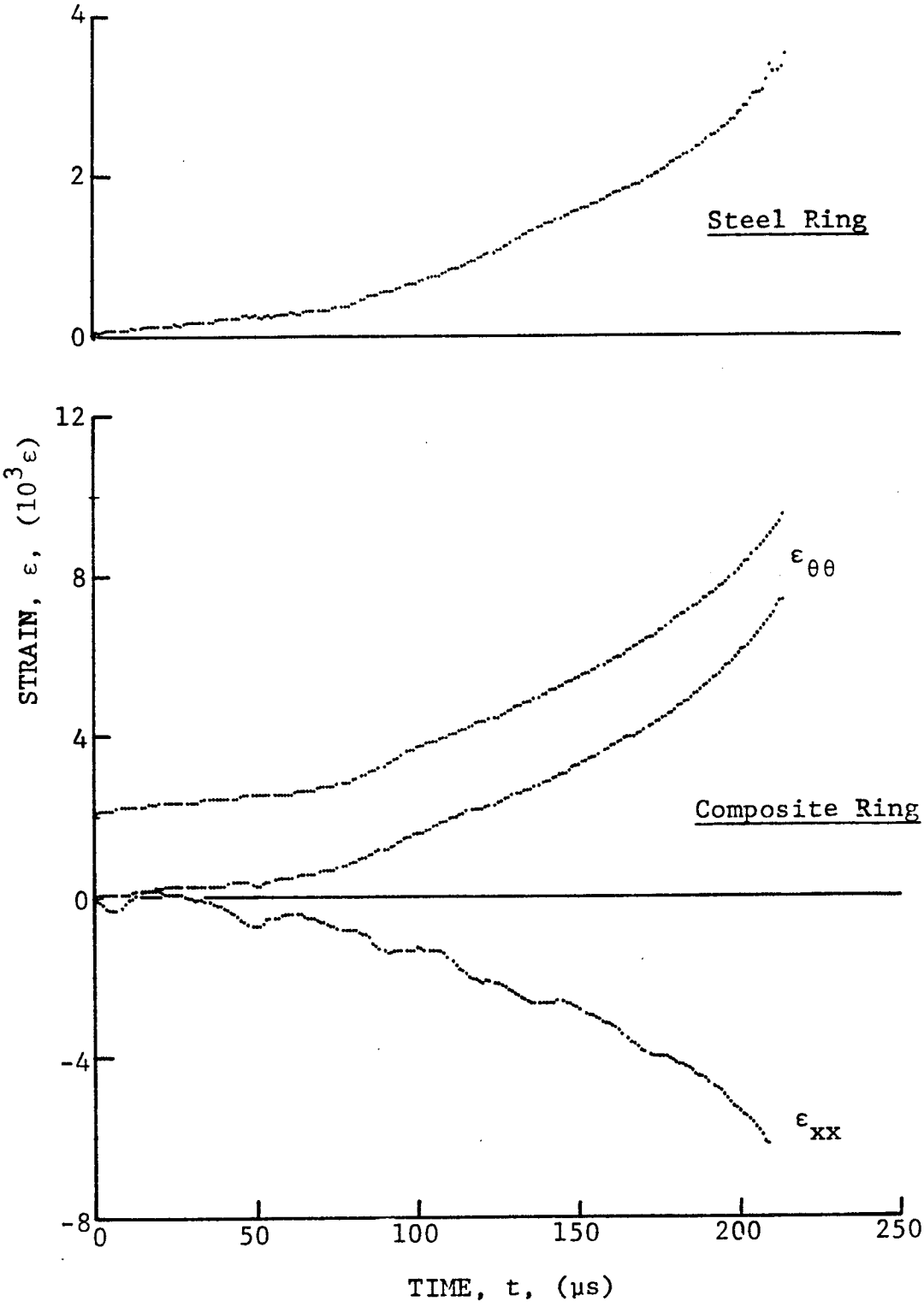

Figure 3-3. Strain records in steel ring and $[\pm 15]_{2s}$ SP288/AS graphite/epoxy ring under dynamic loading for Specimen No. 35-11 (0.65 g shotgun powder).

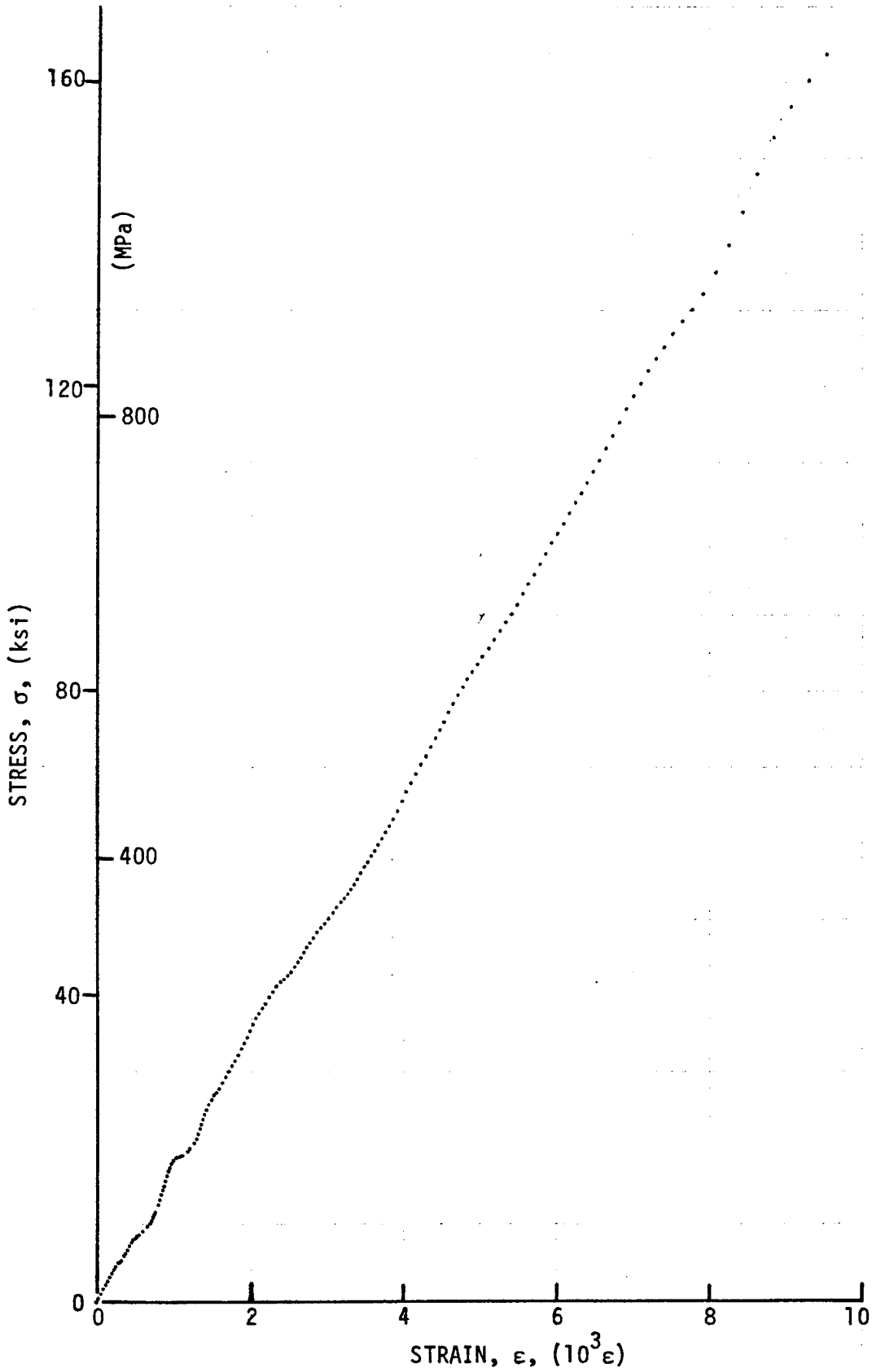

Figure 3-4. Stress-strain curves for dynamically loaded $[\pm 15]_{2s}$ SP288/AS graphite/epoxy ring, Specimen No. 35-7.

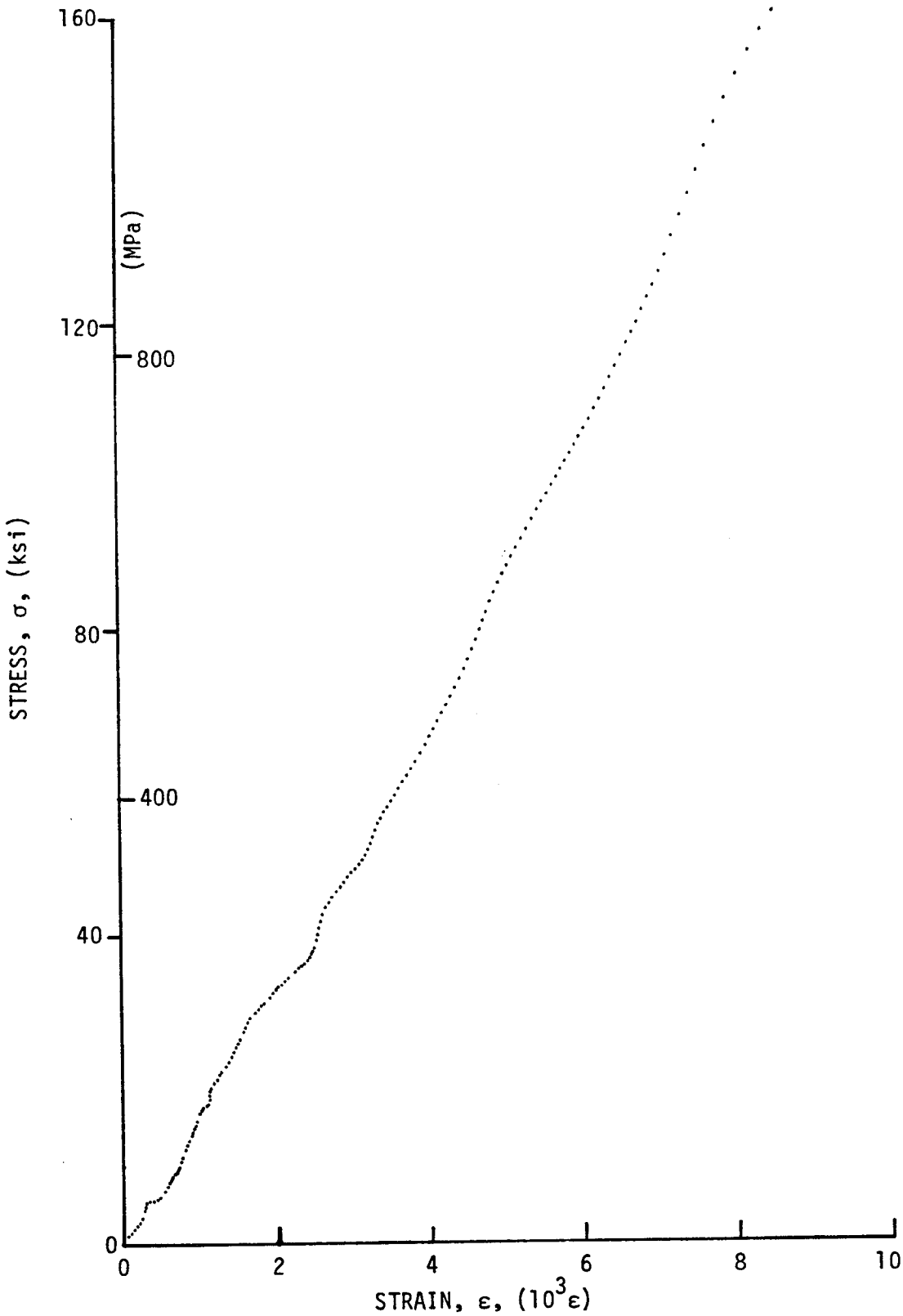

Figure 3-5. Stress-strain curves for dynamically loaded $[\pm 15]_{2s}$ SP288/AS graphite/epoxy ring, Specimen No. 35-10.

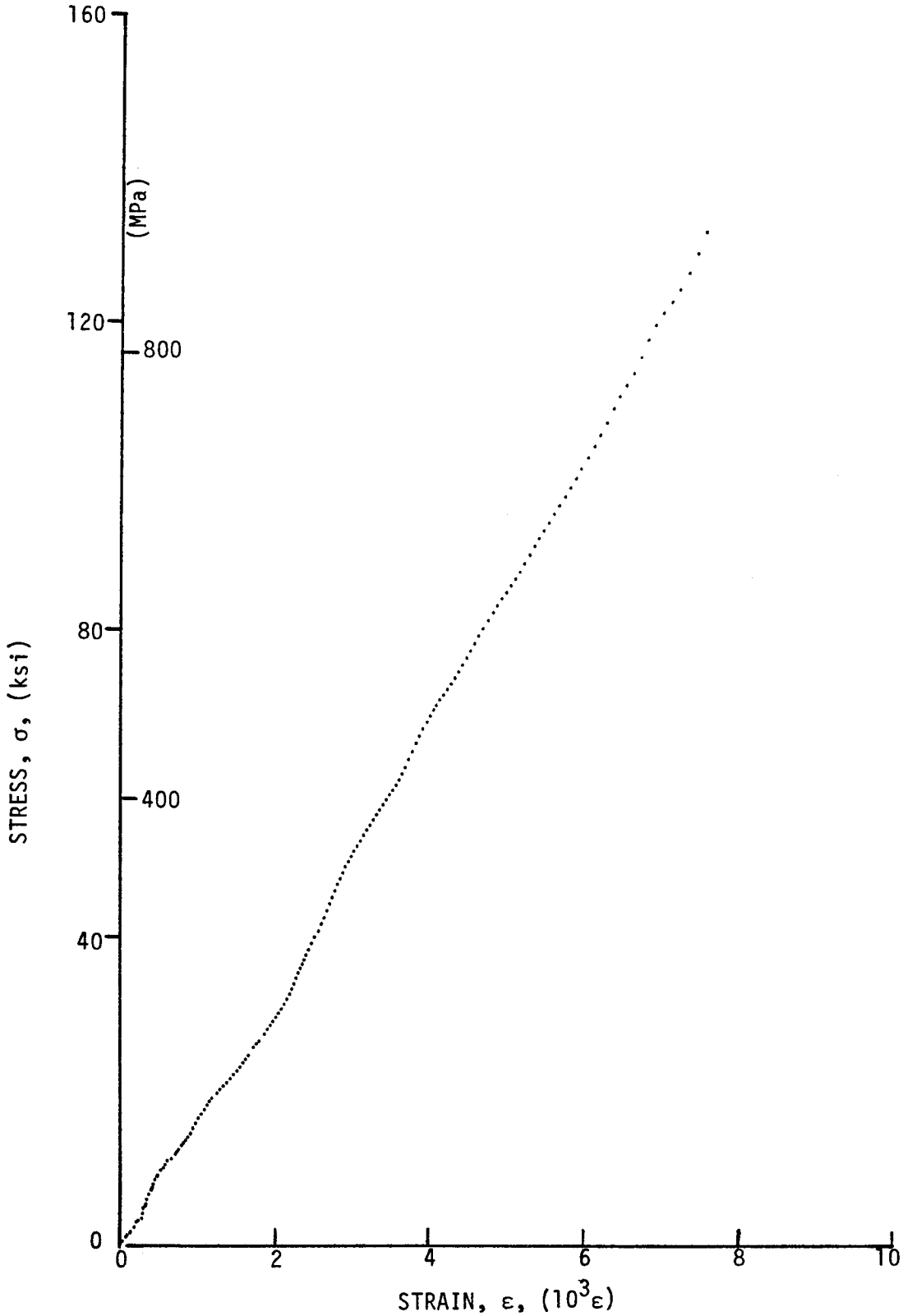

Figure 3-6. Stress-strain curves for dynamically loaded $[\pm 15]_{2s}$ SP288/AS graphite/epoxy ring, Specimen No. 35-11.

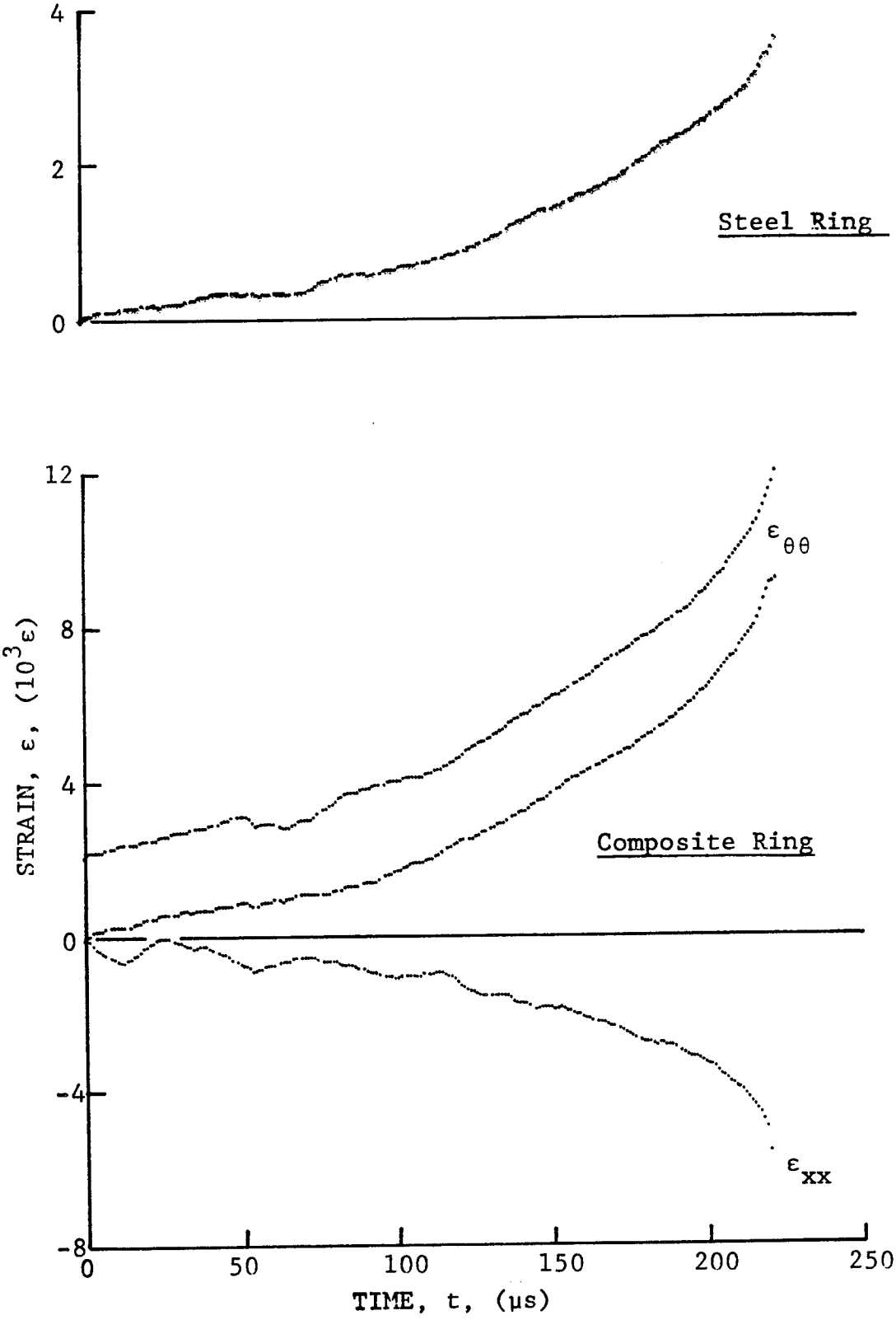

Figure 3-7. Strain records in steel ring and 80AS/20S/PR288 $[\pm 15]_{2s}$ graphite/S-glass/epoxy ring under dynamic loading for Specimen No. 36-6 (0.65 g shotgun powder).

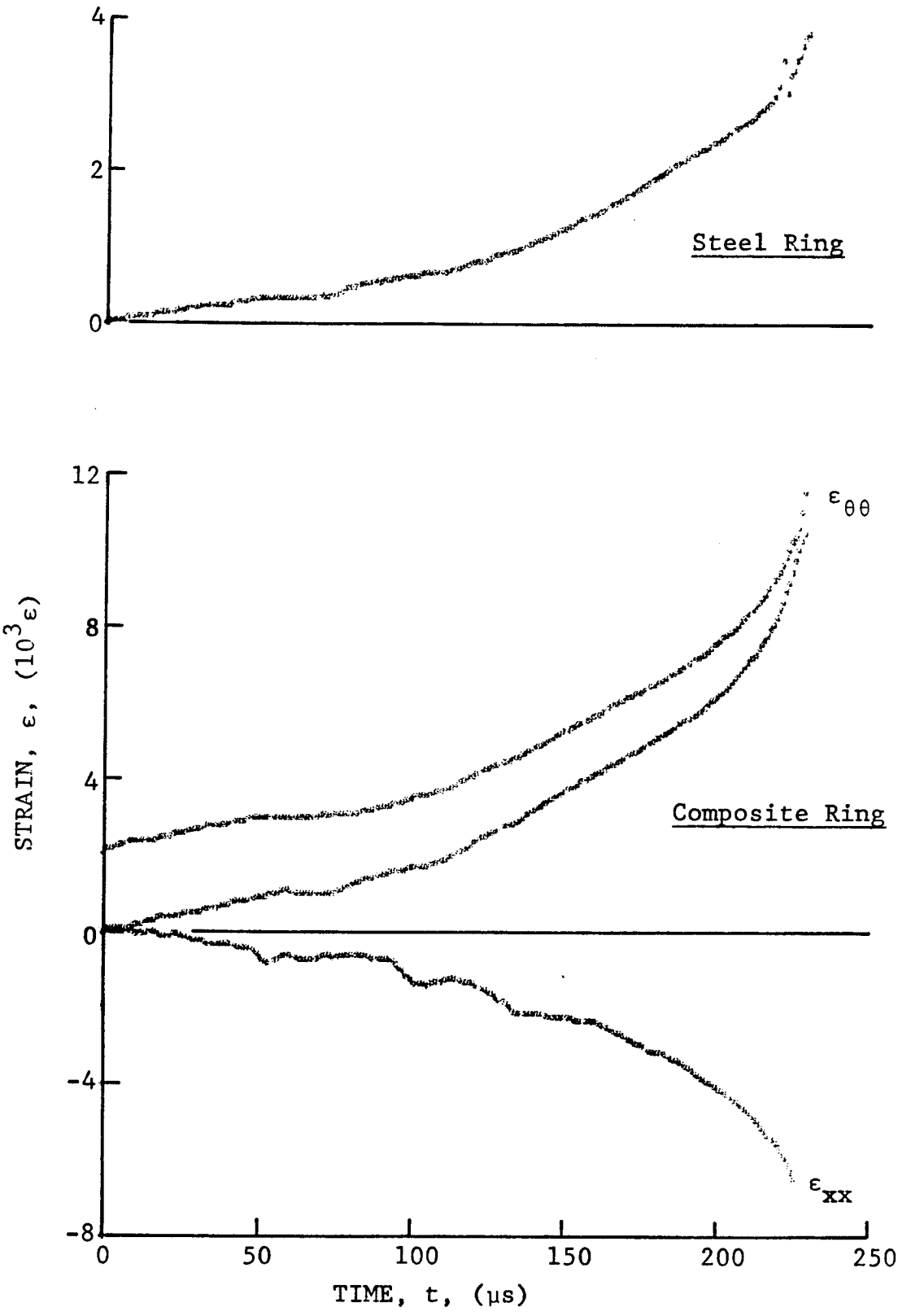

Figure 3-8. Strain records in steel ring and 80AS/20S/PR288 $[\pm 15]_{2s}$ graphite/S-glass/epoxy ring under dynamic loading for Specimen No. 36-10 (0.65 g shotgun powder).

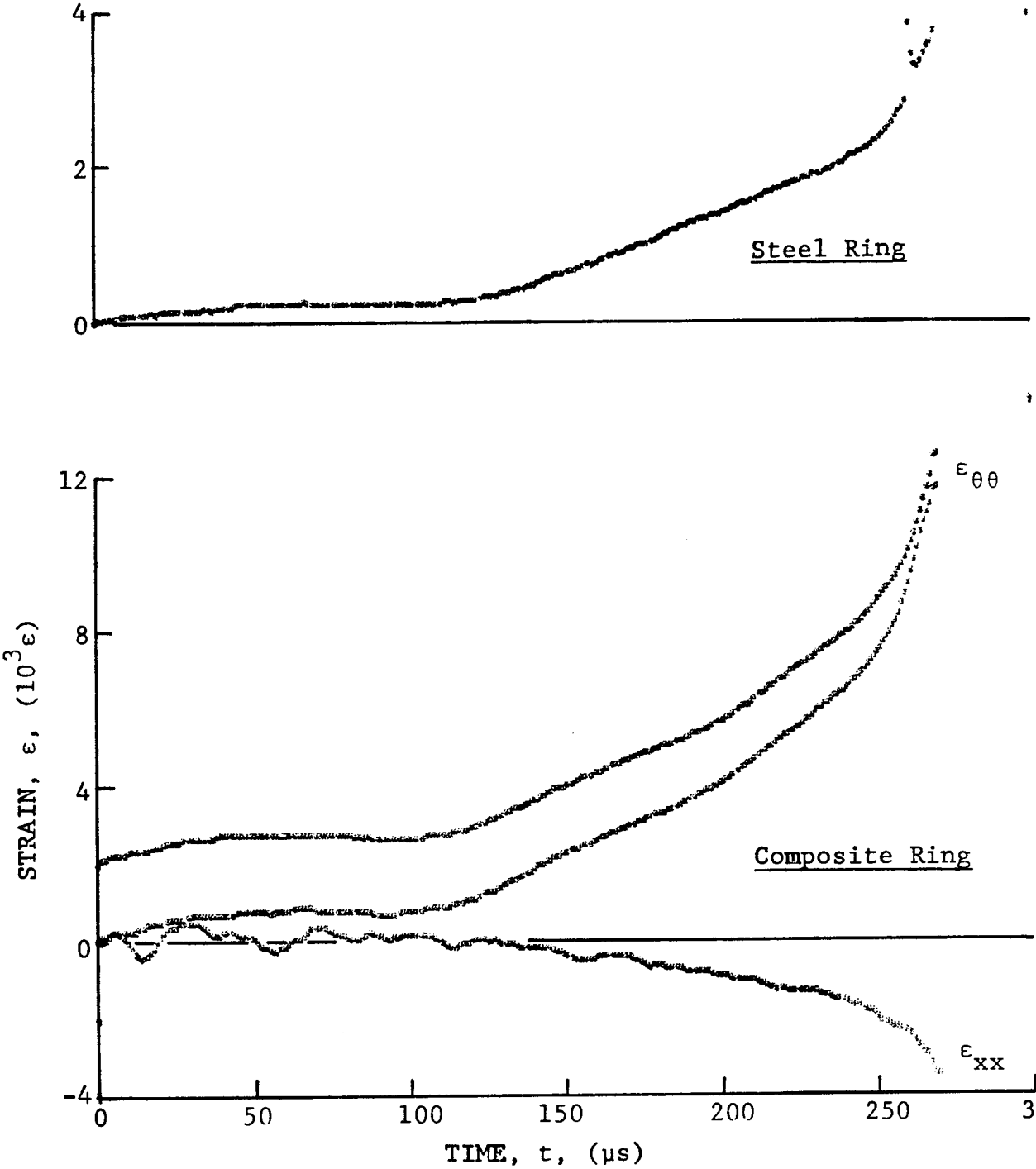

Figure 3-9. Strain records in steel ring and 80AS/20S/PR288 $[\pm 15]_{2s}$ graphite/S-glass/epoxy ring under dynamic loading for Specimen No. 36-11 (0.65 g shotgun powder).

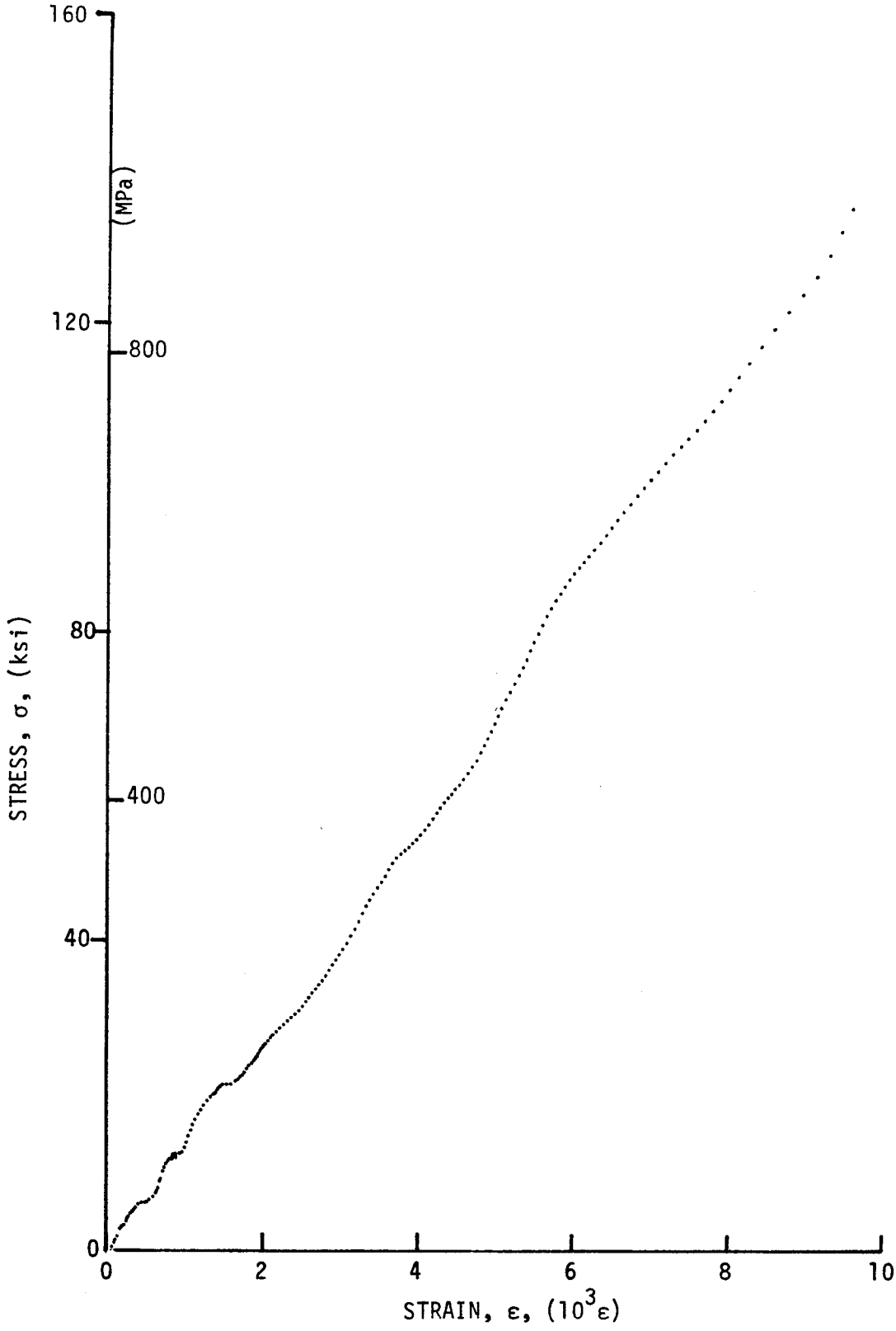

Figure 3-10. Stress-strain curves for dynamically loaded $[\pm 15]_{2s}$ 80AS/20S/PR288 graphite/S-glass/epoxy ring, Specimen No. 36-6.

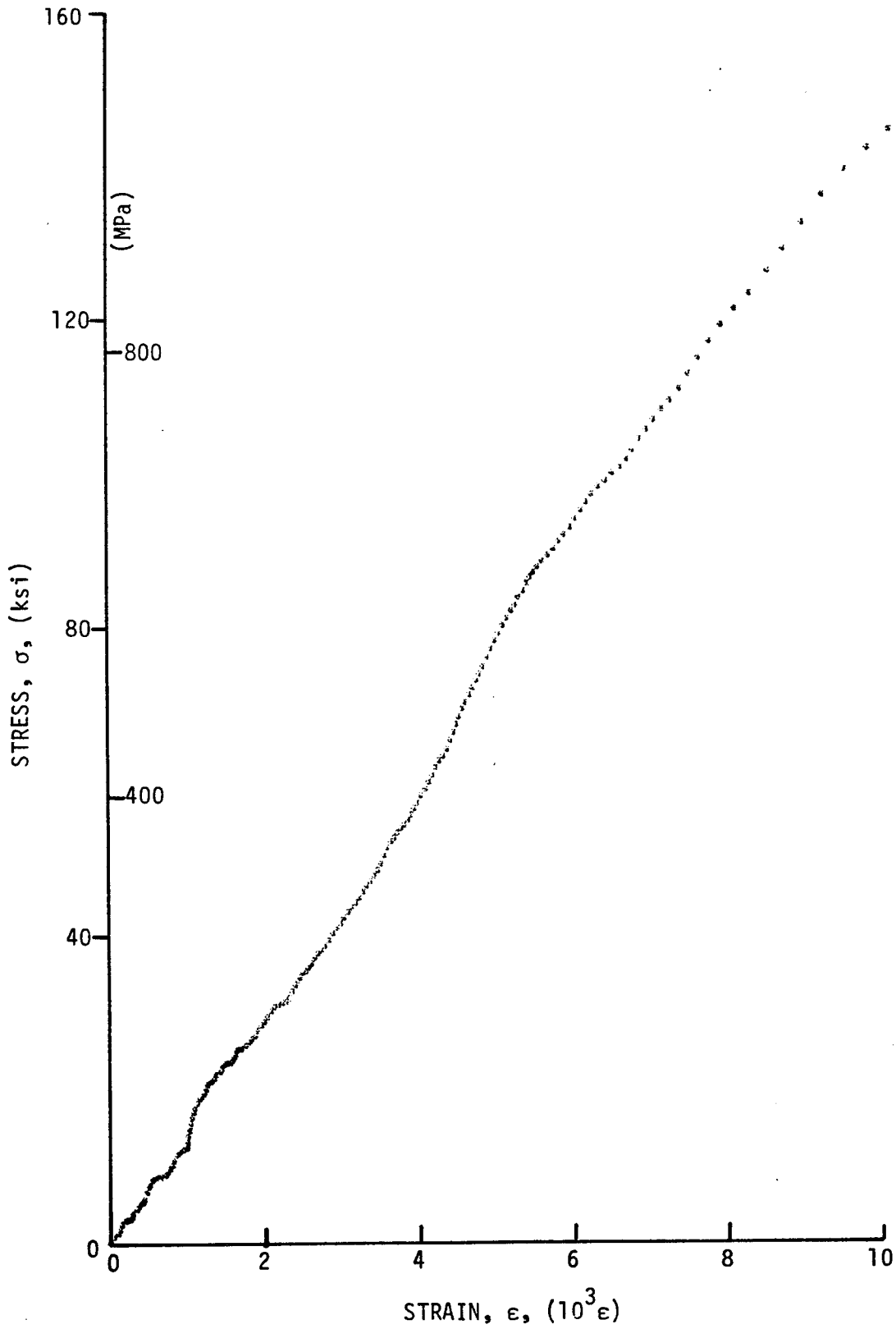

Figure 3-11. Stress-strain curves for dynamically loaded $[\pm 15]_{2s}$ 80AS/20S/PR288 graphite/S-glass/epoxy ring, Specimen No. 36-10.

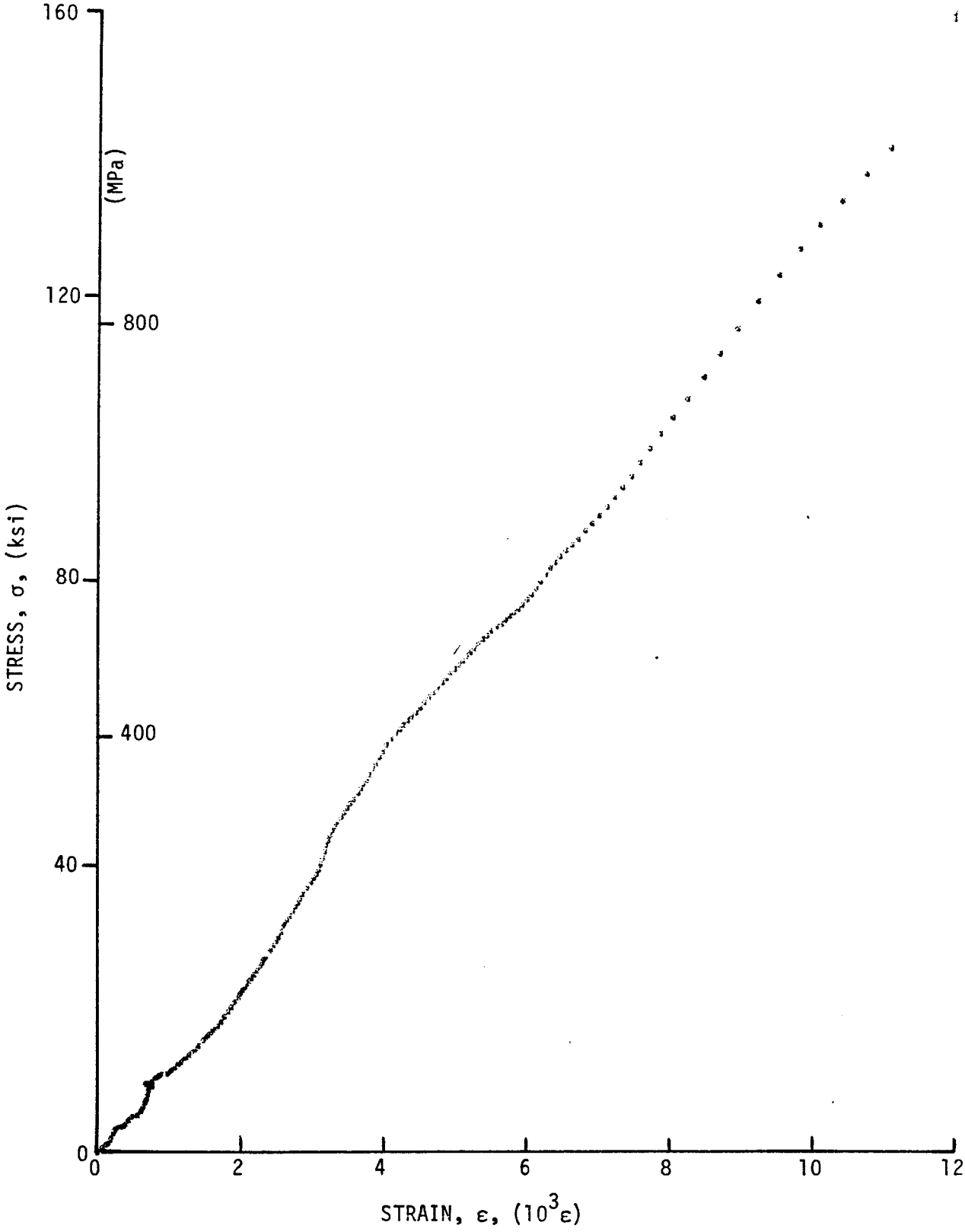

Figure 3-12. Stress-strain curves for dynamically loaded $[\pm 15]_{2s}$ 80AS/20S/PR288 graphite/S-glass/epoxy ring, Specimen No. 36-11.

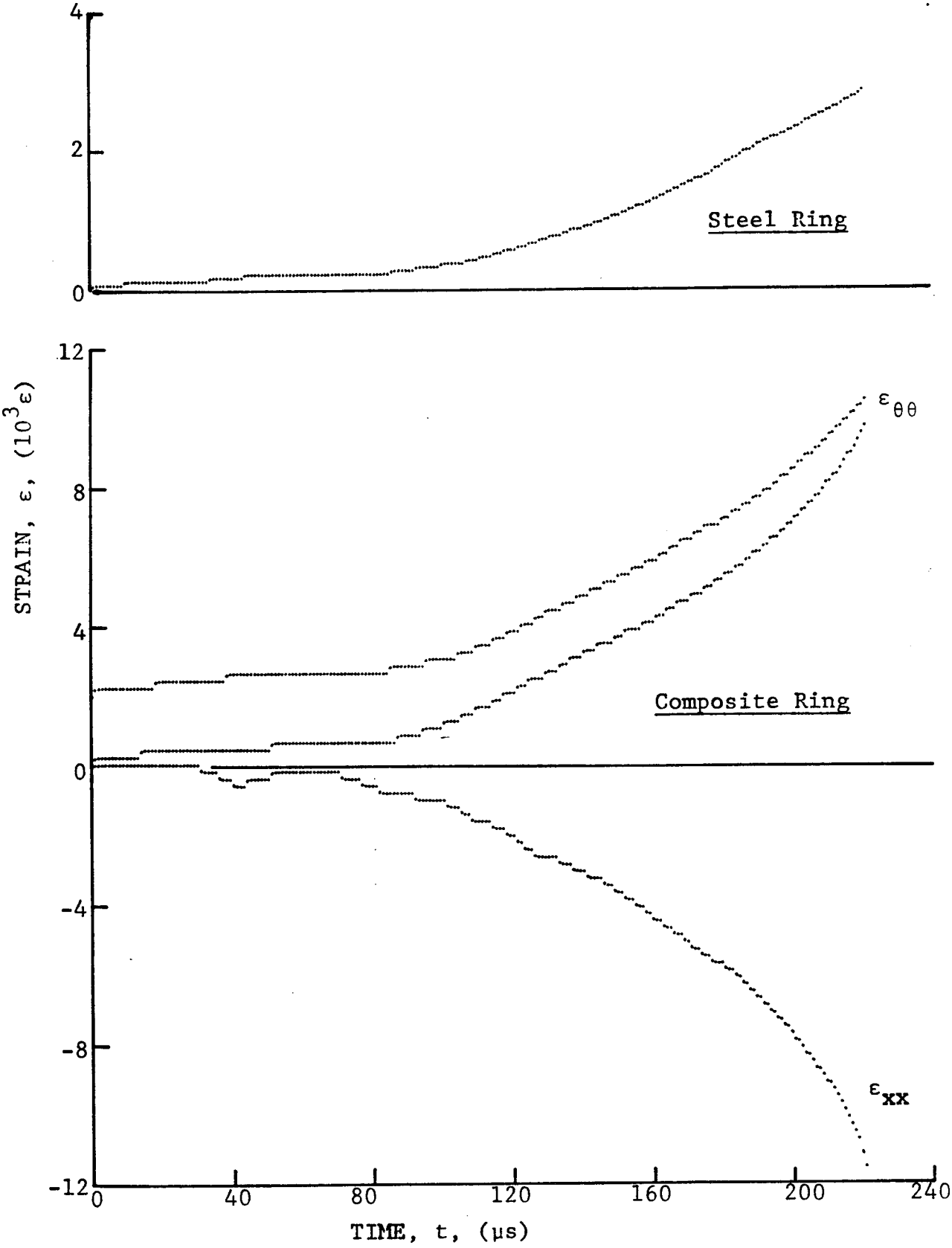

Figure 3-13. Strain records in steel ring and $[\pm 22.5]_{2S}$ SP288/AS graphite/epoxy ring under dynamic loading for Specimen No. 33-10 (0.65 g shotgun powder).

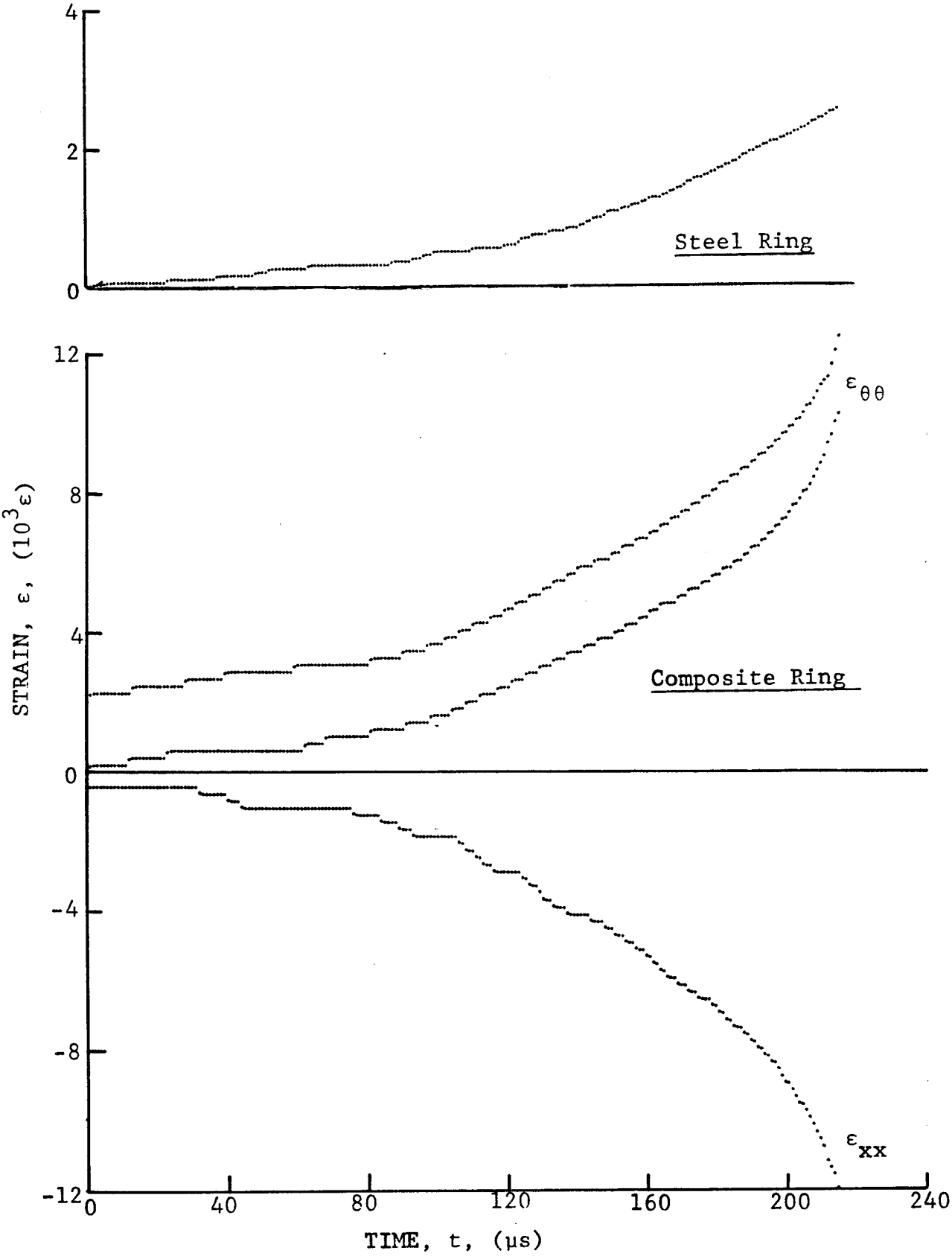

Figure 3-14. Strain records in steel ring and $[\pm 22.5]_{2s}$ SP288/AS graphite/epoxy ring under dynamic loading for Specimen No. 33-11 (0.65 g shotgun powder).

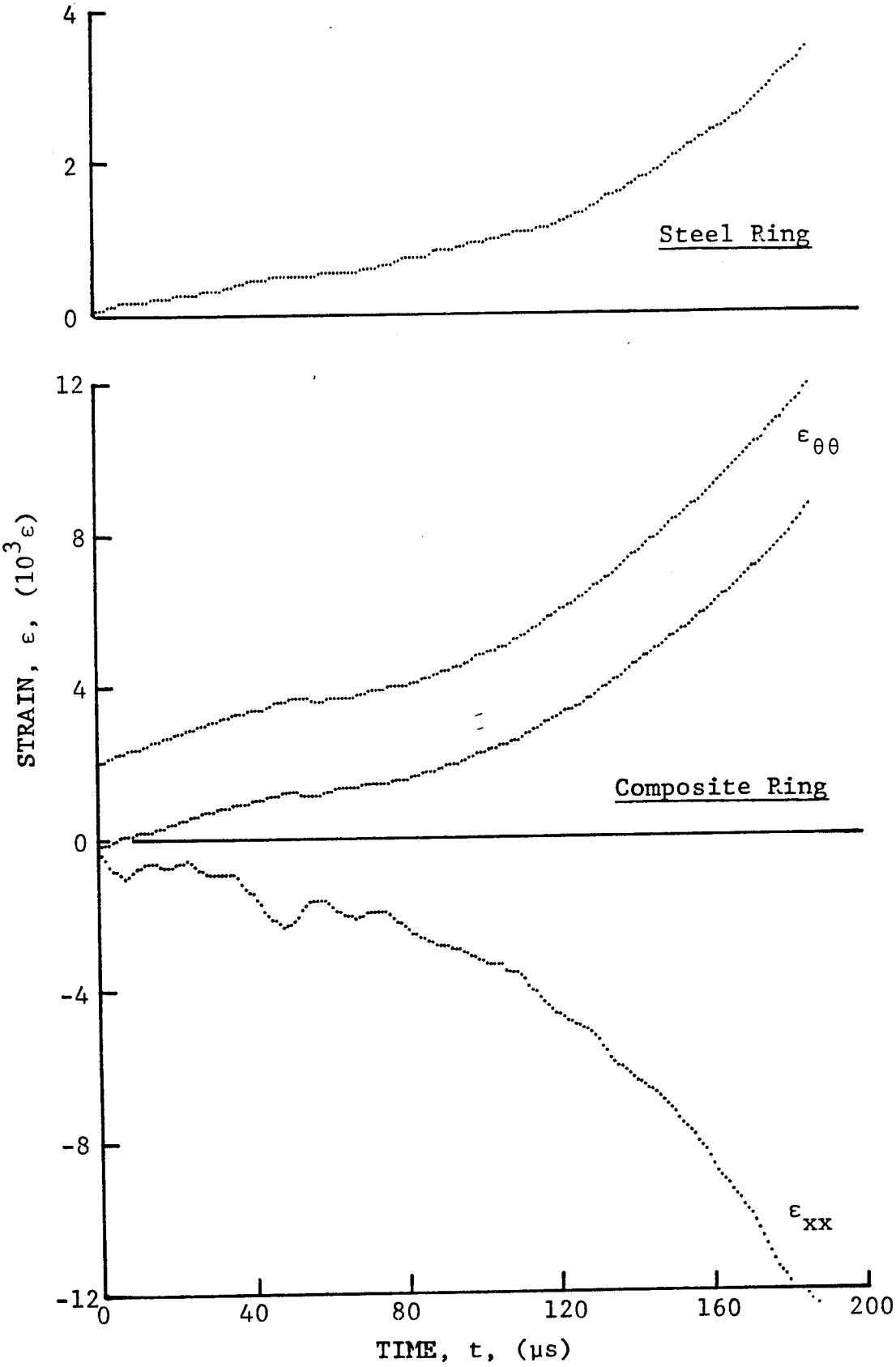

Figure 3-15. Strain records in steel ring and $[\pm 22.5]_{2S}$ SP288/AS graphite/epoxy ring under dynamic loading for Specimen No. 33-13 (0.65 g shotgun powder).

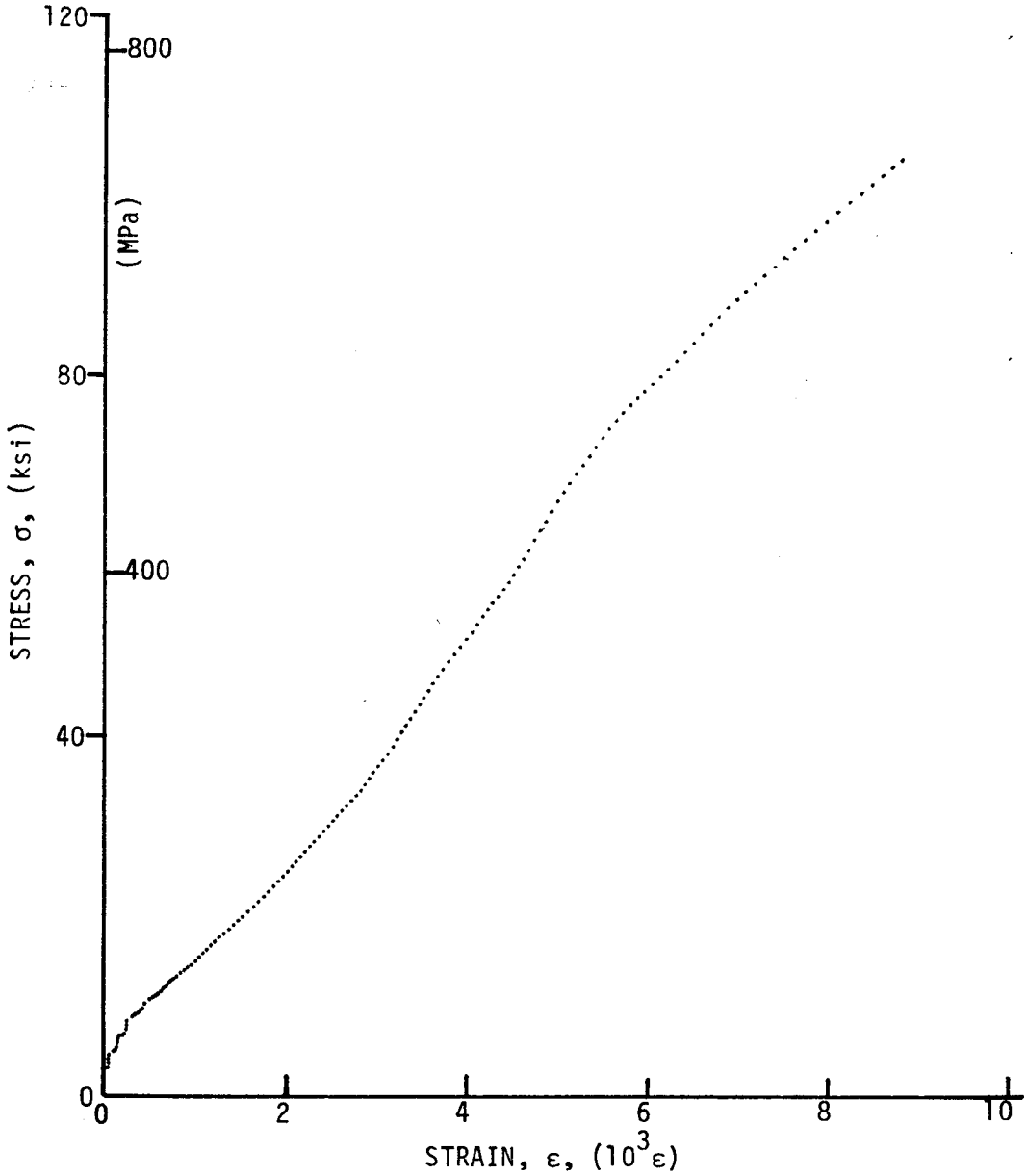

Figure 3-16. Stress-strain curves for dynamically loaded $[\pm 22.5]_{2s}$ SP288/AS graphite/epoxy ring, Specimen No. 33-10.

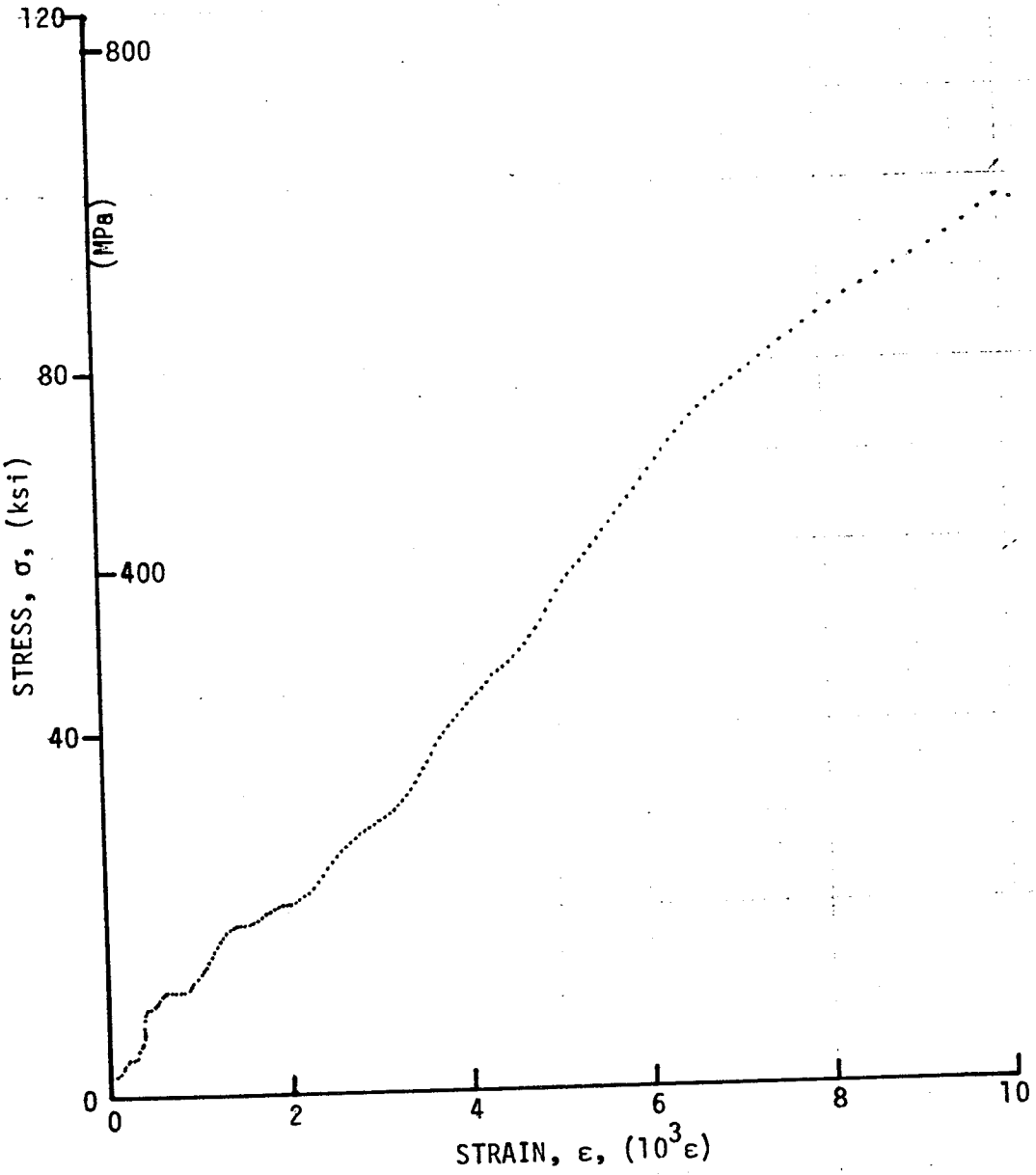

Figure 3-17. Stress-strain curves for dynamically loaded $[\pm 22.5]_{2s}$ SP288/AS graphite/epoxy ring, Specimen No. 33-11.

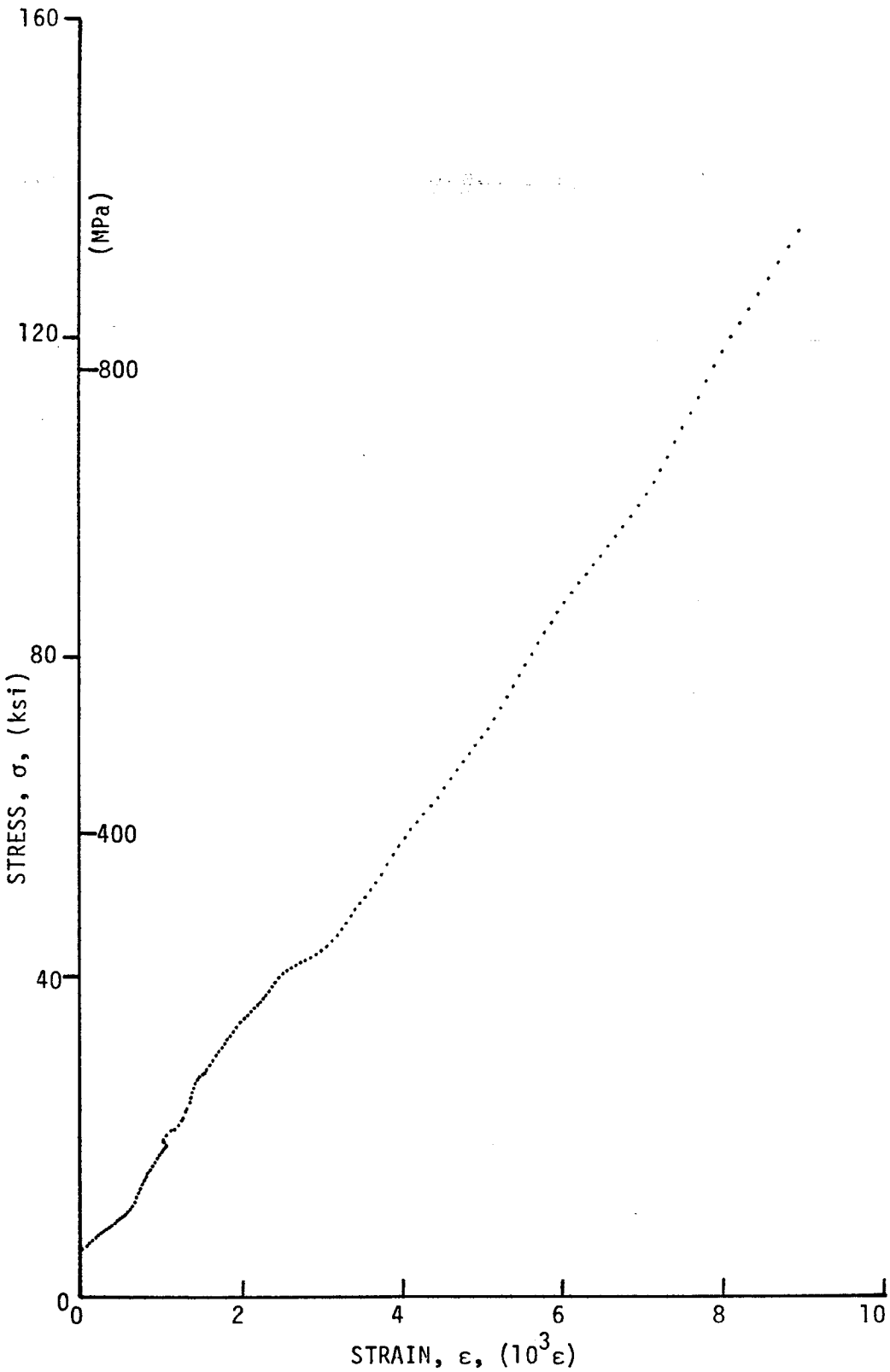

Figure 3-18. Stress-strain curves for dynamically loaded $[\pm 22.5]_{2s}$ SP288/AS graphite/epoxy ring, Specimen No. 33-13.

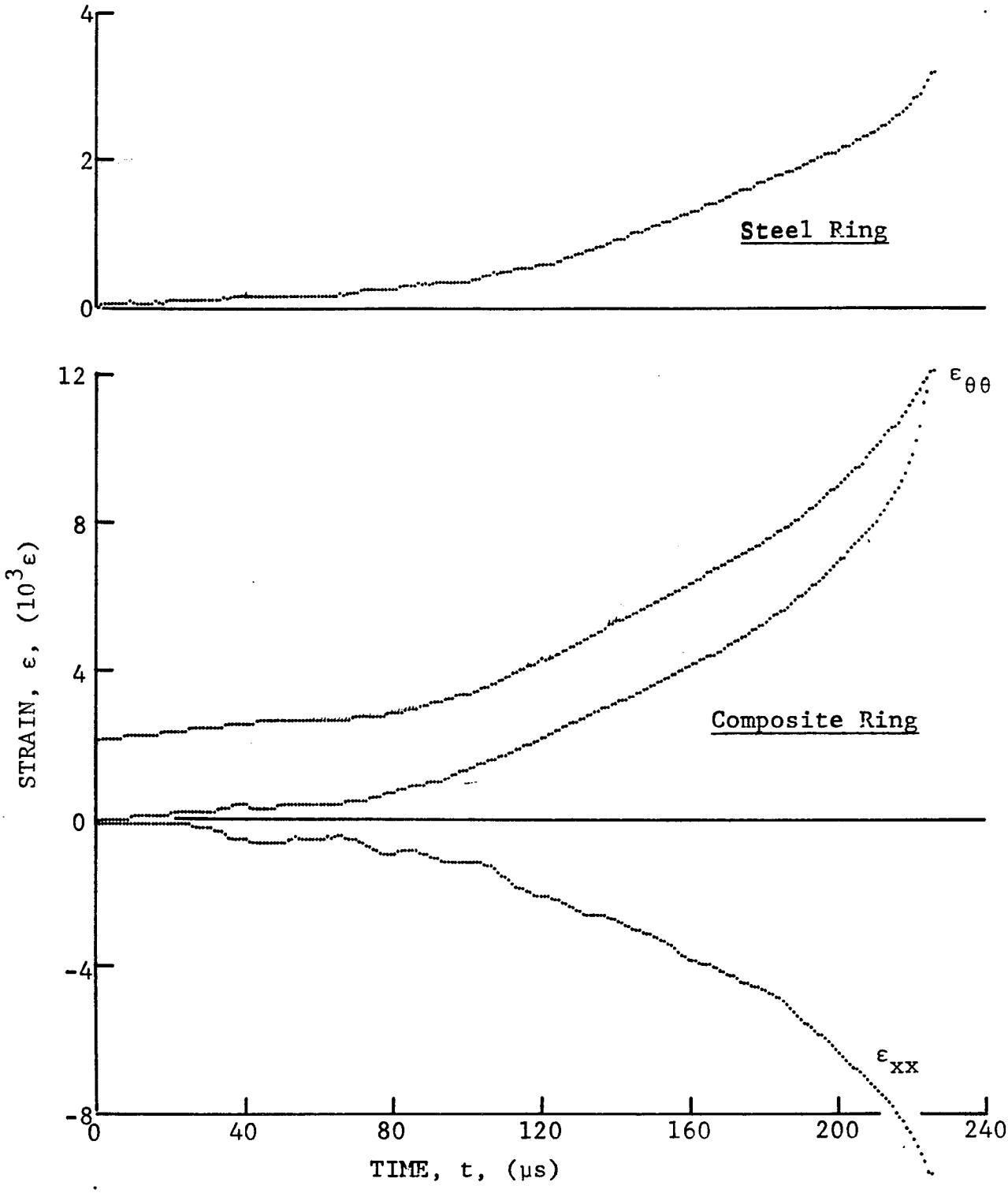

Figure 3-19. Strain records in steel ring and 80AS/20S/PR288 $[\pm 22.5]_{2S}$ graphite/S-glass/epoxy ring under dynamic loading for Specimen No. 34-2 (0.65 g shotgun powder).

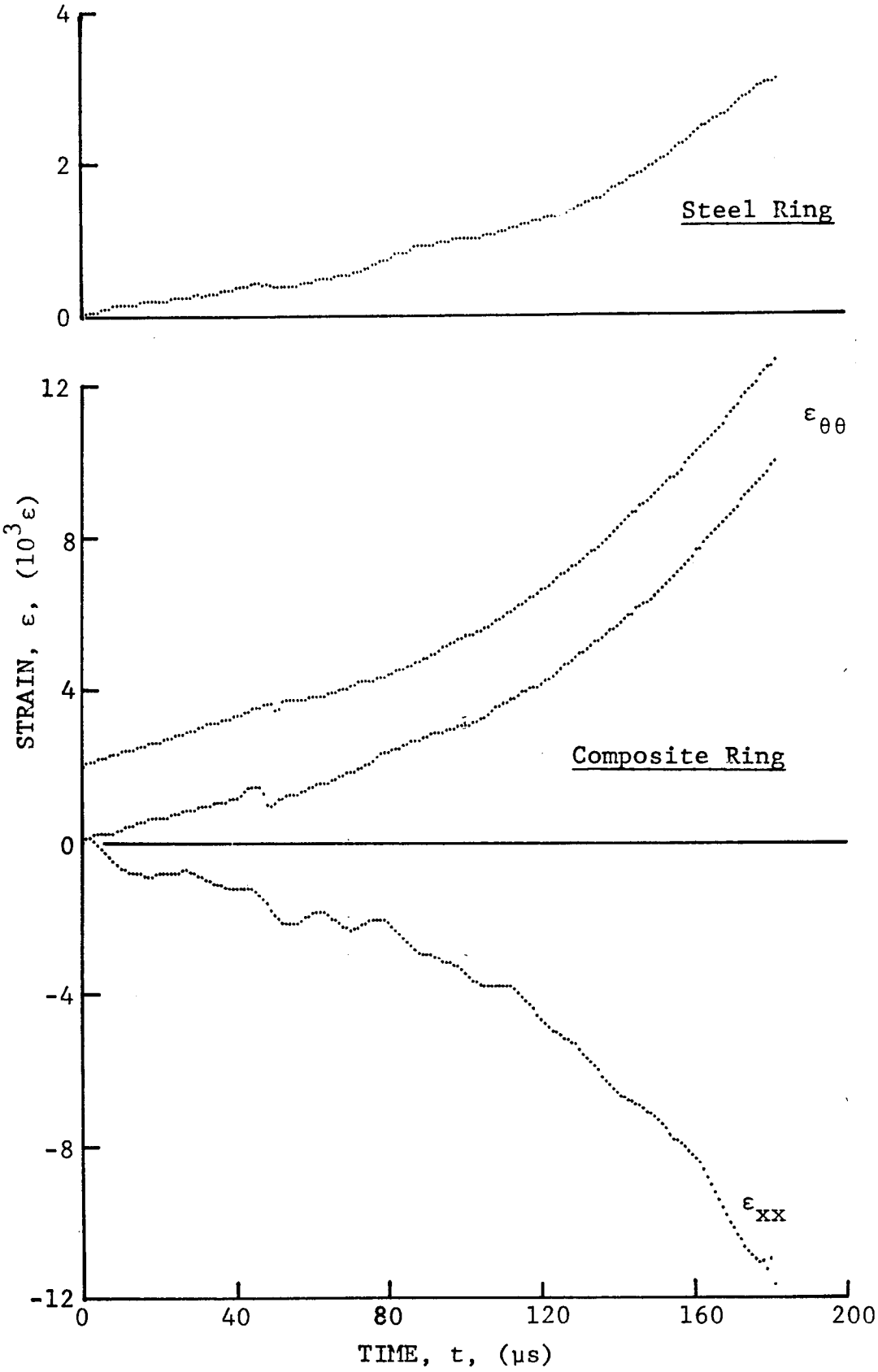

Figure 3-20. Strain records in steel ring and 80AS/20S/PR288 $[\pm 22.5]_{2s}$ graphite/S-glass/epoxy ring under dynamic loading for Specimen No. 34-10 (0.65 g shotgun powder).

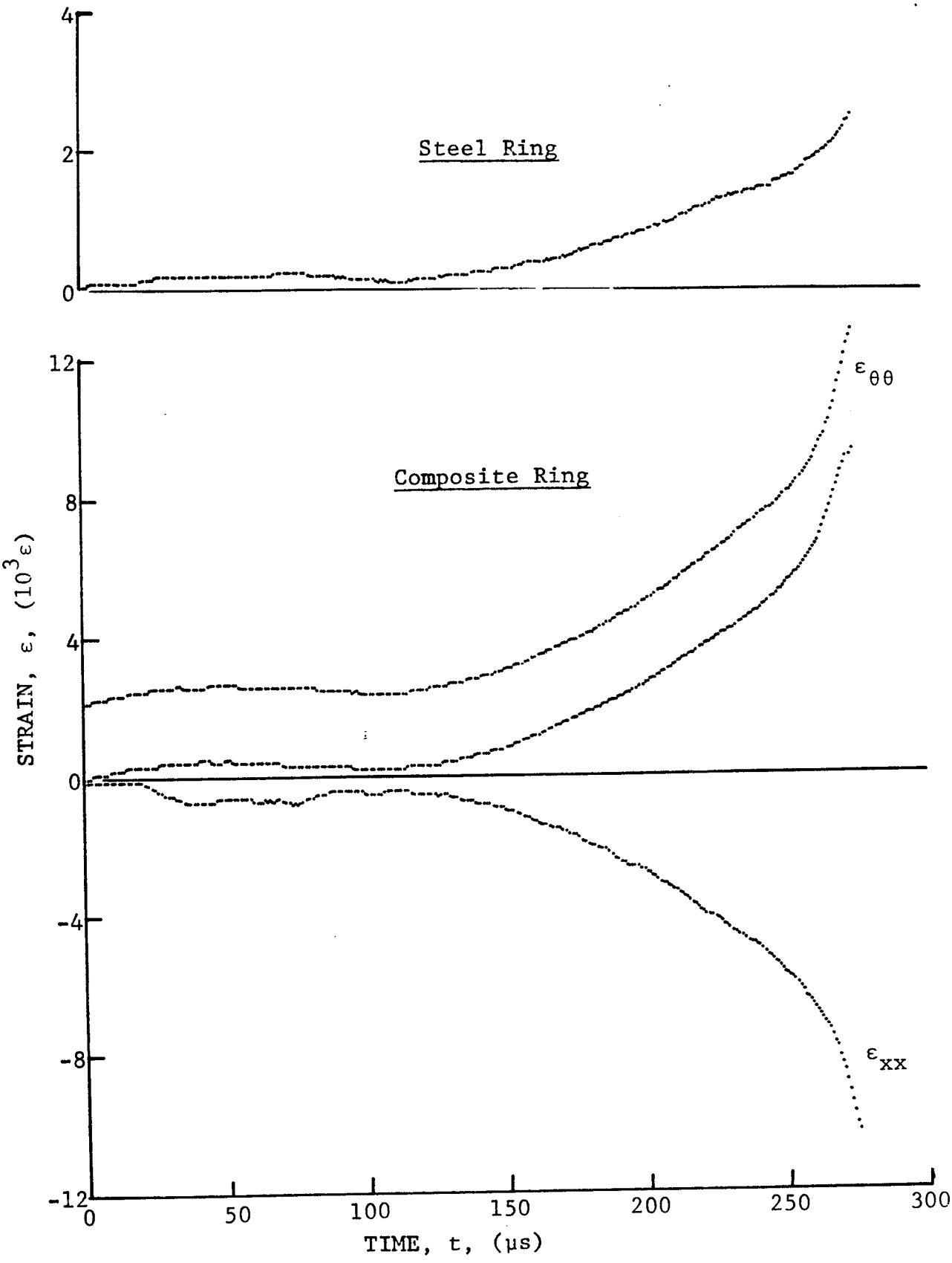

Figure 3-21. Strain records in steel ring and 80AS/20S/PR288 $[\pm 22.5]_{2s}$ graphite/S-glass/epoxy ring under dynamic loading for Specimen No. 34-11 (0.65 g shotgun powder).

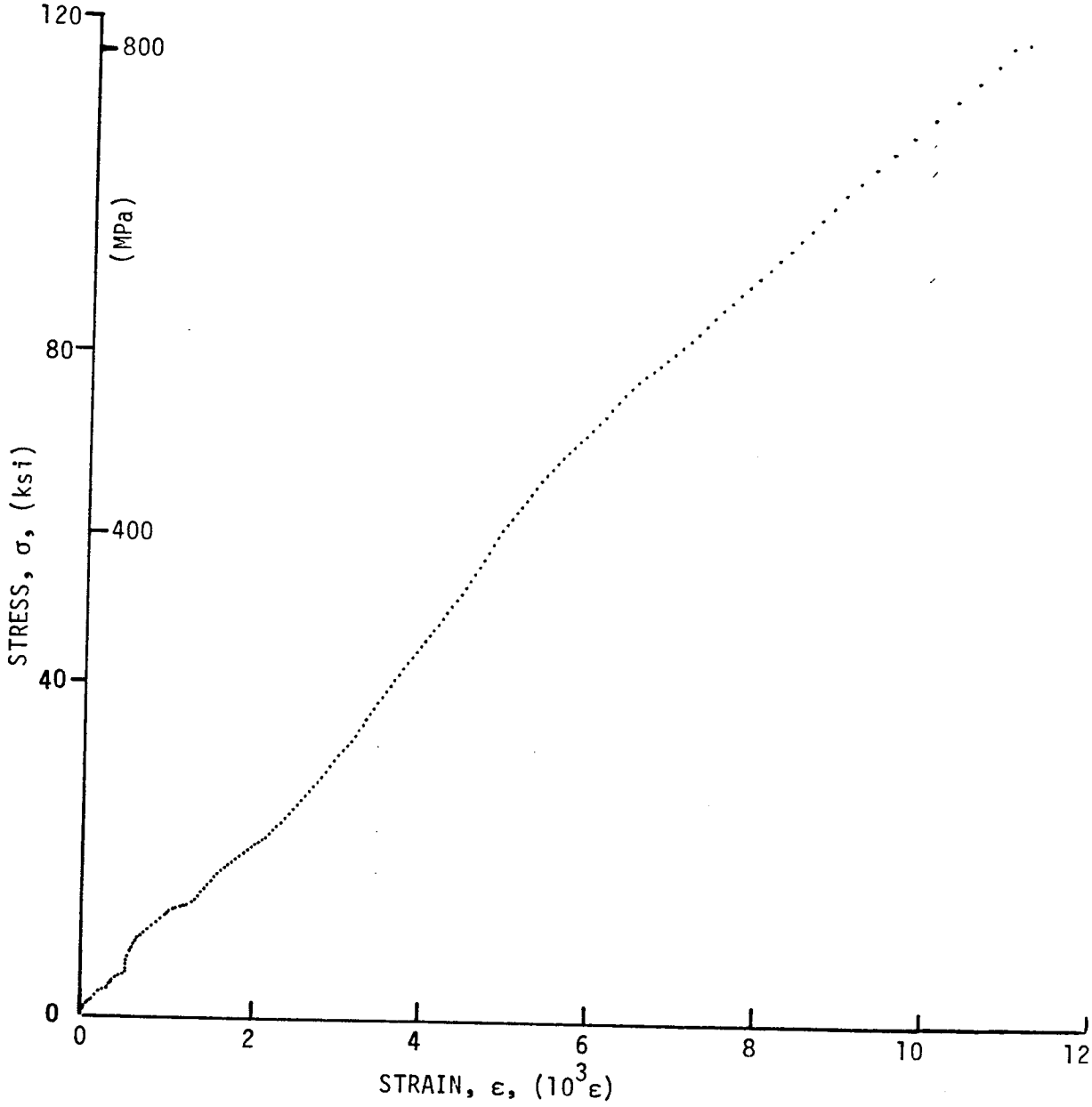

Figure 3-22. Stress-strain curves for dynamically loaded $[\pm 22.5]_{2s}$ 80AS/20S/PR288 graphite/S-glass/epoxy ring, Specimen No. 34-2.

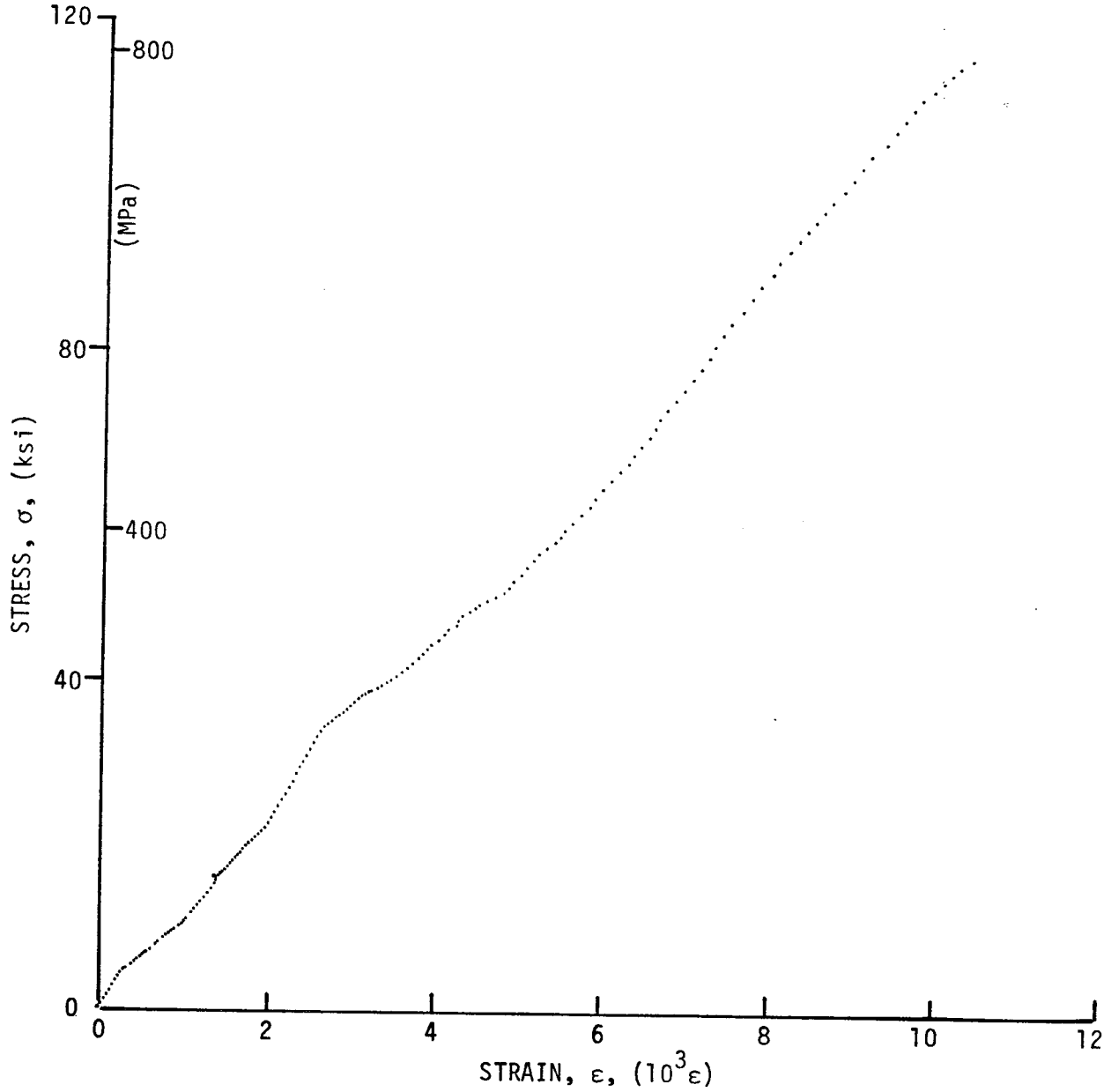

Figure 3-23. Stress-strain curves for dynamically loaded $[\pm 22.5]_{2s}$ 80AS/20S/PR288 graphite/S-glass/epoxy ring, Specimen No. 34-10.

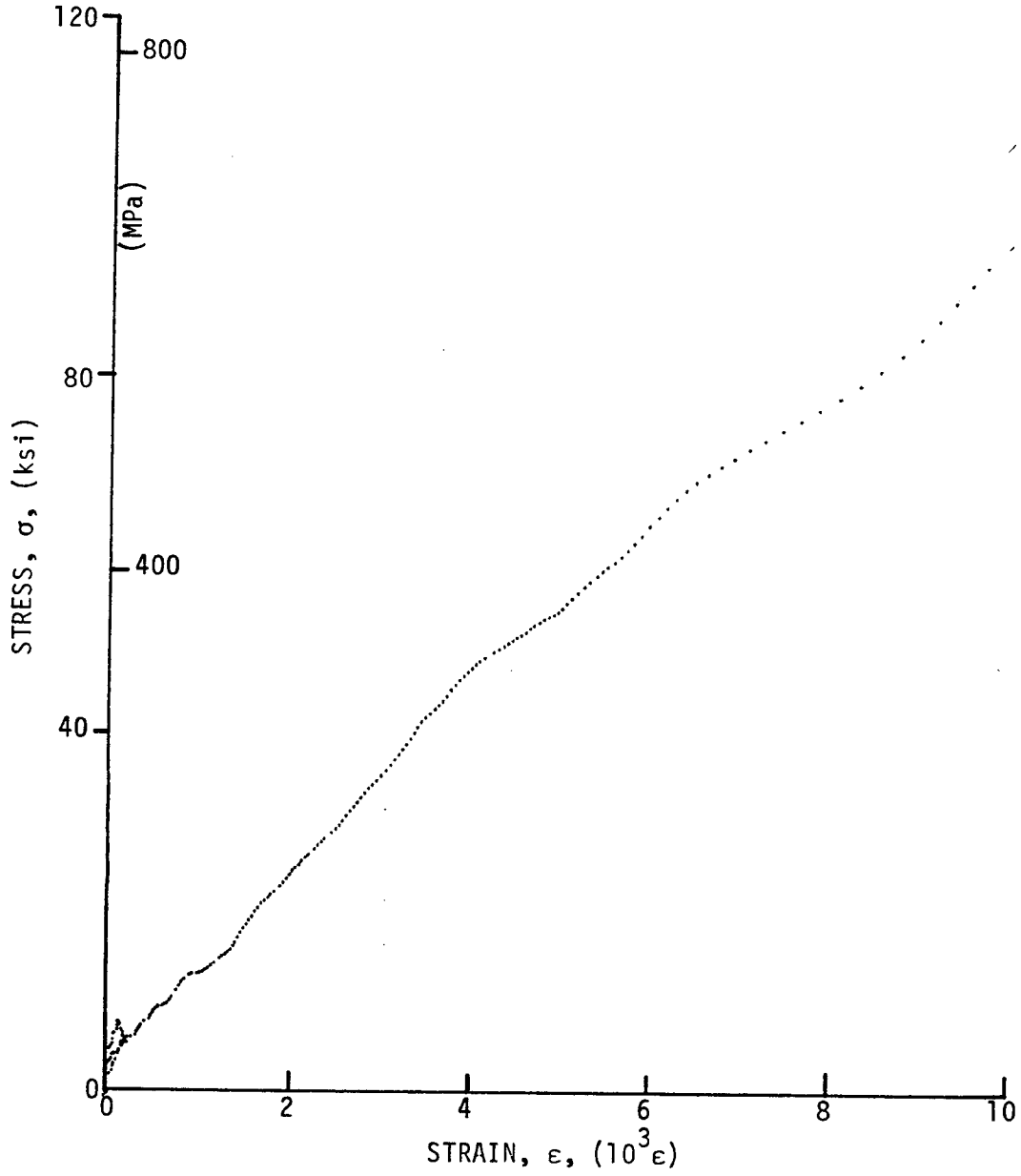

Figure 3-24. Stress-strain curves for dynamically loaded $[\pm 22.5]_{2s}$ 80AS/20S/PR288 graphite/S-glass/epoxy ring, Specimen No. 34-11.

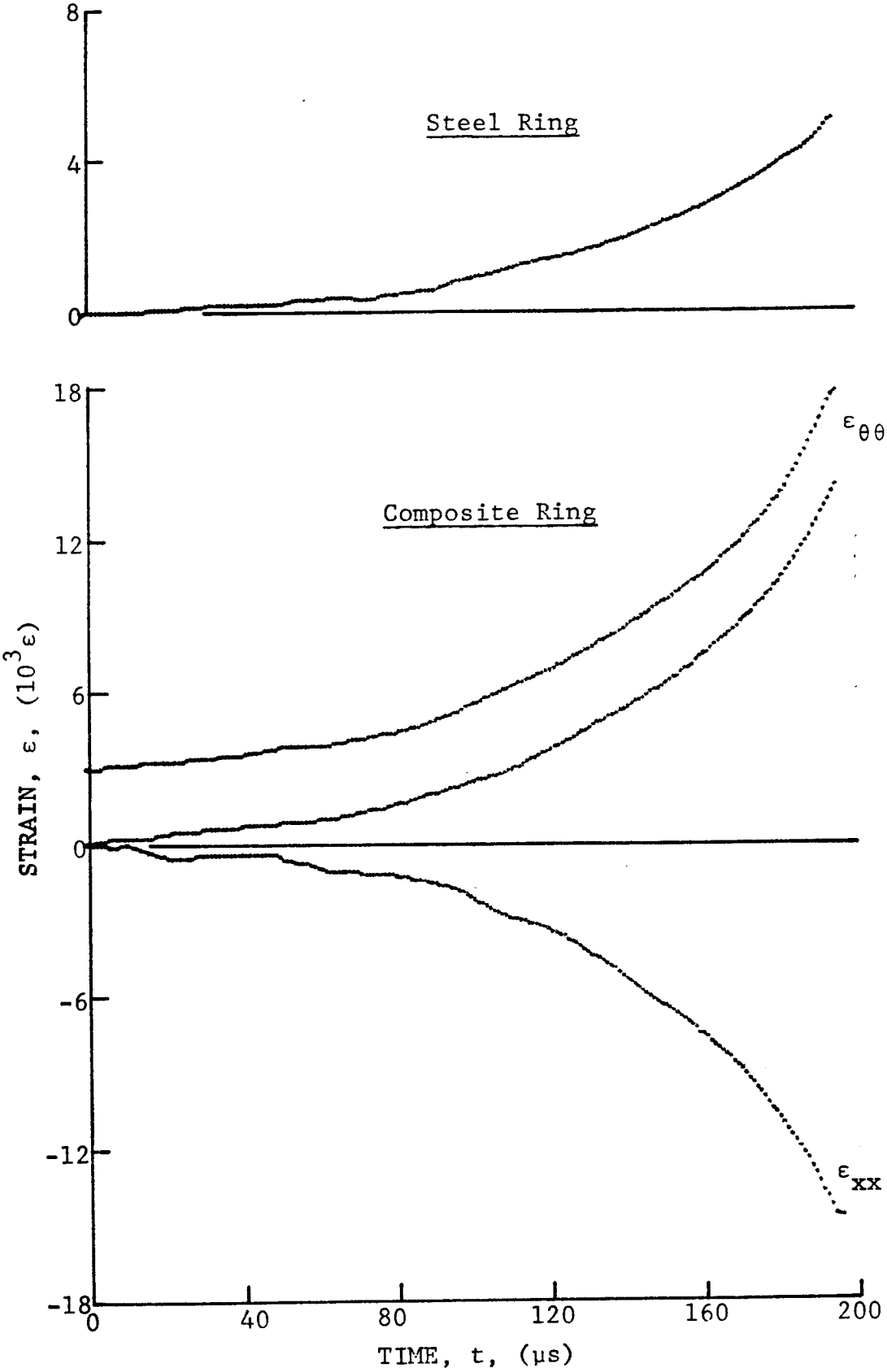

Figure 3-25. Strain records in steel ring and $[\pm 30]_{2s}$ SP288/AS graphite/epoxy ring under dynamic loading for Specimen No. 28-2 (0.65 g shotgun powder).

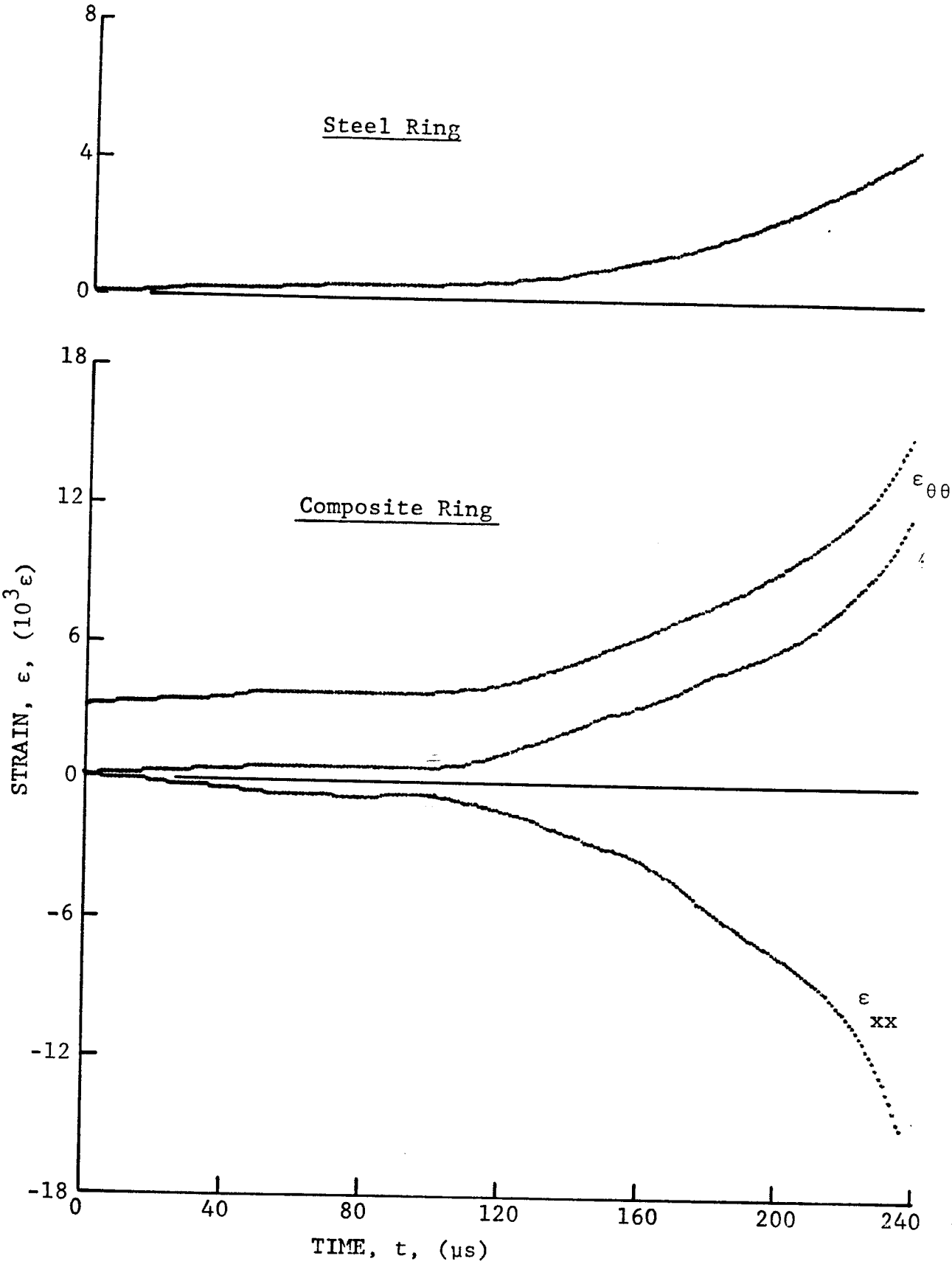

Figure 3-26. Strain records in steel ring and $[\pm 30]_{2s}$ SP288/AS graphite/epoxy ring under dynamic loading for Specimen No. 28-12 (0.65 g shotgun powder).

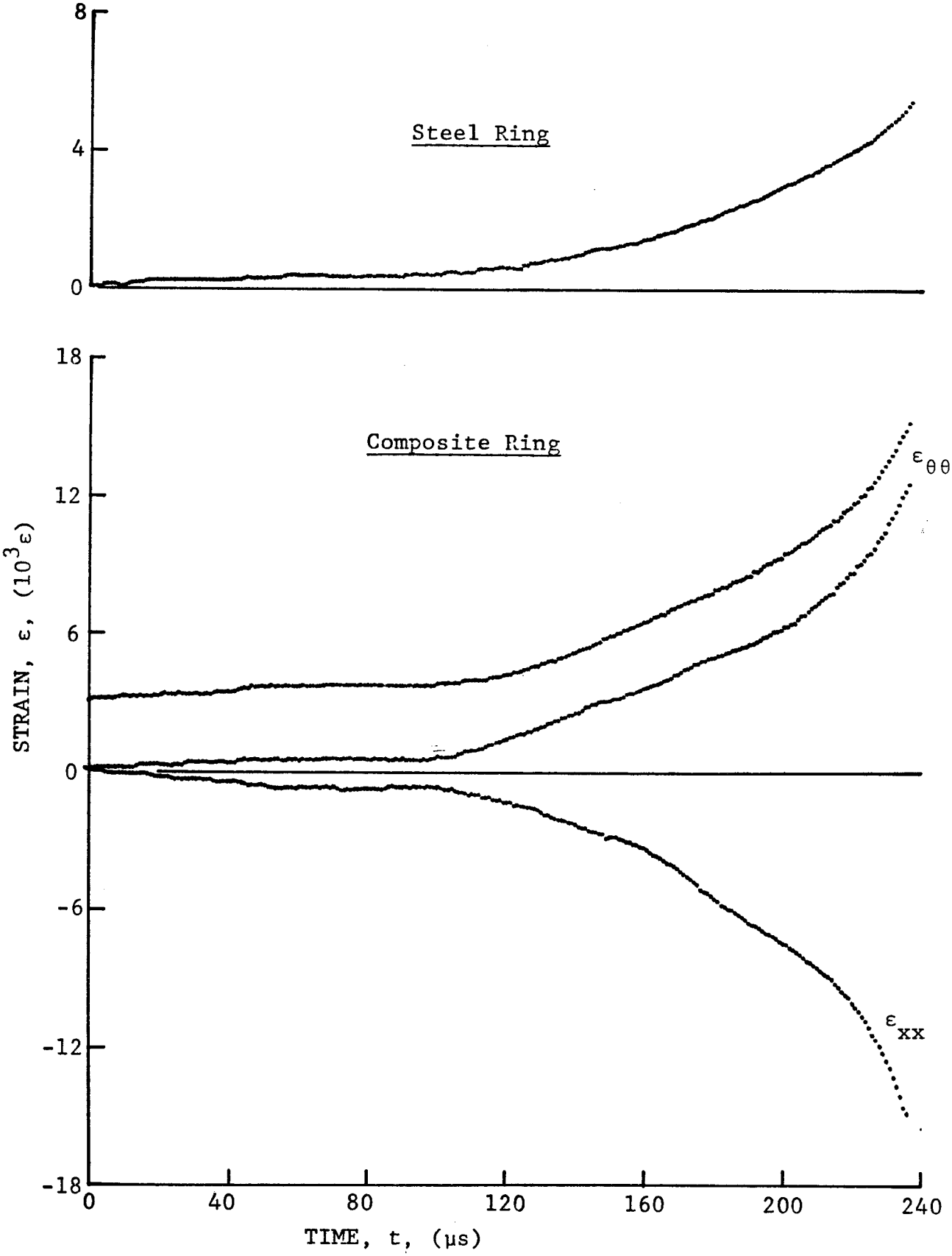

Figure 3-27. Strain records in steel ring and $[\pm 30]_{2s}$ SP288/AS graphite/epoxy ring under dynamic loading for Specimen No. 28-13 (0.65 g shotgun powder).

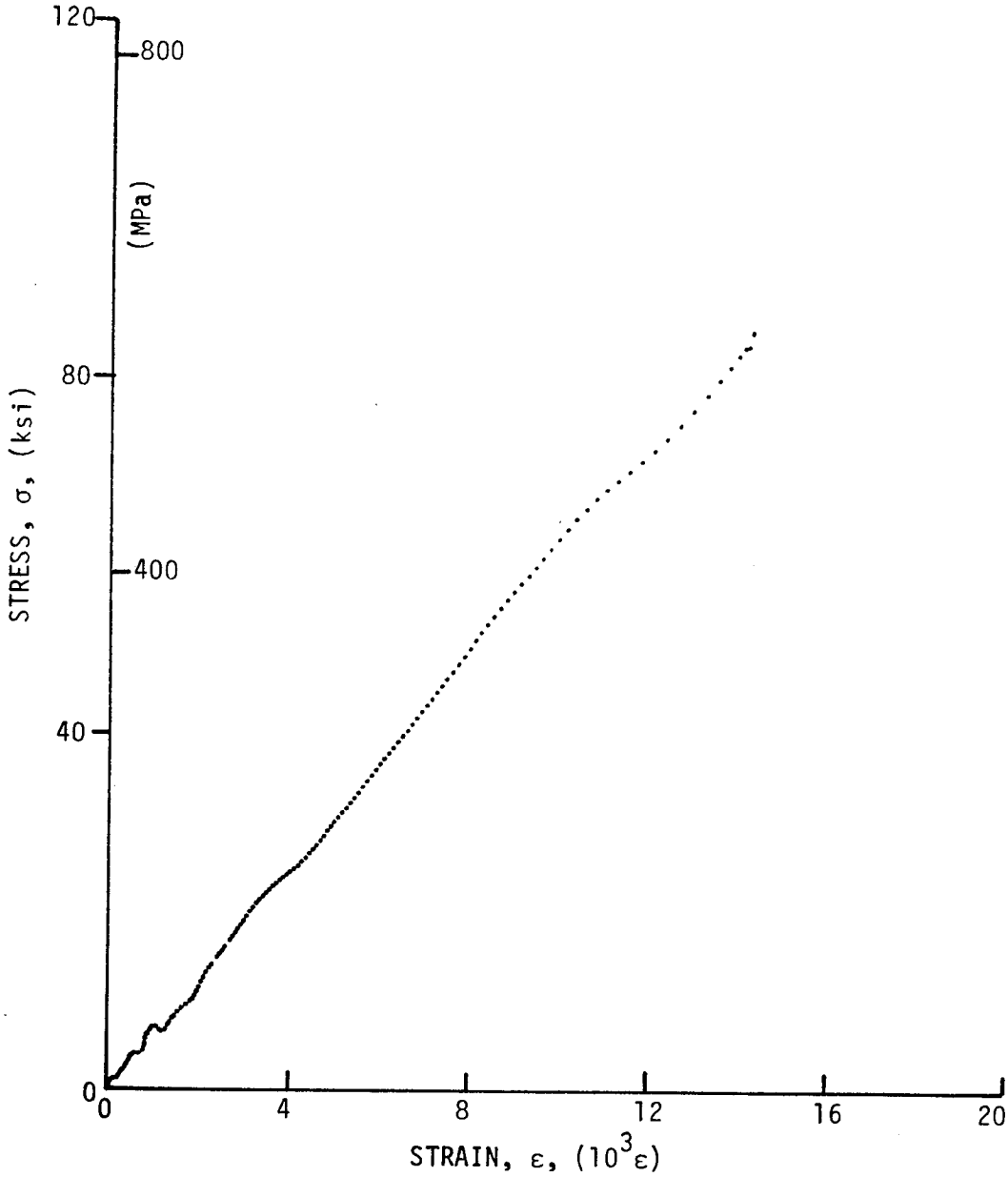

Figure 3-28. Stress-strain curves for dynamically loaded $[\pm 30_{2S}]$ SP288/AS graphite/epoxy ring, Specimen No. 28-2.

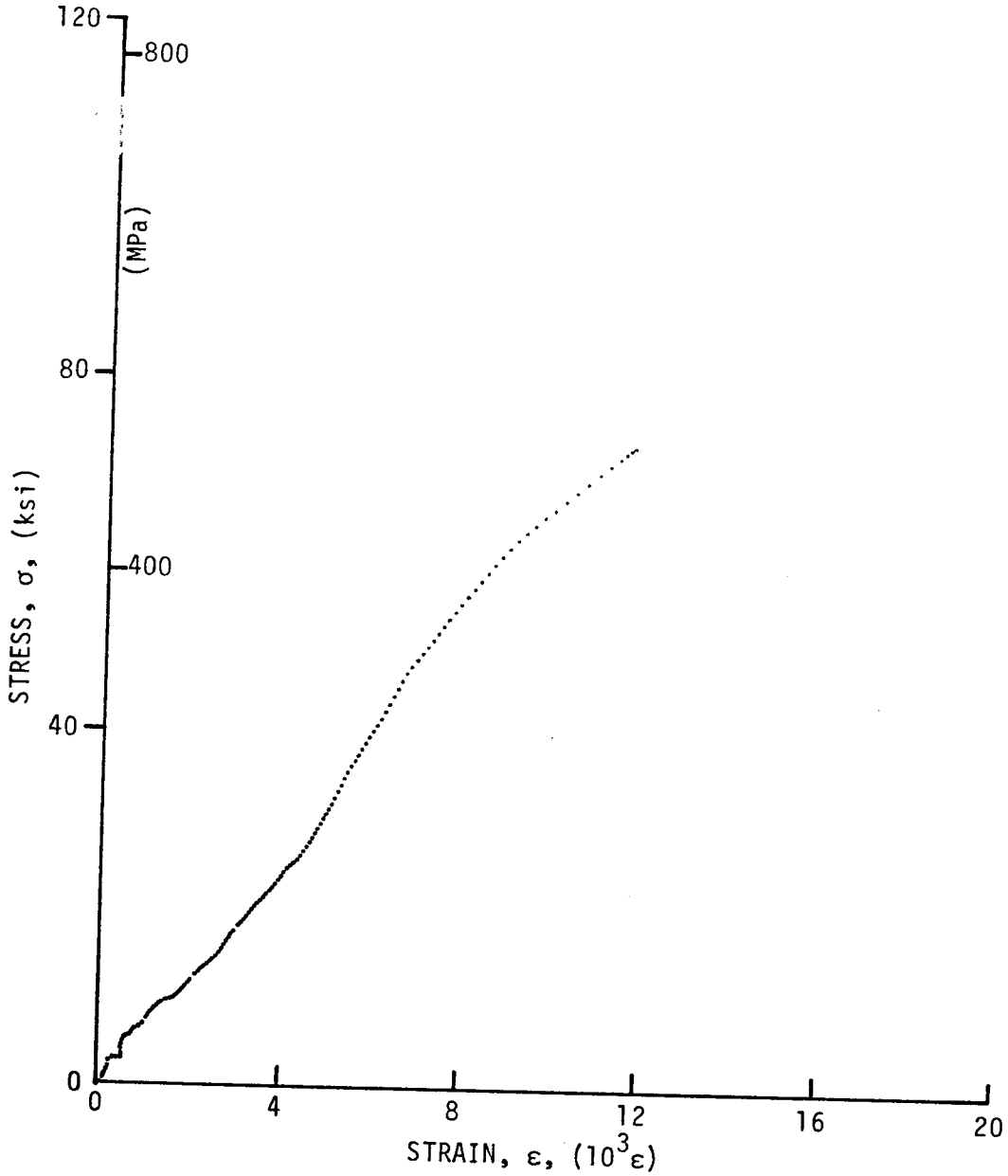

Figure 3-29. Stress-strain curves for dynamically loaded $[\pm 30]_{2s}$ SP288/AS graphite/epoxy ring, Specimen No. 28-12.

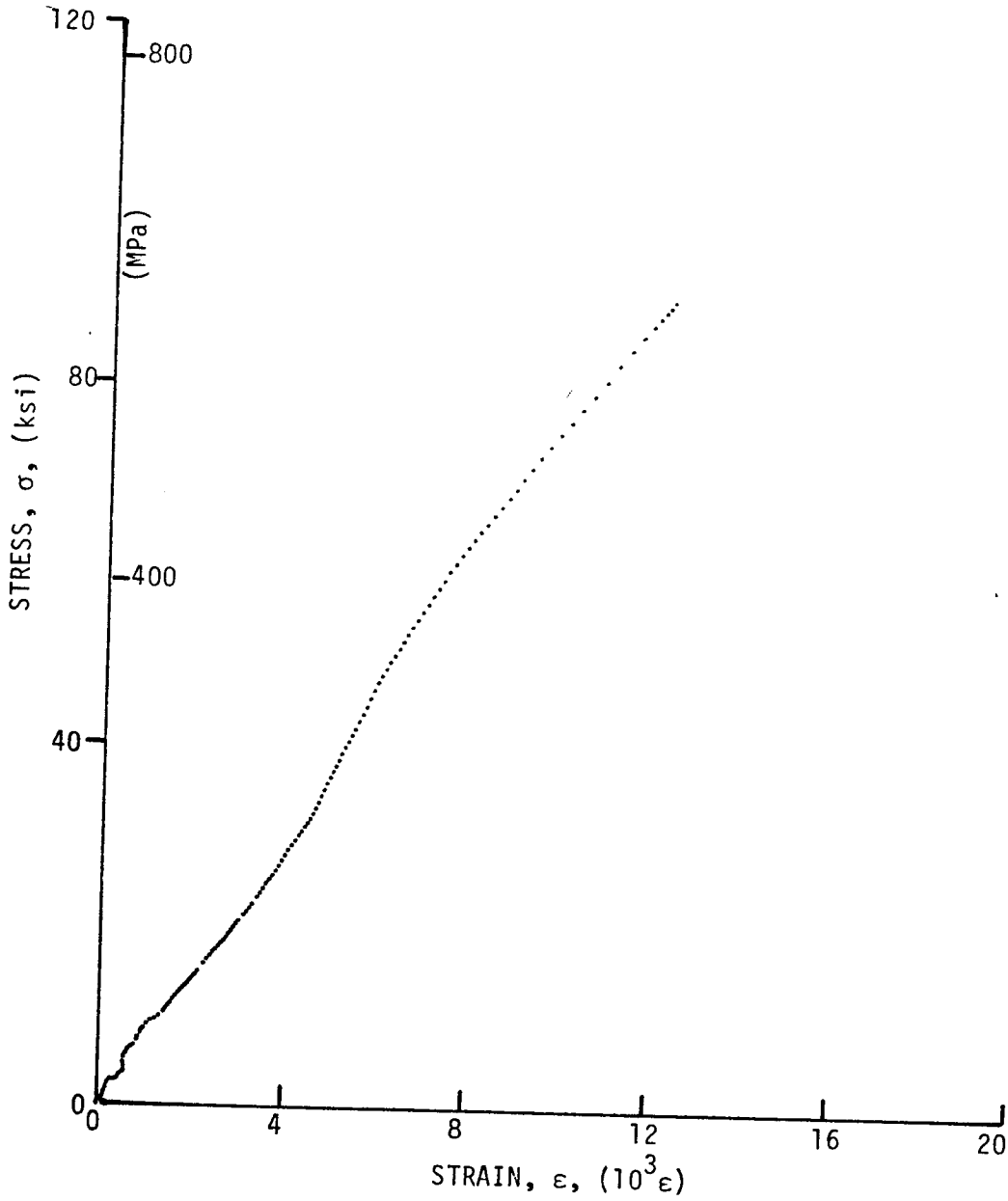

Figure 3-30. Stress-strain curves for dynamically loaded $[\pm 30]_{2s}$ SP288/AS graphite/epoxy ring, Specimen No. 28-13.

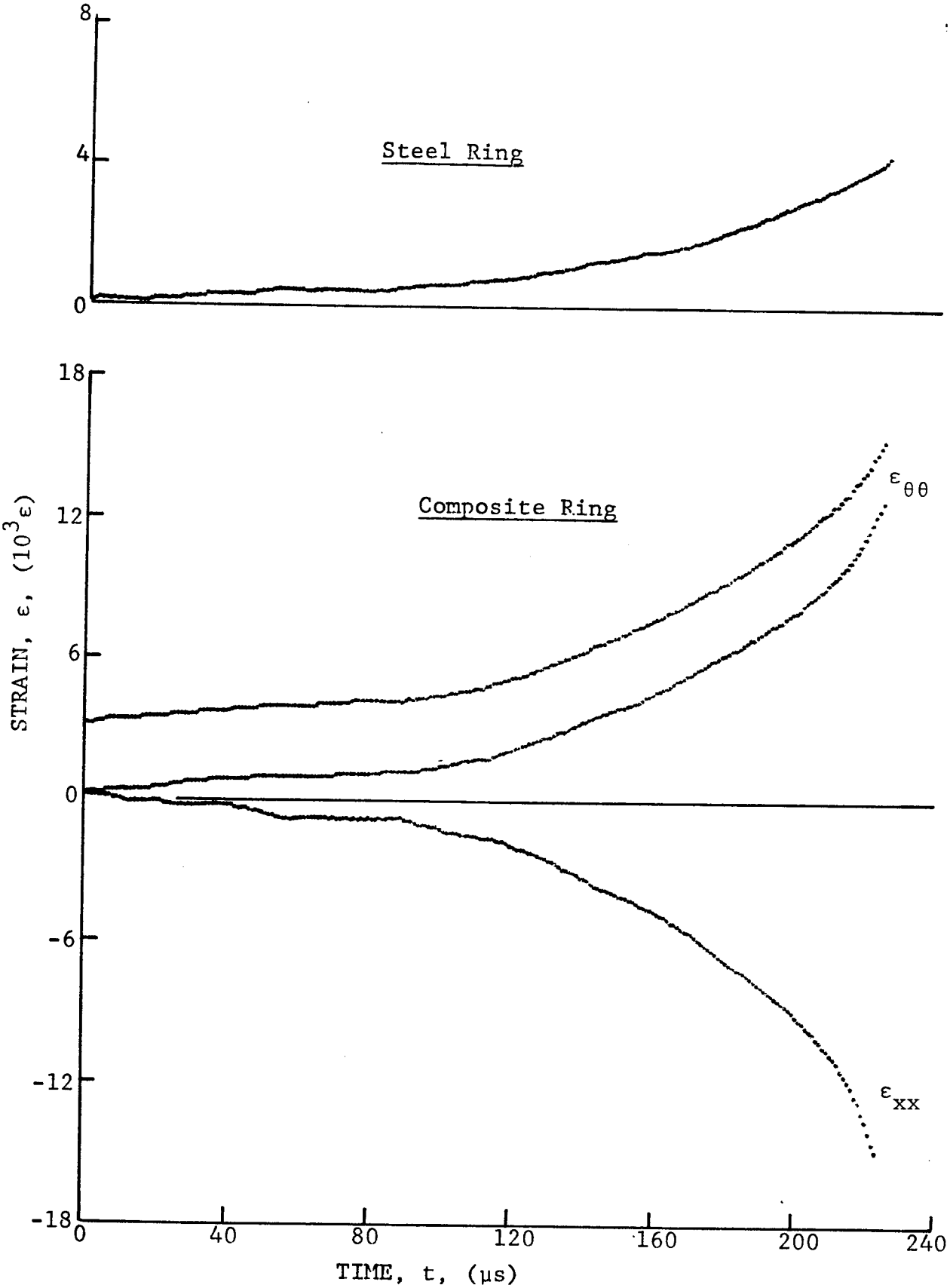

Figure 3-31. Strain records in steel ring and 80AS/20S/PR288 $[\pm 30]_{2s}$ graphite/S-glass/epoxy ring under dynamic loading for Specimen No. 54-2 (0.65 g shotgun powder).

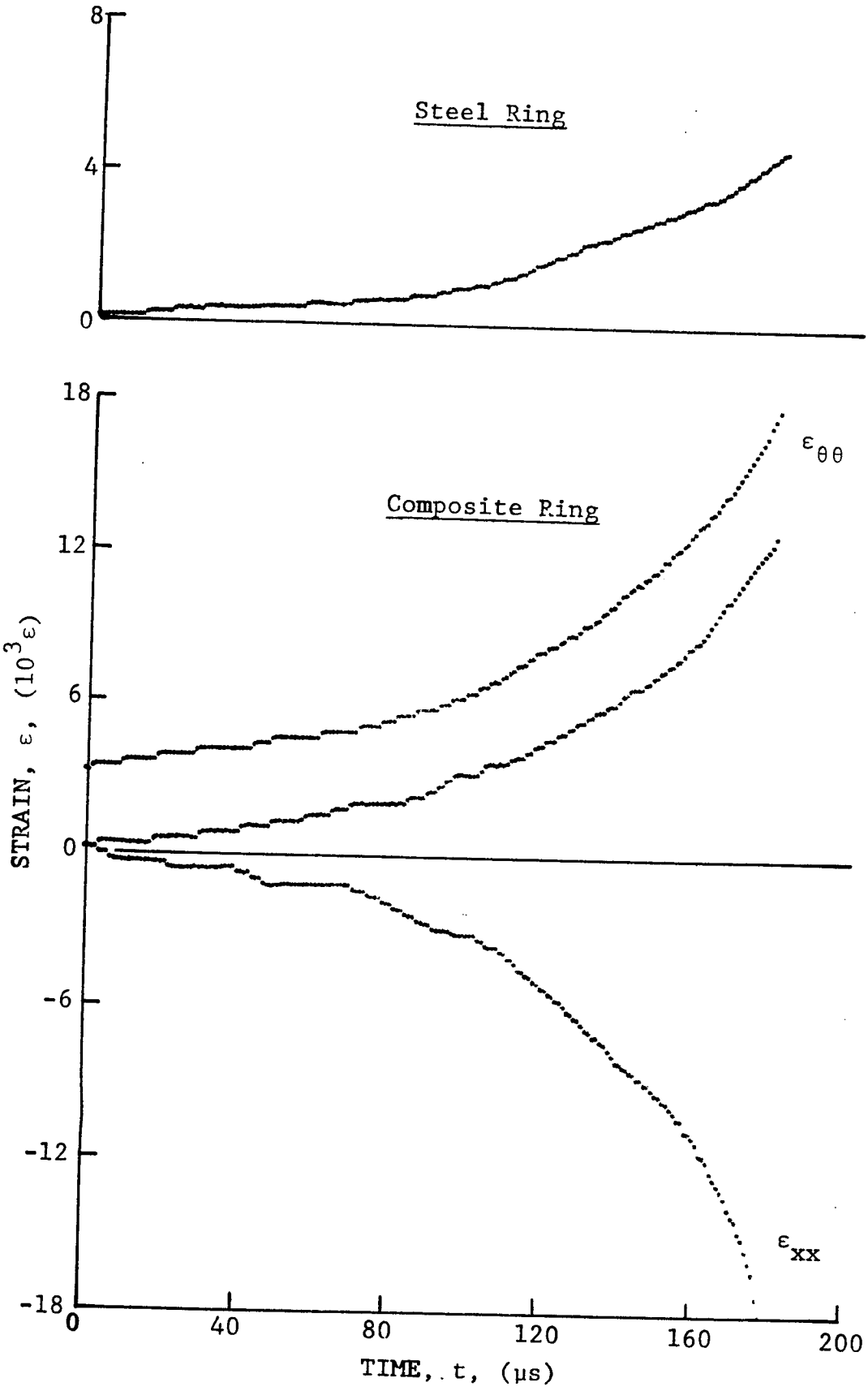

Figure 3-32. Strain records in steel ring and 80AS/20S/PR288 $[\pm 30]_{2s}$ graphite/S-glass/epoxy ring under dynamic loading for Specimen No. 54-3 (0.65 g shotgun powder).

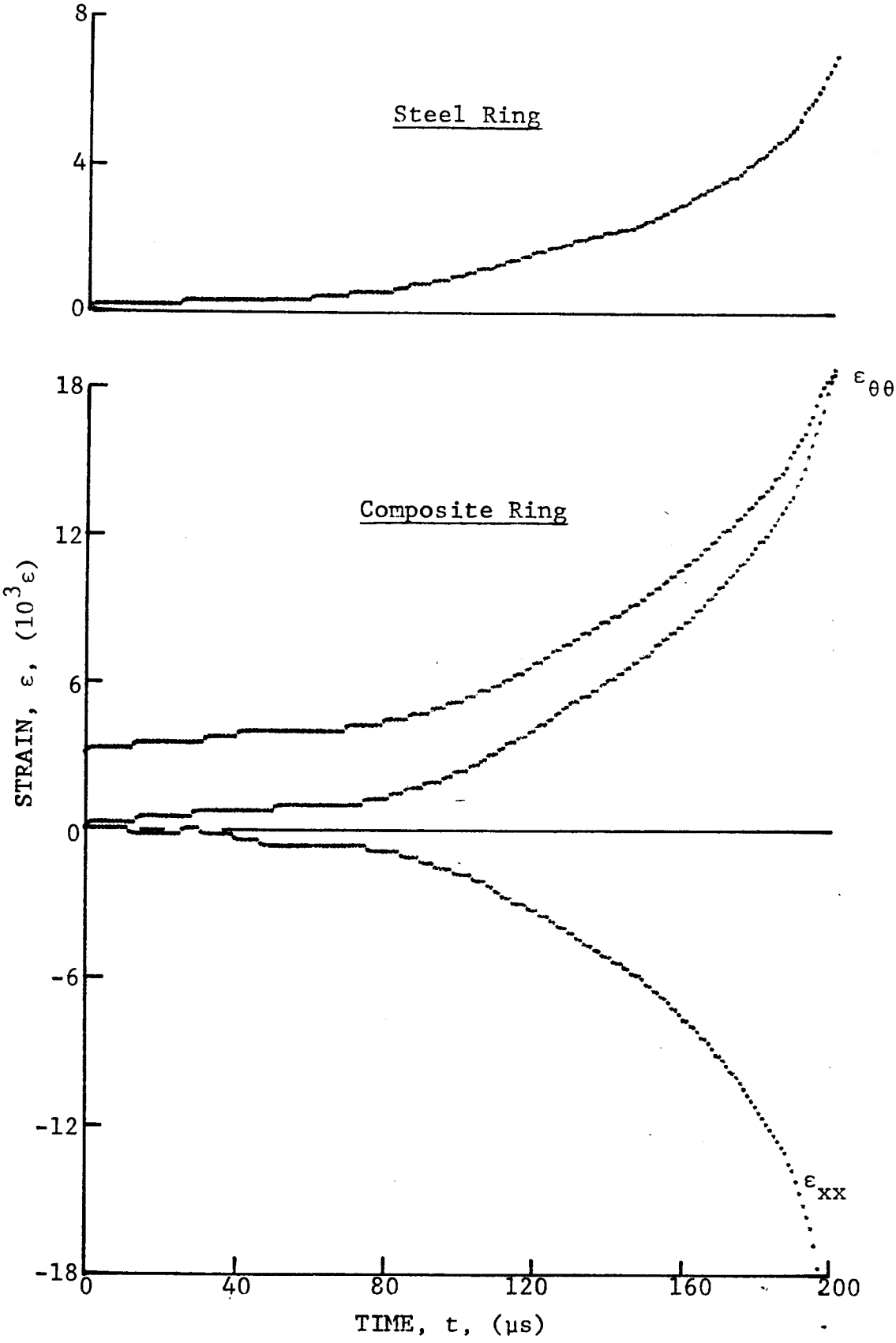

Figure 3-33. Strain records in steel ring and 80AS/20S/PR288 $[\pm 30]_{2s}$ graphite/S-glass/epoxy ring under dynamic loading for Specimen No. 54-5 (0.65 g shotgun powder).

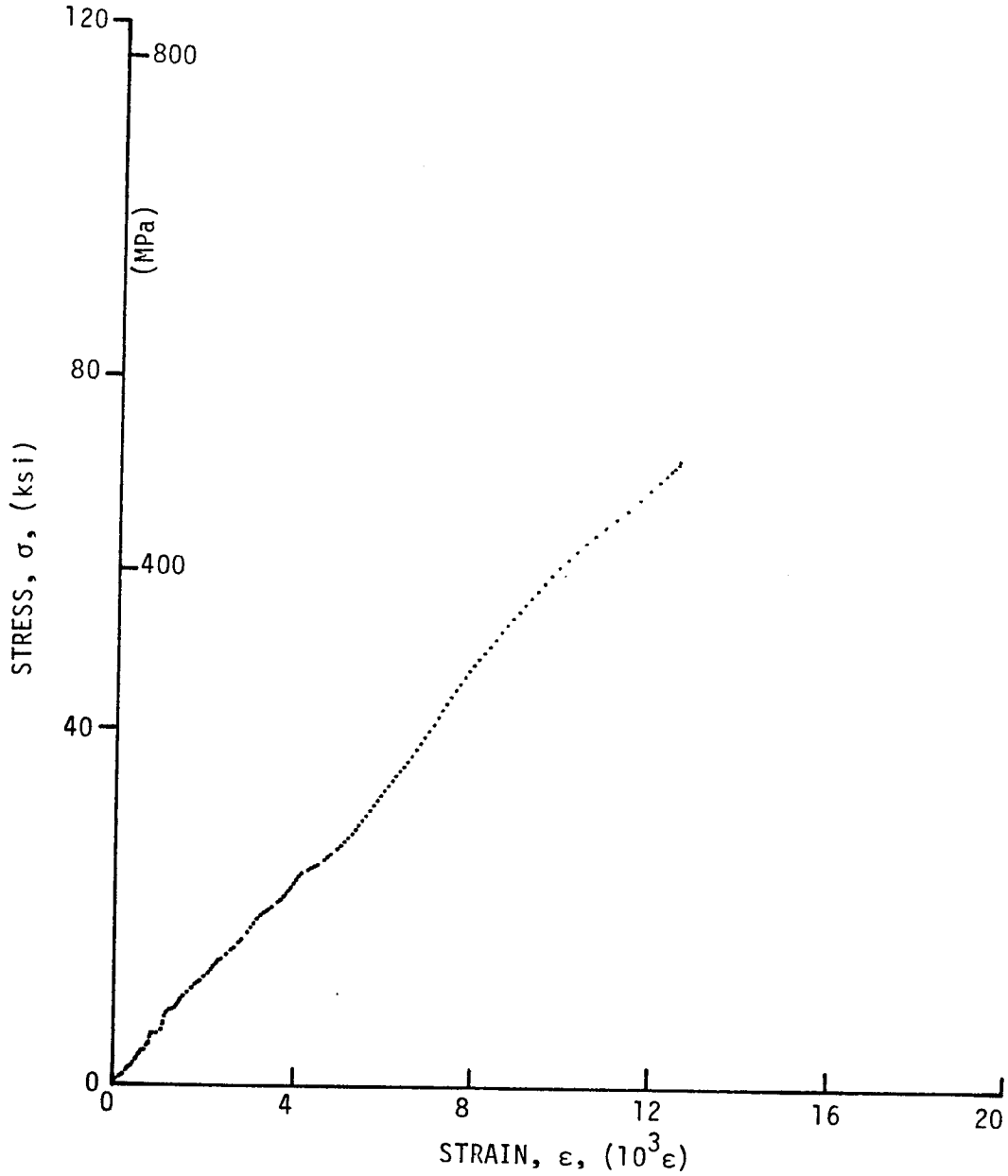

Figure 3-34. Stress-strain curves for dynamically loaded $[\pm 30]_{2s}$ 80AS/20S/PR288 graphite/S-glass/epoxy ring, Specimen No. 54-2.

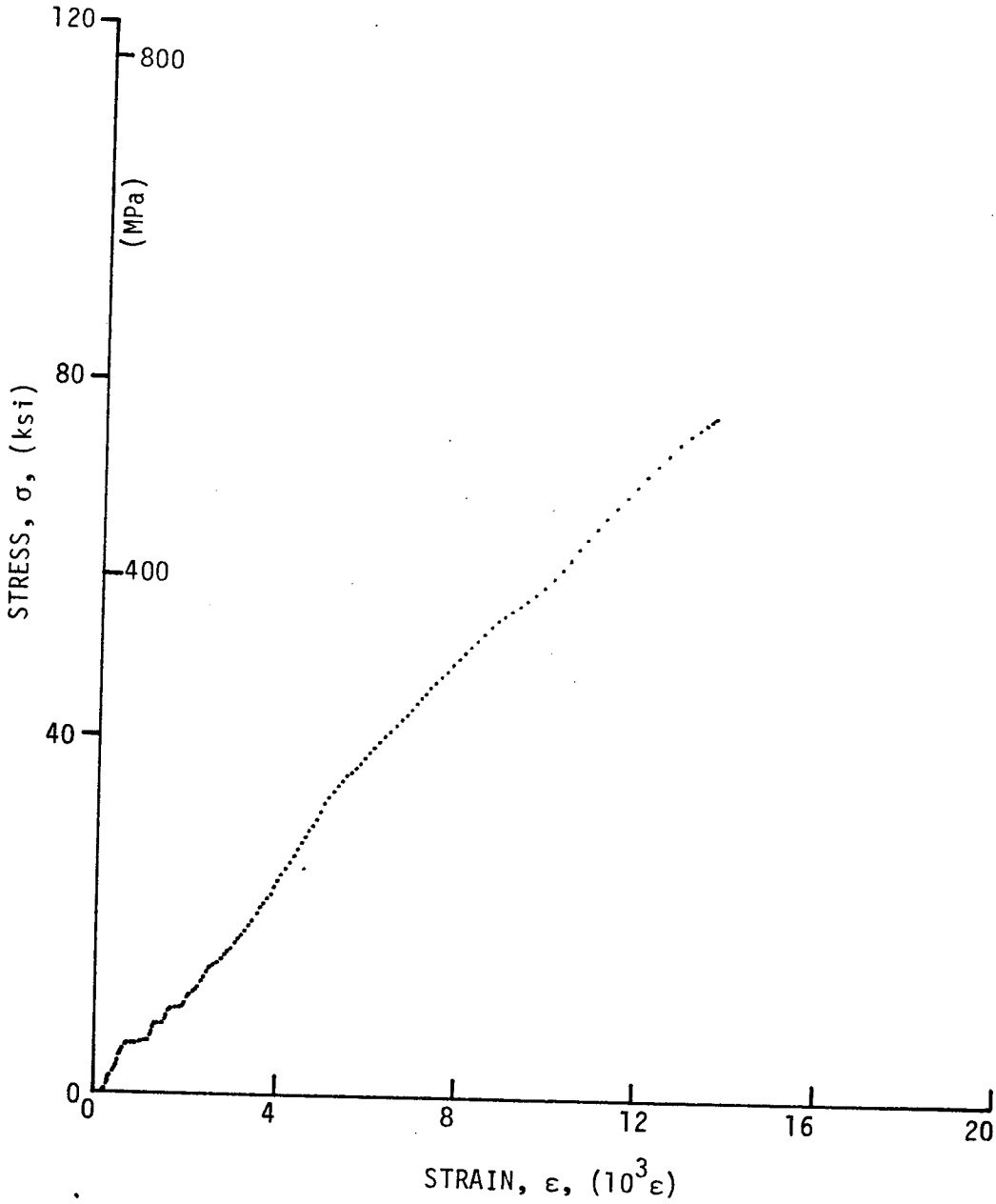

Figure 3-35. Stress-strain curves for dynamically loaded $[\pm 30]_{2s}$ 80AS/20S/PR288 graphite/S-glass/epoxy ring, Specimen No. 54-3.

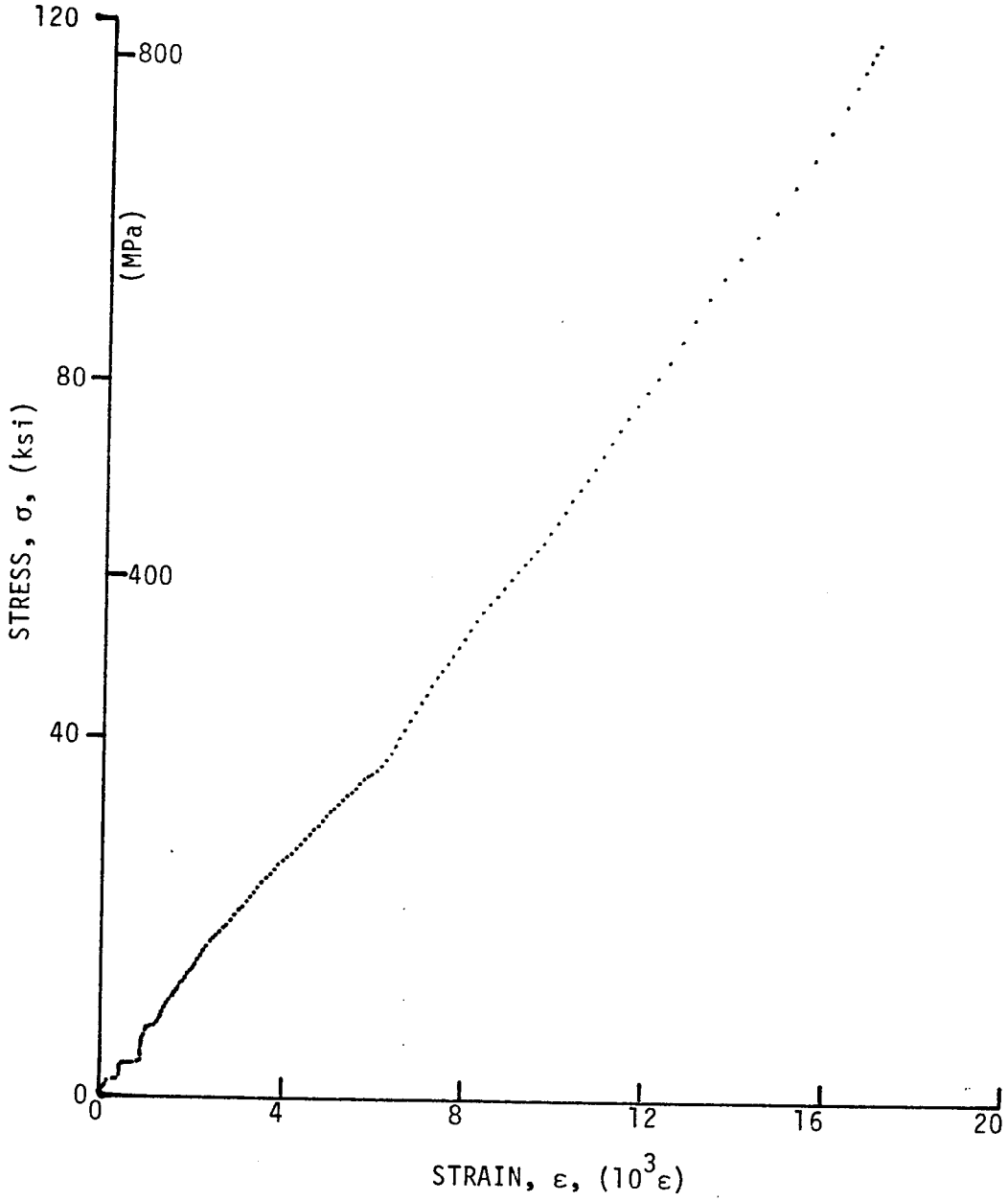

Figure 3-36. Stress-strain curves for dynamically loaded $[\pm 30]_{2s}$ 80AS/20S/PR288 graphite/S-glass/epoxy ring, Specimen No. 54-5.

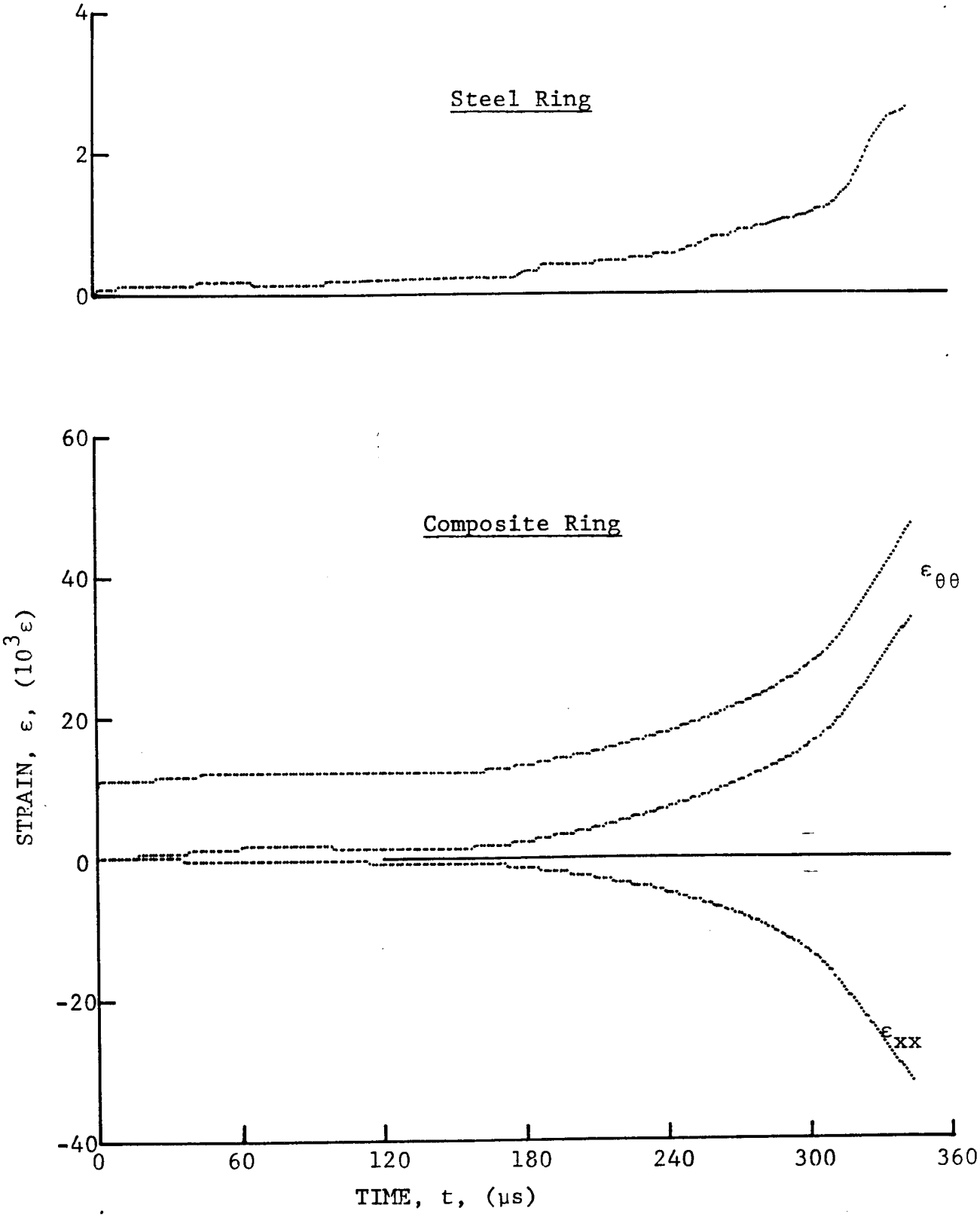

Figure 3-37. Strain records in steel ring and $[\pm 45]_{2s}$ SP288/AS graphite/epoxy ring under dynamic loading for Specimen No. 24-11 (0.65 g shotgun powder).

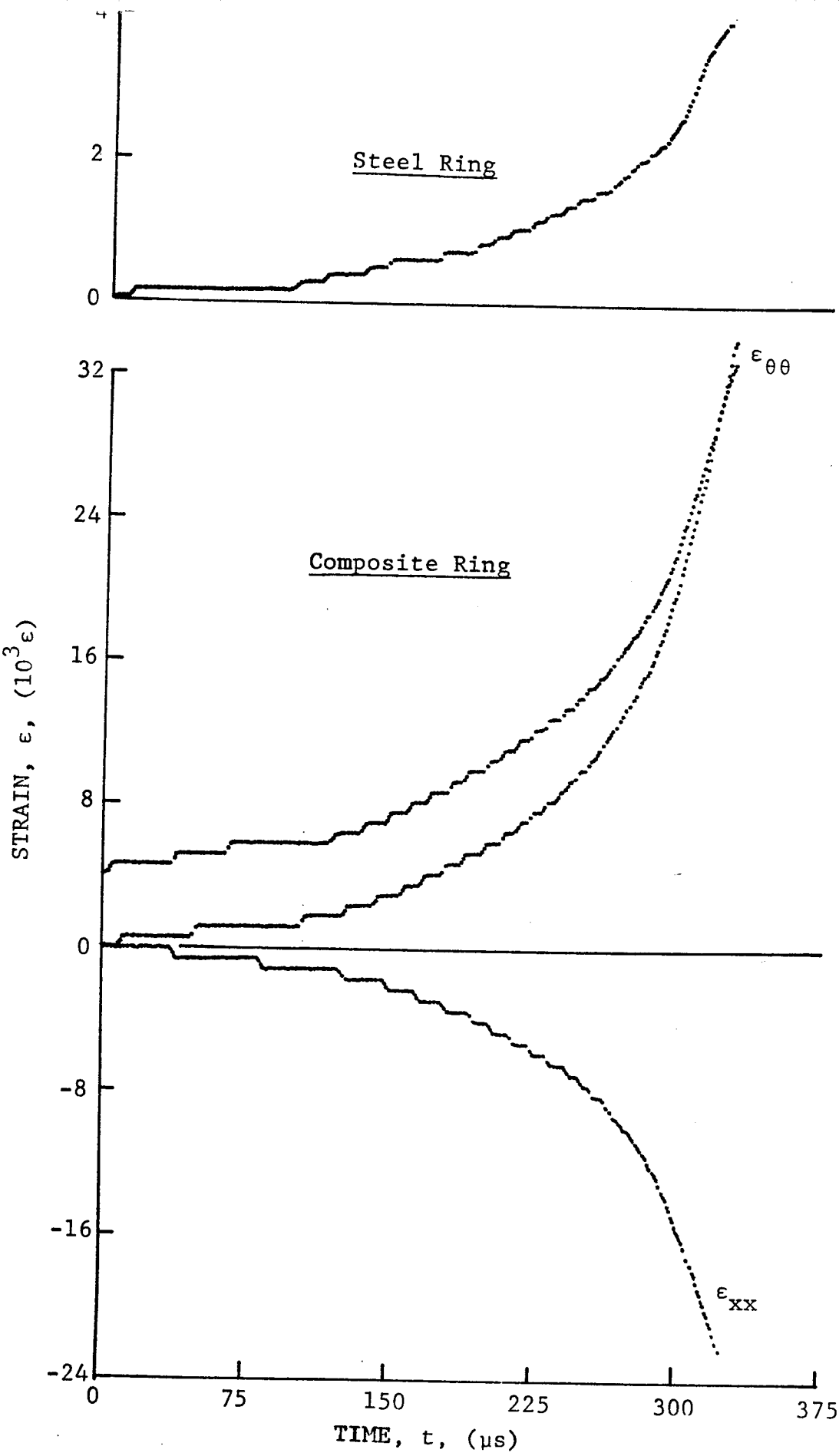

Figure 3-38. Strain records in steel ring and $[\pm 45]_{2S}$ SP288/AS graphite/epoxy ring under dynamic loading for Specimen No. 52-2 (0.65 g shotgun powder).

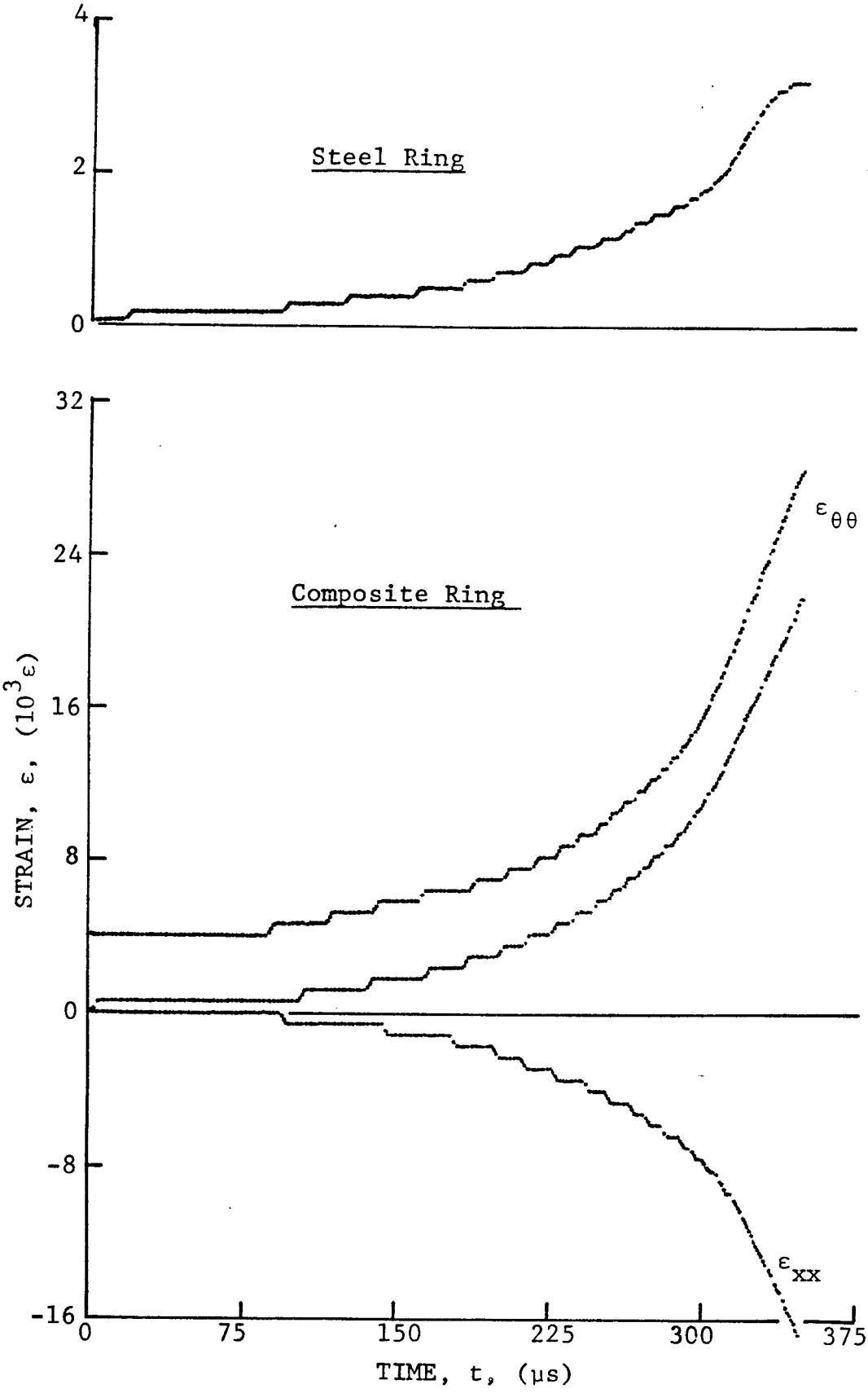

Figure 3-39. Strain records in steel ring and $[\pm 45]_{2s}$ SP288/AS graphite/epoxy ring under dynamic loading for Specimen No. 52-3 (0.65 g shotgun powder).

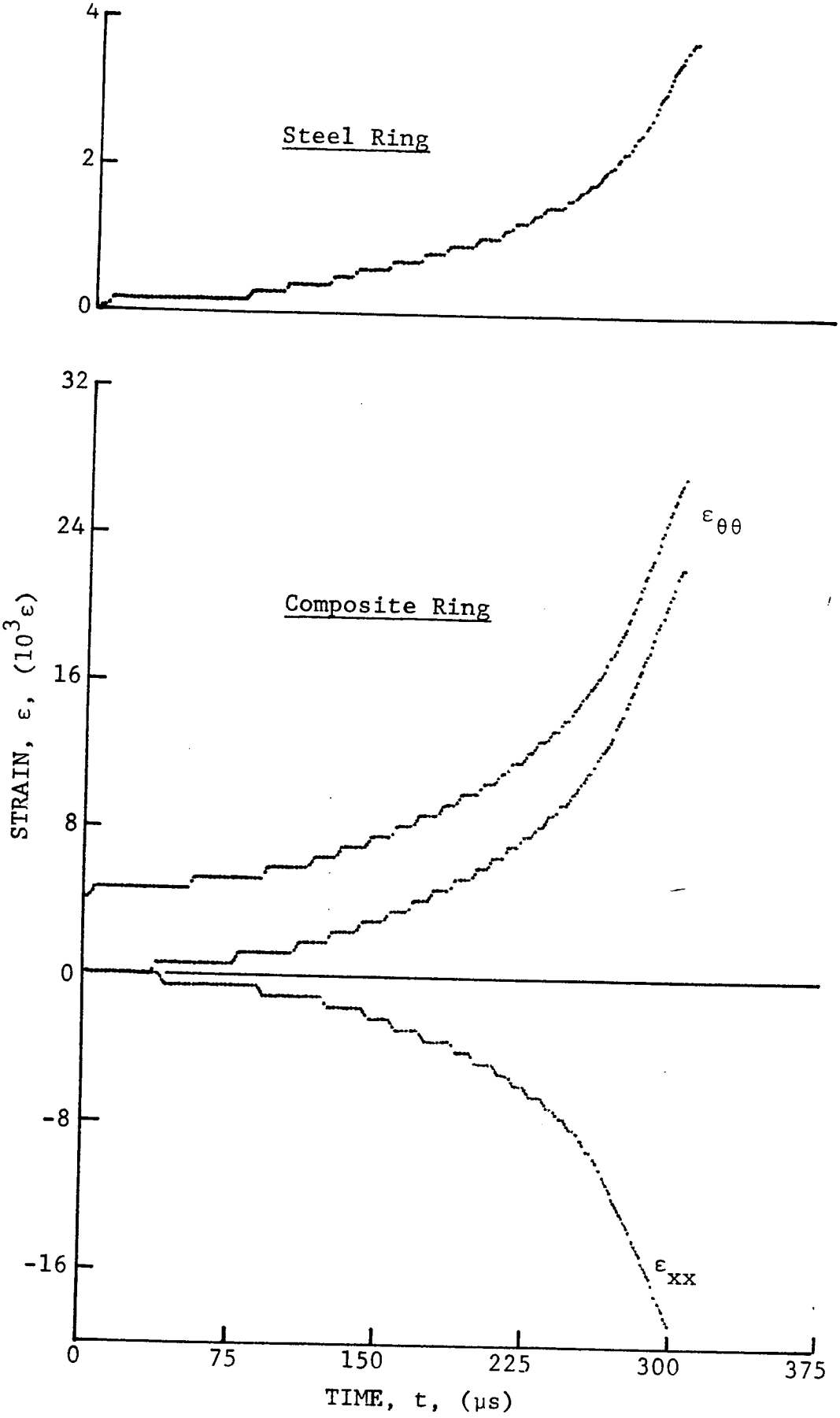

Figure 3-40. Strain records in steel ring and $[\pm 45]_{2s}$ SP288/AS graphite/epoxy ring under dynamic loading for Specimen No. 52-4 (0.65 g shotgun powder).

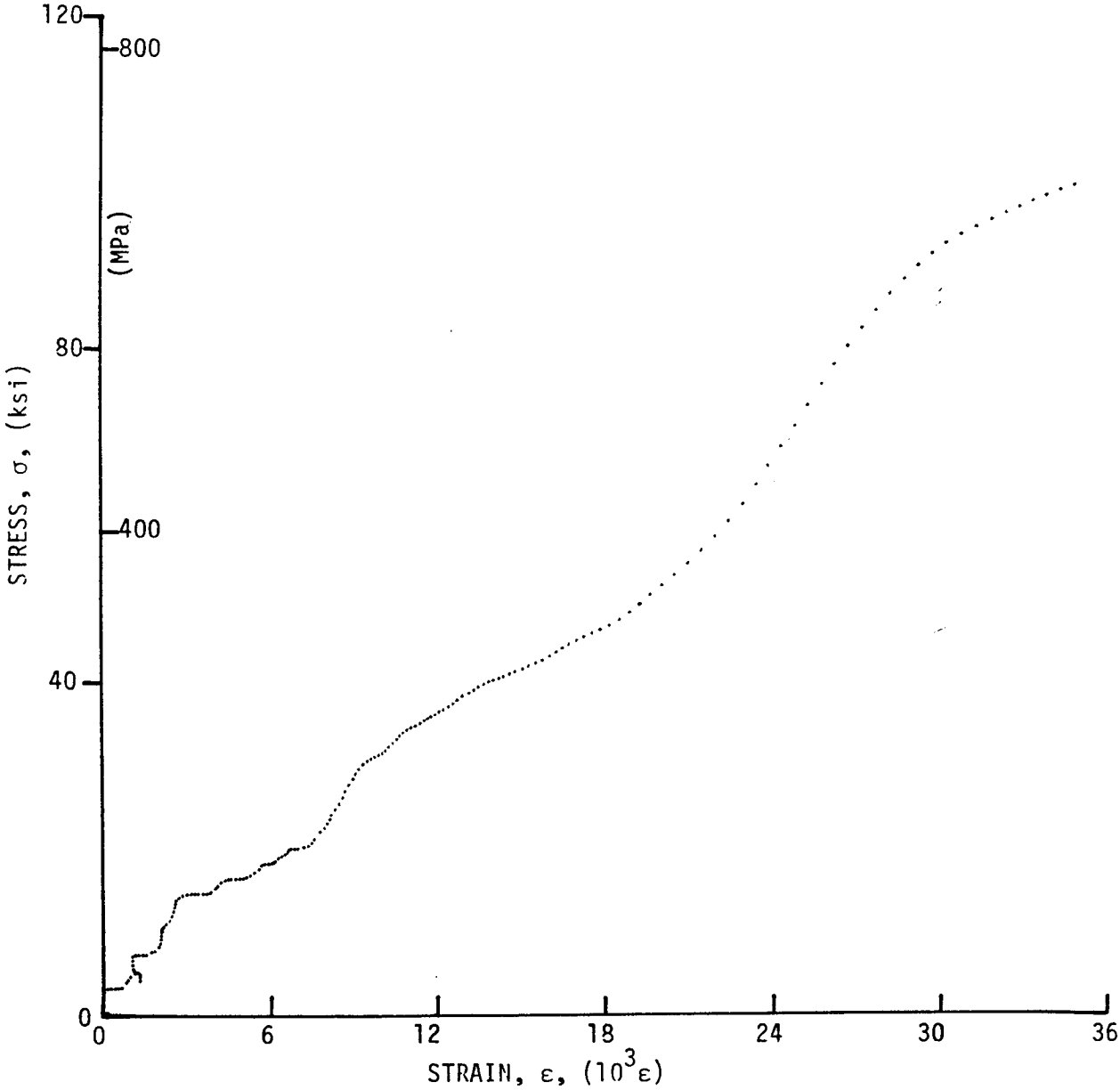

Figure 3-41. Stress-strain curves for dynamically loaded $[\pm 45]_{2s}$ SP288/AS graphite/epoxy ring, Specimen No. 24-11.

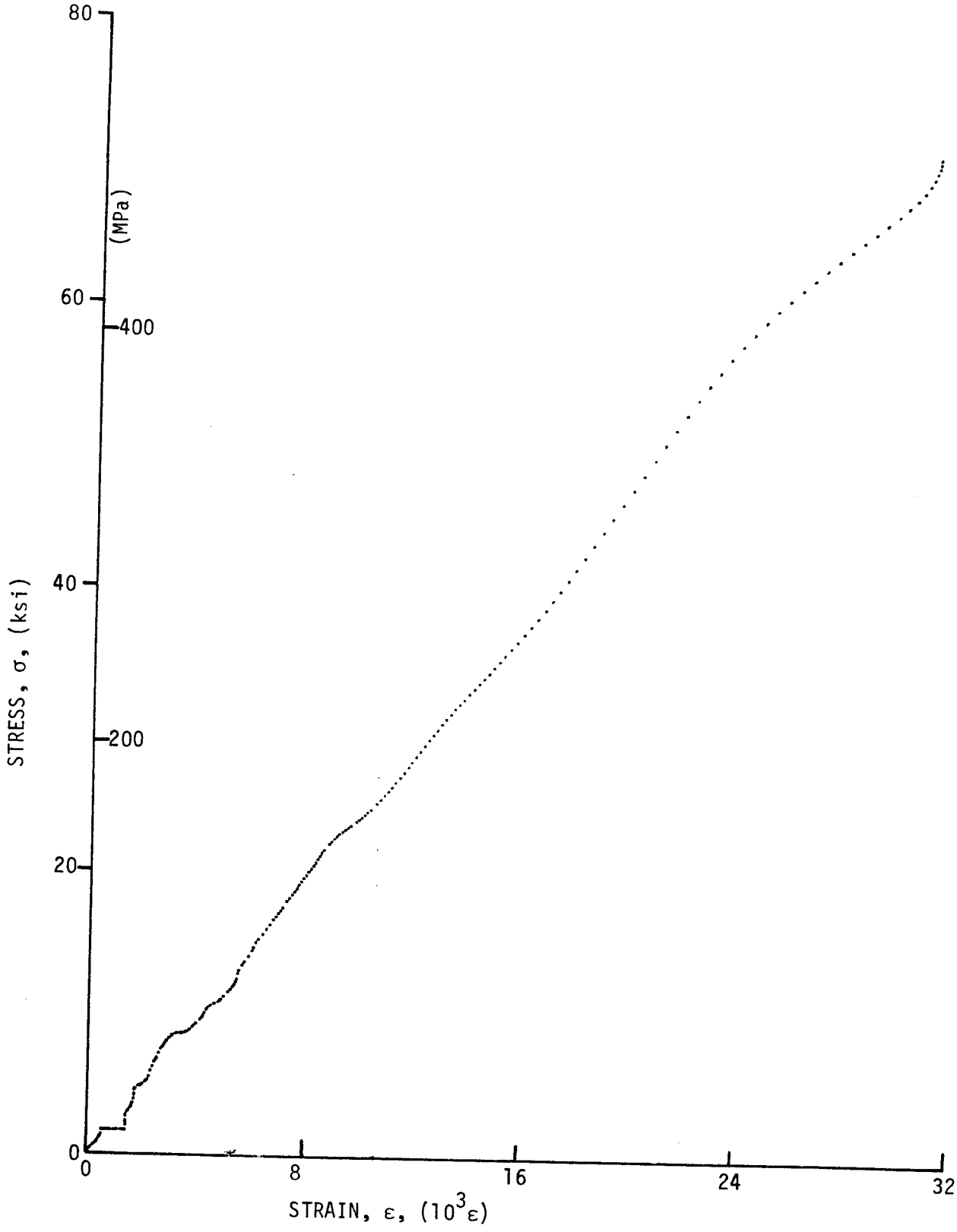

Figure. 3-42. Stress-strain curves for dynamically loaded $[\pm 45]_{2s}$ SP288/AS graphite/epoxy ring, Specimen No. 52-2.

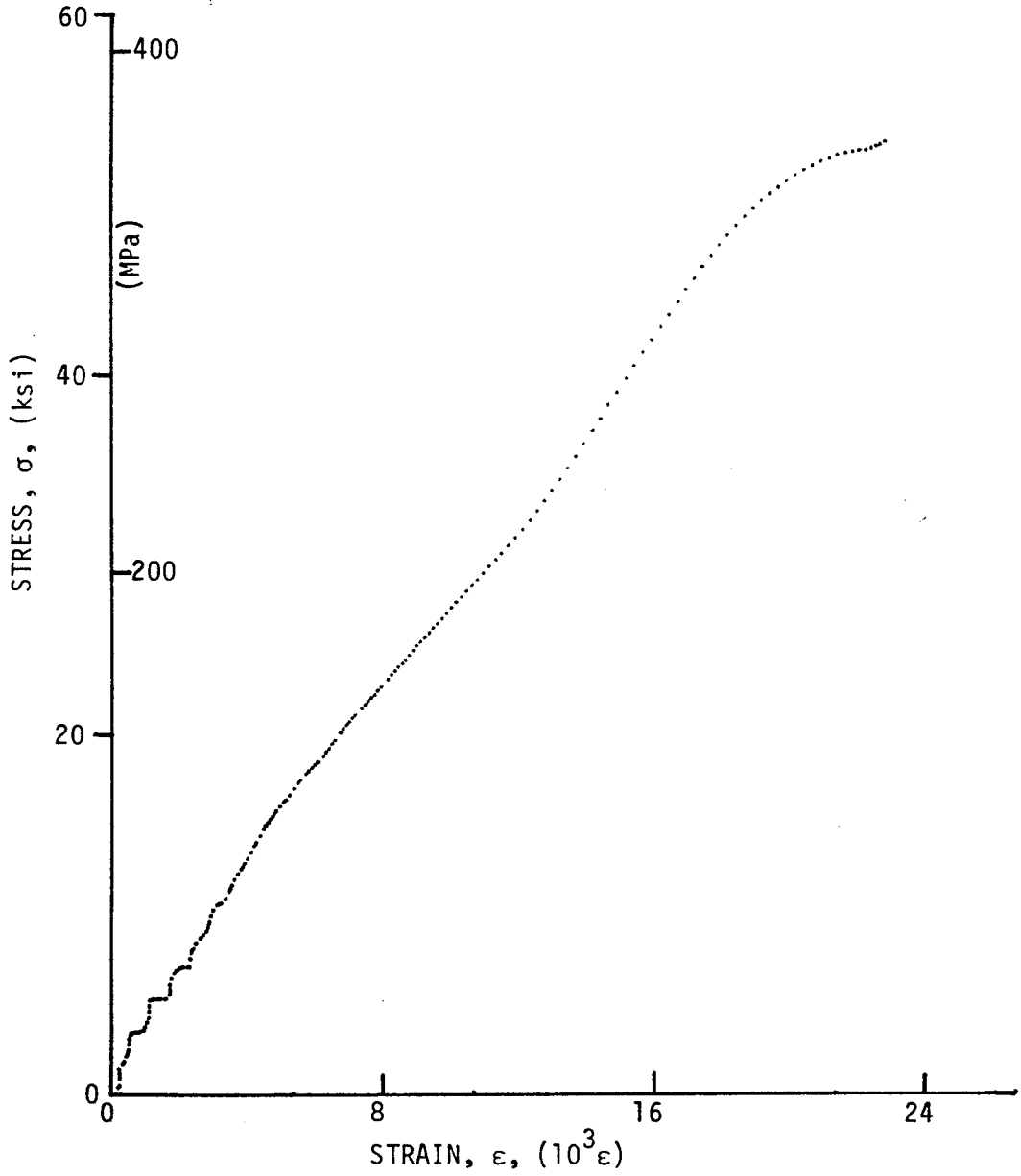

Figure 3-43. Stress-strain curves for dynamically loaded $[\pm 45]_{2s}$ SP288/AS graphite/epoxy ring, Specimen No. 52-3.

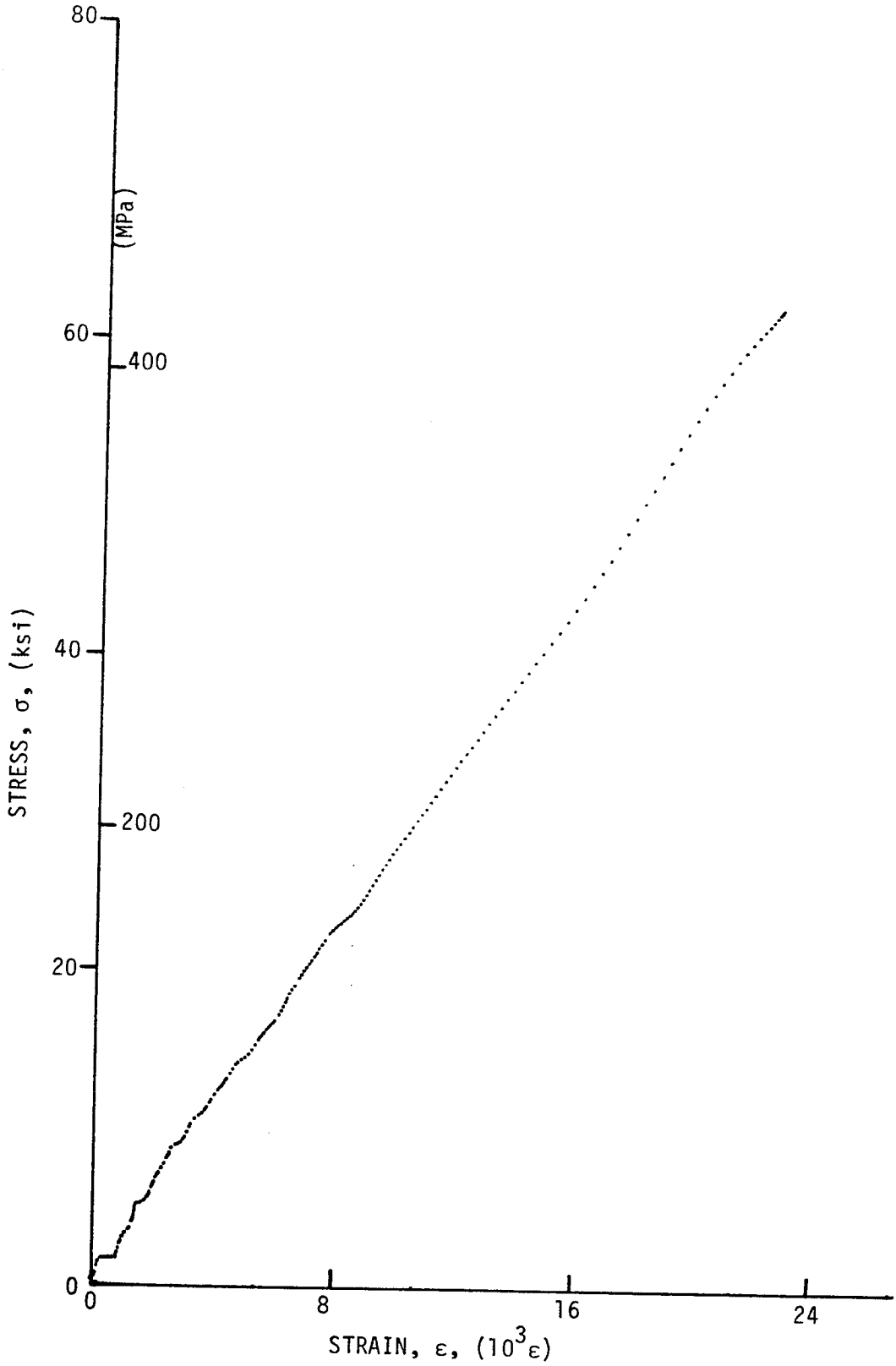

Figure 3-44. Stress-strain curves for dynamically loaded $[\pm 45]_{2s}$ SP288/AS graphite/epoxy ring, Specimen No. 52-4.

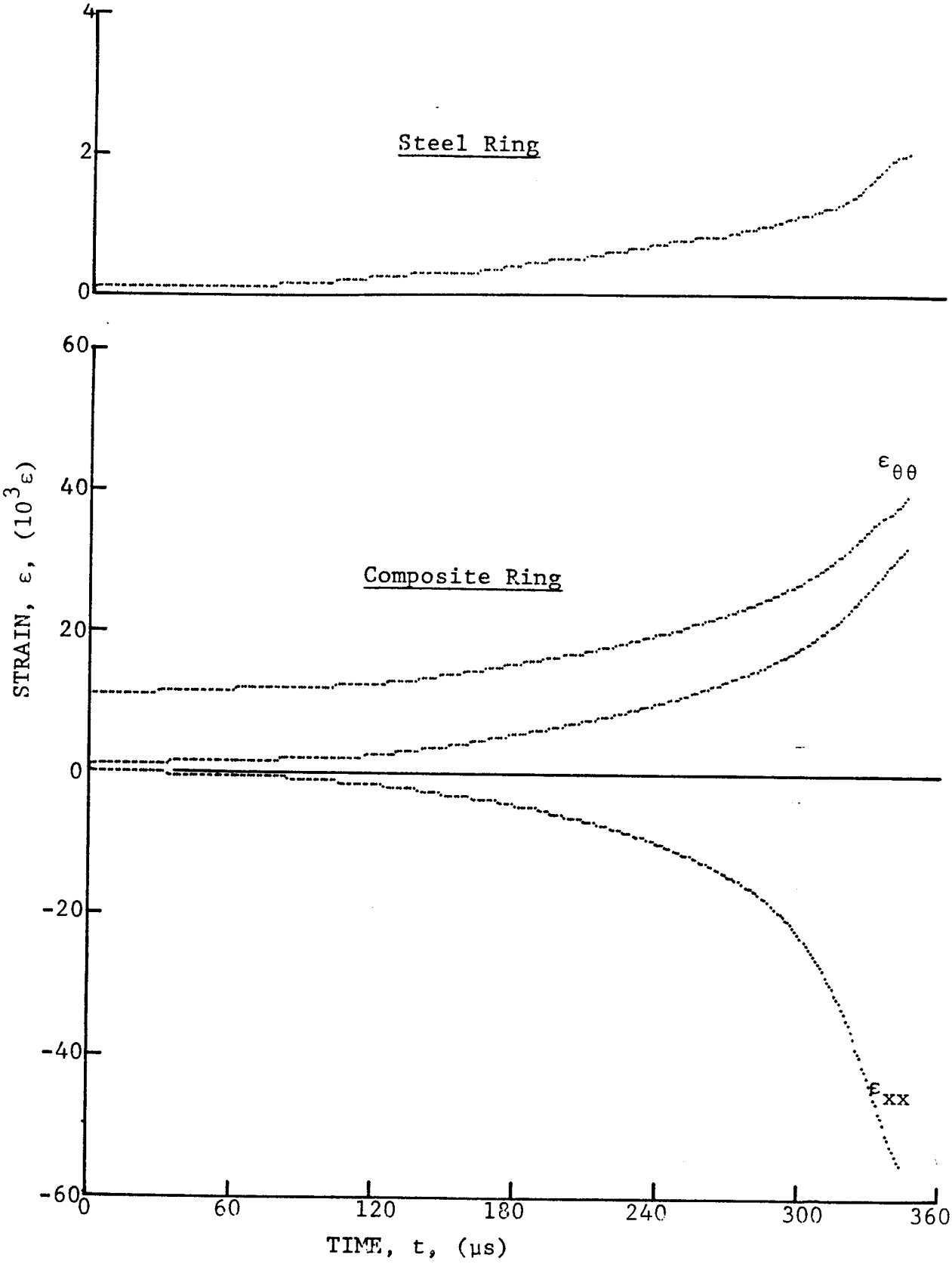

Figure 3-45. Strain records in steel ring and 80AS/20S/PR288 $[\pm 45]_{2S}$ graphite/S-glass/epoxy ring under dynamic loading for Specimen No. 25-9 (0.65 g shotgun powder).

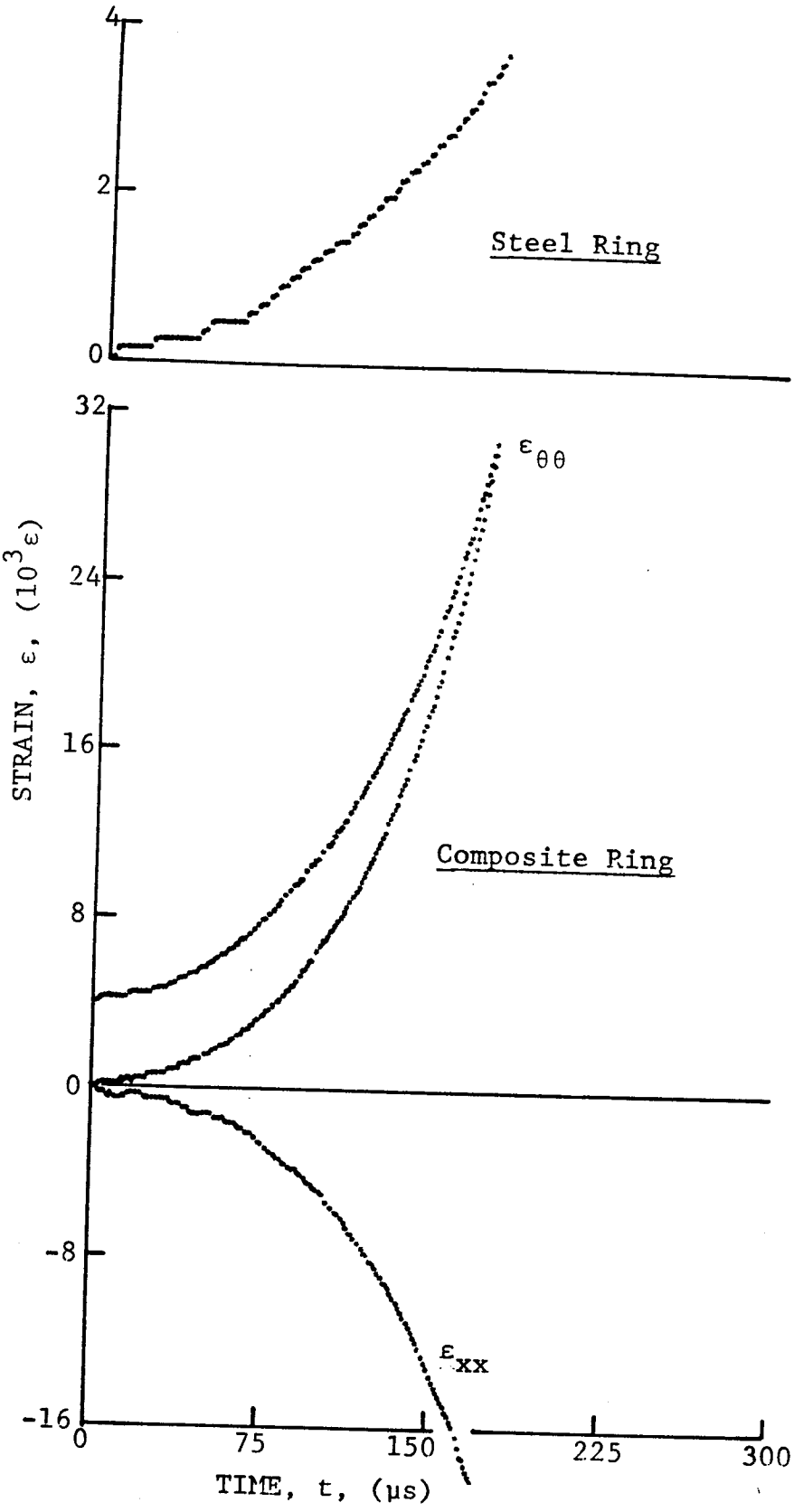

Figure 3-46. Strain records in steel ring and 80AS/20S/PR288 $[\pm 45]_{2S}$ graphite/S-glass/epoxy ring under dynamic loading for Specimen No. 53-1 (0.65 g shotgun powder).

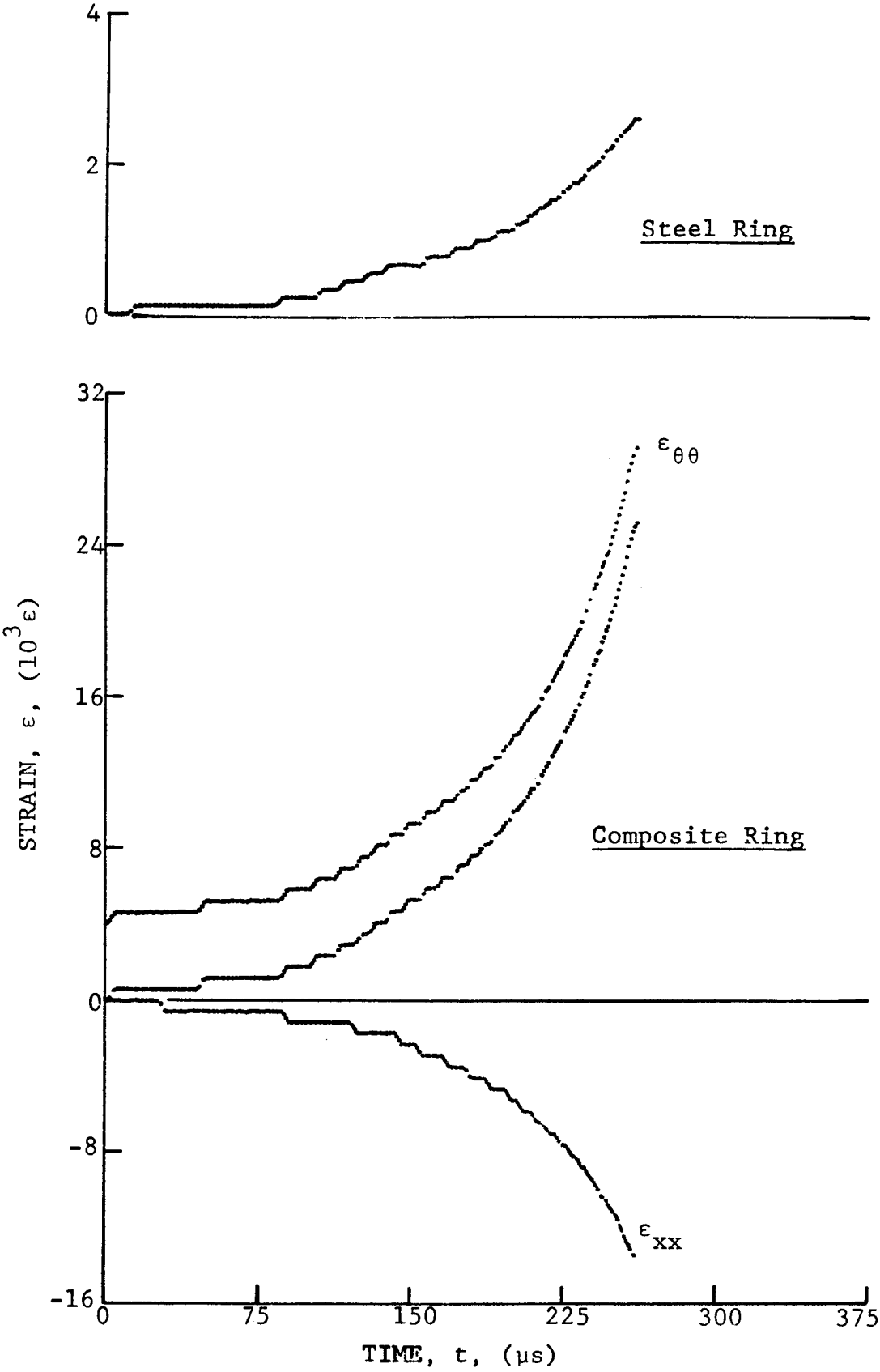

Figure 3-47. Strain records in steel ring and 80AS/20S/PR288 $[\pm 45]_{2s}$ graphite/S-glass/epoxy ring under dynamic loading for Specimen No. 53-4 (0.65 g shotgun powder).

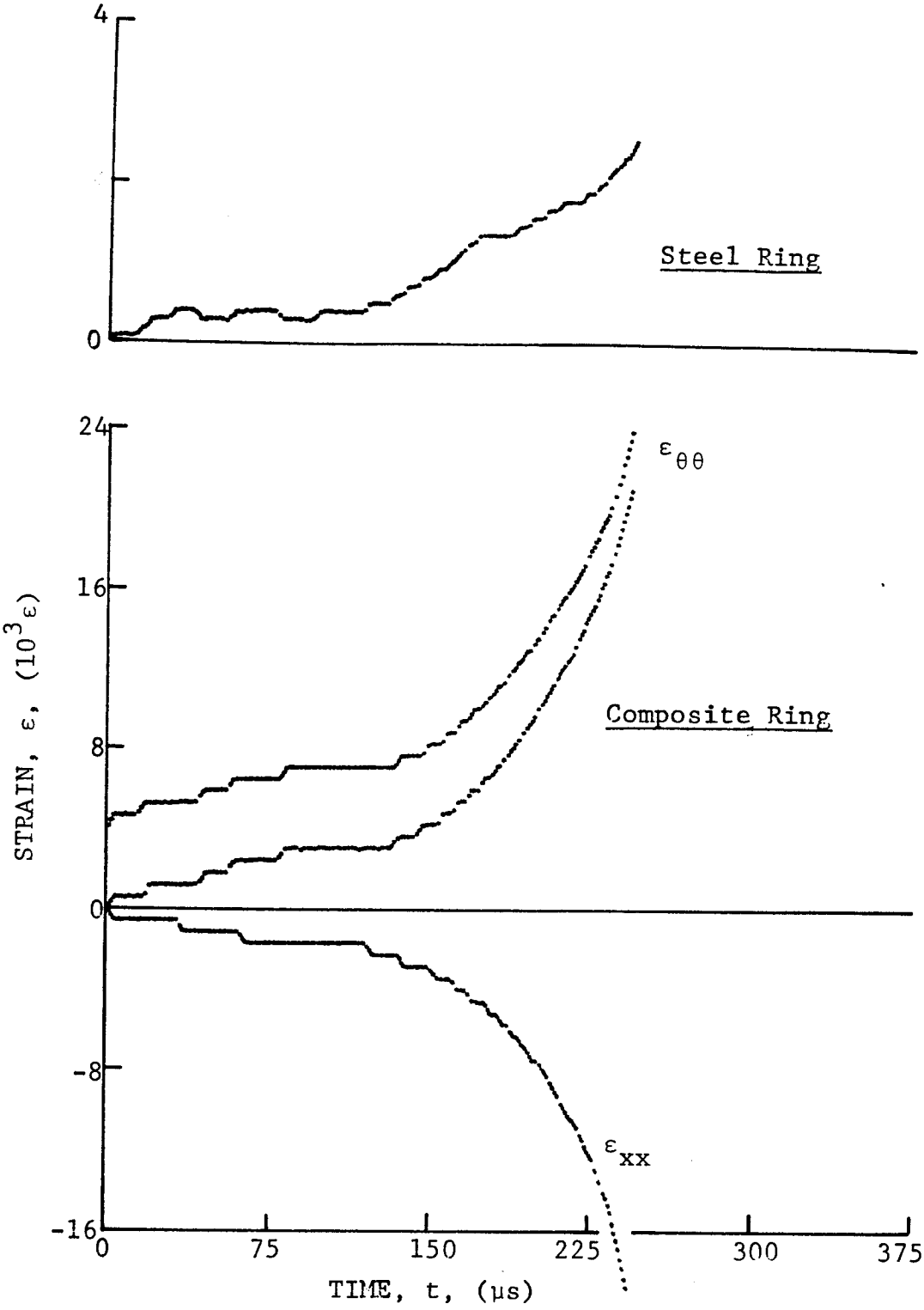

Figure 3-48. Strain records in steel ring and 80AS/20S/PR288 $[\pm 45]_{2s}$ graphite/S-glass/epoxy ring under dynamic loading for Specimen No. 53-5 (0.65 g shotgun powder).

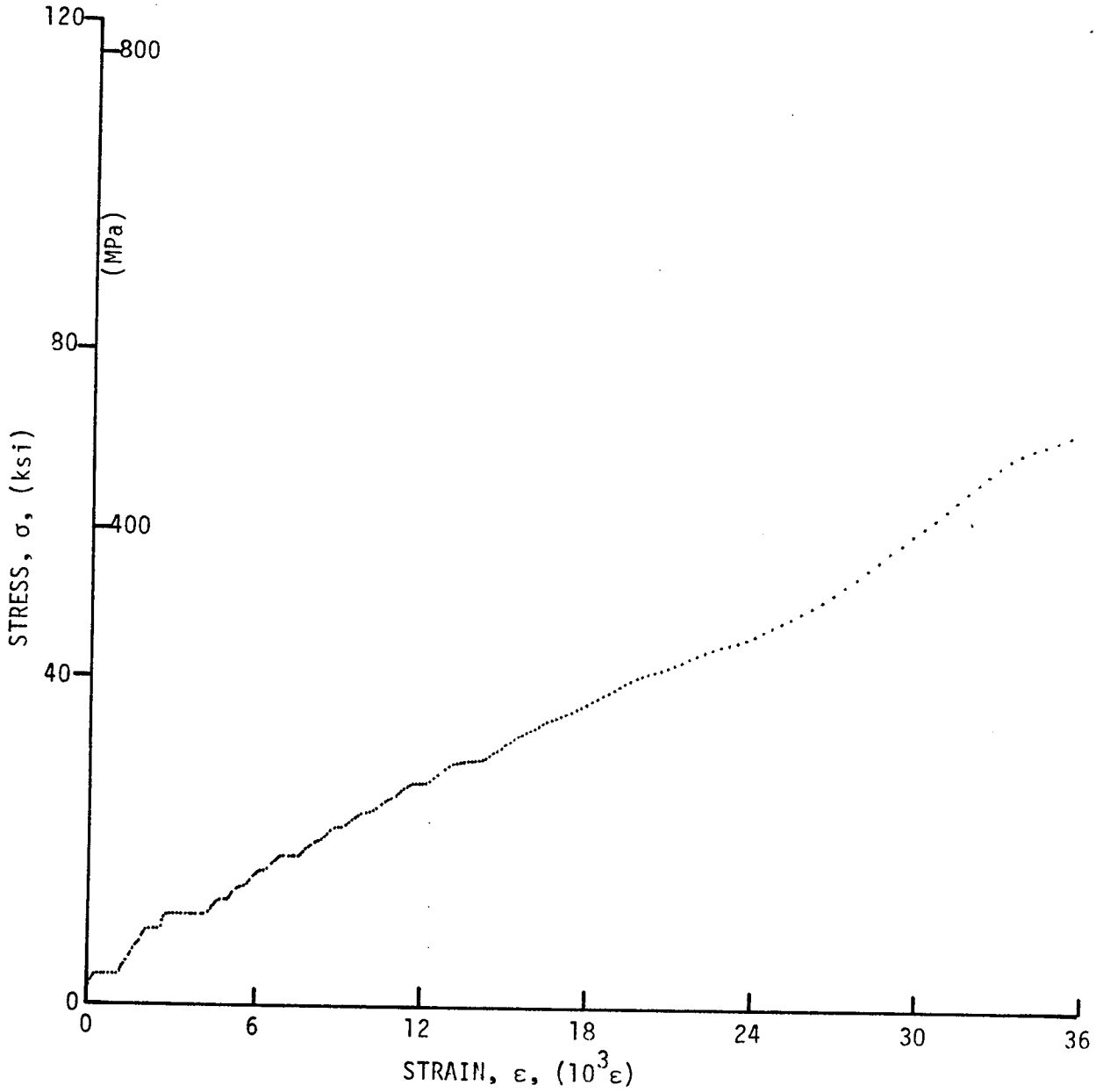

Figure 3-49. Stress-strain curves for dynamically loaded $[\pm 45]_{2s}$ 80AS/20S/PR288 graphite/S-glass/epoxy ring, Specimen No. 25-9.

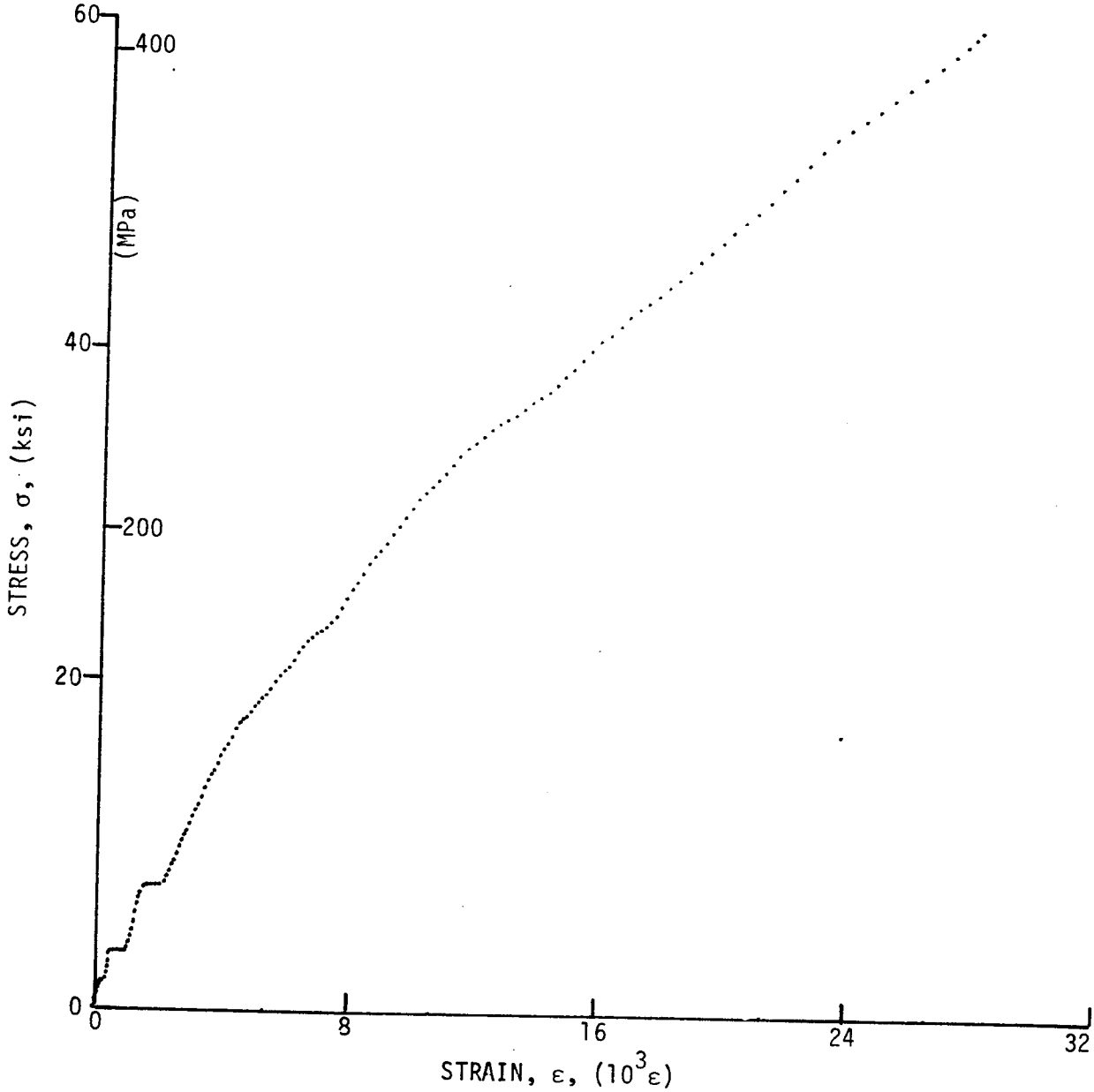

Figure 3-50. Stress-strain curves for dynamically loaded $[\pm 45]_{2s}$ 80AS/20S/PR288 graphite/S-glass/epoxy ring, Specimen No. 53-1.

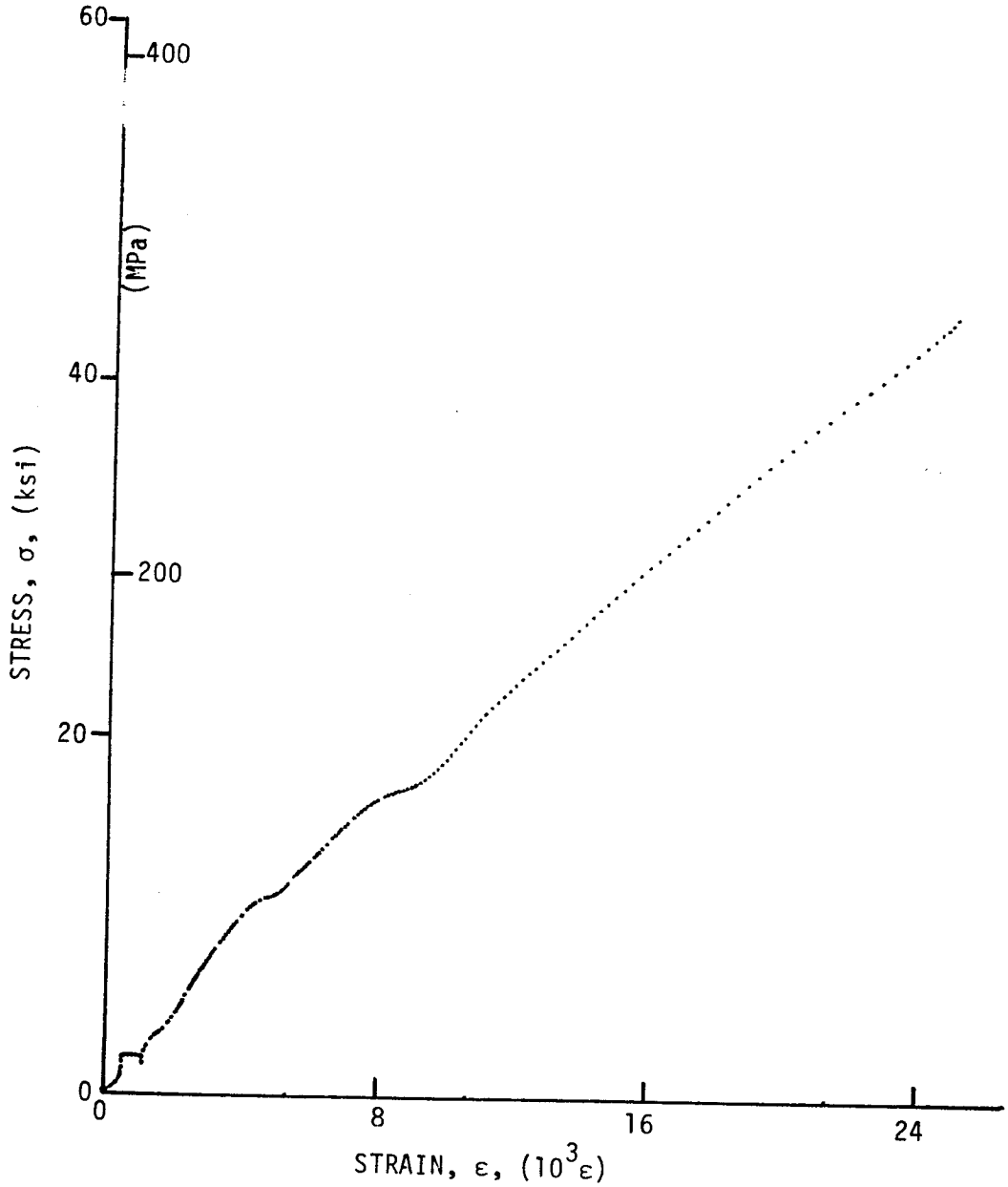

Figure 3-51. Stress-strain curves for dynamically loaded $[\pm 45]_{2s}$ 80AS/20S/PR288 graphite/S-glass/epoxy ring, Specimen No. 53-4.

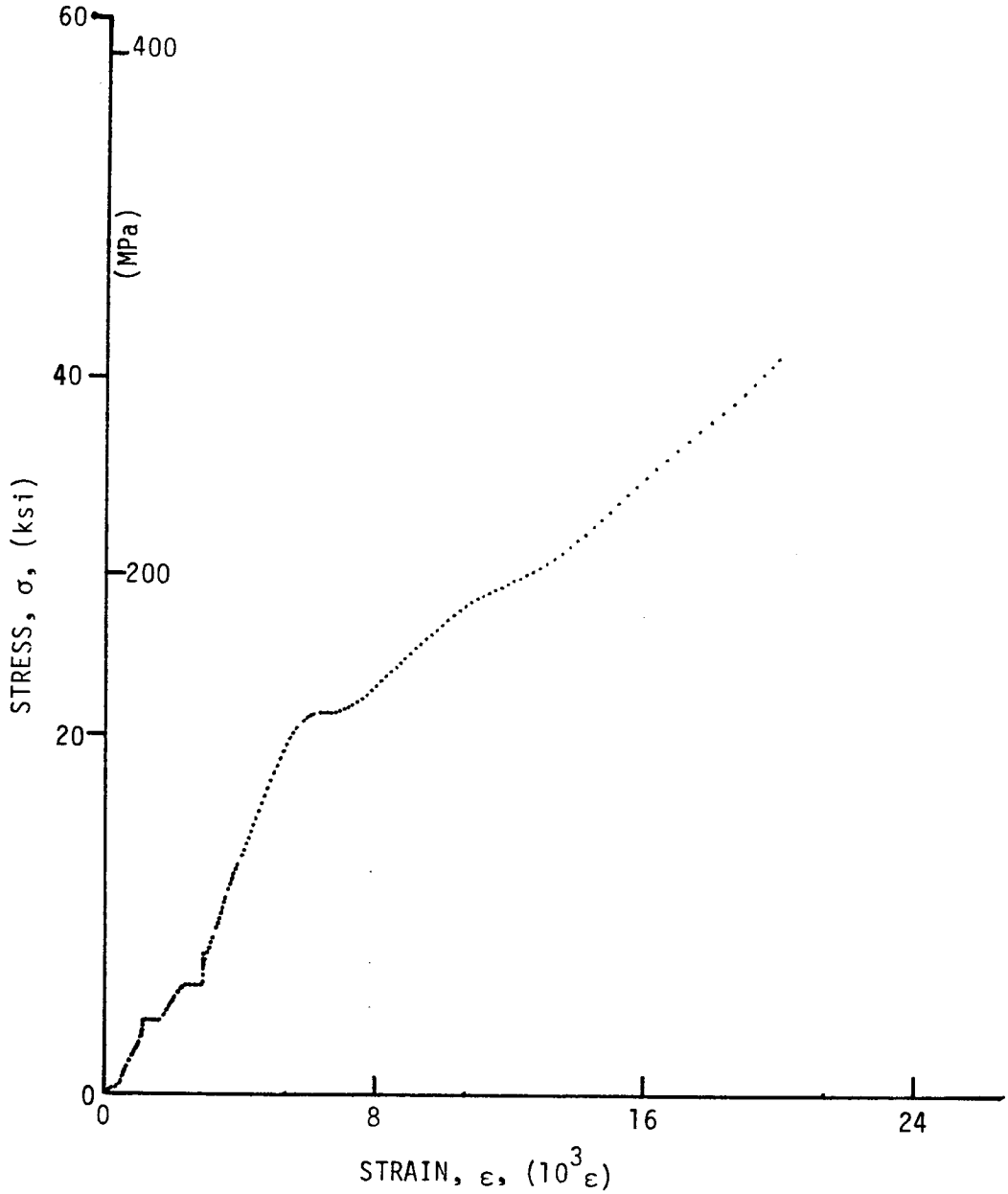

Figure 3-52. Stress-strain curves for dynamically loaded $[\pm 45]_{2s}$ 80AS/20S/PR288 graphite/S-glass/epoxy ring, Specimen No. 53-5.

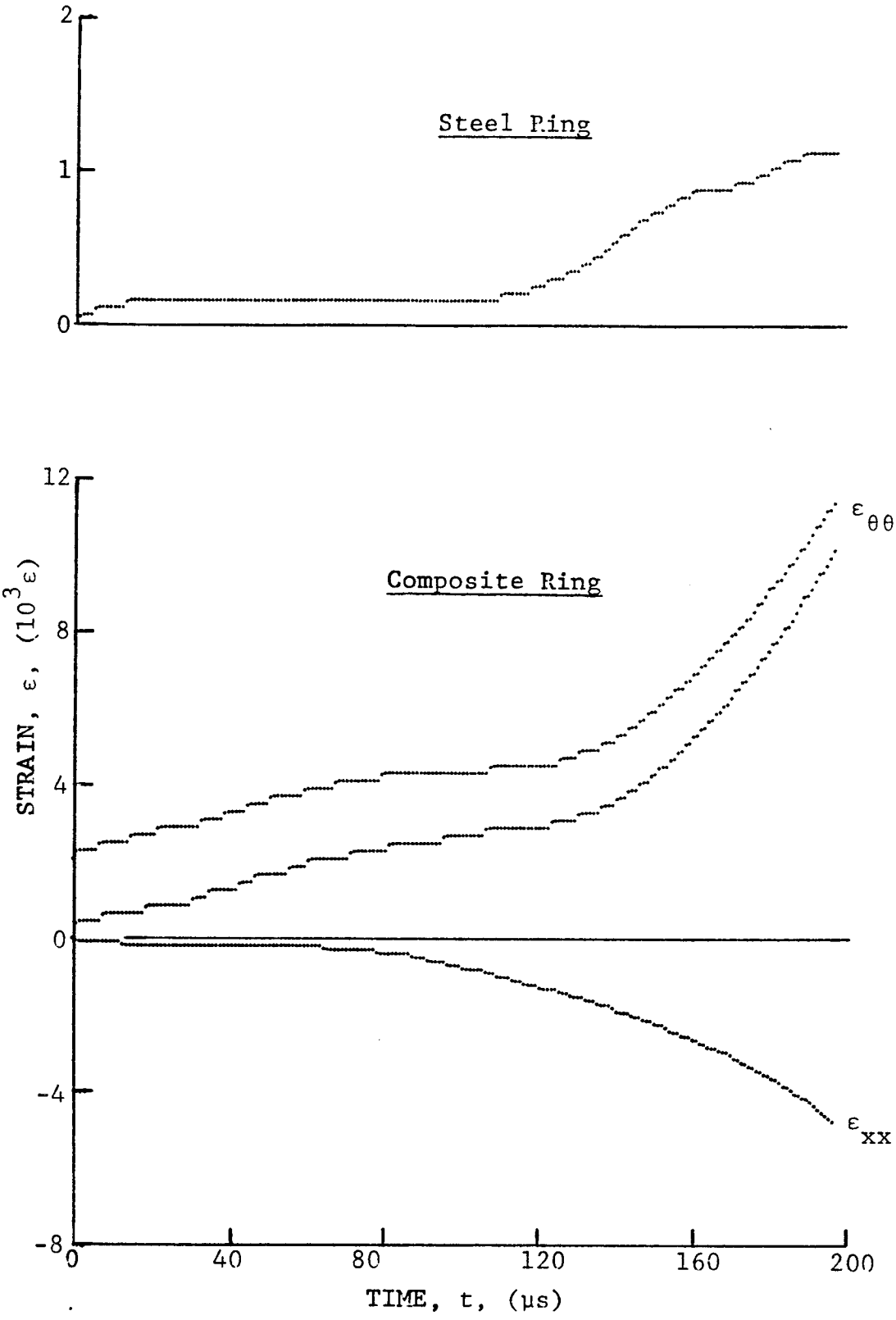

Figure 3-53. Strain records in steel ring and $[\pm 60]_{2s}$ SP288/AS graphite/epoxy ring under dynamic loading for Specimen No. 22-9 (0.65 g shotgun powder).

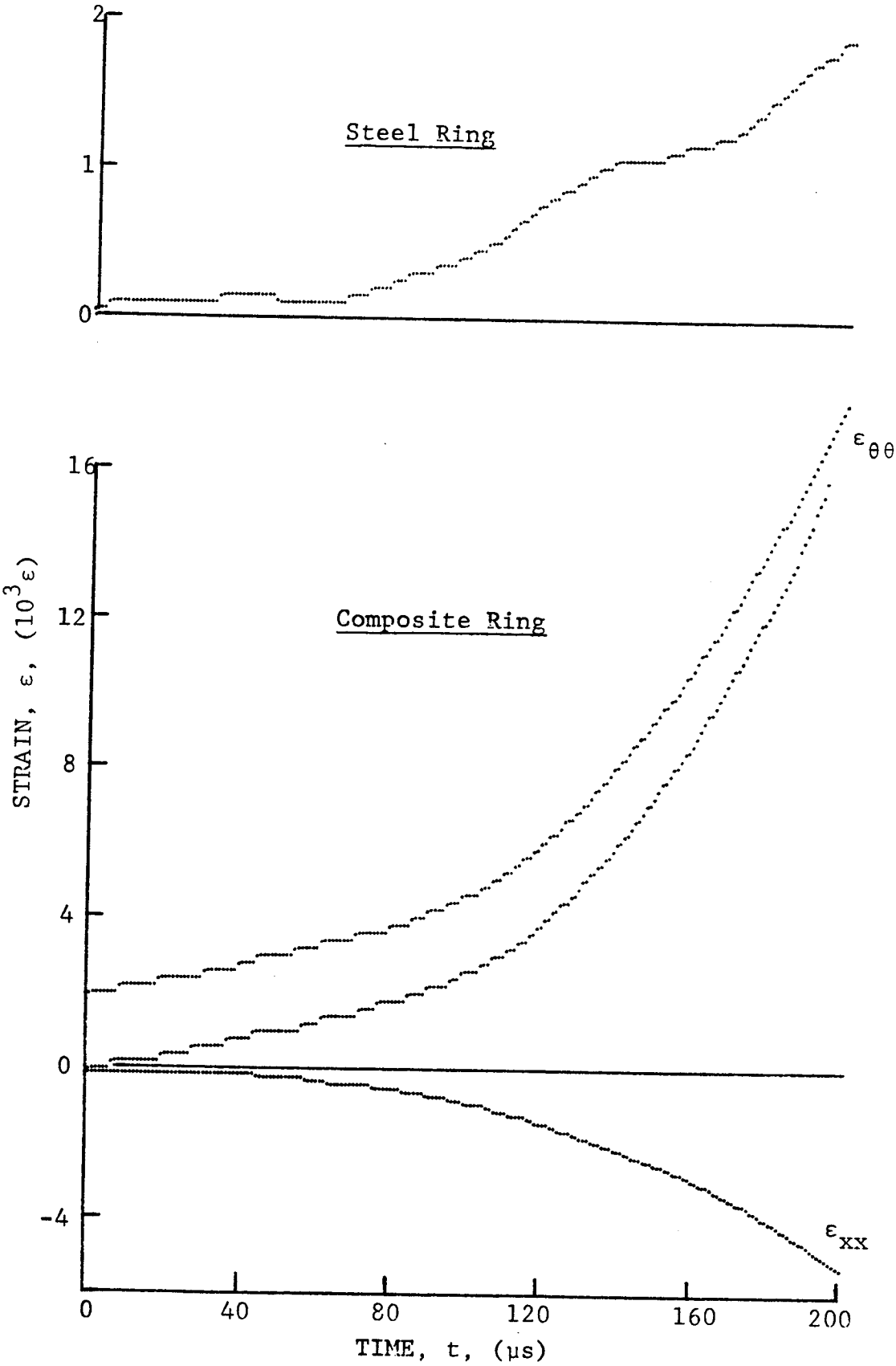

Figure 3-54. Strain records in steel ring and $[\pm 60]_{2S}$ SP288/AS graphite/epoxy ring under dynamic loading for Specimen No. 22-10 (0.65 g shotgun powder).

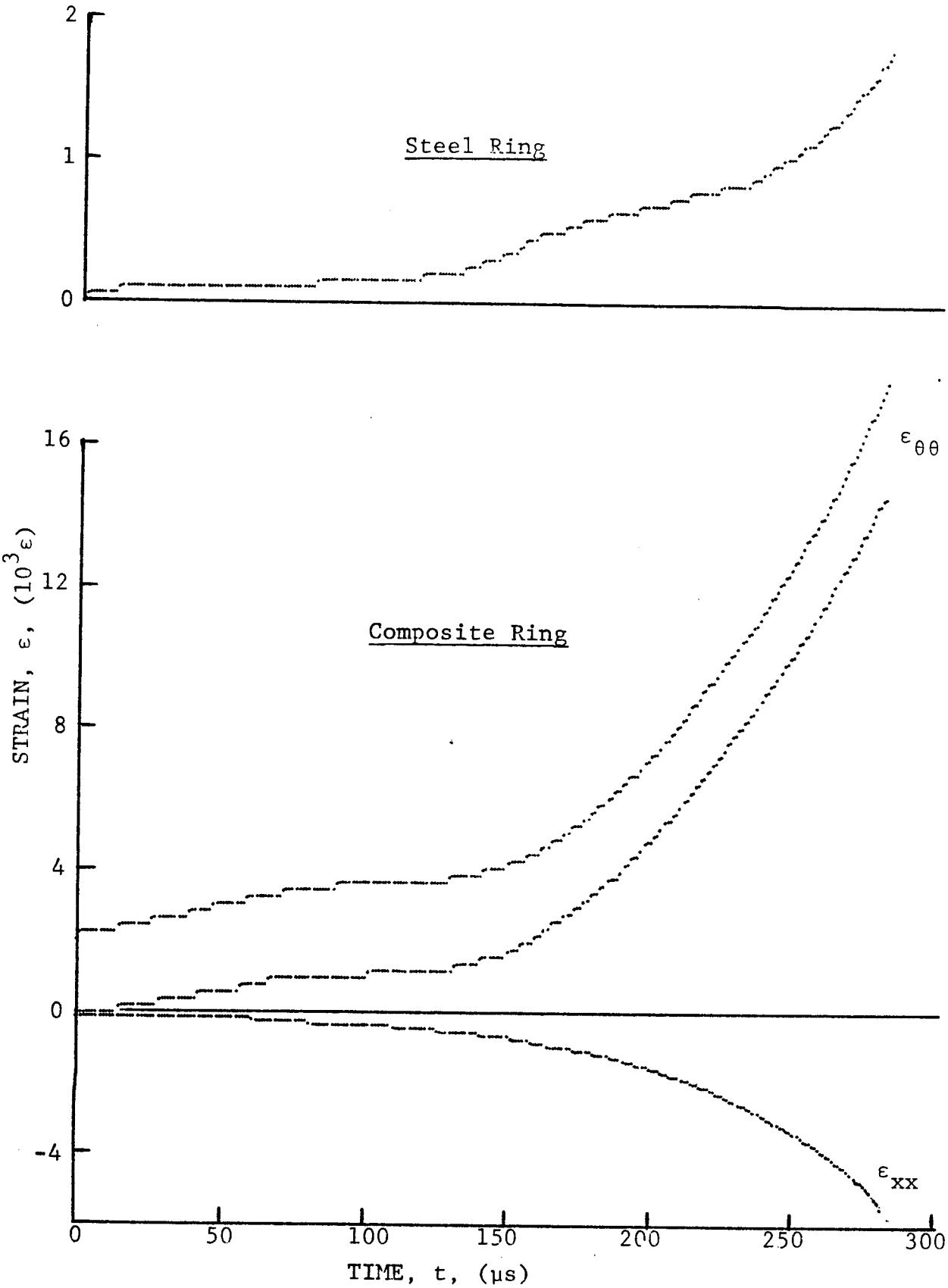

Figure 3-55. Strain records in steel ring and $[\pm 60]_{2S}$ SP288/AS graphite/epoxy ring under dynamic loading for Specimen No. 22-11 (0.65 g shotgun powder).

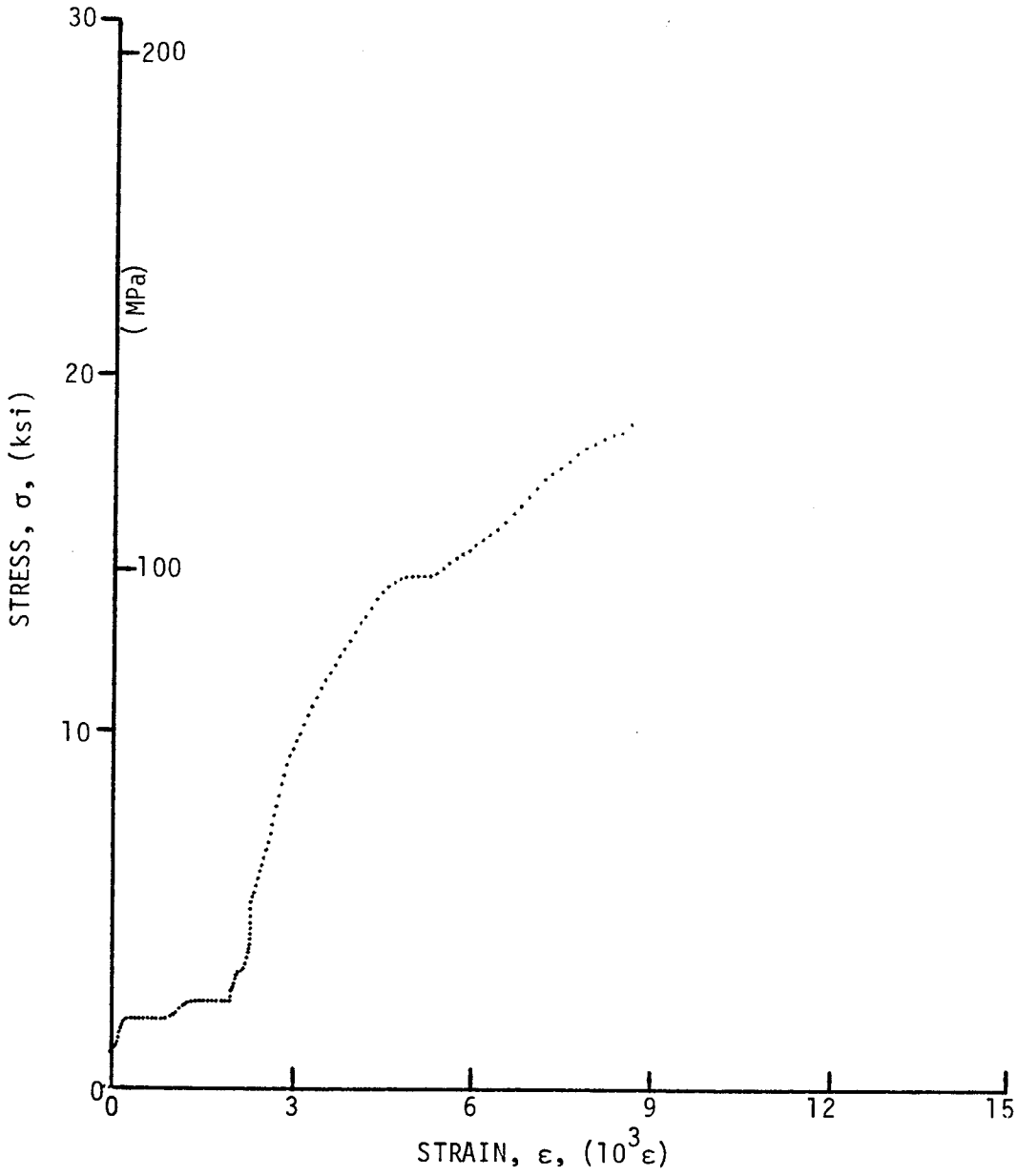

Figure 3-56. Stress-strain curve for dynamically loaded $[\pm 60]_{2s}$ SP288/AS graphite/epoxy ring, Specimen No. 22-9.

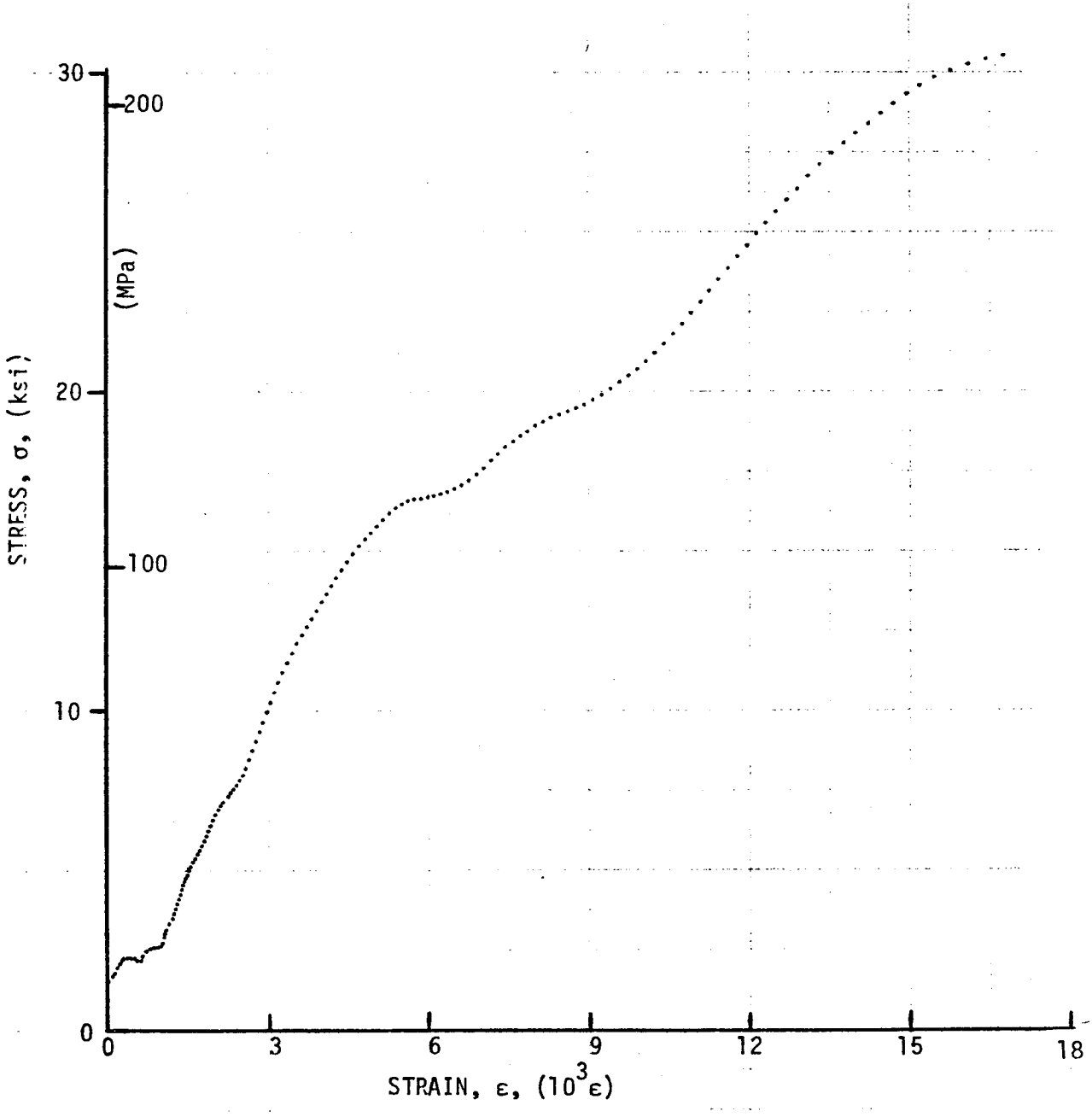

Figure 3-57. Stress-strain curve for dynamically loaded $[\pm 60]_{2s}$ SP288/AS graphite/epoxy ring, Specimen No. 22-10.

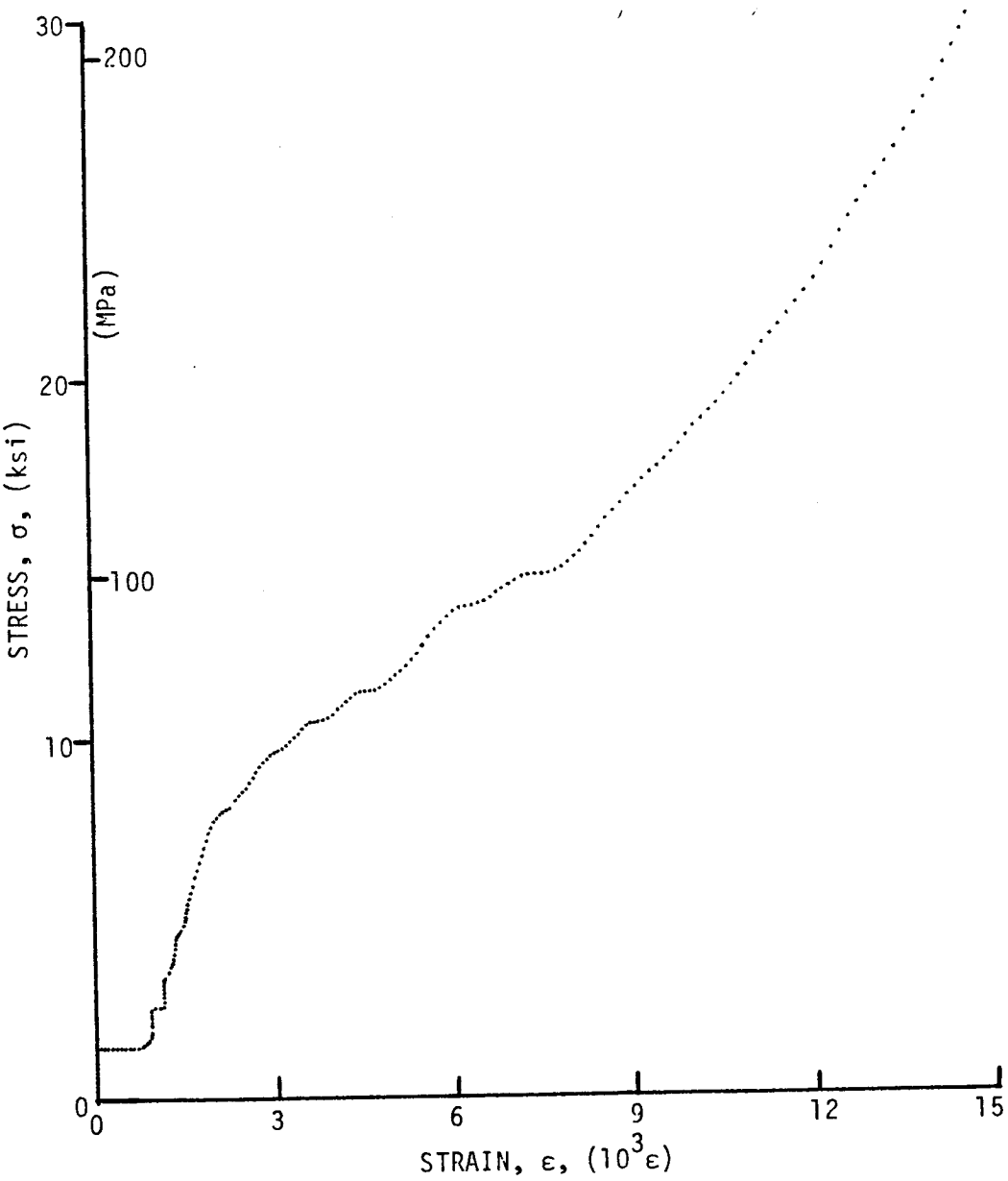

Figure 3-58. Stress-strain curve for dynamically loaded $[\pm 60]_{2s}$ SP288/AS graphite/epoxy ring, Specimen No. 22-11.

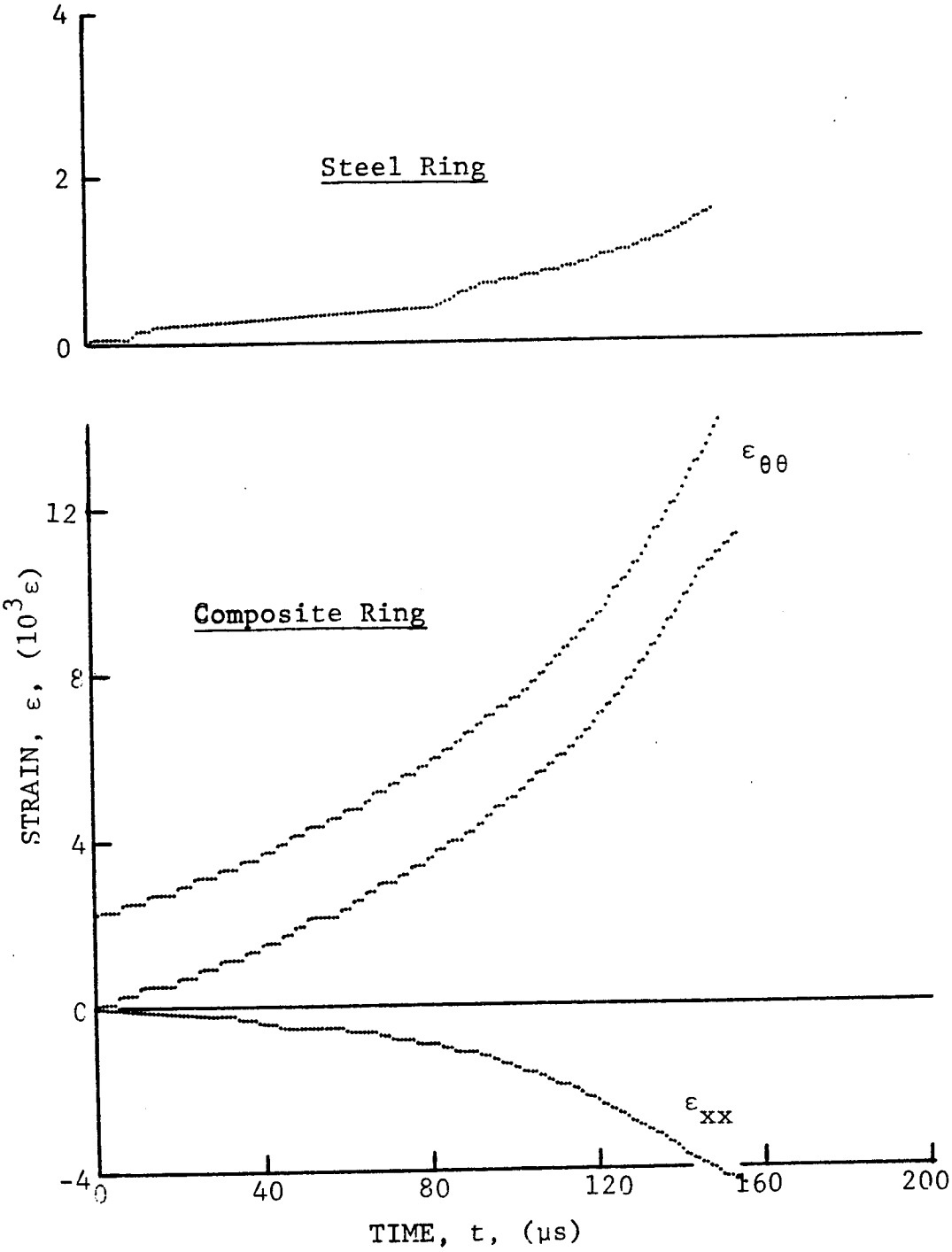

Figure 3-59. Strain records in steel ring and 80AS/20S/PR288 $[\pm 60]_{2s}$ graphite/S-glass/epoxy ring under dynamic loading for Specimen No. 23-7 (0.65 g shotgun powder).

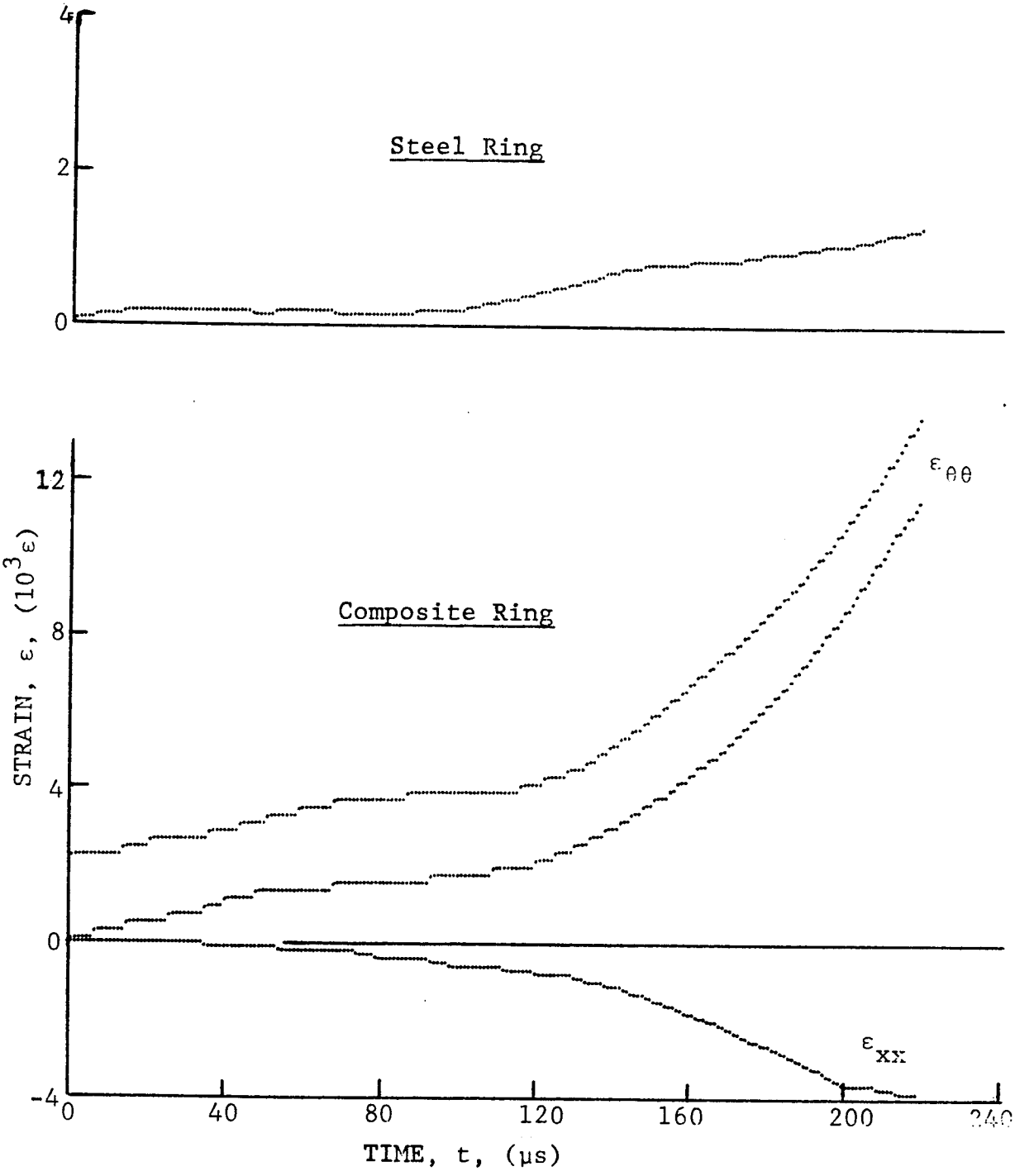

Figure 3-60. Strain records in steel ring and 80AS/20S/PR288 $[\pm 60]_{2s}$ graphite/S-glass/epoxy ring under dynamic loading for Specimen No. 23-10 (0.65 g shotgun powder).

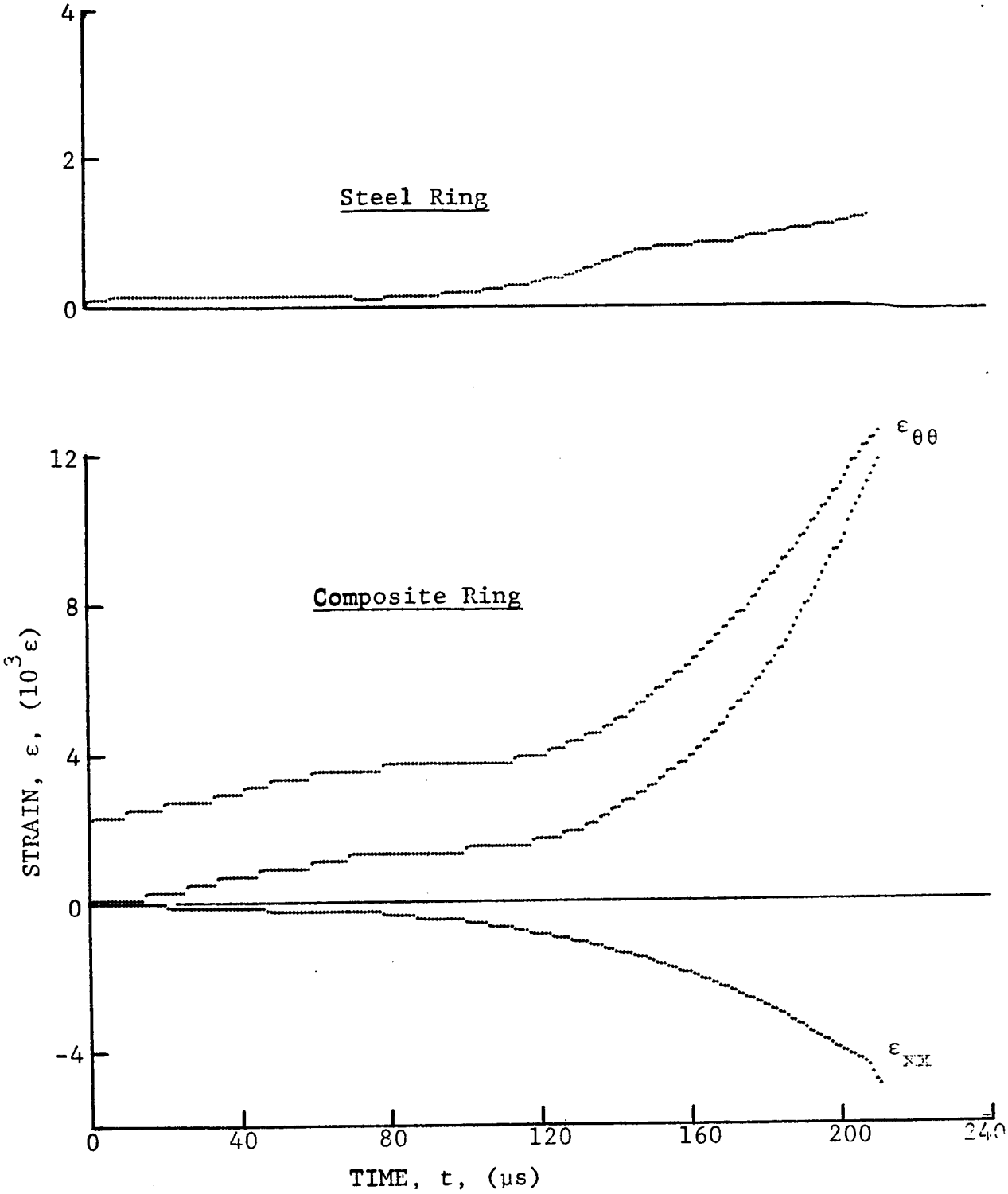

Figure 3-61. Strain records in steel ring and 80AS/20S/PR288 $[\pm 60]_{2s}$ graphite/S-glass/epoxy ring under dynamic loading for Specimen No. 23-11 (0.65 g shotgun powder).

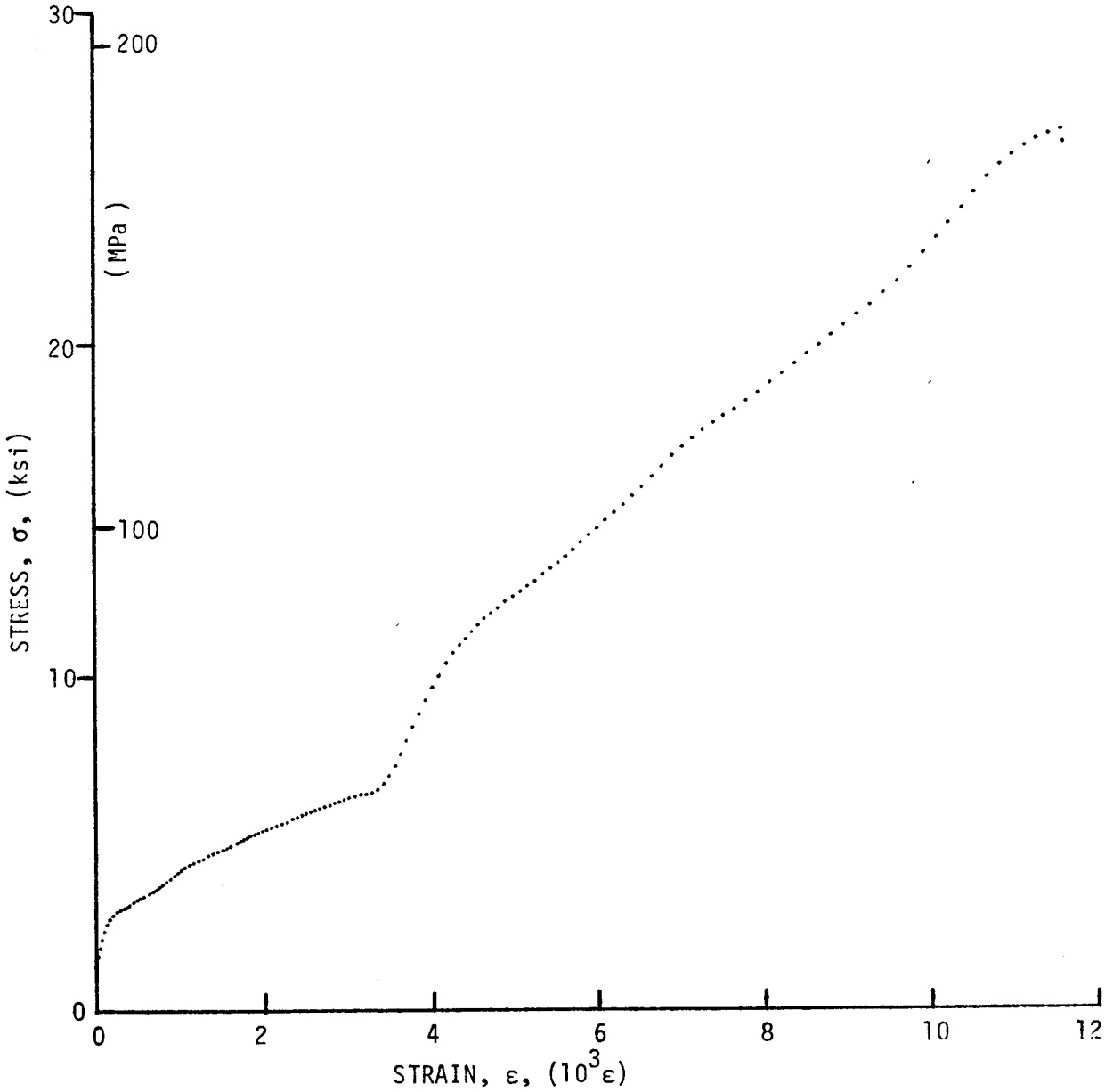

Figure 3-62. Stress-strain curve for dynamically loaded $[\pm 60]_{2s}$ 80AS/20S/PR288 graphite/S-glass/epoxy ring, Specimen No. 23-7.

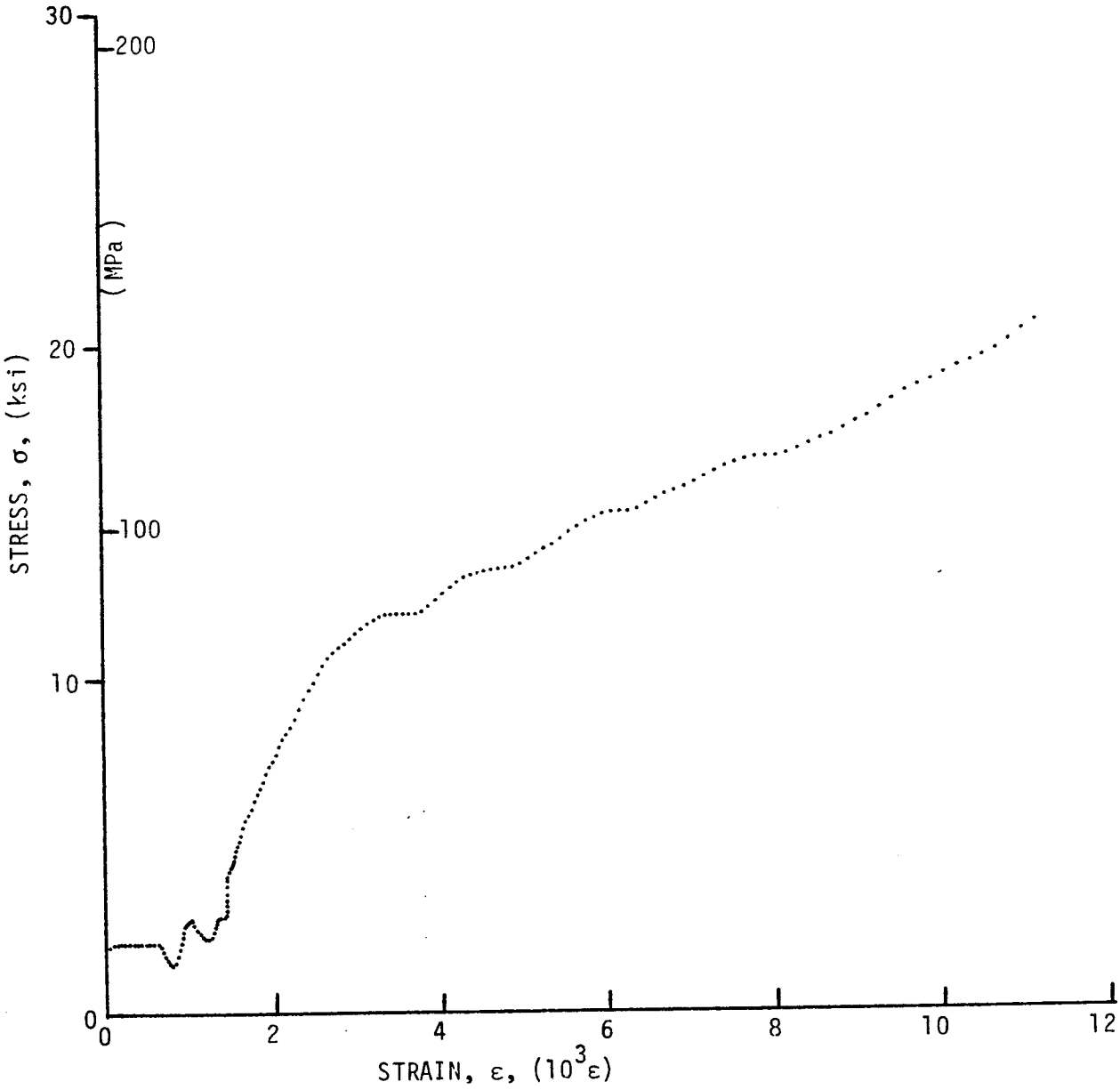

Figure 3-63. Stress-strain curve for dynamically loaded $[\pm 60]_{2s}$ 80AS/20S/PR288 graphite/S-glass/epoxy ring, Specimen No. 23-10.

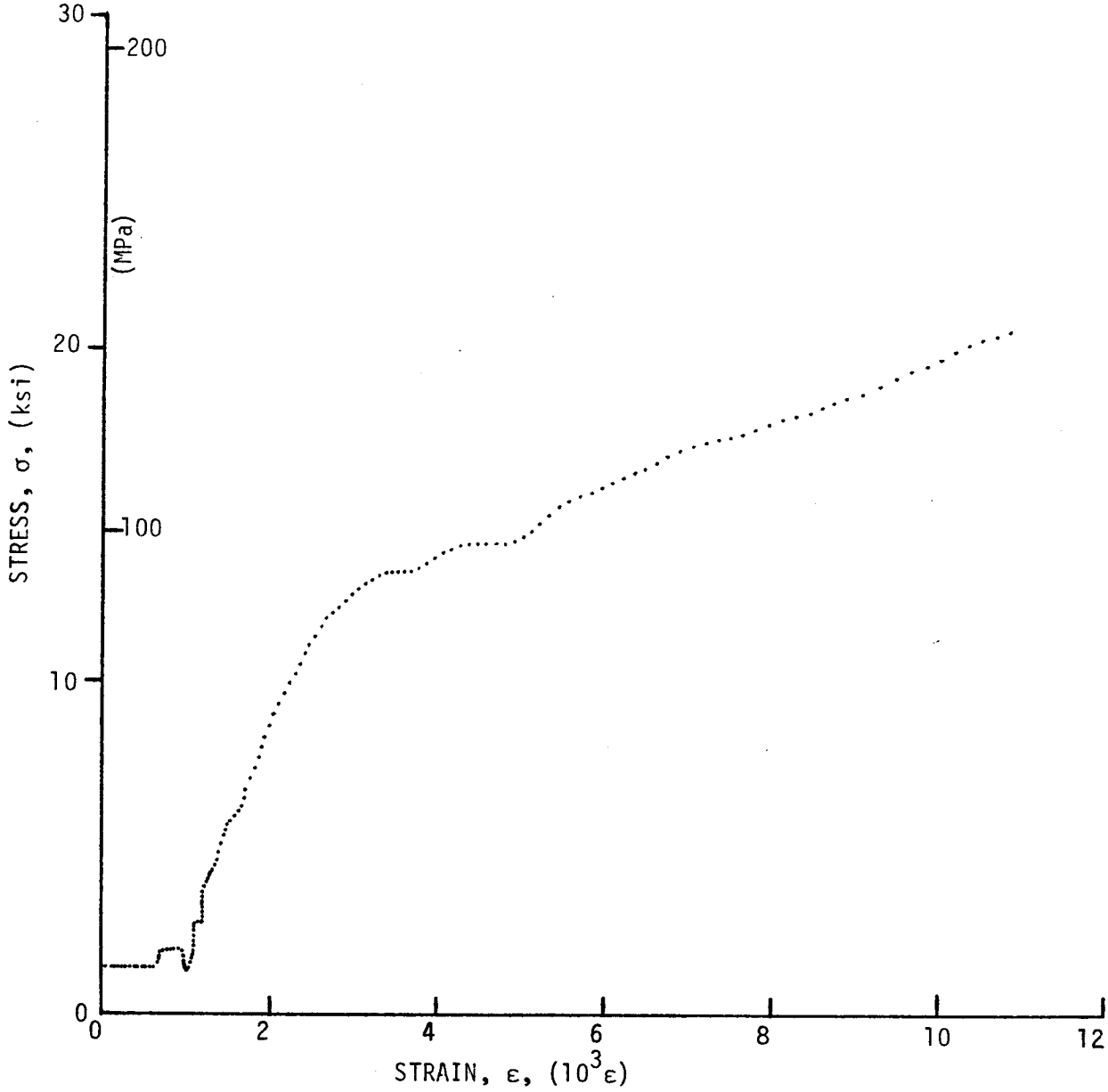

Figure 3-64. Stress-strain curve for dynamically loaded $[\pm 60]_{2s}$ 80AS/20S/PR288 graphite/S-glass/epoxy ring, Specimen No. 23-11.

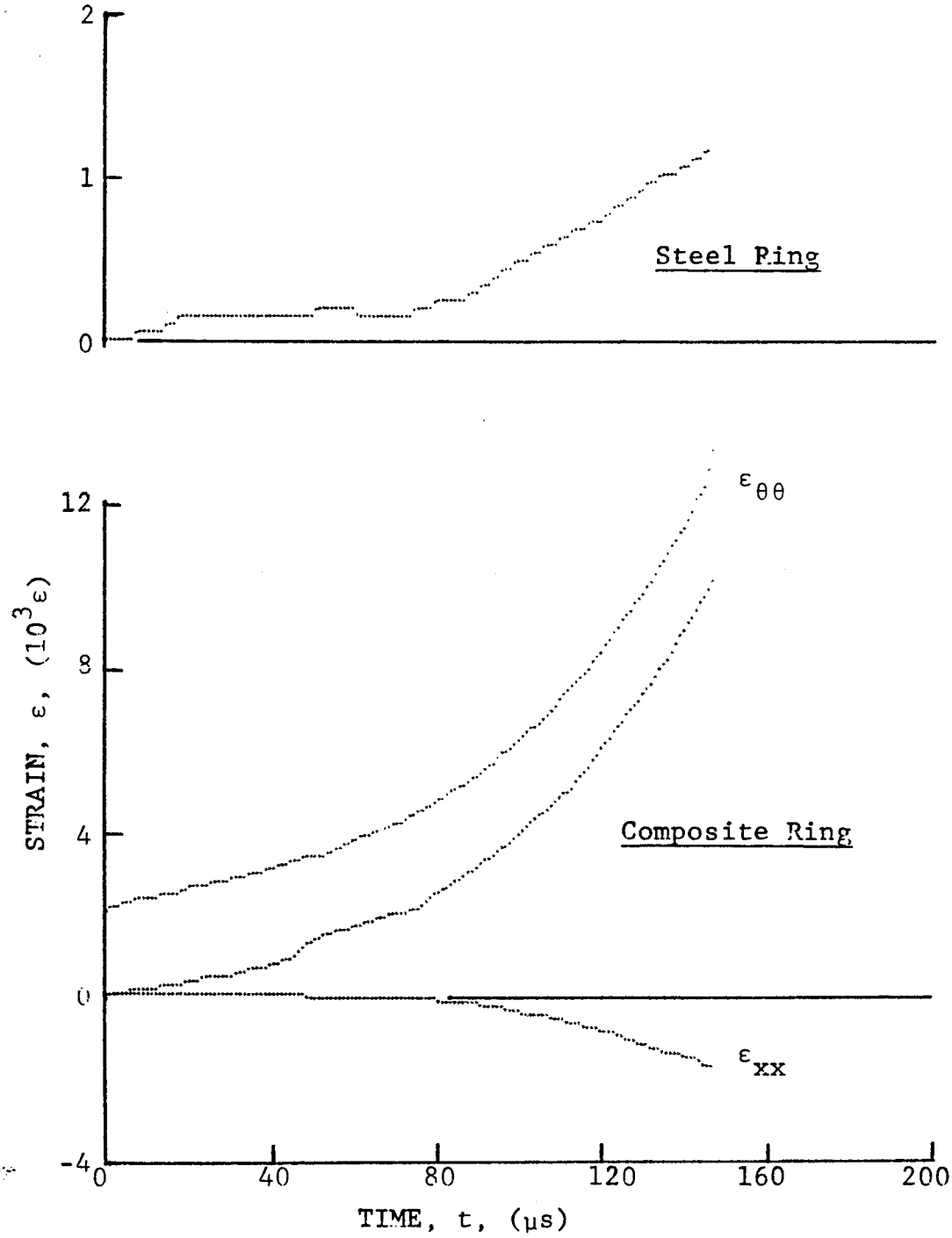

Figure 3-65. Strain records in steel ring and $[\pm 67.5]_{2s}$ SP288/AS graphite/epoxy ring under dynamic loading for Specimen No. 26-10 (0.65 g shotgun powder).

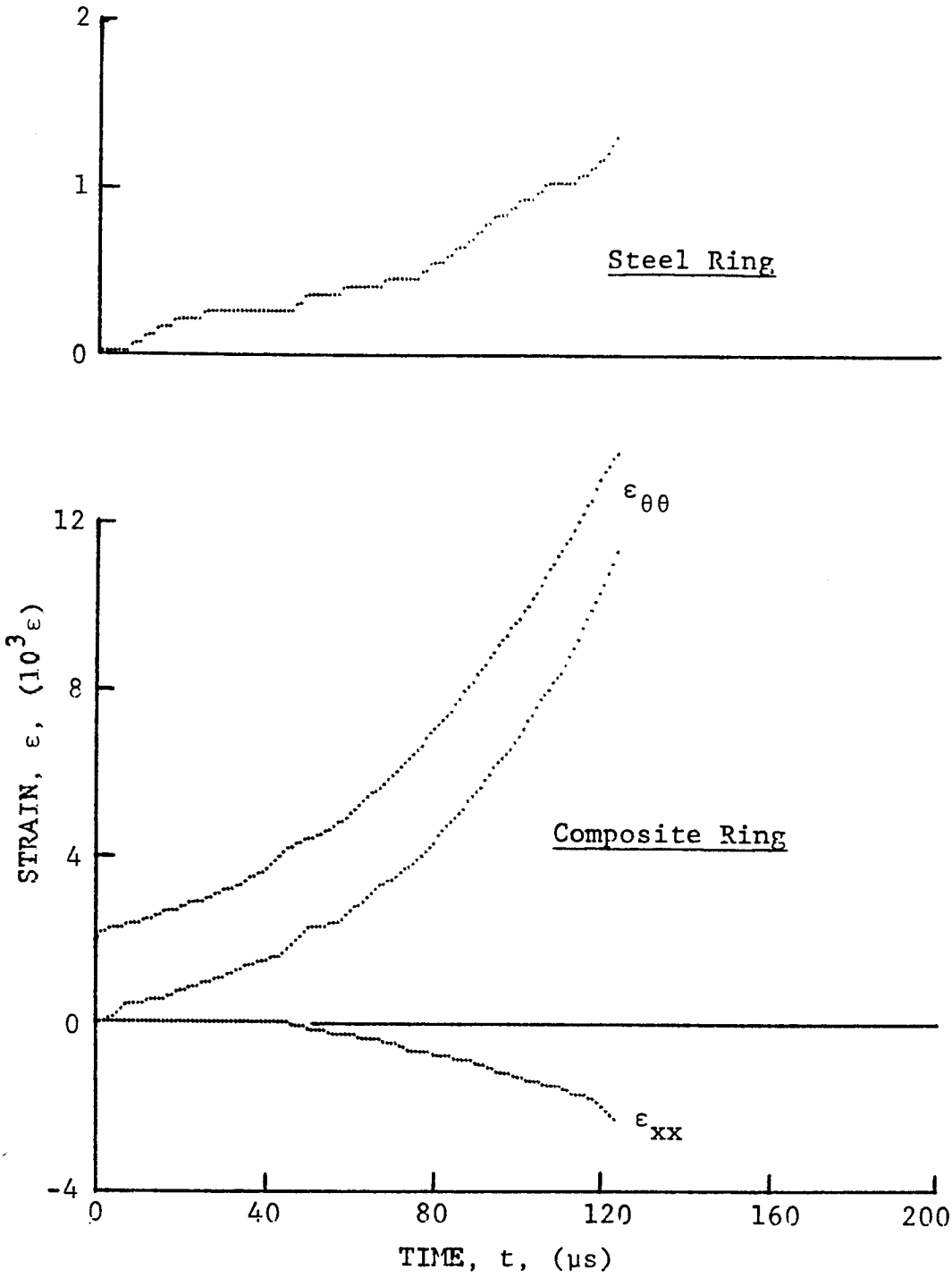

Figure 3-66. Strain records in steel ring and $[\pm 67.5]_{2s}$ SP288/AS graphite/epoxy ring under dynamic loading for Specimen No. 26-11 (0.65 g shotgun powder).

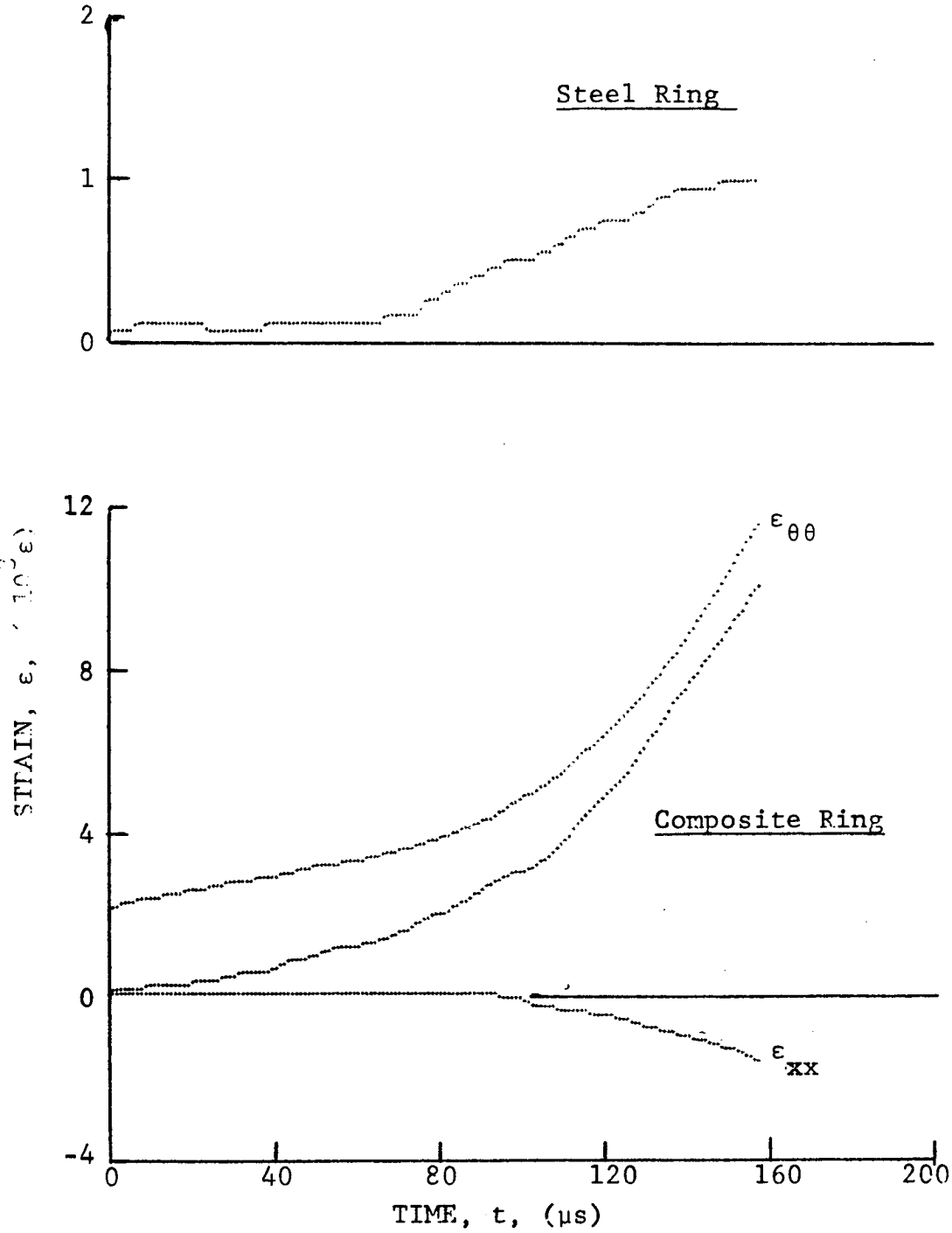

Figure 3-67. Strain records in steel ring and $[\pm 67.5]_{2s}$ SP288/AS graphite/epoxy ring under dynamic loading for Specimen No. 26-13 (0.65 g shotgun powder).

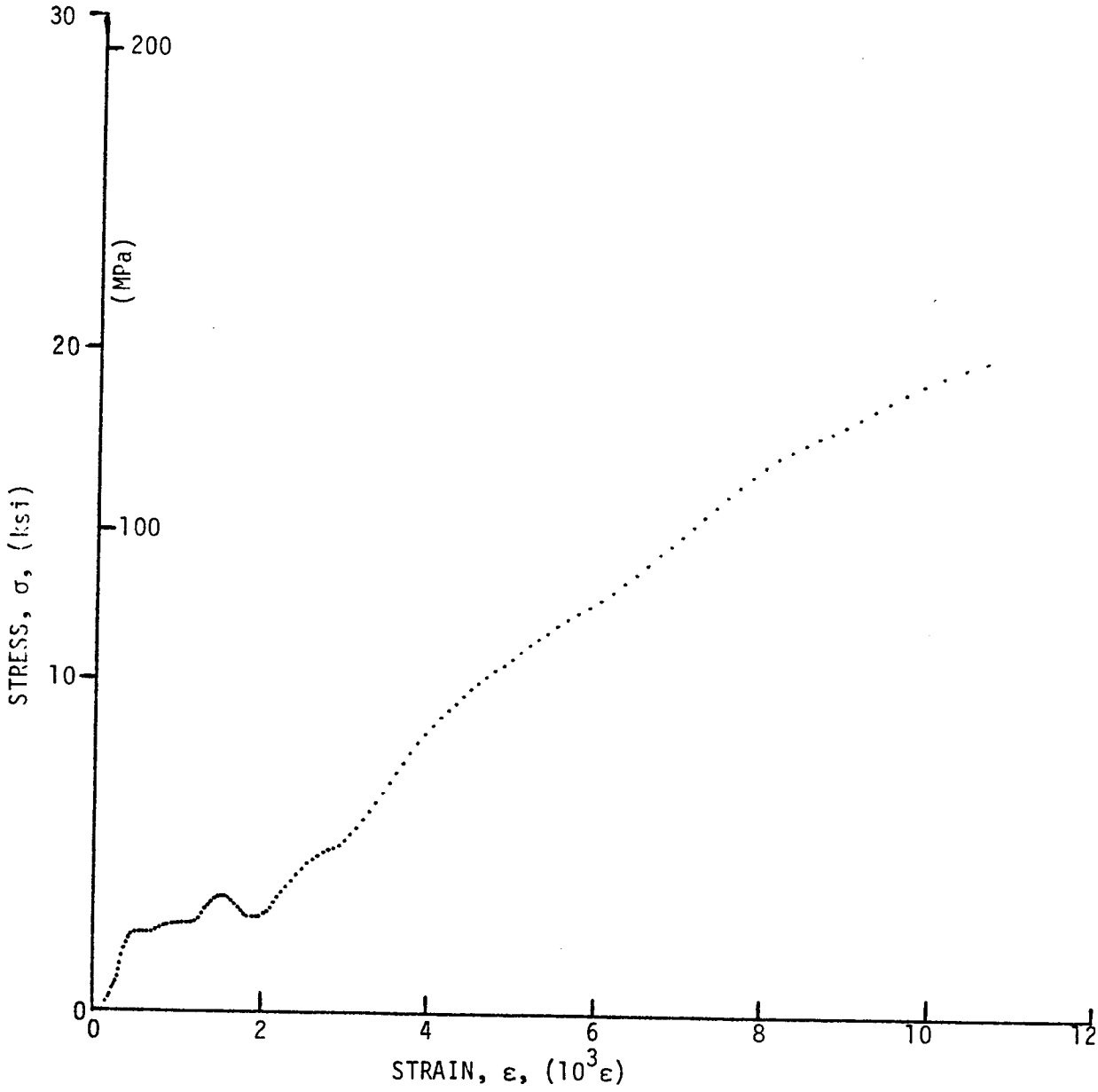

Figure 3-68. Stress-strain curve for dynamically loaded $[\pm 67.5]_{2s}$ SP288/AS graphite/epoxy ring, Specimen No. 26-10.

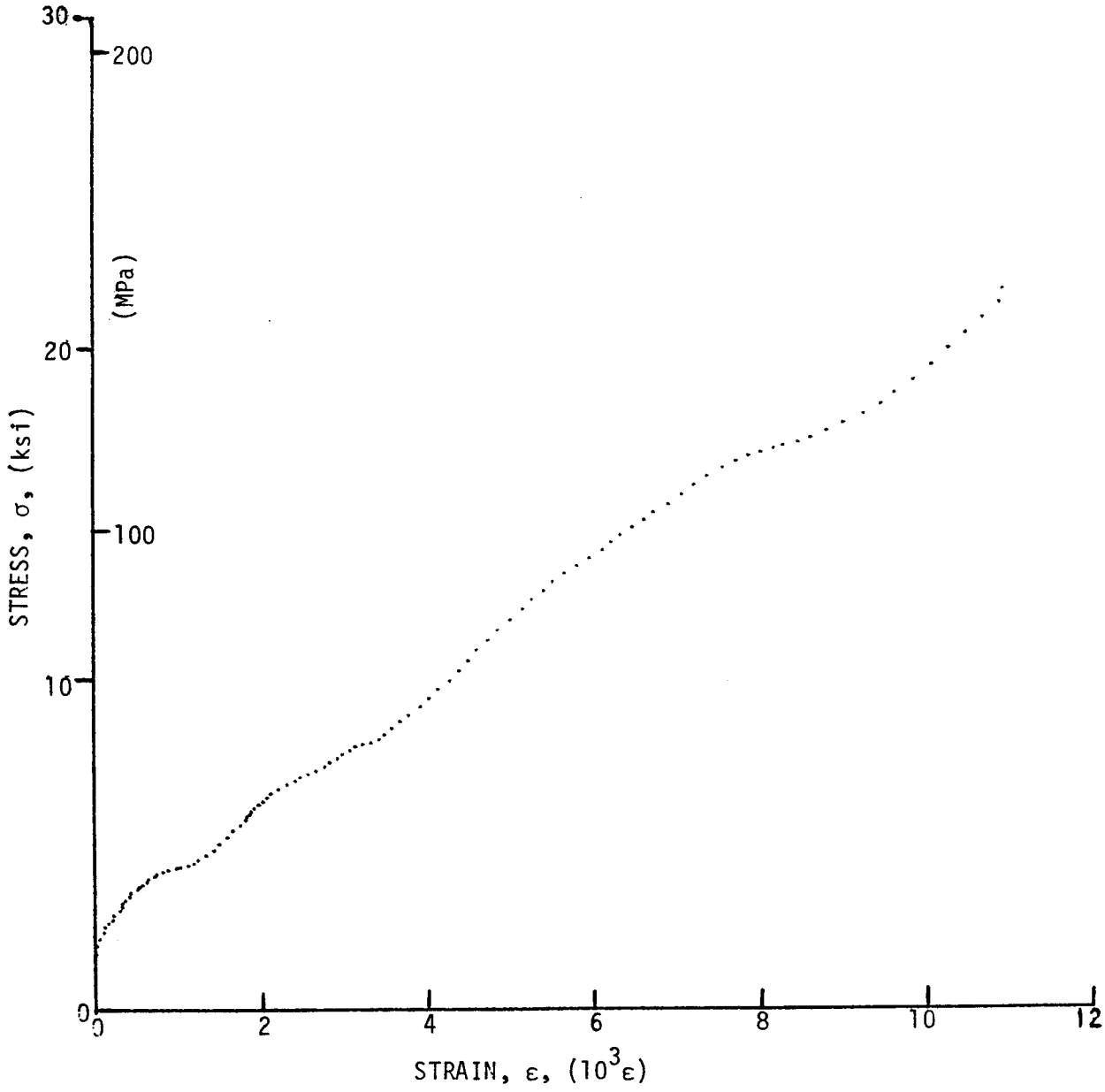

Figure 3-69. Stress-strain curve for dynamically loaded $[\pm 67.5]_{2s}$ SP288/AS graphite/epoxy ring, Specimen No. 26-11.

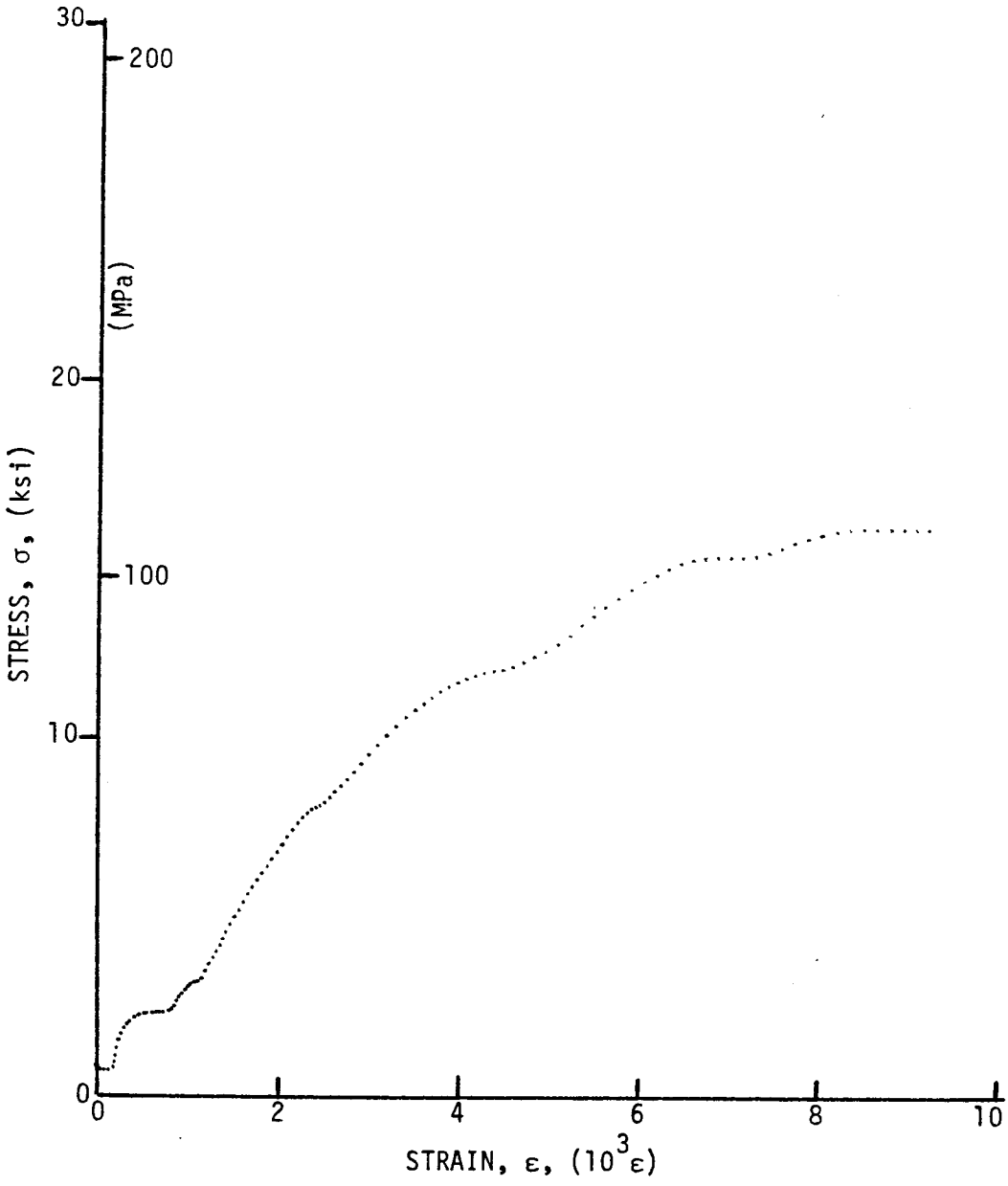

Figure 3-70. Stress-strain curve for dynamically loaded $[\pm 67.5]_{2s}$ SP288/AS graphite/epoxy ring, Specimen No. 26-13.

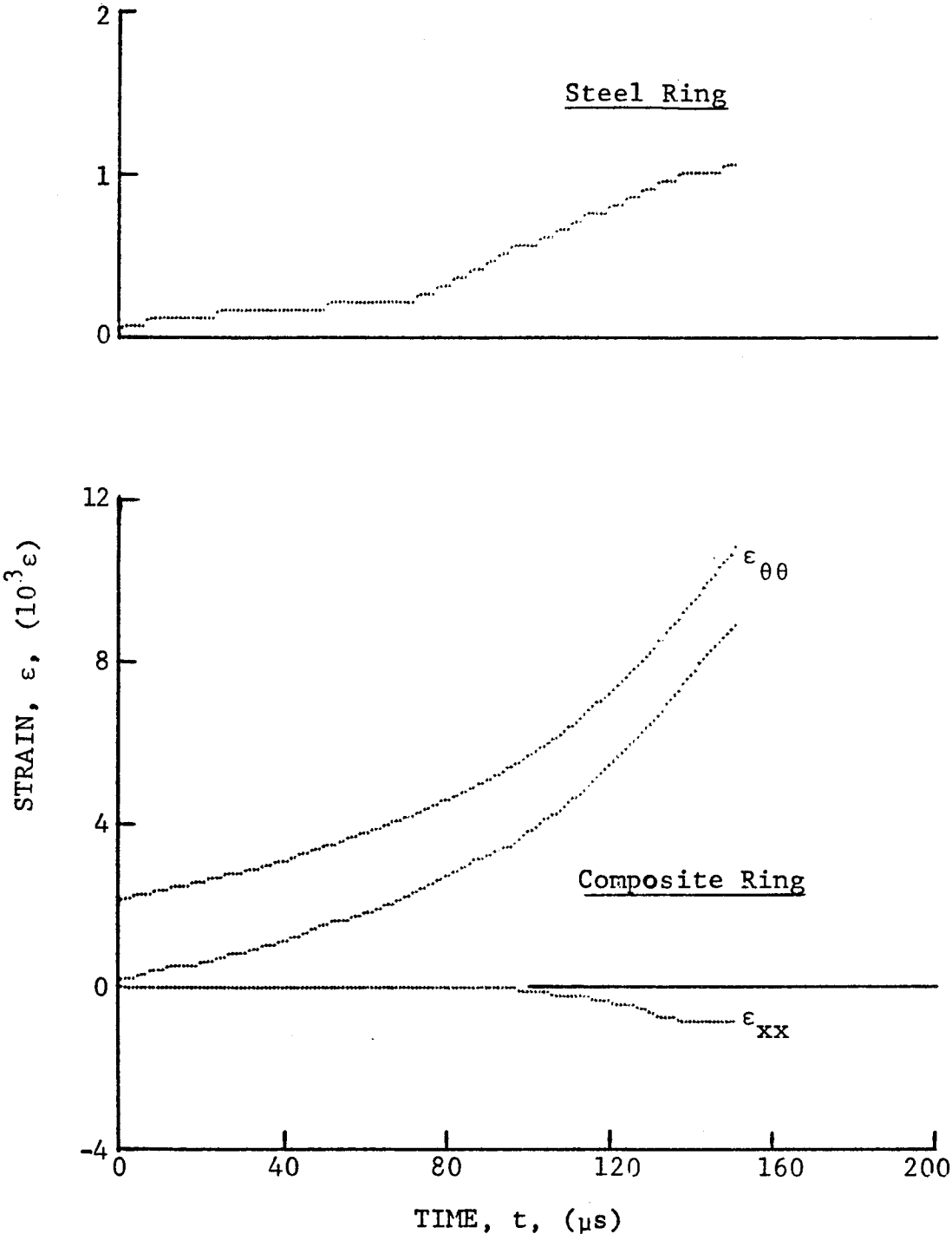

Figure 3-71. Strain records in steel ring and 80AS/20S/PR288 $[\pm 67.5]_{2s}$ graphite/S-glass/epoxy ring under dynamic loading for Specimen No. 27-10 (0.65 g shotgun powder).

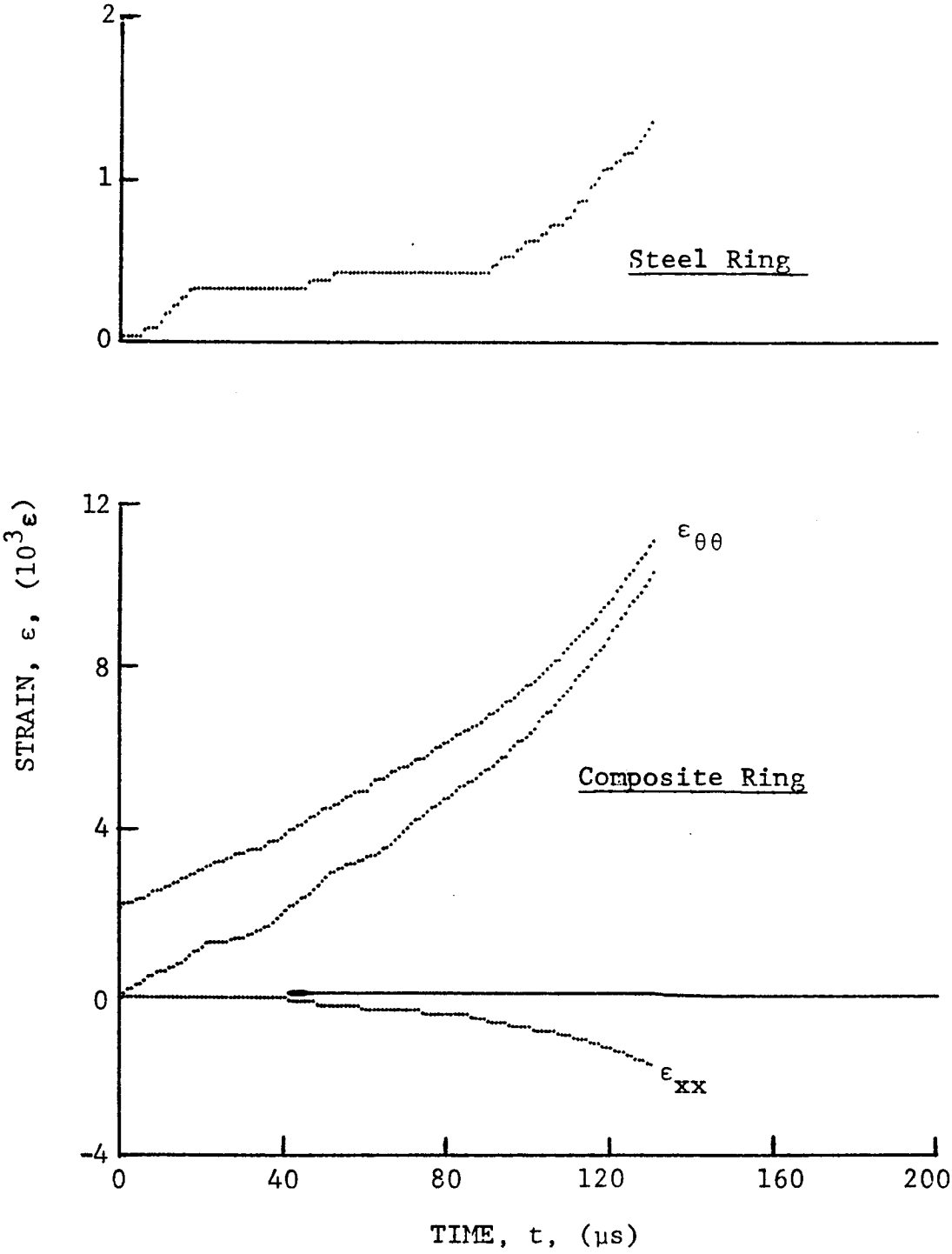

Figure 3-72. Strain records in steel ring and 80AS/20S/PR288 $[\pm 67.5]_{2S}$ graphite/S-glass/epoxy ring under dynamic loading for Specimen No. 27-11 (0.65 g shotgun powder).

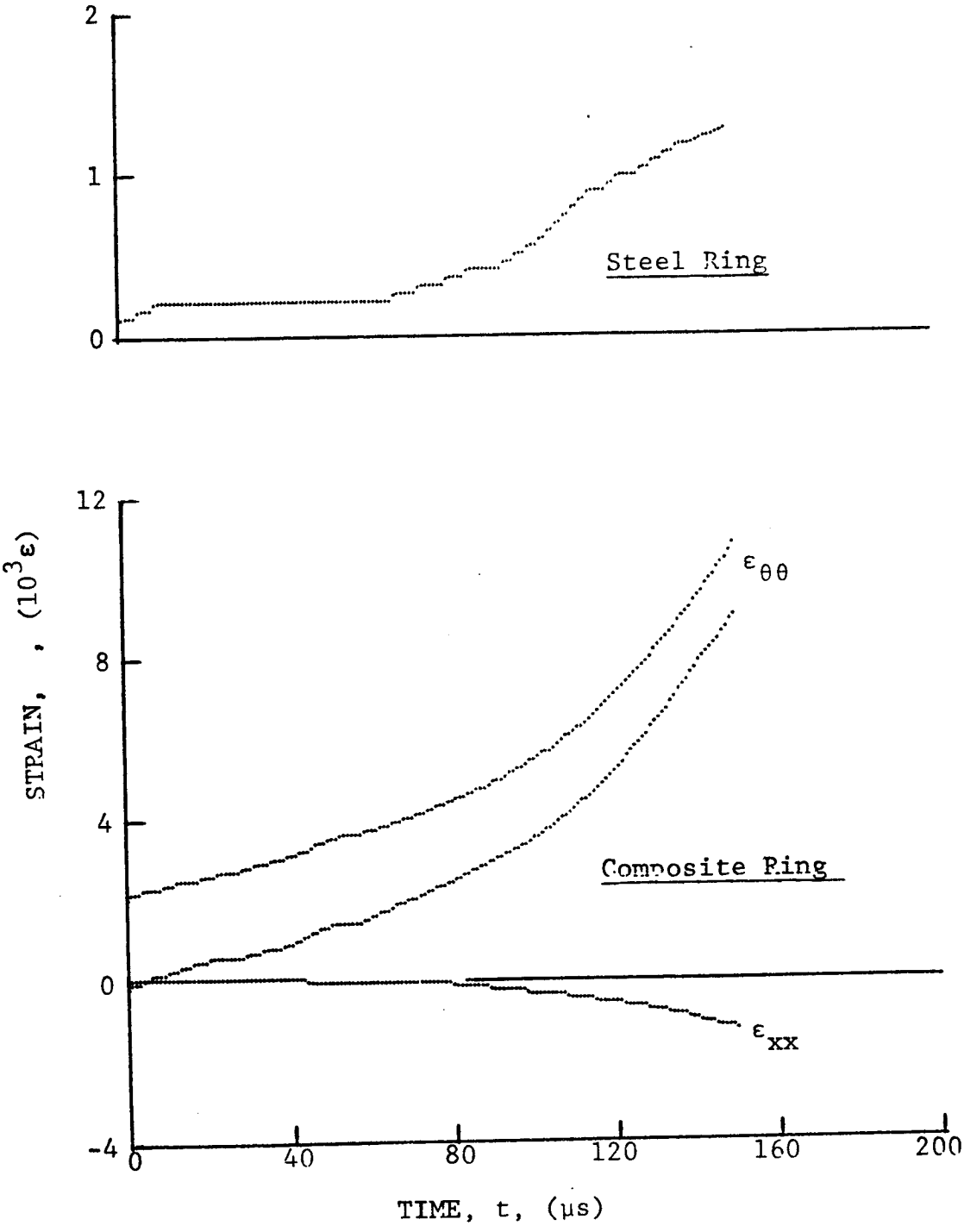

Figure 3-73. Strain records in steel ring and 80AS/20S/PR288 $[\pm 67.5]_{2s}$ graphite/S-glass/epoxy ring under dynamic loading for Specimen No. 27-13 (0.65 g shotgun powder).

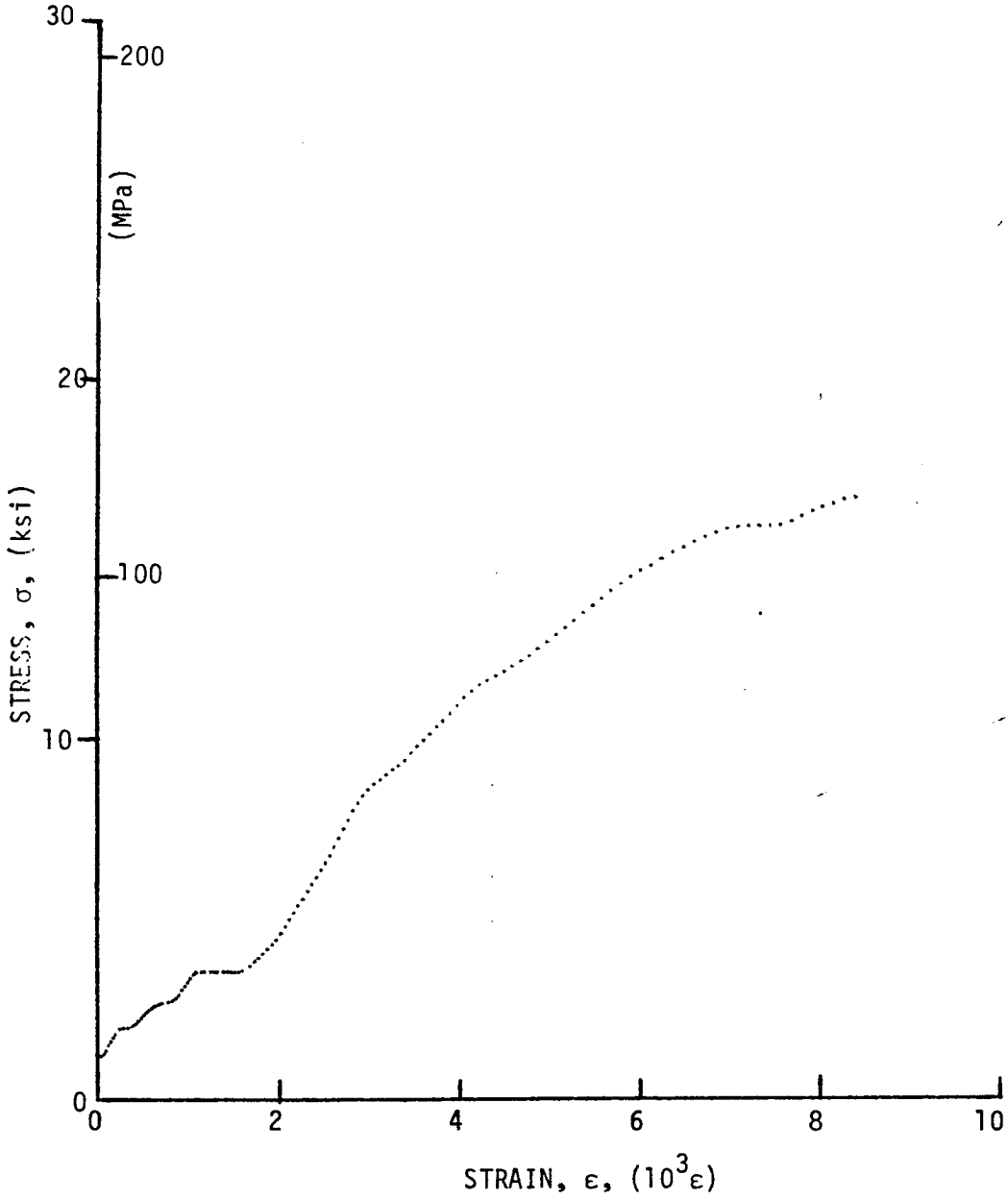

Figure 3-74. Stress-strain curve for dynamically loaded $[\pm 67.5]_{2s}$ 80AS/20S/PR288 graphite/S-glass/epoxy ring, Specimen No. 27-10.

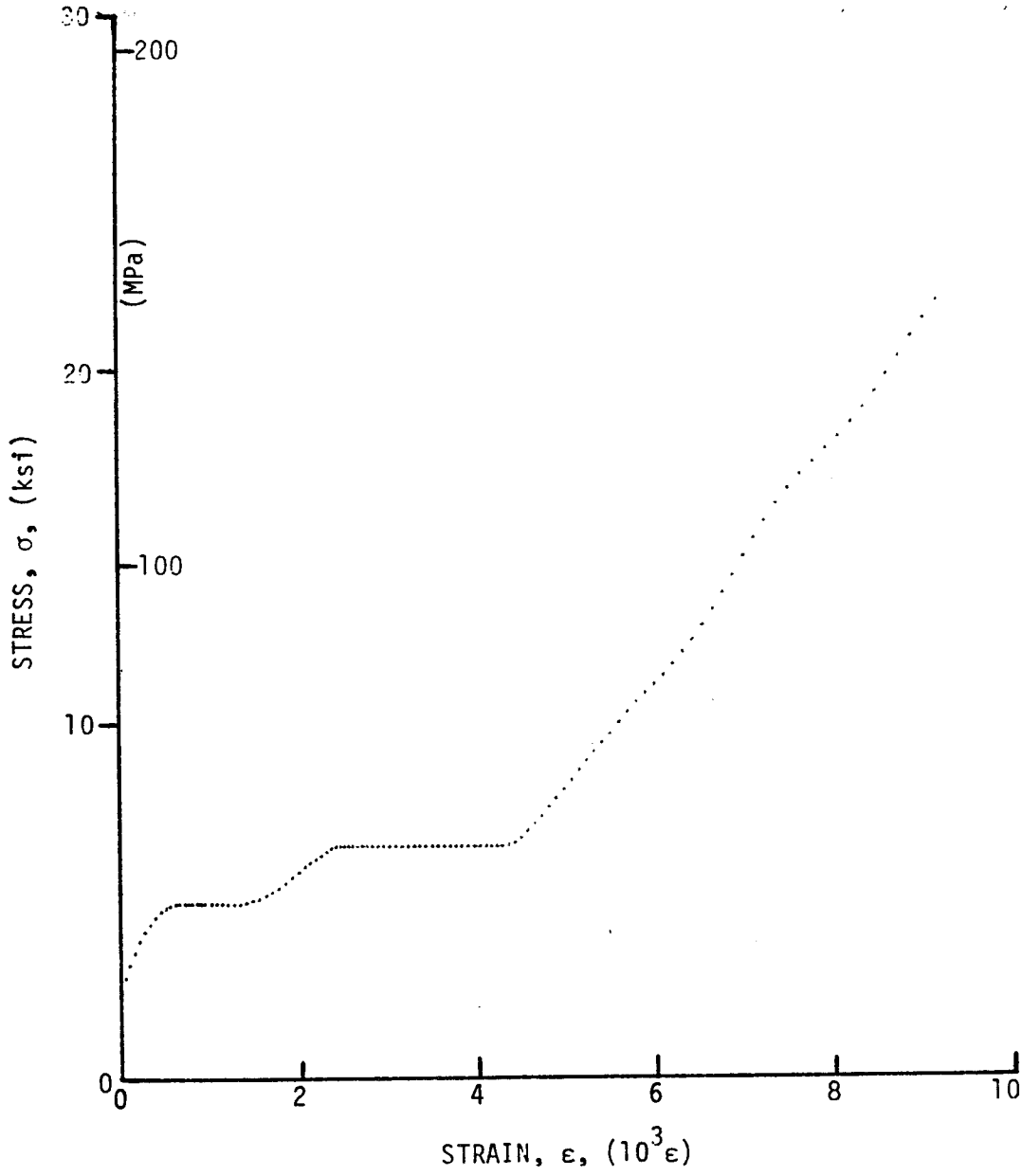

Figure 3-75. Stress-strain curve for dynamically loaded $[\pm 67.5]_{2s}$ 80AS/20S/PR288 graphite/S-glass/epoxy ring, Specimen No. 27-11.

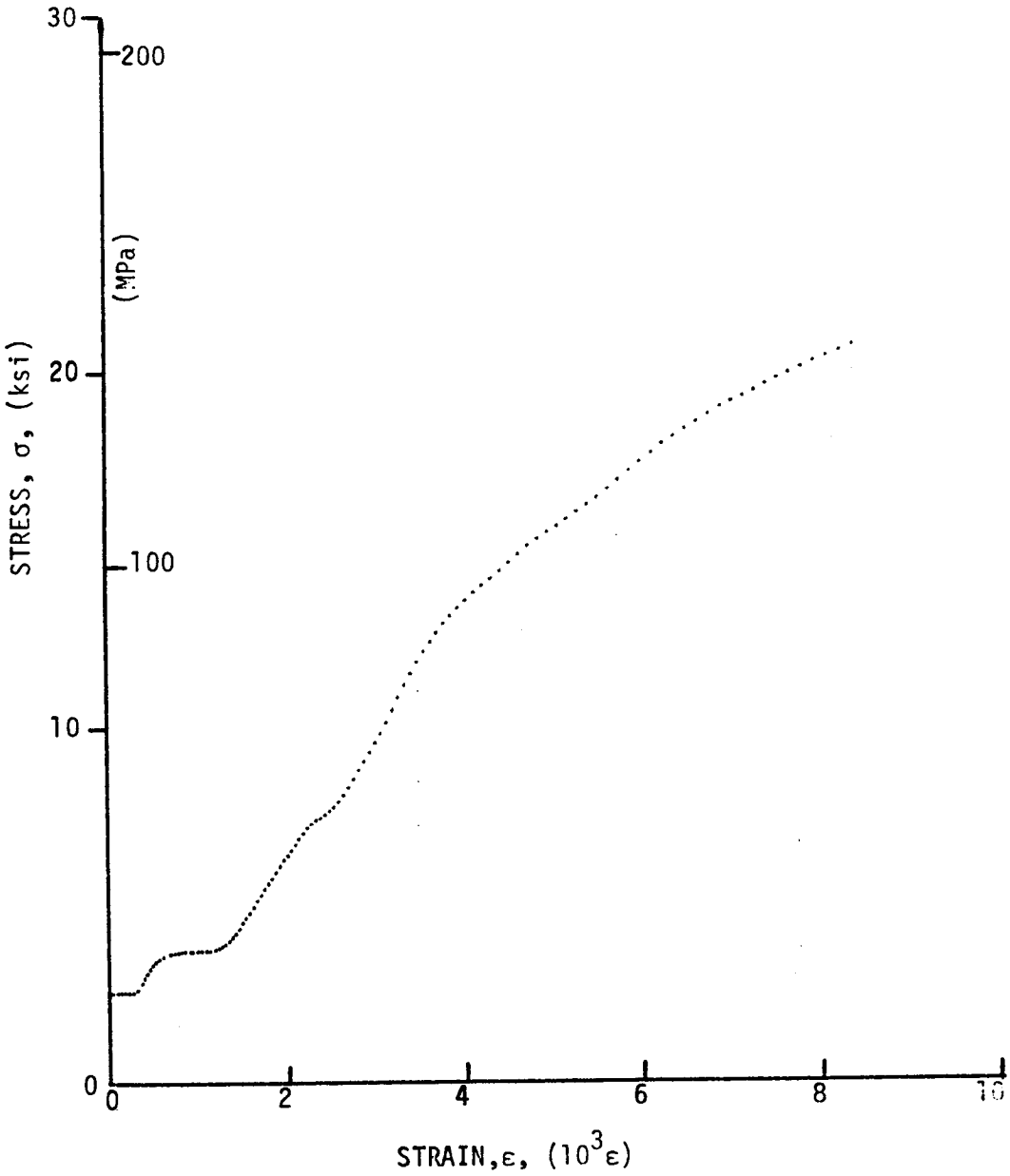

Figure 3-76. Stress-strain curve for dynamically loaded $[\pm 67.5]_{2s}$ 80AS/20S/PR288 graphite/S-glass/epoxy ring, Specimen No. 27-13.

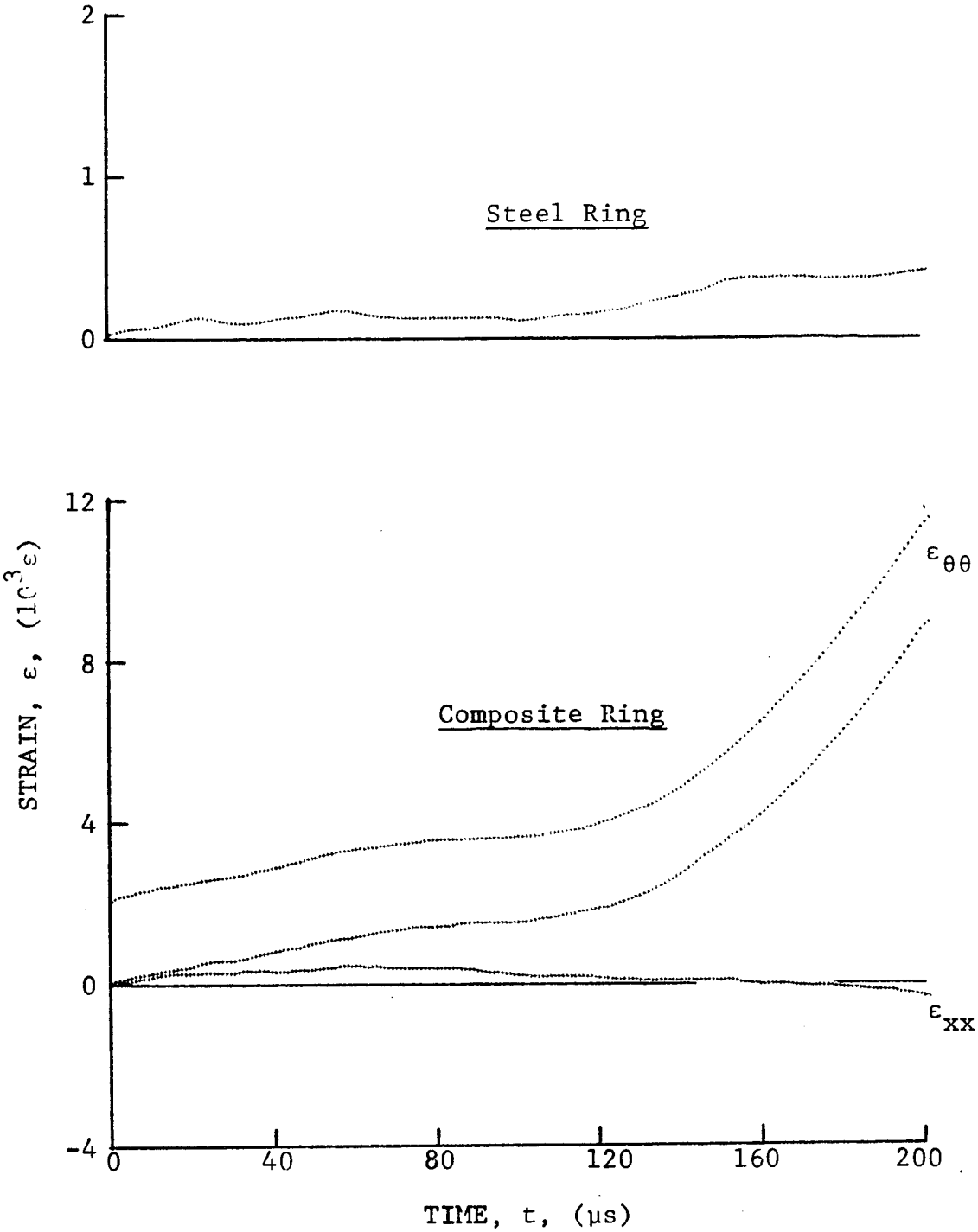

Figure 3-77. Strain records in steel ring and $[\pm 75]_{2s}$ SP288/AS graphite/epoxy ring under dynamic loading for Specimen No. 20-12 (0.65 g shotgun powder).

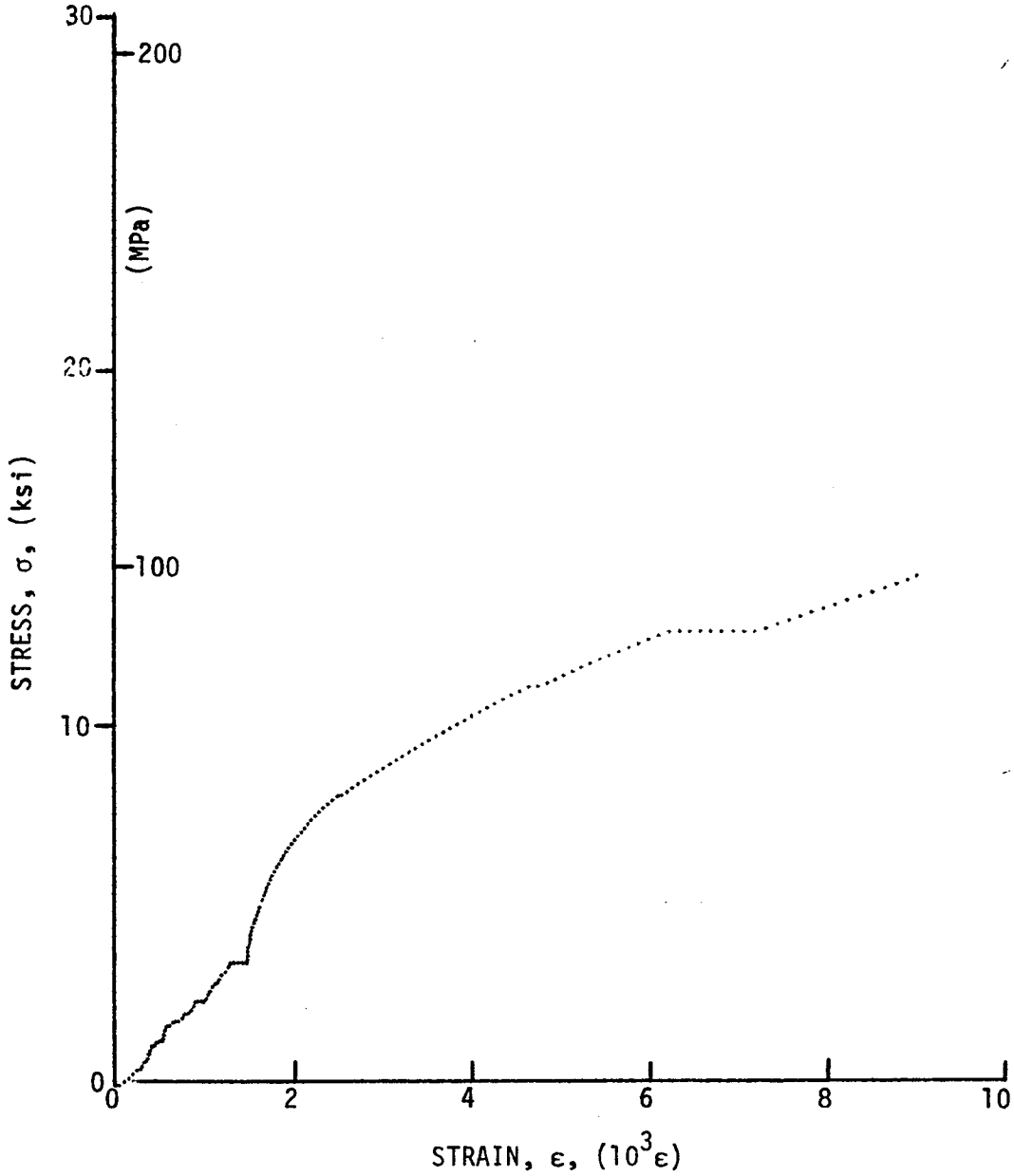

Figure 3-78. Stress-strain curve for dynamically loaded $[\pm 75]_{2s}$ graphite/epoxy ring, Specimen No. 20-12.

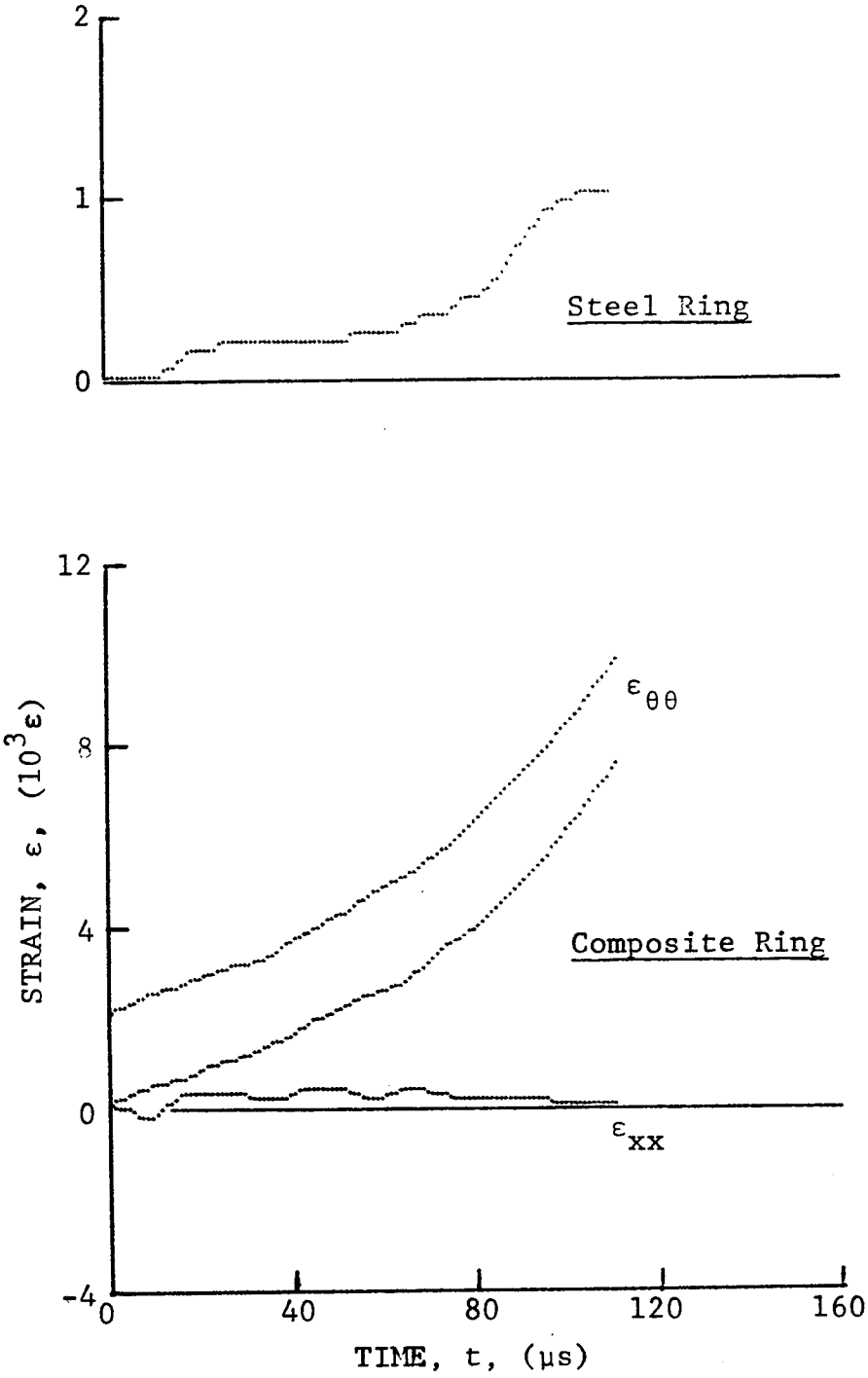

Figure 3-79. Strain records in steel ring and 80AS/20S/PR288 $[\pm 75]_{2S}$ graphite/S-glass/epoxy ring under dynamic loading for Specimen No. 21-10 (0.65 g shotgun powder).

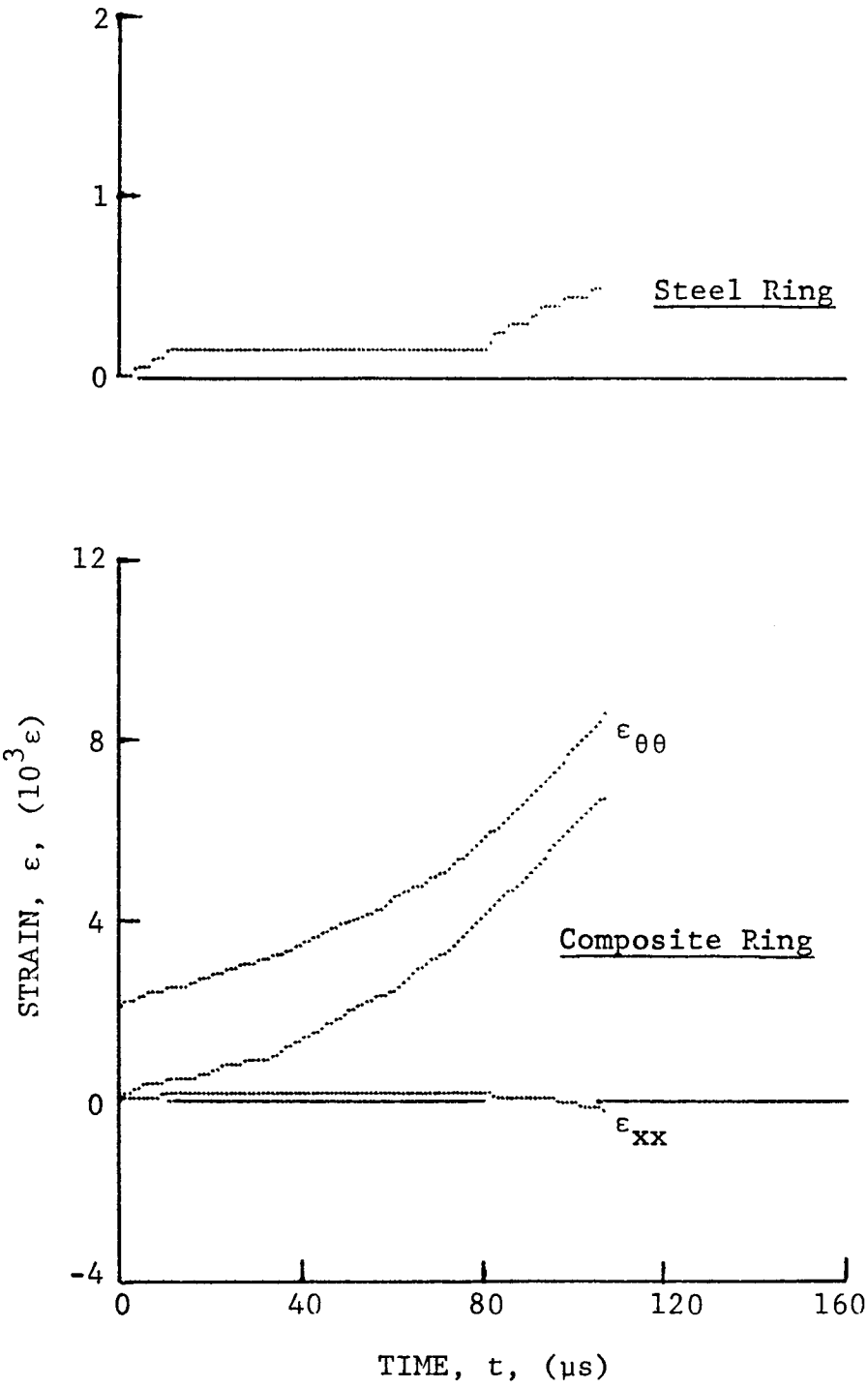

Figure 3-80. Strain records in steel ring and 80AS/20S/PR288 $[\pm 75]_{2S}$ graphite/S-glass/epoxy ring under dynamic loading for Specimen No. 21-11 (0.65 g shotgun powder).

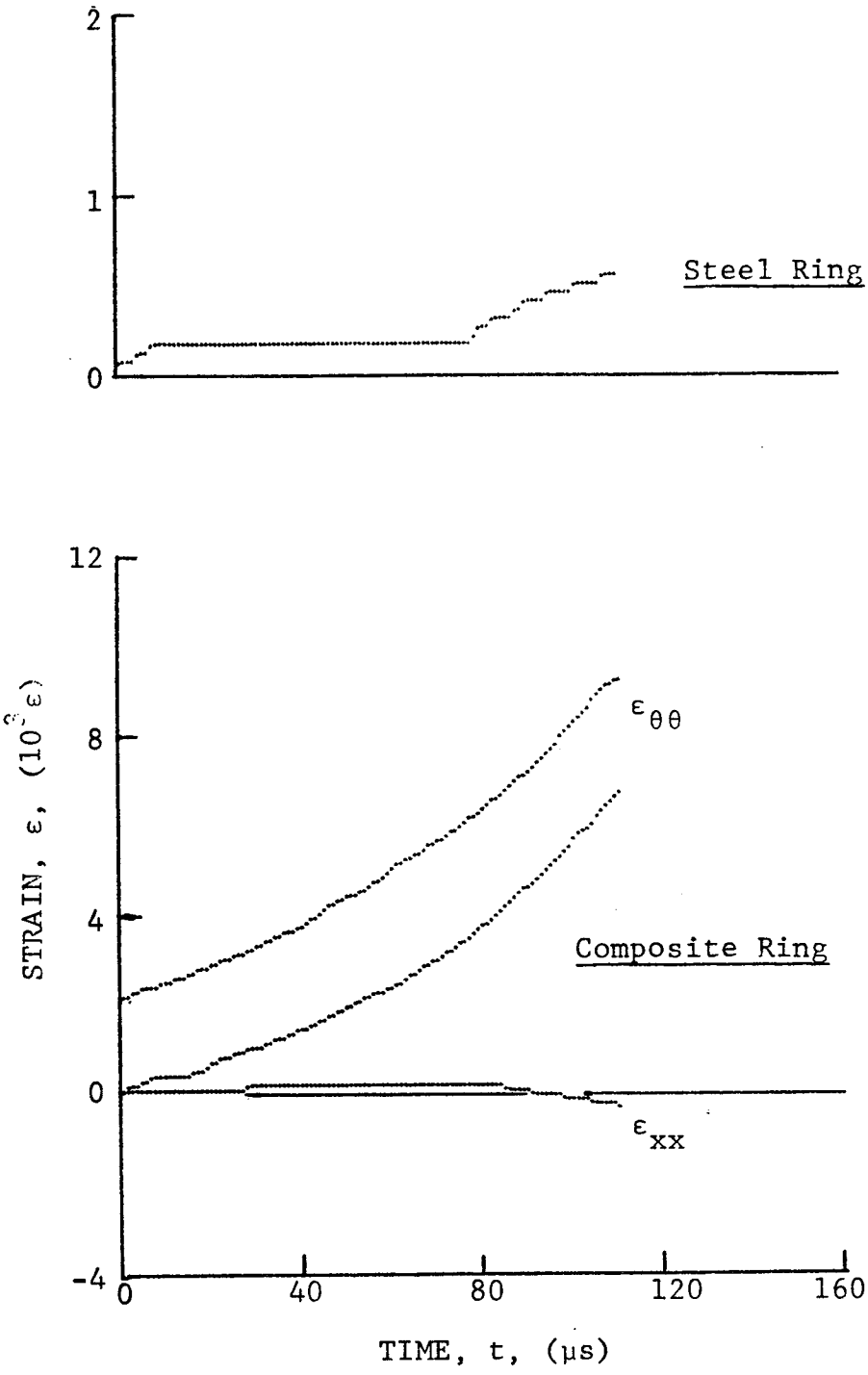

Figure 3-81. Strain records in steel ring and 80AS/20S/PR288 $[\pm 75]_{2S}$ graphite/S-glass/epoxy ring under dynamic loading for Specimen No. 21-12 (0.65 g shotgun powder).

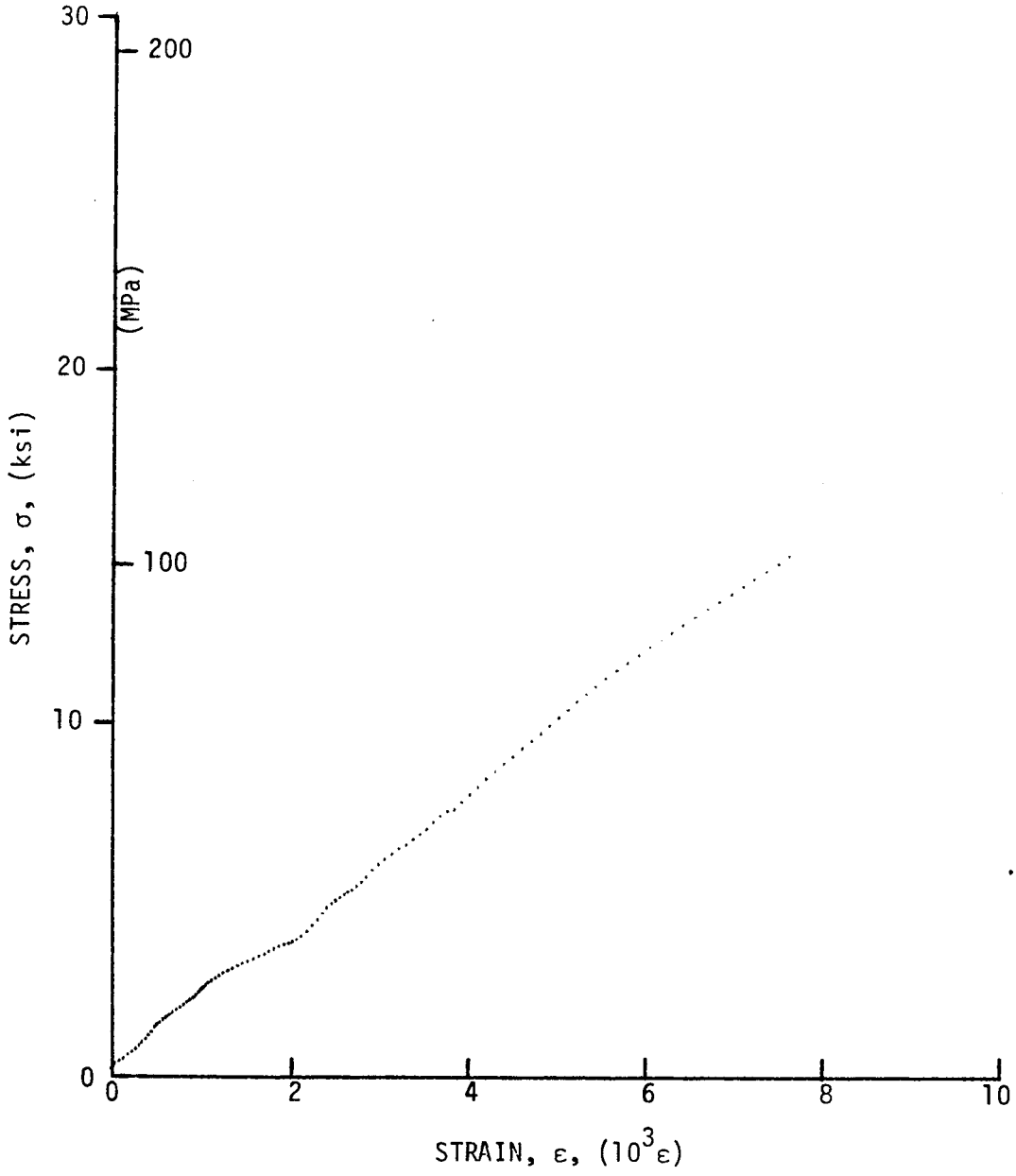

Figure 3-82. Stress-strain curve for dynamically loaded $[\pm 75]_{2S}$ 80AS/20S/PR288 graphite/S-glass/epoxy ring, Specimen No. 21-10.

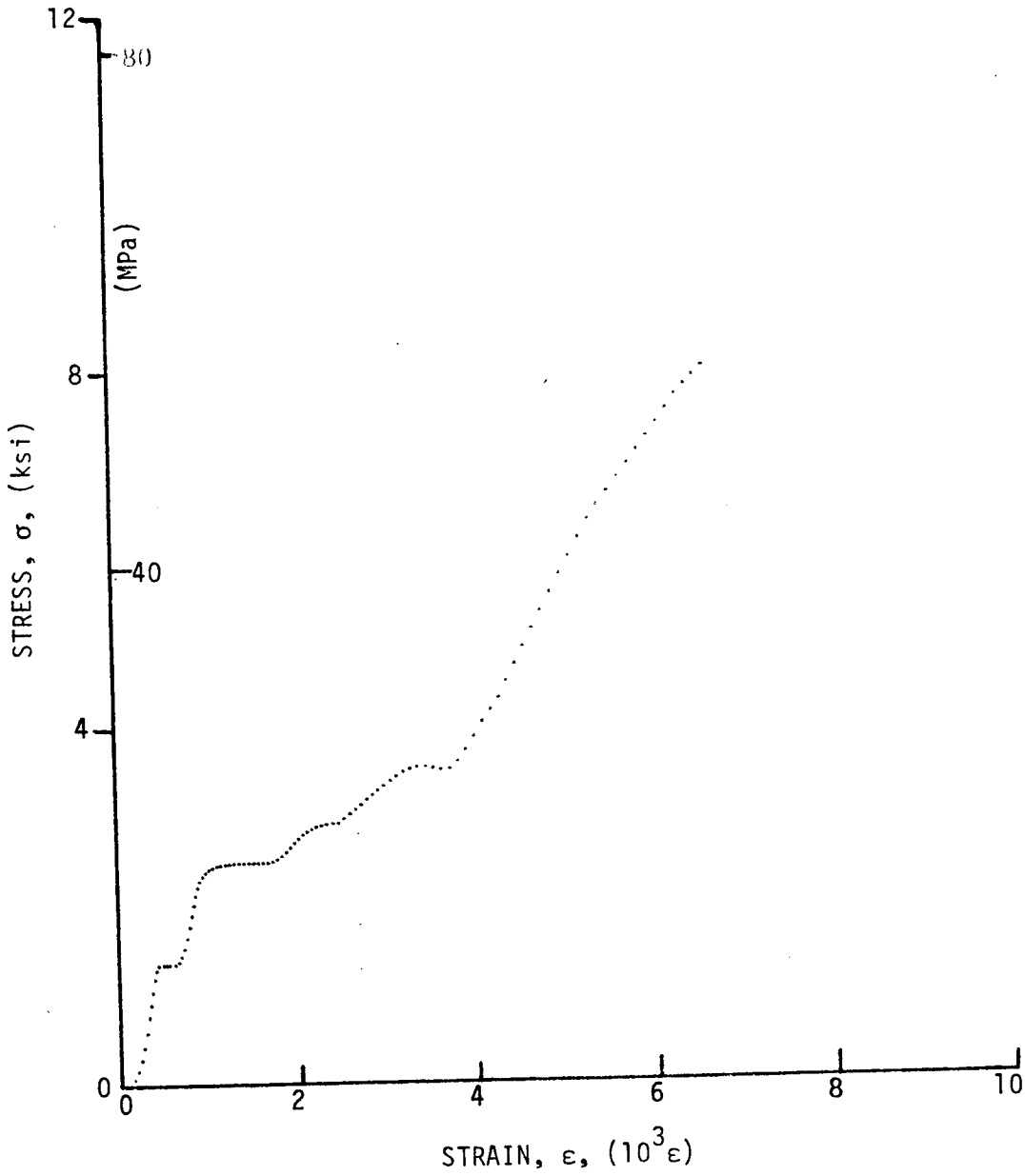

Figure 3-83. Stress-strain curve for dynamically loaded $[\pm 75]_{2s}$ 80AS/20S/PR288 graphite/S-glass/epoxy ring, Specimen No. 21-11.

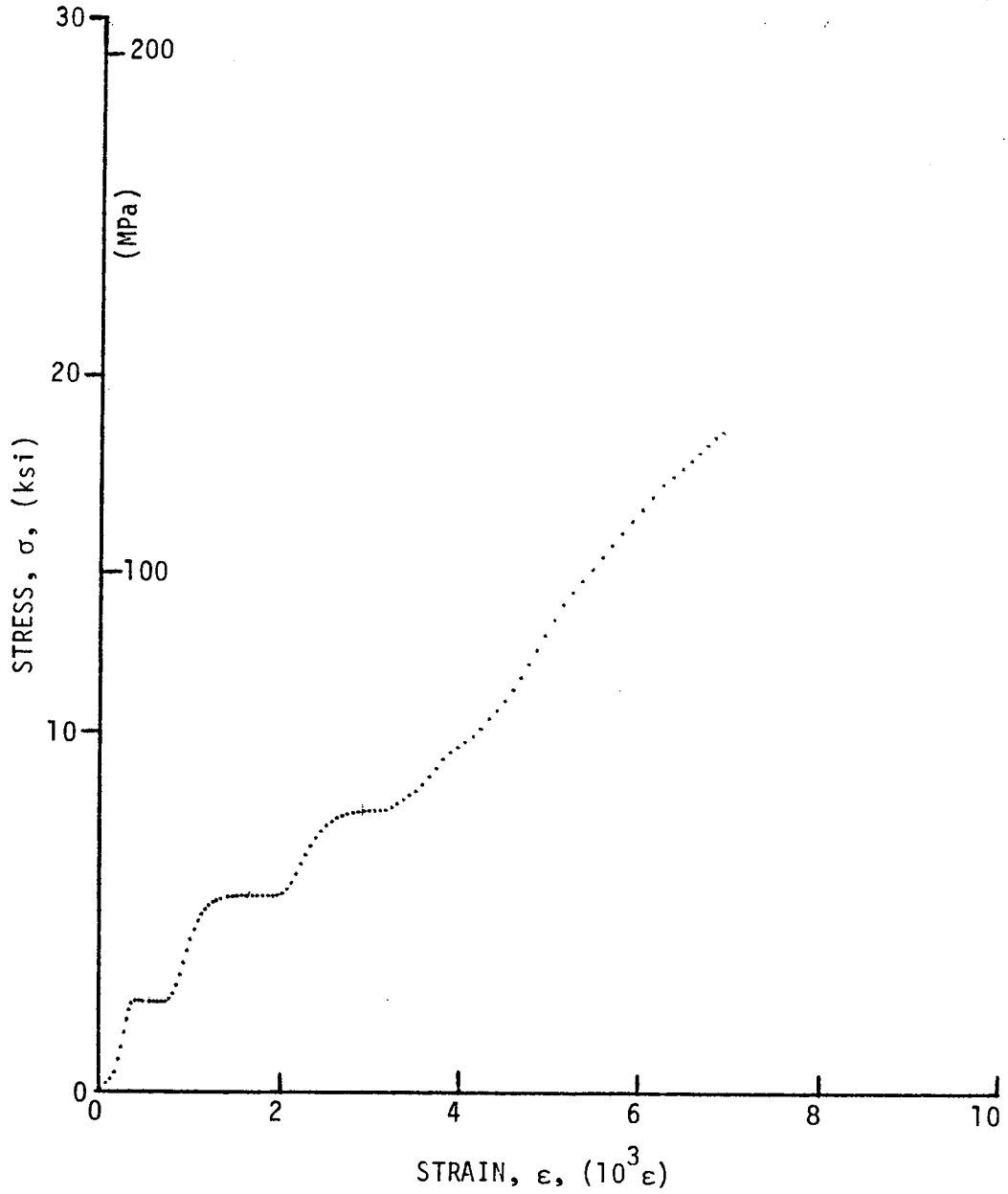

Figure 3-84. Stress-strain curve for dynamically loaded $[\pm 75]_{2s}$ 80AS/20S/PR288 graphite/S-glass/epoxy ring, Specimen No. 21-12.

4. HIGH STRAIN RATE TENSILE PROPERTIES OF ANGLE-PLY LAMINATES

4.1 $[\pm 15]_{2s}$ LAMINATES

High strain rate tensile properties of $[\pm 15]_{2s}$ SP288/AS graphite/epoxy and 80AS/20S/PR288 graphite/S-glass/epoxy were obtained by testing rings under dynamic internal pressure. Three rings of each material were loaded dynamically using 100 mg PETN detonators in the pressure chamber of the fixture. The circumferential and axial strains in the composite ring and the circumferential strain in the calibration steel ring were recorded in every case.

Strain and strain derivative records for the three graphite/epoxy rings tested are shown in Figures 4-1 through 4-9 (Specimen Nos. 35-2, 35-4, and 35-6). These data were analyzed following procedures described in Part I of this report. Dynamic stress-strain curves obtained by the digital processing oscilloscope are shown in Figures 4-10, 4-11, and 4-12. Results for the three rings tested are tabulated in Table 4-1. The initial strain rates range between $130s^{-1}$ and $250s^{-1}$ and the average (secant) rates between $175s^{-1}$ and $254s^{-1}$. The times to failure range between 35 μs and 44 μs. The initial and secant moduli of 113.2 GPa (16.4×10^6 psi) and 117.8 GPa (17.1×10^6 psi), respectively, are higher than the static modulus of 104.5 GPA (15.2×10^6 psi) by 8% and 12%, respectively. The overall average Poisson's ratio of 0.80 is lower than the static value of 0.86. The average dynamic strength of 1029 MPa (149 ksi) is higher than the static strength of 823 MPa (119.3 ksi) by 25%. The increase in dynamic strength is higher than the increase in dynamic modulus. The average dynamic ultimate strain of 0.0088 is higher than the static value of 0.0078. This trend in properties is related to some change in failure modes from those under quasi-static to those under dynamic loading conditions. Quasi-static failure modes include pronounced interlaminar shear failures. Under dynamic conditions, with the higher rate-dependent, matrix-dominated interlaminar shear properties, there is more brittle-like behavior with failures dominated primarily by fiber fractures.

TABLE 4-1. HIGH STRAIN RATE TENSILE PROPERTIES OF $[\pm 15]_{2s}$ SP288/AS GRAPHITE/EPOXY

Specimen Number	Strain Rate ($\dot{\varepsilon}_{\theta\theta}$), s^{-1}	Modulus ($E_{\theta\theta}$), GPa (10^6 psi)	Poisson's Ratio ($\nu_{\theta x}$)
		Initial Properties	
35-2	250	104.9 (15.2)	0.63
35-4	190	116.6 (16.9)	0.92
35-6	130	118.0 (17.1)	0.73
		Secant Properties	
35-2	243	110.4 (16.0)	0.61
35-4	254	109.0 (15.8)	0.89
35-6	175	133.9 (19.4)	1.02
		Terminal Properties	
35-2	270	117.3 (17.0)	0.71
35-4	300	104.2 (15.1)	-
35-6	250	113.9 (16.5)	-
		Ultimate Properties	
	Time to Failure (t_f), μs	Strength ($S_{\theta\theta T}$), MPa (ksi)	Strain ($\varepsilon^u_{\theta\theta T}$)
35-2	40	1080 (156)	0.0097
35-4	35	973 (141)	0.0089
35-6	44	1035 (150)	0.0077

Strain and strain derivative records for the three hybrid rings are shown in Figures 4-13 through 4-21 (Specimen Nos. 36-2, 36-4, and 36-7). Dynamic stress-strain curves are shown in Figures 4-22, 4-23, and 4-24. Results for the three rings tested are tabulated in Table 4-2. The initial strain rates range between $125s^{-1}$ and $150s^{-1}$ and the average (secant) rates between $173s^{-1}$ and $210s^{-1}$. The times to failure range between 40 μs and 45 μs. The initial and secant moduli of 133.2 GPa (19.3×10^6 psi) and 101.2 GPa (14.7×10^6 psi), respectively, are higher than the static modulus of 94.5 GPa (13.7×10^6 psi) by 41% and 7%, respectively. The average Poisson's ratio of 0.90 is higher than the static value of 0.68. The dynamic strength of 837 MPa (121 ksi) is only slightly higher than the static one of 806 MPa (117 ksi). This trend is contrary to the one observed in the graphite/epoxy specimens. The dynamic ultimate strain of 0.0083 is approximately equal to the static value of 0.0084.

4.2 $[\pm 22.5]_{2s}$ LAMINATES

High strain rate tensile properties of $[\pm 22.5]_{2s}$ SP288/AS graphite/epoxy and 80AS/20S/PR288 graphite/S-glass/epoxy were obtained by testing rings under dynamic internal pressure. Three rings of each material were loaded dynamically using 100 mg PETN detonators in the pressure chamber of the fixture. In one case, the pressure on the steel ring was also measured with a Manganin alloy gage.

Strain and strain derivative records for the three graphite/epoxy rings tested are shown in Figures 4-25 through 4-33 (Specimen Nos. 33-4, 33-6, and 33-7). Dynamic stress-strain curves are shown in Figures 4-34, 4-35, and 4-36. Results are tabulated in Table 4-3. The initial strain rates range between $130s^{-1}$ and $150s^{-1}$ and the average (secant) rates between $184s^{-1}$ and $211s^{-1}$. The times to failure range between 38 μs and 46 μs. The initial and secant moduli of 131.7 GPa (19.1×10^6 psi) and 93.4 GPa (13.5×10^6 psi), respectively, are higher than the static modulus of 81.4 GPa (11.8×10^6 psi) by 62% and 15%, respectively. The average dynamic secant Poisson's ratio of 1.22 is slightly higher than the static one of 1.18. The average dynamic strength of 790 MPa (115 ksi) is only slightly higher than the static one of 773 MPa (112 ksi). However, the dynamic ultimate strain of 0.0084 is appreciably lower than the static value of 0.0103.

TABLE 4-2. HIGH STRAIN RATE TENSILE PROPERTIES OF $[\pm 15]_{2s}$ 80AS/20S/PR288 GRAPHITE/S-GLASS/EPOXY

Specimen Number	Strain Rate ($\dot{\varepsilon}_{\theta\theta}$), s^{-1}	Modulus ($E_{\theta\theta}$), GPa (10^6 psi)	Poisson's Ratio ($\nu_{\theta x}$)
		Initial Properties	
36-2	150	131.1 (19.0)	0.97
36-4	145	122.1 (17.7)	0.62
36-7	125	146.3 (21.2)	1.06
		Secant Properties	
36-2	198	98.0 (14.2)	1.06
36-4	210	111.8 (16.2)	0.85
36-7	173	93.8 (13.6)	0.85
		Terminal Properties	
36-2	225	63.5 (9.2)	1.24
36-4	290	58.0 (8.4)	-
36-7	220	28.2 (4.1)	0.93
		Ultimate Properties	
	Time to Failure (t_f), μs	Strength ($S_{\theta\theta T}$), MPa (ksi)	Strain ($\varepsilon^u_{\theta\theta T}$)
36-2	44	849 (123)	0.0087
36-4	40	932 (135)	0.0084
36-7	45	731 (106)	0.0078

TABLE 4-3. HIGH STRAIN RATE TENSILE PROPERTIES OF $[\pm 22.5]_{2s}$ SP288/AS GRAPHITE/EPOXY

Specimen Number	Strain Rate ($\dot{\varepsilon}_{\theta\theta}$), s^{-1}	Modulus ($E_{\theta\theta}$), GPa (10^6 psi)	Poisson's Ratio ($\nu_{\theta x}$)
		Initial Properties	
33-4	135	131.1 (19.0)	1.66
33-6	150	140.2 (20.3)	1.50
33-7	130	123.9 (18.0)	1.54
		Secant Properties	
33-4	196	89.5 (13.0)	1.33
33-6	184	95.9 (13.9)	1.19
33-7	211	94.9 (13.7)	1.13
		Terminal Properties	
33-4	280	45.7 (6.6)	1.26
33-6	190	55.5 (8.1)	1.70
33-7	390	85.9 (12.4)	1.10
		Ultimate Properties	
	Time to Failure (t_f), μs	Strength ($S_{\theta\theta T}$), MPa (ksi)	Strain ($\varepsilon^u_{\theta\theta T}$)
33-4	46	806 (117)	0.0090
33-6	38	673 (98)	0.0070
33-7	44	890 (129)	0.0093

Strain and strain derivative records for the three hybrid rings are shown in Figures 4-37 through 4-45 (Specimen Nos. 34-4, 34-6, and 34-7). Dynamic stress-strain curves are shown in Figures 4-46, 4-47, and 4-48. Results are tabulated in Table 4-4. The initial strain rates range between $130s^{-1}$ and $140s^{-1}$ and the average (secant) rates between $198s^{-1}$ and $246s^{-1}$. The times to failure range between 45 μs and 46 μs. The initial and secant moduli of 126.1 GPa (18.3×10^6 psi) and 76.5 GPa (11.1×10^6 psi), respectively, are higher than the static modulus of 68.5 GPa (9.9×10^6 psi) by 84% and 12%, respectively. The average dynamic Poisson's ratio of 0.97 is higher than the static one of 0.83. The average dynamic strength of 731 MPa (106 ksi) is higher than the static strength of 653 MPa (95 ksi) by 12%. The dynamic ultimate strain of 0.0095 is somewhat lower than the static value of 0.0104.

4.3 $[\pm 30]_{2s}$ LAMINATES

High strain rate tensile properties of $[\pm 30]_{2s}$ SP288/AS graphite/epoxy and 80AS/20S/PR288 graphite/S-glass/epoxy were obtained by testing rings under dynamic internal pressure. Initially, 100 mg PETN detonators were used in the pressure chamber of the fixture. The pressure pulse produced by this loading, as seen from the strain response of the steel ring, reaches its peak in approximately 40 μs. The time to failure, however, is somewhat longer than that, which makes the analysis of the data very difficult. It was decided to modify the explosive detonation to produce a longer, but sufficiently intense, pressure pulse. The originally used black powder, or bullseye powder, was sufficiently slow-burning to produce a long pulse, but the intensity of this pulse was too low and resulted in relatively low strain rates. To boost the explosive energy of the normally fuel-rich bullseye powder potassium perchlorate ($KC\ell O_4$) and aluminum powder were mixed in. All subsequent tests were conducted using 520 mg of each component above in the pressure chamber. The resulting pressure pulse was longer than the time to failure of the $[\pm 30]_{2s}$ specimens and only slightly shorter than that for the $[\pm 45]_{2s}$ specimens.

One difficulty encountered in the past was in pinpointing the exact time of failure of the composite specimens. If initial failure does not happen to occur exactly at a gage location, the strain readings at the unfailed locations

TABLE 4-4. HIGH STRAIN RATE TENSILE PROPERTIES OF $[\ 22.5]_{2s}$ 80AS/20S/PR288 GRAPHITE/S-GLASS/EPOXY

Specimen Number	Strain Rate ($\dot{\varepsilon}_{\theta\theta}$), s^{-1}	Modulus ($E_{\theta\theta}$), GPa (10^6 psi)	Poisson's Ratio ($\nu_{\theta x}$)
		Initial Properties	
34-4	130	134.6 (19.5)	1.15
34-6	140	100.1 (14.5)	0.93
34-7	130	143.7 (20.8)	0.85
		Secant Properties	
34-4	198	73.6 (10.7)	1.06
34-6	246	79.2 (11.5)	0.87
34-7	208	76.6 (11.1)	0.99
		Terminal Properties	
34-4	300	26.9 (3.9)	1.16
34-6	308	50.0 (7.2)	0.84
34-7	280	29.3 (4.3)	1.07
		Ultimate Properties	
	Time to Failure (t_f), μs	Strength ($S_{\theta\theta T}$), MPa (ksi)	Strain ($\varepsilon^u_{\theta\theta T}$)
34-4	45	656 (95)	0.0089
34-6	46	819 (119)	0.0103
34-7	45	716 (104)	0.0094

continue to increase for some time after initial failure. To overcome this uncertainty a conductive ribbon was bonded around the entire circumference of the ring and connected to one of the tabs of one strain gage. The ribbon is a Micromeasurements Ni-clad copper ribbon of 0.025 mm x 0.397 mm (0.001 in. x 1/64 in.) cross section. This ribbon is first bonded on a strip of 104 type glass scrimcloth with Epon 815/V40 adhesive. After curing, the ribbon with the scrimcloth strip is bonded on the composite ring with Micromeasurements AE10 adhesive and connected in series with one of the leads of a circumferential strain gage. When the specimen fails at any point around the circumference the ribbon breaks and strain readings from the gage connected to the ribbon are interrupted.

Tests on the $[\ 30]_{2s}$ laminates were repeated using a 1560 mg mixture of equal amounts of bullseye pistol powder, potassium perchlorate ($KC\ell O_4$), and aluminum dust. Strain and strain derivative records for the three graphite/epoxy rings tested are shown in Figures 4-49 through 4-55 (Specimen Nos. 28-9, 28-10, and 28-11). Stress-strain curves are shown in Figures 4-56, 4-57, and 4-58. Results are tabulated in Table 4-5. The initial strain rates range between $200s^{-1}$ and $230s^{-1}$ and the average (secant) rates between $285s^{-1}$ and $320s^{-1}$. The times to failure range between 44 μs and 45 μs. The initial and secant moduli of 85.7 GPa (12.4×10^6 psi) and 49.8 GPa (7.2×10^6 psi), respectively, are higher and lower than the static modulus of 58.6 GPa (8.5×10^6 psi) by 46% and 15%, respectively. The average dynamic Poissons's ratio of 1.21 is only slightly lower than the static one of 1.25. The average dynamic strength of 660 MPa (96 ksi) is higher than the static one of 566 MPa (82 ksi) by 17%. The dynamic ultimate strain of 0.0133 is almost equal to the static value of 0.0132.

Strain and strain derivative records for the three hybrid rings are shown in Figures 4-59 through 4-64 (Specimen Nos. 29-10, 29-11, and 29-12). Stress-strain curves are shown in Figures 4-65, 4-66, and 4-67. Results are tabulated in Table 4-6. The initial strain rates range between $190s^{-1}$ and $230s^{-1}$ and the average (secant) rates between $300s^{-1}$ and $340s^{-1}$. The times to failure range between 40 μs and 43 μs. The initial and secant moduli of 93.5 GPa (13.6×10^6 psi) and 51.5 GPa (7.5×10^6 psi), respectively, are higher than the static modulus of 44.9 GPa (6.51×10^6 psi) by 108% and 15%, respectively.

TABLE 4-5. HIGH STRAIN RATE TENSILE PROPERTIES OF $[\pm 30]_{2s}$ SP288/AS GRAPHITE/EPOXY

Specimen Number	Strain Rate ($\dot{\varepsilon}_{\theta\theta}$), s^{-1}	Modulus ($E_{\theta\theta}$), GPa (10^6 psi)	Poisson's Ratio ($\nu_{\theta x}$)
		Initial Properties	
28-9	230	84.0 (12.2)	-
28-10	230	82.8 (12.0)	1.09
28-11	200	90.2 (13.1)	1.35
		Secant Properties	
28-9	320	46.8 (6.8)	-
28-10	285	49.1 (7.1)	1.19
28-11	286	53.5 (7.8)	1.21
		Terminal Properties	
28-9	465	41.0 (5.9)	-
28-10	400	27.3 (4.0)	1.25
28-11	420	37.3 (5.4)	1.07
		Ultimate Properties	
	Time to Failure (t_f), μs	Strength ($S_{\theta\theta T}$), MPa (ksi)	Strain ($\varepsilon^u_{\theta\theta T}$)
28-9	44	664 (96)	0.0142
28-10	45	626 (91)	0.0128
28-11	45	690 (100)	0.0129

TABLE 4-6. HIGH STRAIN RATE TENSILE PROPERTIES OF $[\pm 30]_{2s}$ 80AS/20S/PR288 GRAPHITE/S-GLASS/EPOXY

Specimen Number	Strain Rate ($\dot{\varepsilon}_{\theta\theta}$), s^{-1}	Modulus ($E_{\theta\theta}$), GPa (10^6 psi)	Poisson's Ratio ($\nu_{\theta x}$)
		Initial Properties	
29-10	200	100.6 (14.6)	1.08
29-11	190	95.9 (13.9)	1.18
29-12	230	84.0 (12.2)	1.09
		Secant Properties	
29-10	300	59.8 (8.7)	1.13
29-11	340	48.1 (7.0)	1.00
29-12	333	46.6 (6.8)	1.05
		Terminal Properties	
29-10	400	48.8 (7.1)	1.79
29-11	440	41.1 (6.0)	1.48
29-12	480	39.2 (5.7)	1.25
		Ultimate Properties	
	Time to Failure (t_f), μs	Strength ($S_{\theta\theta T}$), MPa (ksi)	Strain ($\varepsilon^u_{\theta\theta T}$)
29-10	40	699 (101)	0.0116
29-11	43	707 (102)	0.0147
29-12	43	666 (97)	0.0143

The average dynamic Poisson's ratio of 1.09 is lower than the static one of 1.26. The average dynamic strength of 690 MPa (100 ksi) is much higher than the static one of 503 MPa (73 ksi) by 37%. The dynamic ultimate strain of 0.0135 is only slightly lower than the static value of 0.0139.

Comparison of the results for the graphite/epoxy and hybrid $[\pm 30]_{2s}$ specimens (Tables 4-5 and 4-6) shows that the hybrid specimens have higher dynamic moduli and strength than the graphite/epoxy ones. This is contrary to the trend in static values. This phenomenon, for which no ready explanation is available, was not noticed in the $[\pm 22.5]_{2s}$ specimens.

4.4 $[\pm 45]_{2s}$ LAMINATES

High strain rate tensile properties of $[\pm 45]_{2s}$ SP288/AS graphite/epoxy and 80AS/20S/PR288 graphite/S-glass/epoxy were obtained by testing rings under dynamic internal pressure using a 1.56 g mixture of pistol powder, $KC\ell O_4$, and aluminum dust in the pressure chamber of the fixture.

Strain and strain derivative records for the three graphite/epoxy rings tested are shown in Figures 4-68 through 4-76 (Specimen Nos. 24-11, 24-12, and 24-13). The corresponding stress-strain curves are shown in Figures 4-77, 4-78, and 4-79. These curves were extrapolated up to the maximum strain measured in the composite ring (ultimate strain). Results are tabulated in Table 4-7. The initial strain rates range between $140s^{-1}$ and $200s^{-1}$ and the average (secant) rates between $220s^{-1}$ and $440s^{-1}$. The times to failure range between 68 μs and 91 μs. The initial and secant moduli of 111.4 GPa (16.15 x 10^6 psi) and 40.3 GPa (5.83 x 10^6 psi), respectively, are much higher than the static modulus of 20.4 GPa (2.95 x 10^6 psi). The secant modulus above was based on the extrapolated stress-strain curve. The average initial Poisson's ratio of 0.78 is also higher than the static value of 0.69. The average dynamic strength obtained approximately by extrapolation of the stress-strain curve is 927 MPa (134 ksi) which is much higher than the static strength of 224 MPa (32.5 ksi). The average dynamic ultimate strain of 0.0245 is lower than the static value of 0.0305.

Strain and strain derivative records for the three hybrid rings tested are shown in Figures 4-80 through 4-88 (Specimen Nos. 25-11, 25-12, and 25-13). The corresponding stress-strain curves are shown in Figures 4-89, 4-90, and

TABLE 4-7. HIGH STRAIN RATE TENSILE PROPERTIES OF $[\pm 45]_{2s}$ SP288/AS GRAPHITE/EPOXY

Specimen Number	Strain Rate ($\dot{\varepsilon}_{\theta\theta}$), s^{-1}	Modulus ($E_{\theta\theta}$), GPa (10^6 psi)	Poisson's Ratio ($\nu_{\theta x}$)
		Initial Properties	
24-11	200	98.3 (14.25)	0.95
24-12	140	111.8 (16.20)	0.68
24-13	165	124.2 (18.00)	0.72
		Secant Properties	
24-11	440	23.8 (3.45)	0.90
24-12	330	44.5 (6.45)	0.89
24-13	220	52.4 (7.60)	0.69
		Terminal Properties	
24-11	550	8.6 (1.25)	0.91
24-12	435	26.9 (3.90)	0.99
24-13	260	25.9 (3.75)	0.75
		Ultimate Properties	
	Time to Failure (t_f), μs	Strength ($S_{\theta\theta T}$), MPa (ksi)	Strain ($\varepsilon^u_{\theta\theta T}$)
24-11	>70	738 (107)	0.0310
24-12	68	1000 (145)	0.0225
24-13	91	1042 (151)	0.0200

4-91. Results are tabulated in Table 4-8. The initial strain rates range between $250s^{-1}$ and $300s^{-1}$ and the average (secant) rates between $550s^{-1}$ and $560s^{-1}$. The times to failure range between 52 μs and 70 μs.

The initial dynamic modulus of 50.8 GPa (7.37×10^6 psi) is much higher than the static modulus of 21.5 GPa (3.12×10^6 psi). The average Poisson's ratio (initial and secant) of 0.76 is slightly higher than the static value of 0.74. The average dynamic strength of 711 MPa (103 ksi) is much higher than the static strength of 191 MPa (28 ksi). The average dynamic ultimate strain, based on the larger recorded values in each specimen, of 0.0353 is also higher than the highest static value recorded (0.0265). It should be noted that the static value for strength and ultimate strain are lower bounds since the specimens could not be tested to ultimate failure.

4.5 $[\pm 60]_{2s}$ LAMINATES

High strain rate tensile properties of $[\pm 60]_{2s}$ SP288/AS graphite/epoxy and 80AS/20S/PR288 graphite/S-glass/epoxy were obtained in a similar manner as before.

Strain and strain derivative records for the three graphite/epoxy rings tested are shown in Figures 4-92 through 4-100 (Specimen Nos. 22-6, 22-7, and 22-8). The corresponding stress-strain curves are shown in Figures 4-101, 4-102, and 4-103. Results are tabulated in Table 4-9. The initial strain rates range between $220s^{-1}$ and $280s^{-1}$ and the average (secant) rates between $307s^{-1}$ and $398s^{-1}$. The times to failure range between 41 μs and 44 μs. The initial and secant moduli of 45.5 GPa (6.59×10^6 psi) and 34.6 GPa (5.02×10^6 psi), respectively, are much higher than the static modulus of 13.4 GPa (1.95×10^6 psi). The average secant Poisson's ratio of 0.34 is only slightly higher than the static value of 0.32. The average dynamic strength of 511 MPa (74 ksi) is much higher than the static strength of 105 MPa (15.2 ksi). The average dynamic ultimate strain of 0.0145 is higher than the static value of 0.0120.

Strain and strain derivative records for the three hybrid rings are shown in Figures 4-104 through 4-112 (Specimen Nos. 23-2, 23-4, and 23-6). The corresponding stress-strain curves are shown in Figures 4-113, 4-114, and 4-115. Results are tabulated in Table 4-10. The initial strain rates range

TABLE 4-8. HIGH STRAIN RATE TENSILE PROPERTIES OF $[\pm 45]_{2s}$ 80AS/20S/PR288 GRAPHITE/S-GLASS/EPOXY

Specimen Number	Strain Rate ($\dot{\varepsilon}_{\theta\theta}$), s^{-1}	Modulus ($E_{\theta\theta}$), GPa (10^6 psi)	Poisson's Ratio ($\nu_{\theta x}$)
		Initial Properties	
25-11	280	43.1 (6.25)	0.85
25-12	300	59.3 (8.60)	0.73
25-13	250	50.0 (7.25)	0.69
		Secant Properties	
25-11	555	19.1 (2.77)	0.96
25-12	560	22.9 (3.32)	0.56
25-13	550	19.0 (2.75)	0.80
		Terminal Properties	
25-11	1000	4.1 (0.60)	0.59
25-12	800	6.6 (0.95)	0.63
25-13	760	3.7 (0.53)	0.59
		Ultimate Properties	
	Time to Failure (t_f), μs	Strength ($S_{\theta\theta T}$), MPa (ksi)	Strain ($\varepsilon^u_{\theta\theta T}$)
25-11	70	745 (108)	0.0390
25-12	52	662 (96)	0.0290
25-13	69	725 (105)	0.0380

TABLE 4-9. HIGH STRAIN RATE TENSILE PROPERTIES OF $[\pm 60]_{2s}$ SP288/AS GRAPHITE/EPOXY

Specimen Number	Strain Rate ($\dot{\varepsilon}_{\theta\theta}$), s^{-1}	Modulus ($E_{\theta\theta}$), GPa (10^6 psi)	Poisson's Ratio ($\nu_{\theta x}$)
		Initial Properties	
22-6	280	46.1 (6.68)	0.50
22-7	220	43.1 (6.25)	0.45
22-8	250	47.3 (6.85)	0.50
		Secant Properties	
22-6	398	37.8 (5.47)	0.32
22-7	307	27.3 (3.96)	0.33
22-8	320	38.8 (5.62)	0.36
		Terminal Properties	
22-6	640	28.6 (4.15)	0.34
22-7	520	17.3 (2.58)	0.35
22-8	480	31.2 (4.52)	0.34
		Ultimate Properties	
	Time to Failure (t_f), μs	Strength ($S_{\theta\theta T}$), MPa (ksi)	Strain ($\varepsilon^u_{\theta\theta T}$)
22-6	41	621 (90)	0.0163
22-7	44	367 (53)	0.0135
22-8	43	543 (79)	0.0138

TABLE 4-10. HIGH STRAIN RATE TENSILE PROPERTIES OF $[\pm 60]_{2s}$ 80AS/20S/PR288 GRAPHITE/S-GLASS/EPOXY

Specimen Number	Strain Rate ($\dot{\varepsilon}_{\theta\theta}$), s^{-1}	Modulus ($E_{\theta\theta}$), GPa (10^6 psi)	Poisson's Ratio ($\nu_{\theta x}$)
		Initial Properties	
23-2	140	45.2 (6.55)	0.32
23-4	270	56.4 (8.17)	0.39
23-6	250	42.4 (6.15)	0.30
		Secant Properties	
23-2	200	52.9 (7.67)	0.31
23-4	288	47.4 (6.87)	0.32
23-6	352	41.7 (6.05)	0.24
		Terminal Properties	
23-2	330	55.5 (8.05)	0.27
23-4	390	34.0 (4.93)	0.28
23-6	600	38.0 (5.50)	0.16
		Ultimate Properties	
	Time to Failure (t_f), μs	Strength ($S_{\theta\theta T}$), MPa (ksi)	Strain ($\varepsilon^u_{\theta\theta T}$)
23-2	51	535 (78)	0.0102
23-4	40	545 (79)	0.0115
23-6	42	618 (89)	0.0148

between $140s^{-1}$ and $270s^{-1}$ and the average (secant) rates between $200s^{-1}$ and $352s^{-1}$. The times to failure range between 40 μs and 51 μs. The initial and secant moduli of 48.0 GPa (6.96 x 10^6 psi) and 47.4 GPa (6.86 x 10^6 psi), respectively, are much higher than the static modulus of 15.2 GPa (2.20 x 10^6 psi). The average secant Poisson's ratio of 0.29 is exactly equal to the static value. The average dynamic strength of 566 MPa (82 ksi) is much higher than the static strength of 94.8 MPa (13.7 ksi). The average dynamic ultimate strain of 0.0122 is appreciably higher than the static value of 0.0087.

Comparison of the results above with those for the similarly oriented graphite/epoxy specimens shows that the hybrid specimens have higher dynamic moduli and strength than the graphite/epoxy specimens. This is contrary to the trend in static strength values.

4.6 $[\pm 67.5]_{2S}$ LAMINATES

High strain rate tensile properties of $[\pm 67.5]_{2S}$ SP288/AS graphite/epoxy and 80AS/20S/PR288 graphite/S-glass/epoxy were obtained as for the other laminates before.

Strain and strain derivative records for the three graphite/epoxy rings tested are shown in Figures 4-116 through 4-124 (Specimen Nos. 26-2, 26-4, and 26-6). The corresponding stress-strain curves are shown in Figures 4-125, 4-126, and 4-127. Results are tabulated in Table 4-11. The initial strain rates range between $200s^{-1}$ and $290s^{-1}$ and the average (secant) rates between $230s^{-1}$ and $310s^{-1}$. The times to failure range between 30 μs and 44 μs. The initial and secant moduli of 48.8 GPa (7.07 x 10^6 psi) and 36.2 GPa (5.24 x 10^6 psi), respectively, are much higher than the static modulus of 12.0 GPa (1.74 x 10^6 psi). The average Poisson's ratio of 0.19 is only slightly higher than the static value of 0.17. The average dynamic strength of 339 MPa (49 ksi) is much higher than the static strength of 85.1 MPa (12.3 ksi). The average dynamic ultimate strain of 0.0096 is somewhat higher than the static value of 0.0081.

Strain and strain derivative records for the three hybrid rings tested are shown in Figures 4-128 through 4-136 (Specimen Nos. 27-2, 27-4, and 27-6). The corresponding stress-strain curves are shown in Figures 4-137, 3-138, and 4-139. Results are tabulated in Table 4-12. The initial strain rates range

TABLE 4-11. HIGH STRAIN RATE TENSILE PROPERTIES OF $[\pm 67.5]_{2s}$ SP288/AS GRAPHITE/EPOXY

Specimen Number	Strain Rate ($\dot{\varepsilon}_{\theta\theta}$), s^{-1}	Modulus ($E_{\theta\theta}$), GPa (10^6 psi)	Poisson's Ratio ($\nu_{\theta x}$)
		Initial Properties	
26-2	290	52.2 (7.56)	0.18
26-4	240	50.9 (7.37)	0.20
26-6	200	43.3 (6.28)	0.13
		Secant Properties	
26-2	310	36.4 (5.27)	0.19
26-4	270	43.6 (6.32)	0.18
26-6	230	28.5 (4.12)	0.19
		Terminal Properties	
26-2	350	22.4 (3.25)	0.13
26-4	320	22.9 (3.31)	0.11
26-6	370	23.4 (3.39)	0.37
		Ultimate Properties	
	Time to Failure (t_f), μs	Strength ($S_{\theta\theta T}$), MPa (ksi)	Strain ($\varepsilon^u_{\theta\theta T}$)
26-2	30	334 (48)	0.0095
26-4	34	395 (57)	0.0092
26-6	44	289 (42)	0.0102

TABLE 4-12. HIGH STRAIN RATE TENSILE PROPERTIES OF $[\pm 67.5]_{2s}$ 80AS/20S/PR288 GRAPHITE/S-GLASS/EPOXY

Specimen Number	Strain Rate ($\dot{\varepsilon}_{\theta\theta}$), s^{-1}	Modulus ($E_{\theta\theta}$), GPa (10^6 psi)	Poisson's Ratio ($\nu_{\theta x}$)
		Initial Properties	
27-2	280	45.3 (6.56)	0.26
27-4	204	44.7 (6.48)	0.19
27-6	300	80.2 (11.62)	0.23
		Secant Properties	
27-2	224	54.3 (7.86)	0.21
27-4	204	36.5 (5.29)	0.24
27-6	280	37.3 (5.40)	0.16
		Terminal Properties	
27-2	180	75.9 (11.00)	0.21
27-4	205	26.9 (3.90)	0.21
27-6	375	22.4 (3.25)	0.08
		Ultimate Properties	
	Time to Failure (t_f), μs	Strength ($S_{\theta\theta T}$), MPa (ksi)	Strain ($\varepsilon^u_{\theta\theta T}$)
27-2	39	474 (69)	0.0087
27-4	38	280 (41)	0.0078
27-6	30	311 (45)	0.0085

between $204s^{-1}$ and $300s^{-1}$ and the average (secant) rates between $204s^{-1}$ and $280s^{-1}$. The times to failure range between 30 μs and 39 μs. The initial modulus for Specimen No. 27-6 is excessively high as seen also in the stress-strain curve of Figure 4-139. In comparing dynamic and static values for the moduli, the value for Specimen No. 27-6 was not considered. The initial and secant dynamic moduli of 45.0 GPa (6.52 x 10^6 psi) and 42.7 GPa (6.18 x 10^6 psi), respectively, are much higher than the static modulus of 14.4 GPa (2.08 x 10^6 psi). The average Poisson's ratio of 0.20 is also higher than the static value of 0.16. The average dynamic strength of 356 MPa (52 ksi) is much higher than the static strength of 76.1 MPa (11.0 ksi). The average dynamic ultimate strain of 0.0083 is higher than the static value of 0.0062.

Comparison of these results with those of the graphite/epoxy specimens show that the hybrid specimens have higher dynamic moduli and strength than the graphite/epoxy specimens. This is contrary to the trend in static strength values.

4.7 $[\pm 75]_{2s}$ LAMINATES

High strain rate properties of $[\pm 75]_{2s}$ SP288/AS graphite/epoxy and 80AS/20S/PR288 graphite/S-glass/epoxy were obtained as for the other laminates before.

Strain and strain derivative records for the three graphite/epoxy rings tested are shown in Figures 4-140 through 4-148 (Specimen Nos. 20-2, 20-4, and 20-7). The corresponding stress-strain curves are shown in Figures 4-149, 4-150, and 4-151. Results are tabulated in Table 4-13. The initial strain rates range between $220s^{-1}$ and $245s^{-1}$ and the average (secant) rates between $253s^{-1}$ and $286s^{-1}$. The times to failure range between 29 μs and 30 μs. The initial and secant dynamic moduli of 45.2 GPa (6.55 x 10^6 psi) and 36.1 GPa (5.24 x 10^6 psi), respectively, are much higher than the static modulus of 11.2 GPa (1.63 x 10^6 psi). It was difficult to obtain reliable values for dynamic Poisson's ratio because of the large scatter in the transverse strain data. The average dynamic strength of 290 MPa (42 ksi) is much higher than the static strength of 75 MPa (10.8 ksi). The average dynamic ultimate strain of 0.0081 is slightly higher than the static value of 0.0076.

TABLE 4-13. HIGH STRAIN RATE TENSILE PROPERTIES OF $[\pm 75]_{2s}$ SP288/AS GRAPHITE/EPOXY

Specimen Number	Strain Rate ($\dot{\varepsilon}_{\theta\theta}$), s^{-1}	Modulus ($E_{\theta\theta}$), GPa (10^6 psi)	Poisson's Ratio ($\nu_{\theta x}$)
		Initial Properties	
20-2	220	43.3 (6.28)	-
20-4	245	54.7 (7.93)	-
20-7	225	37.6 (5.45)	-
		Secant Properties	
20-2	277	36.6 (5.30)	0.18
20-4	253	38.1 (5.53)	-
20-7	286	33.6 (4.87)	0.12
		Terminal Properties	
20-2	320	30.5 (4.42)	-
20-4	295	26.6 (3.85)	-
20-7	330	32.1 (4.65)	-
		Ultimate Properties	
	Time to Failure (t_f), μs	Strength ($S_{\theta\theta T}$), MPa (ksi)	Strain ($\varepsilon^u_{\theta\theta T}$)
20-2	30	304 (44)	0.0083
20-4	30	290 (42)	0.0076
20-7	29	278 (40)	0.0083

Strain and strain derivative records for the three hybrid rings tested are shown in Figures 4-152 through 4-160 (Specimen Nos. 21-2, 21-4, and 21-6). The corresponding stress-strain curves are shown in Figures 4-161, 4-162, and 4-163. Results are tabulated in Table 4-14. The initial strain rates range between $140s^{-1}$ and $260s^{-1}$ and the average (secant) rates between $215s^{-1}$ and $290s^{-1}$. The times to failure range between 24 μs and 27 μs. The initial and secant moduli of 45.1 GPa (6.53×10^6 psi) and 35.1 GPa (5.09×10^6 psi), respectively, are much higher than the static modulus of 15.5 GPa (2.25×10^6 psi). It was difficult to obtain reliable values for dynamic Poisson's ratio, because of the large scatter in the transverse strain data. The average dynamic strength of 223 MPa (32 ksi) is much higher than the static strength of 61.4 GPa (8.9×10^6 psi). The average dynamic ultimate strain of 0.0066 is also higher than the static value of 0.0047.

TABLE 4-14. HIGH STRAIN RATE TENSILE PROPERTIES OF $[\pm 75]_{2s}$ 80AS/20S/PR288 GRAPHITE/S-GLASS/EPOXY

Specimen Number	Strain Rate ($\dot{\varepsilon}_{\theta\theta}$), s^{-1}	Modulus ($E_{\theta\theta}$), GPa (10^6 psi)	Poisson's Ratio ($\nu_{\theta x}$)
		Initial Properties	
21-2	250	46.6 (6.75)	-
21-4	140	56.2 (8.14)	0.03
21-6	260	32.4 (4.70)	-
		Secant Properties	
21-2	263	31.8 (4.61)	-
21-4	215	46.5 (6.74)	0.017
21-6	290	27.0 (3.91)	0.02
		Terminal Properties	
21-2	280	16.8 (2.43)	-
21-4	230	42.0 (6.08)	-
21-6	375	18.4 (2.66)	-
		Ultimate Properties	
	Time to Failure (t_f), μs	Strength ($S_{\theta\theta T}$), MPa (ksi)	Strain ($\varepsilon^u_{\theta\theta T}$)
21-2	27	214 (31)	0.0071
21-4	27	270 (39)	0.0058
21-6	24	186 (27)	0.0069

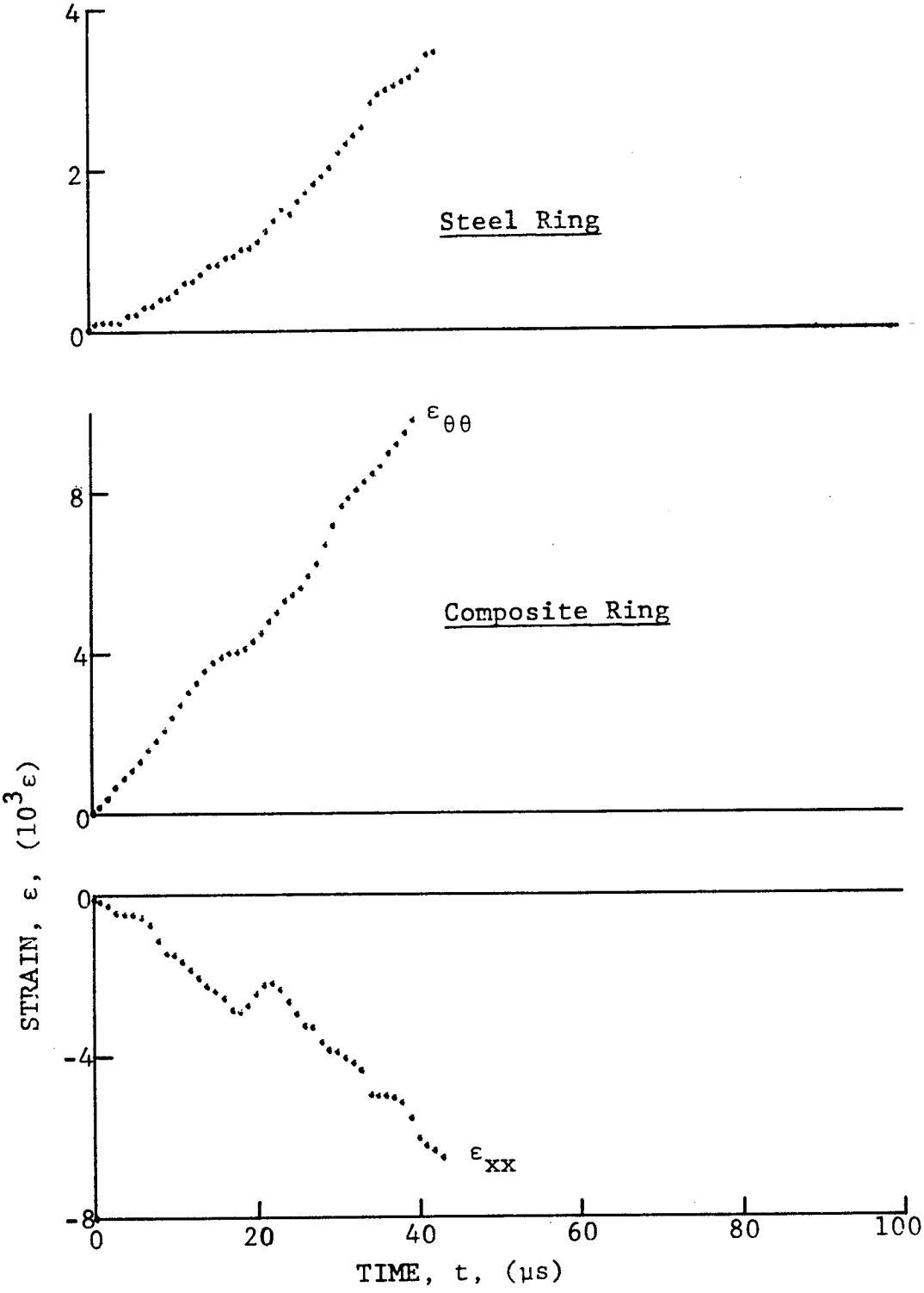

Figure 4-1. Strain records in steel ring and $[\pm 15]_{2s}$ SP288/AS graphite/epoxy ring under dynamic loading for Specimen No. 35-2 (100 mg PETN detonator).

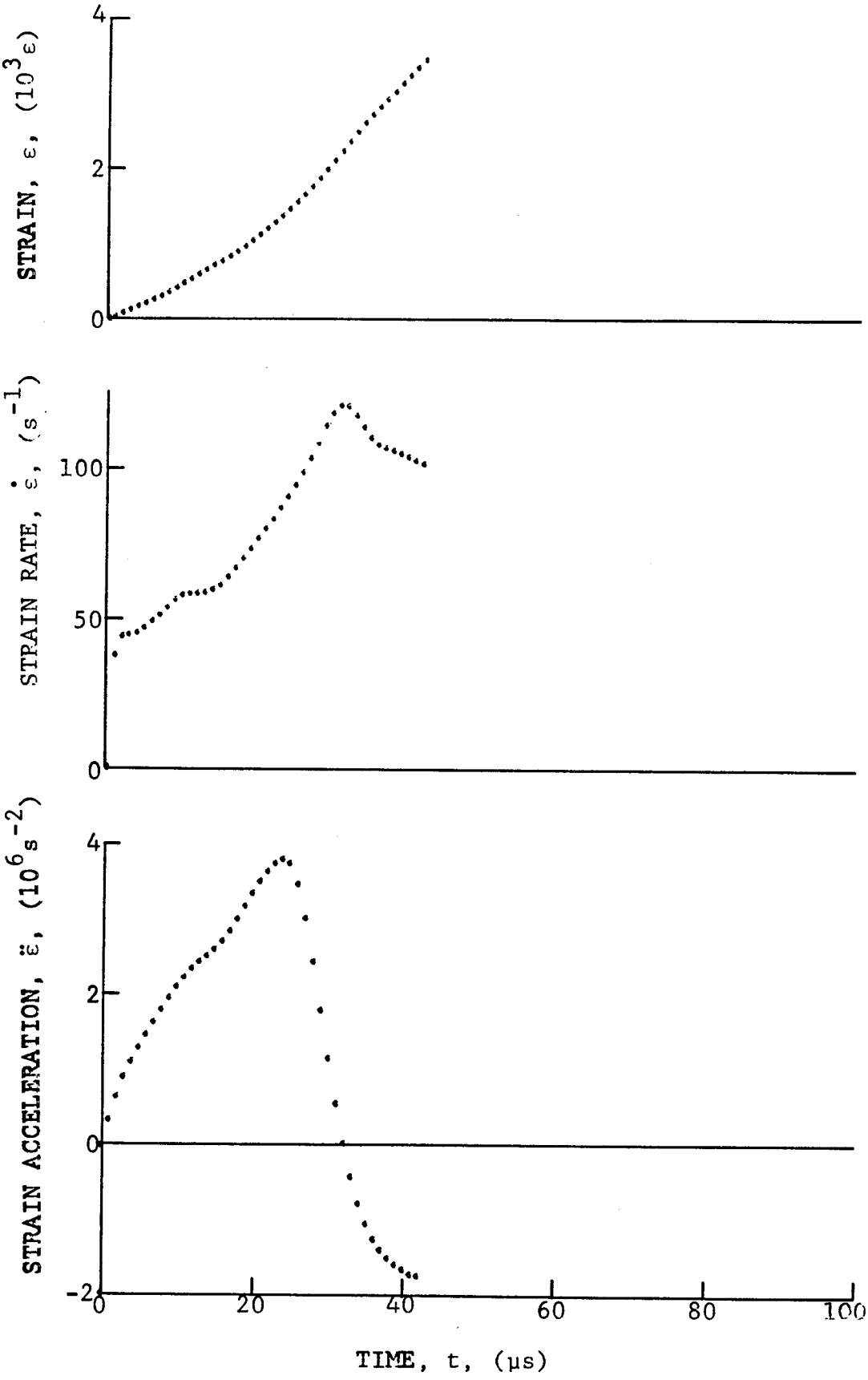

Figure 4-2. Strain and its derivatives in steel ring for Specimen No. 35-2.

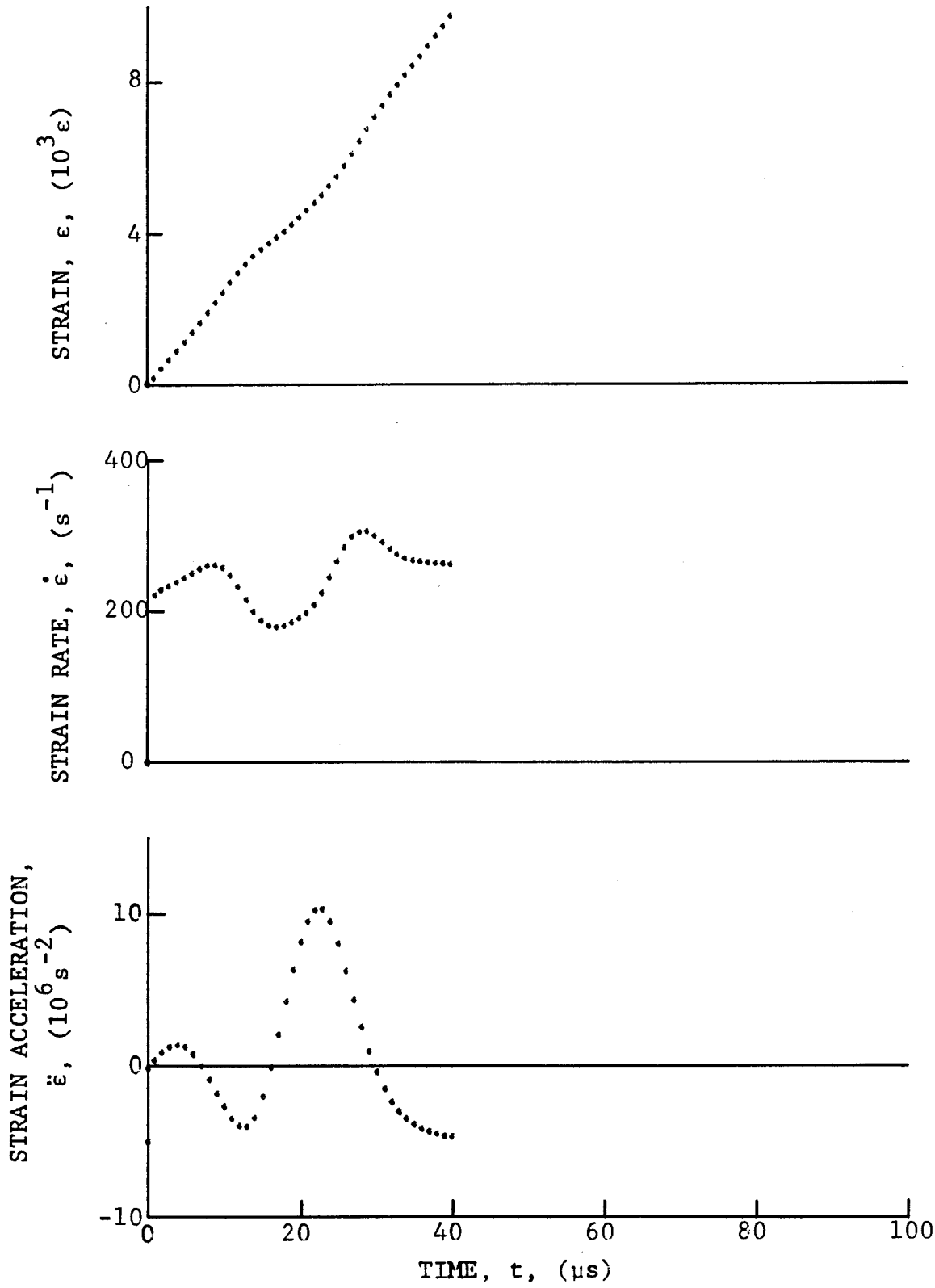

Figure 4-3. Circumferential strain and its derivatives in $[\pm 15]_{2s}$ SP288/AS graphite/epoxy ring under dynamic loading for Specimen No. 35-2.

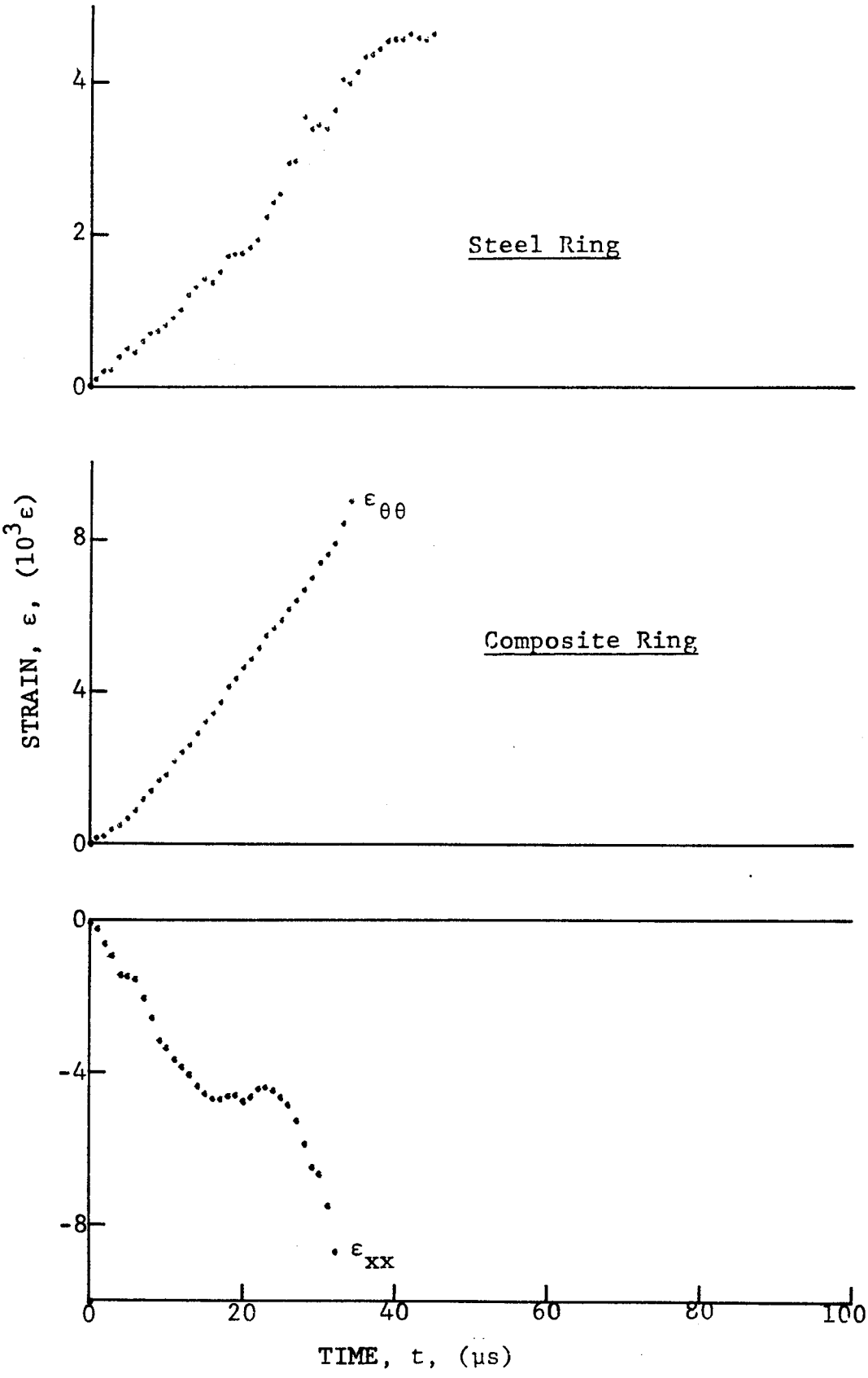

Figure 4-4. Strain records in steel ring and $[\pm 15]_{2s}$ SP288/AS graphite/epoxy ring under dynamic loading for Specimen No. 35-4 (100 mg PETN detonator).

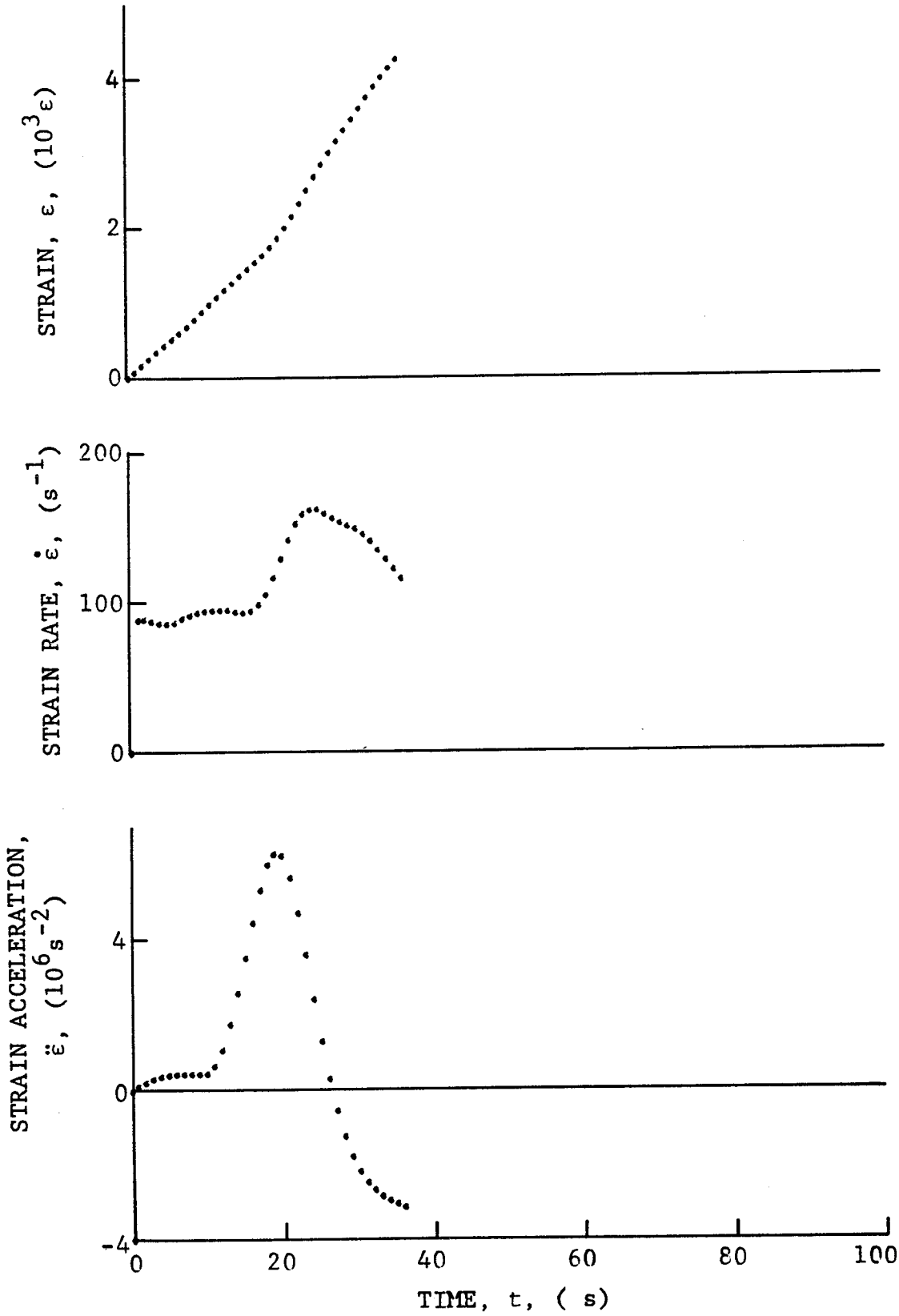

Figure 4-5. Strain and its derivatives in steel ring for Specimen No. 35-4.

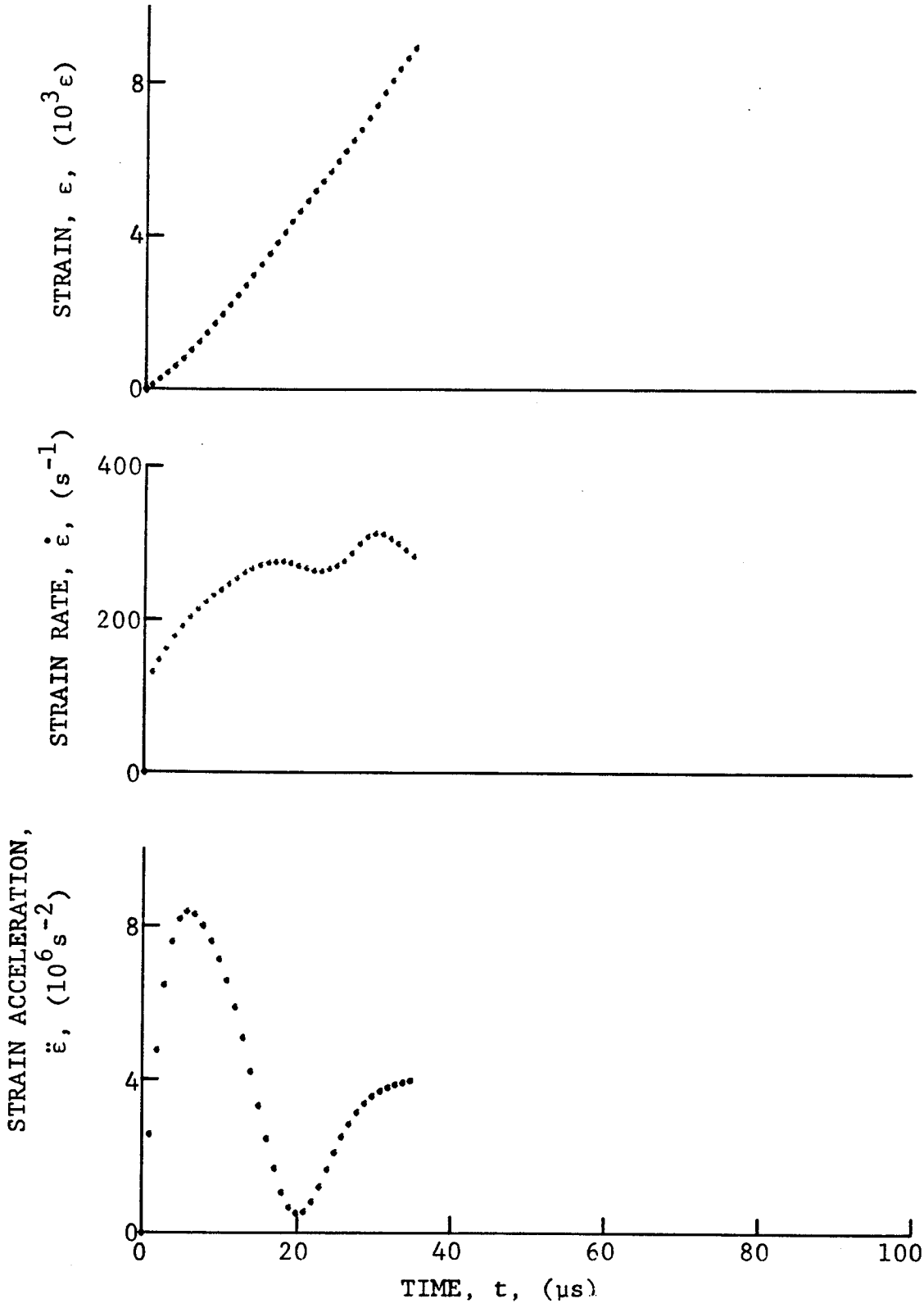

Figure 4-6. Circumferential strain and its derivatives in $[\pm 15]_{2s}$ SP288/AS graphite/epoxy ring under dynamic loading for Specimen No. 35-4.

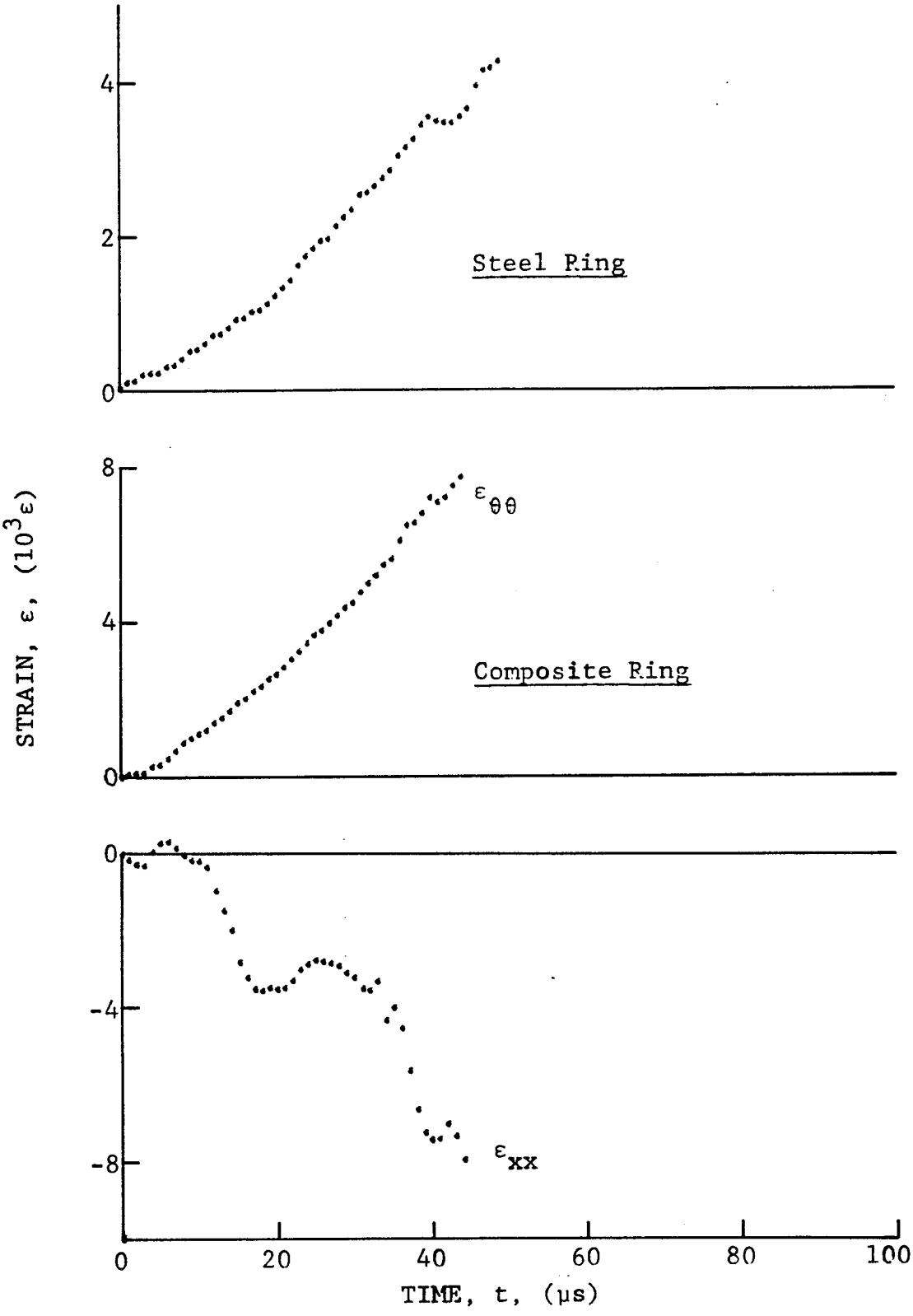

Figure 4-7. Strain records in steel ring and $[\pm 15]_{2s}$ SP288/AS graphite/epoxy ring under dynamic loading for Specimen No. 35-6 (100 mg PETN detonator).

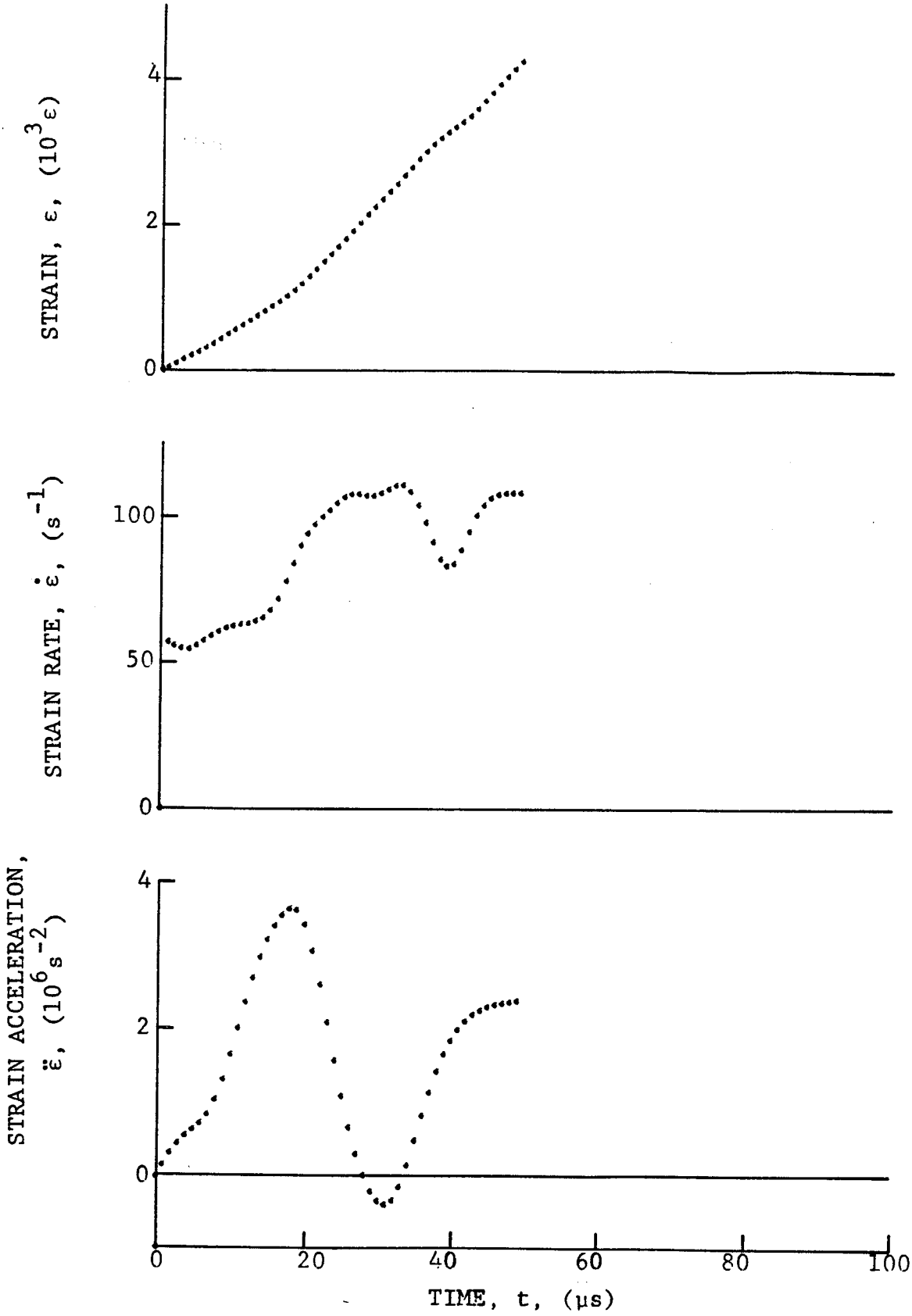

Figure 4-8. Strain and its derivatives in steel ring in Specimen No. 35-6.

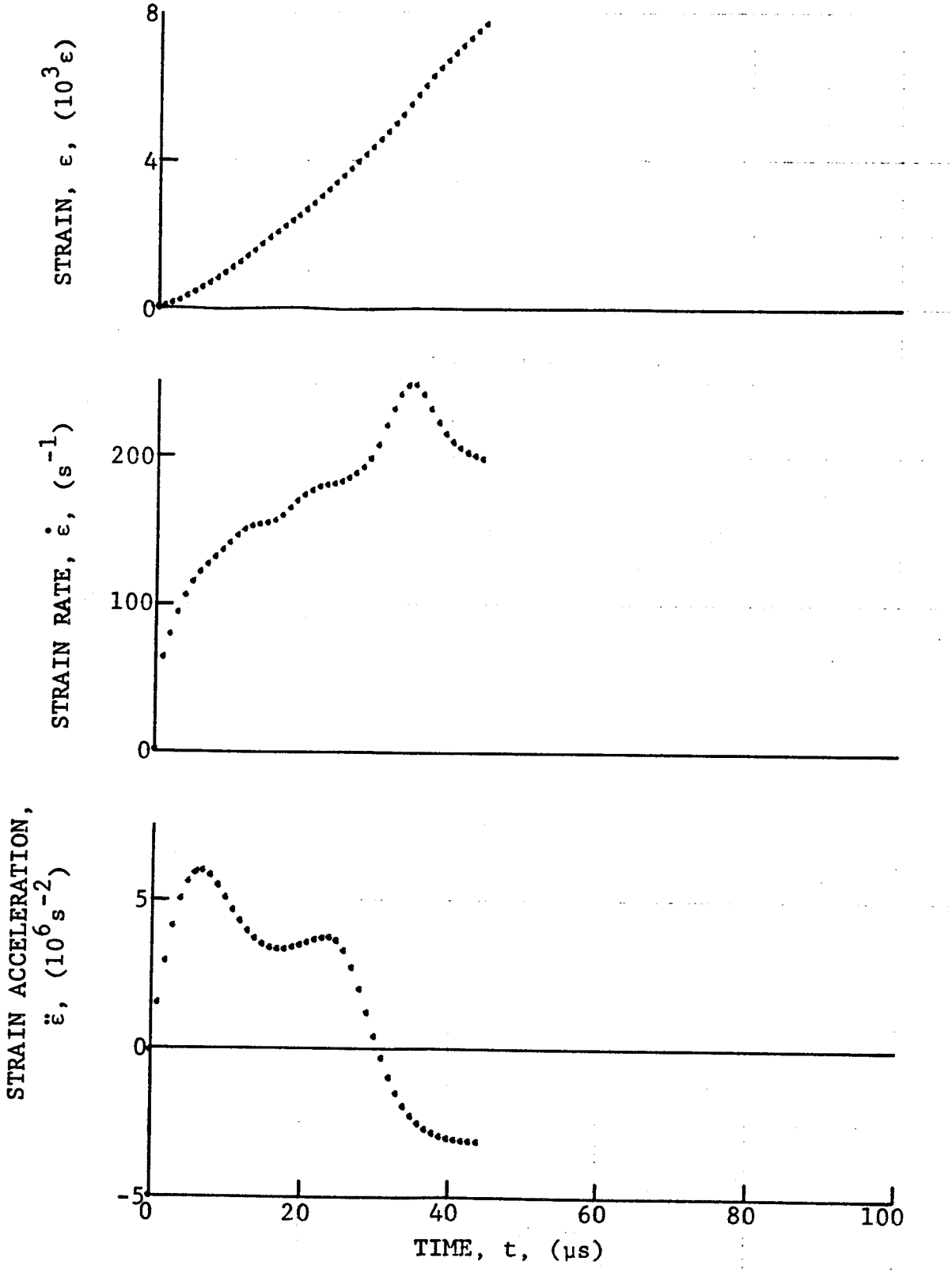

Figure 4-9. Circumferential strain and its derivatives in $[\pm 15]_{2s}$ SP288/AS graphite/epoxy ring under dynamic loading for Specimen No. 35-6.

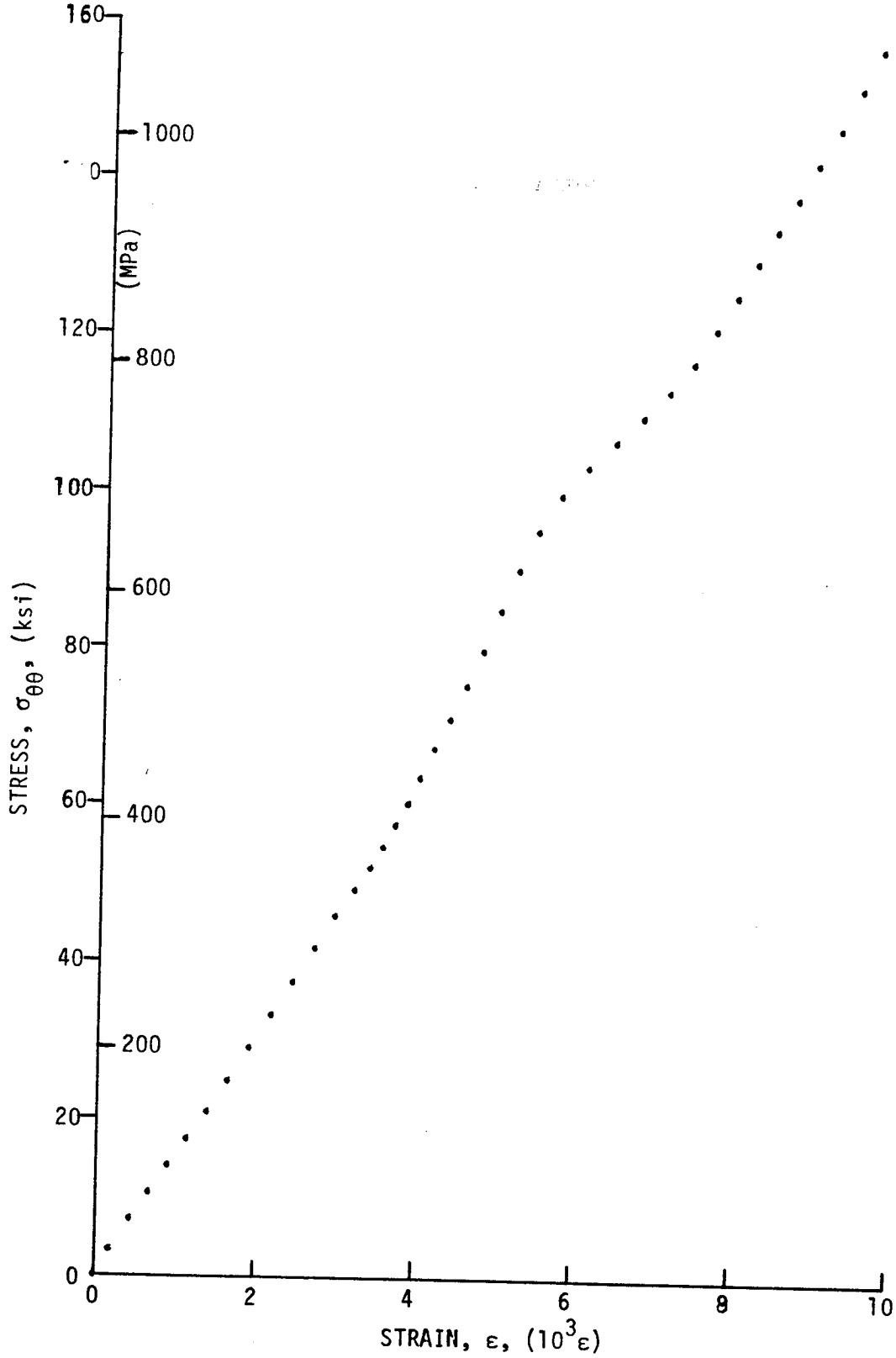

Figure 4-10. Stress-strain curve for dynamically loaded $[\pm 15]_{2s}$ SP288/AS graphite/epoxy ring, Specimen No. 35-2.

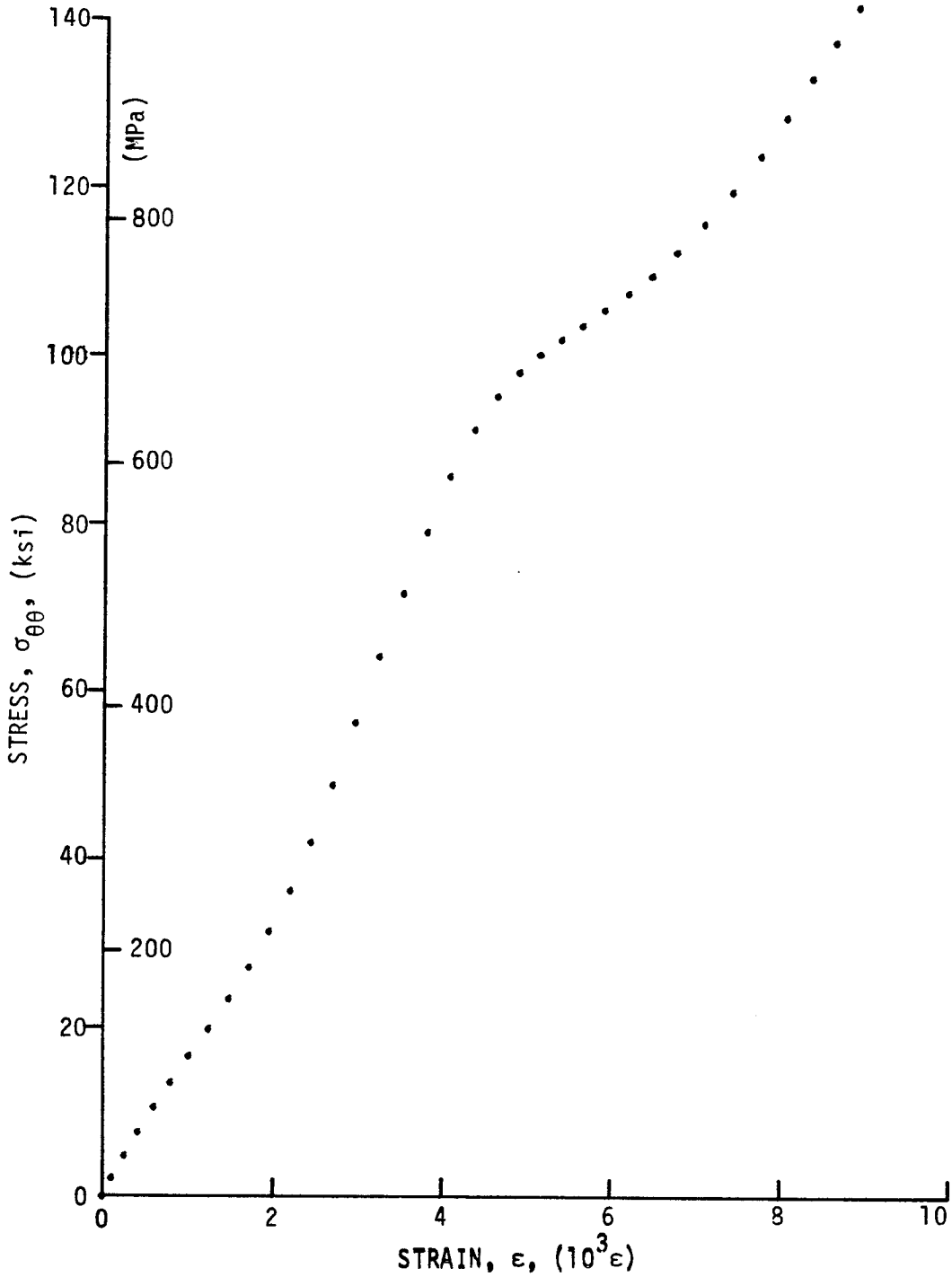

Figure 4-11. Stress-strain curve for dynamically loaded $[\pm 15]_{2s}$ SP288/AS graphite/epoxy ring, Specimen No. 35-4.

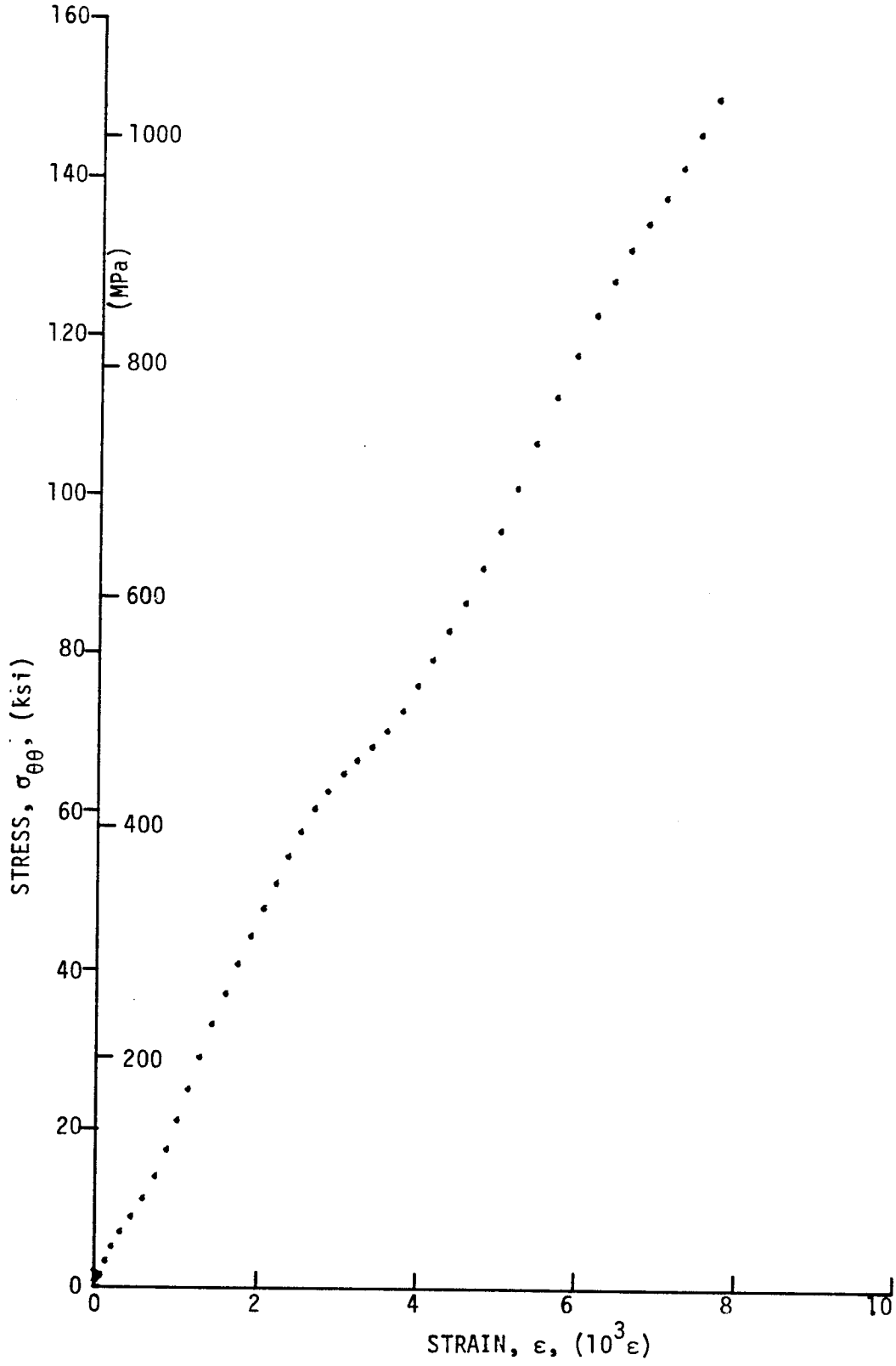

Figure 4-12. Stress-strain curve for dynamically loaded $[\pm 15]_{2s}$ SP288/AS graphite/epoxy ring, Specimen No. 35-6.

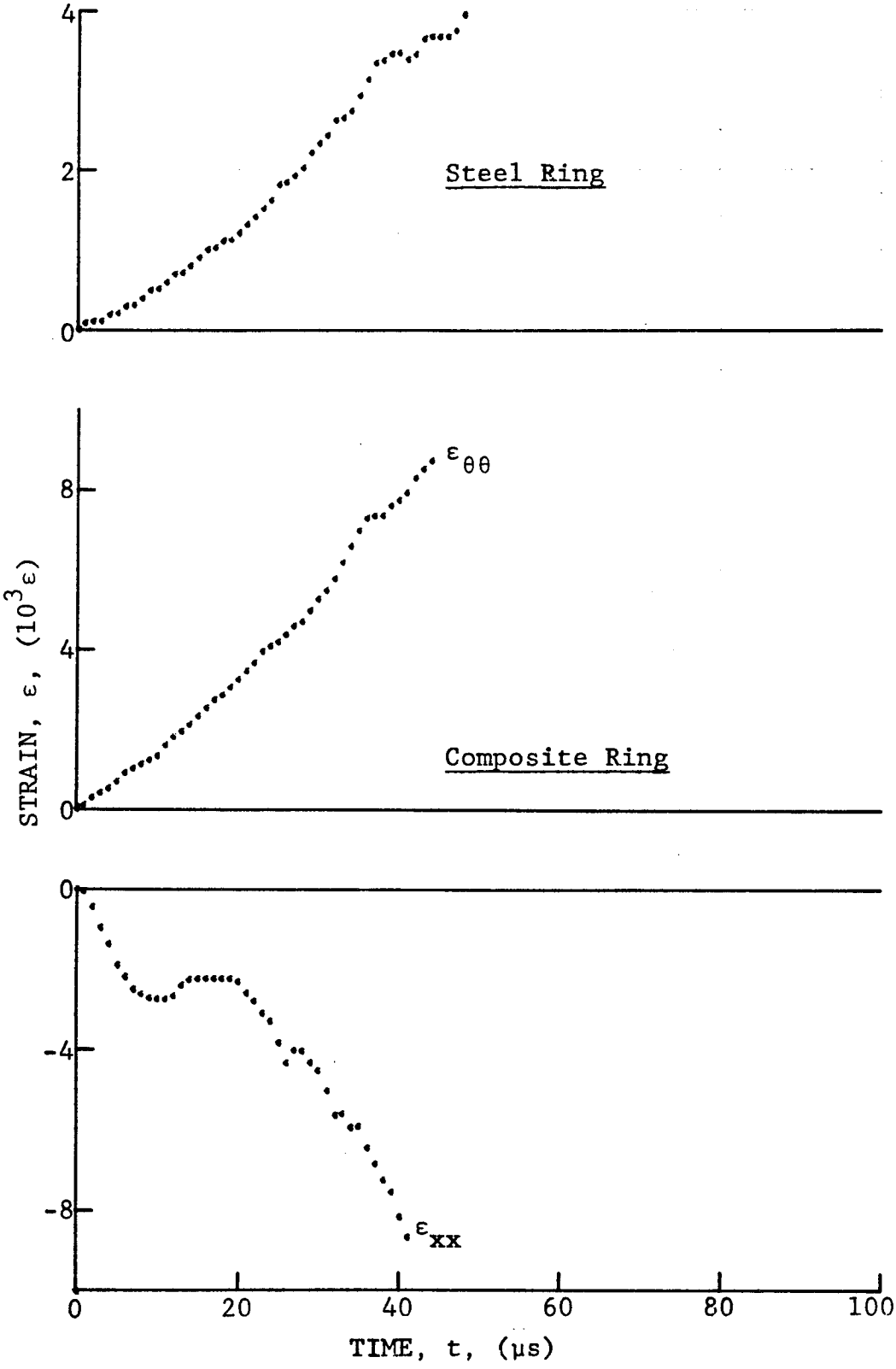

Figure 4-13. Strain records in steel ring and 80AS/20S/PR288 $[\pm 15]_{2s}$ graphite/S-glass/epoxy ring under dynamic loading for Specimen No. 36-2 (100 mg PETN detonator).

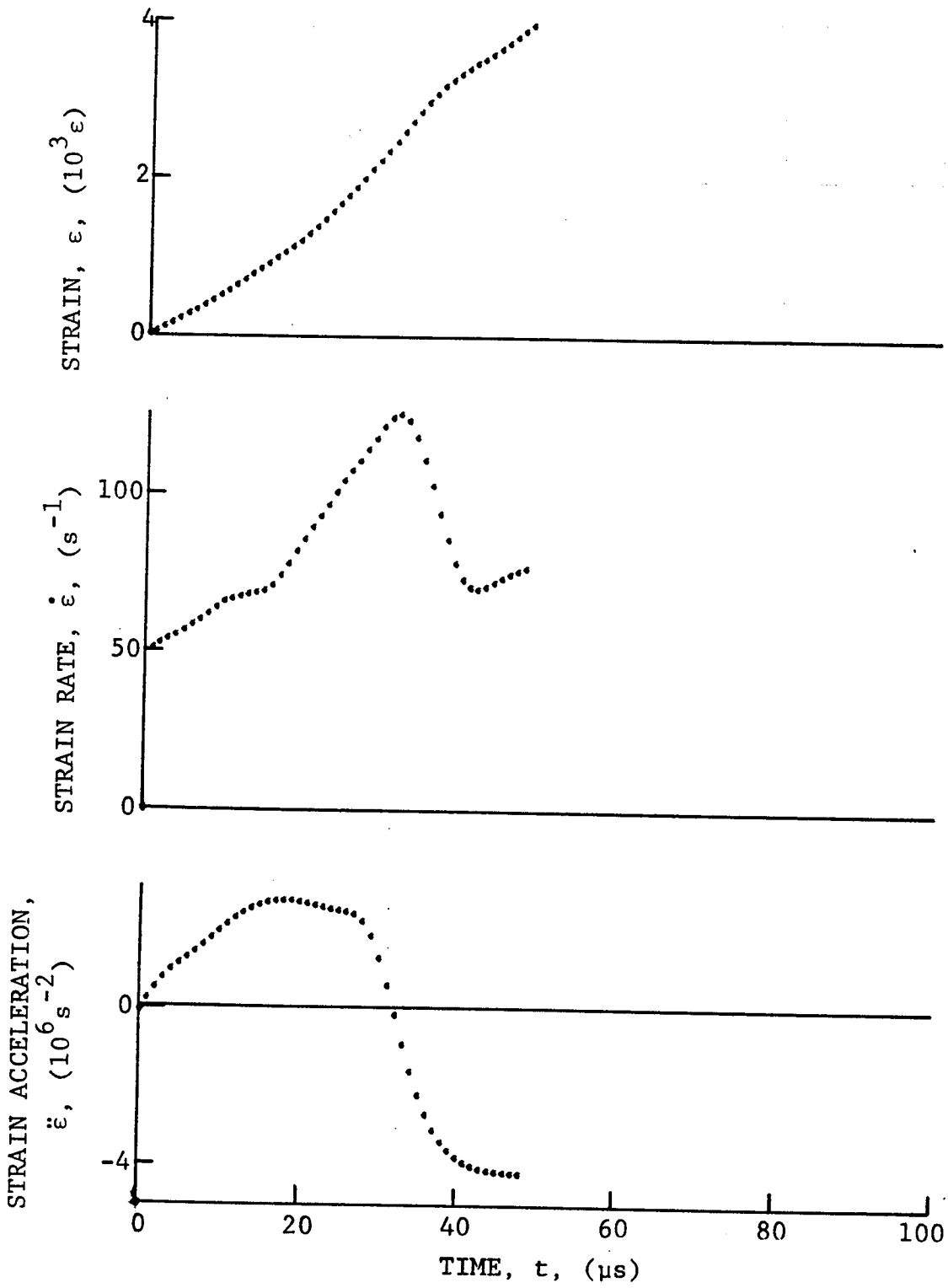

Figure 4-14. Strain and its derivatives in steel ring for Specimen No. 36-2.

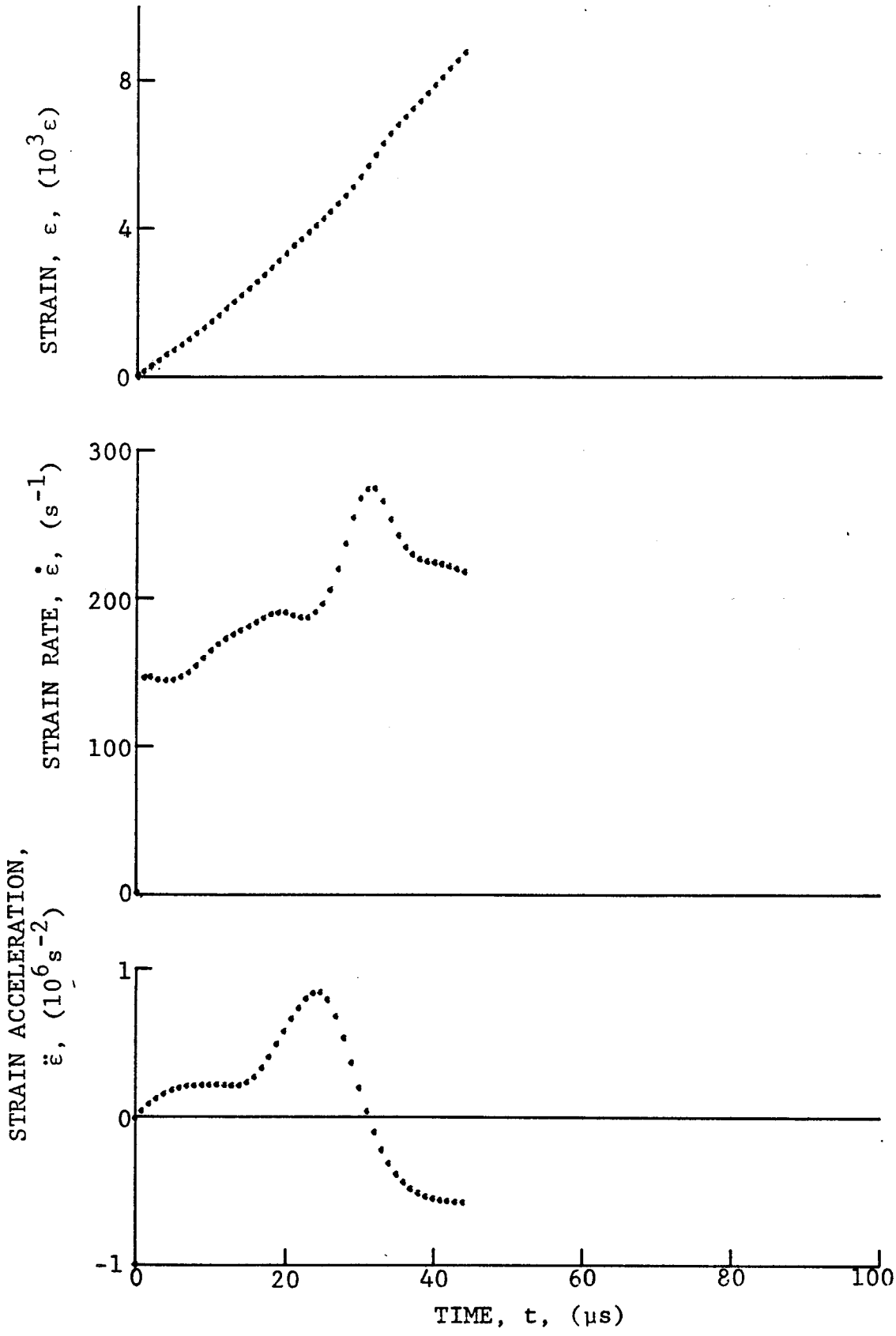

Figure 4-15. Circumferential strain and its derivatives in 80AS/20S/PR288 $[\pm 15]_{2S}$ graphite/S-glass/epoxy ring under dynamic loading for Specimen No. 36-2.

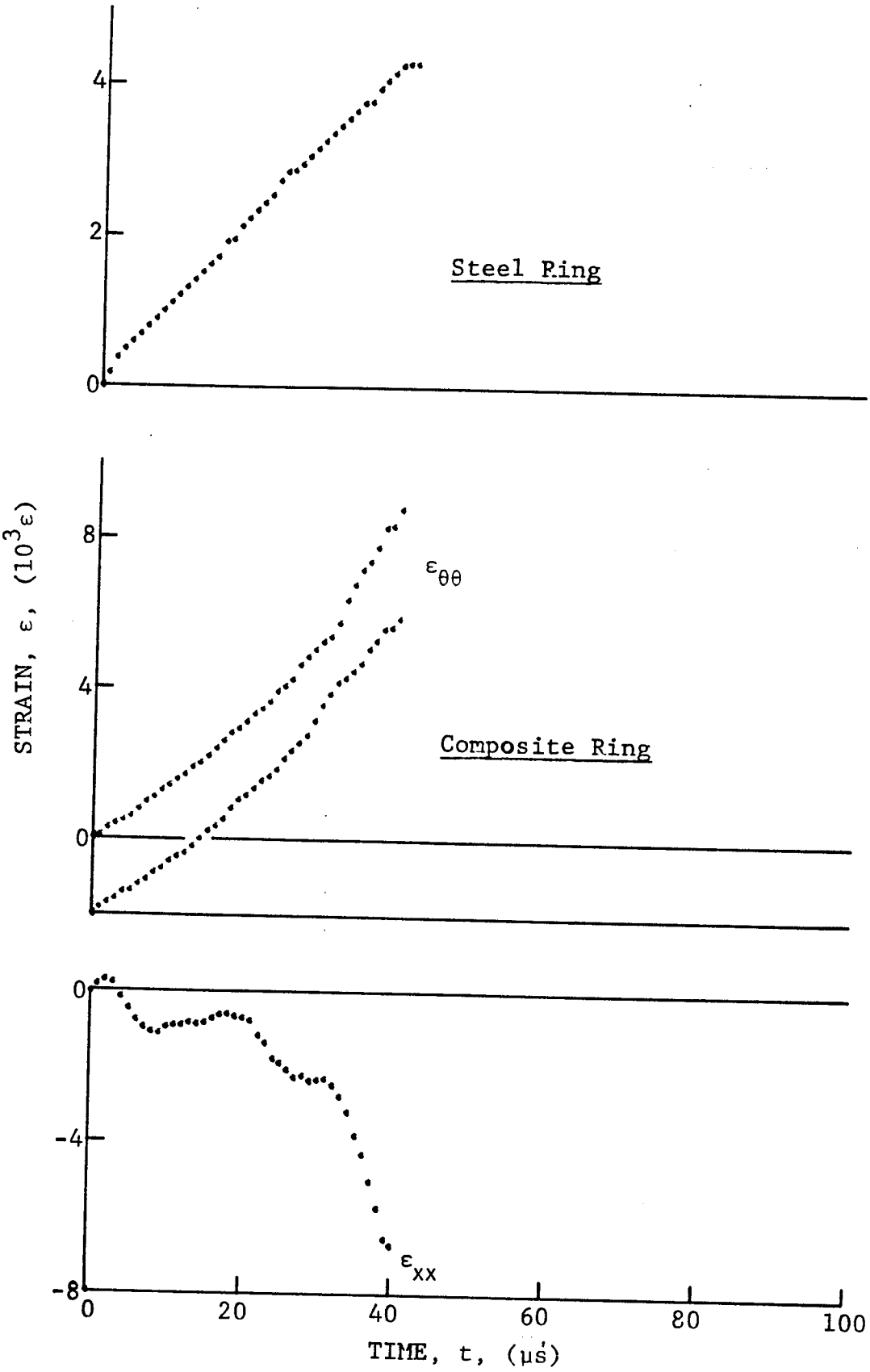

Figure 4-16. Strain records in steel ring and 80AS/20S/PR288 $[\pm 15]_{2s}$ graphite/S-glass/epoxy ring under dynamic loading for Specimen No. 36-4 (100 mg PETN detonator).

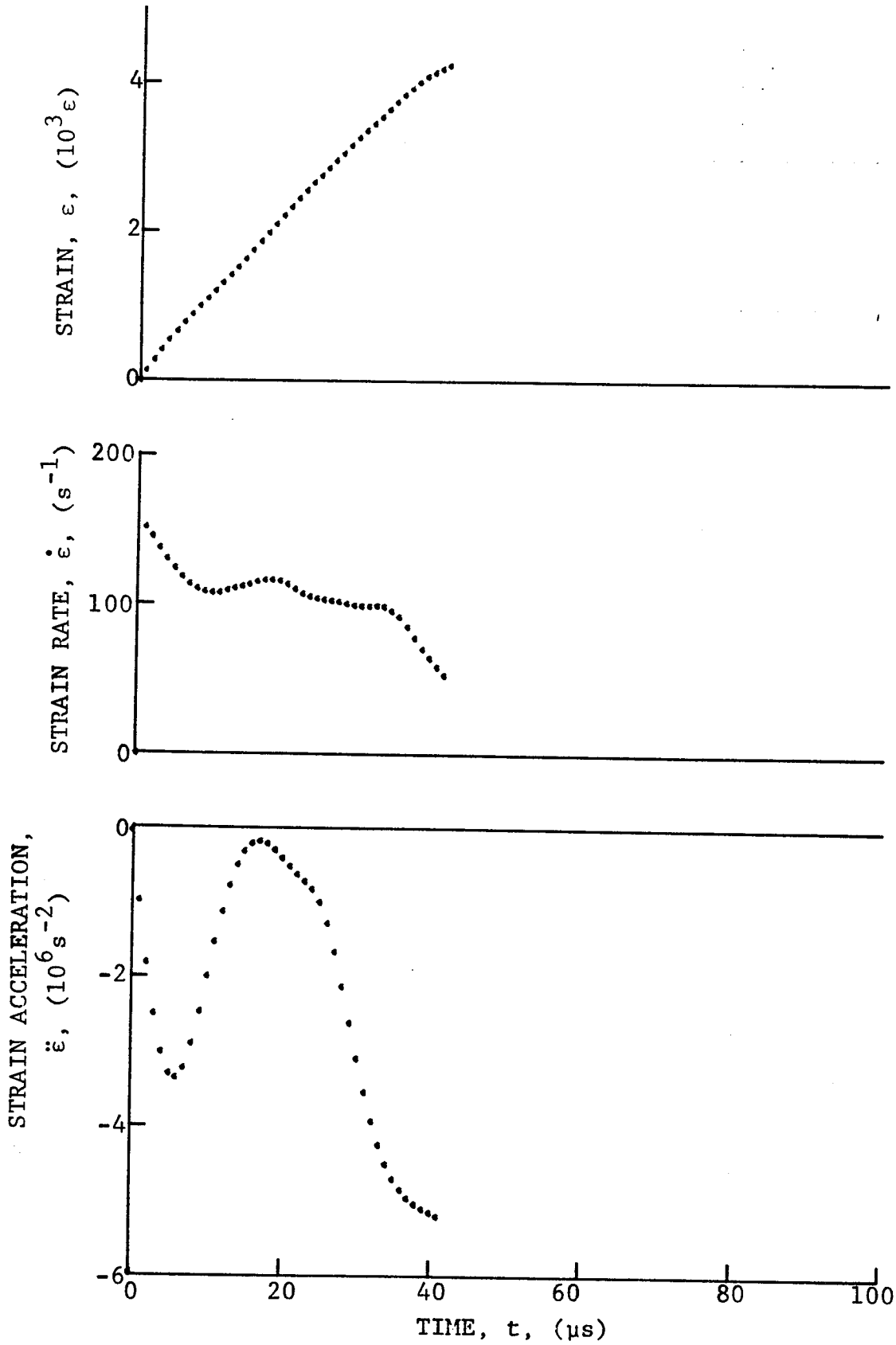

Figure 4-17. Strain and its derivatives in steel ring for Specimen No. 36-4.

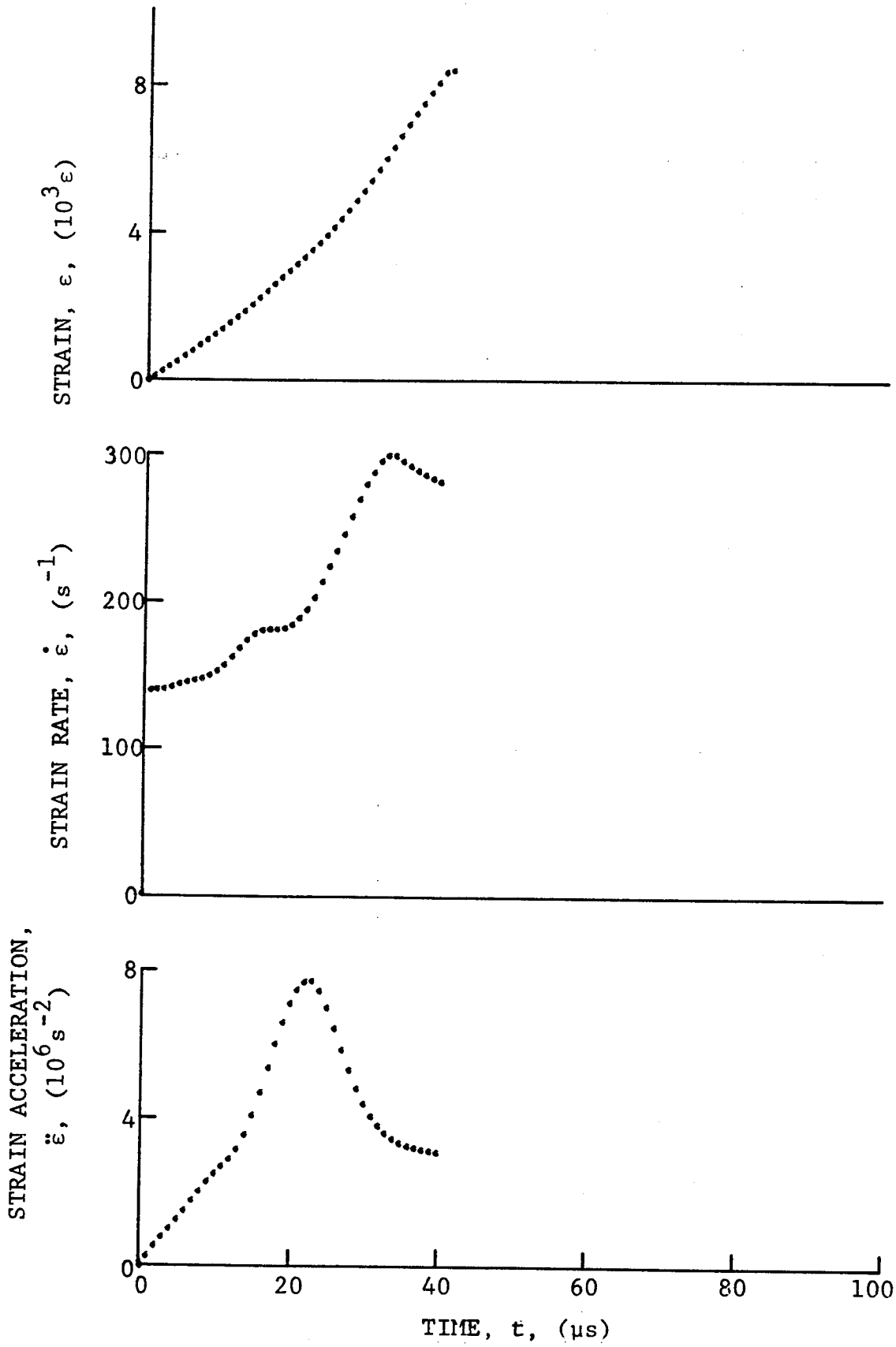

Figure 4-18. Circumferential strain and its derivatives in 80AS/20S/PR288 $[\pm 15]_{2S}$ graphite/S-glass/epoxy ring under dynamic loading for Specimen No. 36-4.

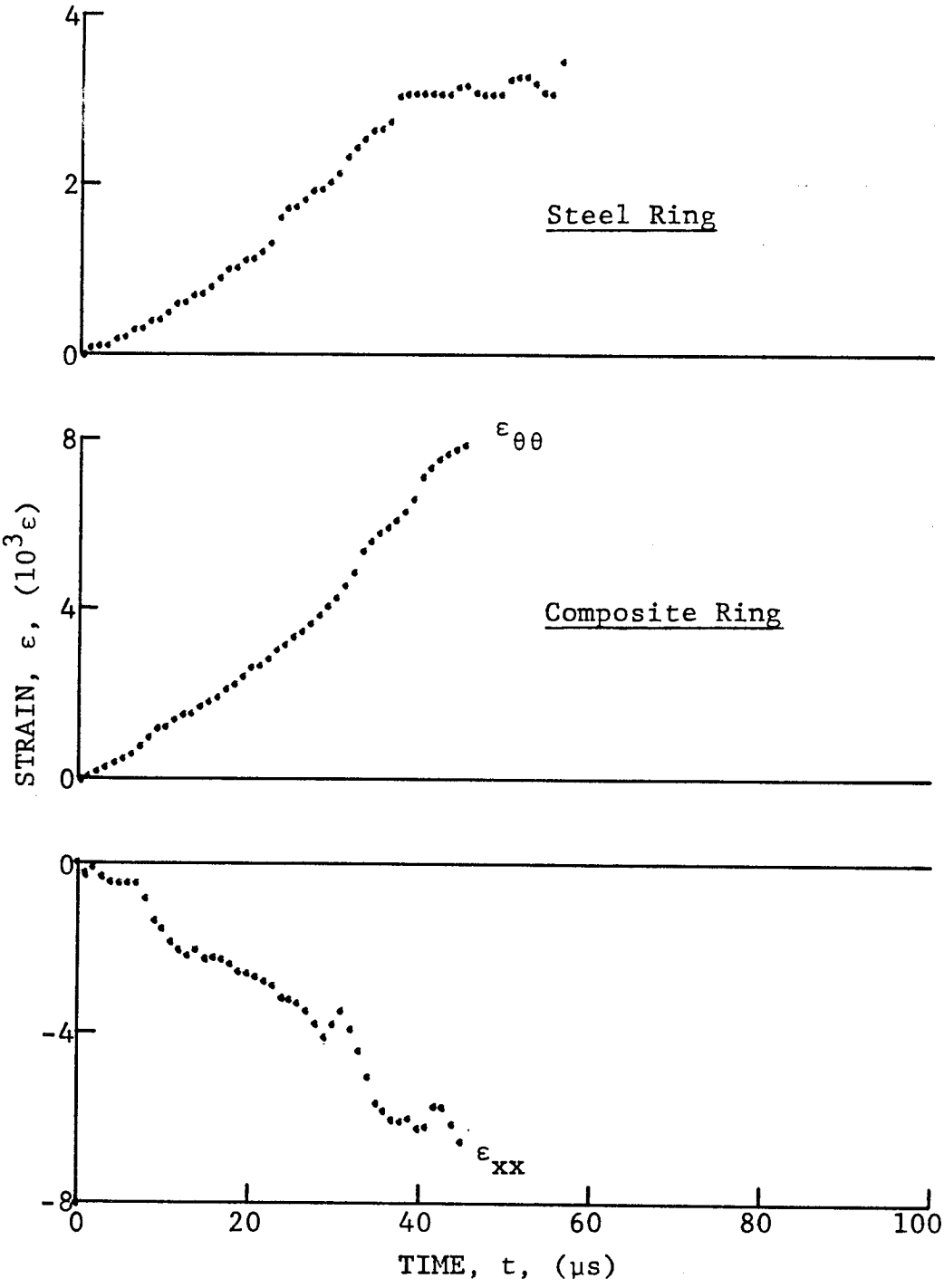

Figure 4-19. Strain records in steel ring and 80AS/20S/PR288 $[\pm 15]_{2s}$ graphite/S-glass/epoxy ring under dynamic loading for Specimen No. 36-7 (100 mg PETN detonator).

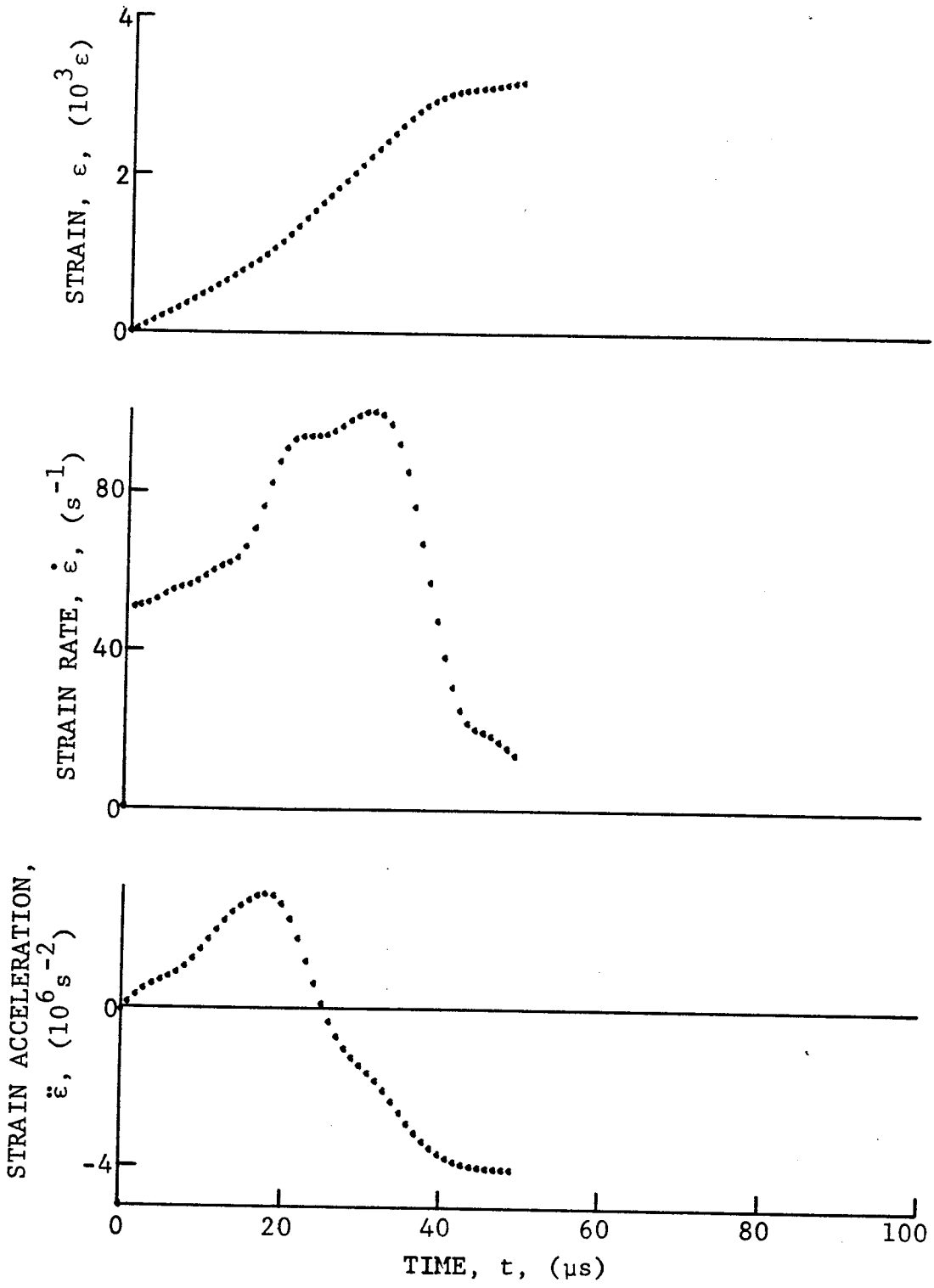

Figure 4-20. Strain and its derivatives in steel ring for Specimen No. 36-7.

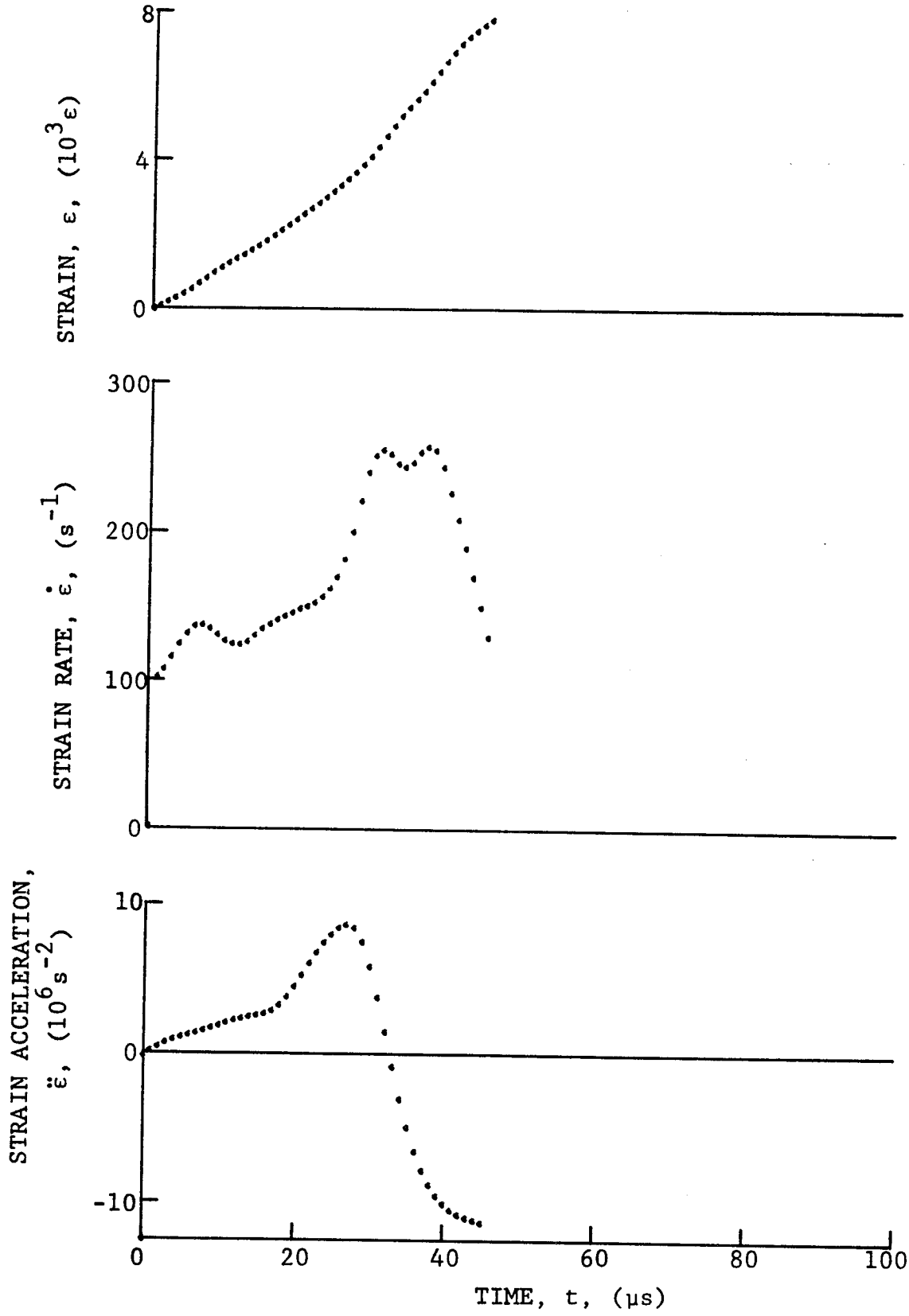

Figure 4-21. Circumferential strain and its derivatives in 80AS/20S/PR288 $[\pm 15]_{2s}$ graphite/S-glass/epoxy ring under dynamic loading for Specimen No. 36-7.

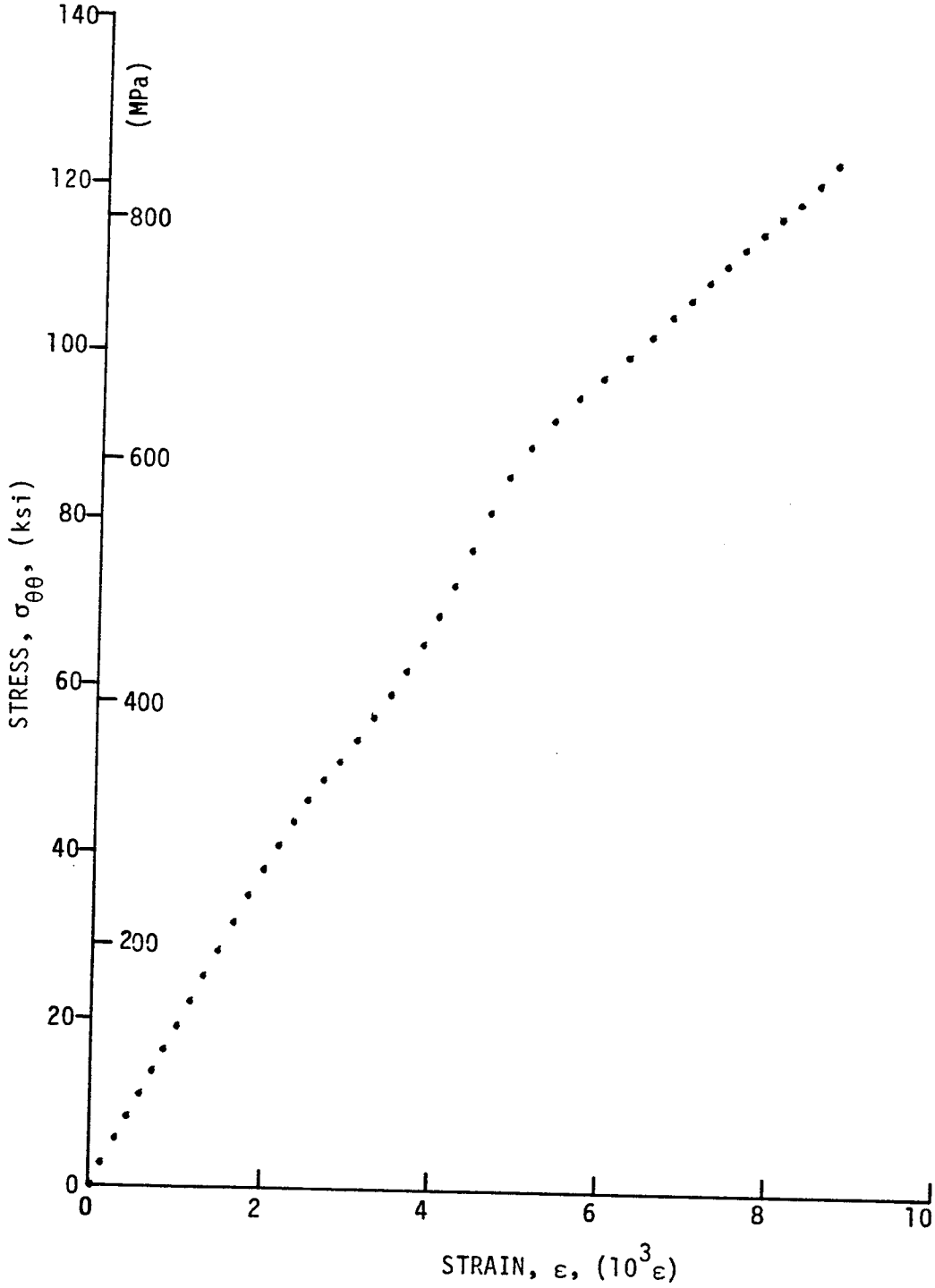

Figure 4-22. Stress-strain curve for dynamically loaded 80AS/20S/PR288 $[\pm 15]_{2S}$ graphite/S-glass/epoxy ring, Specimen No. 36-2.

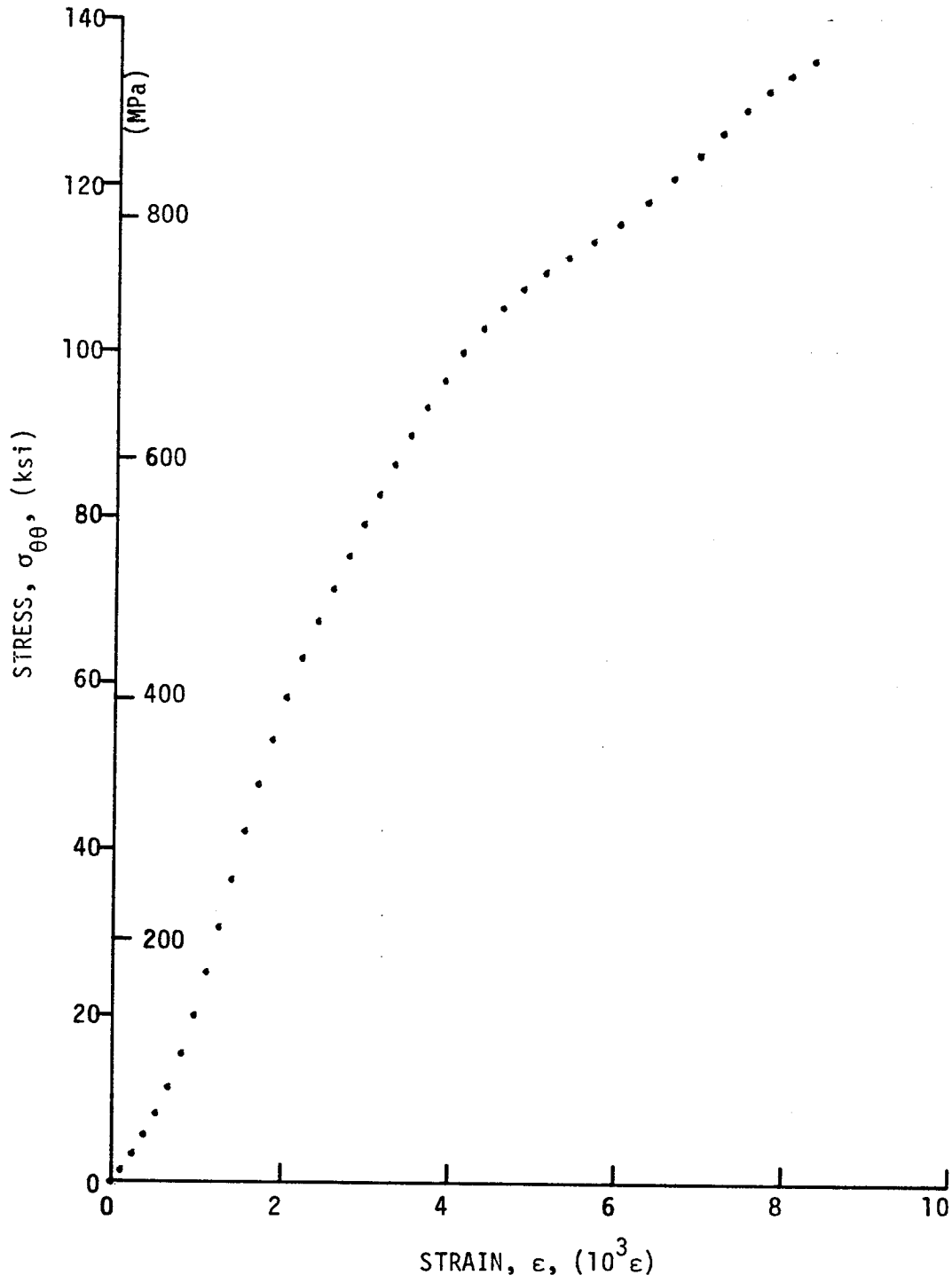

Figure 4-23. Stress-strain curve for dynamically loaded 80AS/20S/PR288 $[\pm 15]_{2S}$ graphite/S-glass/epoxy ring, Specimen No. 36-4.

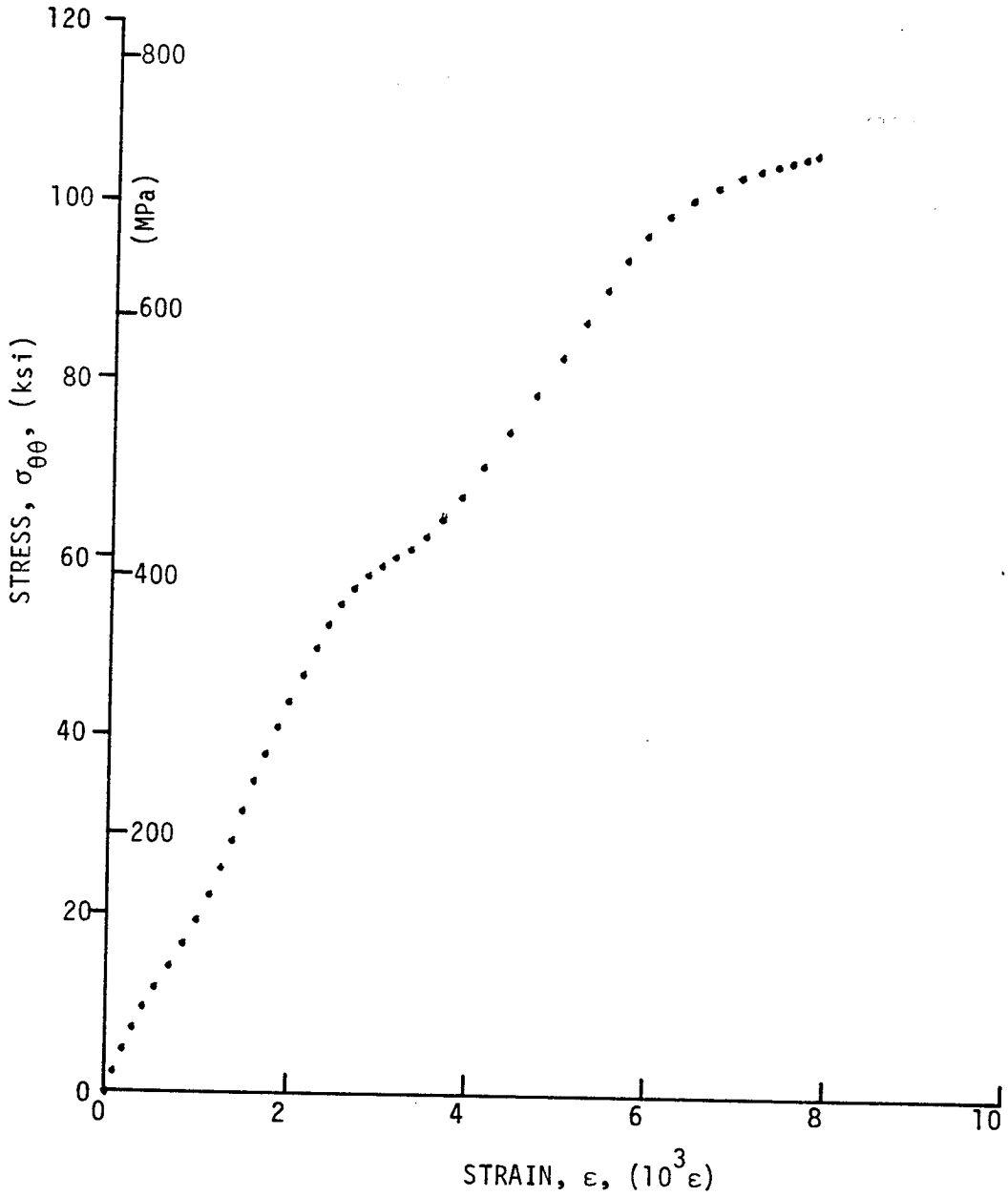

Figure 4-24. Stress-strain curve for dynamically loaded 80AS/20S/PR288 $[\pm 15]_{2S}$ graphite/S-glass/epoxy ring, Specimen No. 36-7.

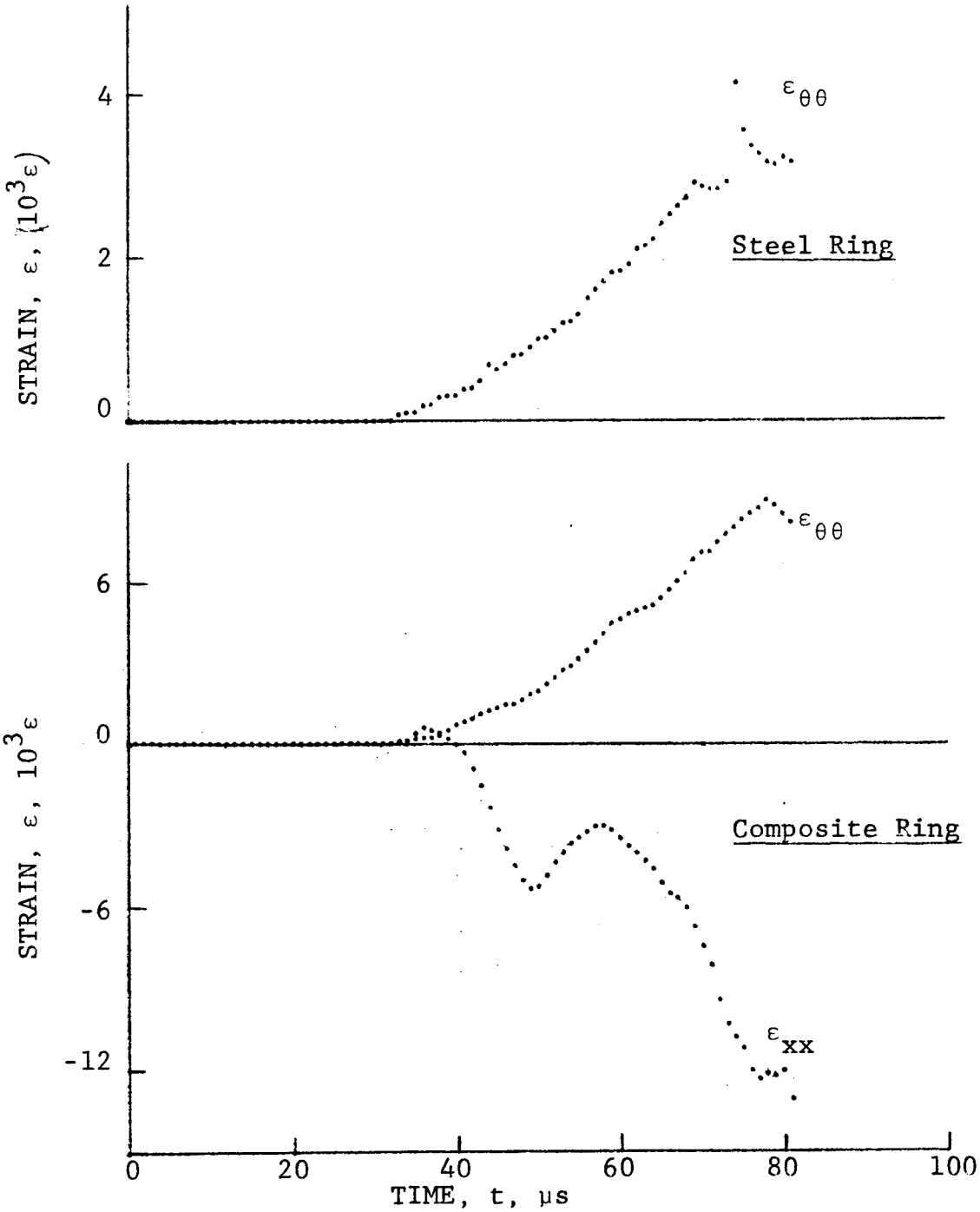

Figure 4-25. Strain records in steel ring and SP288/AS $[\pm 22.5]_{2S}$ graphite/epoxy ring under dynamic loading for Specimen No. 33-4 (100 mg PETN detonator).

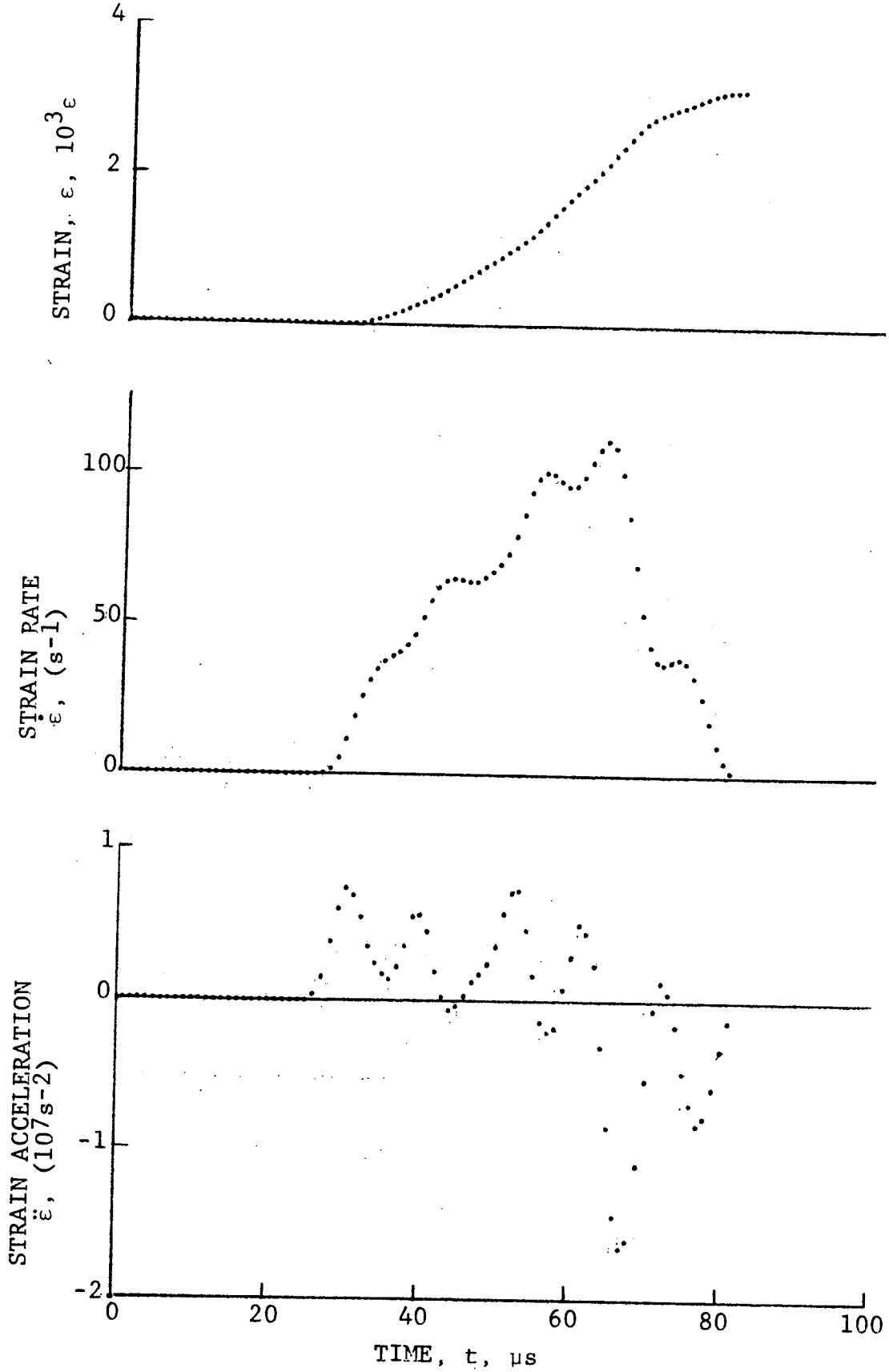

Figure 4-26. Strain in steel ring and its derivatives for Specimen No. 33-4.

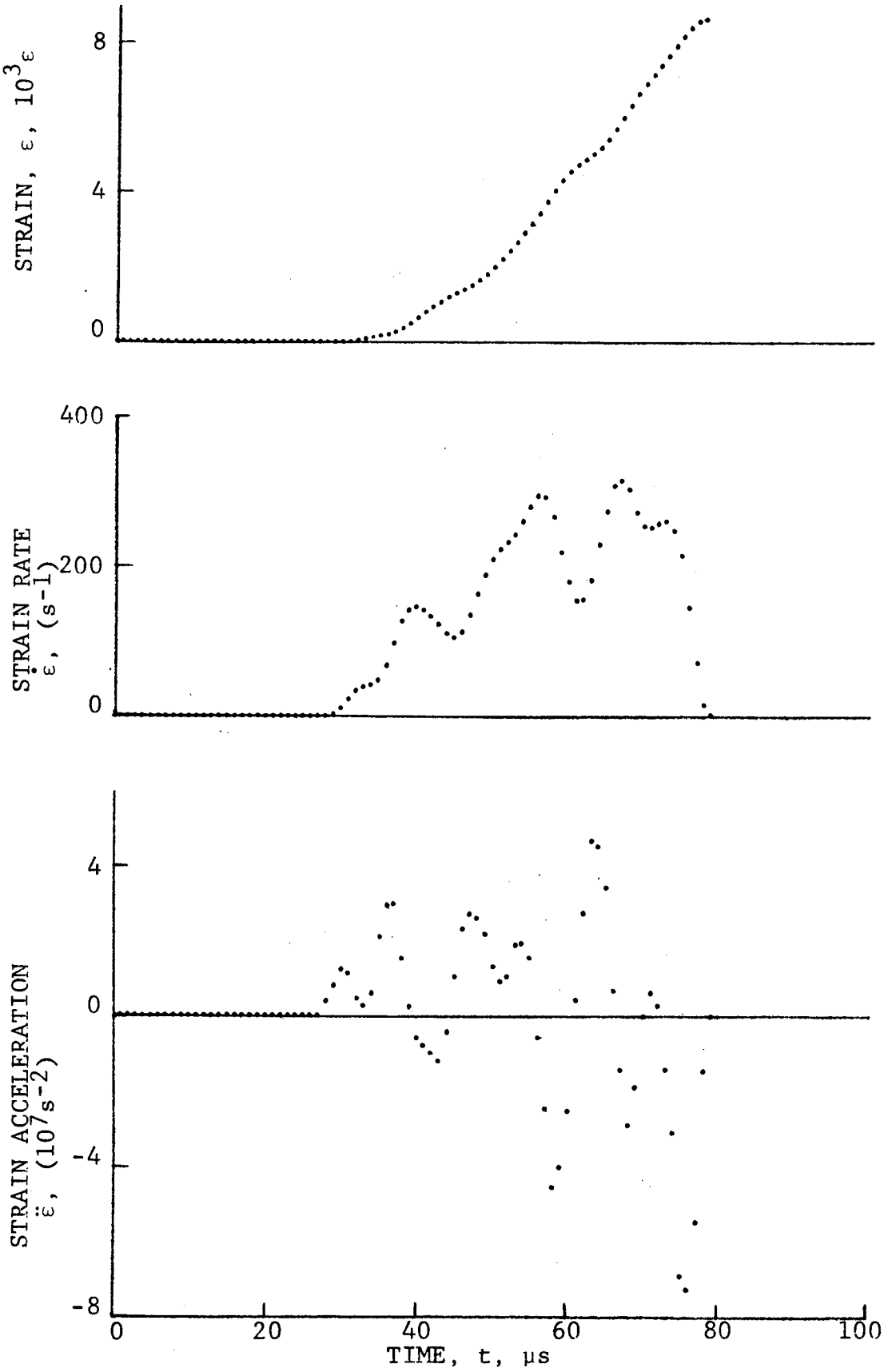

Figure 4-27. Circumferential strain and its derivatives in SP288/AS $[\pm 22.5]_{2s}$ graphite/epoxy ring under dynamic loading, Specimen No. 33-4.

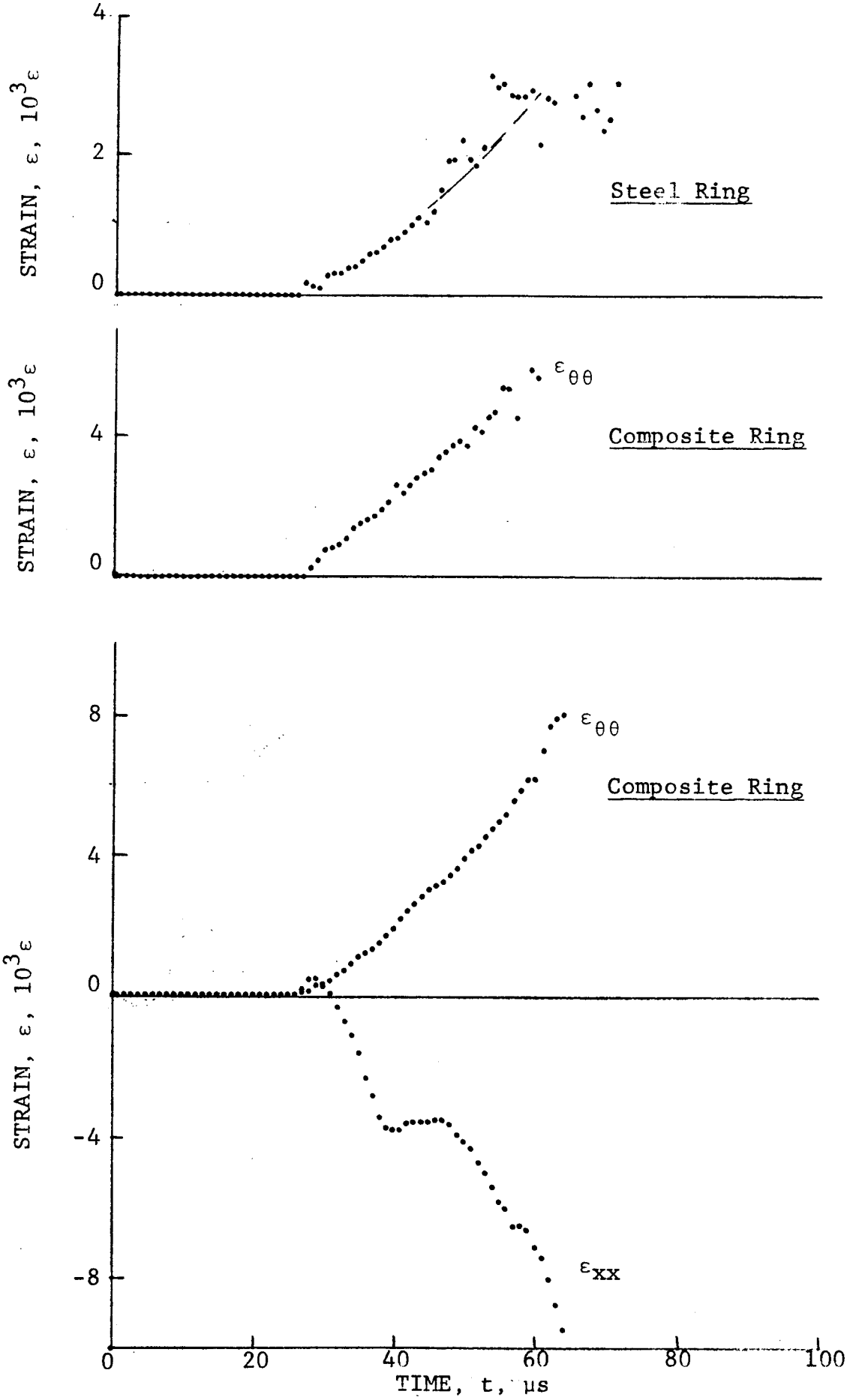

Figure 4-28. Strain records in steel ring and SP288/AS $[\pm 22.5]_{2s}$ graphite/epoxy ring under dynamic loading for Specimen No. 33-6 (100 mg PETN detonator).

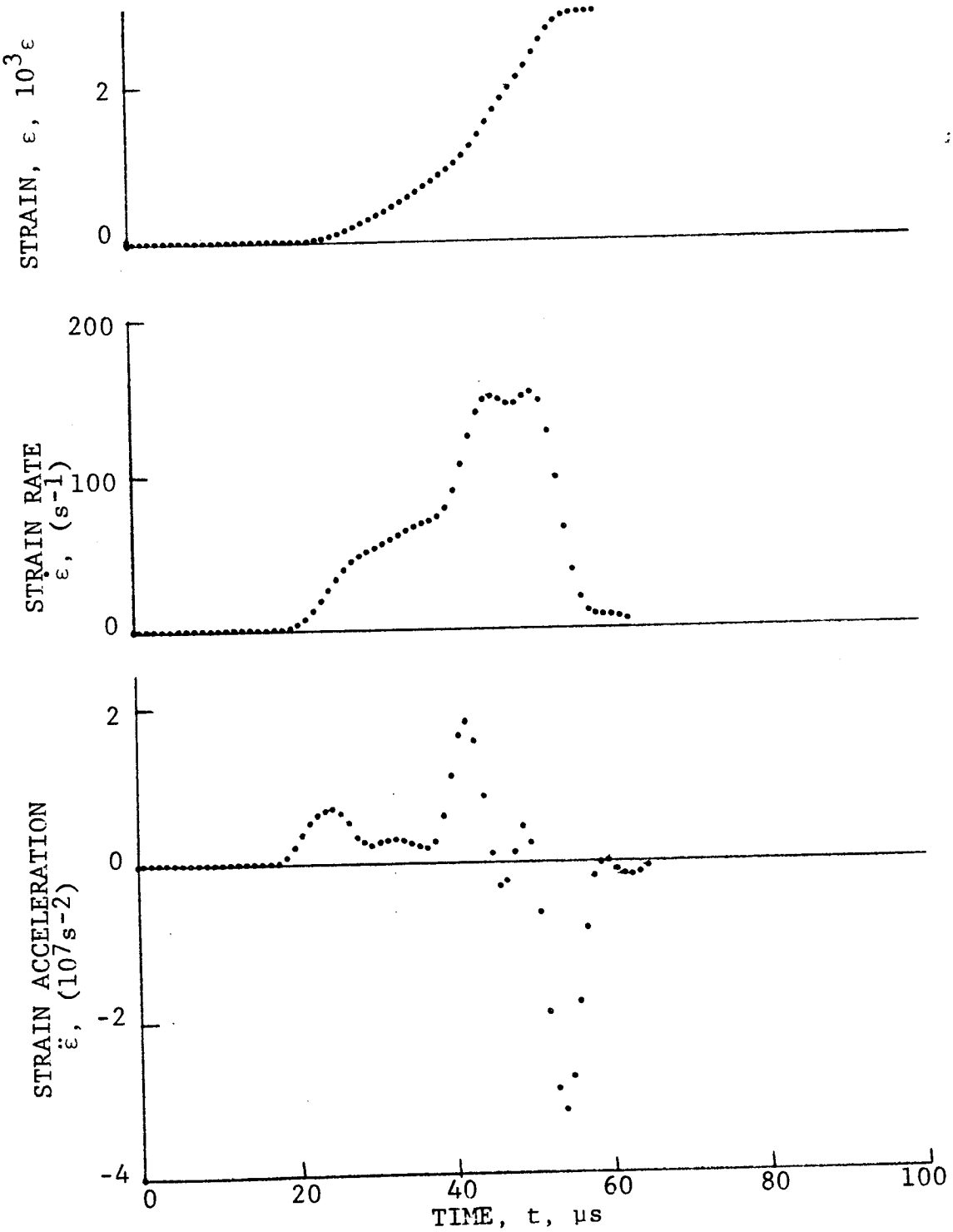

Figure 4-29. Strain in steel ring and its derivatives for Specimen No. 33-6.

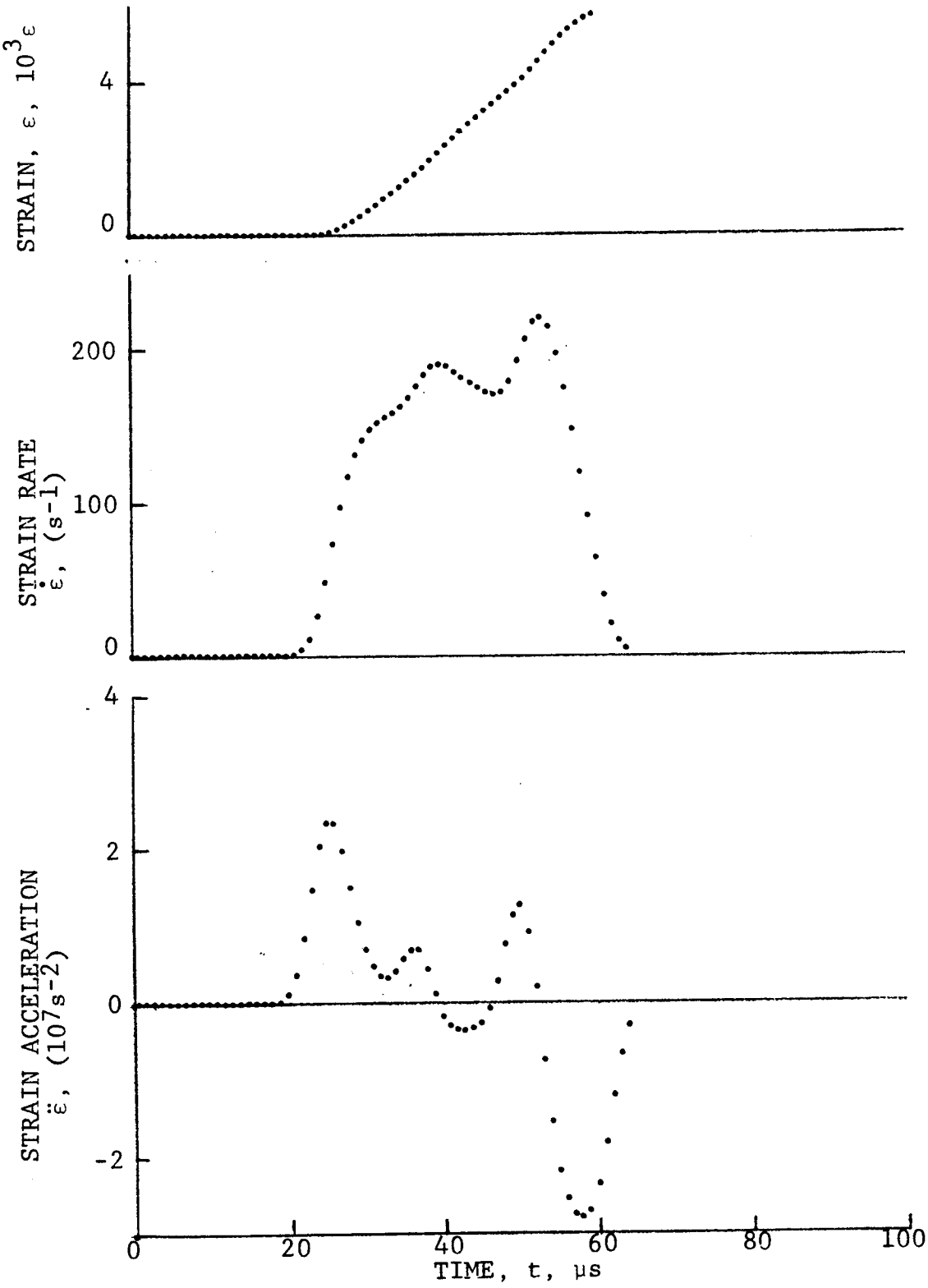

Figure 4-30. Circumferential strain and its derivatives in SP288/AS $[\pm 22.5]_{2s}$ graphite/epoxy ring under dynamic loading, Specimen No. 33-6.

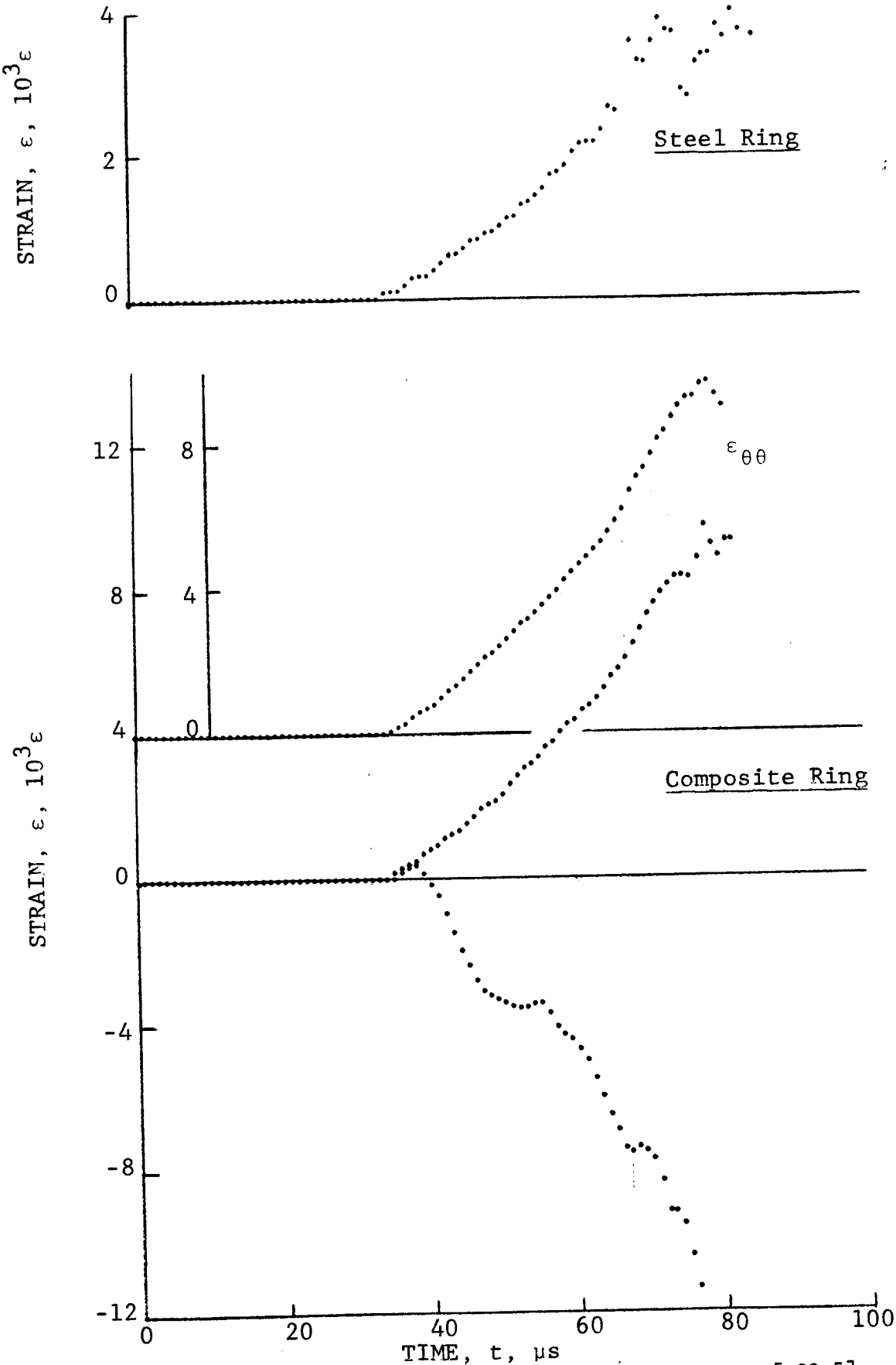

Figure 4-31. Strain records in steel ring and SP288/AS $[\pm 22.5]_{2s}$ graphite/epoxy ring under dynamic loading for Specimen No. 33-7 (100 mg PETN detonator).

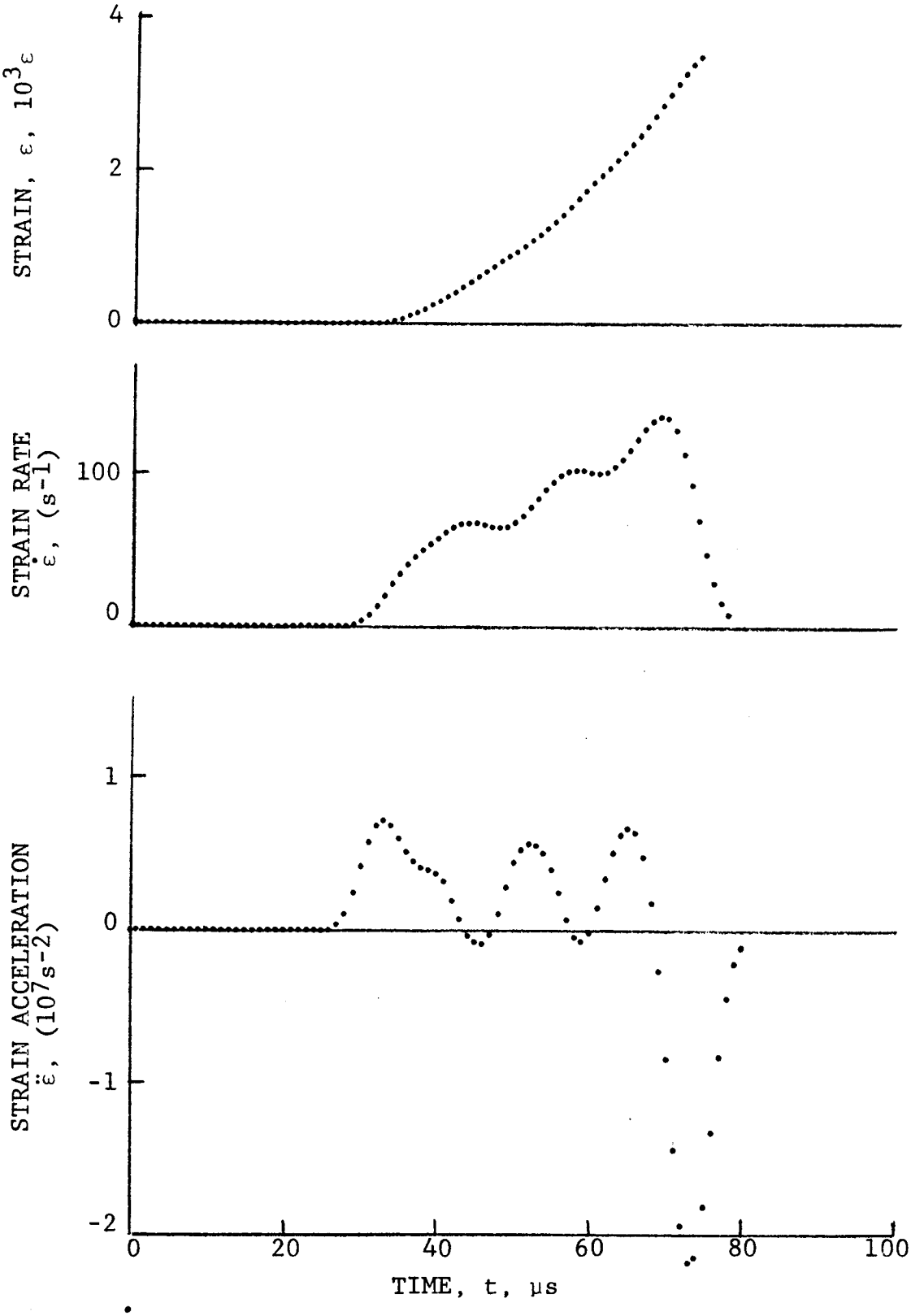

Figure 4-32. Strain in steel ring and its derivatives for Specimen No. 33-7.

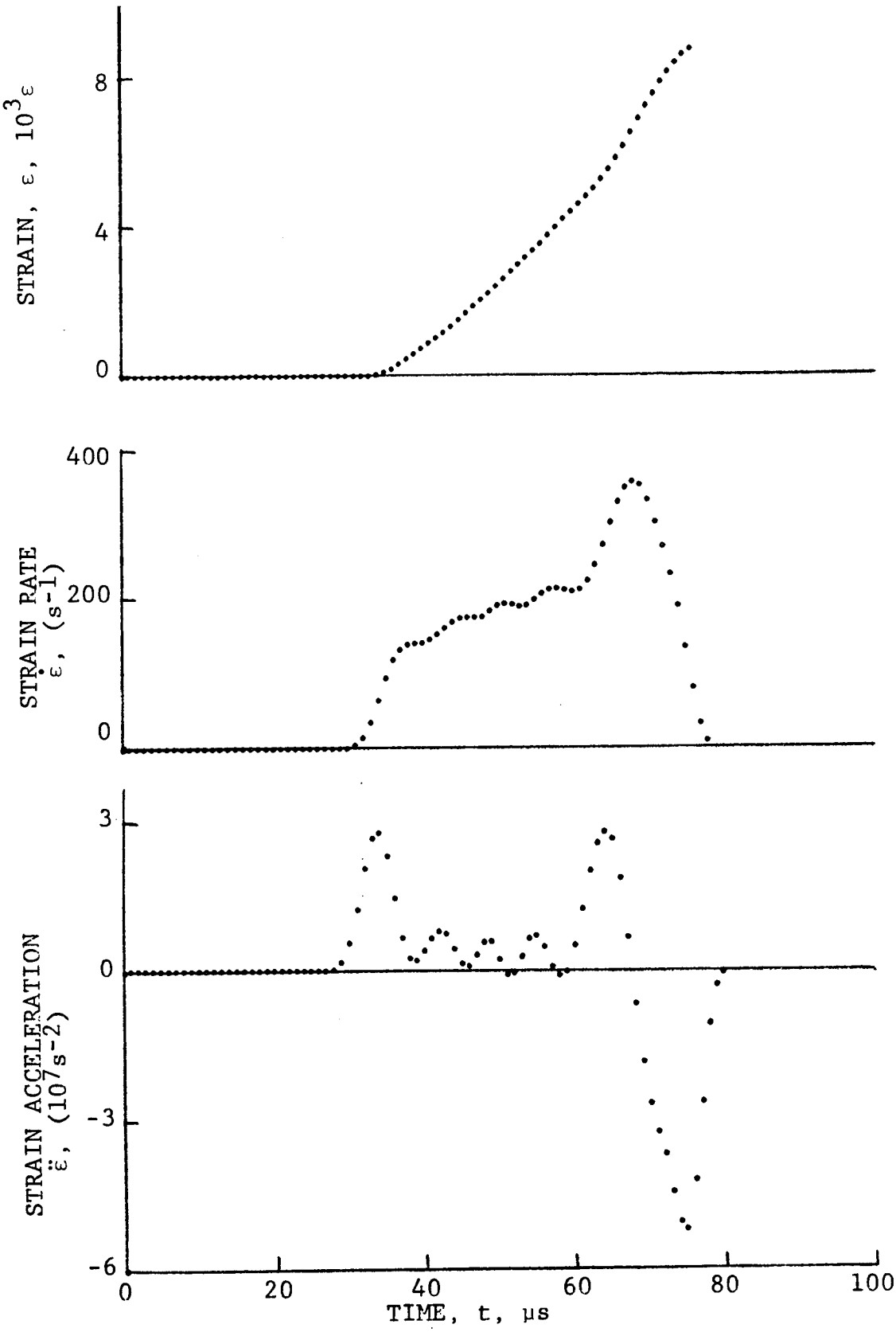

Figure 4-33. Circumferential strain and its derivatives in SP288/AS $[\pm 22.5]_{2s}$ graphite/epoxy ring under dynamic loading, Specimen No. 33-7.

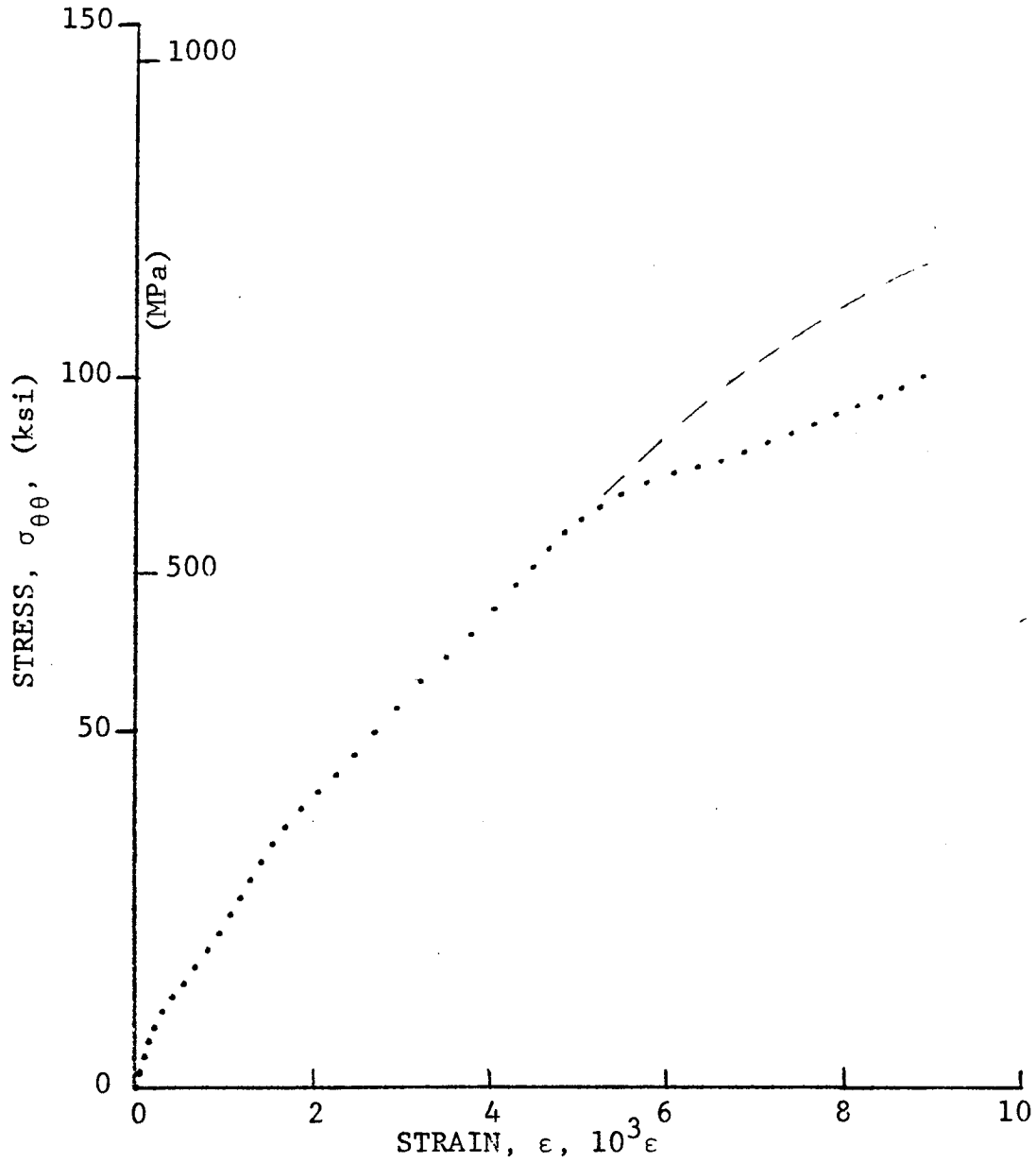

Figure 4-34. Stress-strain curve for dynamically loaded SP288/AS $[\pm 22.5]_{2s}$ graphite/epoxy ring, Specimen No. 33-4 (100 mg PETN detonator).

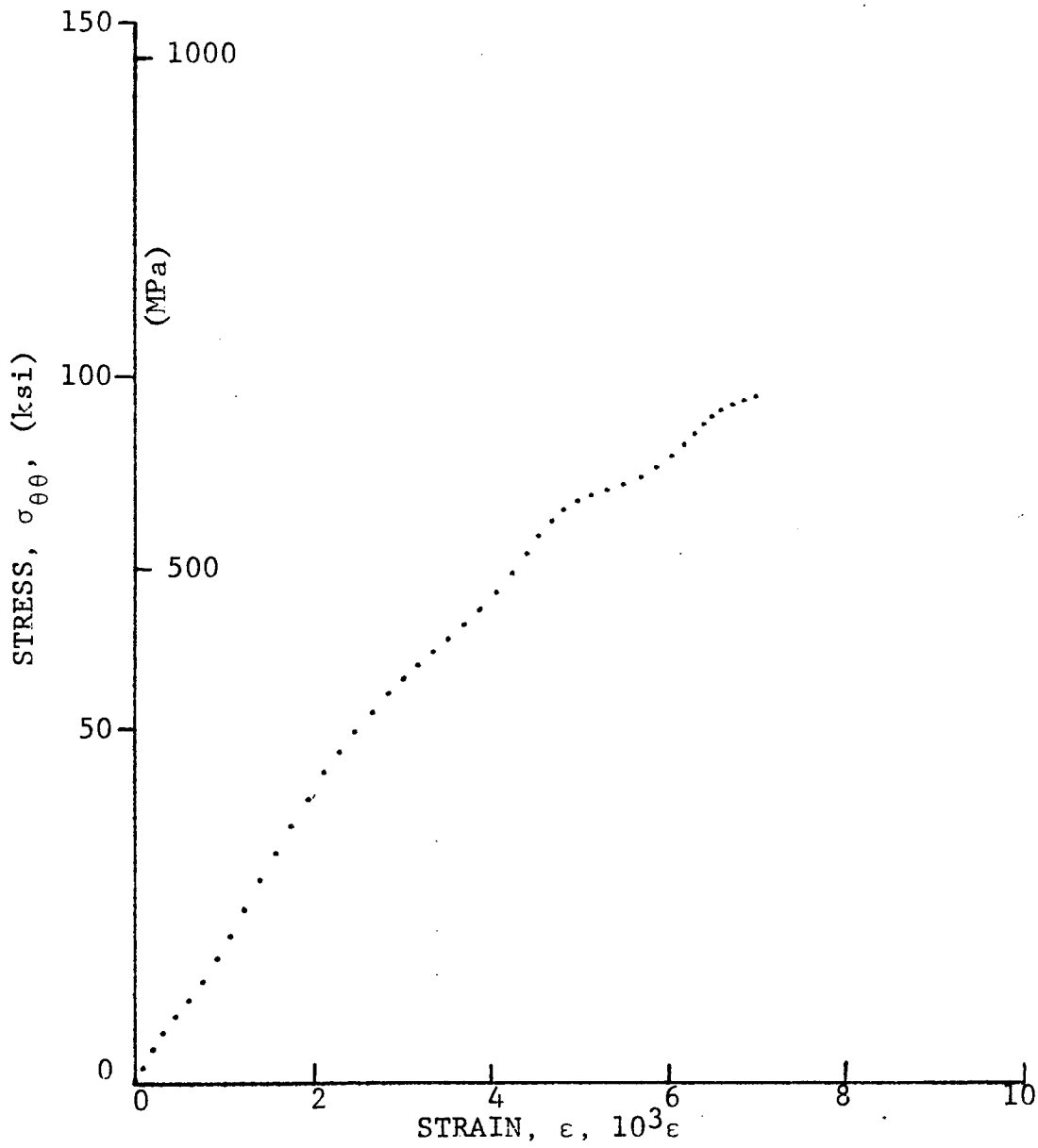

Figure 4-35. Stress-strain curve for dynamically loaded SP288/AS $[\pm 22.5]_{2s}$ graphite/epoxy ring, Specimen No. 33-6 (100 mg PETN detonator).

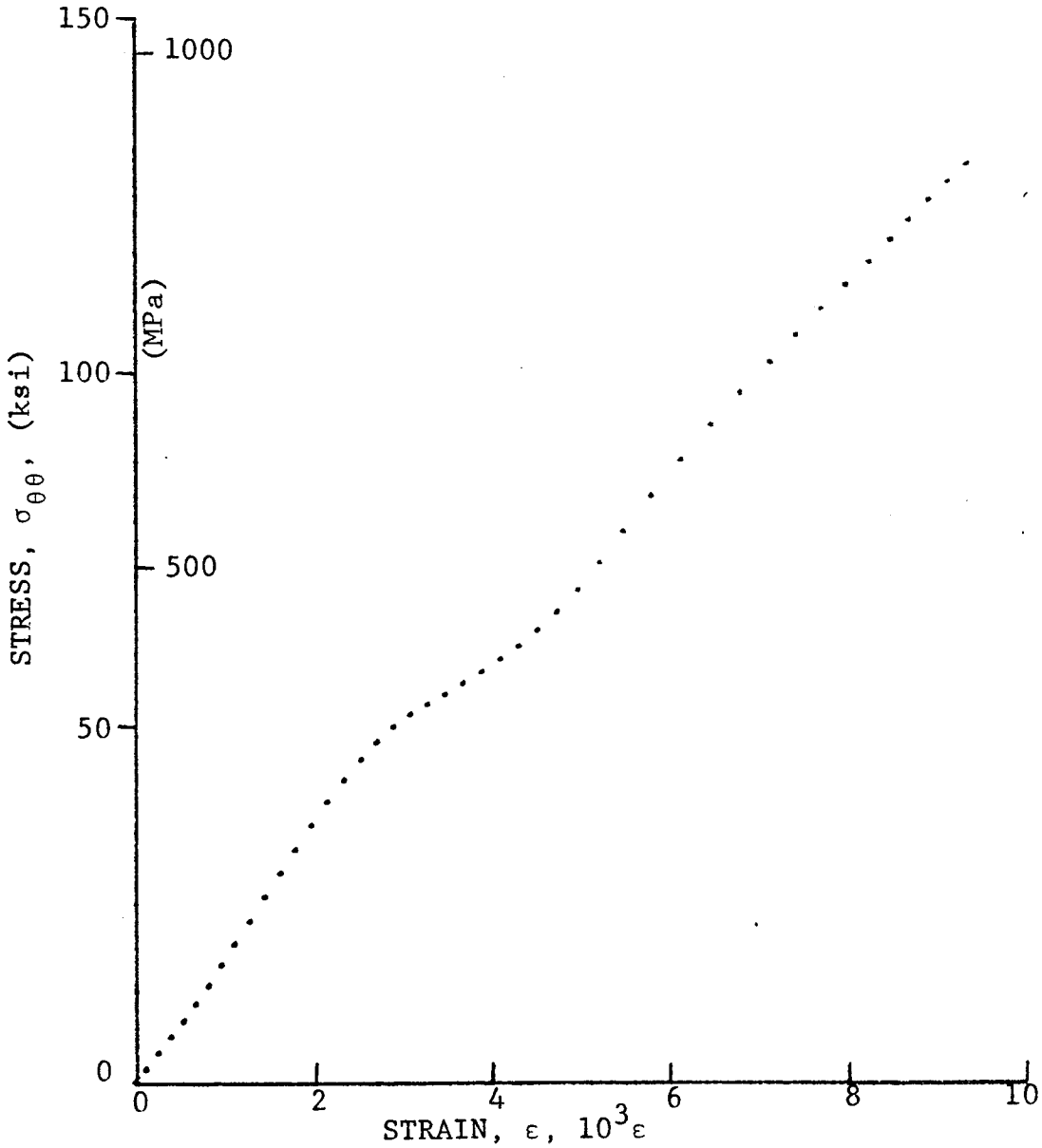

Figure 4-36. Stress-strain curve for dynamically loaded SP288/AS $[\pm 22.5]_{2s}$ graphite/epoxy ring, Specimen No. 33-7 (100 mg PETN detonator).

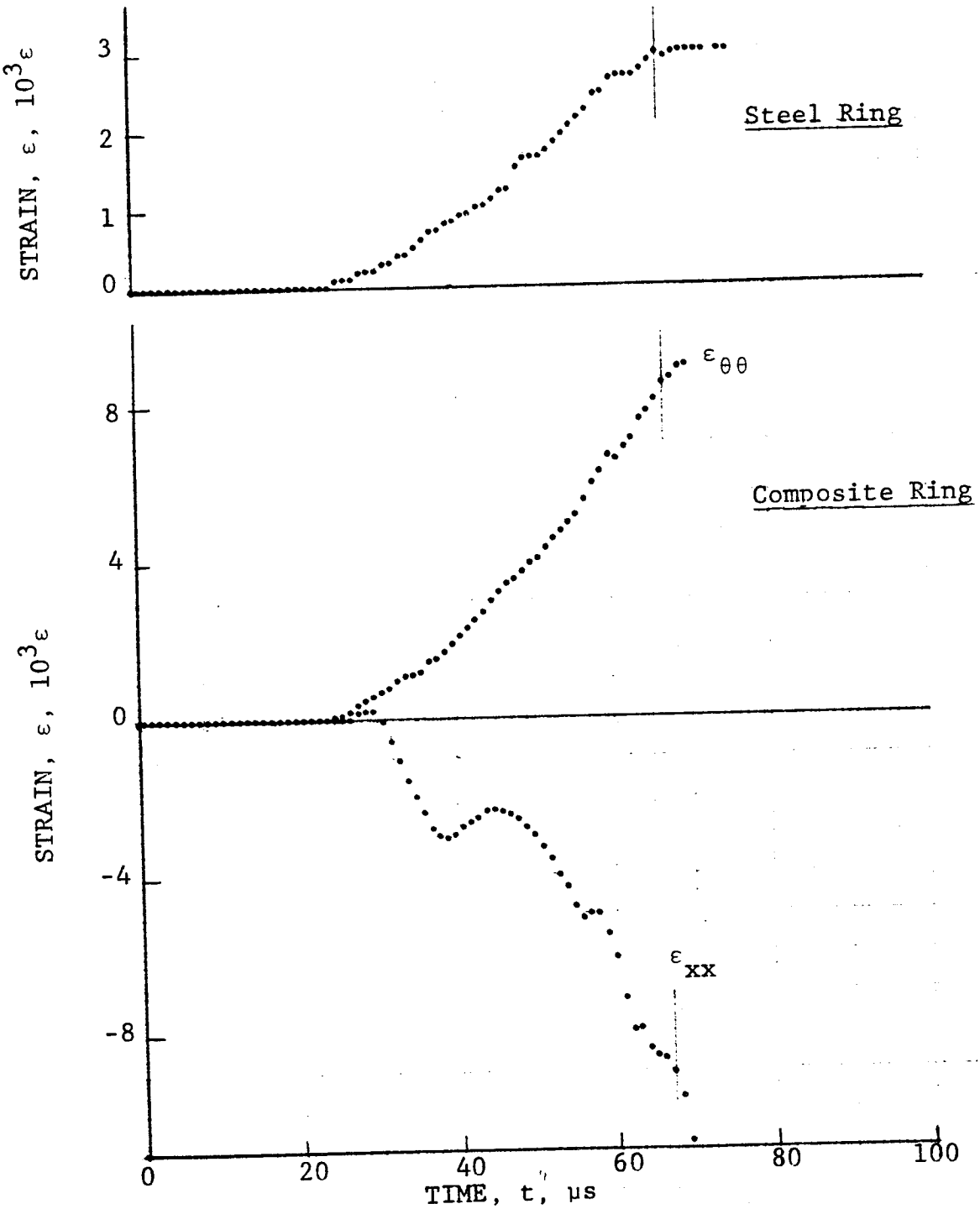

Figure 4-37. Strain records in steel ring and in 80AS/20S/PR288 $[\pm 22.5]_{2s}$ graphite/S-glass/epoxy ring under dynamic loading for Specimen No. 34-4 (100 mg PETN detonator).

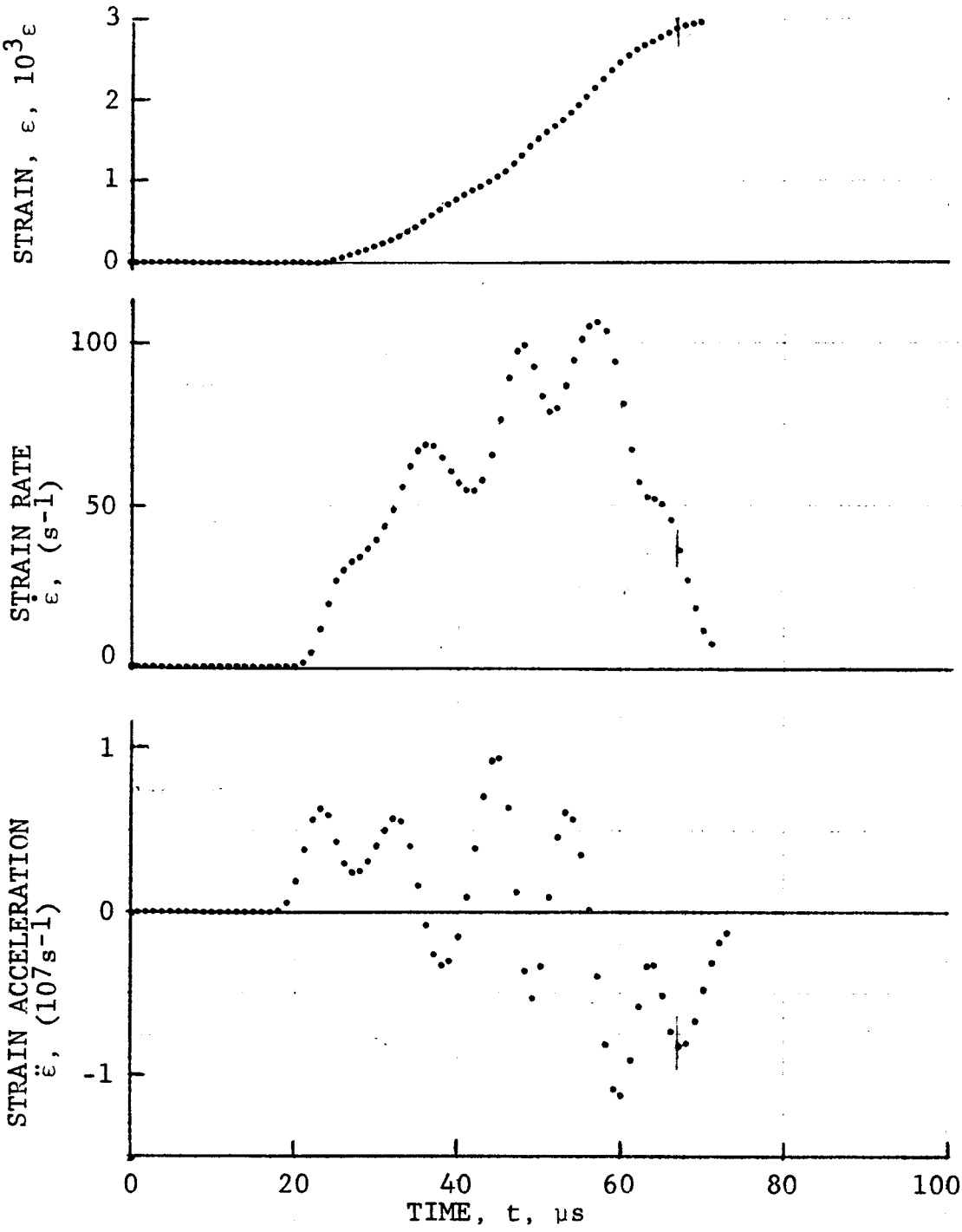

Figure 4-38. Strain and its derivatives in steel ring for Specimen No. 34-4.

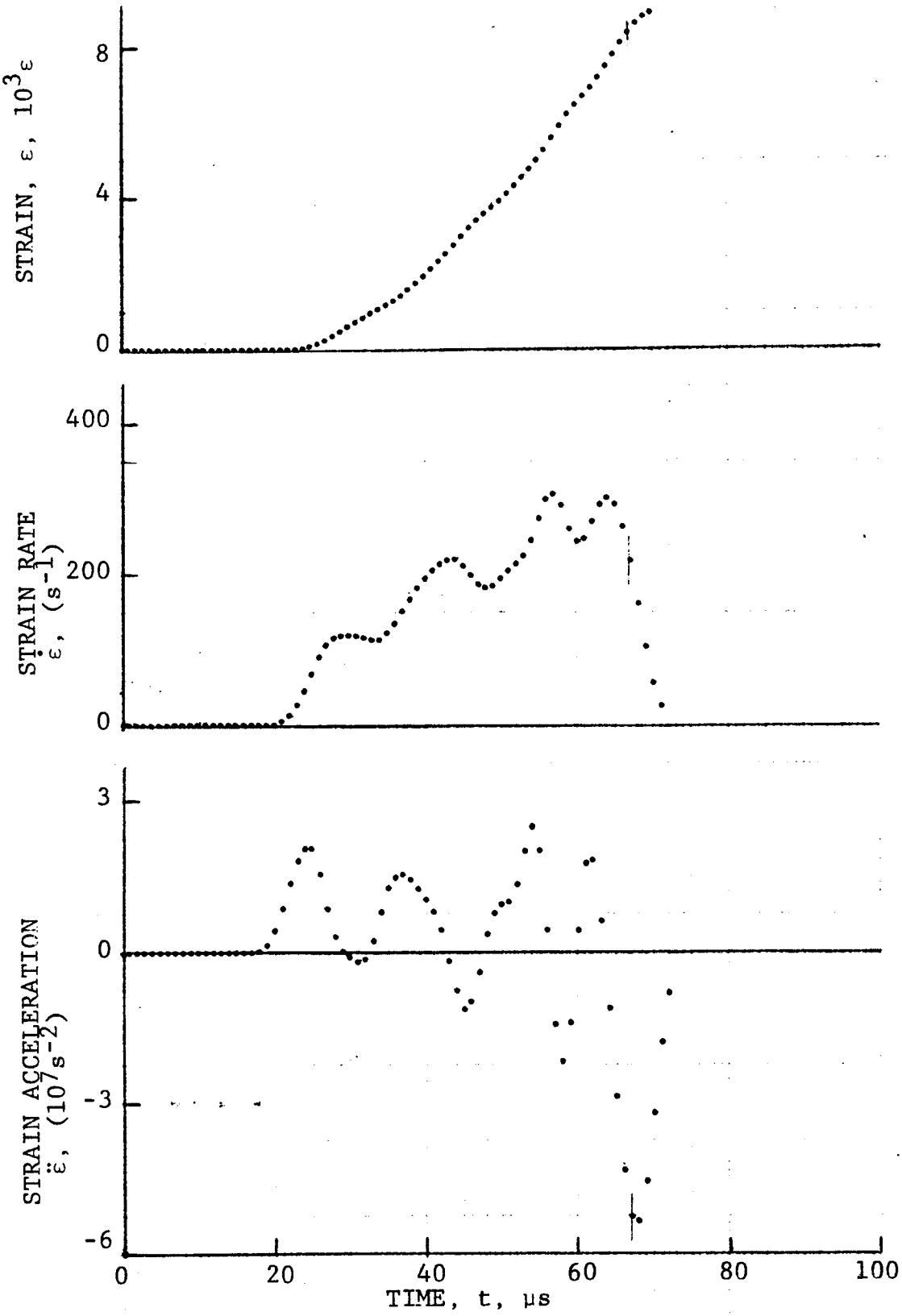

Figure 4-39. Circumferential strain and its derivatives in 80AS/20S/PR288 $[\pm 22.5]_{2s}$ graphite/S-glass/epoxy ring under dynamic loading, Specimen No. 34-4.

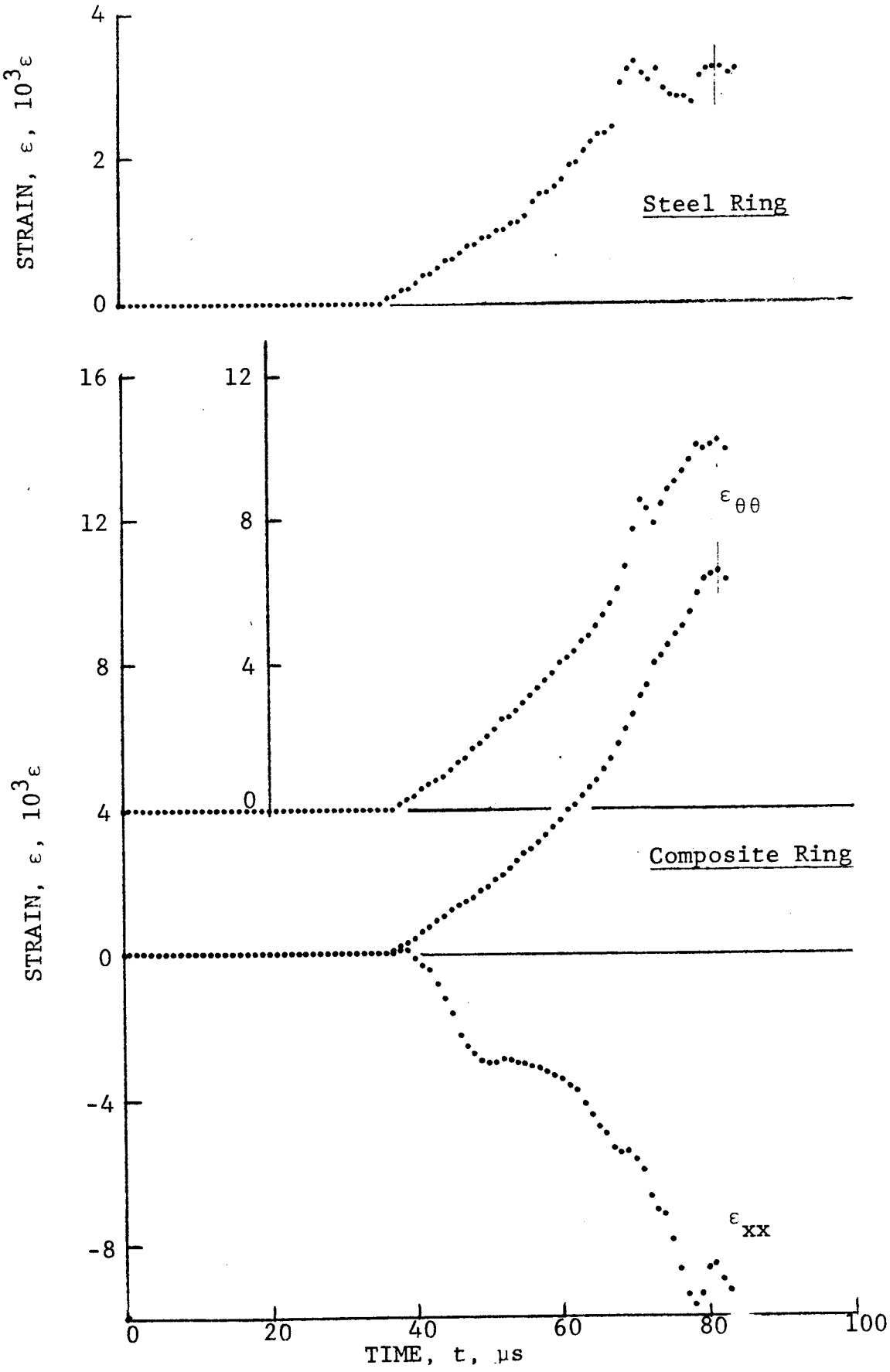

Figure 4-40. Strain records in steel ring and in 80AS/20S/PR288 $[\pm 22.5]_{2S}$ graphite/S-glass/epoxy ring under dynamic loading, Specimen No. 34-6 (100 mg PETN detonator).

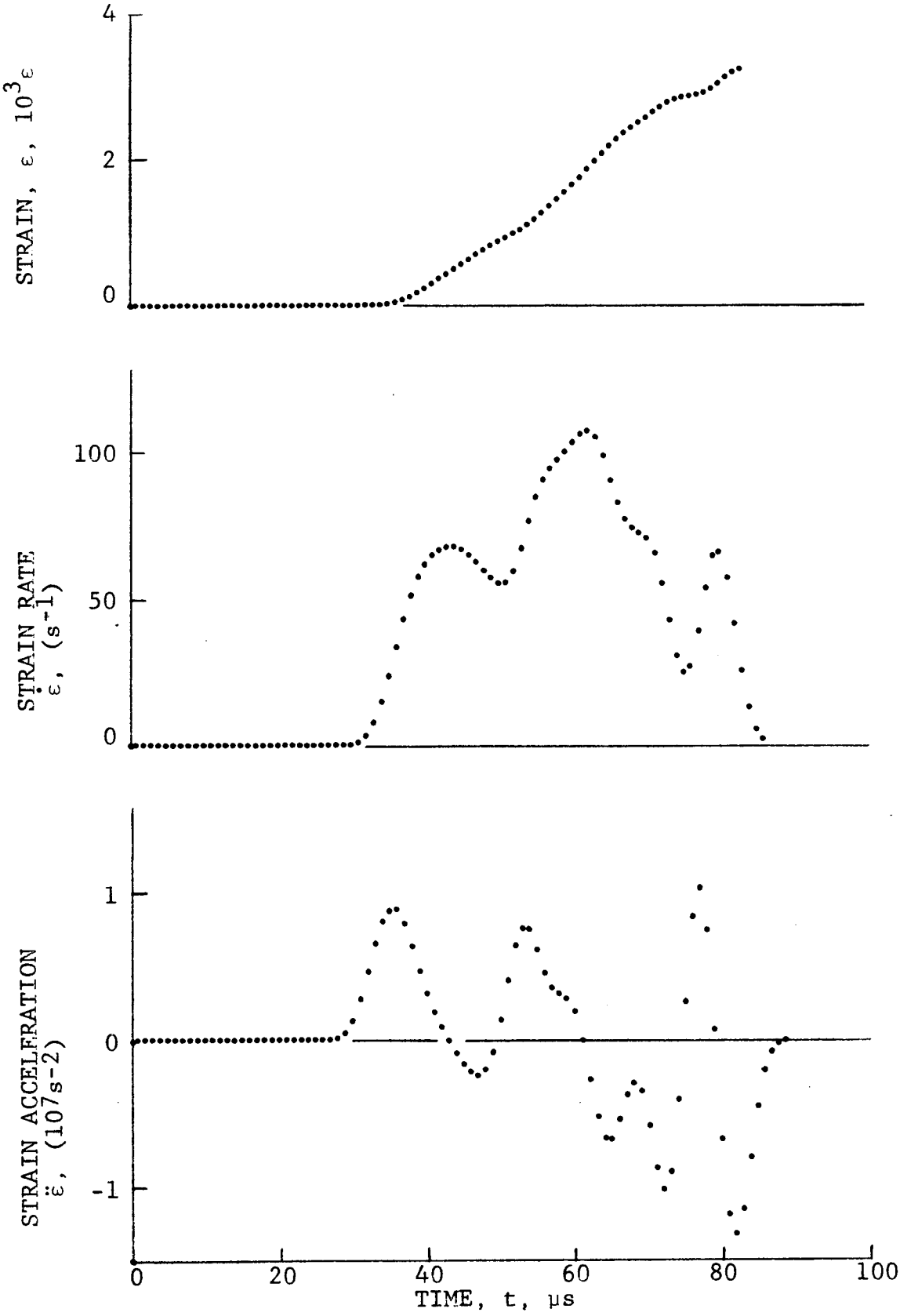

Figure 4-41. Strain and its derivatives in steel ring for Specimen No. 34-6.

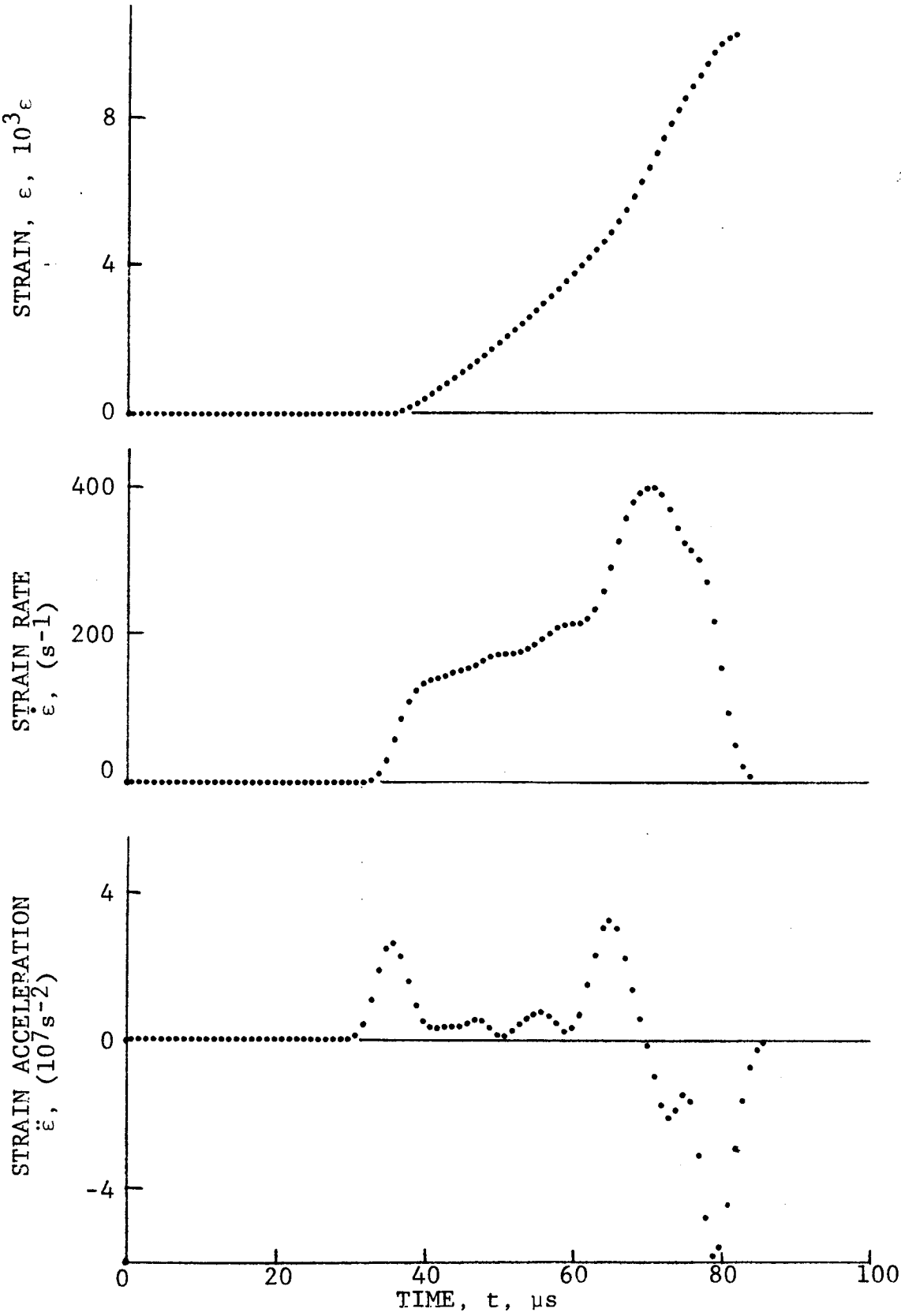

Figure 4-42. Circumferential strain and its derivatives in 80AS/20S/PR288 $[\pm 22.5]_{2S}$ graphite/S-glass/epoxy ring under dynamic loading, Specimen No. 34-6.

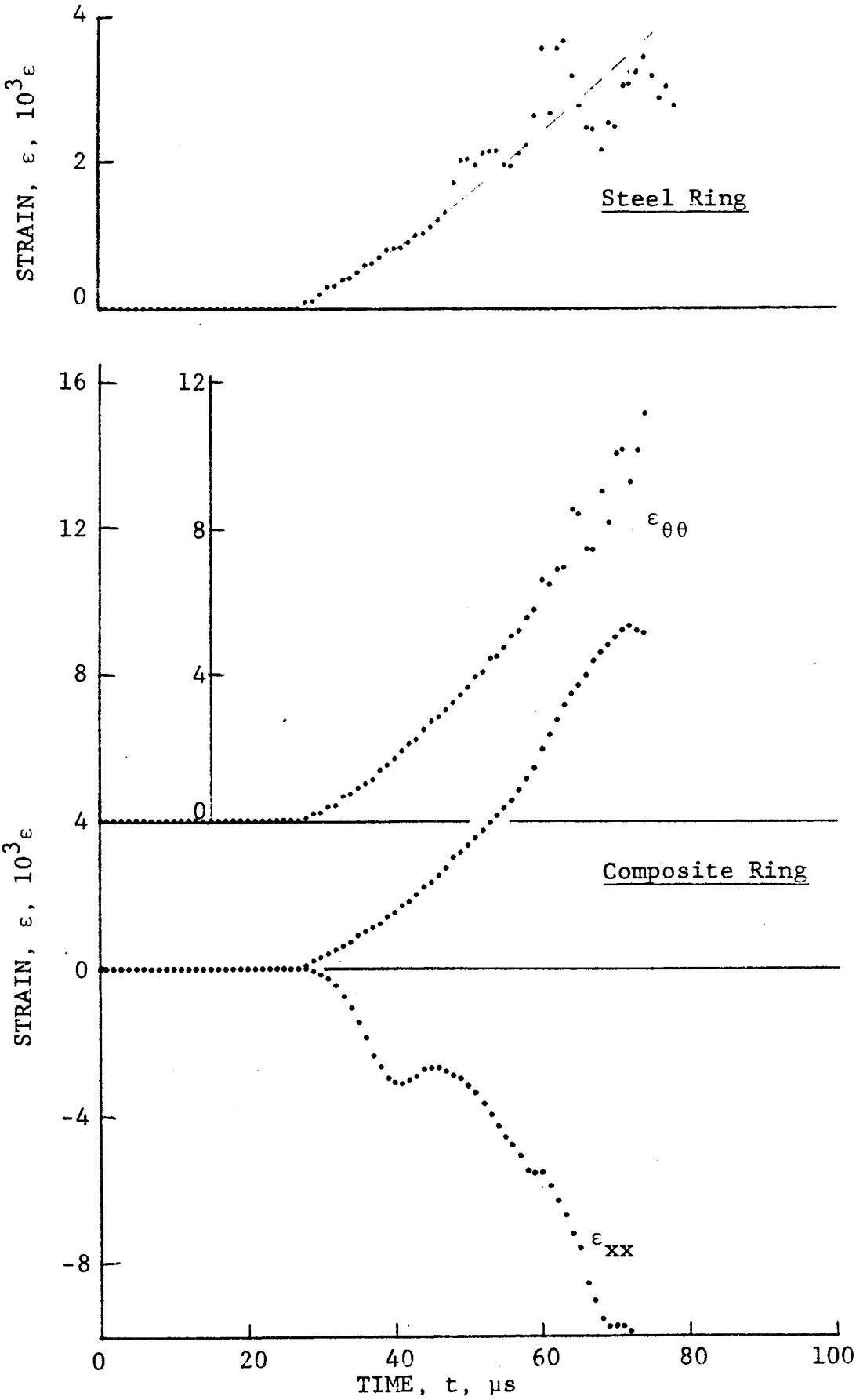

Figure 4-43. Strain records in steel ring and in 80AS/20S/PR288 $[\pm 22.5]_{2S}$ graphite/S-glass/epoxy ring under dynamic loading, Specimen No. 34-7 (100 mg PETN detonator).

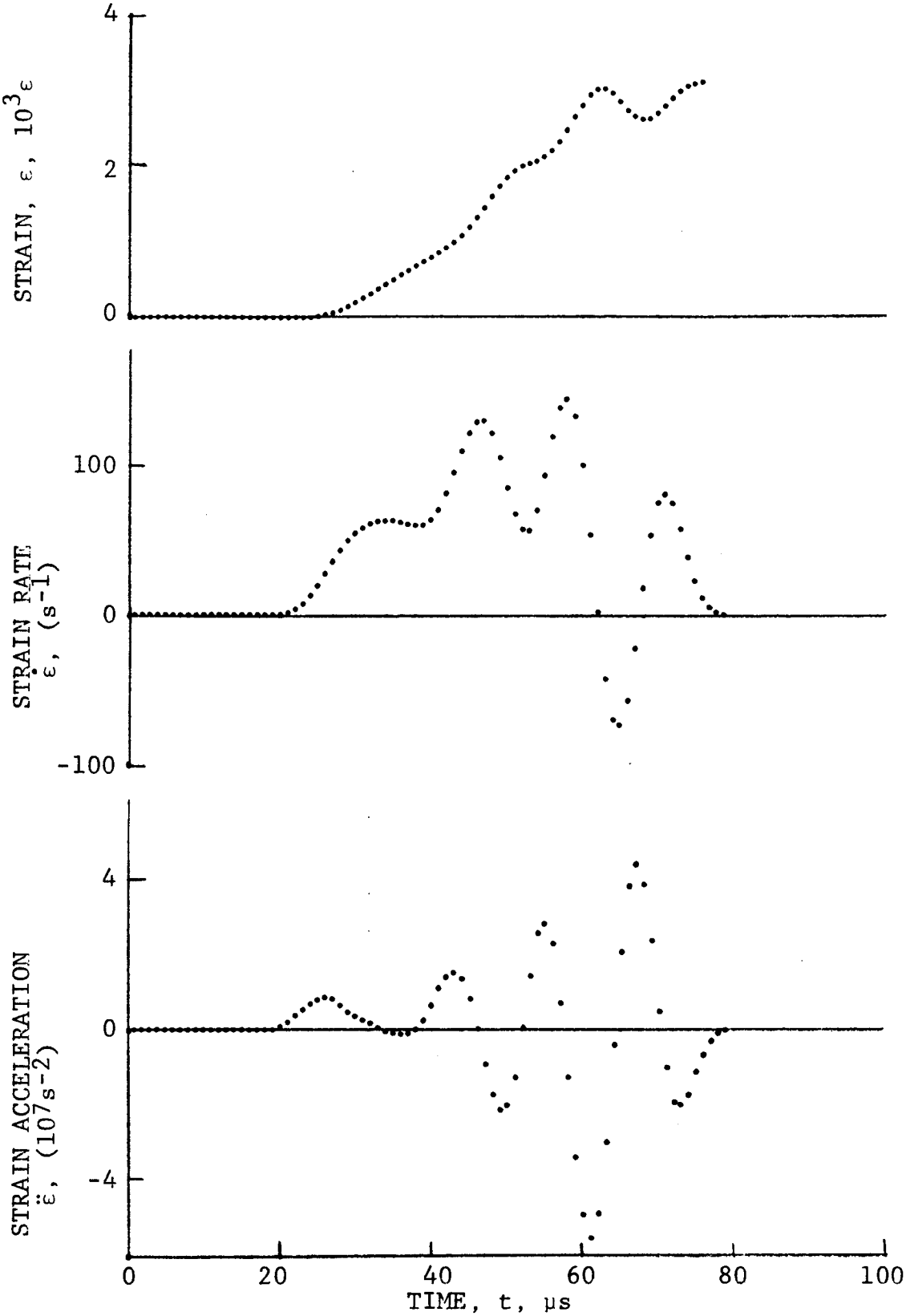

Figure 4-44. Strain and its derivatives in steel ring for Specimen No. 34-7.

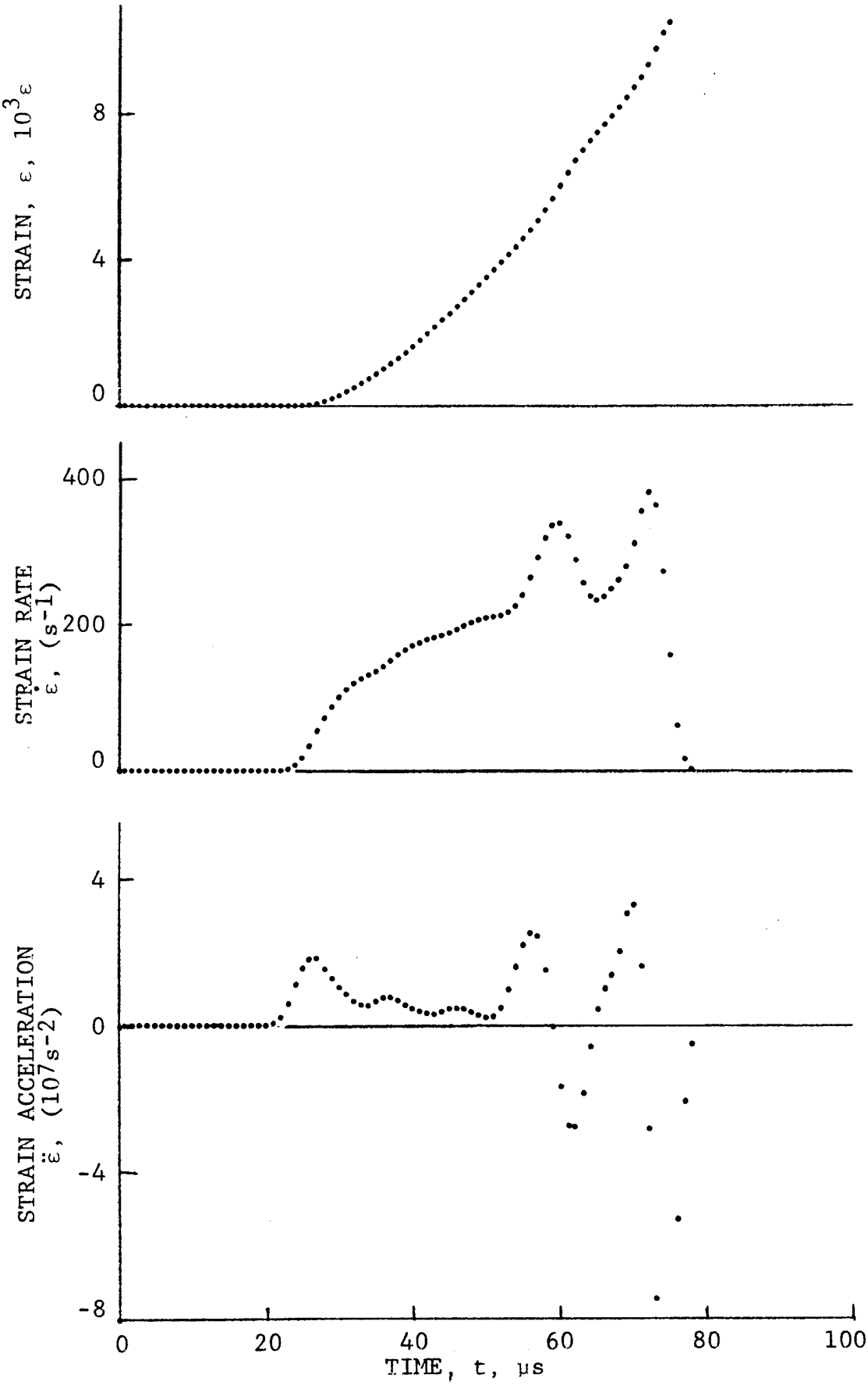

Figure 4-45. Circumferential strain and its derivatives in 80AS/20S/PR288 $[\pm 22.5]_{2S}$ graphite/S-glass/epoxy ring under dynamic loading, Specimen No. 34-7.

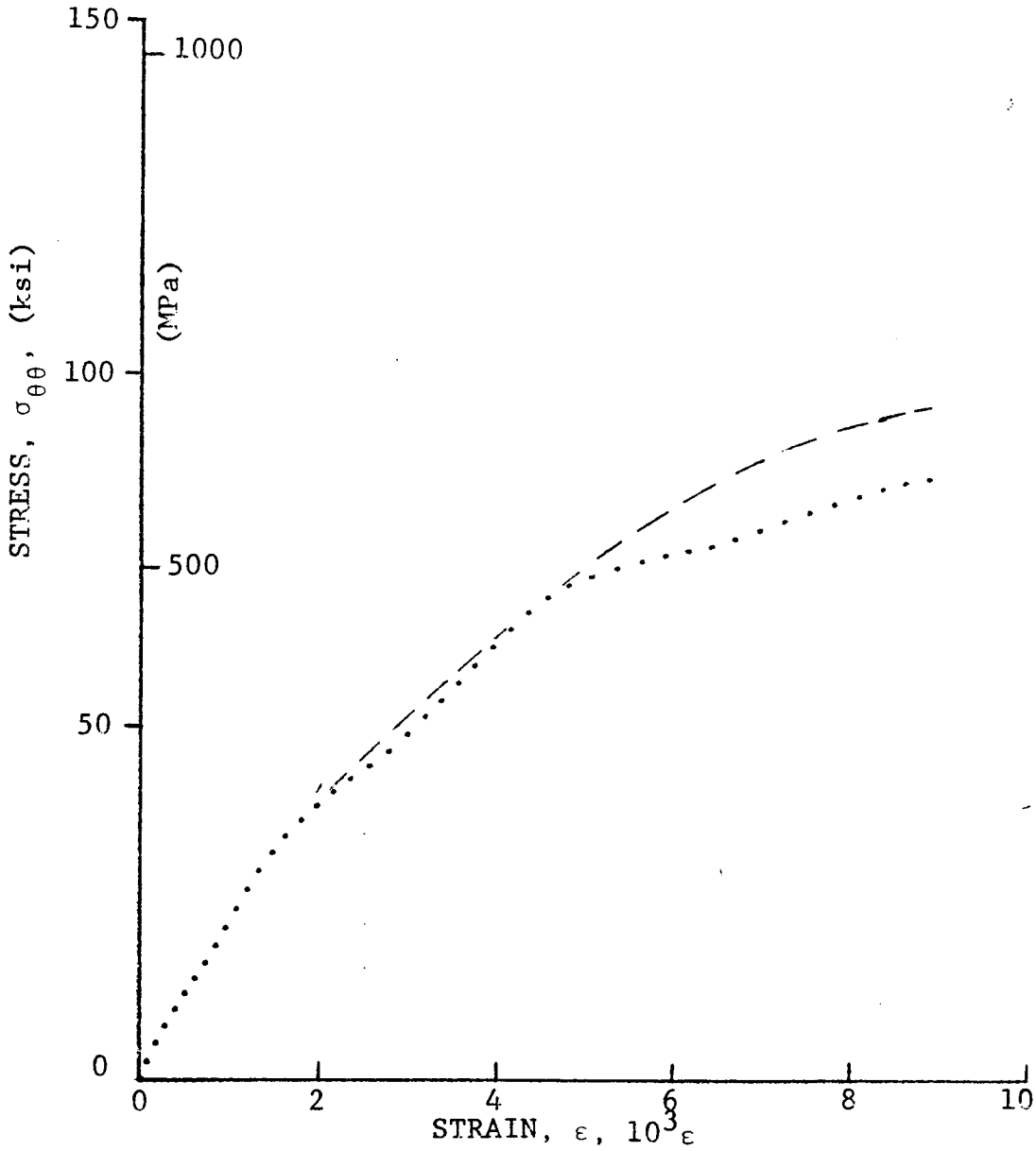

Figure 4-46. Stress-strain curve for dynamically loaded 80AS/20S/PR288 $[\pm 22.5]_{2S}$ graphite/S-glass/epoxy ring, Specimen No. 34-4 (100 mg PETN detonator).

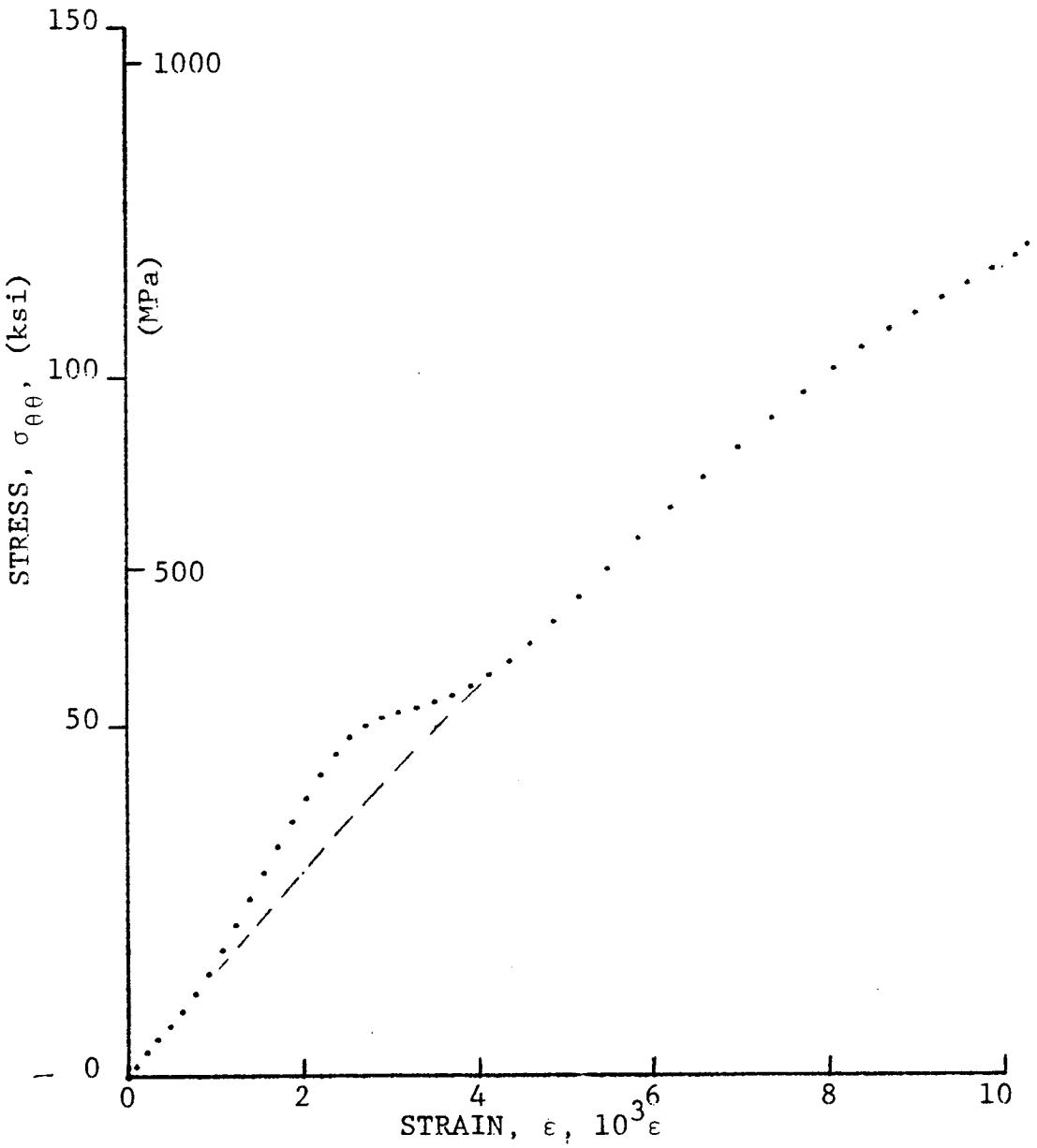

Figure 4-47. Stress-strain curve for dynamically loaded 80AS/20S/PR288 $[\pm 22.5]_{2S}$ graphite/S-glass/epoxy ring, Specimen No. 34-6 (100 mg PETN detonator).

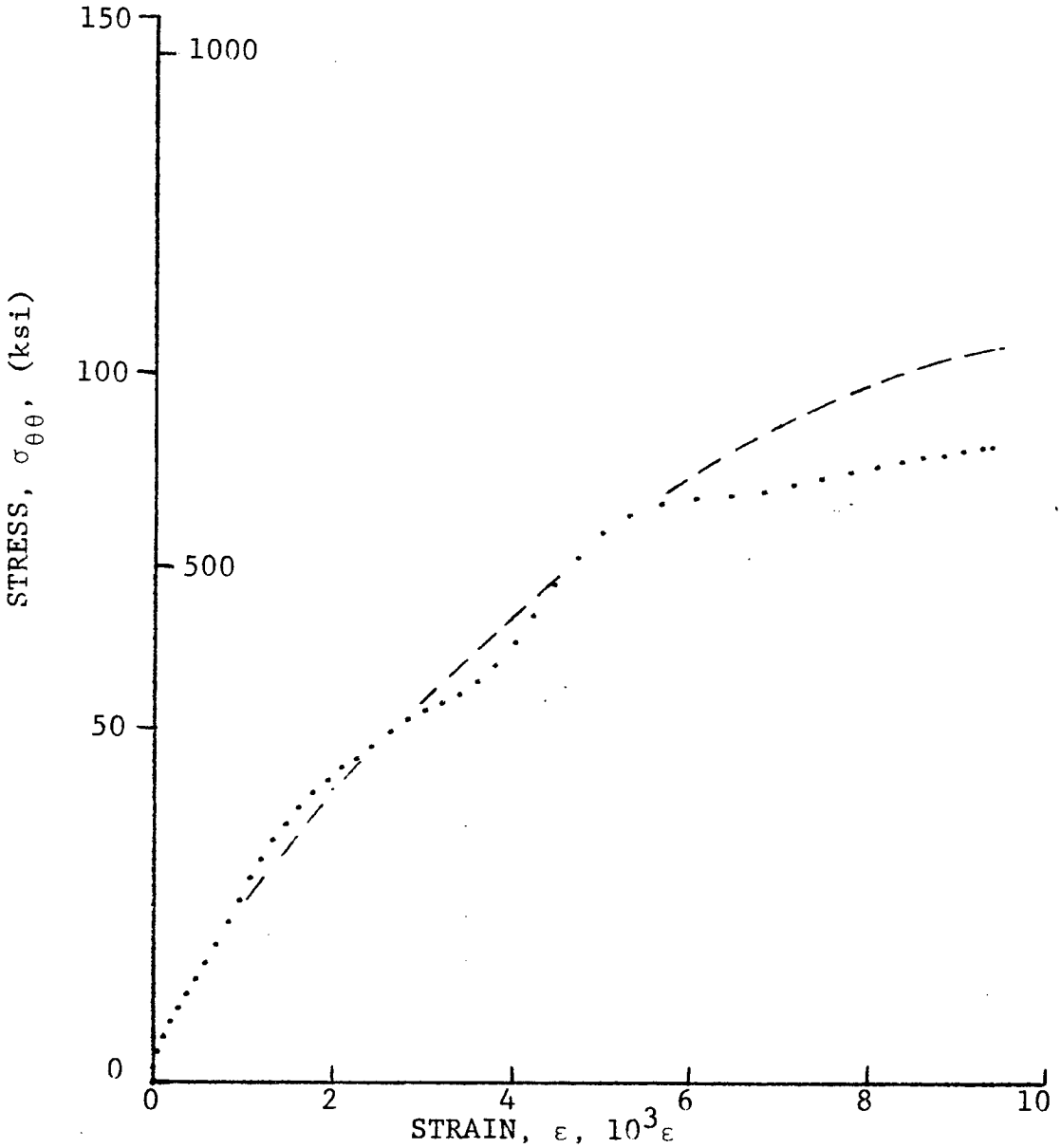

Figure 4-48. Stress-strain curve for dynamically loaded 80AS/20S/PR288 $[\pm 22.5]_{2s}$ graphite/S-glass/epoxy ring, Specimen No. 34-7 (100 mg PETN detonator).

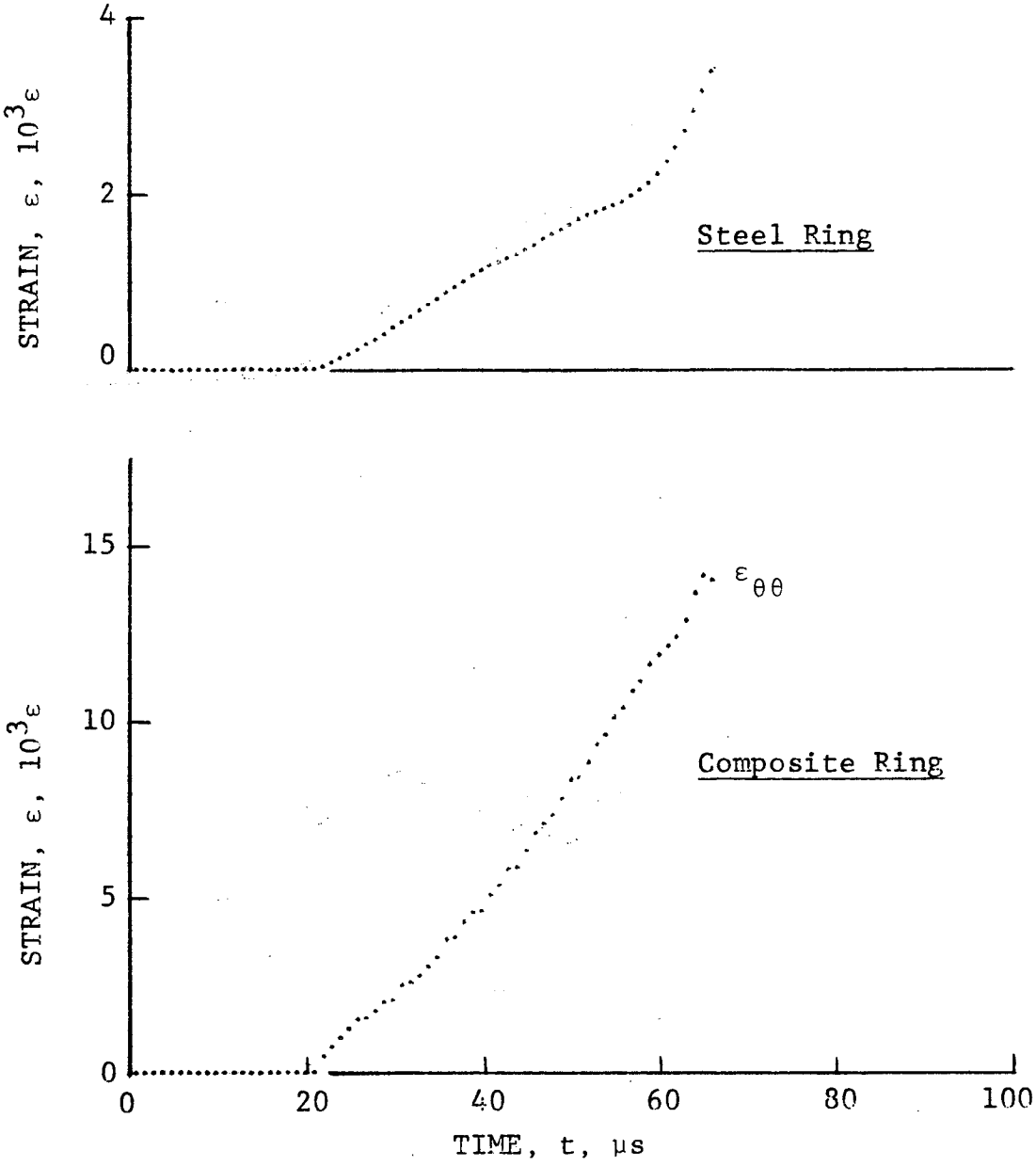

Figure 4-49. Strain records in steel ring and SP288/AS $[\pm 30]_{2s}$ graphite/epoxy ring under dynamic loading, Specimen No. 28-9 (1.56 g bullseye powder, $KC\ell O_4$, and aluminum dust).

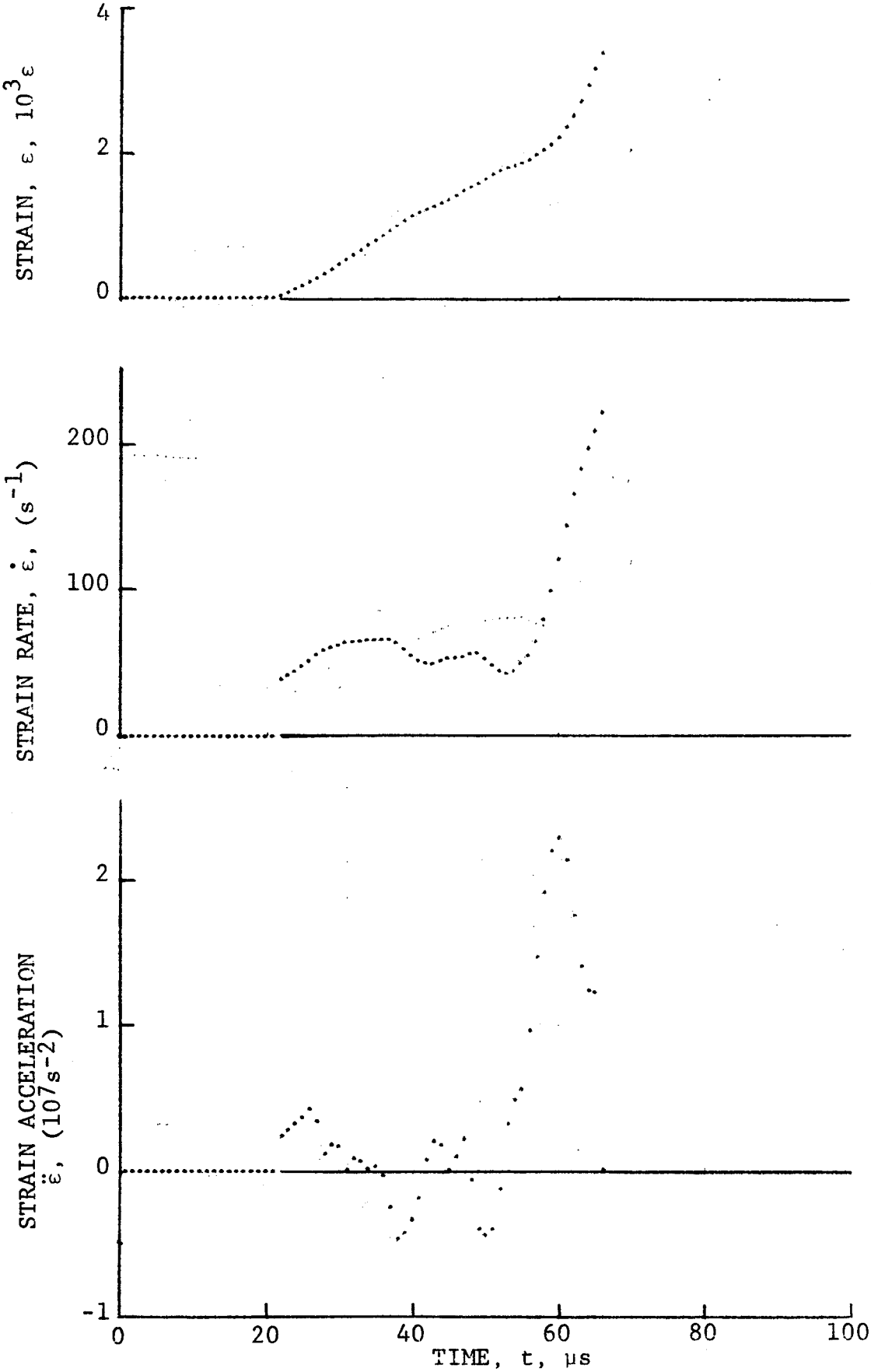

Figure 4-50. Strain and its derivatives in steel ring for Specimen No. 28-9.

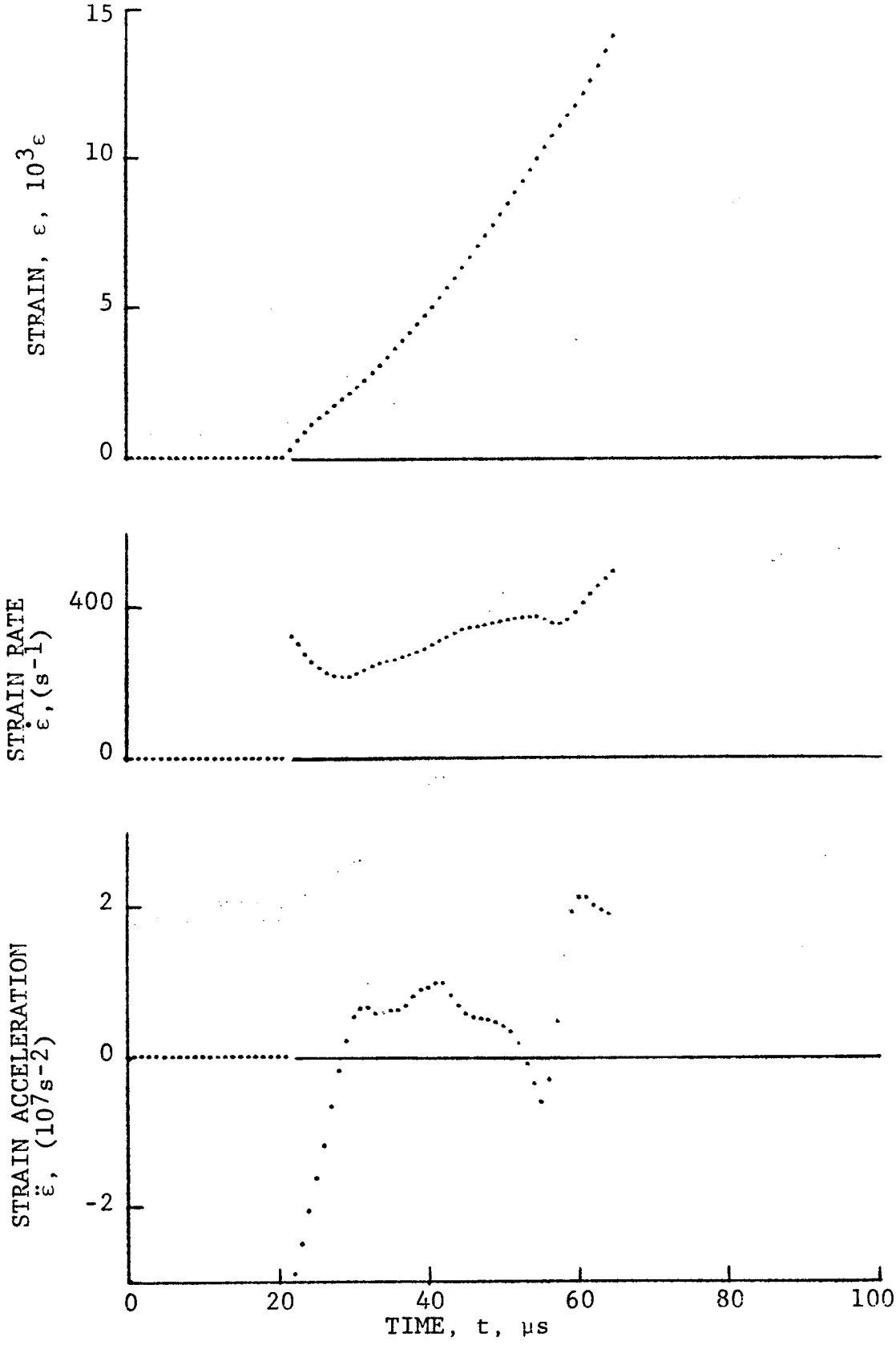

Figure 4-51. Circumferential strain and its derivatives in SP288/AS $[\pm 30]_{2S}$ graphite/epoxy ring under dynamic loading, Specimen No. 28-9.

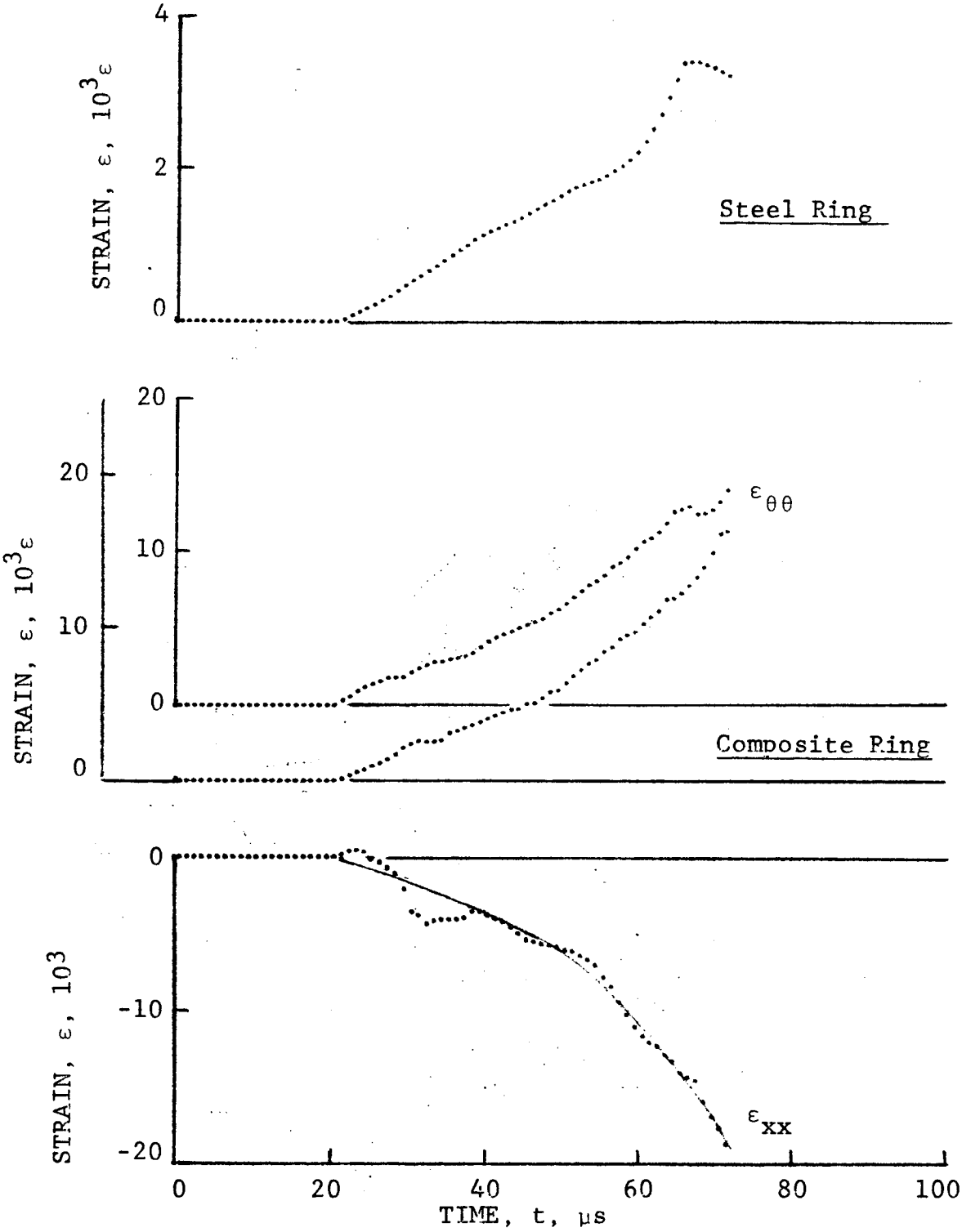

Figure 4-52. Strain records in steel ring and SP288/AS $[\pm 30]_{2s}$ graphite/epoxy ring under dynamic loading, Specimen No. 28-10 (1.56 g bullseye powder, $KC\ell O_4$, and aluminum dust).

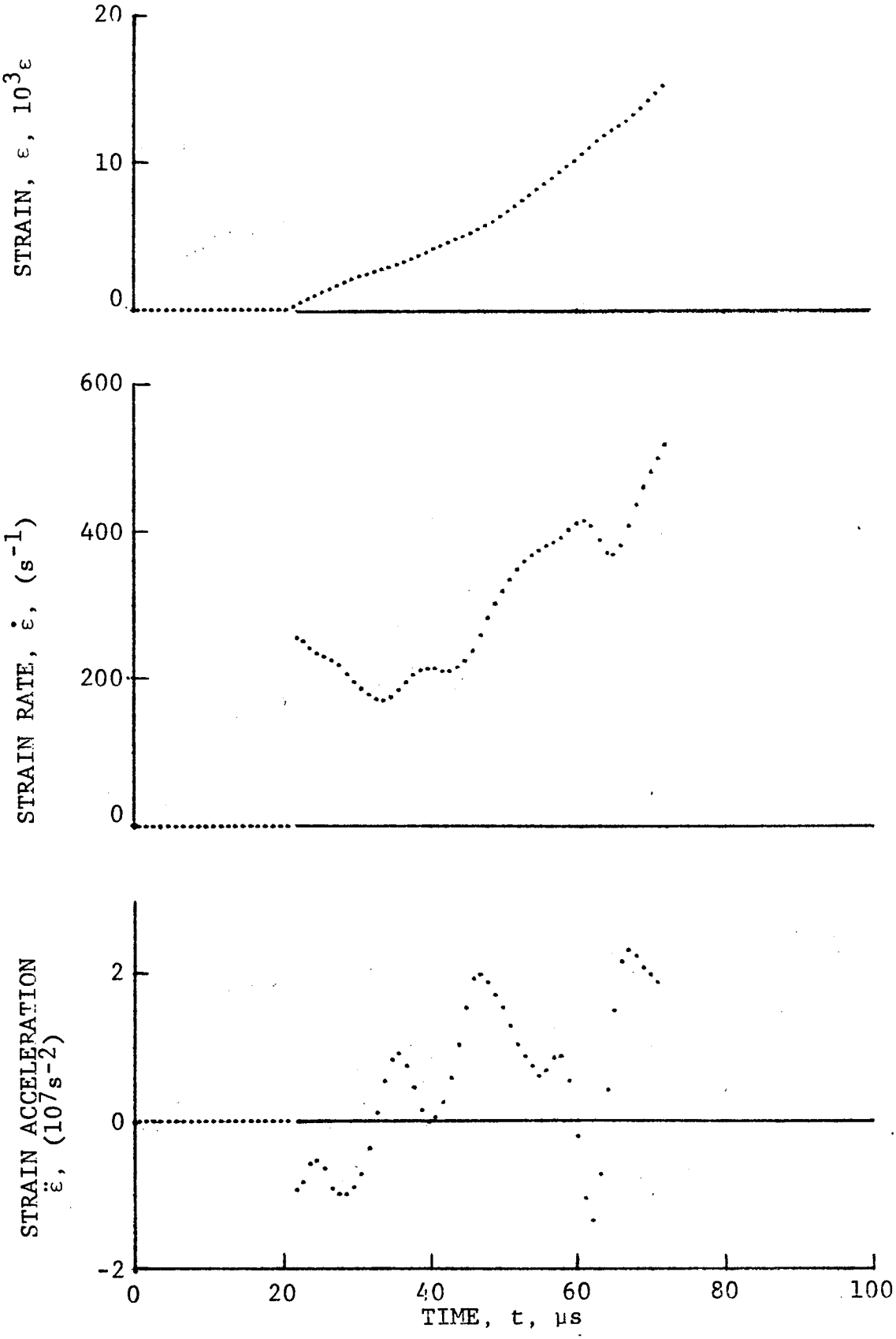

Figure 4-53. Circumferential strain and its derivatives in SP288/AS $[\pm 30]_{2s}$ graphite/epoxy ring under dynamic loading, Specimen No. 28-10.

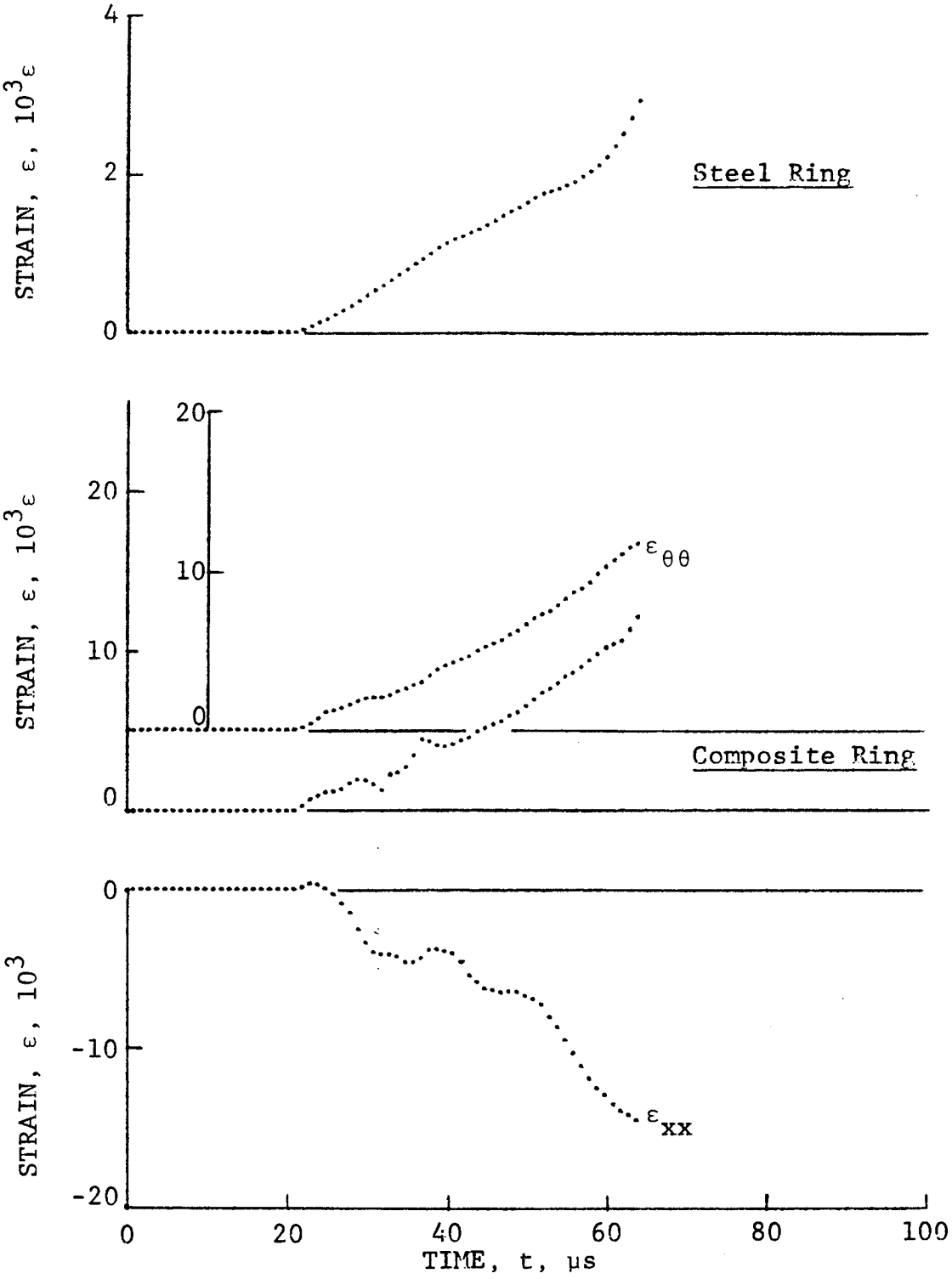

Figure 4-54. Strain records in steel ring and SP288/AS $[\pm 30]_{2S}$ graphite/epoxy ring under dynamic loading, Specimen No. 28-11 (1.56 g bullseye powder, $KC\ell O_4$, and aluminum dust).

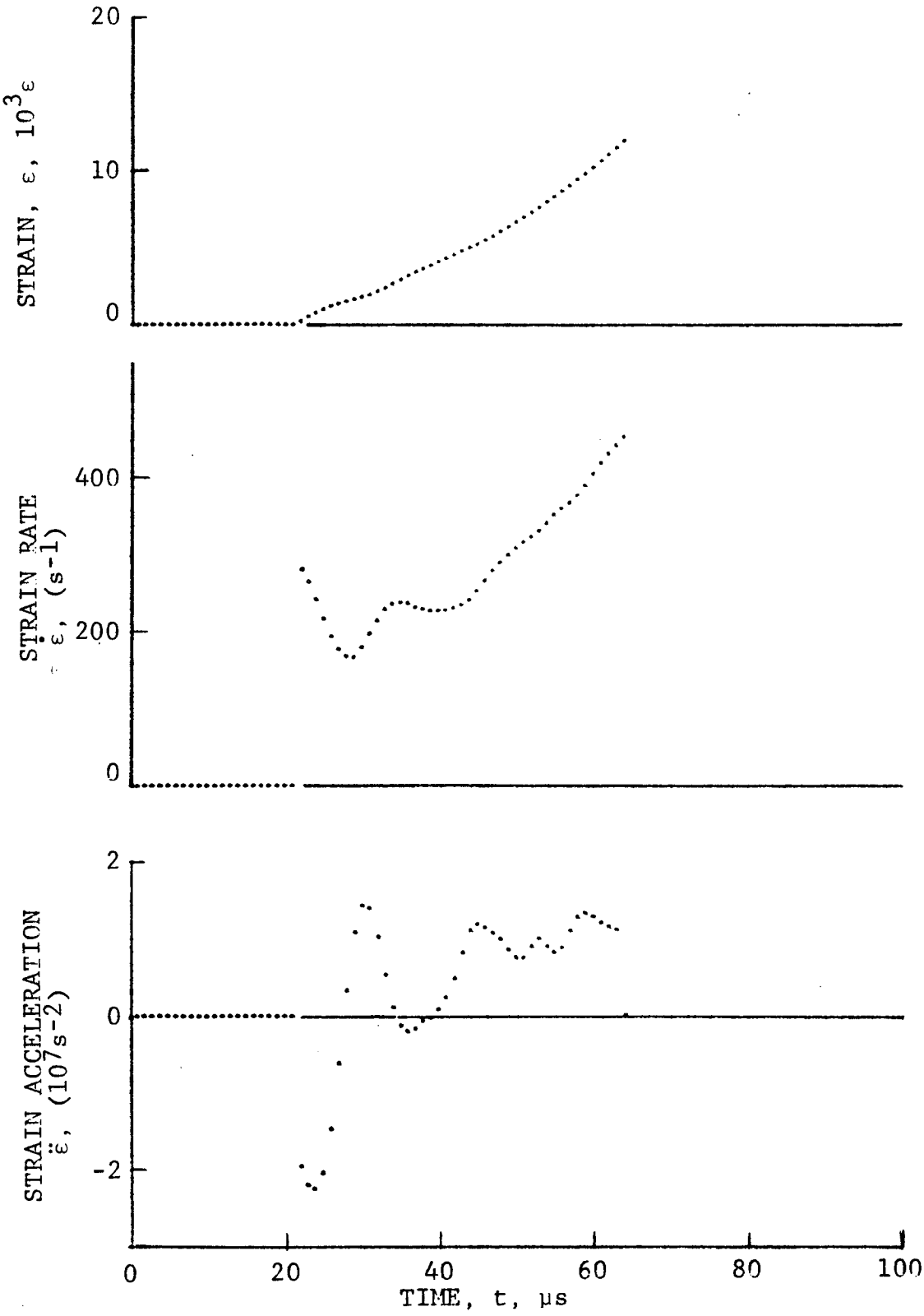

Figure 4-55. Circumferential strain and its derivatives in SP288/AS $[\pm 30]_{2S}$ graphite/epoxy ring under dynamic loading, Specimen No. 28-11.

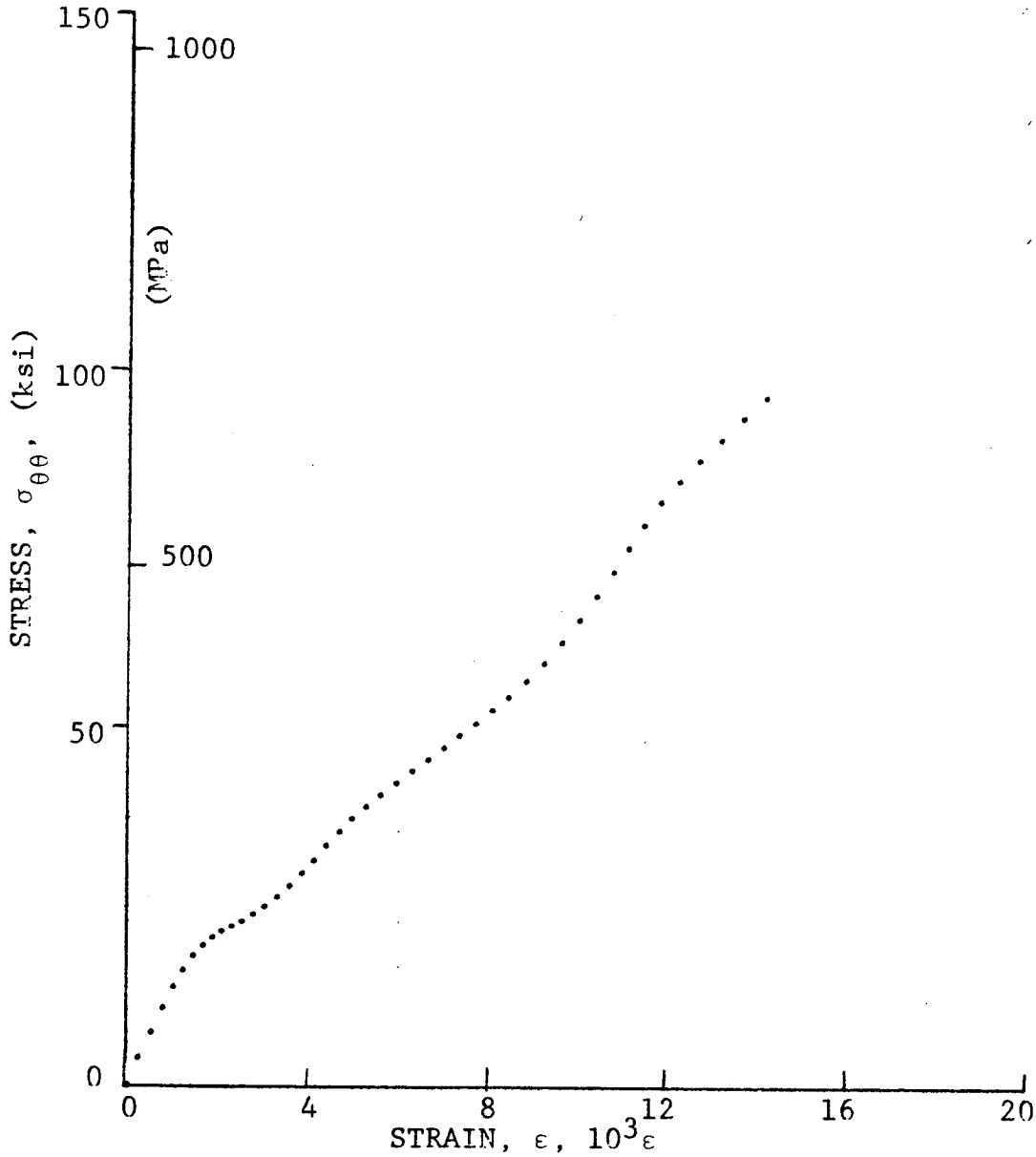

Figure 4-56. Stress-strain curve for dynamically loaded SP288/AS $[\pm 30]_{2S}$ graphite/epoxy ring, Specimen No. 28-9 (1.56 g bullseye powder, $KC\ell O_4$, and aluminum dust).

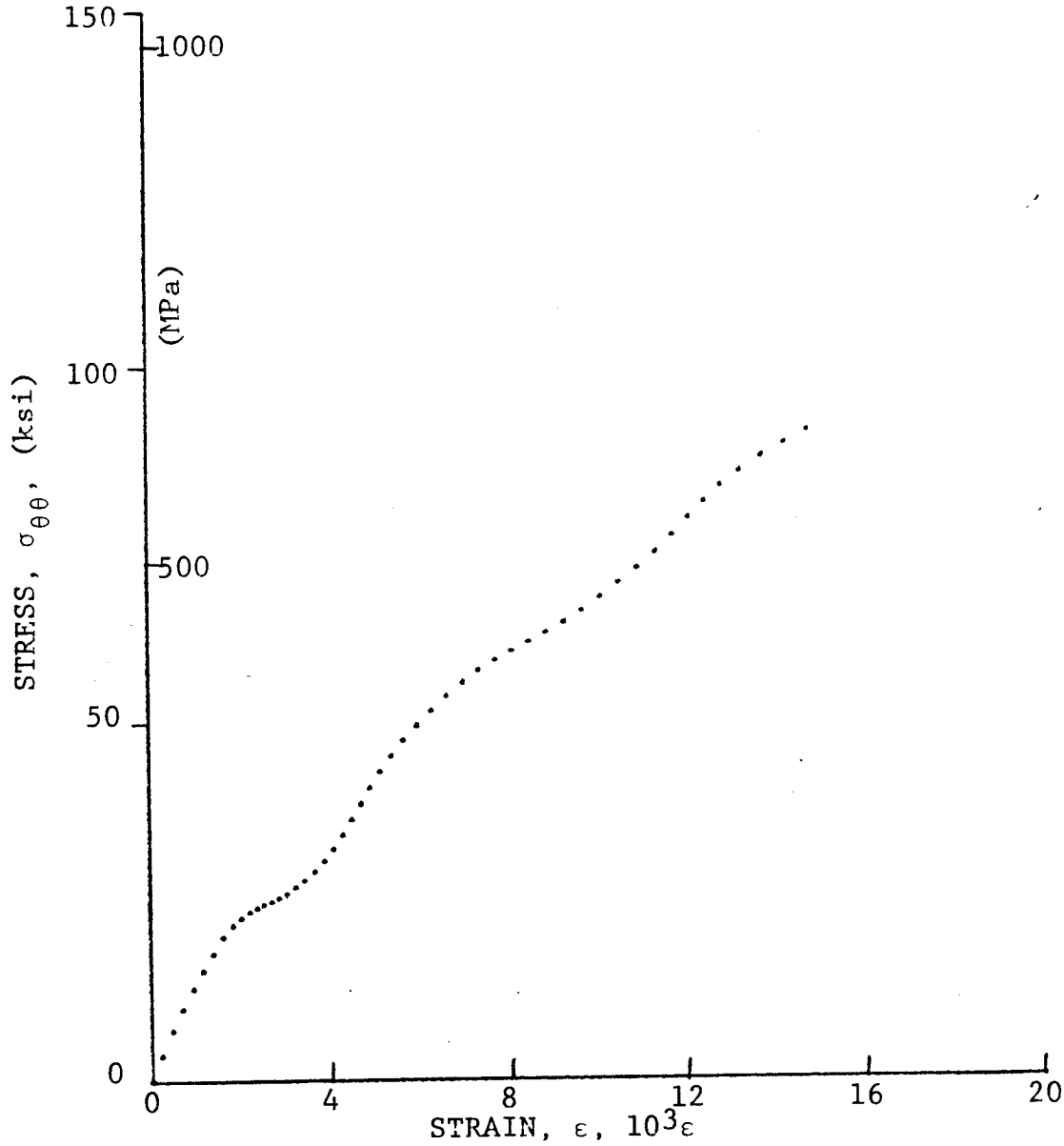

Figure 4-57. Stress-strain curve for dynamically loaded SP288/AS $[\pm 30]_{2S}$ graphite/epoxy ring, Specimen No. 28-10 (1.56 g bullseye powder, $KC\ell O_4$, and aluminum dust).

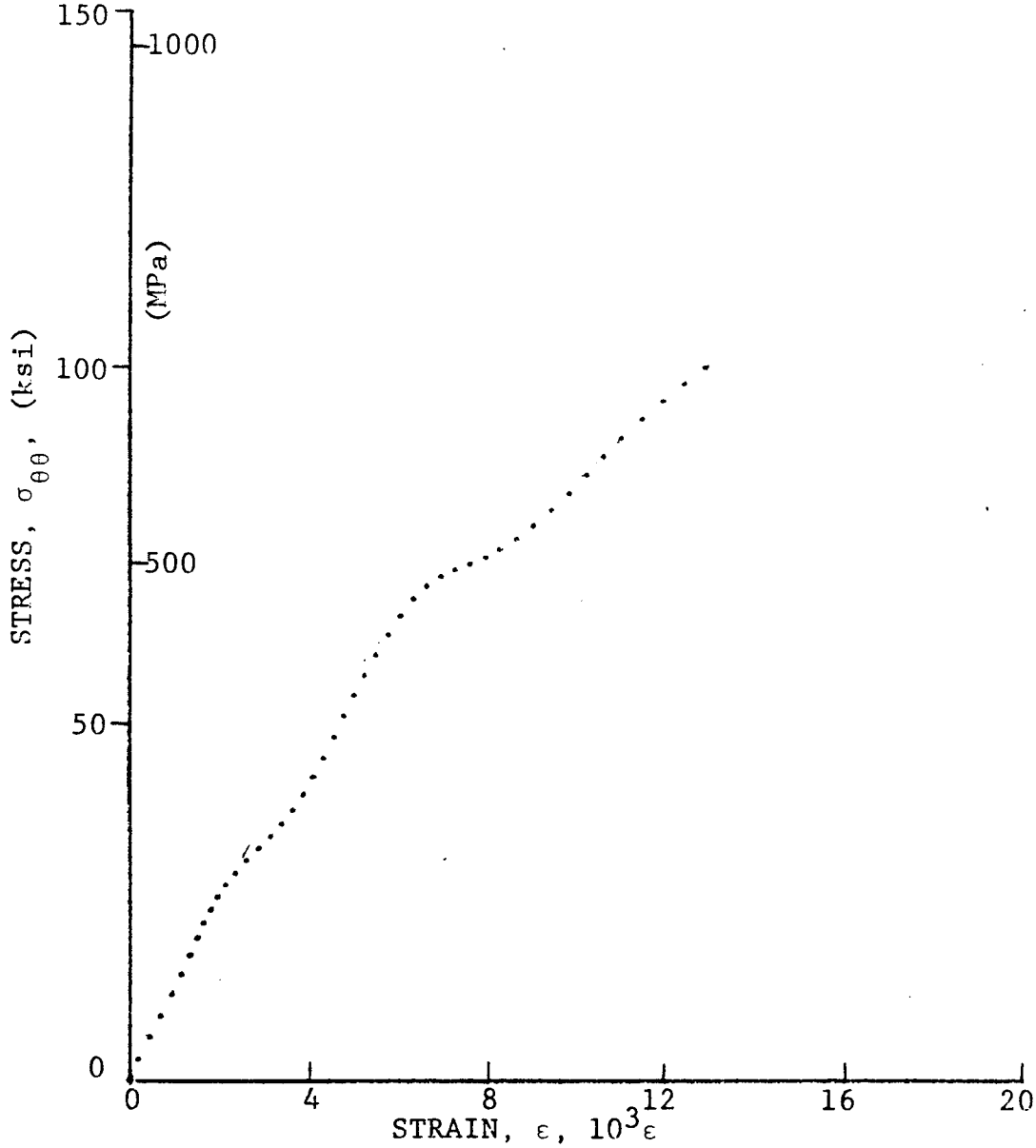

Figure 4-58. Stress-strain curve for dynamically loaded SP288/AS $[\pm 30]_{2s}$ graphite/epoxy ring, Specimen No. 28-11 (1.56 g bullseye powder, $KC\ell O_4$, and aluminum dust).

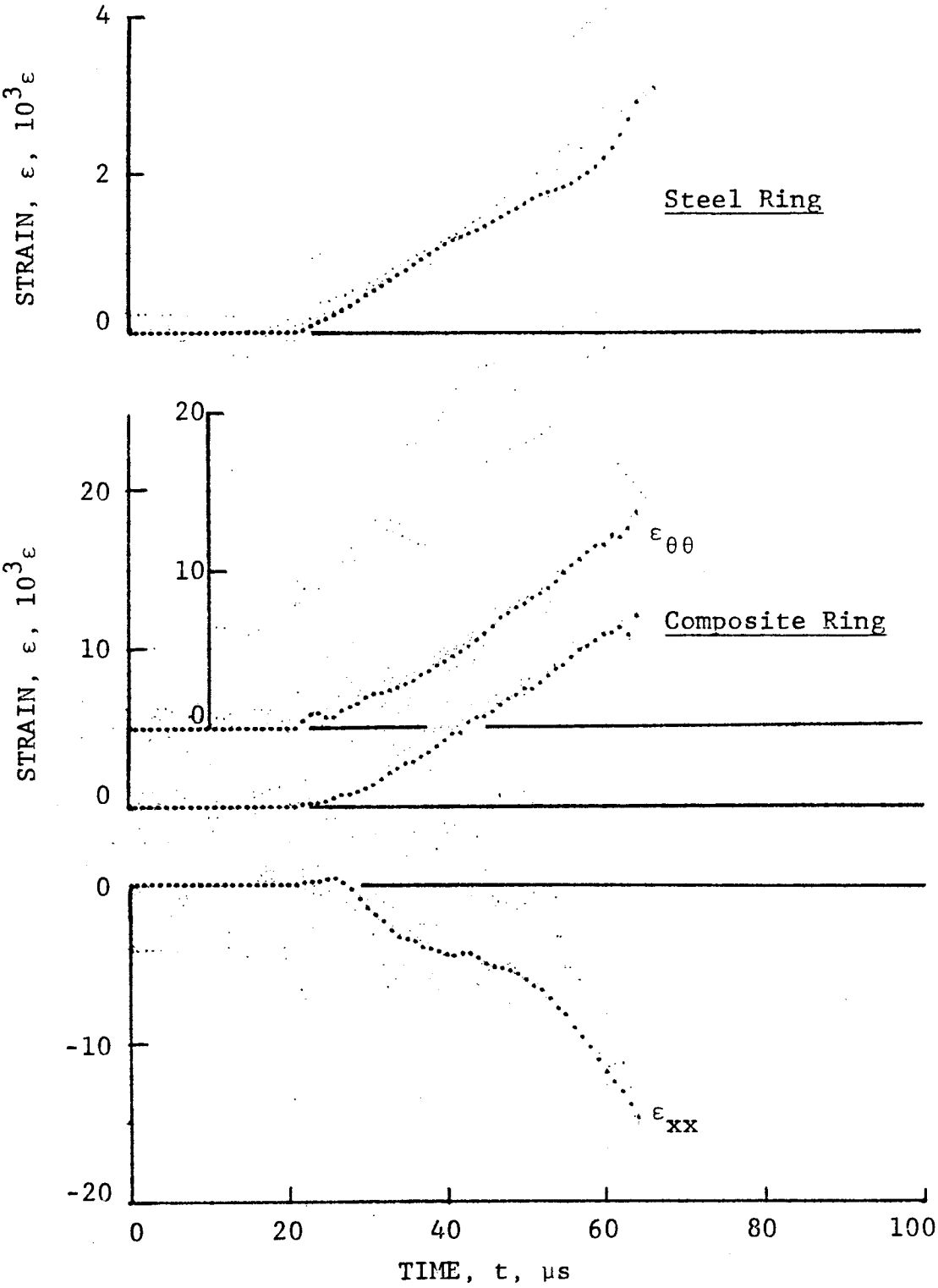

Figure 4-59. Strain records in steel ring and in 80AS/20S/PR288 $[\pm 30]_{2S}$ graphite/S-glass/epoxy ring under dynamic loading, Specimen No. 29-10 (1.56 g bullseye powder, $KC\ell O_4$, and aluminum dust).

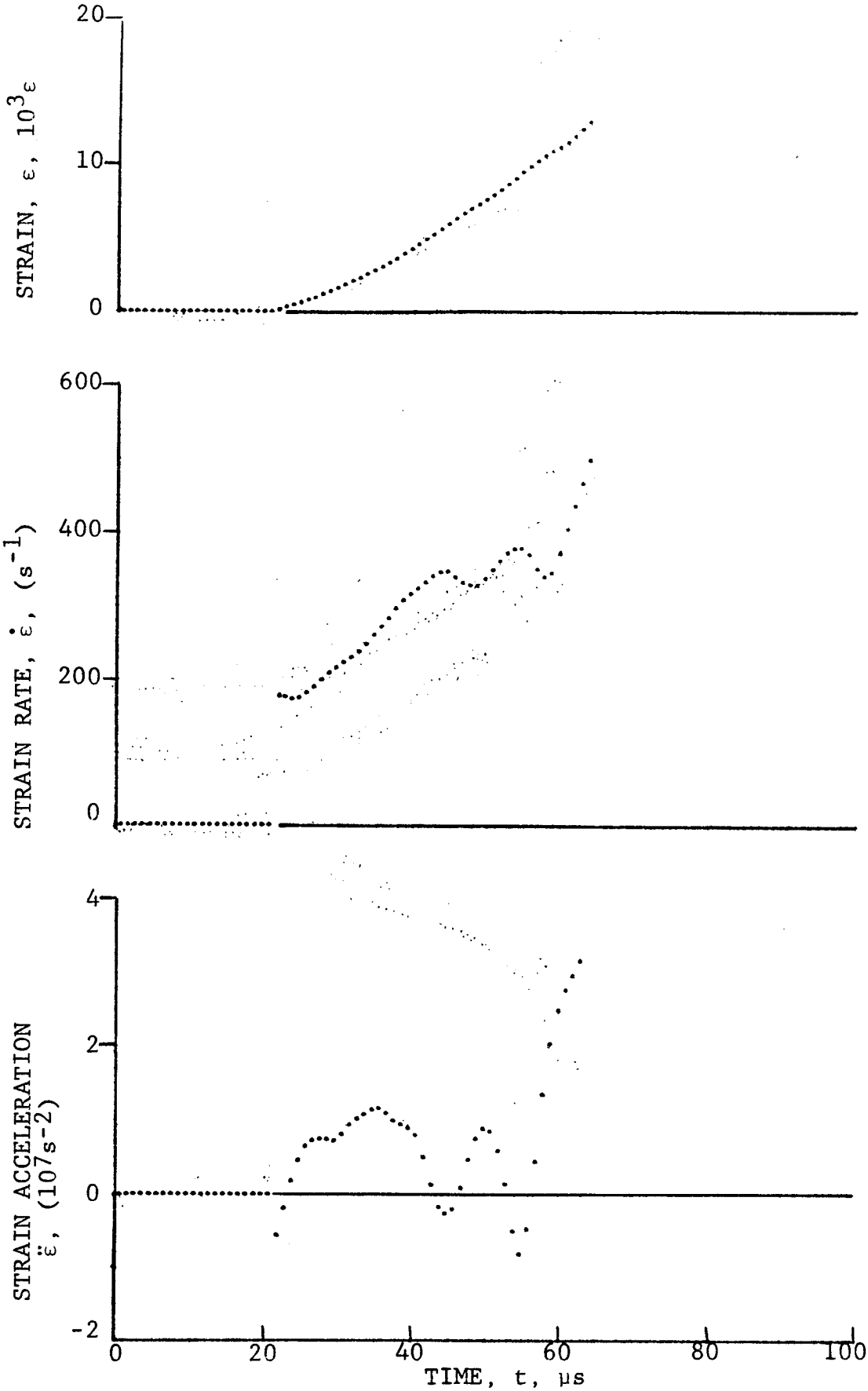

Figure 4-60. Circumferential strain and its derivatives in 80AS/20S/PR288 $[\pm 30]_{2s}$ graphite/S-glass/epoxy ring under dynamic loading, Specimen No. 29-10.

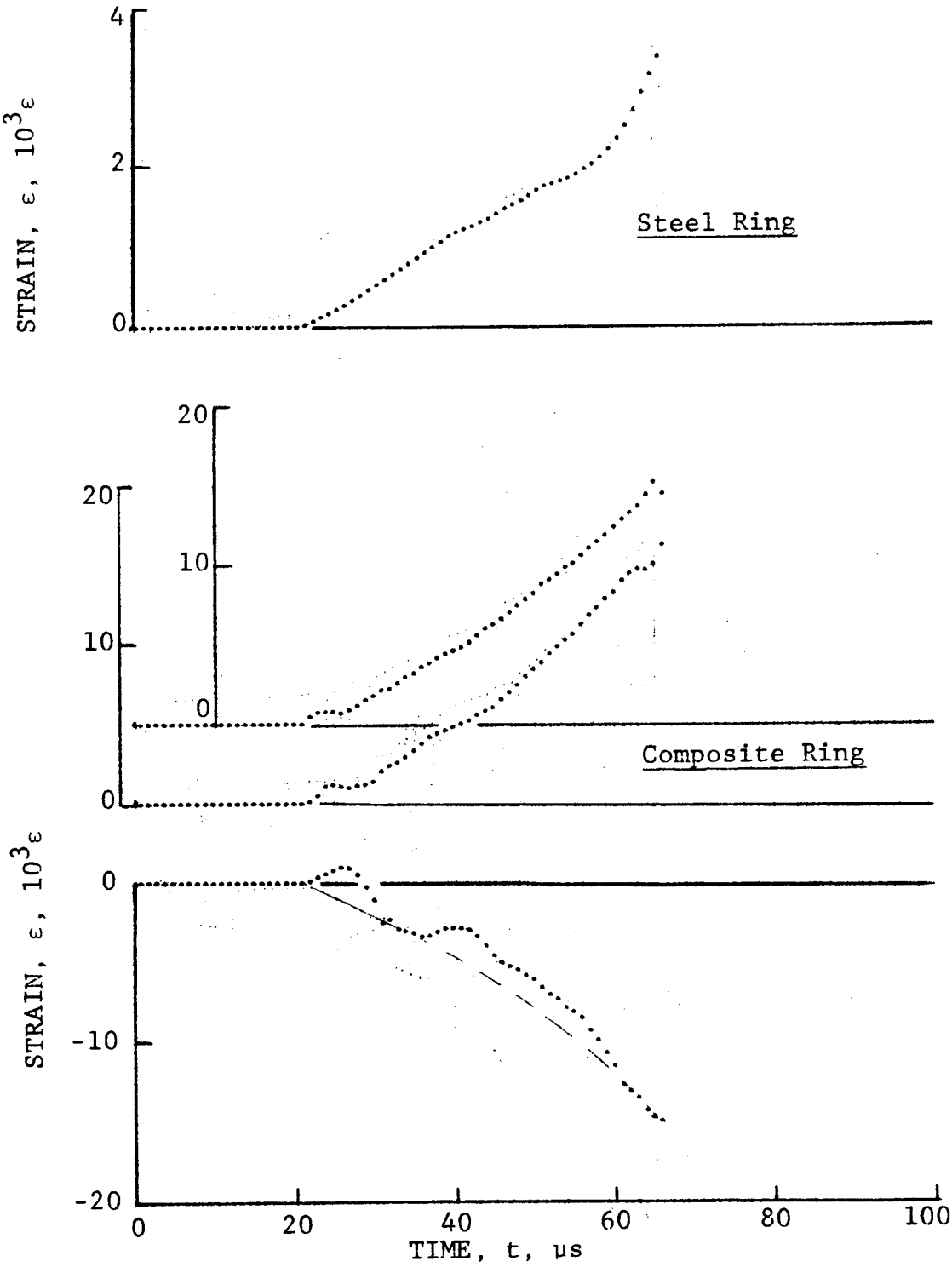

Figure 4-61. Strain records in steel ring and in 80AS/20S/PR288 $[\pm 30]_{2S}$ graphite/S-glass/epoxy ring under dynamic loading, Specimen No. 29-11 (1.56 g bullseye powder, $KC\ell O_4$, and aluminum dust).

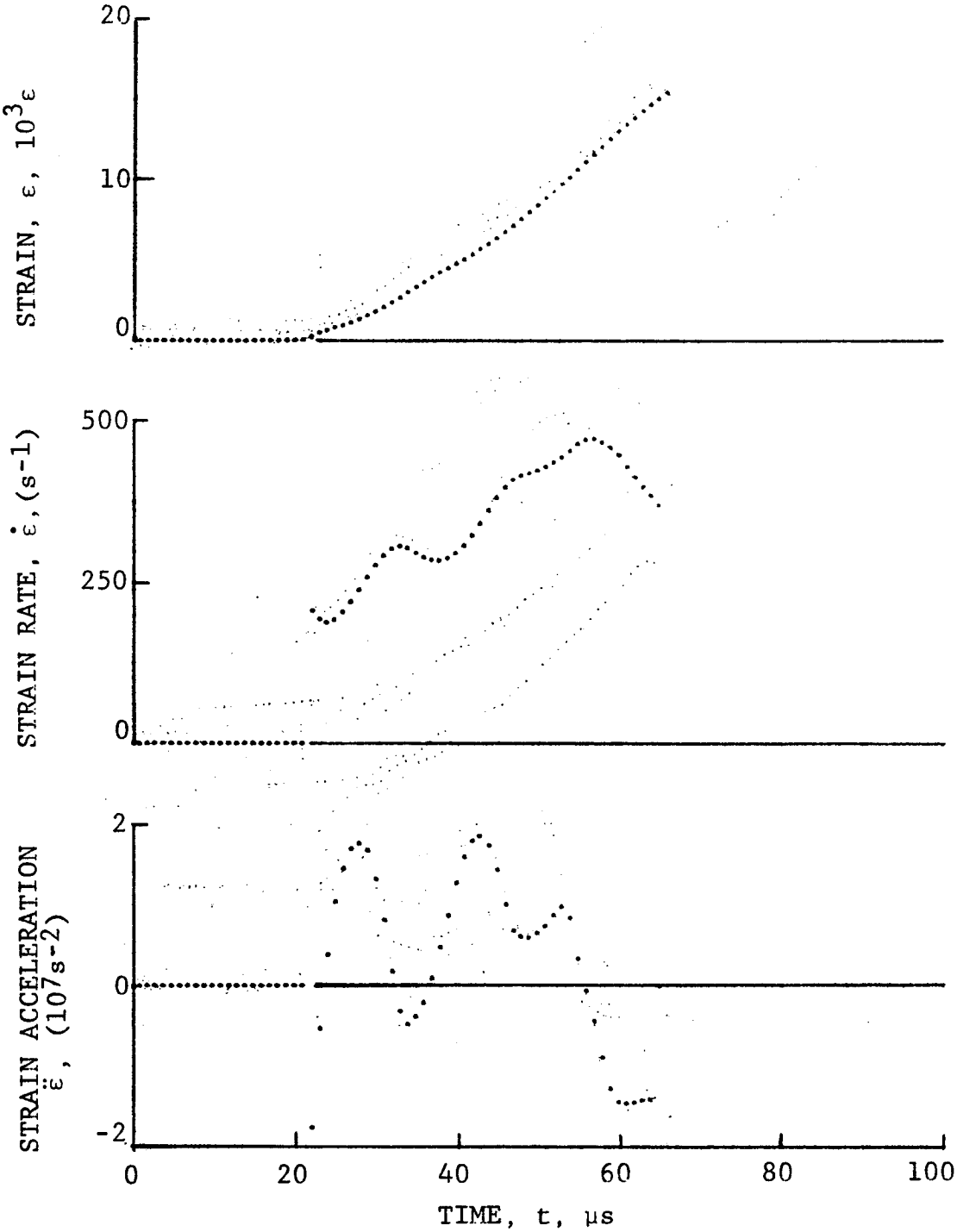

Figure 4-62. Circumferential strain and its derivatives in 80AS/20S/PR288 $[\pm 30]_{2S}$ graphite/S-glass/epoxy ring under dynamic loading, Specimen No. 29-11.

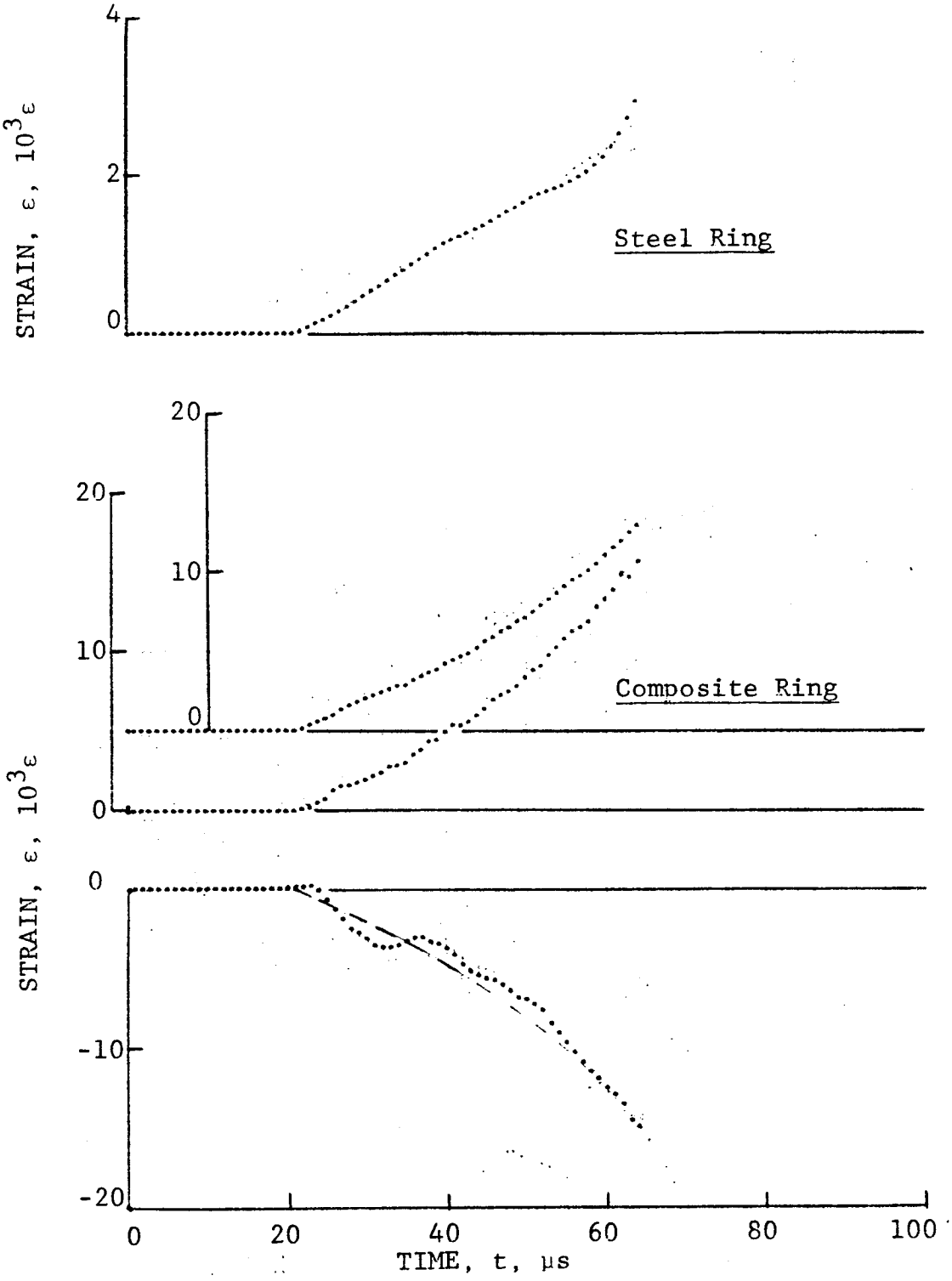

Figure 4-63. Strain records in steel ring and in 80AS/20S/PR288 $[\pm 30]_{2S}$ graphite/S-glass/epoxy ring under dynamic loading, Specimen No. 29-12 (1.56 g bullseye powder, $KC\ell O_4$, and aluminum dust).

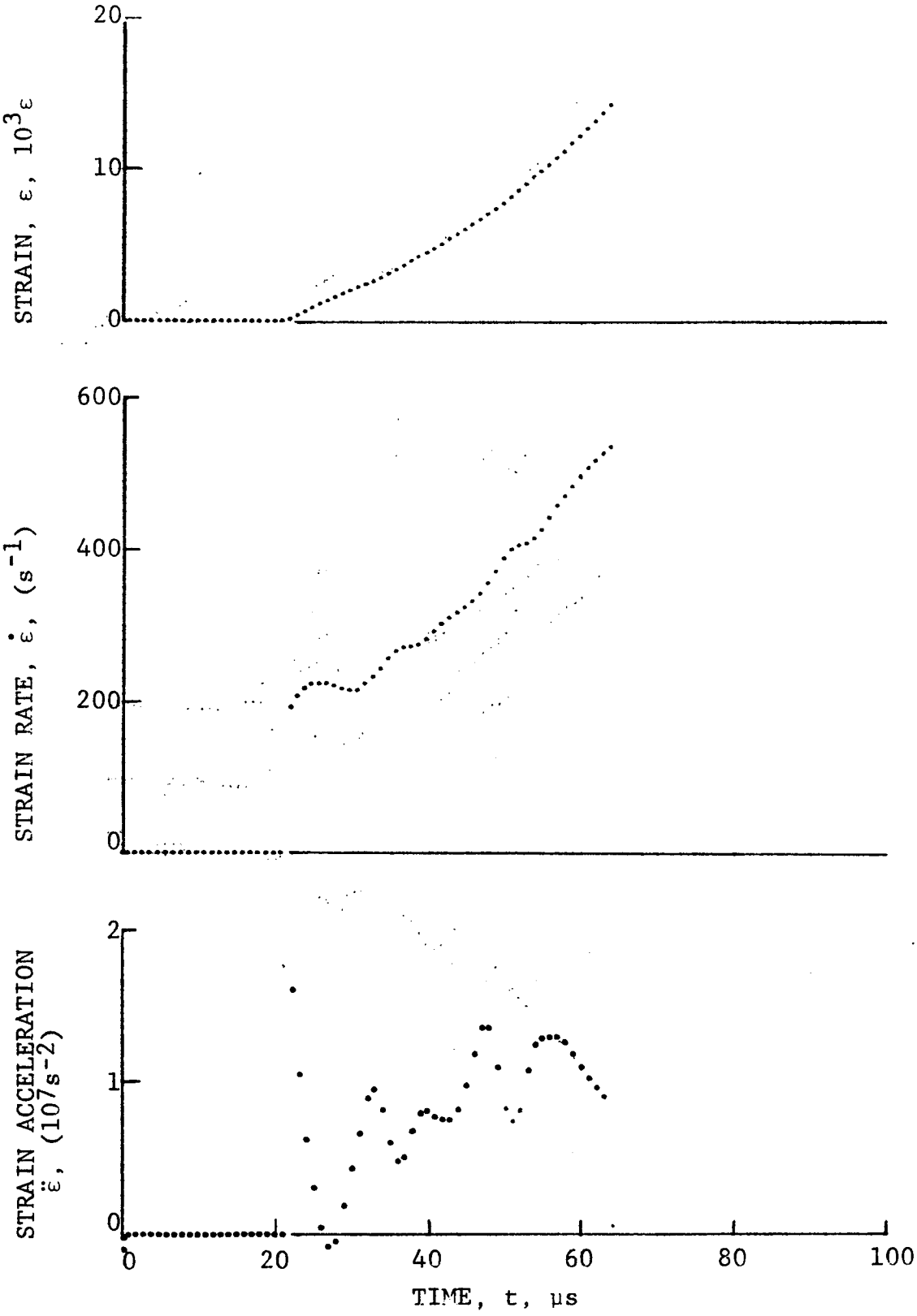

Figure 4-64. Circumferential strain and its derivatives in 80AS/20S/PR288 $[\pm 30]_{2s}$ graphite/S-glass/epoxy ring under dynamic loading, Specimen No. 29-12.

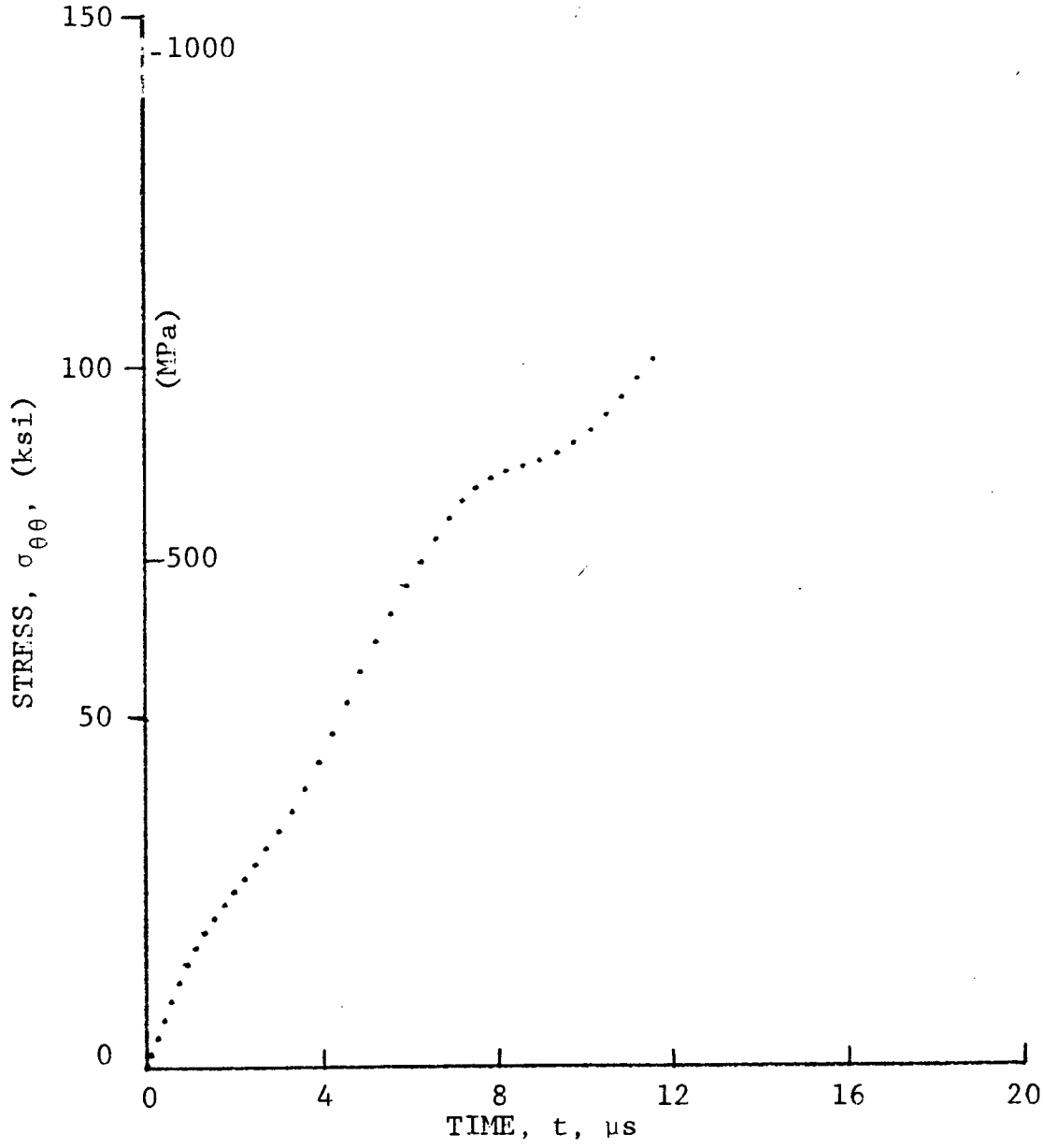

Figure 4-65. Stress-strain curve for dynamically loaded 80AS/20S/PR288 $[\pm 30]_{2s}$ graphite/S-glass/epoxy ring, Specimen No. 29-10 (1.56 g bullseye powder, $KC\ell O_4$, and aluminum dust).

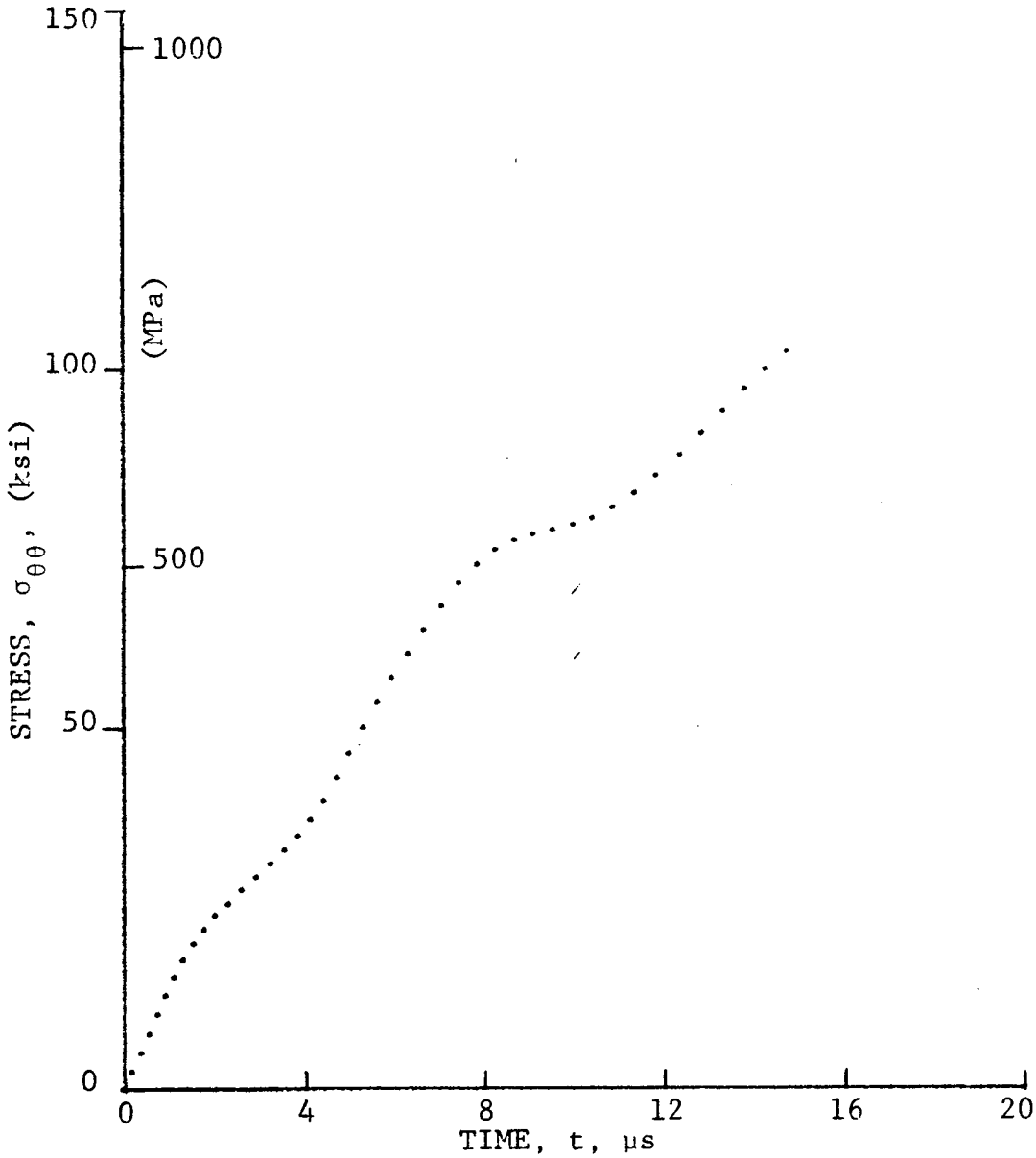

Figure 4-66. Stress-strain curve for dynamically loaded 80AS/20S/PR288 $[\pm 30]_{2S}$ graphite/S-glass/epoxy ring, Specimen No. 29-11 (1.56 g bullseye powder, $KC\ell O_4$, and aluminum dust).

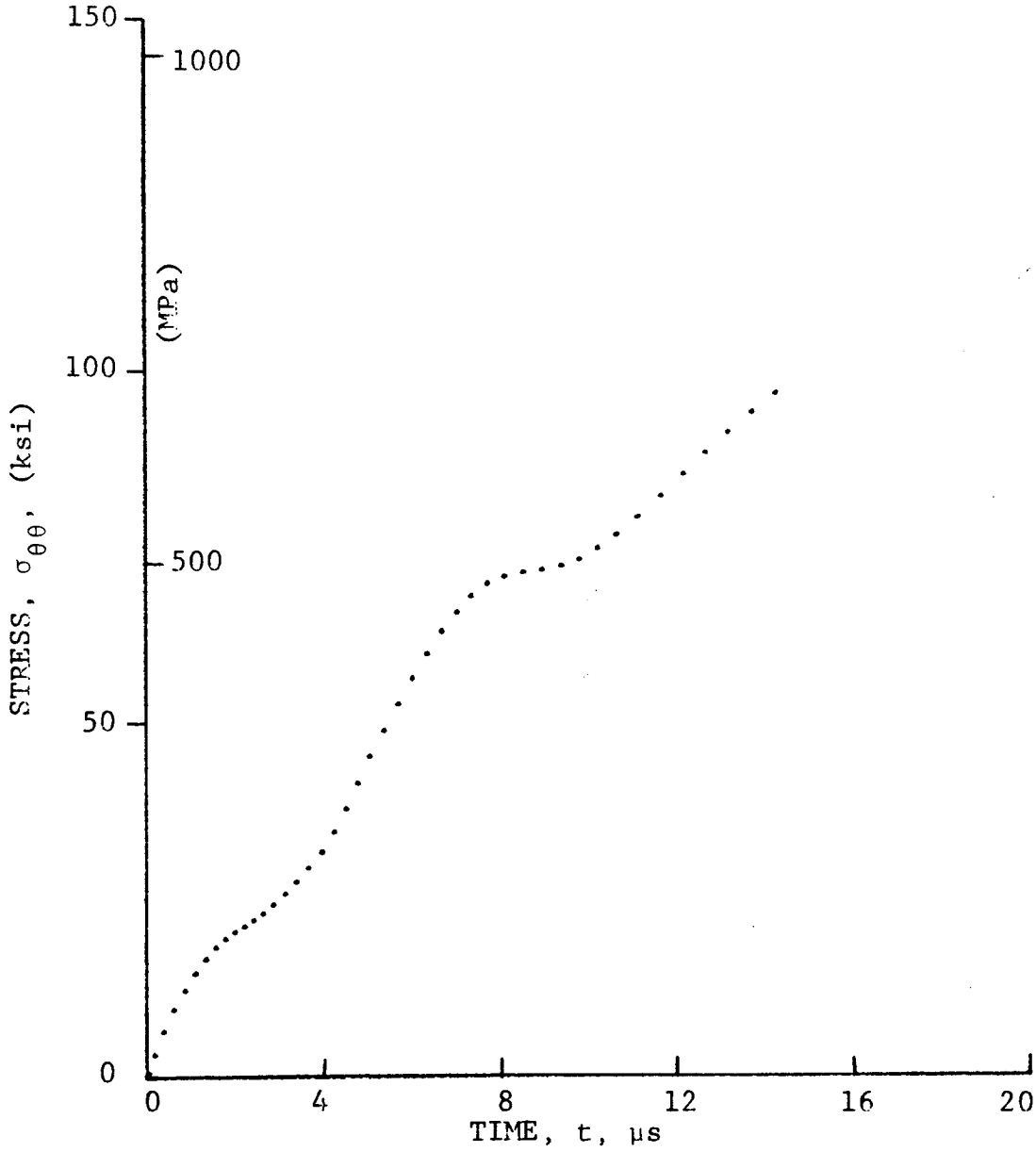

Figure 4-67. Stress-strain curve for dynamically loaded 80AS/20S/PR288 $[\pm 30]_{2S}$ graphite/S-glass/epoxy ring, Specimen No. 29-12 (1.56 g bullseye powder, $KC\ell O_4$, and aluminum dust).

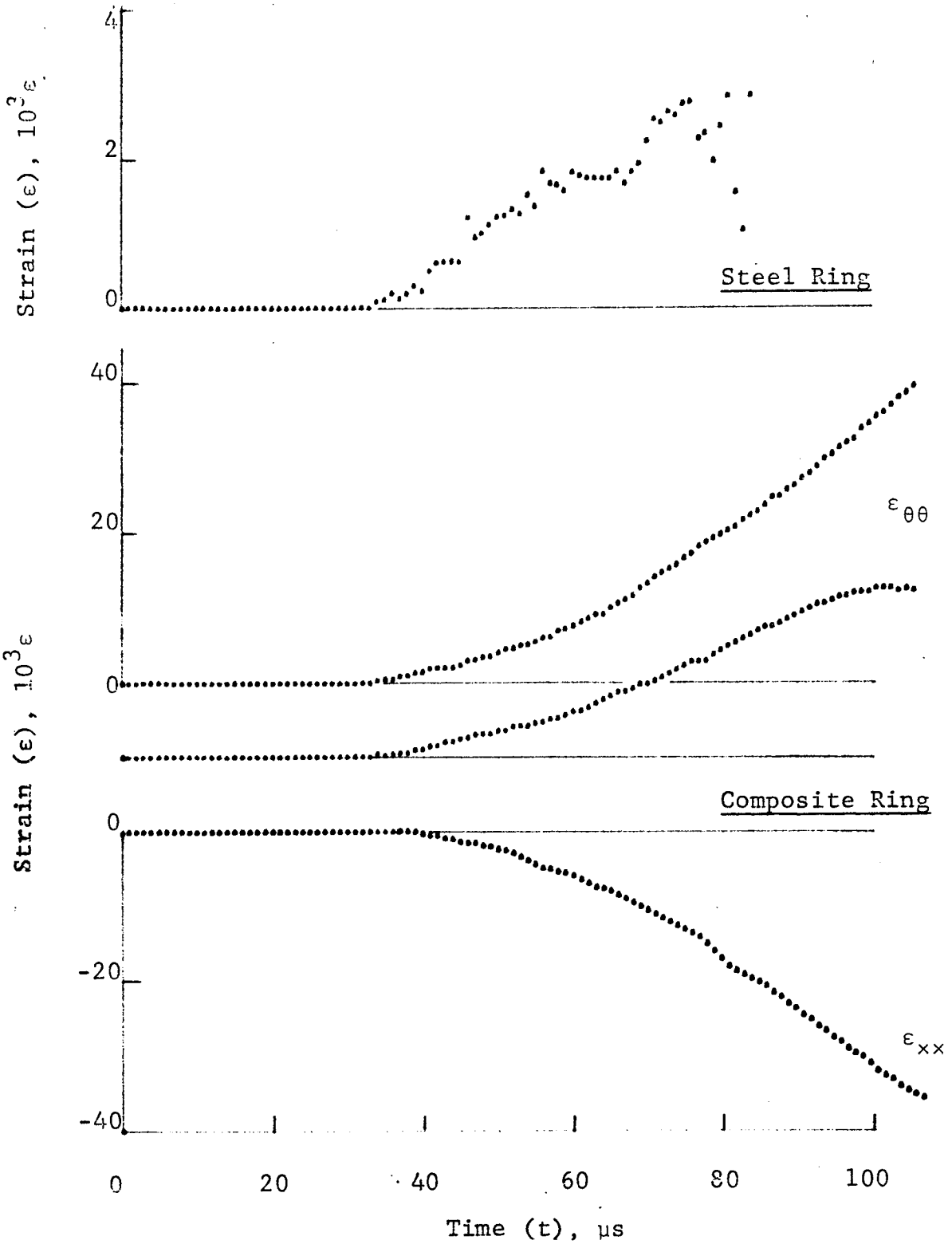

Figure 4-68. Strain records in steel ring and SP288/AS $[\pm 45]_{2s}$ graphite/epoxy ring under dynamic loading for Specimen No. 24-11 (1.56 g pistol powder, $KC\ell O_4$, and aluminum dust).

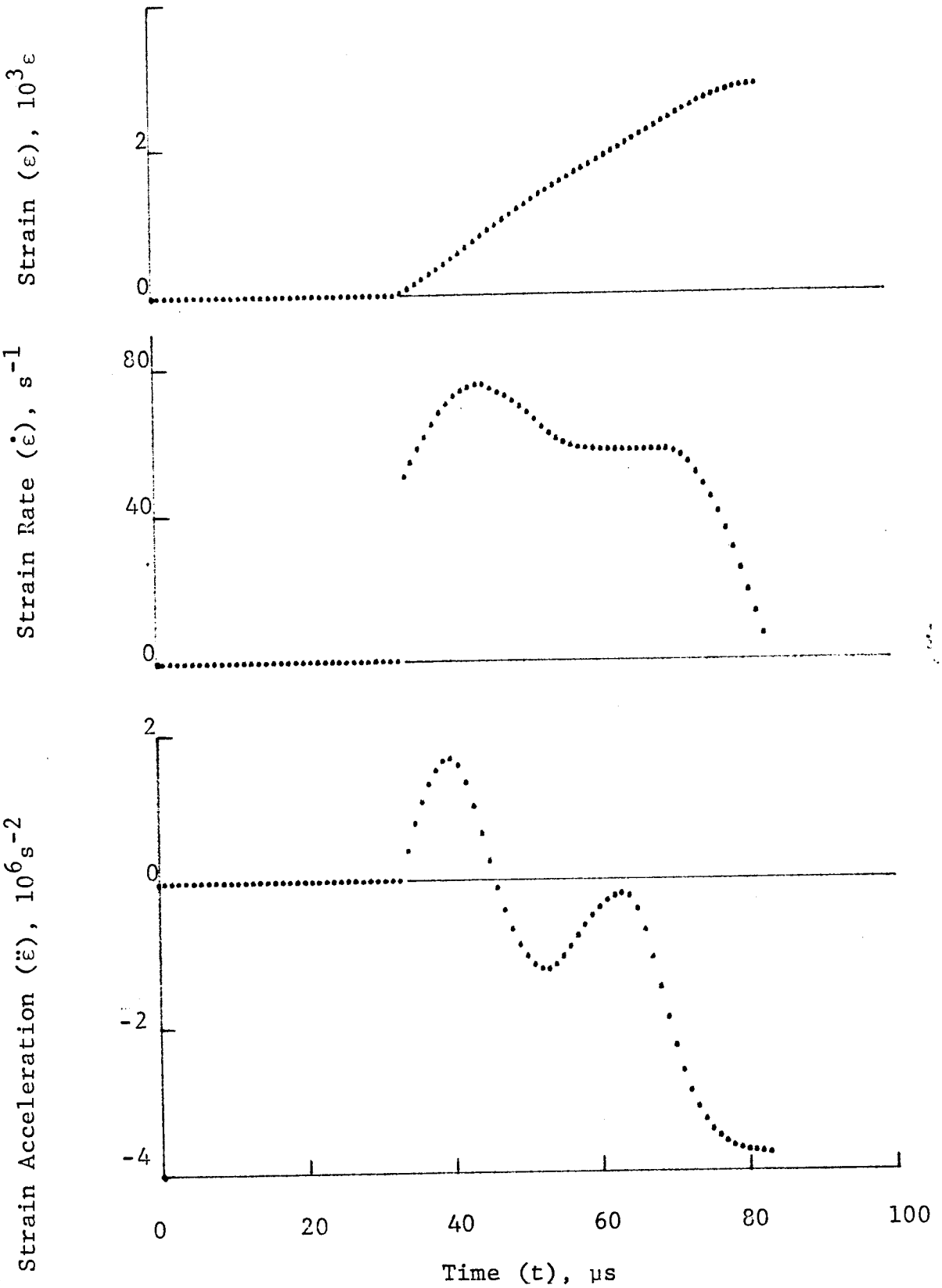

Figure 4-69. Strain and its derivatives in steel ring for Specimen No. 24-11.

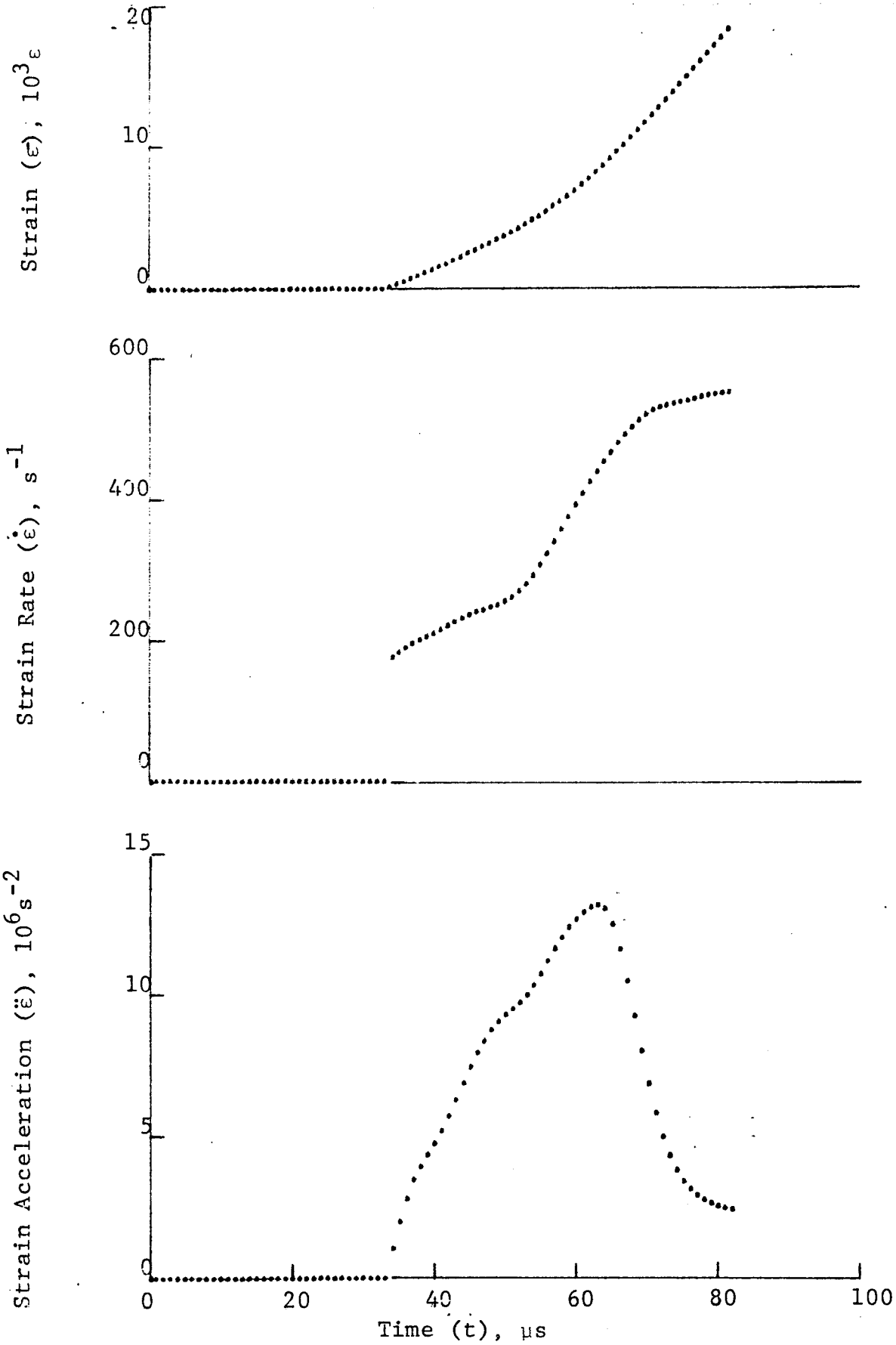

Figure 4-70. Circumferential strain and its derivatives in SP288/AS $[\pm 45]_{2S}$ graphite/epoxy ring under dynamic loading for Specimen No. 24-11 (1.56 g pistol powder, $KC\ell O_4$, and aluminum dust).

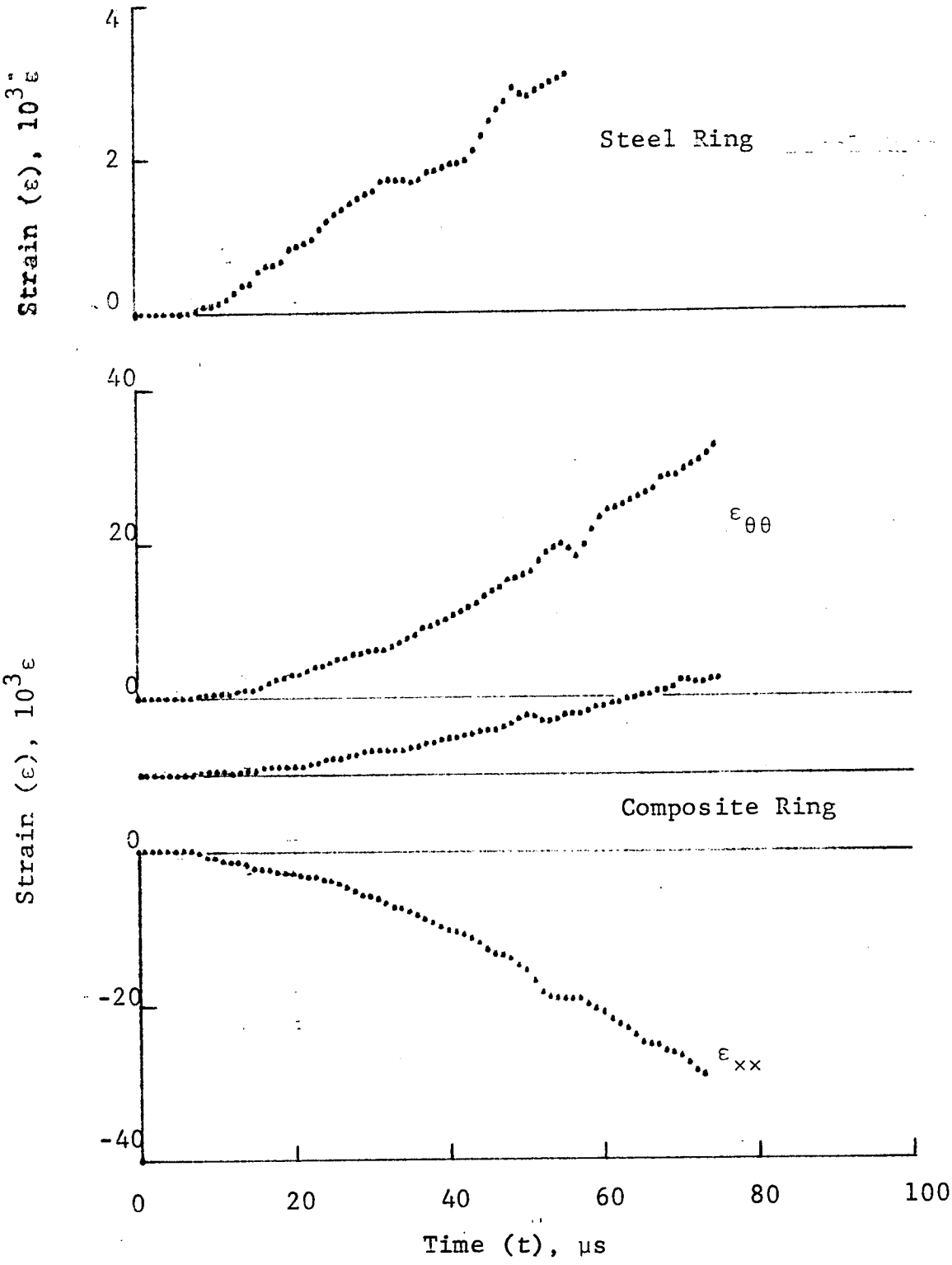

Figure 4-71. Strain records in steel ring and SP288/AS $[\pm 45]_{2s}$ graphite/epoxy ring under dynamic loading for Specimen No. 24-12 (1.56 g pistol powder, $KC\ell O_4$, and aluminum dust).

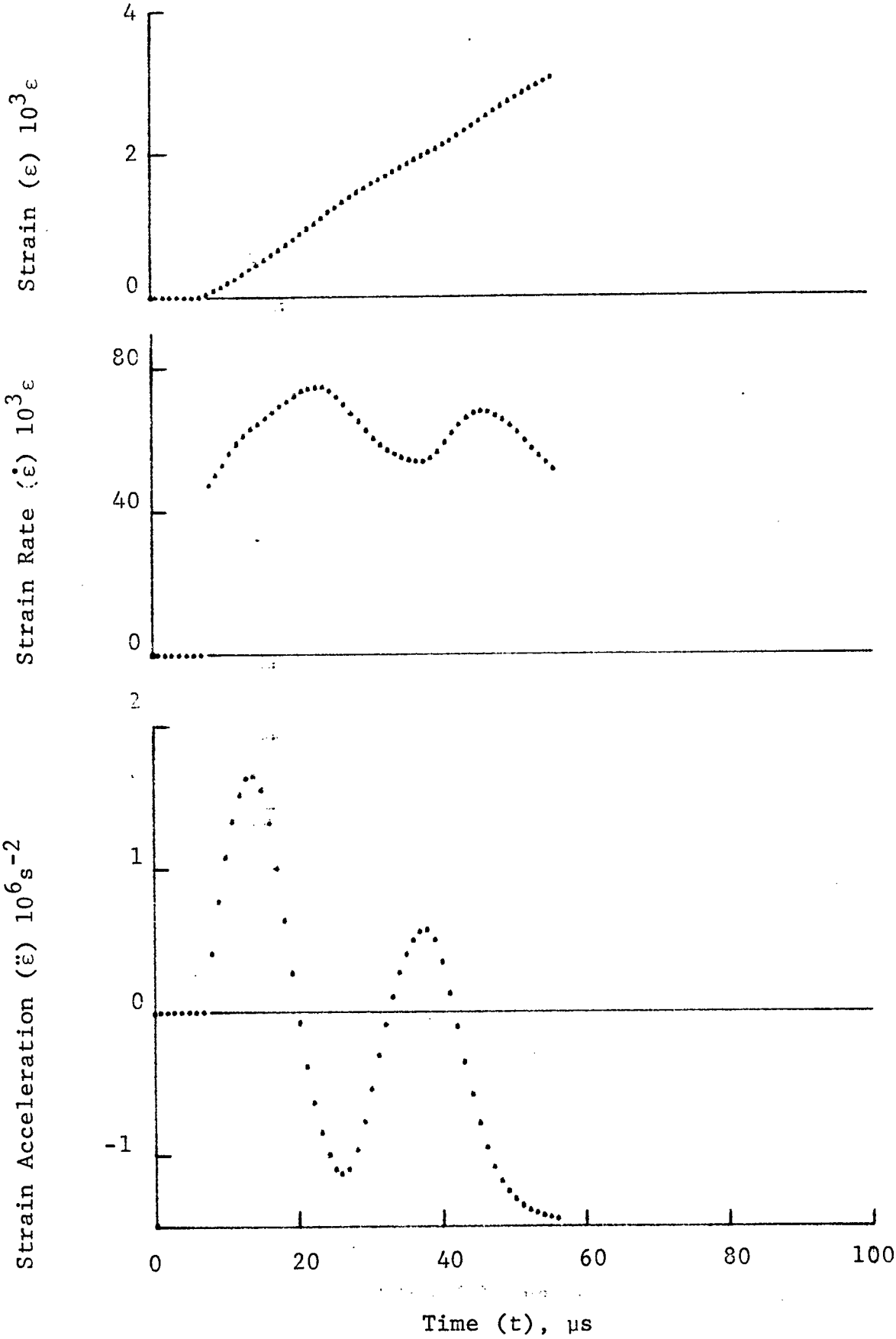

Figure 4-72. Strain and its derivatives in steel ring for Specimen No. 24-12.

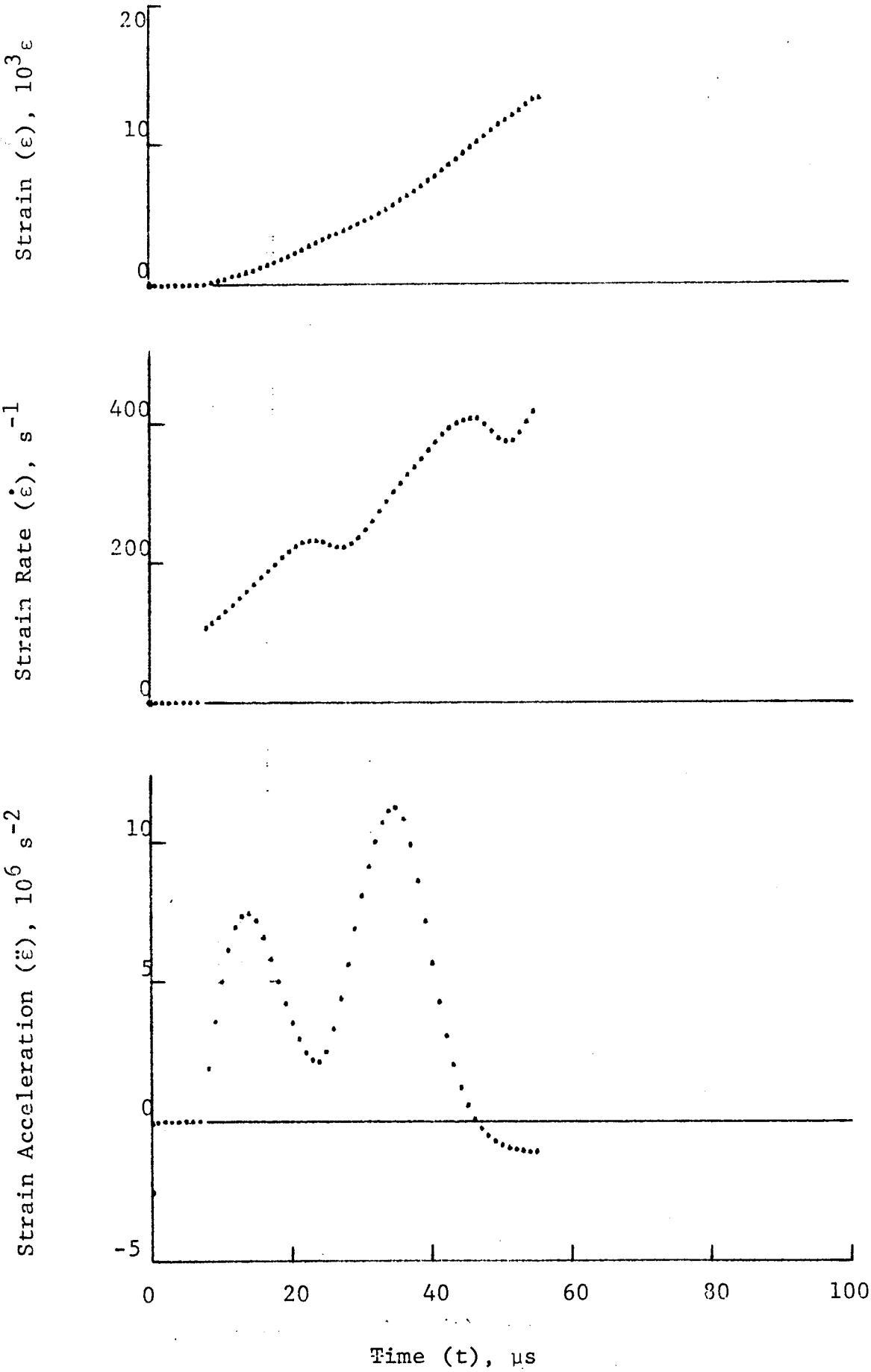

Figure 4-73. Circumferential strain and its derivatives in SP288/AS $[\pm 45]_{2s}$ graphite/epoxy ring under dynamic loading for Specimen No. 24-12.

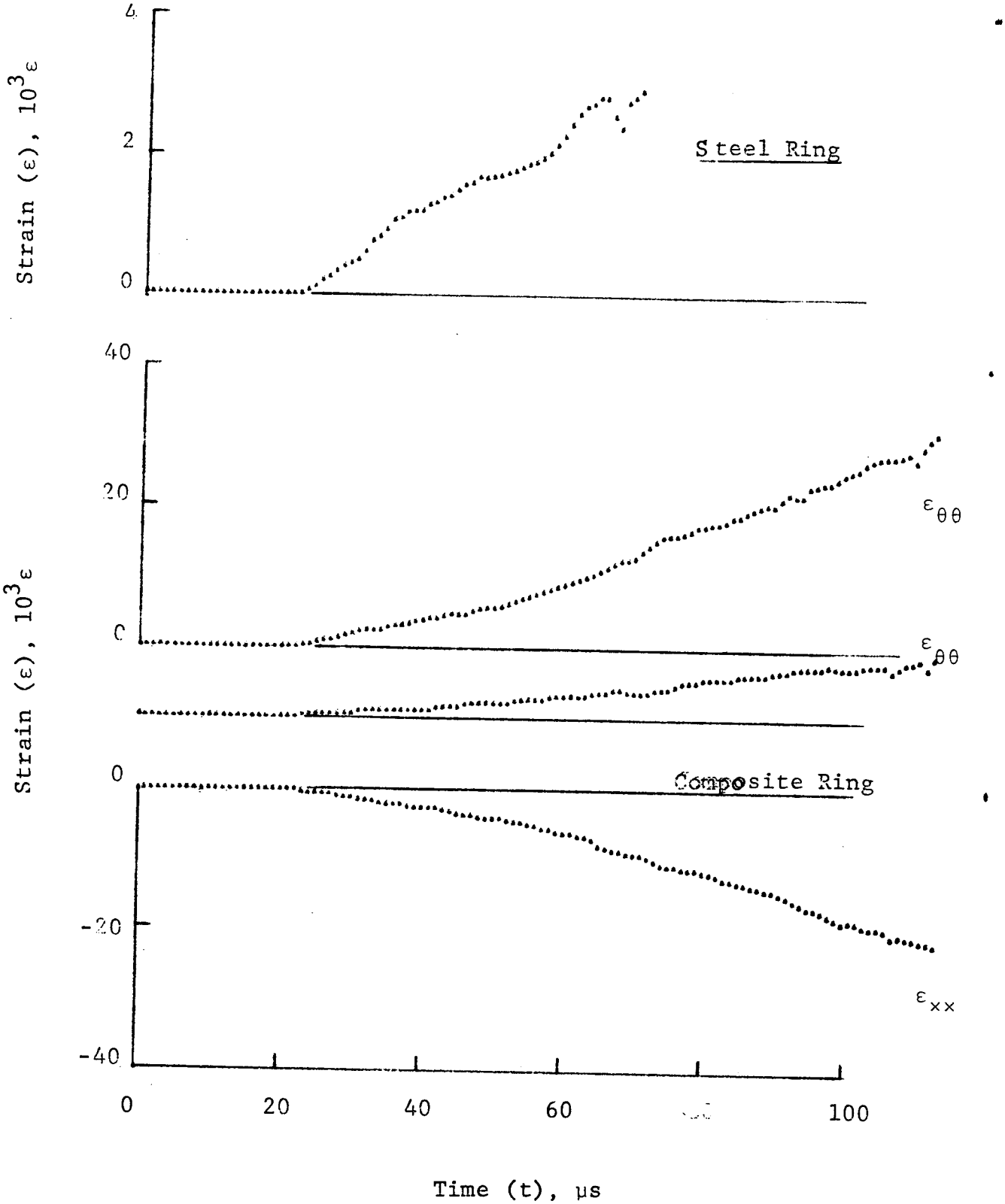

Figure 4-74. Strain records in steel ring and SP288/AS $[\pm 45]_{2s}$ graphite/epoxy ring under dynamic loading for Specimen No. 24-13 (1.56 g pistol powder, $KC\ell O_4$, and aluminum dust).

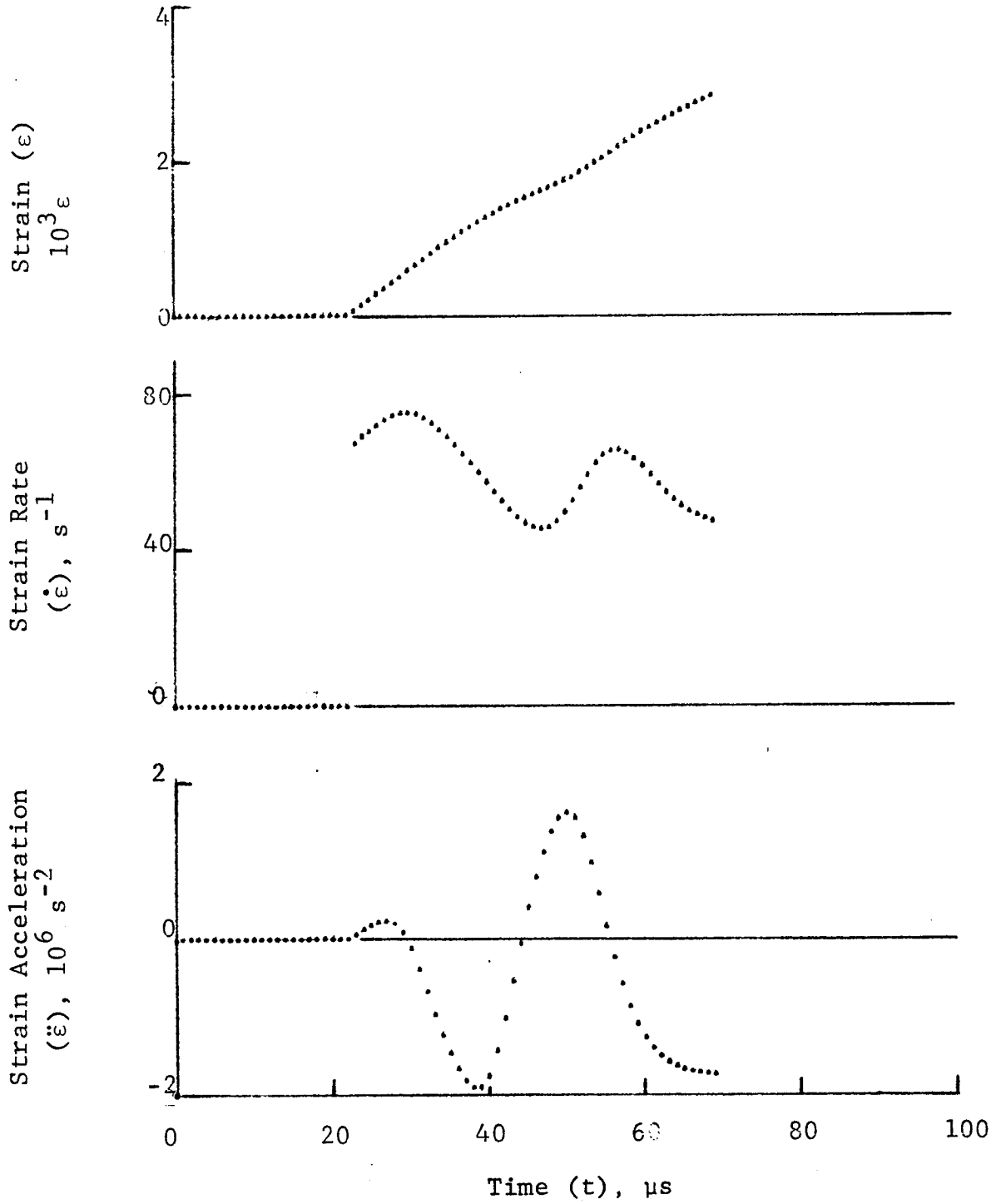

Figure 4-75. Circumferential strain and its derivatives in steel ring for Specimen No. 24-13.

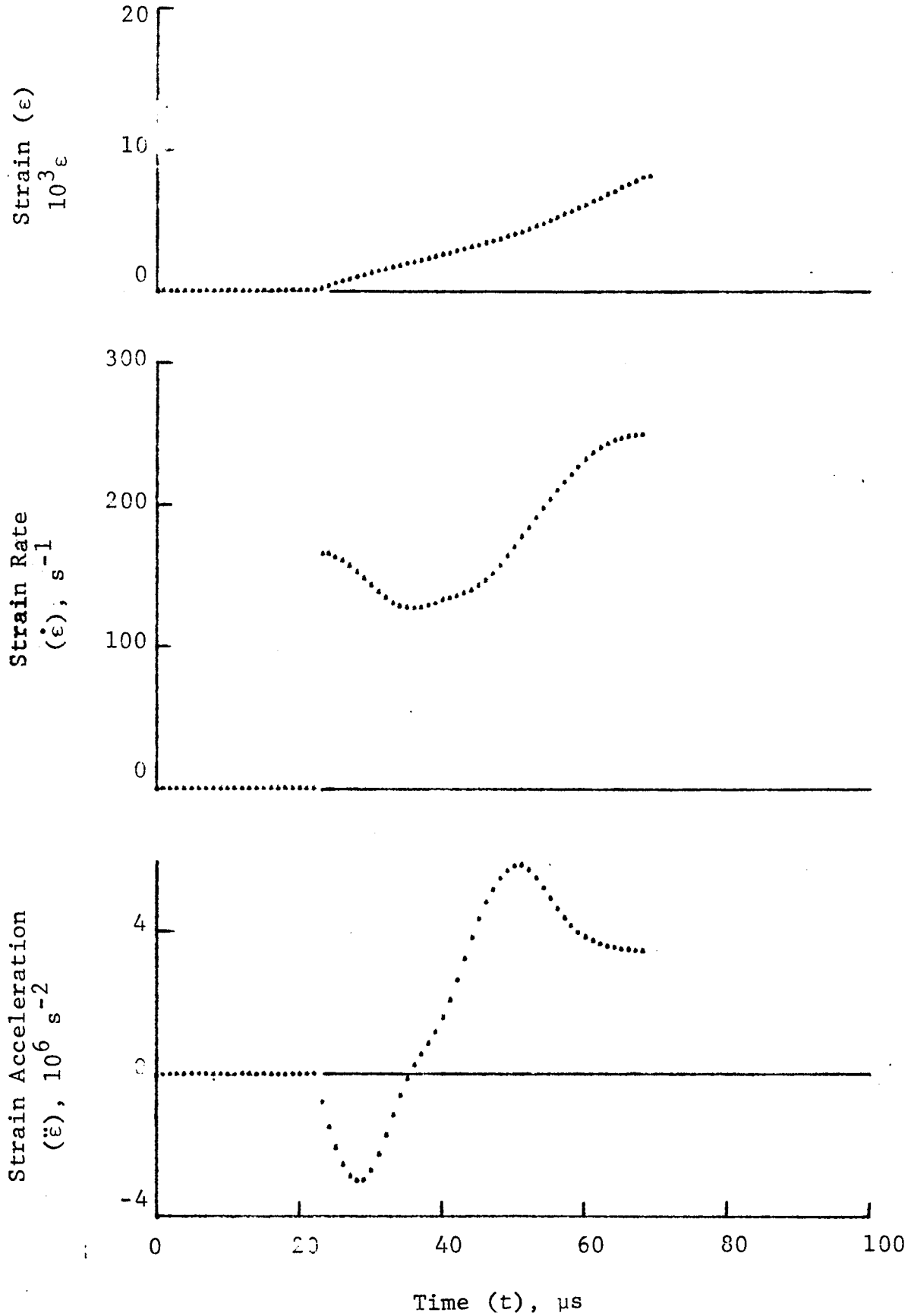

Figure 4-76. Circumferential strain and its derivatives in SP288/AS $[\pm 45]_{2S}$ graphite/epoxy ring under dynamic loading for Specimen No. 24-13 (1.56 g pistol powder, $KC\ell O_4$, and aluminum dust).

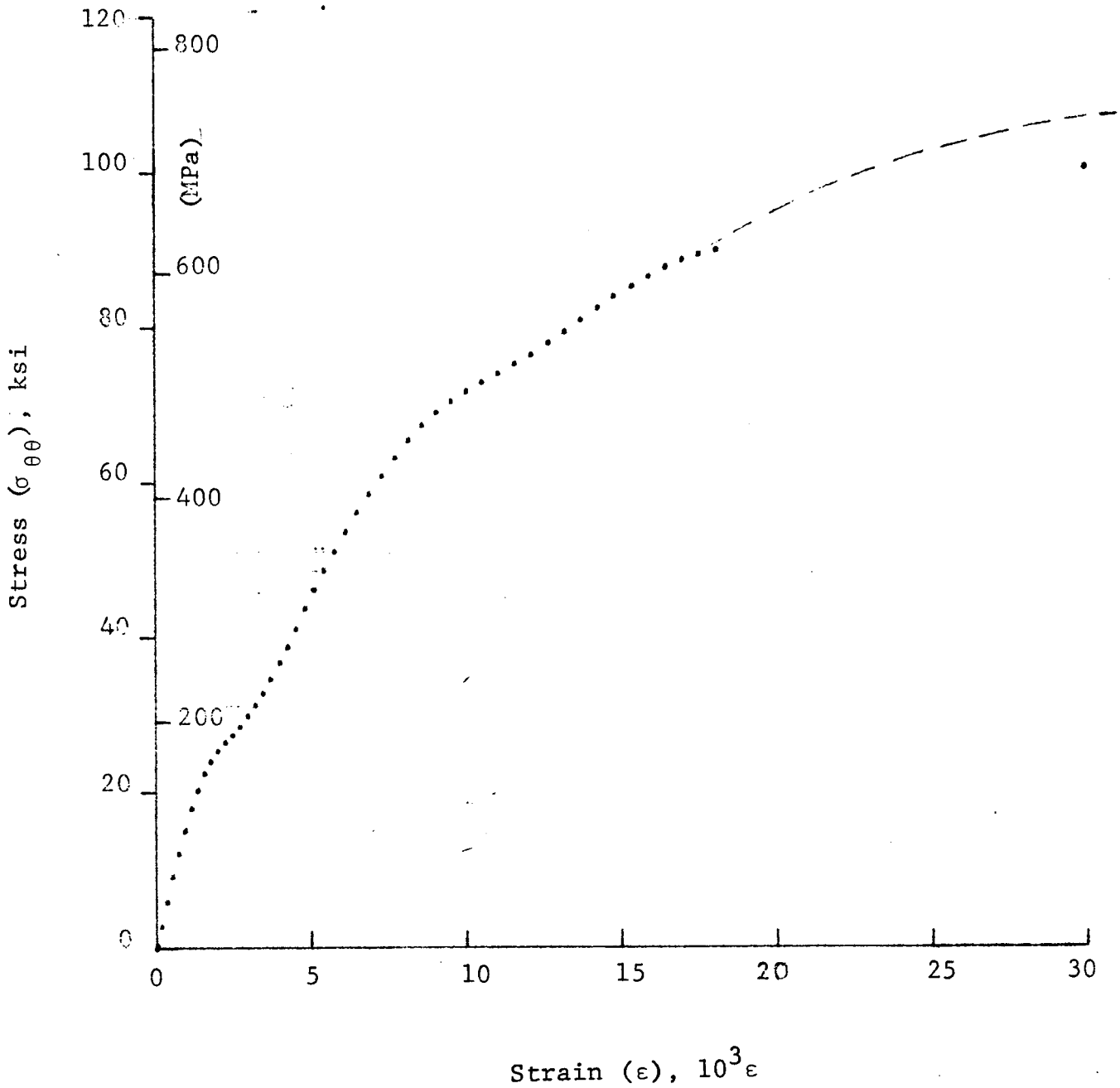

Figure 4-77. Stress-strain curve for dynamically loaded SP288/AS $[\pm 45]_{2s}$ graphite/epoxy ring, Specimen No. 24-11 (1.56 g pistol powder, $KC\ell O_4$, and aluminum dust).

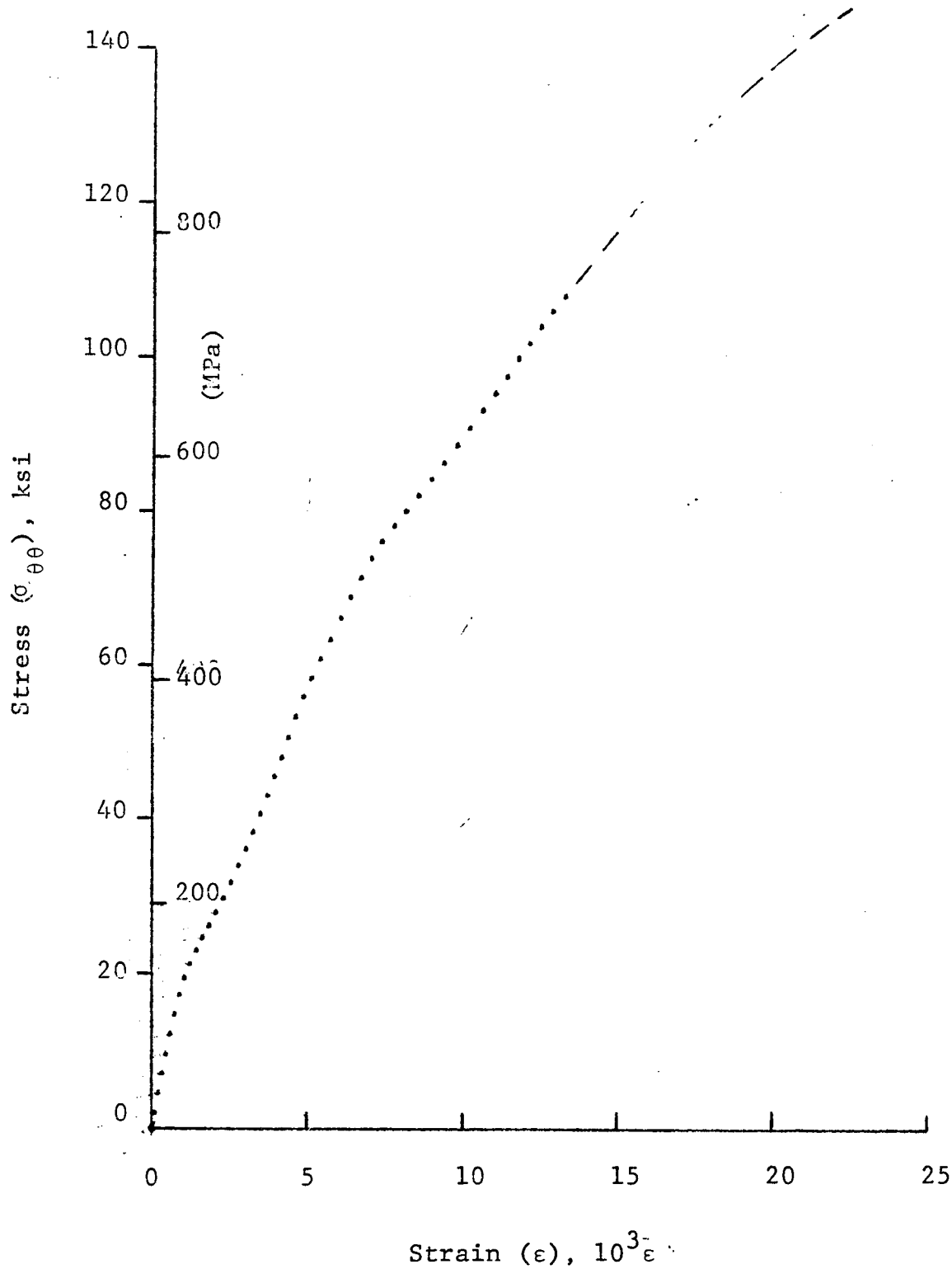

Figure 4-78. Stress-strain curve for dynamically loaded SP288/AS $[\pm 45]_{2s}$ graphite/epoxy ring, Specimen No. 24-12 (1.56 g pistol powder, $KC\ell O_4$, and aluminum dust).

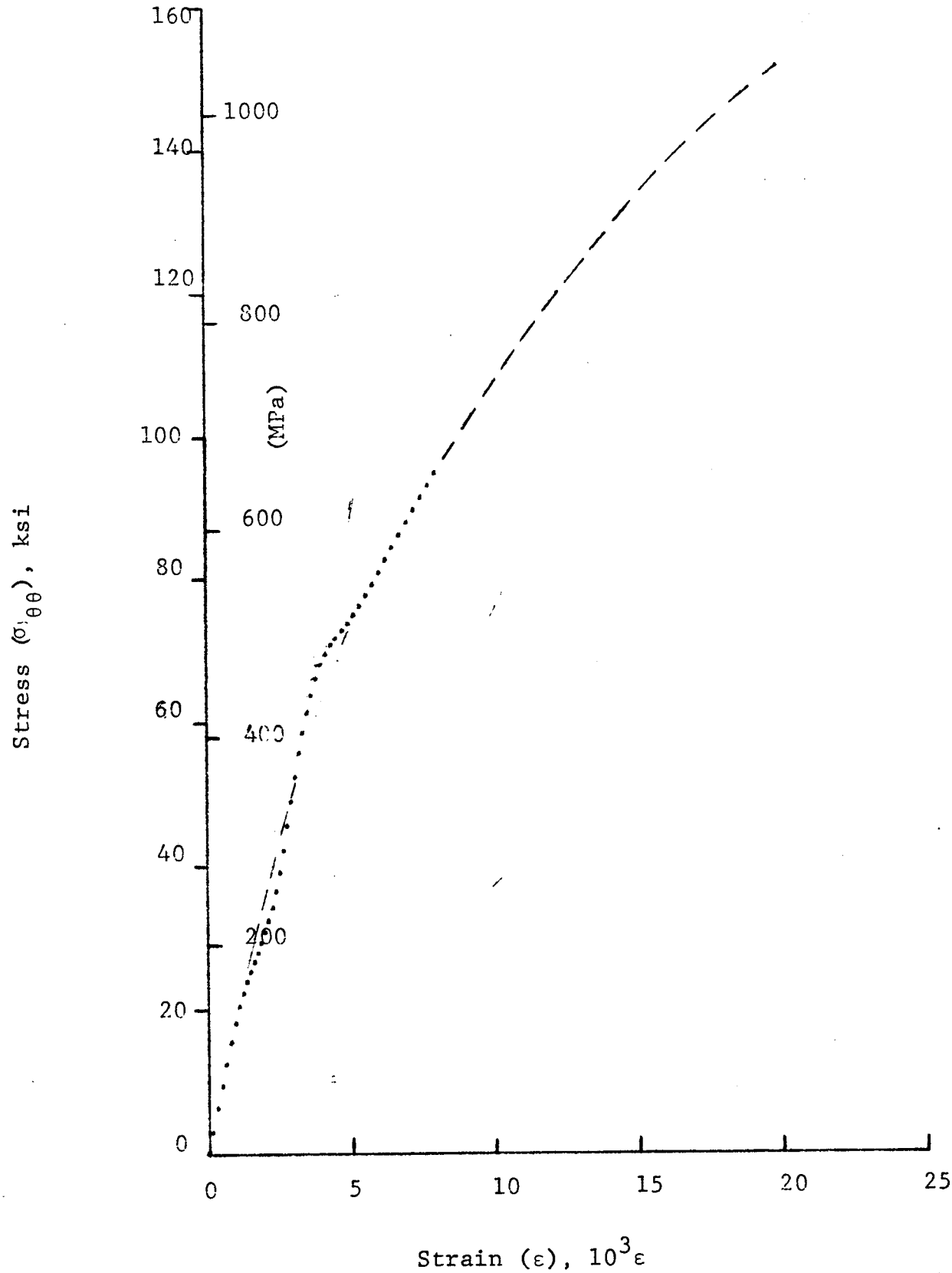

Figure 4-79. Stress-strain curve for dynamically loaded SP288/AS $[\pm 45]_{2s}$ graphite/epoxy ring, Specimen No. 24-13 (1.56 g pistol powder, $KC\ell O_4$, and aluminum dust).

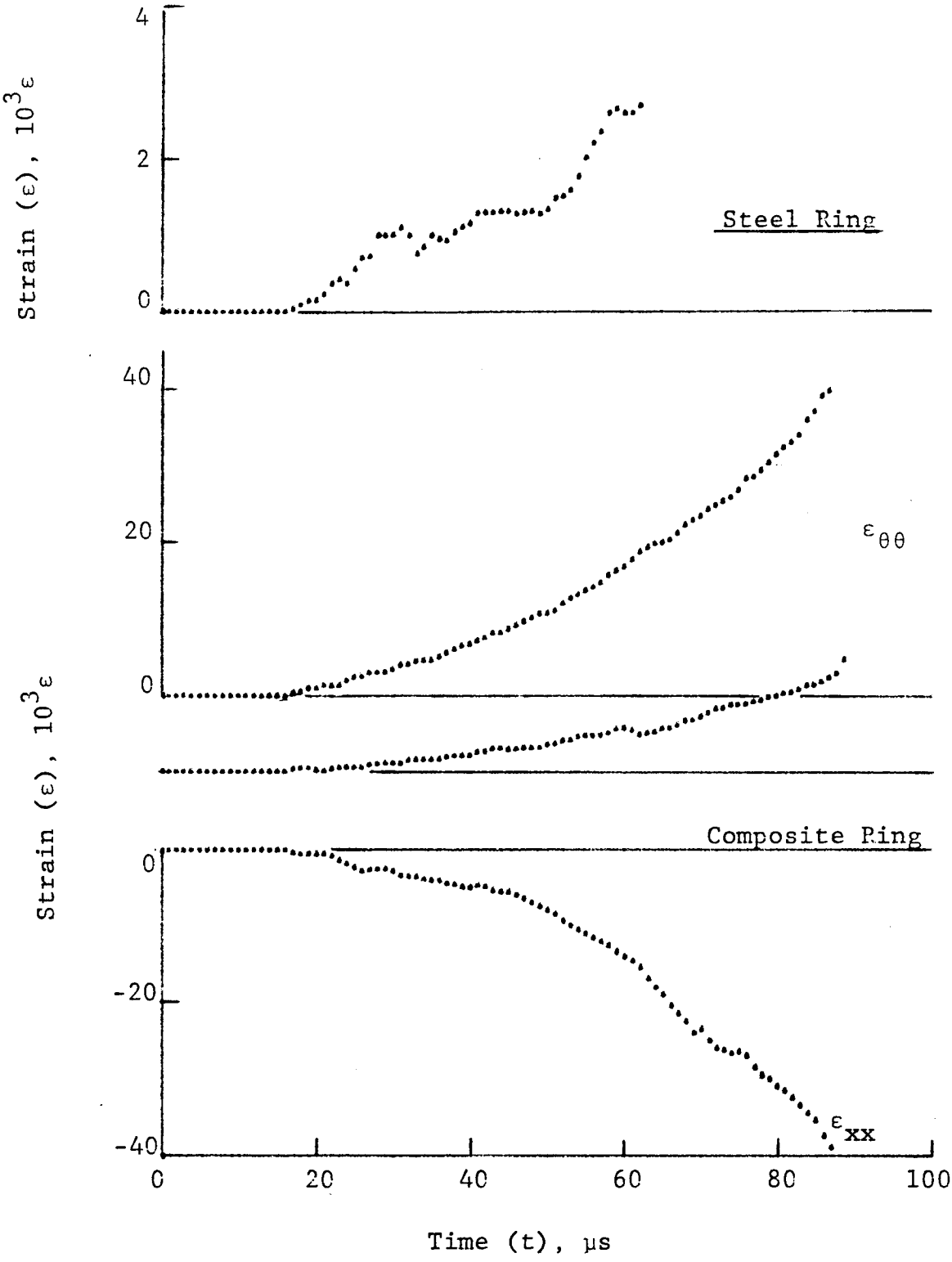

Figure 4-80. Strain records in steel ring and 80AS/20S/PR288 $[\pm 45]_{2s}$ graphite/S-glass/epoxy ring under dynamic loading for Specimen No. 25-11 (1.56 g pistol powder, $KC\ell O_4$, and aluminum dust).

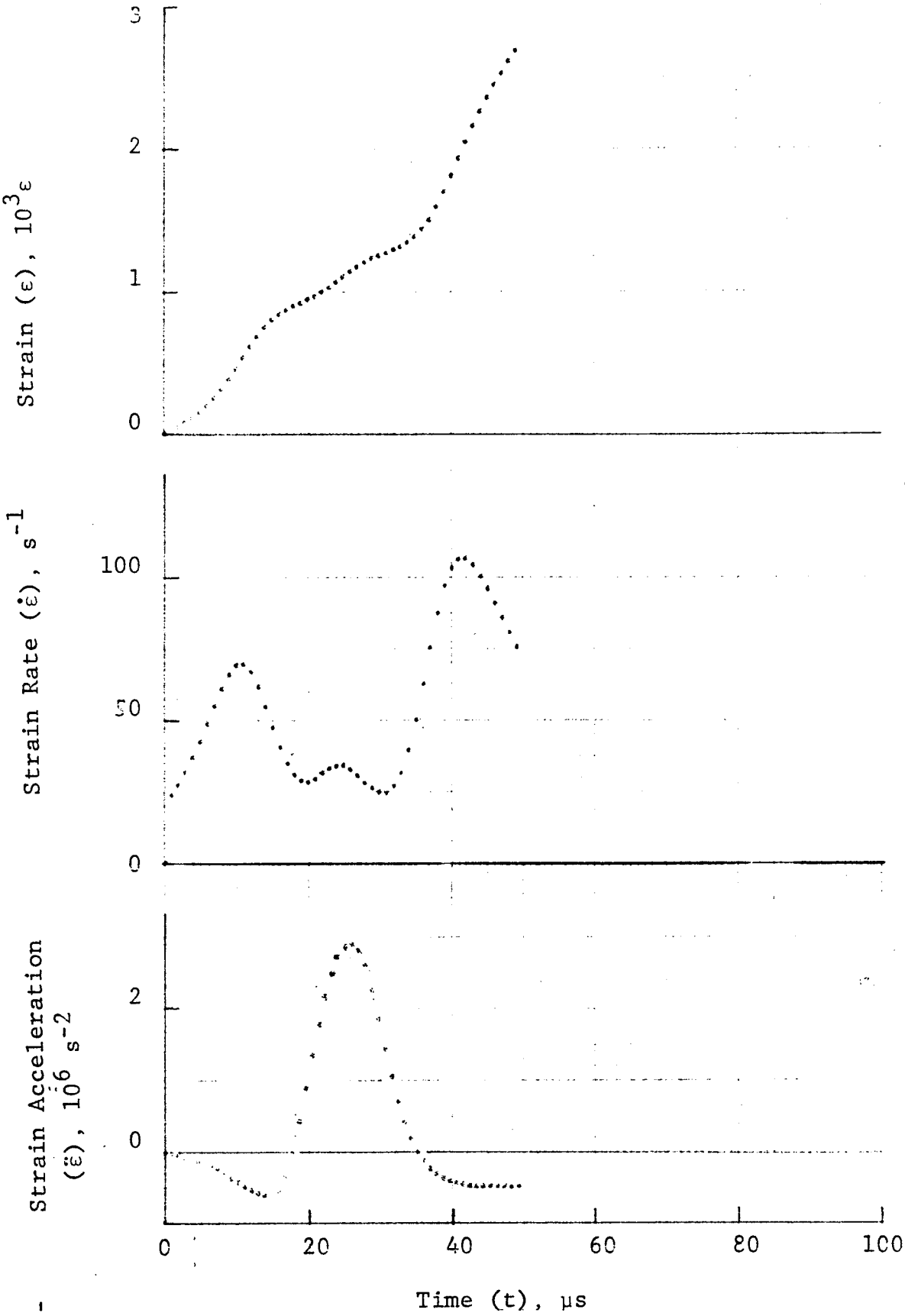

Figure 4-81. Strain and its derivatives in steel ring for Specimen No. 25-11.

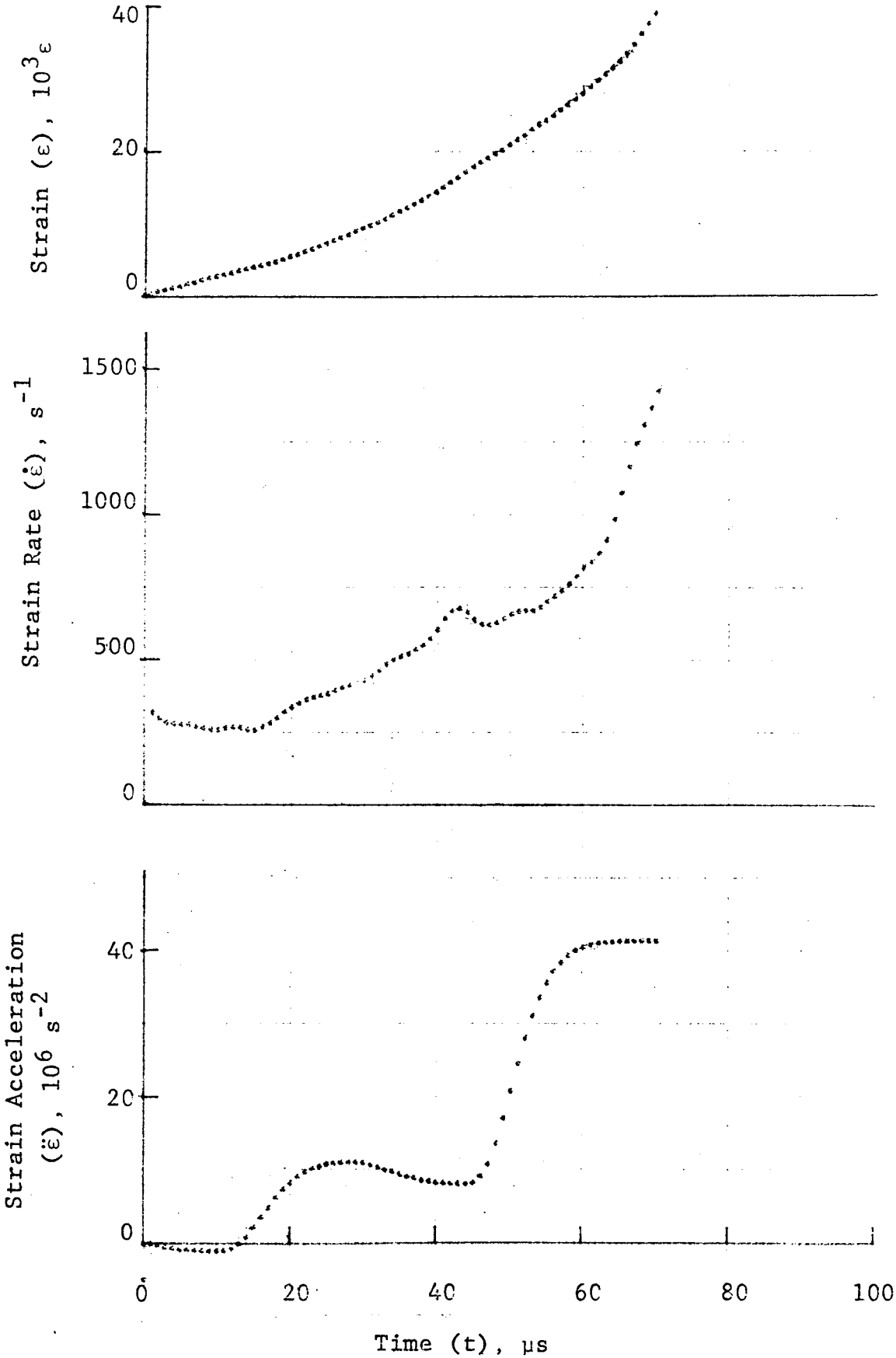

Figure 4-82. Circumferential strain and its derivatives in 80AS/20S/PR288 $[\pm 45]_{2s}$ graphite/S-glass/epoxy ring under dynamic loading for Specimen No. 25-11 (1.56 g pistol powder, $KC\ell O_4$, and aluminum dust).

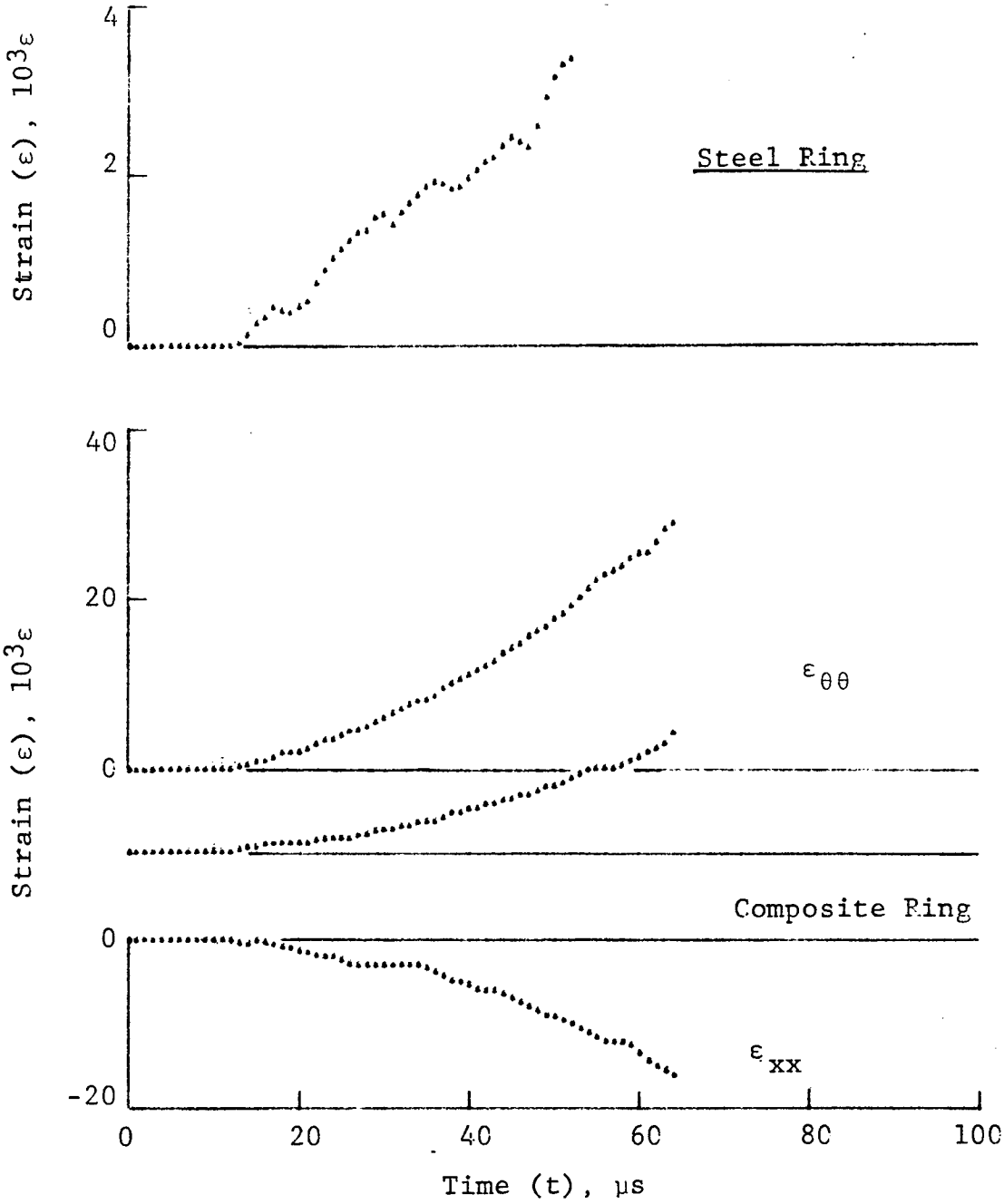

Figure 4-83. Strain records in steel ring and 80AS/20S/PR288 $[\pm 45]_{2s}$ graphite/S-glass/epoxy ring under dynamic loading for Specimen No. 25-12 (1.56 g pistol powder, $KC\ell O_4$, and aluminum dust).

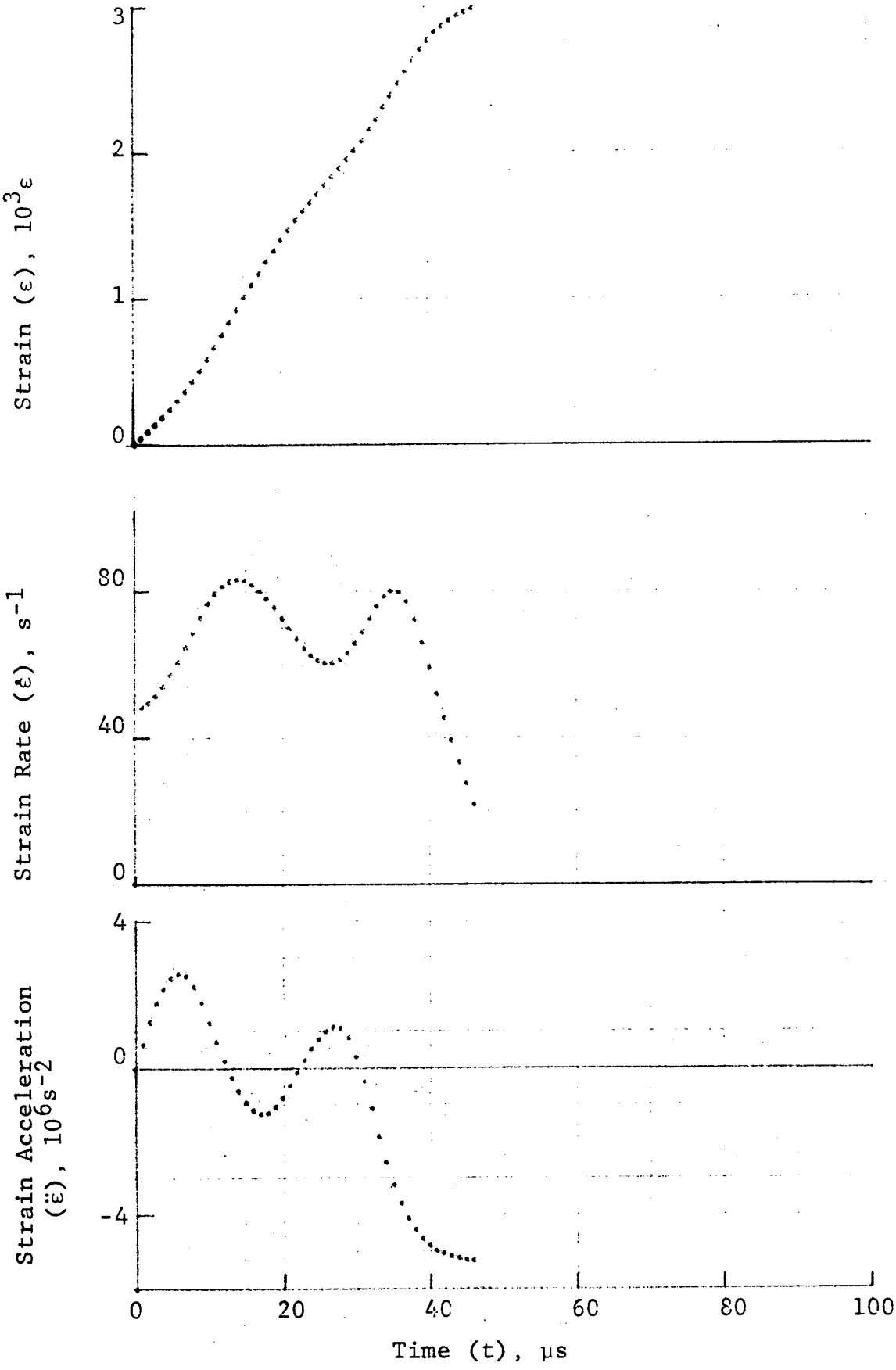

Figure 4-84. Strain and its derivatives in steel ring for Specimen No. 25-12.

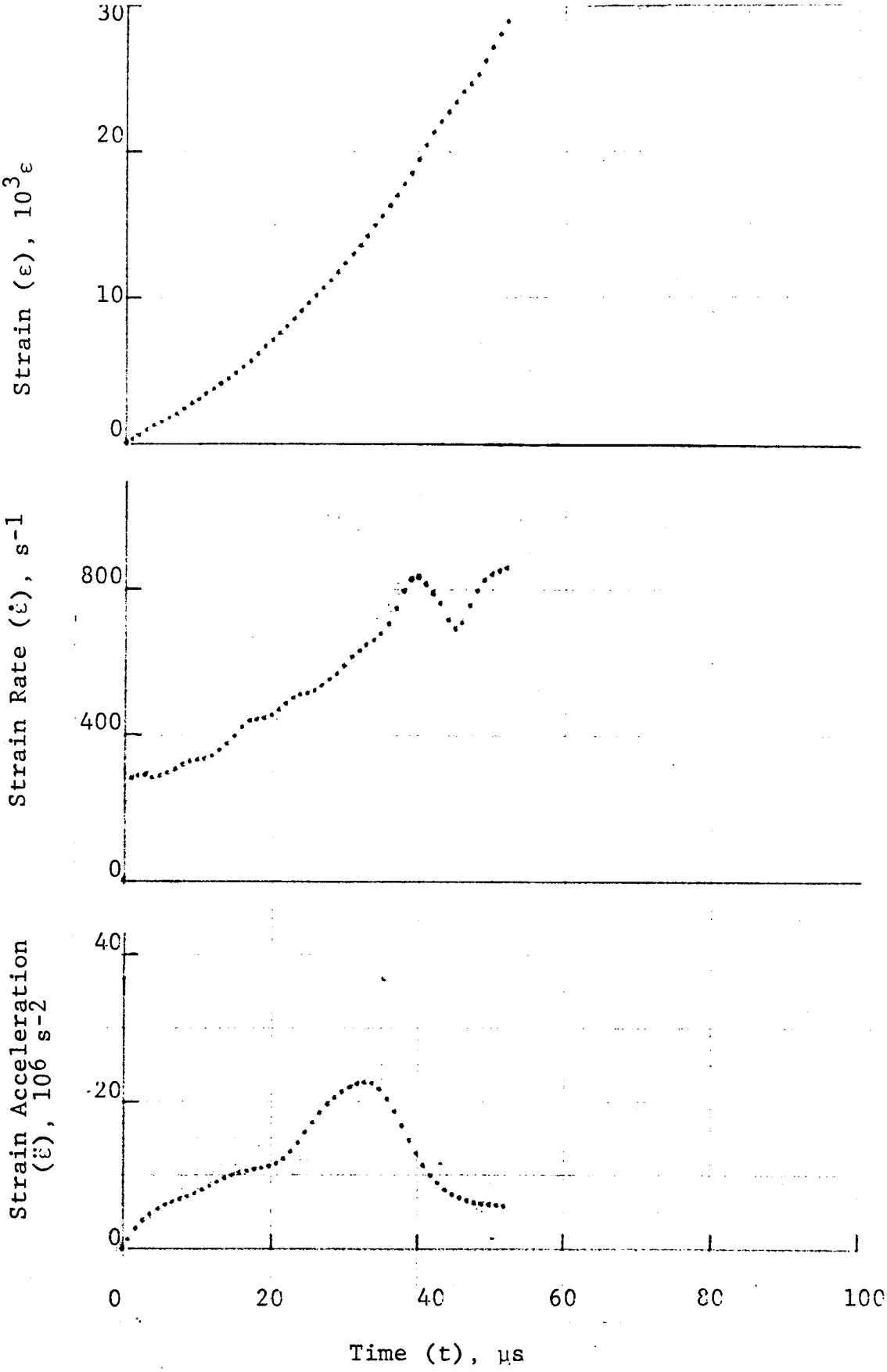

Figure 4-85. Circumferential strain and its derivatives in 80AS/20S/PR288 $[\pm 45]_{2s}$ graphite/S-glass/epoxy ring under dynamic loading for Specimen No. 25-12 (1.56 g pistol powder, $KC\ell O_4$, and aluminum dust).

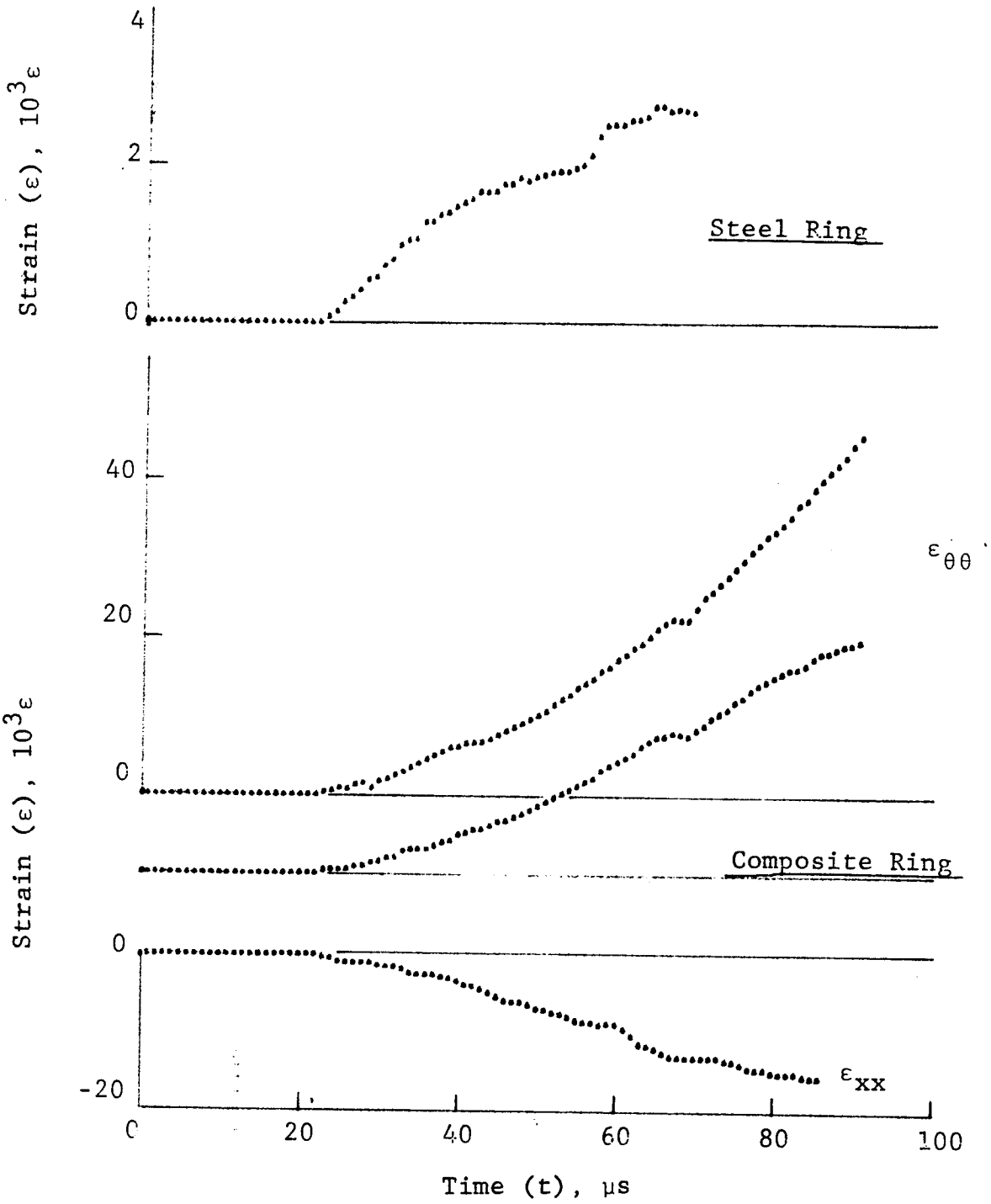

Figure 4-86. Strain records in steel ring and 80AS/20S/PR288 $[\pm 45]_{2s}$ graphite/S-glass/epoxy ring under dynamic loading for Specimen No. 25-13 (1.56 g pistol powder, $KC\ell O_4$, and aluminum dust).

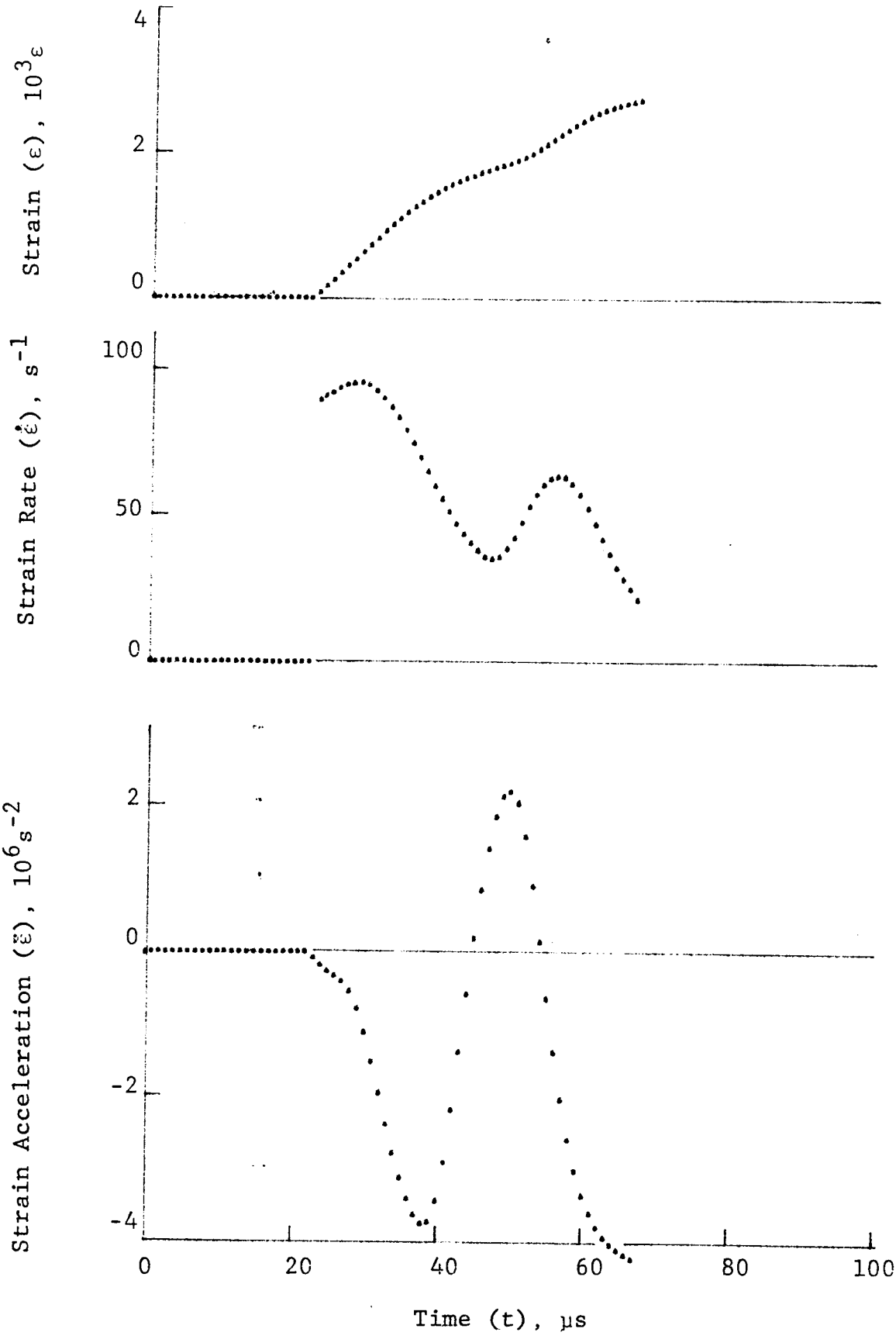

Figure 4-87. Strain and its derivatives in steel ring for Specimen No. 25-13.

C-4

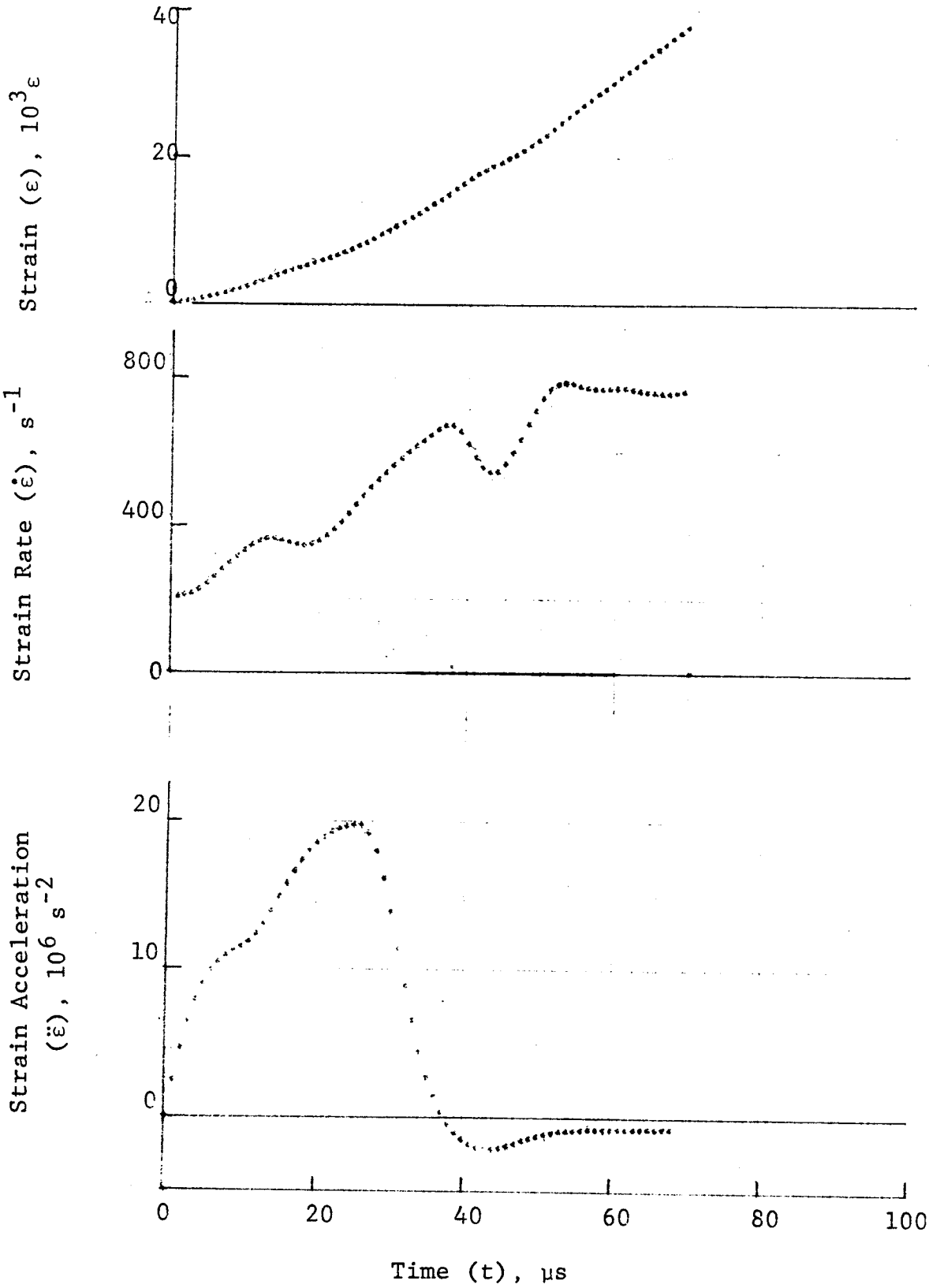

Figure 4-88. Circumferential strain and its derivatives in 80AS/20S/PR288 $[\pm 45]_{2s}$ graphite/S-glass/epoxy ring under dynamic loading for Specimen No. 25-13 (1.56 g pistol powder, $KC\ell O_4$, and aluminum dust).

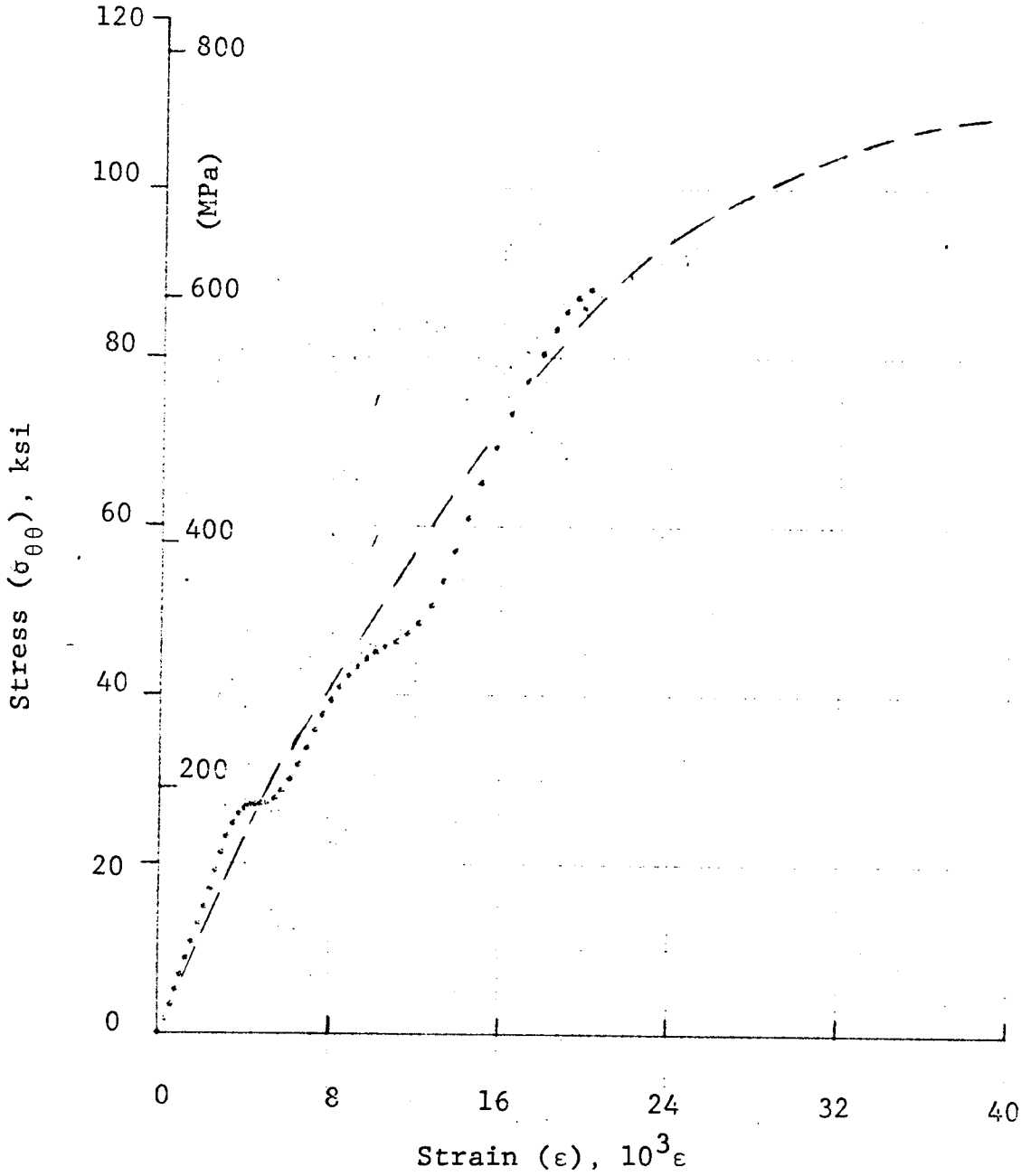

Figure 4-89. Stress-strain curve for dynamically loaded 80AS/20S/PR288 $[\pm 45]_{2s}$ graphite/S-glass/epoxy ring, Specimen No. 25-11 (1.56 g pistol powder, $KC\ell O_4$, and aluminum dust).

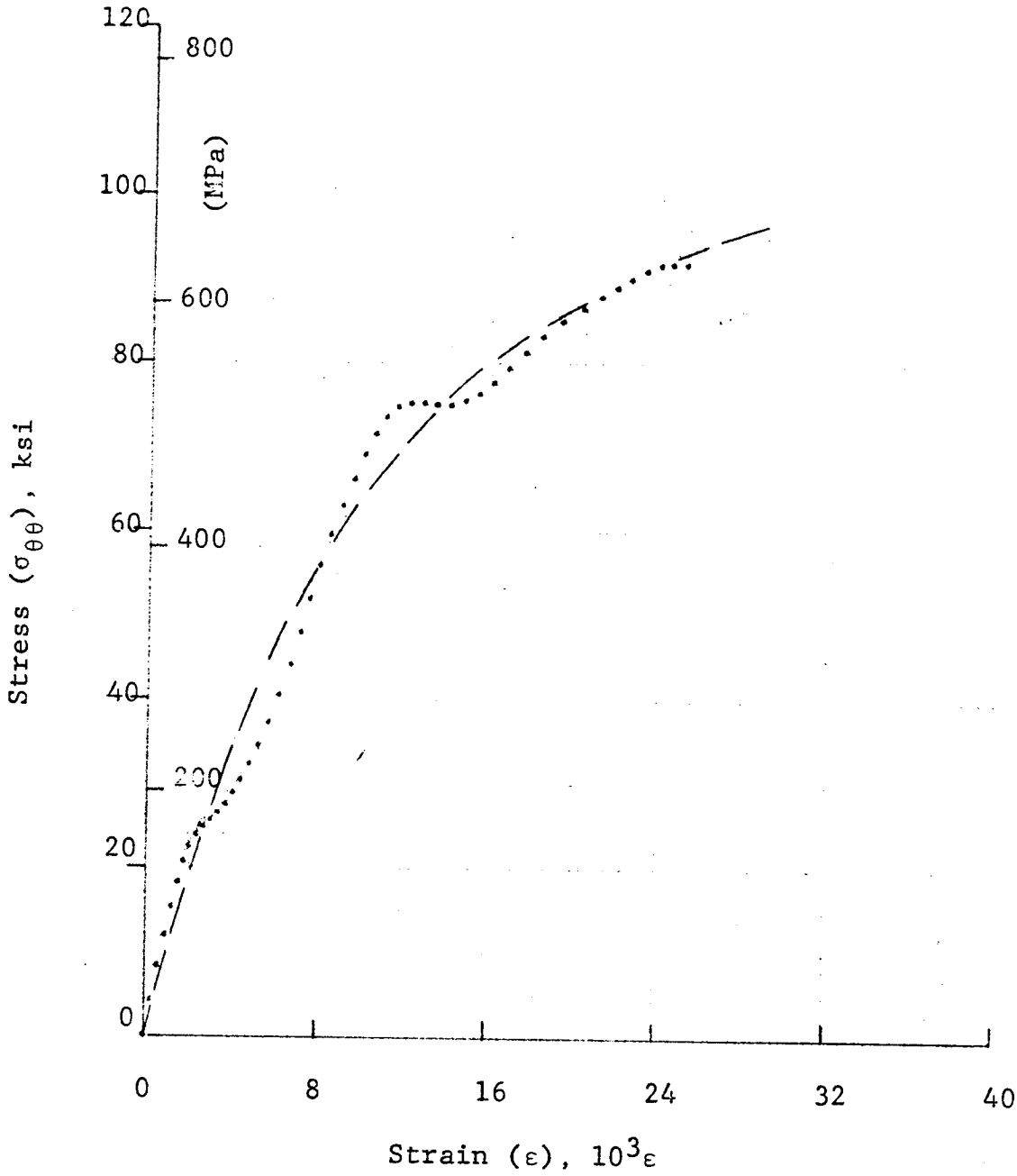

Figure 4-90. Stress-strain curve for dynamically loaded 80AS/20S/PR288 $[\pm 45]_{2s}$ graphite/S-glass/epoxy ring, Specimen No. 25-12 (1.56 g pistol powder, $KC\ell O_4$, and aluminum dust).

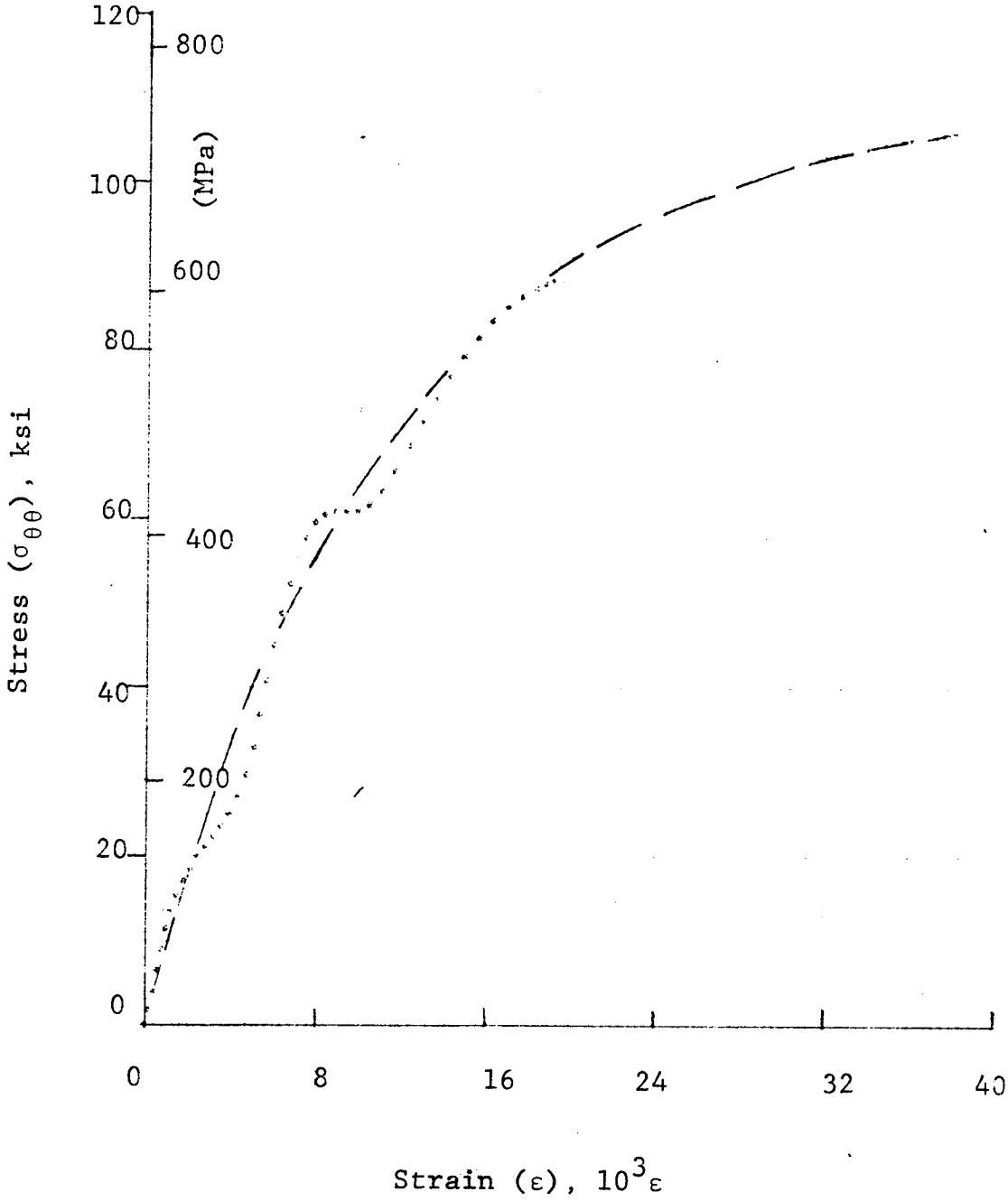

Figure 4-91. Stress-strain curve for dynamically loaded 80AS/20S/PR288 $[\pm 45]_{2s}$ graphite/S-glass/epoxy ring, Specimen No. 25-13 (1.56 g pistol powder, $KC\ell O_4$, and aluminum dust).

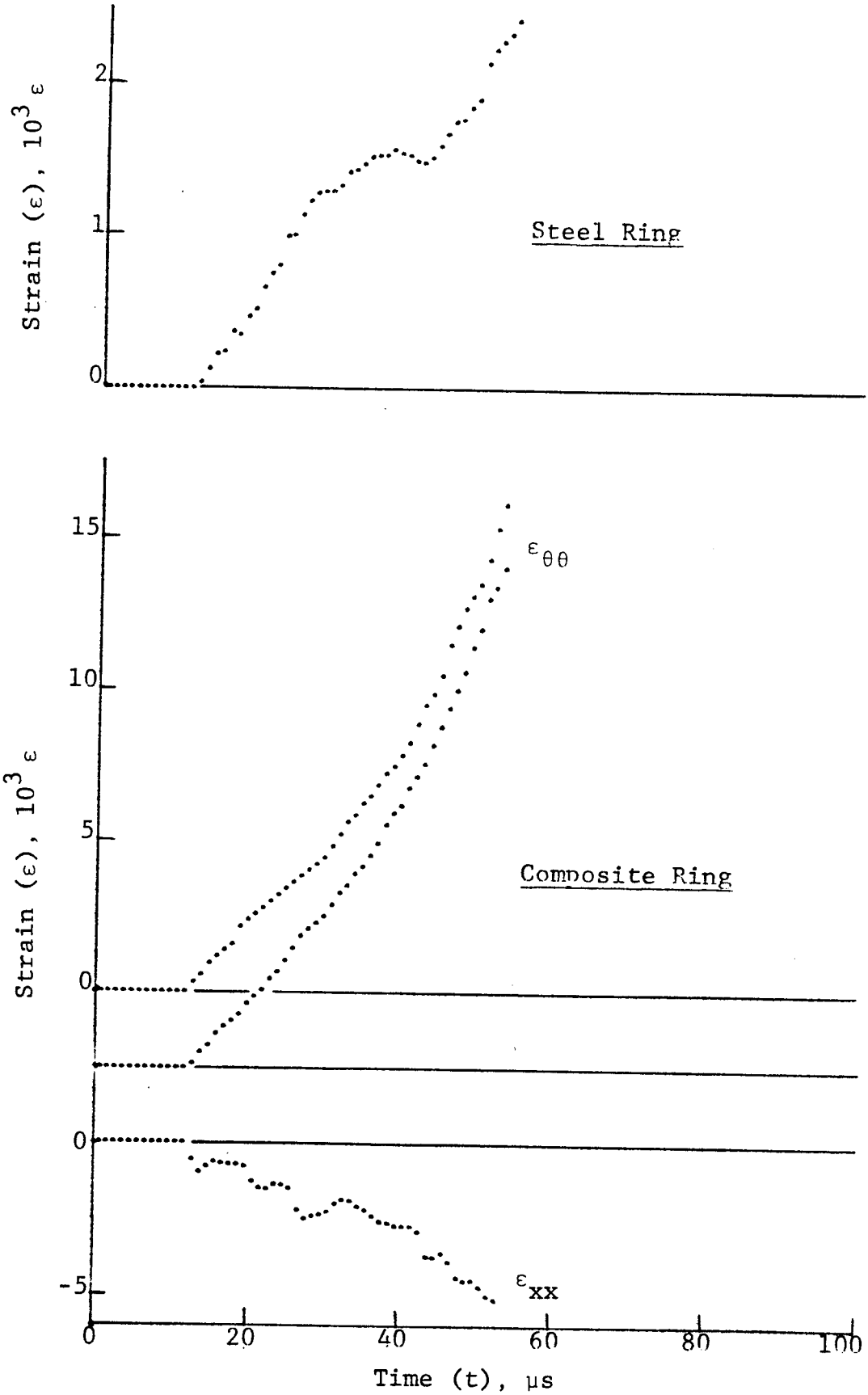

Figure 4-92. Strain records in steel ring and SP288/AS $[\pm 60]_{2S}$ graphite/epoxy ring under dynamic loading for Specimen No. 22-6 (1.56 g pistol powder, $KC\ell O_4$, and aluminum dust).

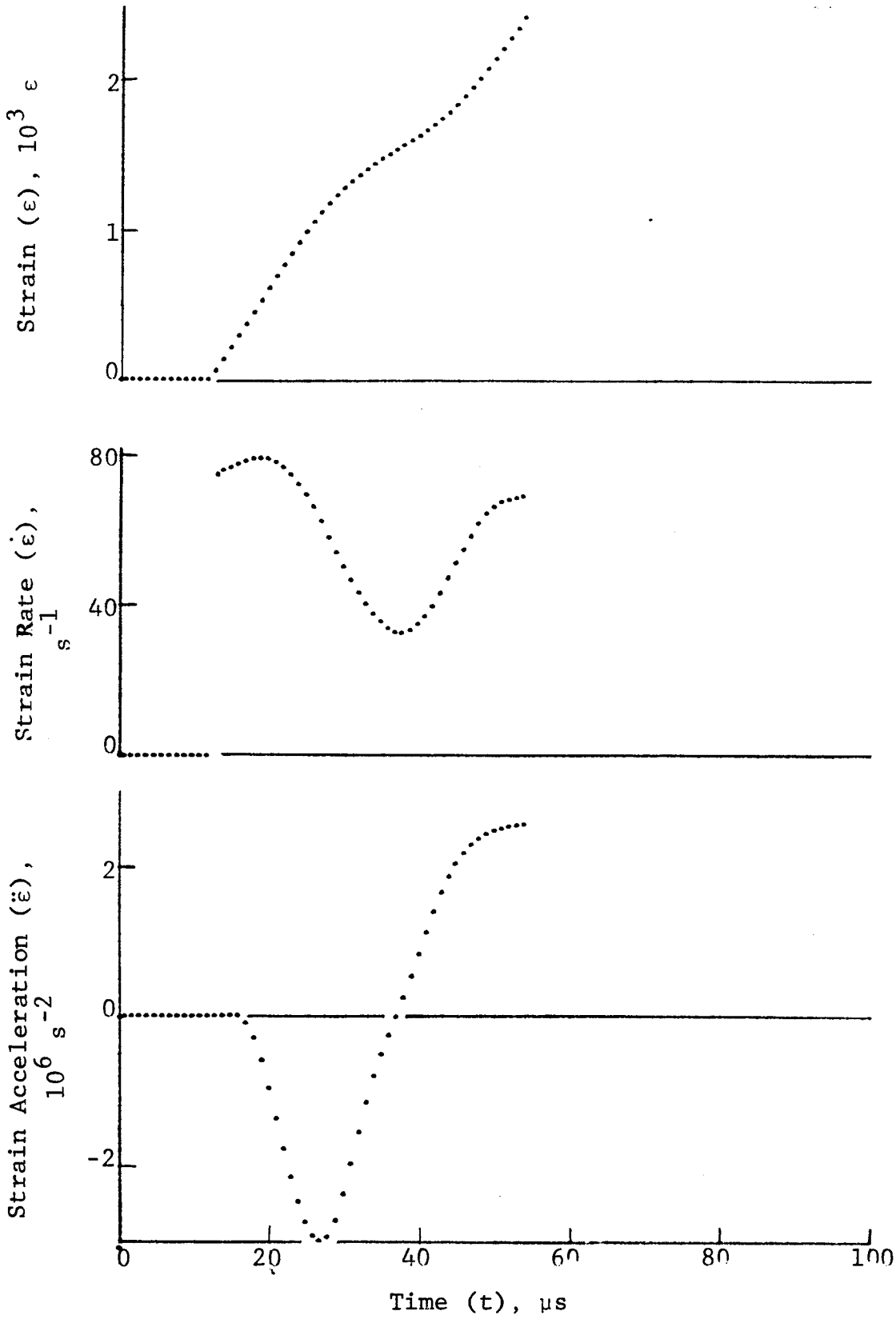

Figure 4-93. Strain and its derivatives in steel ring for Specimen No. 22-6.

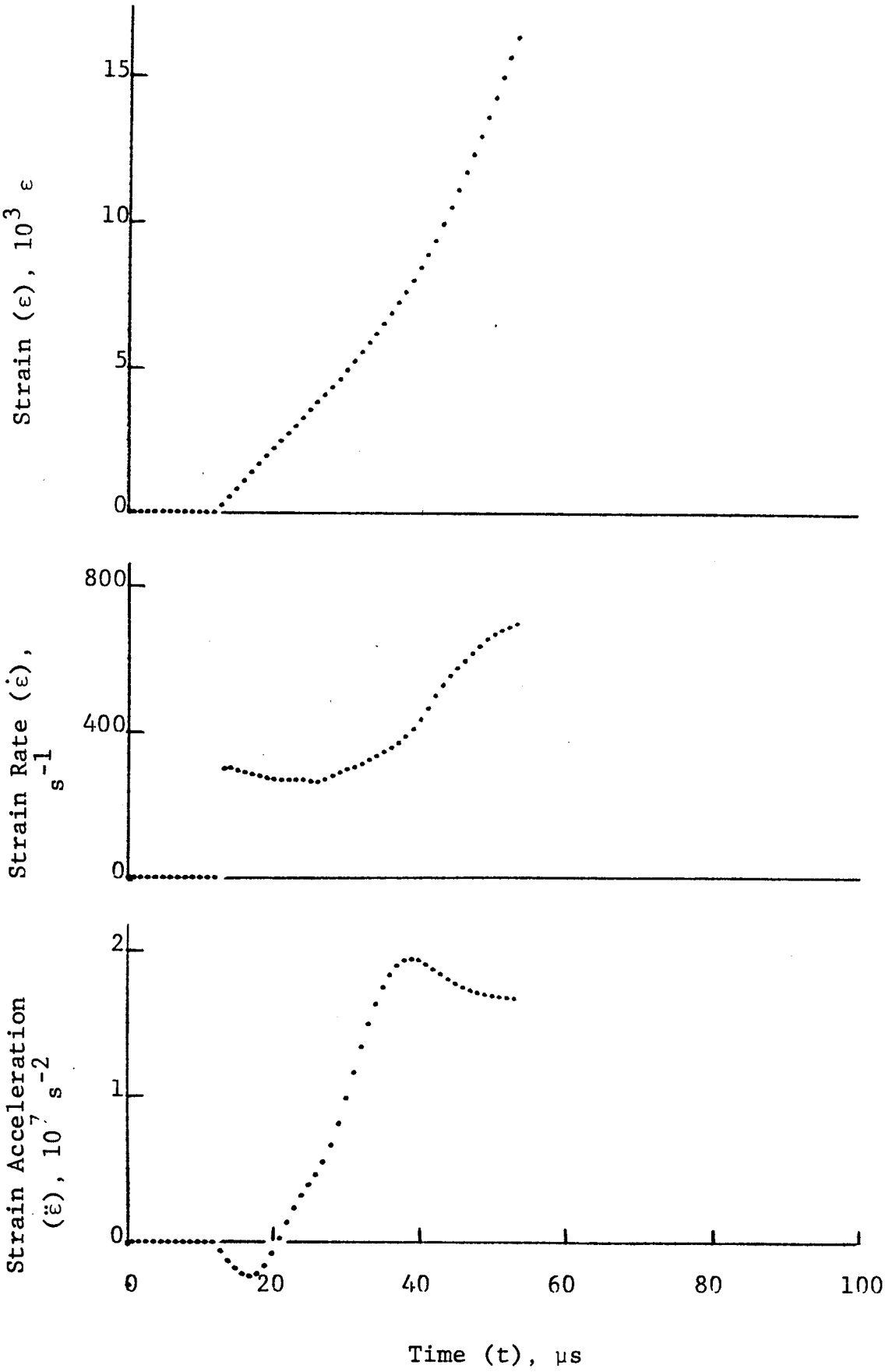

Figure 4-94. Circumferential strain and its derivatives in SP288/AS $[\pm 60]_{2s}$ graphite/epoxy ring under dynamic loading for Specimen No. 22-6.

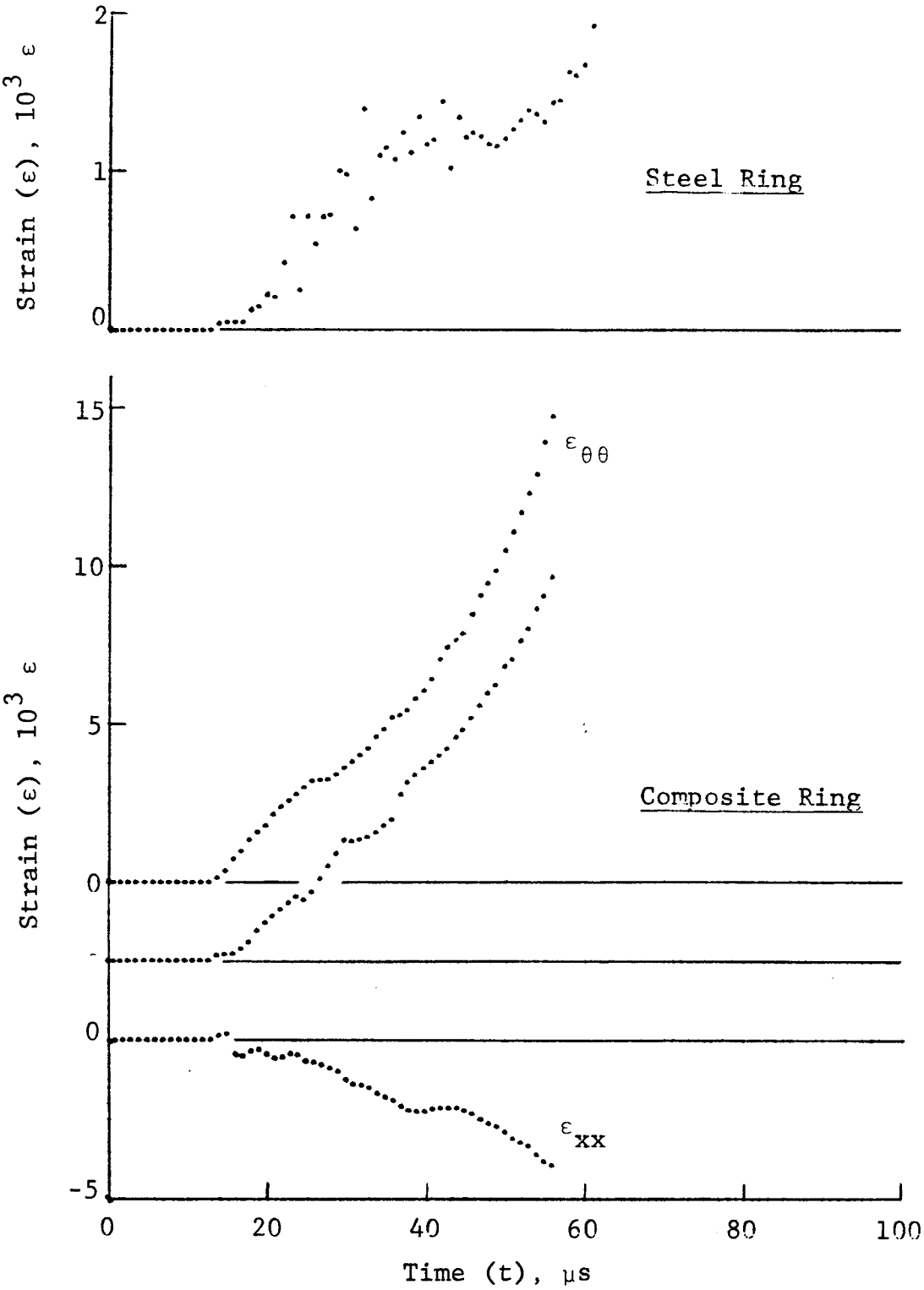

Figure 4-95. Strain records in steel ring and SP288/AS $[\pm 60]_{2S}$ graphite/epoxy ring under dynamic loading for Specimen No. 22-7 (1.56 g pistol powder, $KC\ell O_4$, and aluminum dust).

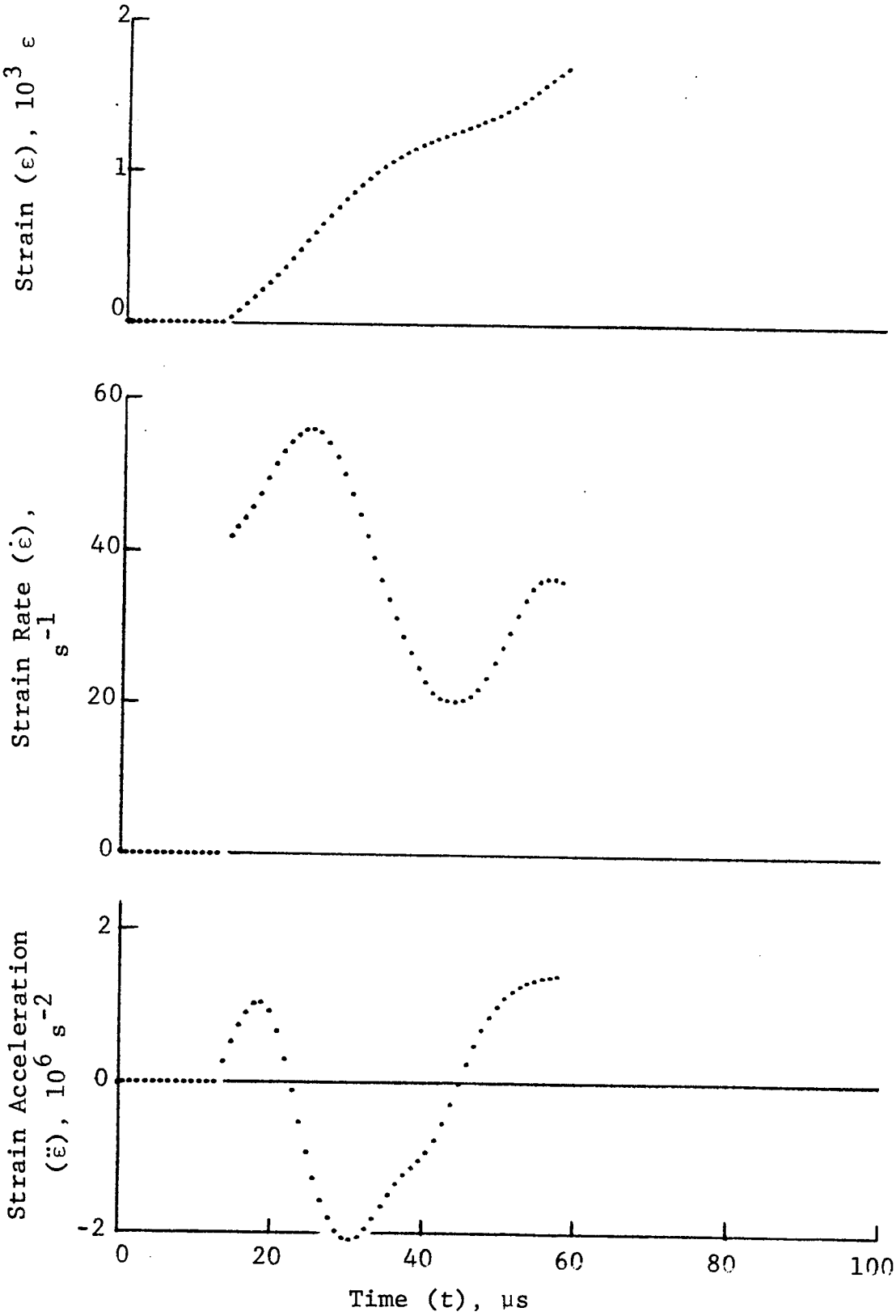

Figure 4-96. Strain and its derivatives in steel ring for Specimen No. 22-7.

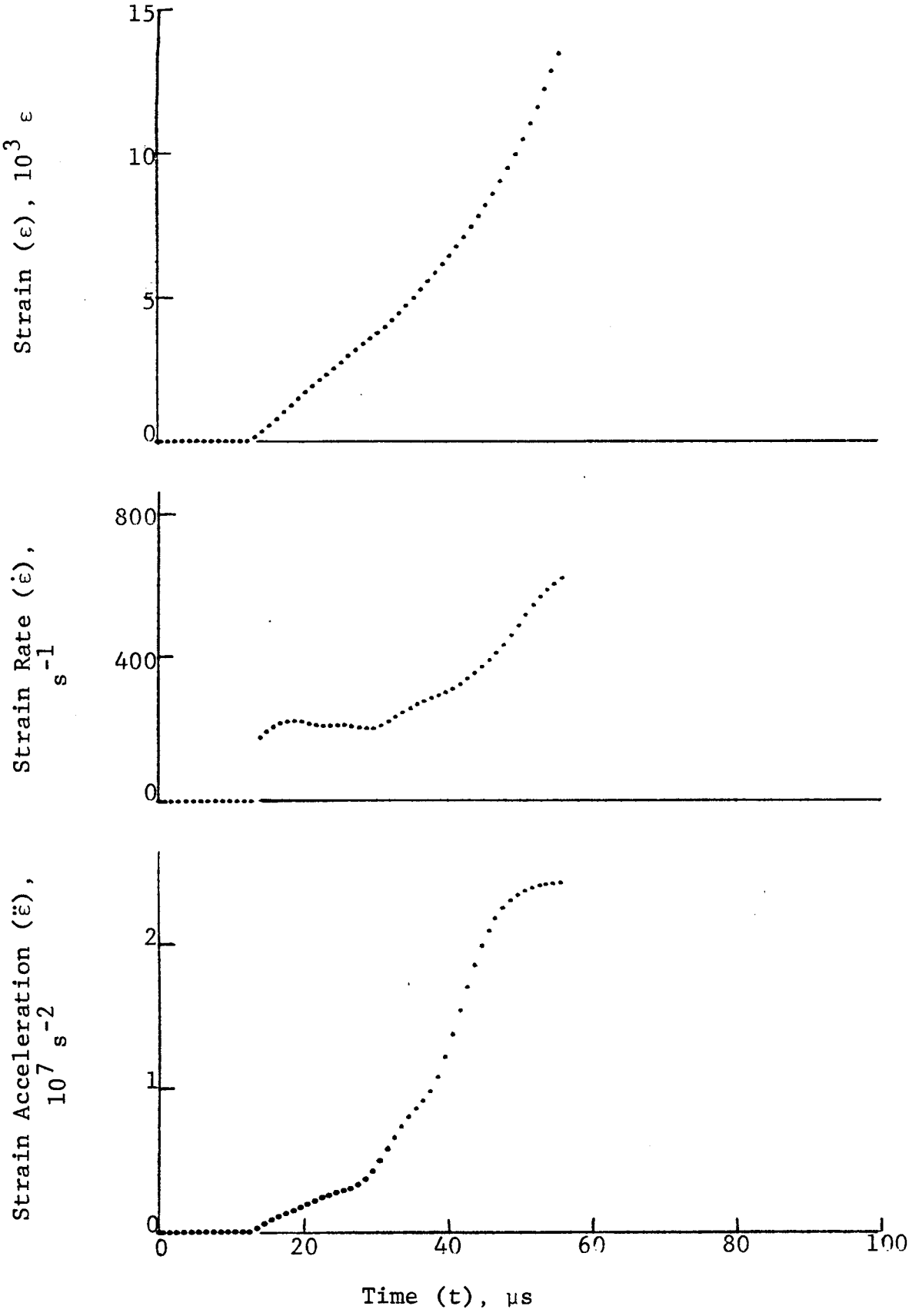

Figure 4-97. Circumferential strain and its derivatives in SP288/AS $[\pm 60]_{2s}$ graphite/epoxy ring under dynamic loading for Specimen No. 22-7.

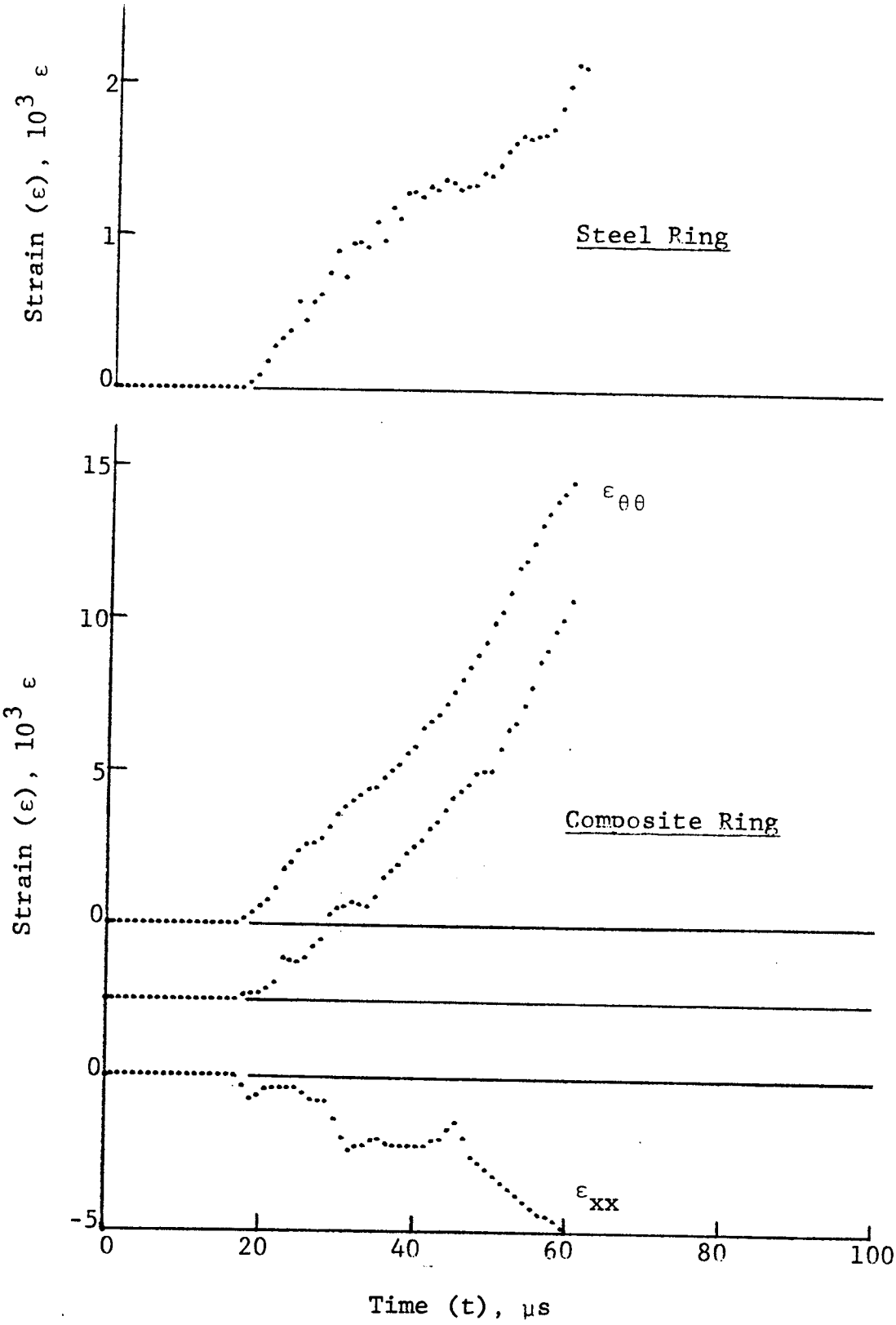

Figure 4-98. Strain records in steel ring and SP288/AS $[\pm 60]_{2S}$ graphite/epoxy ring under dynamic loading for Specimen No. 22-8 (1.56 g pistol powder, $KC\ell O_4$, and aluminum dust).

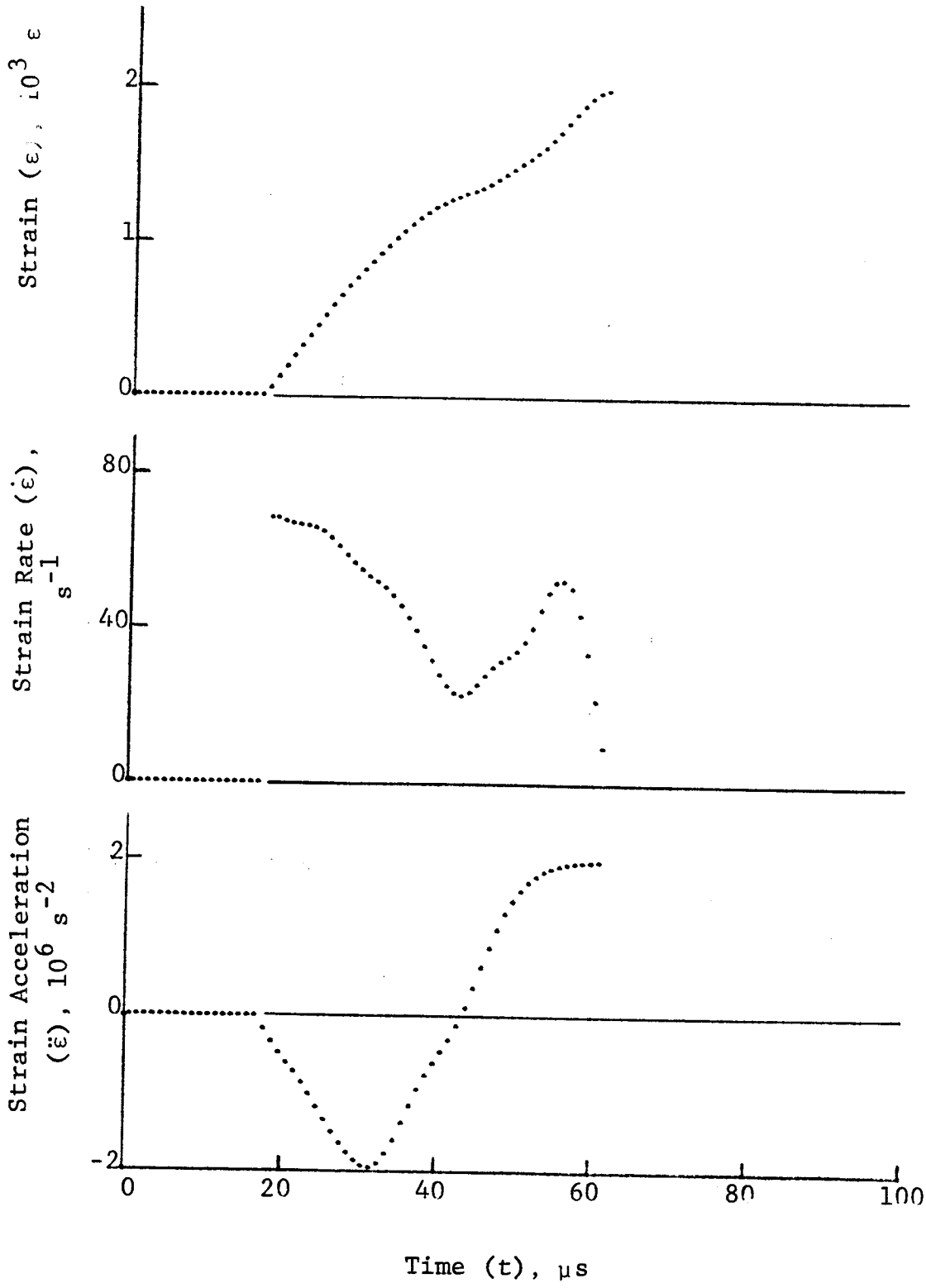

Figure 4-99. Strain and its derivatives in steel ring for Specimen No. 22-8.

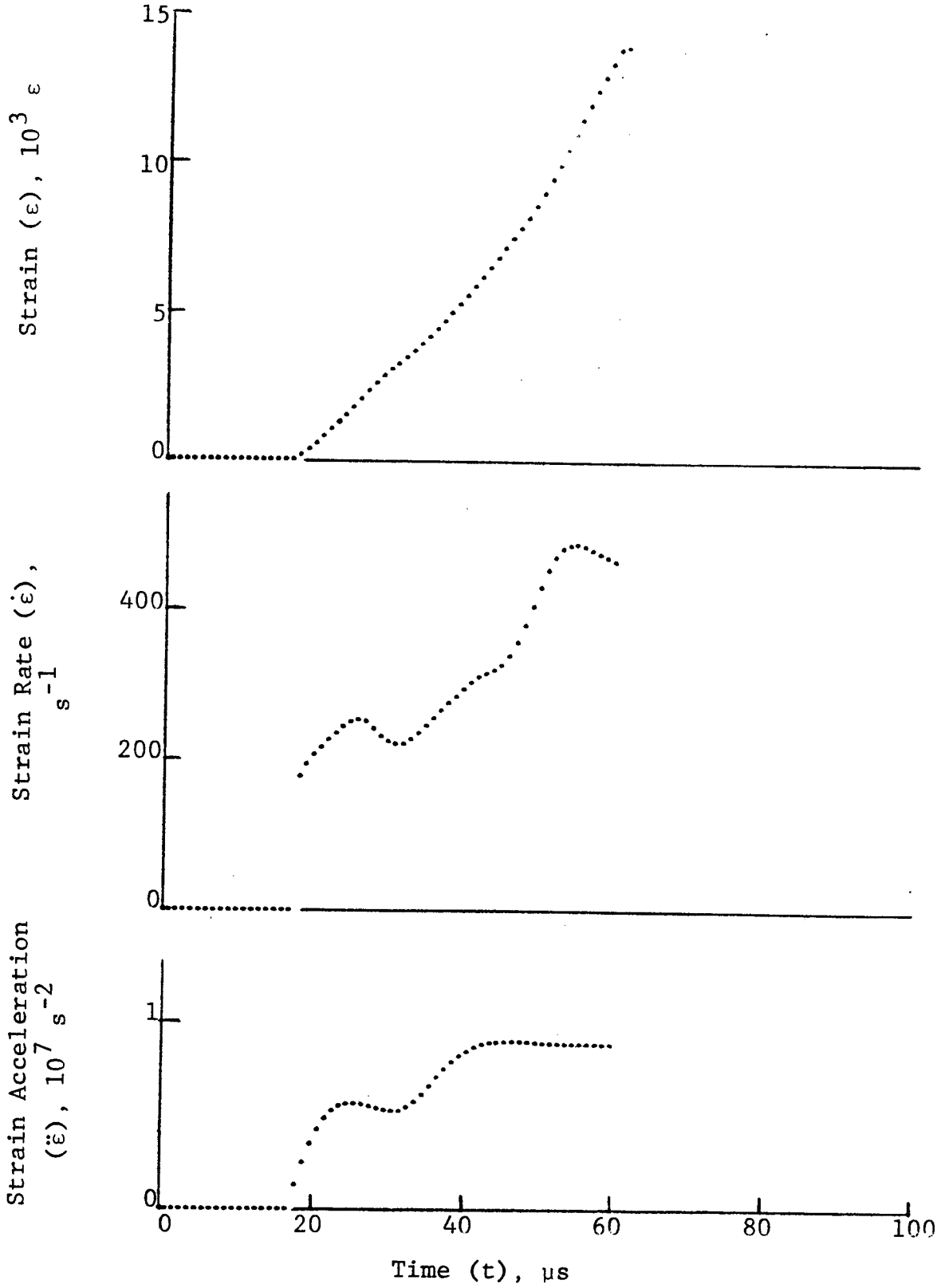

Figure 4-100. Circumferential strain and its derivatives in SP288/AS $[\pm 60]_{2S}$ graphite/epoxy ring under dynamic loading for Specimen No. 22-8.

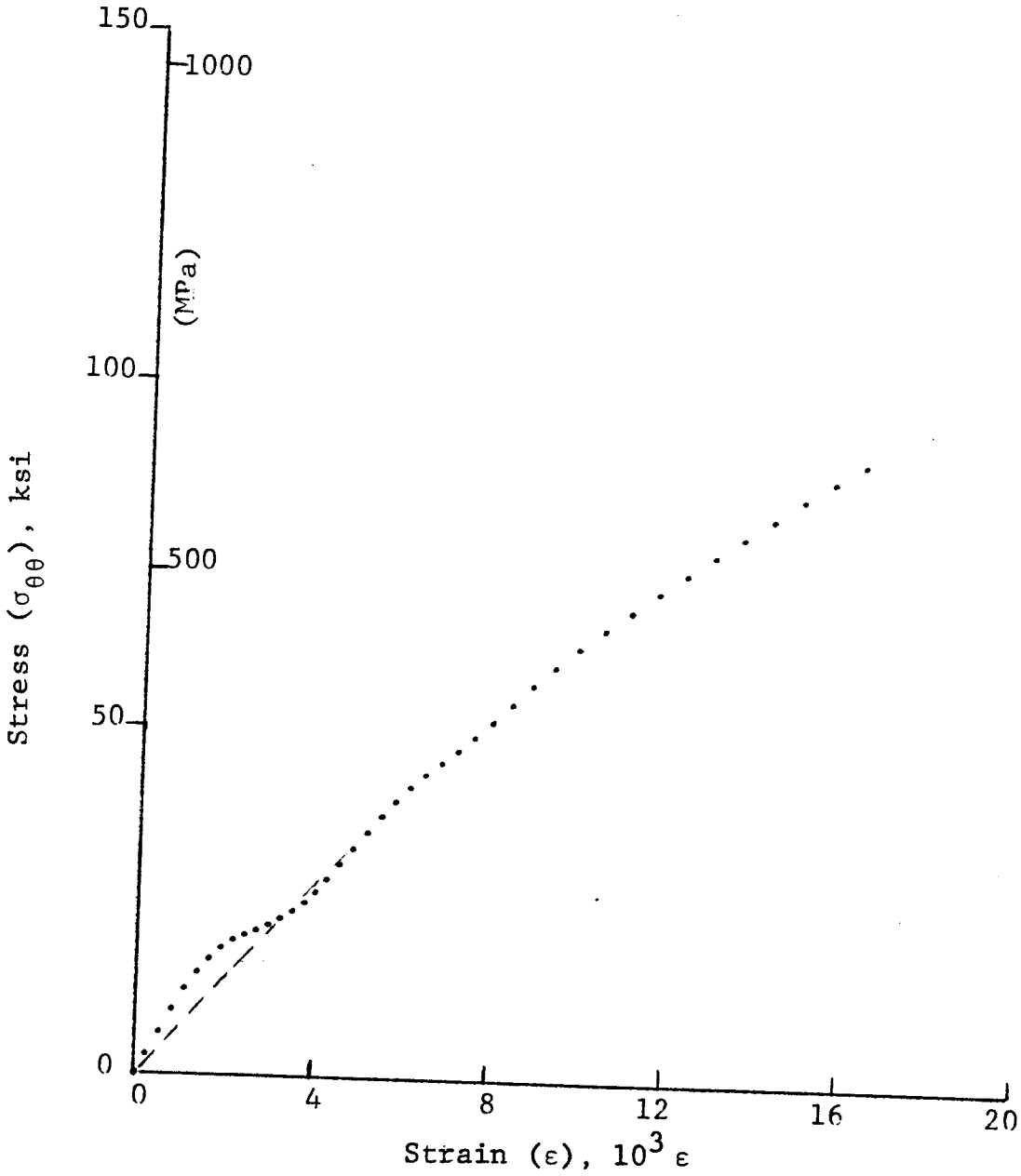

Figure 4-101. Stress-strain curve for dynamically loaded SP288/AS $[\pm 60]_{2s}$ graphite/epoxy ring, Specimen No. 22-6 (1.56 g pistol powder, $KC\ell O_4$, and aluminum dust).

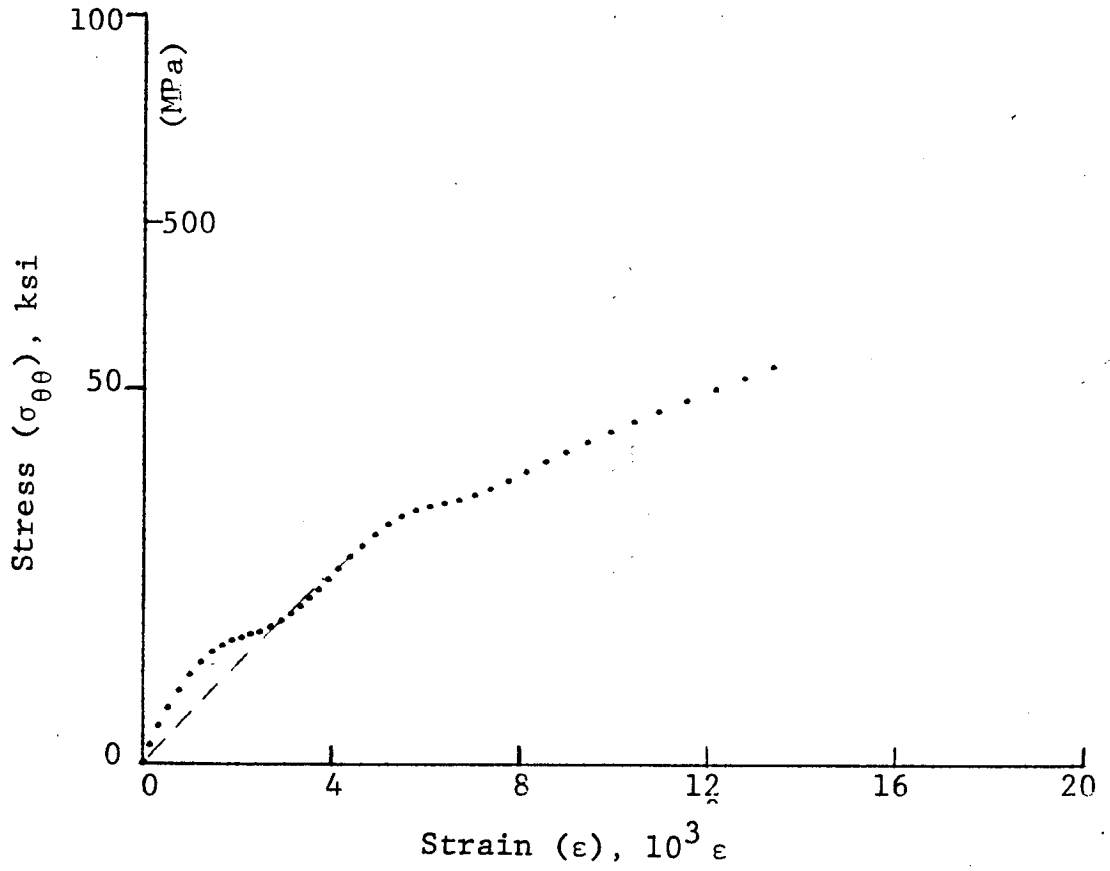

Figure 4-102. Stress-strain curve for dynamically loaded SP288/AS $[\pm 60]_{2s}$ graphite/epoxy ring, Specimen No. 22-7 (1.56 g pistol powder, $KC\ell O_4$, and aluminum dust).

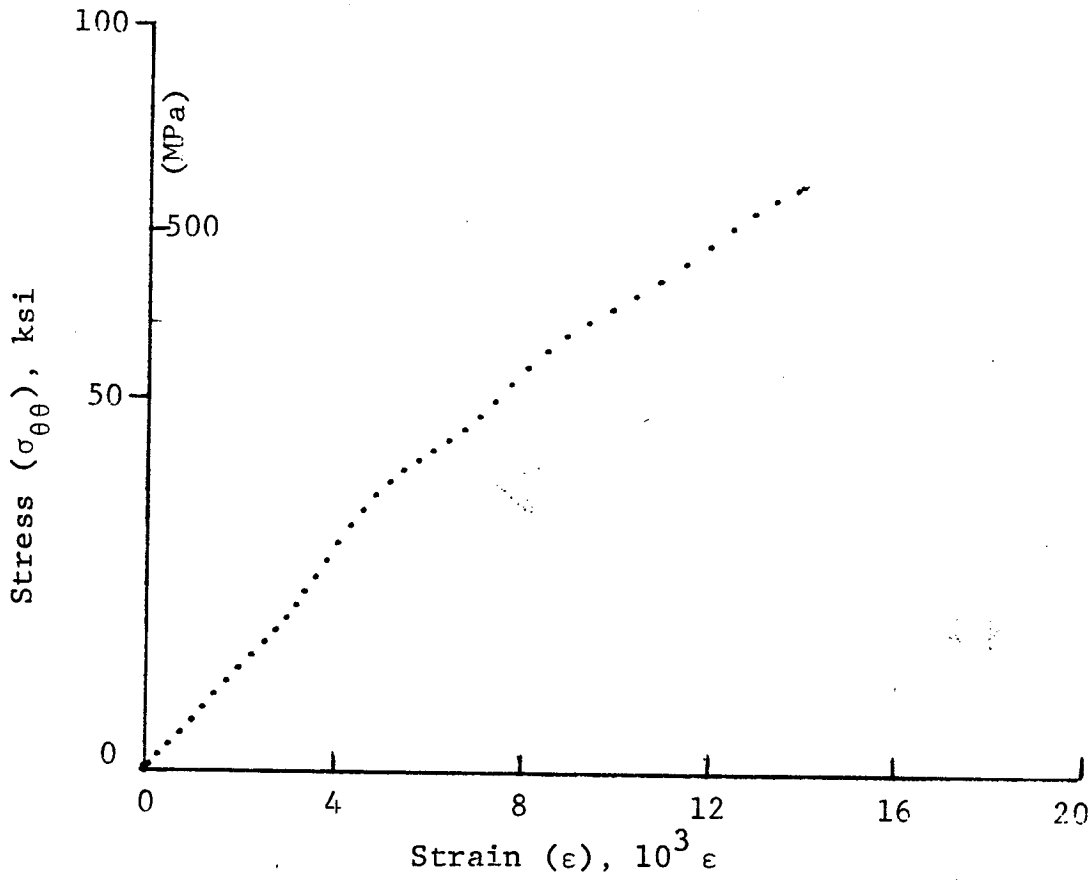

Figure 4-103. Stress-strain curve for dynamically loaded SP288/AS $[\pm 60]_{2s}$ graphite/epoxy ring, Specimen No. 22-8 (1.56 g pistol powder, $KC\ell O_4$, and aluminum dust).

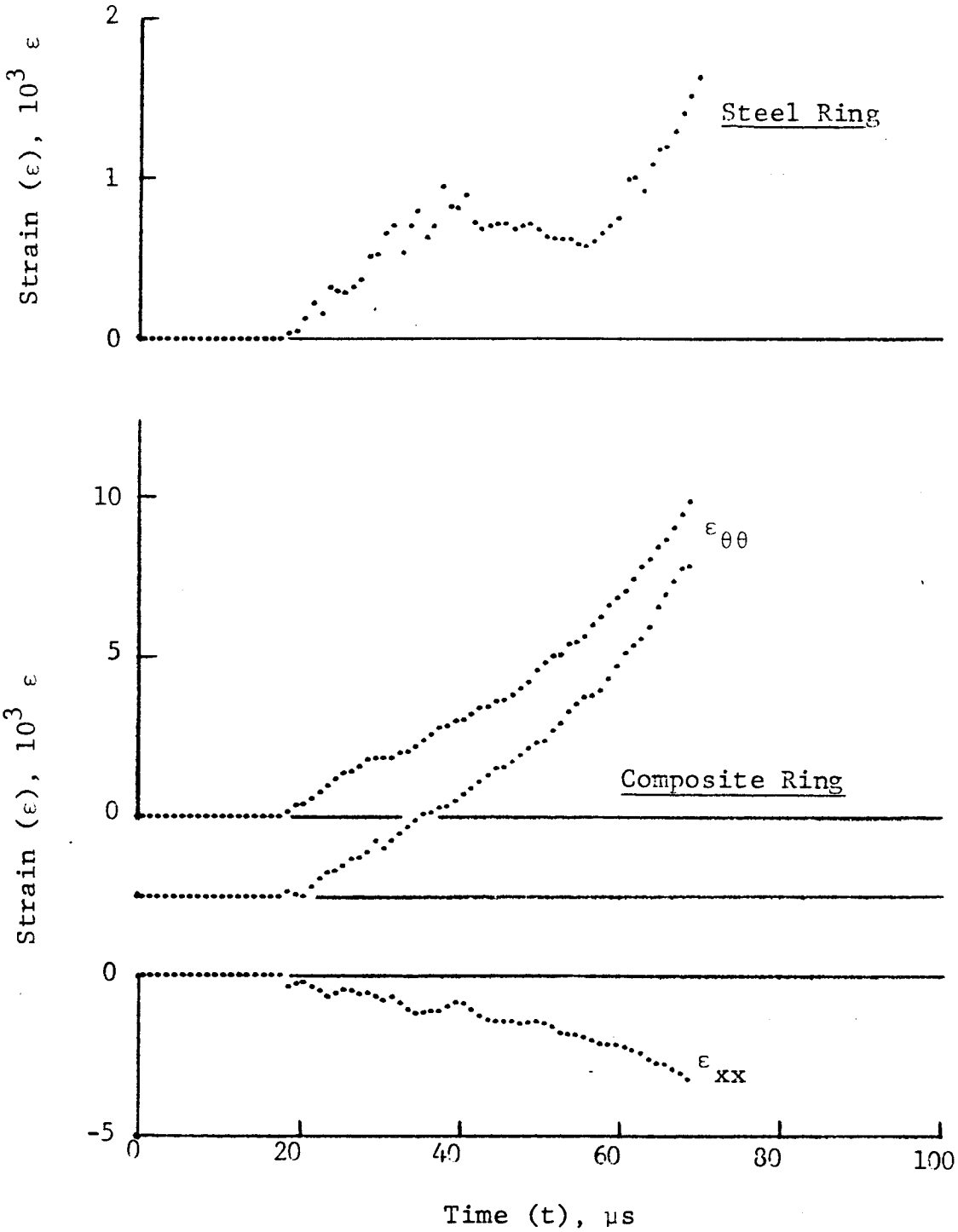

Figure 4-104. Strain records in steel ring and $[\pm 60]_{2S}$ 80AS/20S/PR288 graphite/S-glass/epoxy ring under dynamic loading for Specimen No. 23-2 (1.56 g pistol powder, $KC\ell O_4$, and aluminum dust).

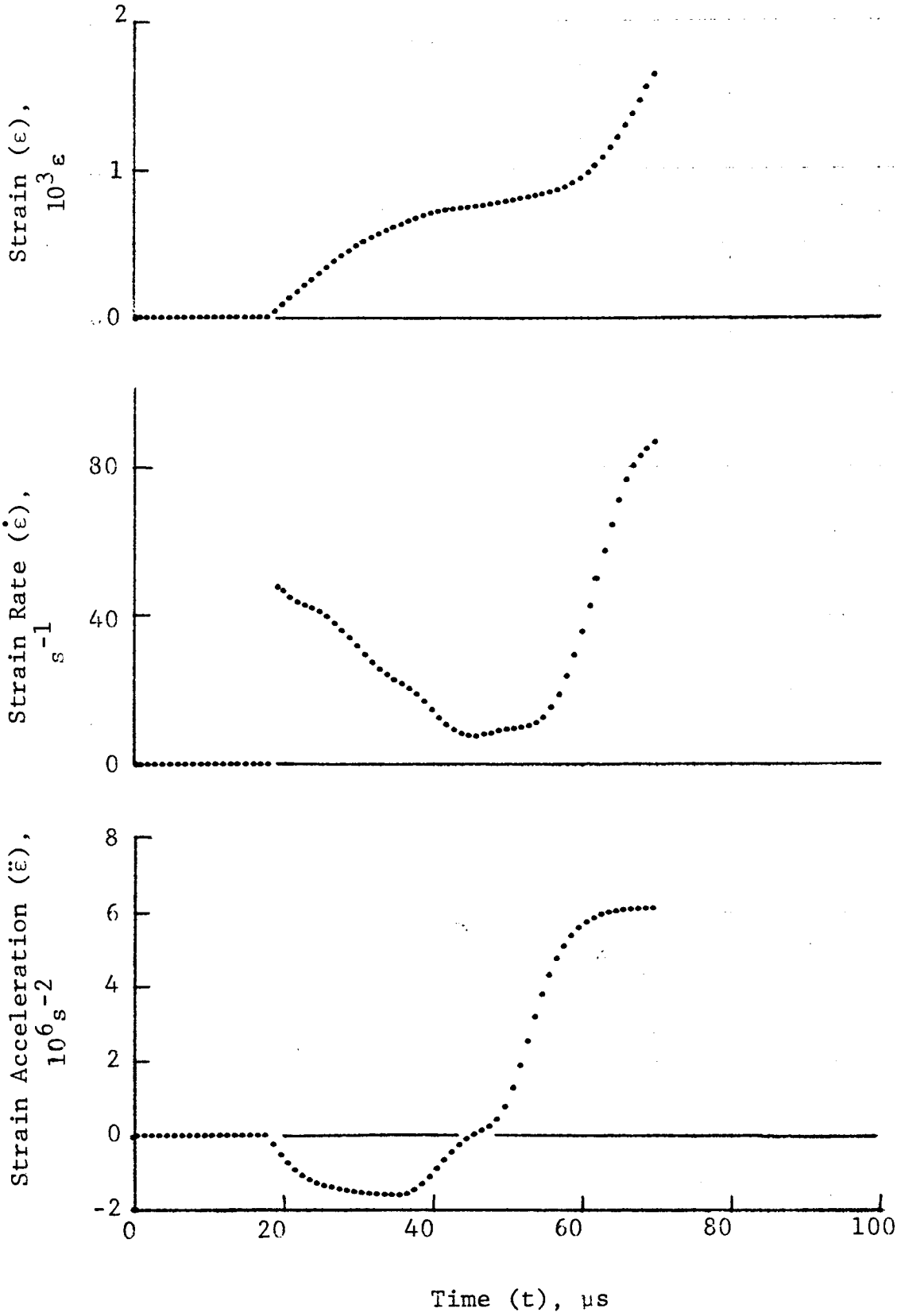

Figure 4-105. Strain and its derivatives in steel ring for Specimen No. 23-2.

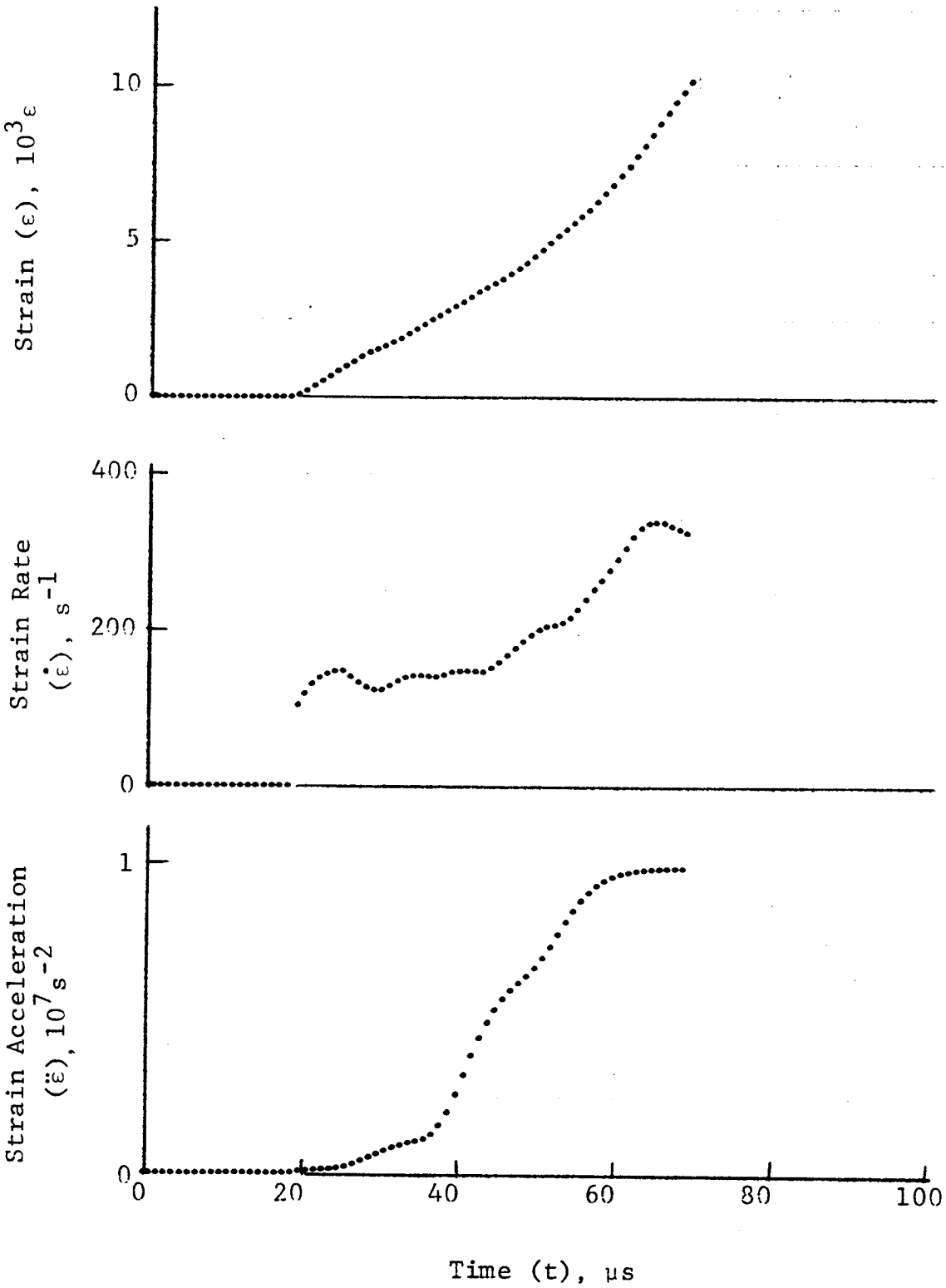

Figure 4-106. Circumferential strain and its derivatives in $[\pm 60]_{2s}$ 80AS/20S/PR288 graphite/S-glass/epoxy ring under dynamic loading for Specimen No. 23-2.

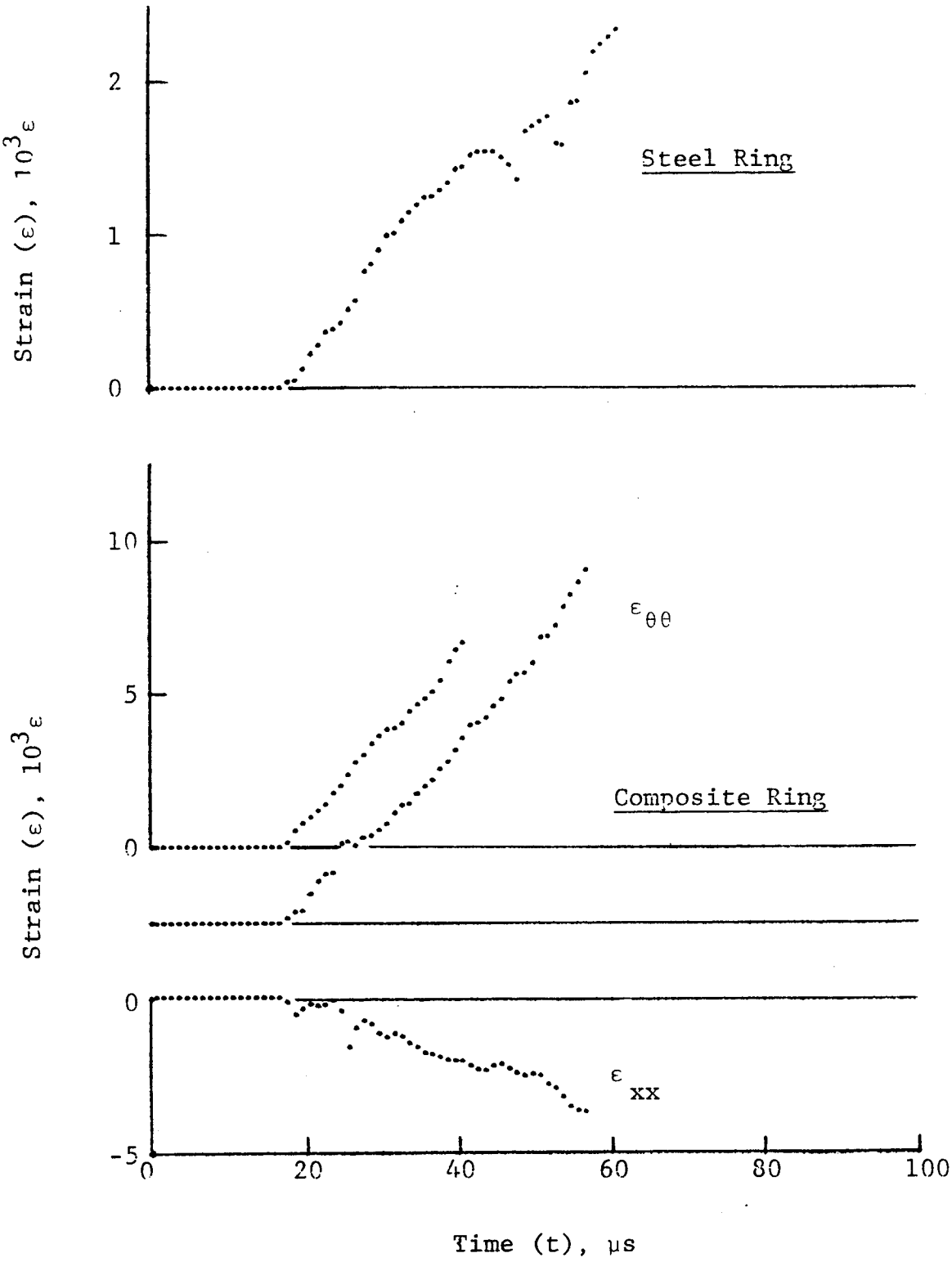

Figure 4-107. Strain records in steel ring and $[\pm 60]_{2S}$ 80AS/20S/PR288 graphite/S-glass/epoxy ring under dynamic loading for Specimen No. 23-4 (1.56 g pistol powder, $KC\ell O_4$, and aluminum dust).

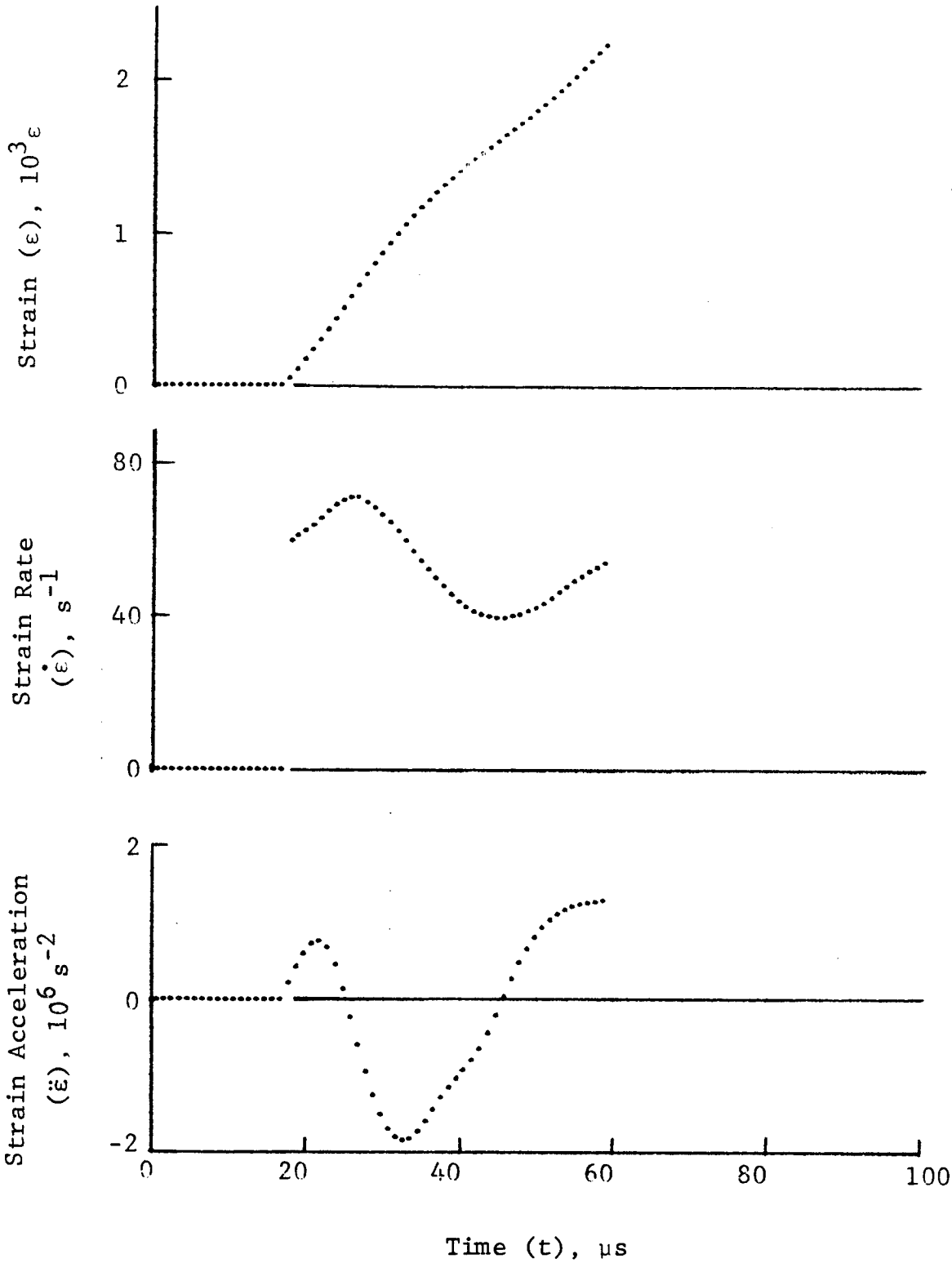

Figure 4-108. Strain and its derivatives in steel ring for Specimen No. 23-4.

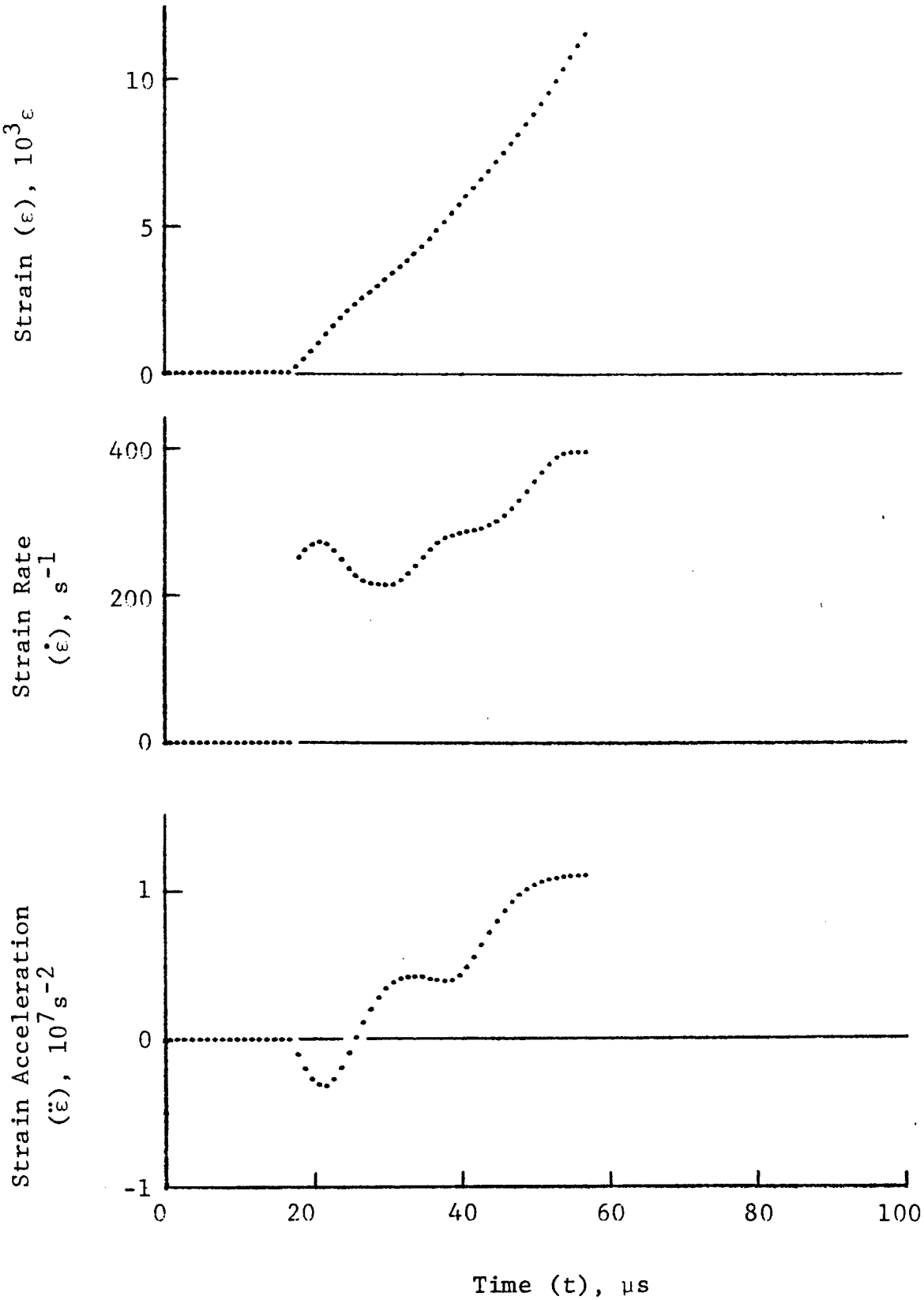

Figure 4-109. Circumferential strain and its derivatives in $[\pm 60]_{2S}$ 80AS/20S/PR288 graphite/S-glass/epoxy ring under dynamic loading for Specimen No. 23-4.

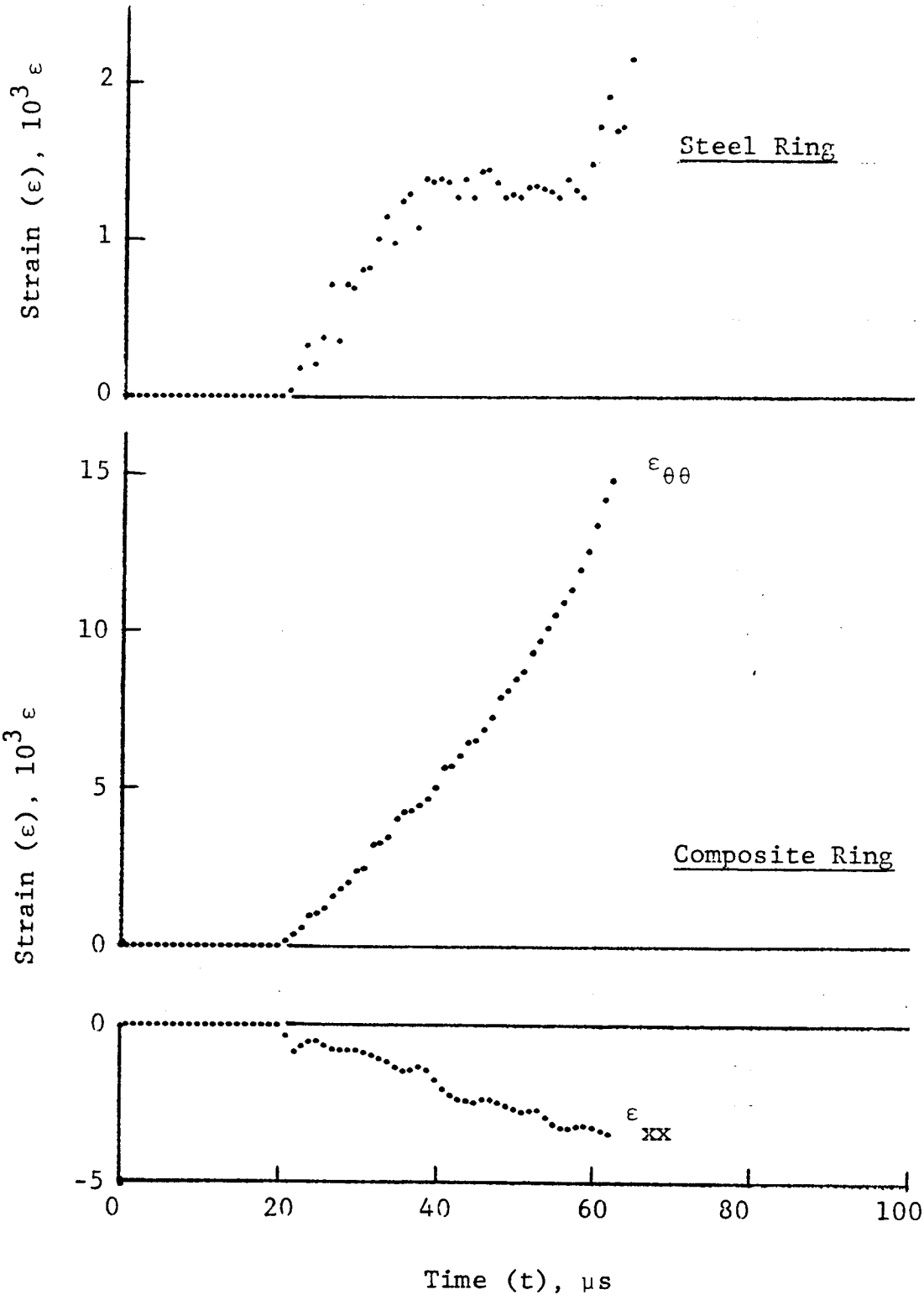

Figure 4-110. Strain records in steel ring and $[\pm 60]_{2S}$ 80AS/20S/PR288 graphite/S-glass/epoxy ring under dynamic loading for Specimen No. 23-6 (1.56 g pistol powder, $KC\ell O_4$, and aluminum dust).

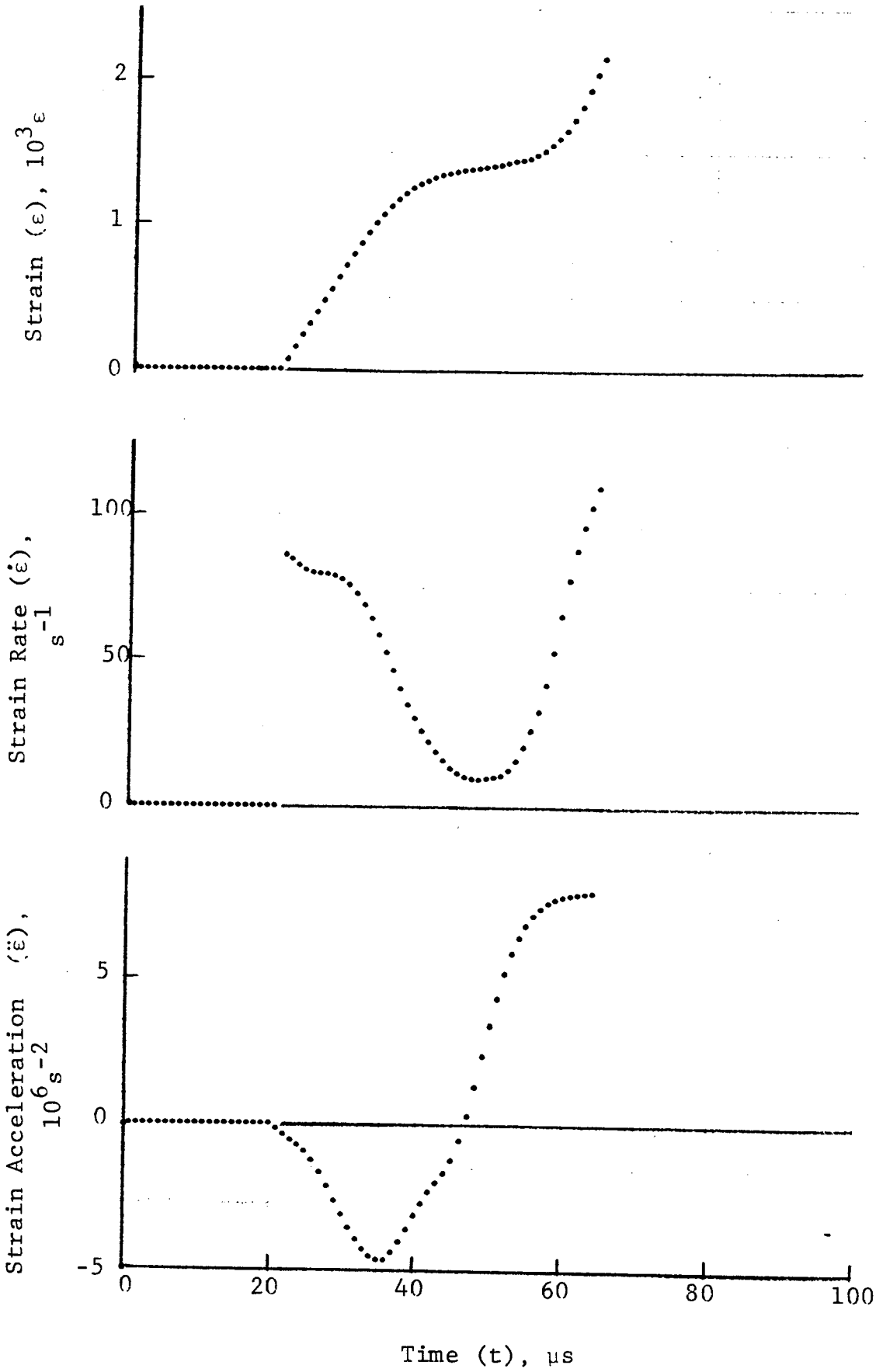

Figure 4-111. Strain and its derivatives in steel ring for Specimen No. 23-6.

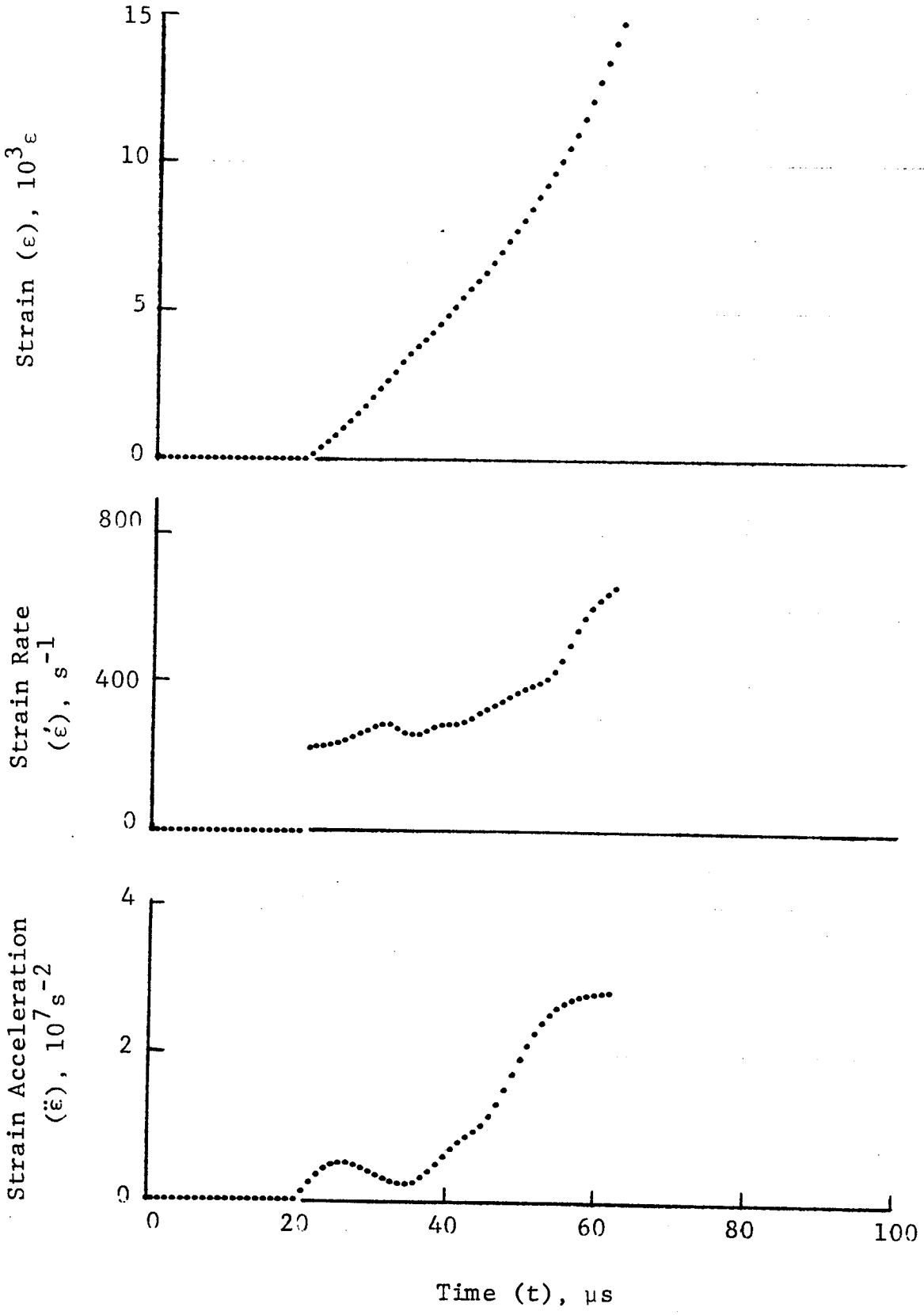

Figure 4-112. Circumferential strain and its derivatives in $[\pm 60]_{2s}$ 80AS/20S/PR288 graphite/S-glass/epoxy ring under dynamic loading for Specimen No. 23-6.

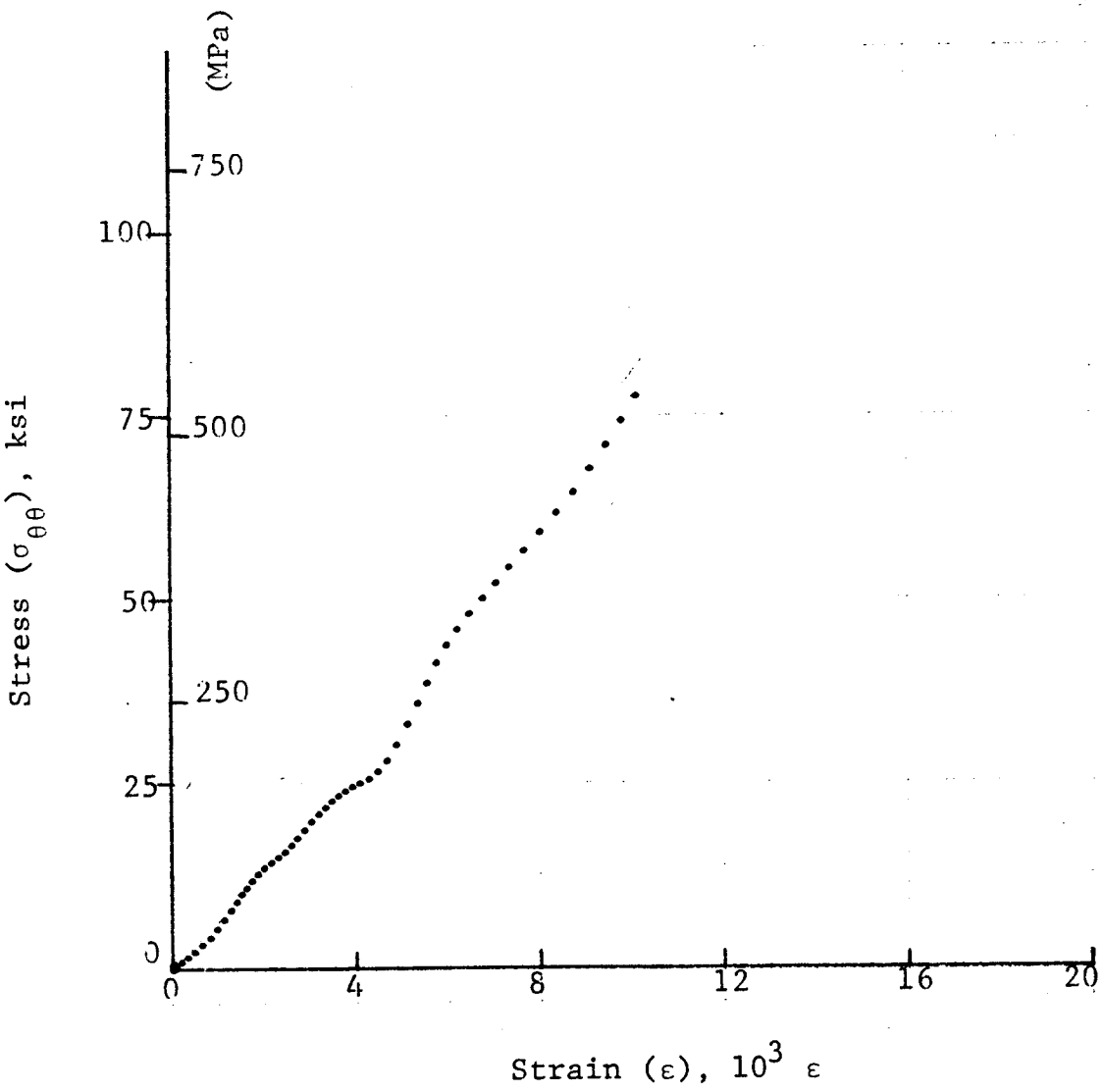

Figure 4-113. Stress-strain curve for dynamically loaded $[\pm 60]_{2s}$ 80AS/20S/PR288 graphite/S-glass/epoxy ring, Specimen No. 23-2 (1.56 g pistol powder, $KC\ell O_4$, and aluminum dust).

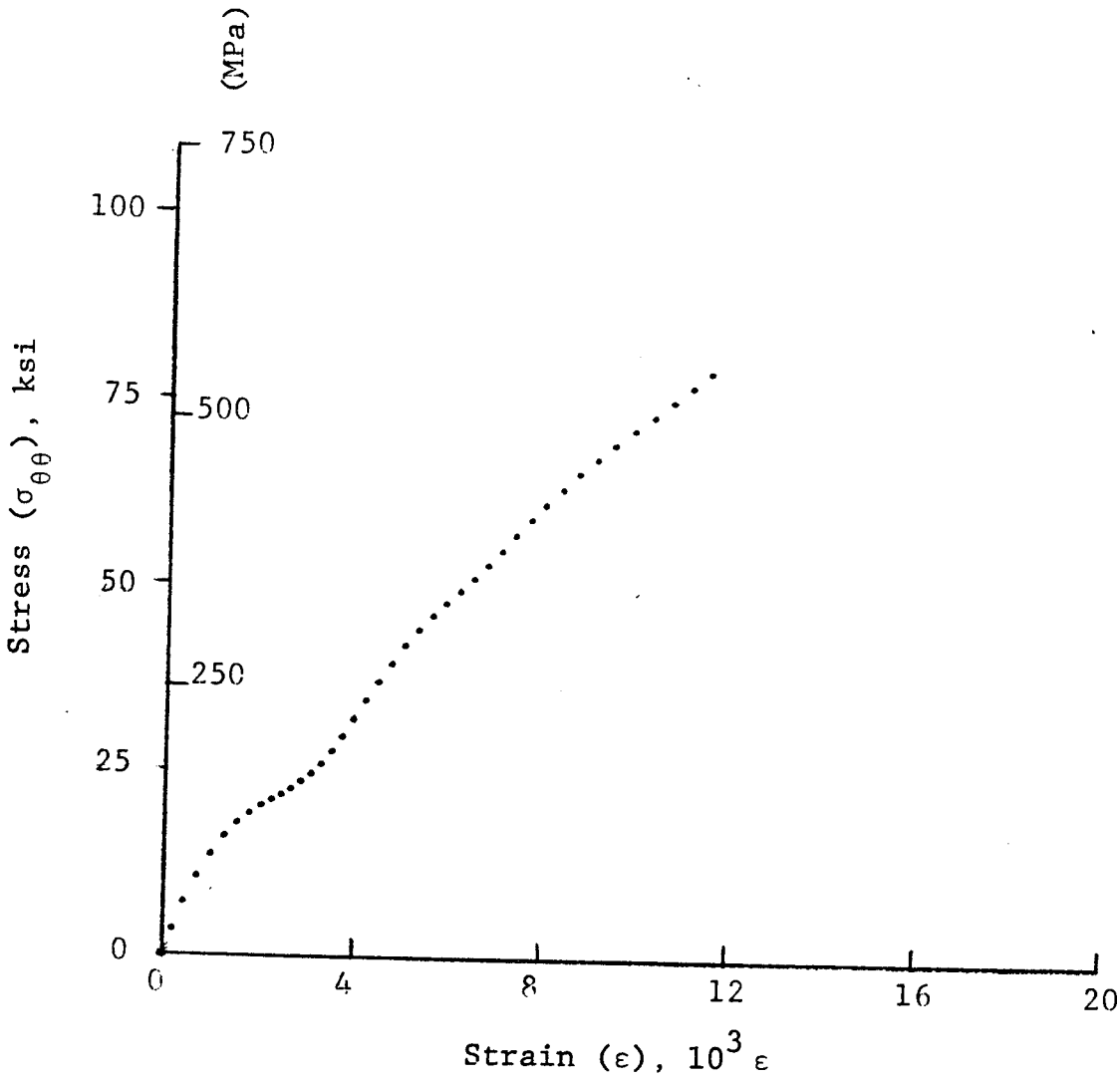

Figure 4-114. Stress-strain curve for dynamically loaded $[\pm 60]_{2s}$ 80AS/20S/PR288 graphite/S-glass/epoxy ring, Specimen No. 23-4 (1.56 g pistol powder, $KC\ell O_4$, and aluminum dust).

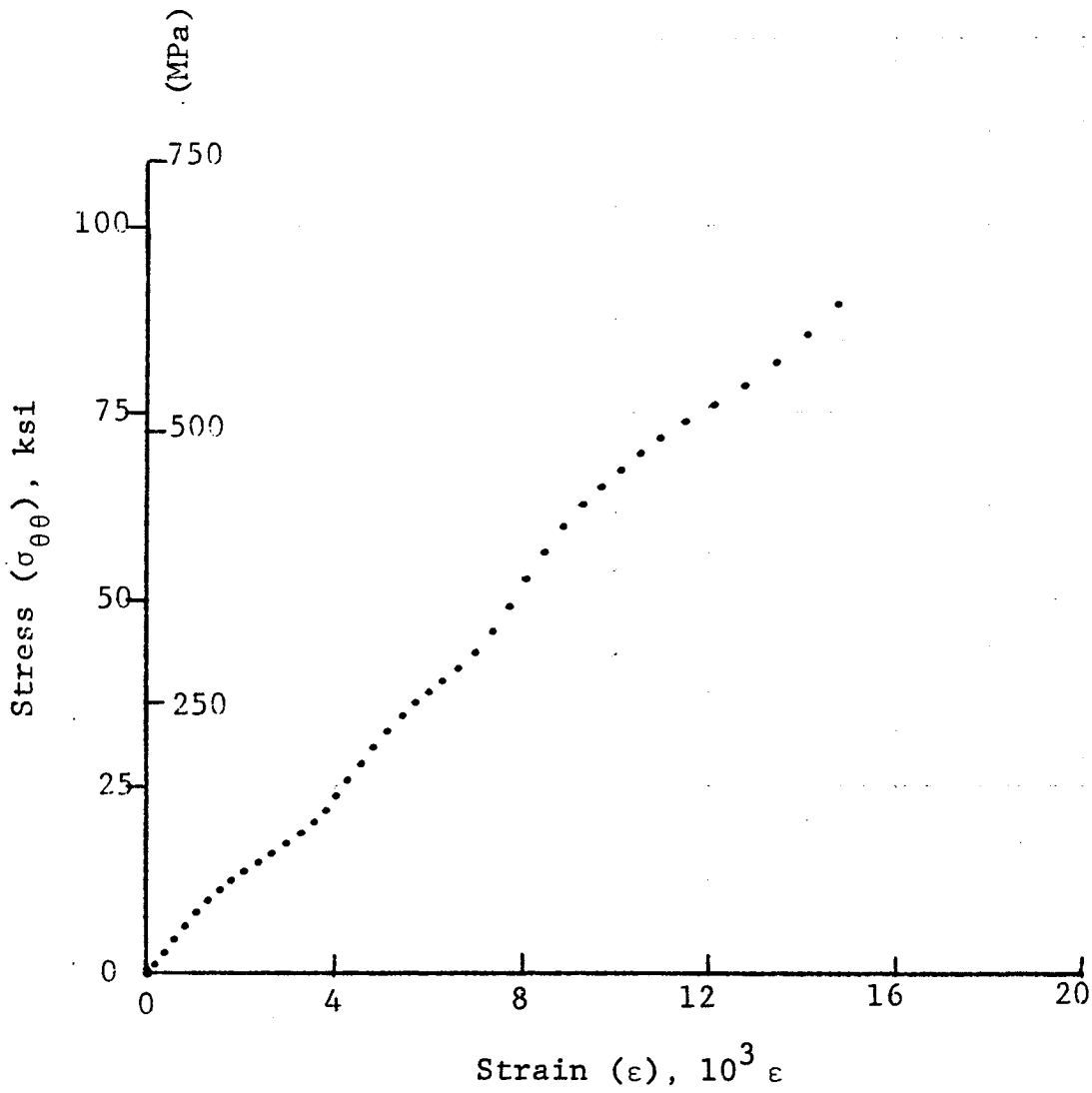

Figure 4-115. Stress-strain curve for dynamically loaded $[\pm 60]_{2s}$ 80AS/20S/PR288 graphite/S-glass/epoxy ring, Specimen No. 23-6 (1.56 g pistol powder, $KC\ell O_4$, and aluminum dust).

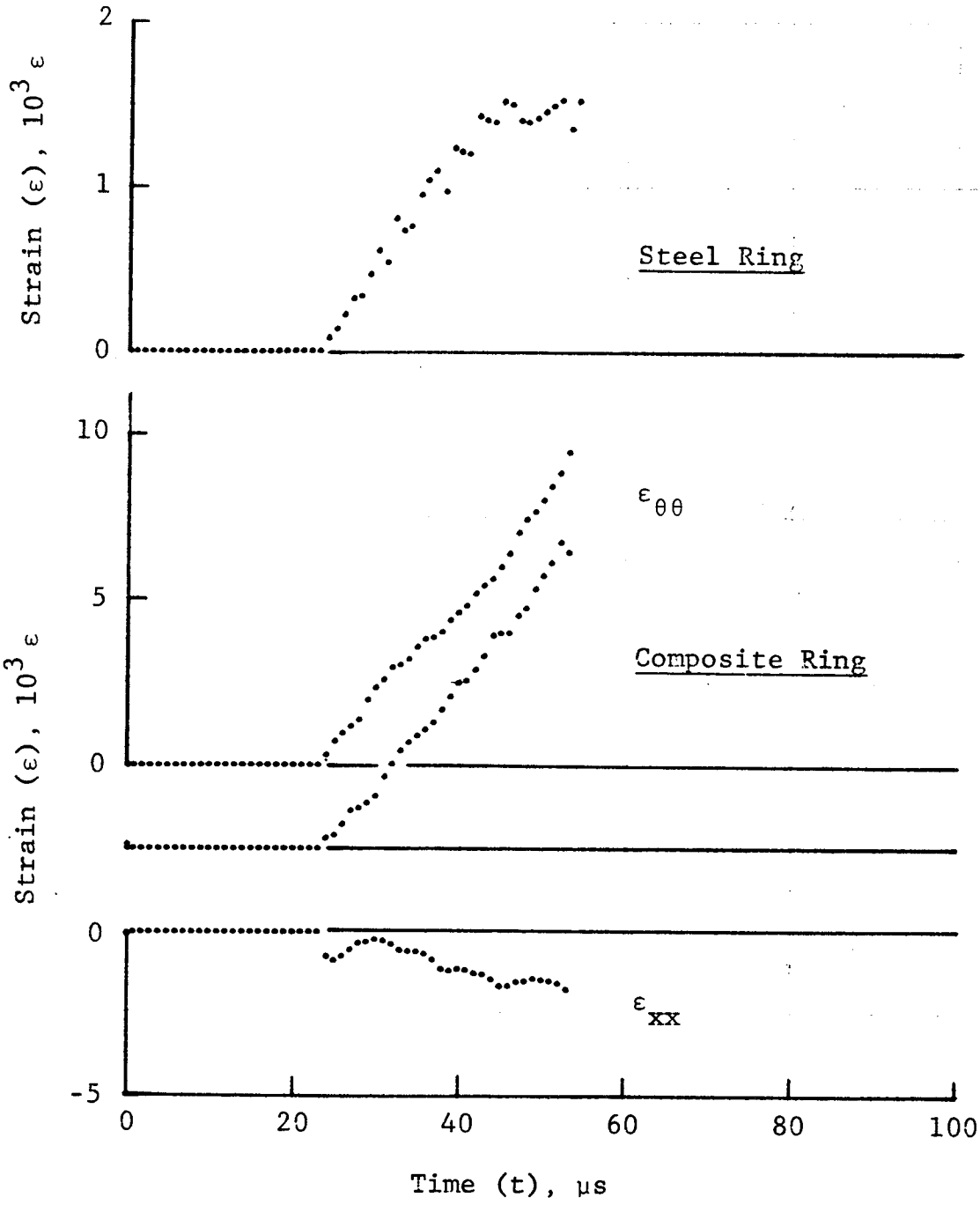

Figure 4-116. Strain records in steel ring and $[\pm 67.5]_{2S}$ SP288/AS graphite/epoxy ring under dynamic loading for Specimen No. 26-2 (1.56 g pistol powder, $KC\ell O_4$, and aluminum dust).

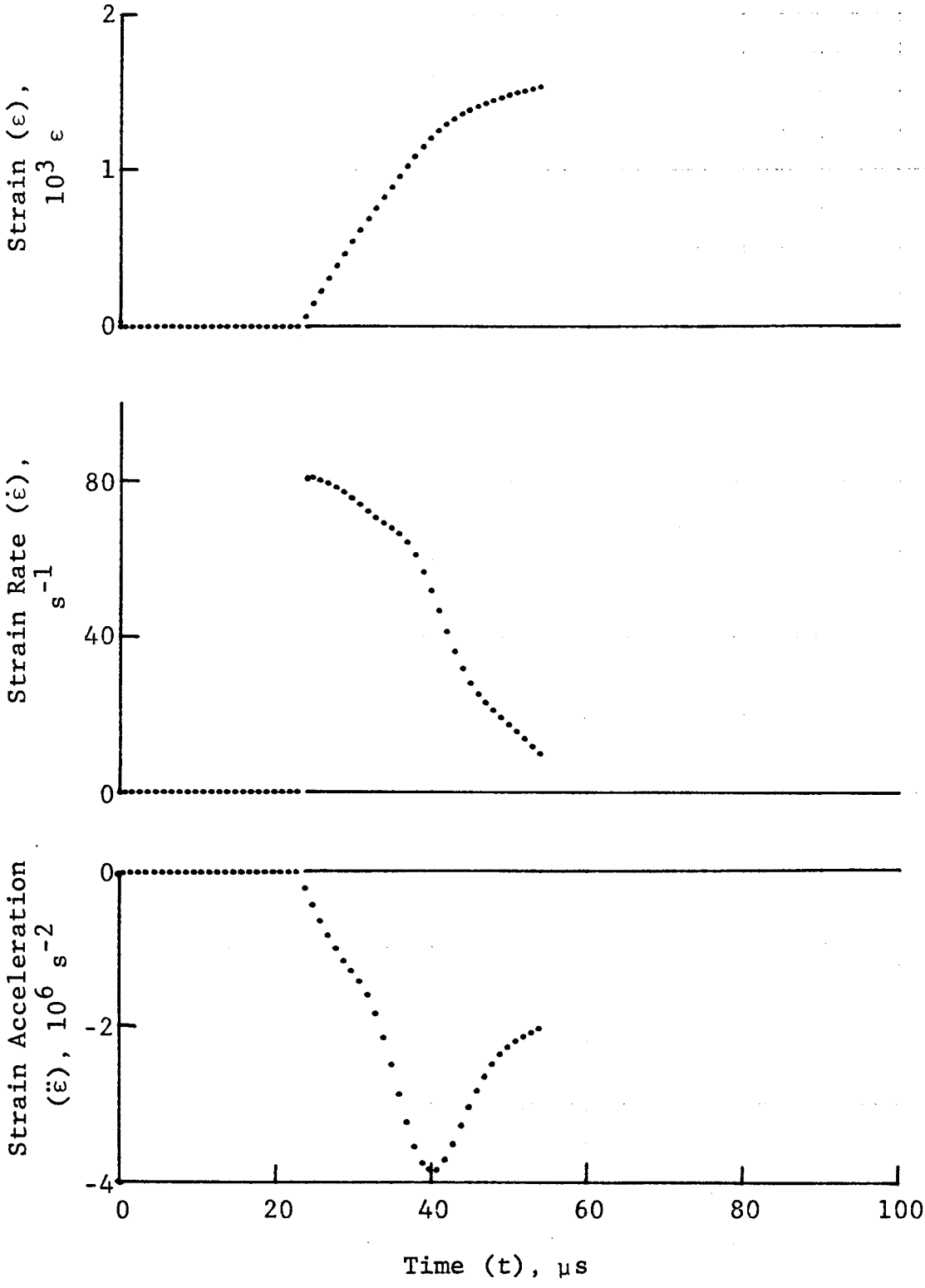

Figure 4-117. Strain and its derivatives in steel ring for Specimen No. 26-2.

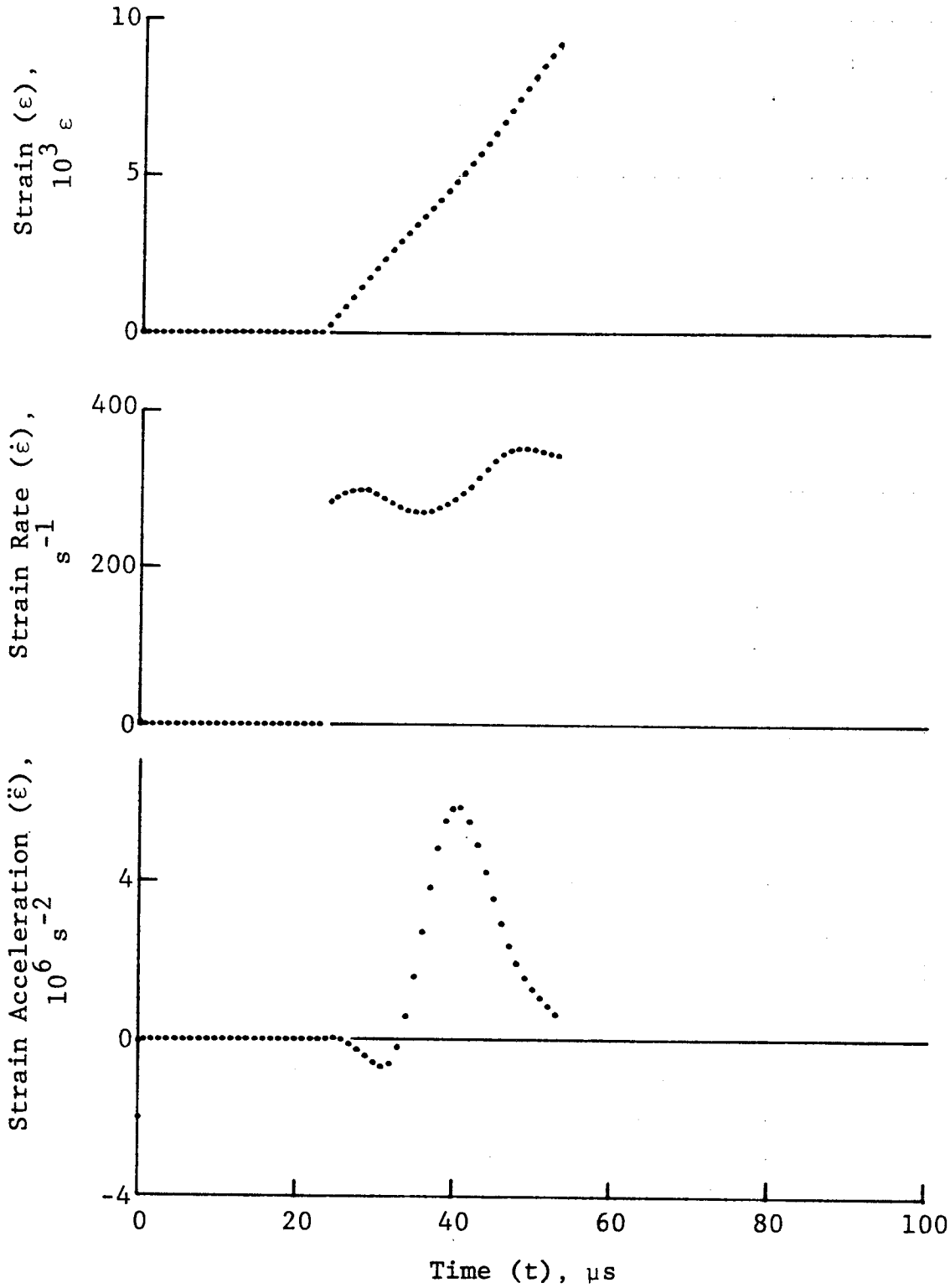

Figure 4-118. Circumferential strain and its derivatives in $[\pm 67.5]_{2s}$ SP288/AS graphite/epoxy ring under dynamic loading for Specimen No. 26-2.

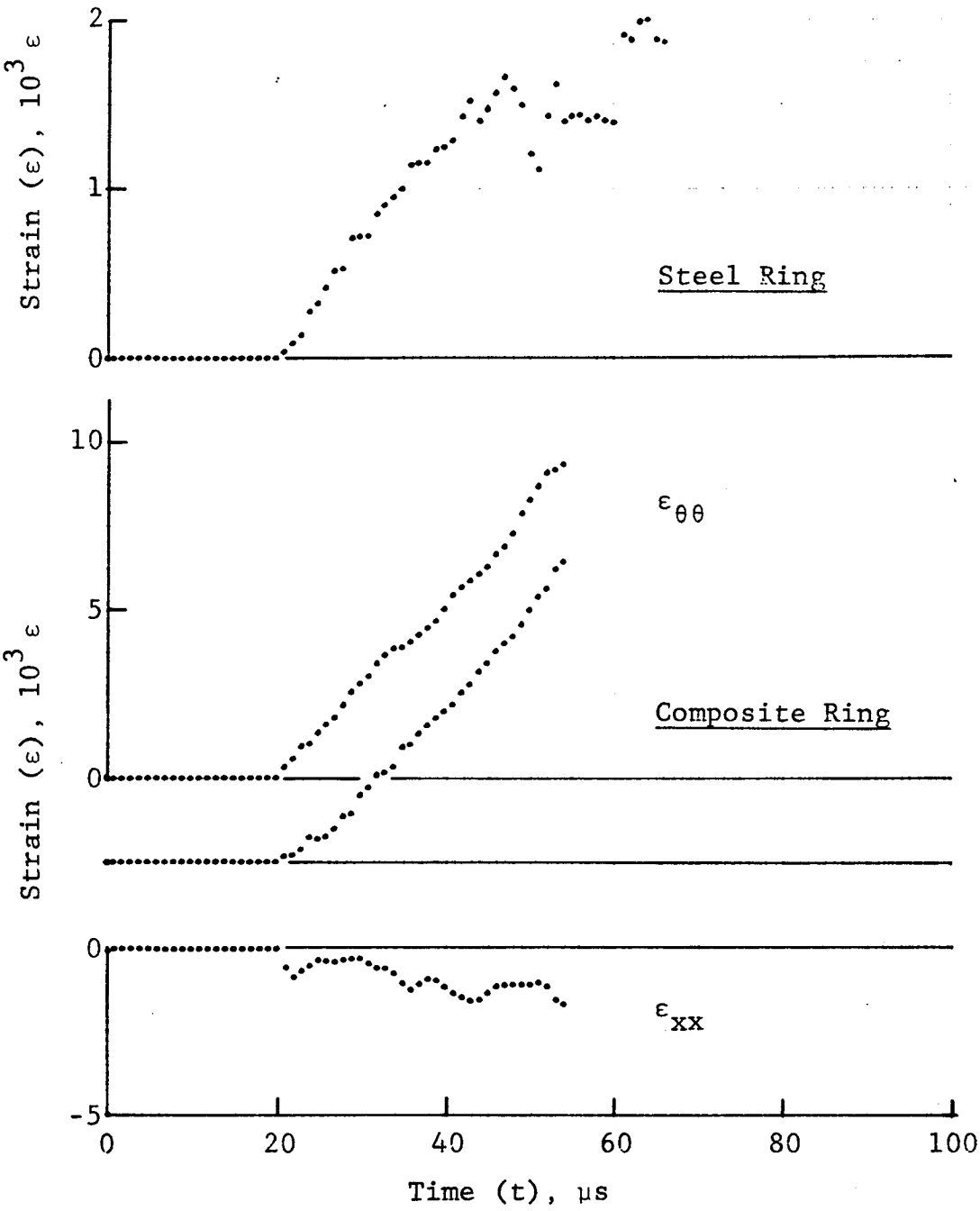

Figure 4-119. Strain records in steel ring and $[\pm 67.5]_{2S}$ SP288/AS graphite/epoxy ring under dynamic loading for Specimen No. 26-4 (1.56 g psitol powder, $KC\ell O_4$, and aluminum dust).

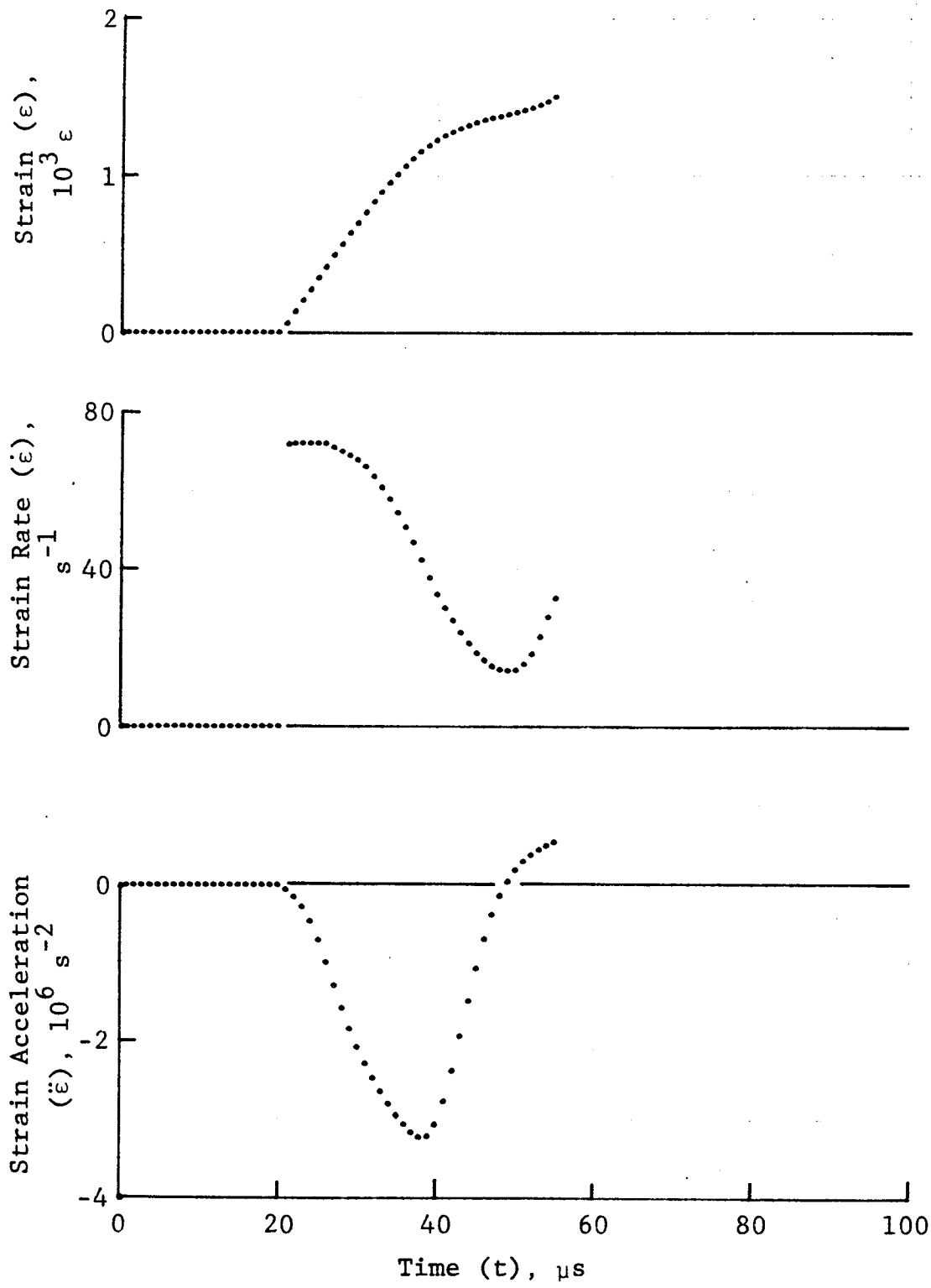

Figure 4-120. Strain and its derivatives in steel ring for Specimen No. 26-4.

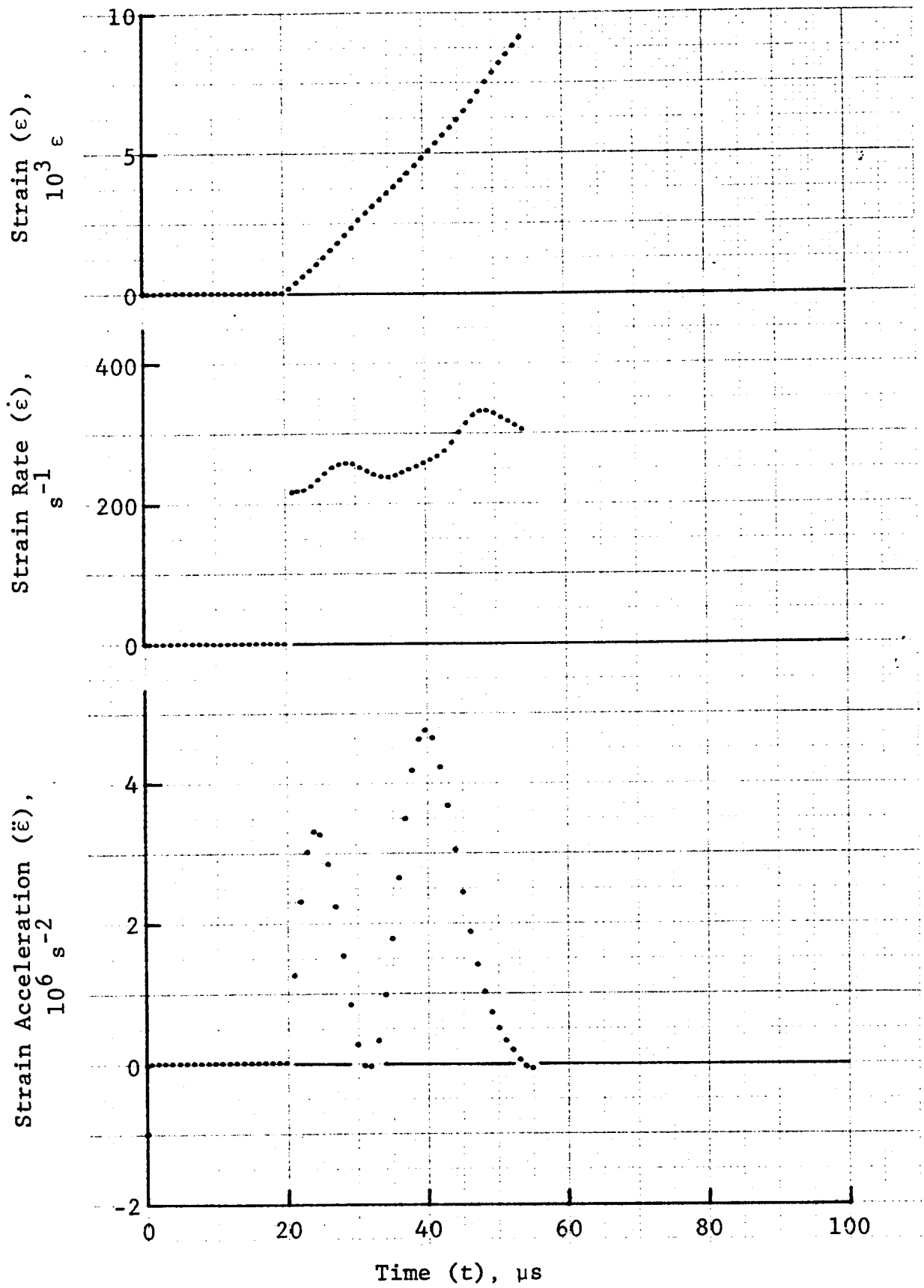

Figure 4-121. Circumferential strain and its derivatives in $[\pm 67.5]_{2s}$ SP288/AS graphite/epoxy ring under dynamic loading for Specimen No. 26-4.

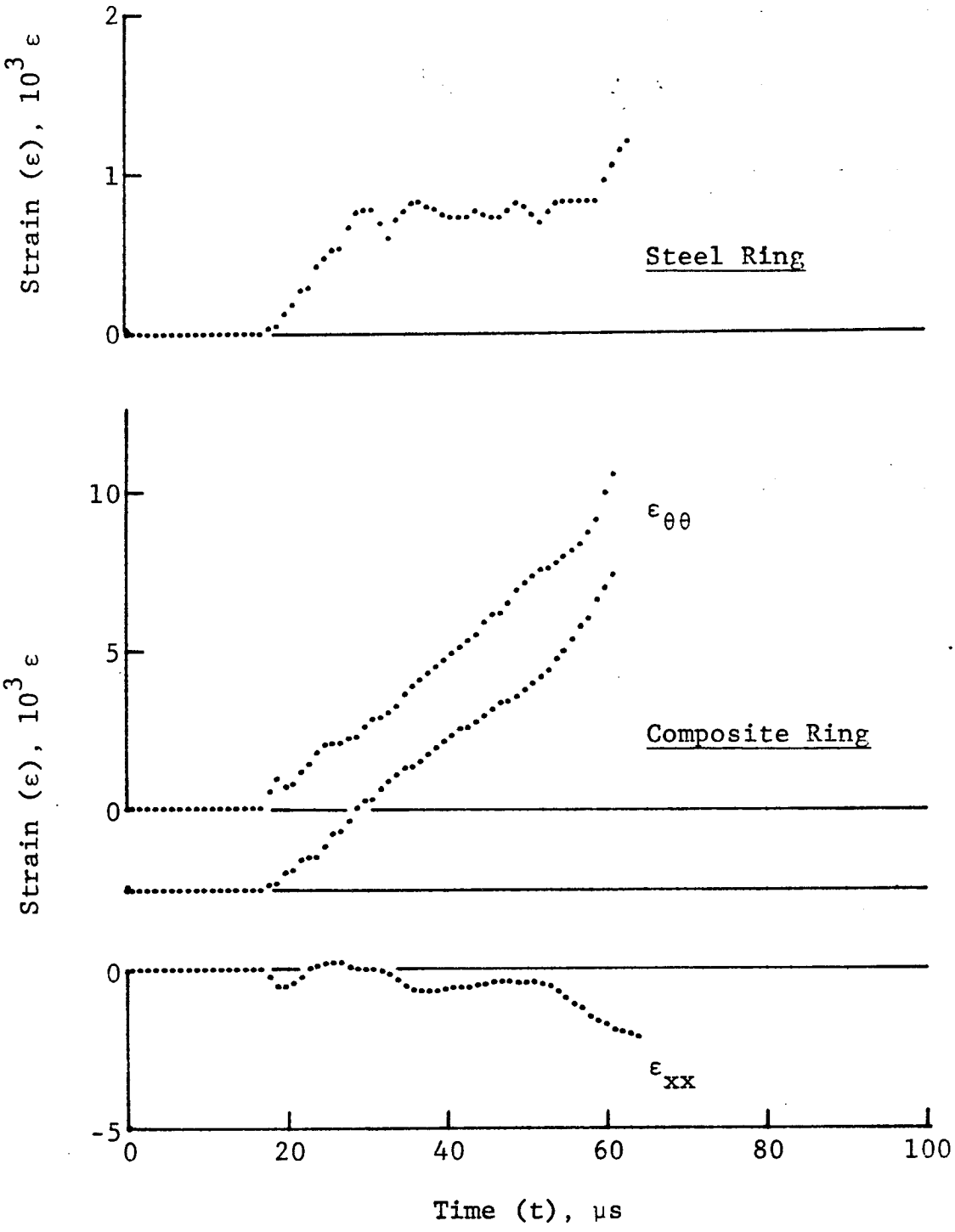

Figure 4-122. Strain records in steel ring and $[\pm 67.5]_{2s}$ SP288/AS graphite/epoxy ring under dynamic loading for Specimen No. 26-6 (1.56 g pistol powder, $KC\ell O_4$, and aluminum dust).

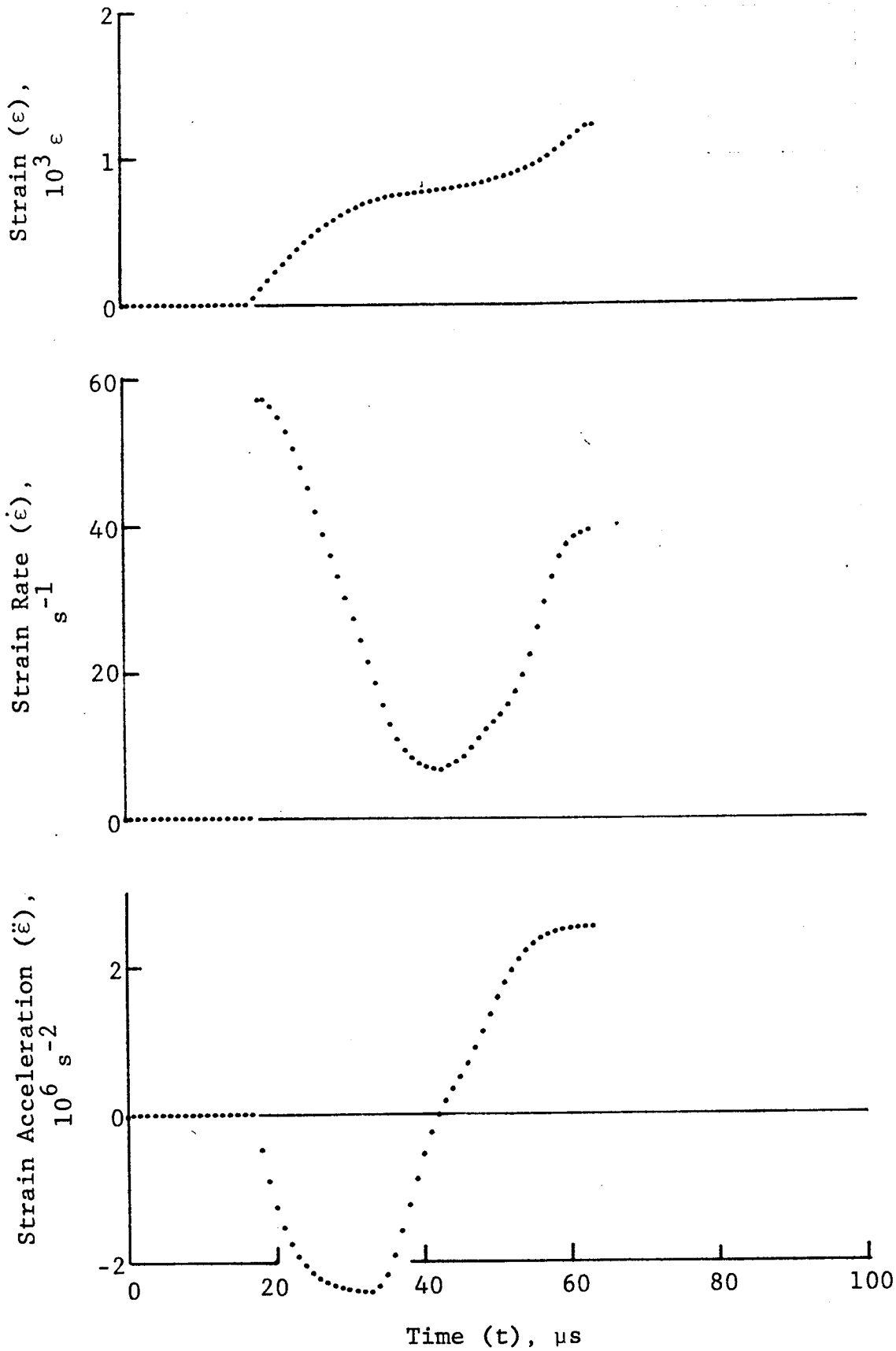

Figure 4-123. Strain and its derivatives in steel ring for Specimen No. 26-6.

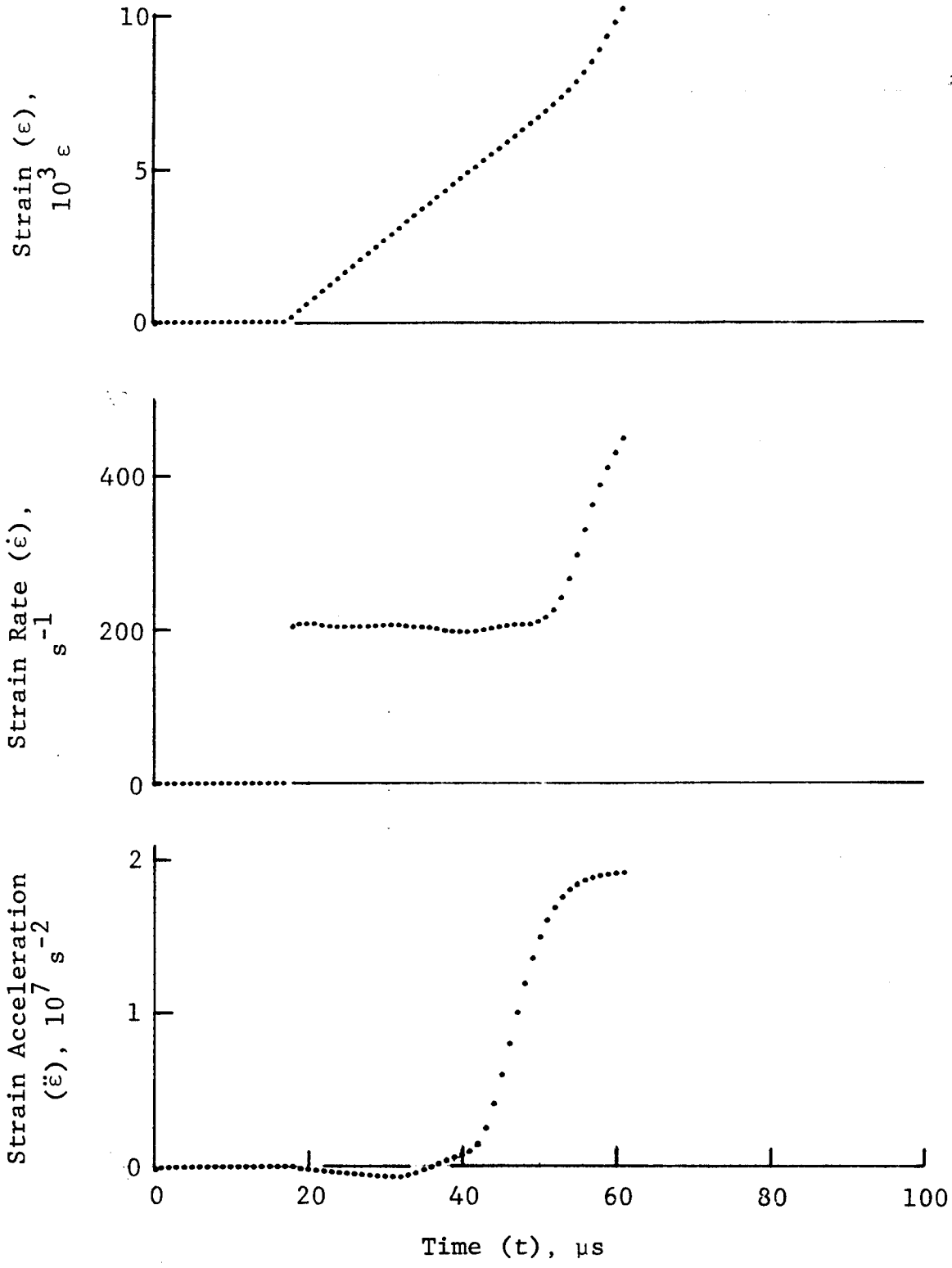

Figure 4-124. Circumferential strain and its derivatives in $[\pm 67.5]_{2s}$ SP288/AS graphite/epoxy ring under dynamic loading for Specimen No. 26-6.

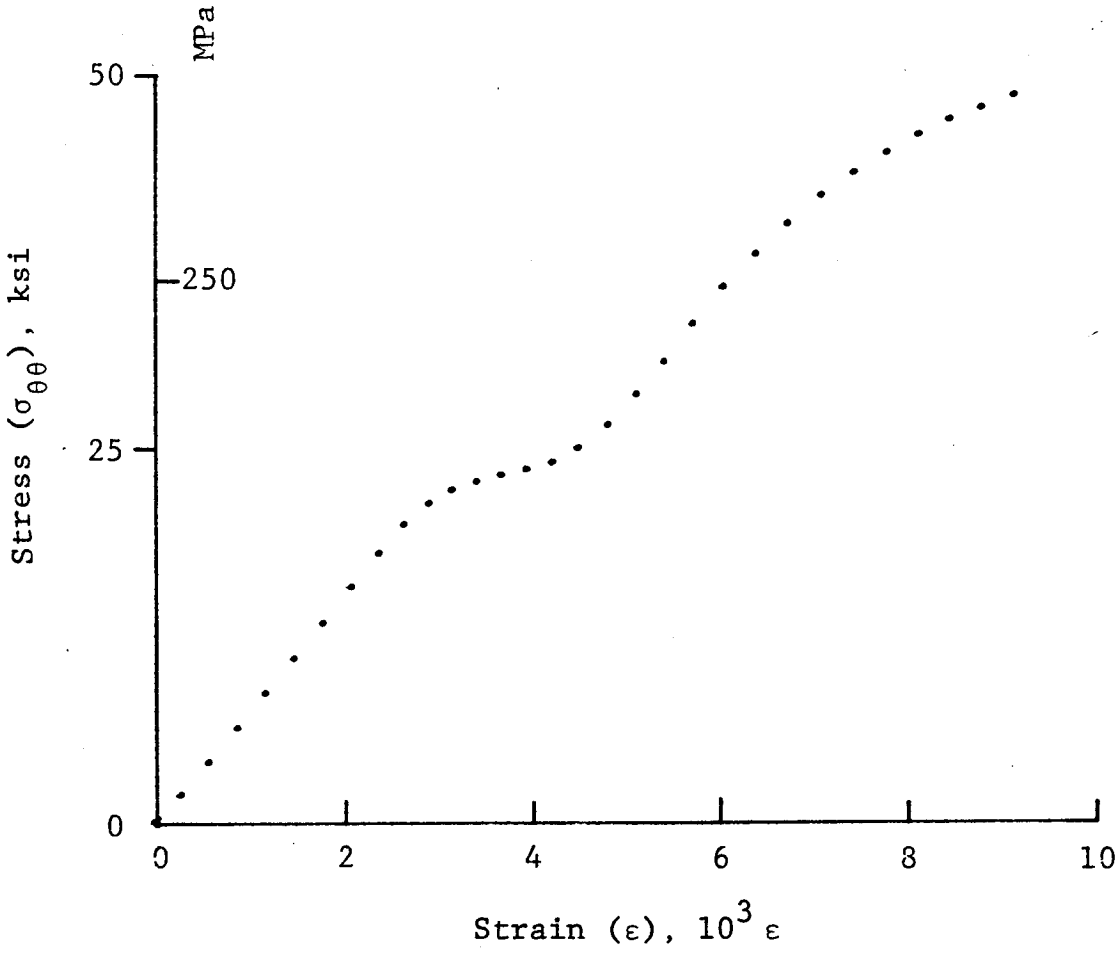

Figure 4-125. Stress-strain curve for dynamically loaded $[\pm 67.5]_{2s}$ SP288/AS graphite/epoxy ring, Specimen No. 26-2 (1.56 g pistol powder, $KC\ell O_4$, and aluminum dust).

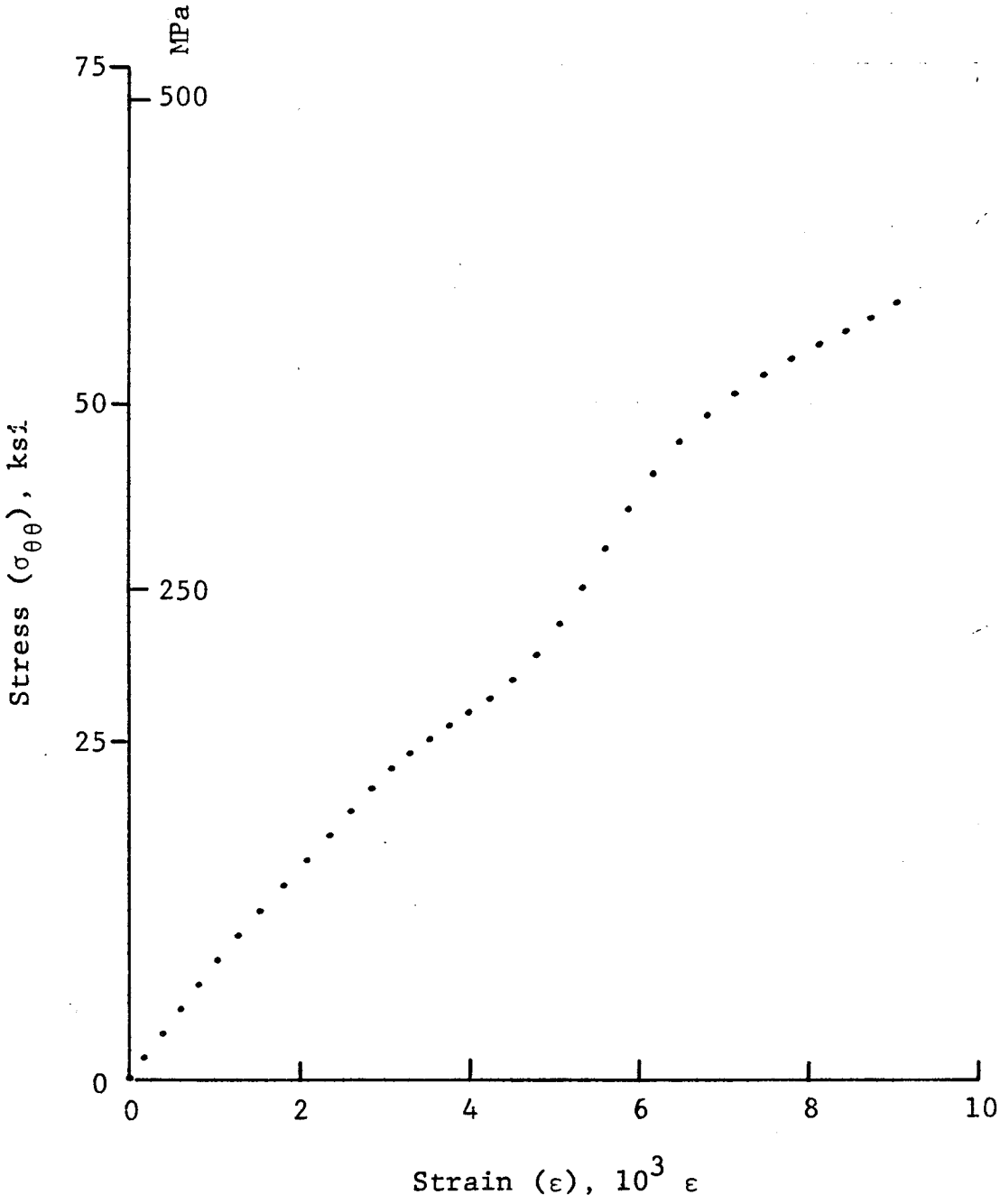

Figure 4-126. Stress-strain curve for dynamically loaded $[\pm 67.5]_{2s}$ SP288/AS graphite/epoxy ring, Specimen No. 26-4 (1.56 g pistol powder, $KC\ell O_4$, and aluminum dust).

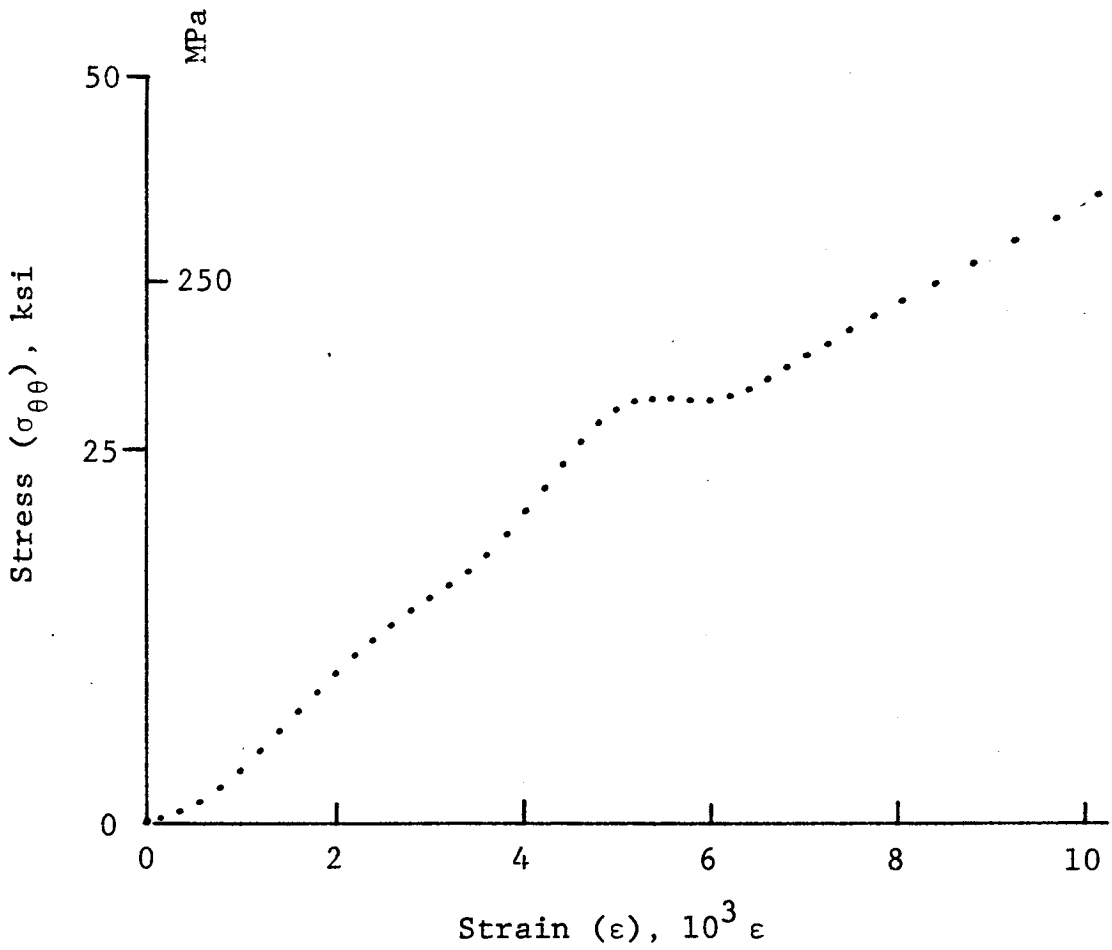

Figure 4-127. Stress-strain curve for dynamically loaded $[\pm 67.5]_{2s}$ SP288/AS graphite/epoxy ring, Specimen No. 26-6 (1.56 g pistol powder, $KC\ell O_4$, and aluminum dust).

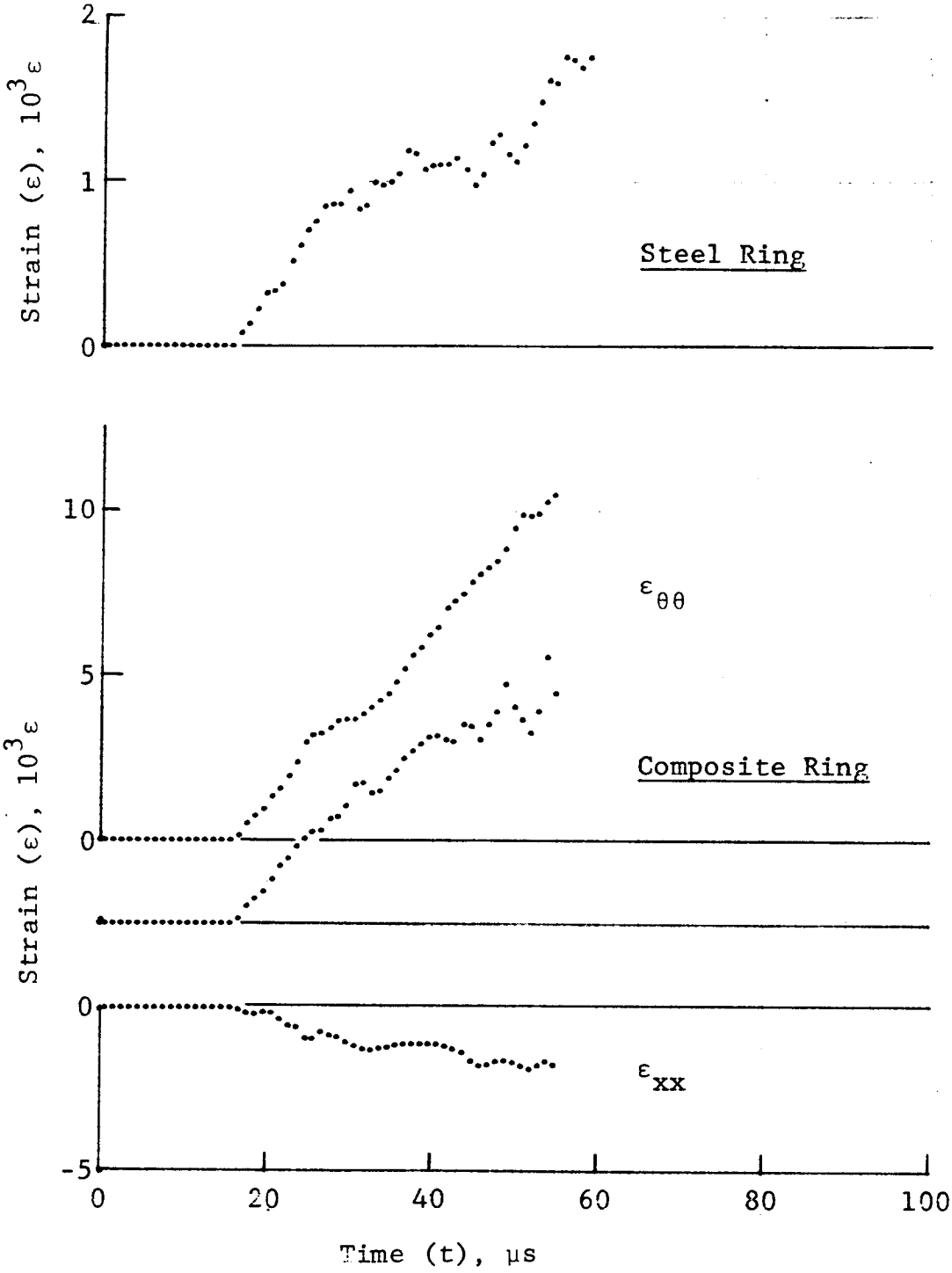

Figure 4-128. Strain records in steel ring and 80AS/20S/PR288 $[\pm 67.5]_{2S}$ graphite/S-glass/epoxy ring under dynamic loading for Specimen No. 27-2 (1.56 g pistol powder, $KC\ell O_4$, and aluminum dust).

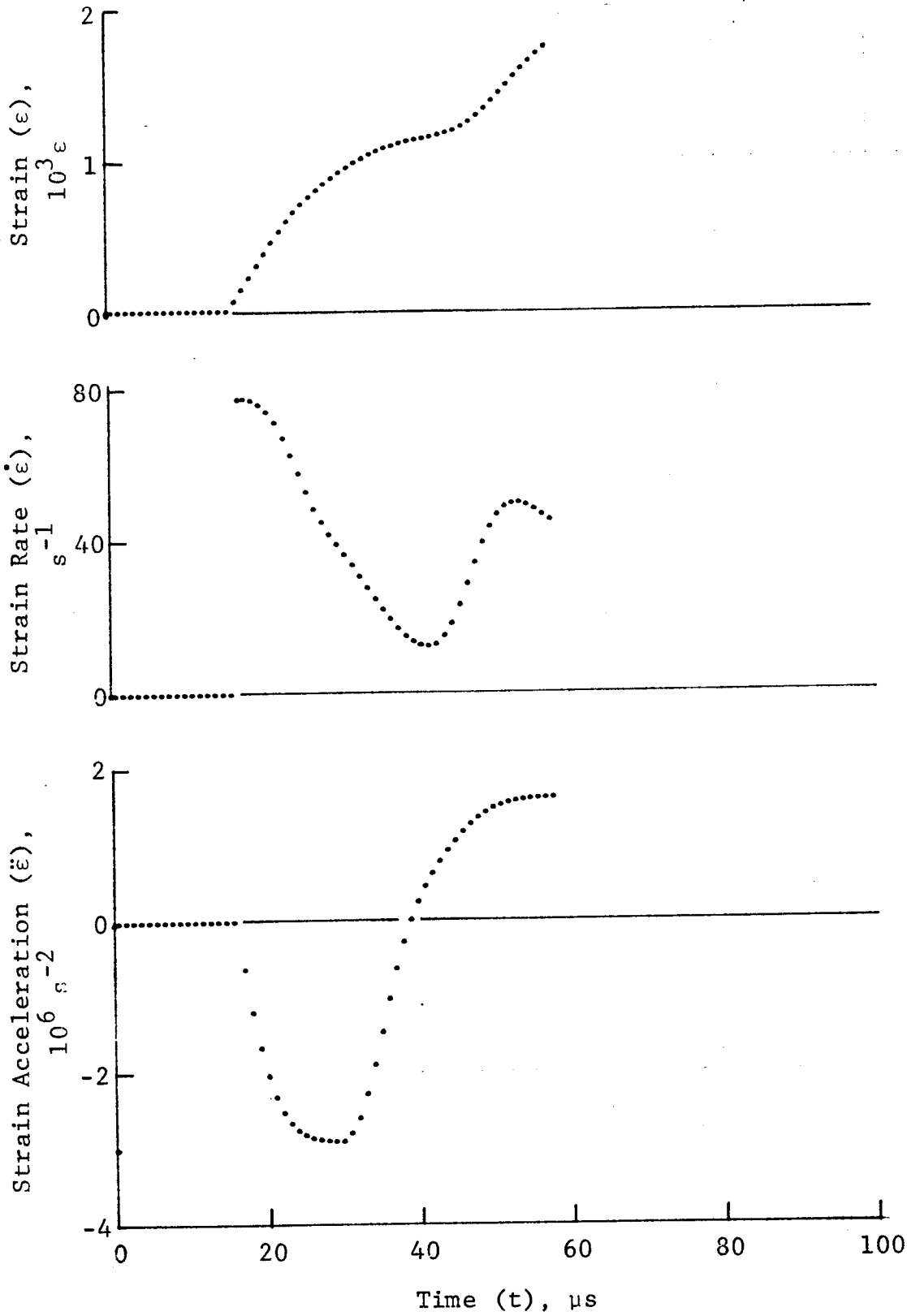

Figure 4-129. Strain and its derivatives in steel ring for Specimen No. 27-2.

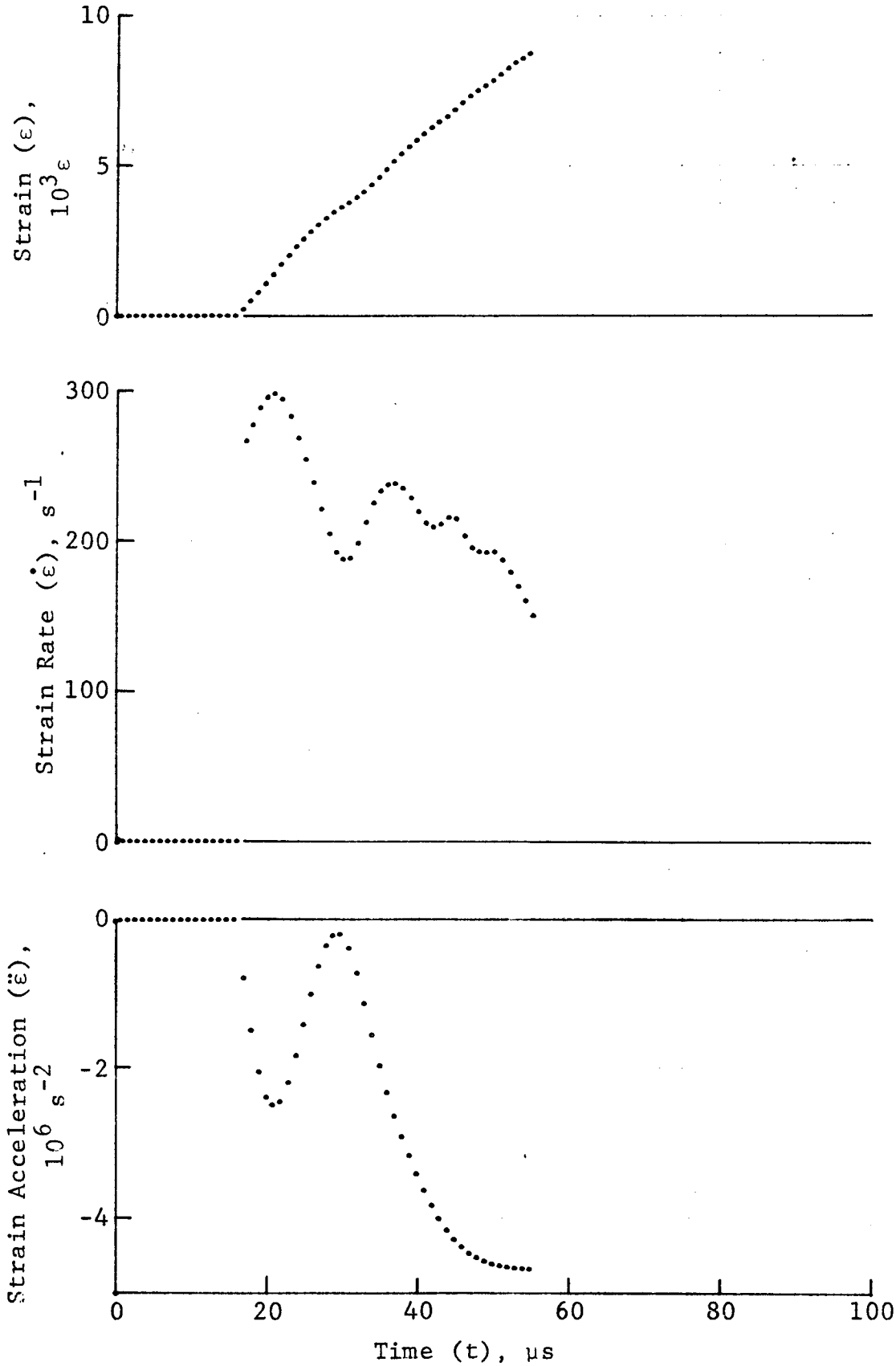

Figure 4-130. Circumferential strain and its derivatives in 80AS/20S/PR288 $[\pm 67.5]_{2S}$ graphite/S-glass/epoxy ring under dynamic loading for Specimen No. 27-2 (1.56 g pistol powder, $KC\ell O_4$, and aluminum dust).

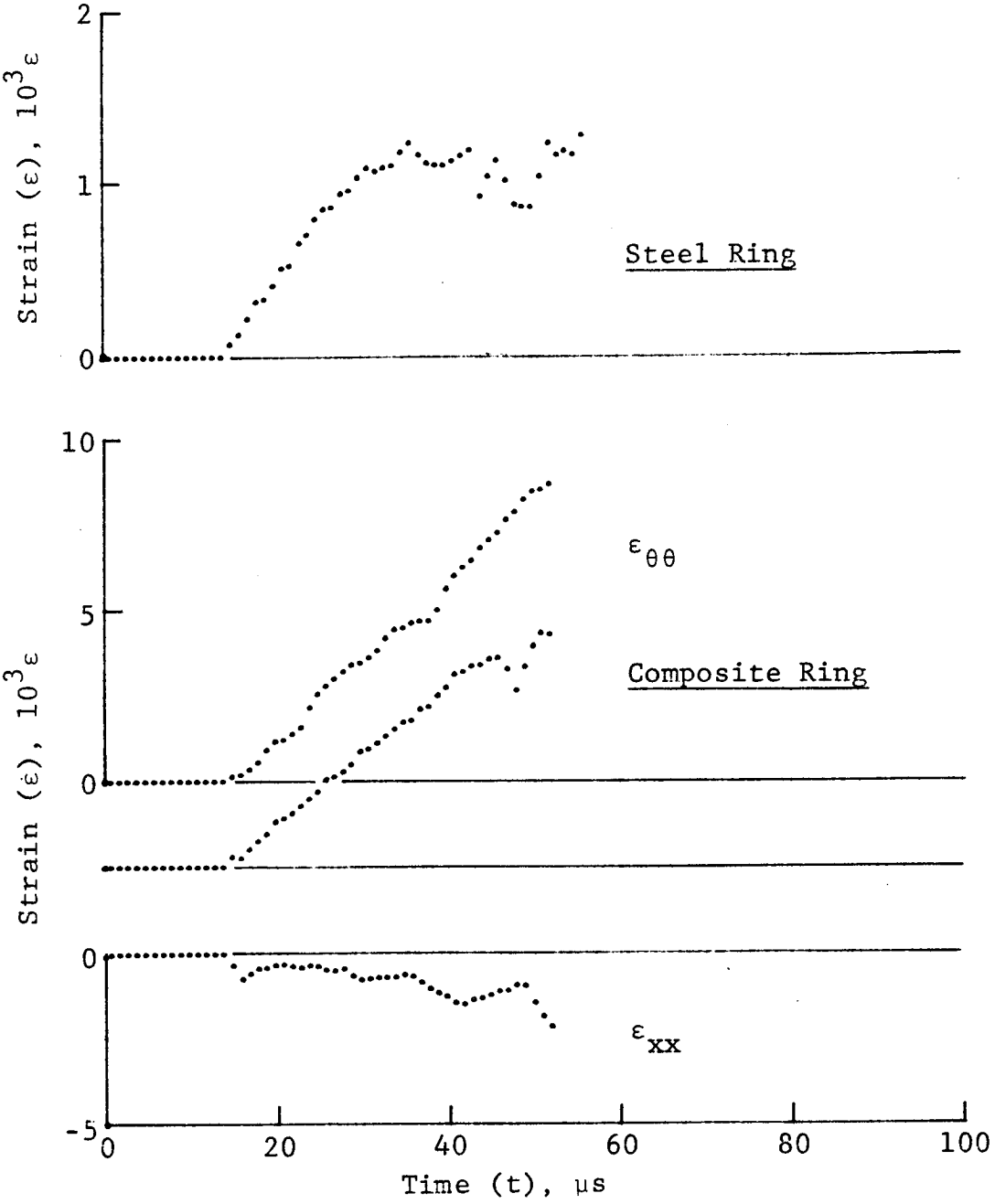

Figure 4-131. Strain records in steel ring and 80AS/20S/PR288 $[\pm 67.5]_{2S}$ graphite/S-glass/epoxy ring under dynamic loading for Specimen No. 27-4 (1.56 g pistol powder, $KC\ell O_4$, and aluminum dust).

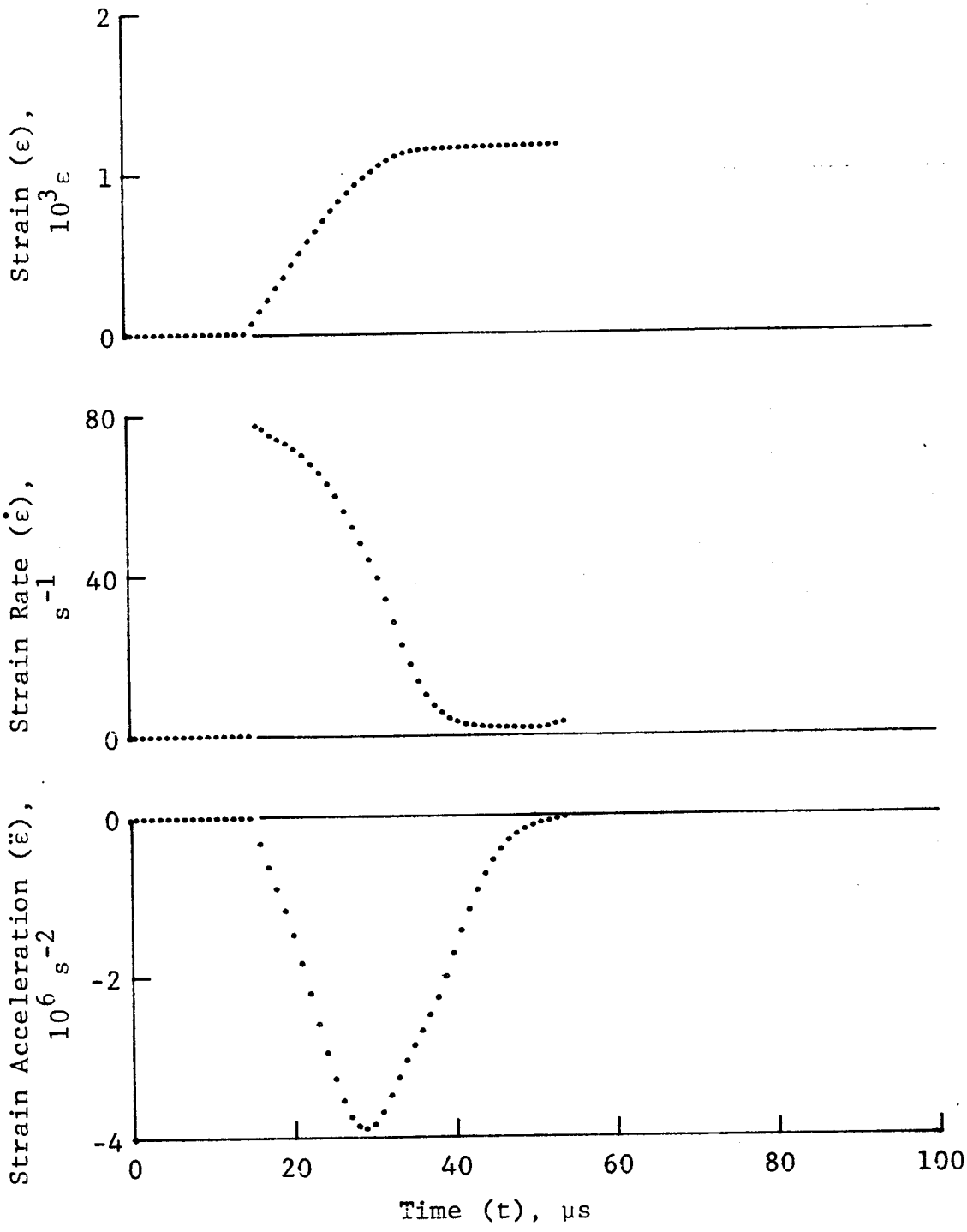

Figure 4-132. Strain and its derivatives in steel ring for Specimen No. 27-4.

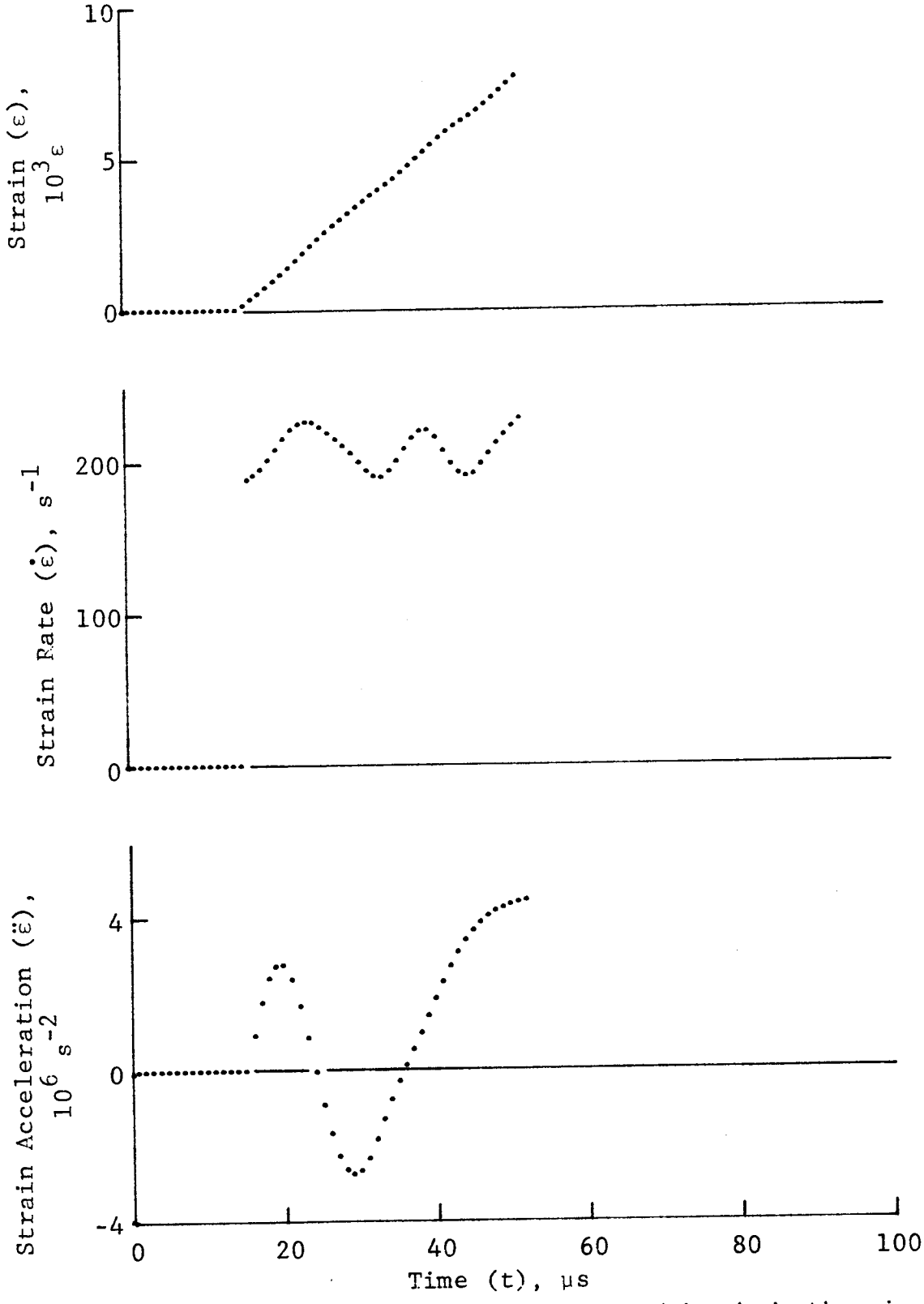

Figure 4-133. Circumferential strain and its derivatives in 80AS/20S/PR288 $[\pm 67.5]_{2S}$ graphite/S-glass/epoxy ring under dynamic loading for Specimen No. 27-4 (1.56 g pistol powder $KC\ell O_4$, and aluminum dust).

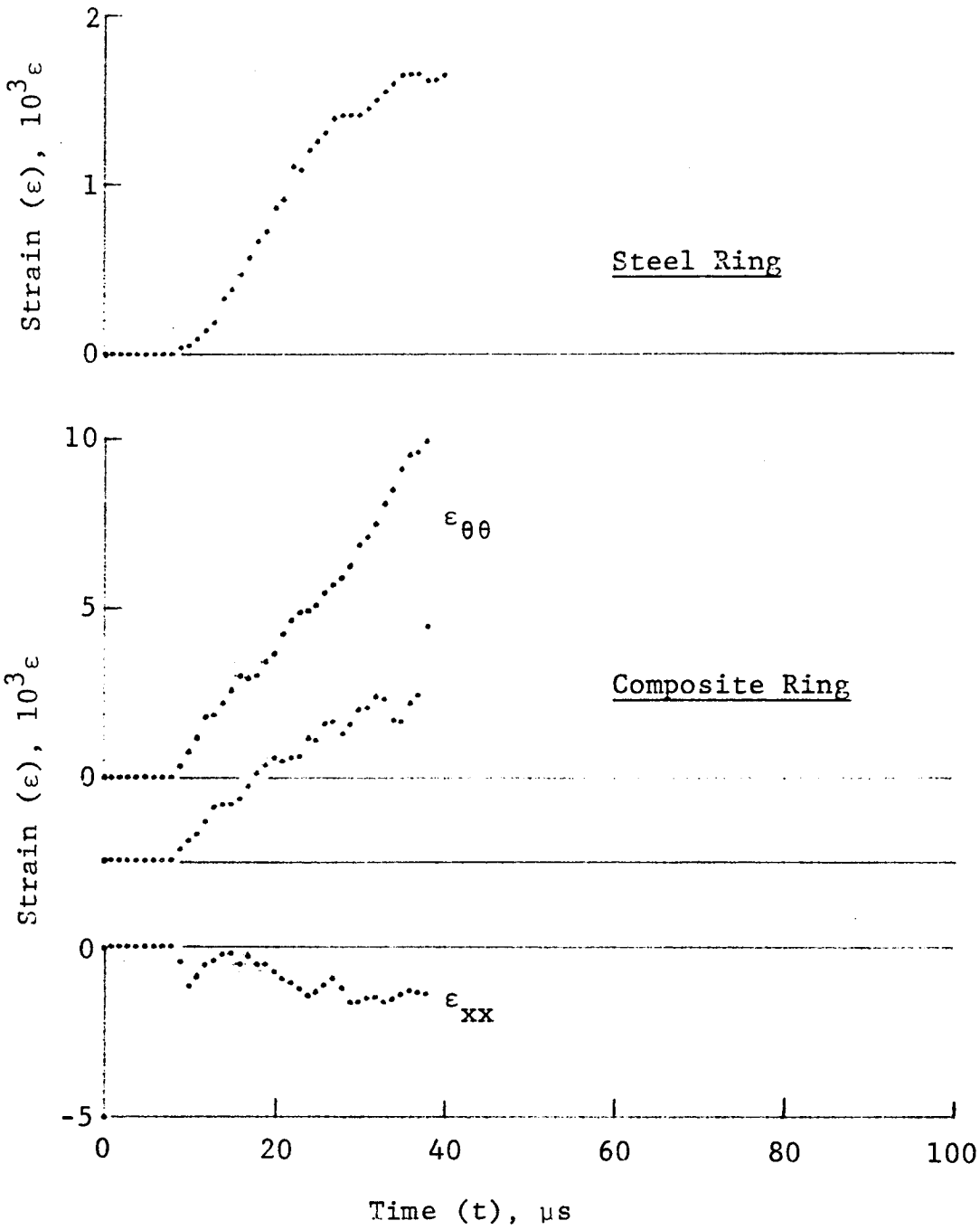

Figure 4-134. Strain records in steel ring and 80AS/20S/PR288 $[\pm 67.5]_{2S}$ graphite/S-glass/epoxy ring under dynamic loading for Specimen No. 27-6 (1.56 g pistol powder, $KC\ell O_4$, and aluminum dust).

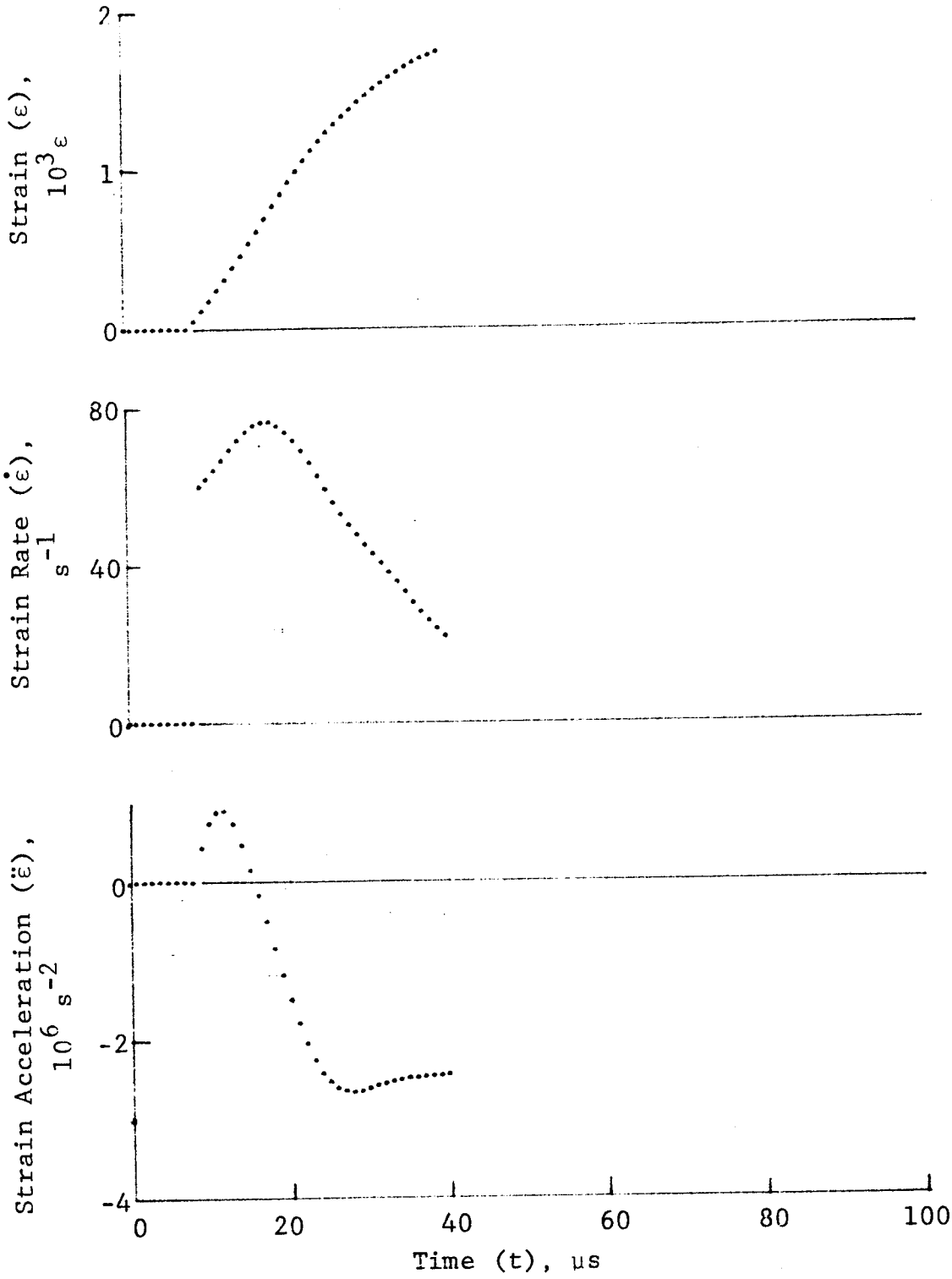

Figure 4-135. Strain and its derivatives in steel ring for Specimen No. 27-6.

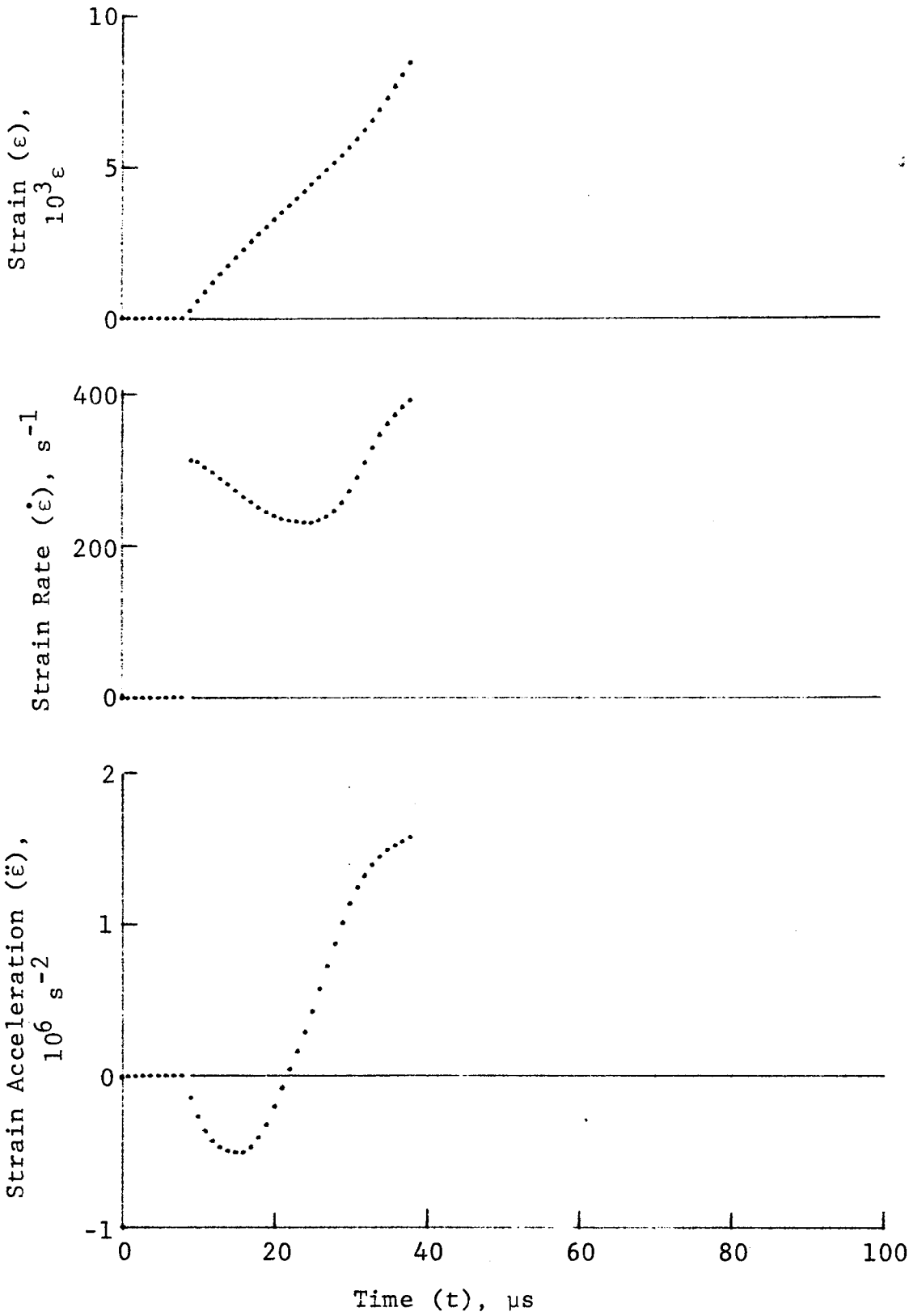

Figure 4-136. Circumferential strain and its derivatives in 80AS/20S/PR288 $[\pm 67.5]_{2S}$ graphite/S-glass/epoxy ring under dynamic loading for Specimen No. 27-6 (1.56 g pistol powder, $KC\ell O_4$, and aluminum dust).

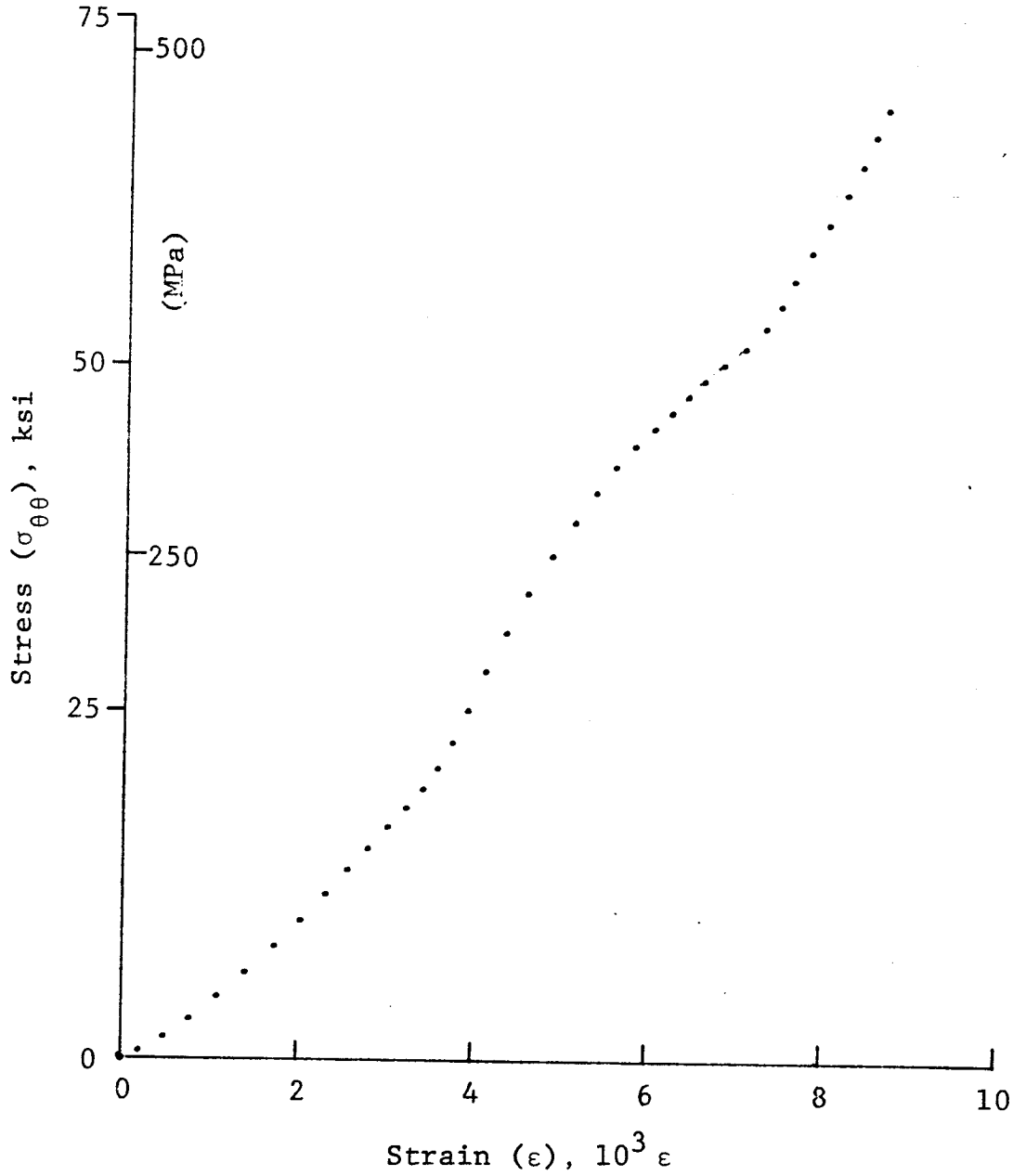

Figure 4-137. Stress-strain curve for dynamically loaded 80AS/20S/PR288 $[\pm 67.5]_{2S}$ graphite/S-glass/epoxy ring, Specimen No. 27-2 (1.56 g pistol powder, $KC\ell O_4$, and aluminum dust).

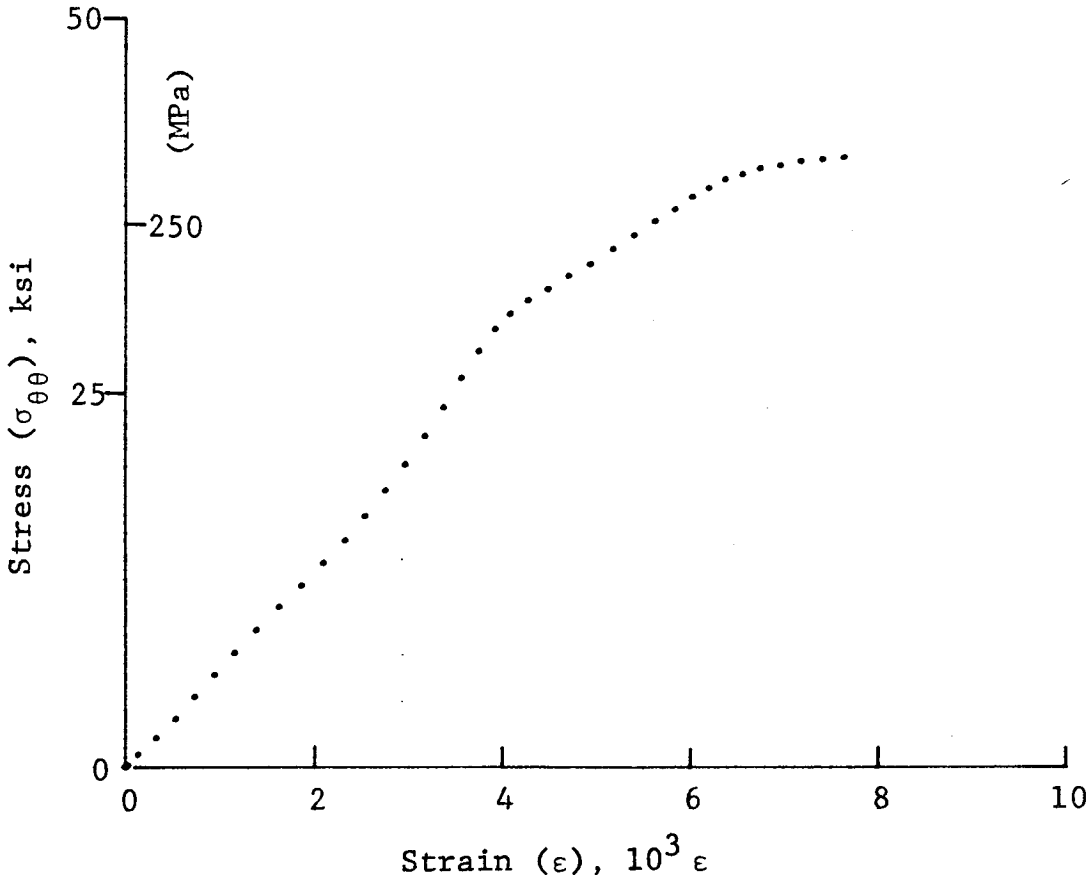

Figure 4-138. Stress-strain curve for dynamically loaded 80AS/20S/PR288 $[\pm 67.5]_{2S}$ graphite/S-glass/epoxy ring, Specimen No. 27-4 (1.56 g pistol powder, $KC\ell O_4$, and aluminum dust).

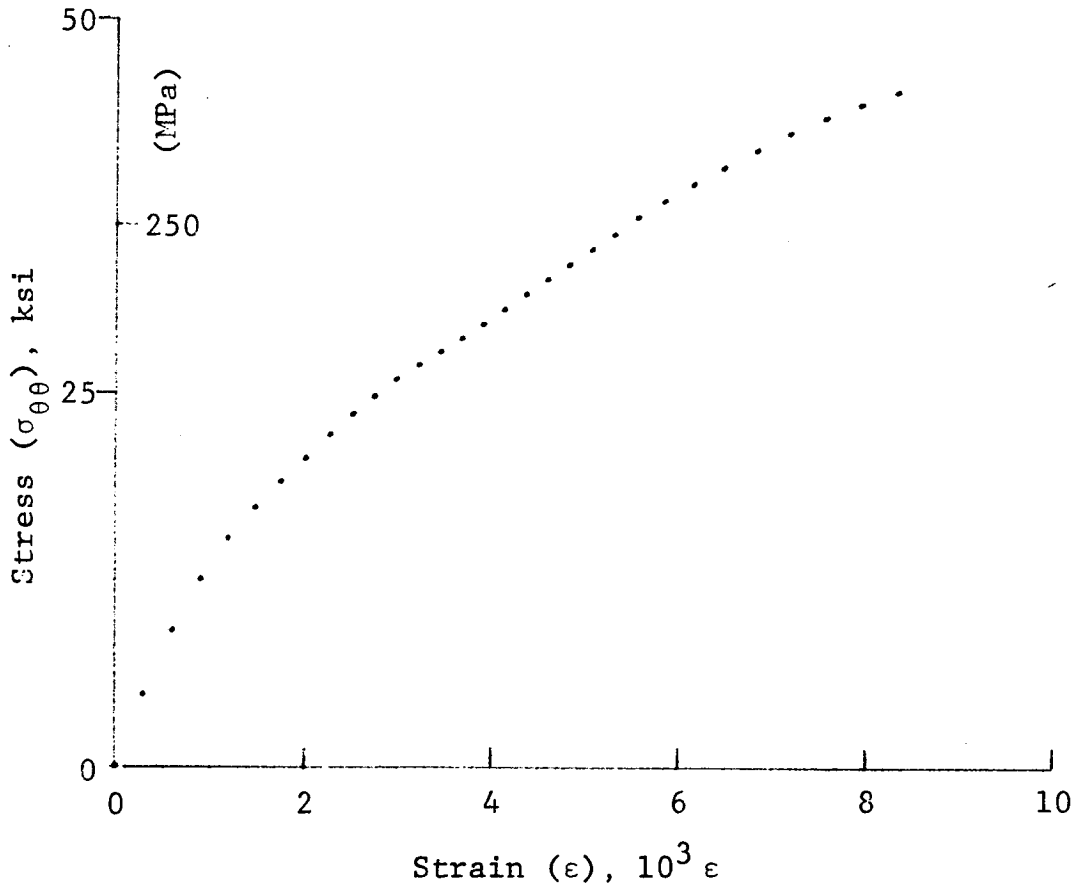

Figure 4-139. Stress-strain curve for dynamically loaded 80AS/20S/PR288 $[\pm 67.5]_{2s}$ graphite/S-glass/epoxy ring, Specimen No. 27-6 (1.56 g pistol powder, $KC\ell O_4$, and aluminum dust).

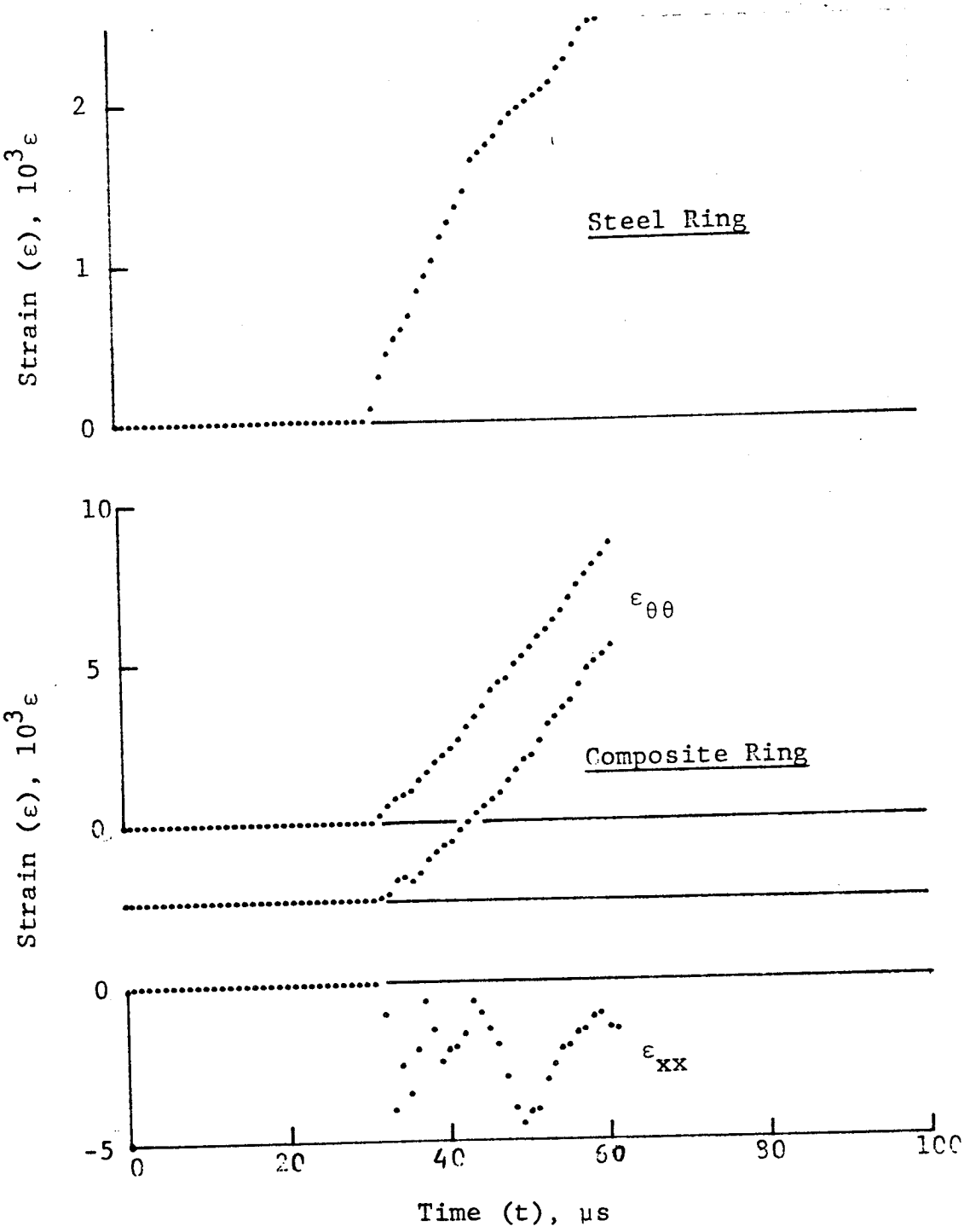

Figure 4-140. Strain records in steel ring and SP288/AS $[\pm 75]_{2s}$ graphite/epoxy ring under dynamic loading for Specimen No. 20-2 (1.56 g pistol powder, $KC\ell O_4$, and aluminum dust).

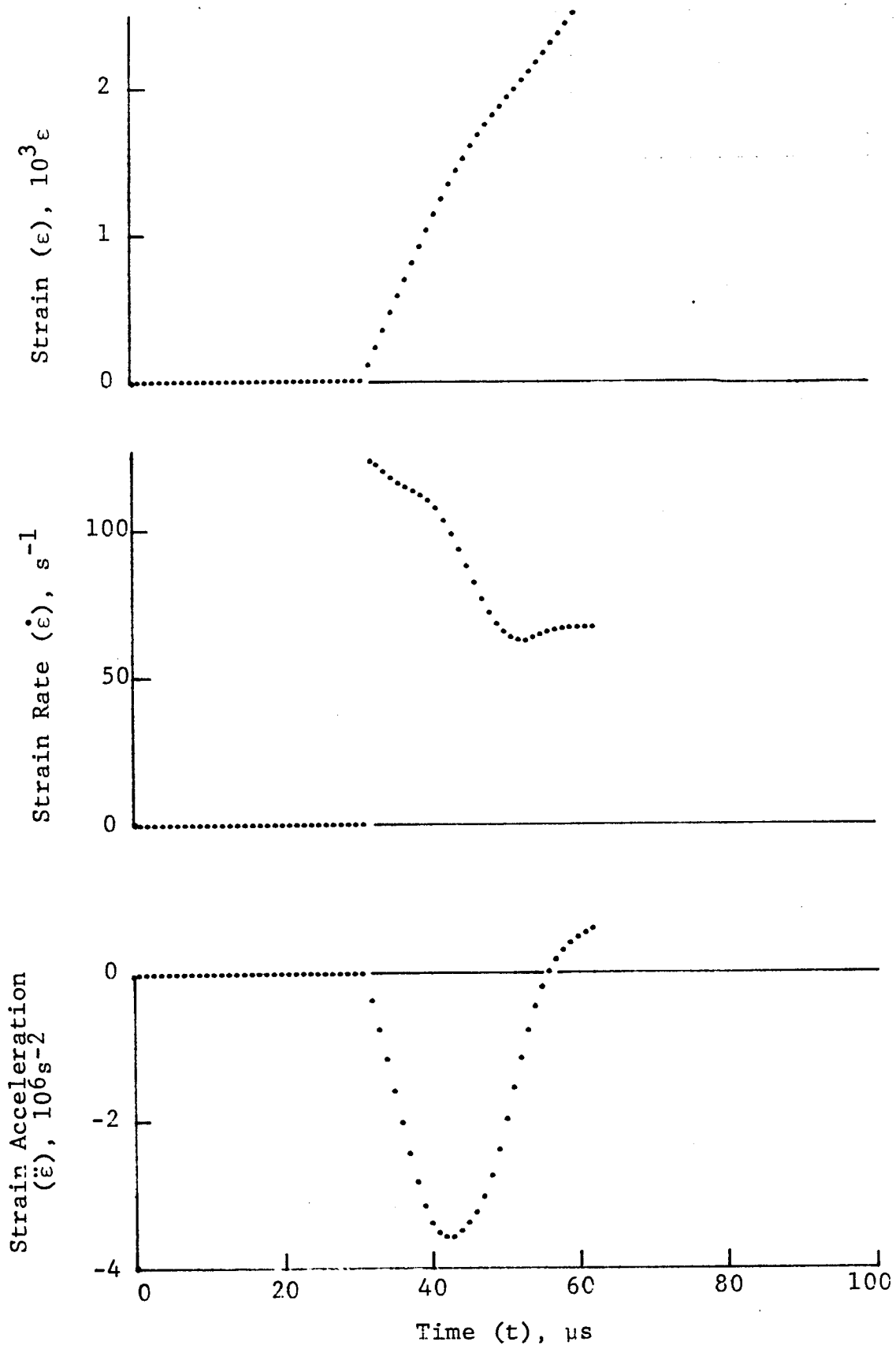

Figure 4-141. Strain and its derivatives in steel ring for Specimen No. 20-2.

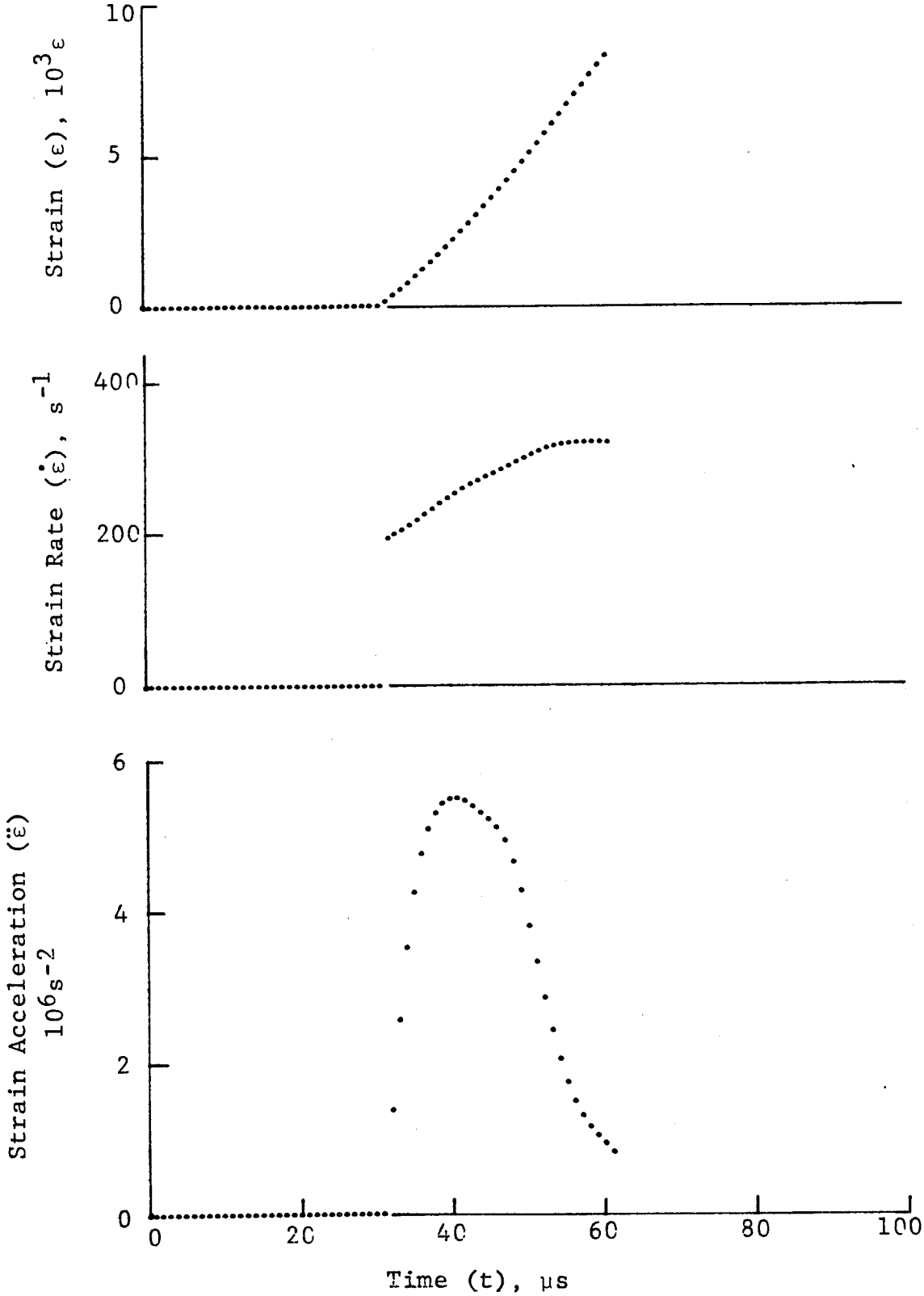

Figure 4-142. Circumferential strain and its derivatives in SP288/AS $[\pm 75]_{2S}$ graphite/epoxy ring under dynamic loading for Specimen No. 20-2 (1.56 g pistol powder, $KC\ell O_4$, and aluminum dust).

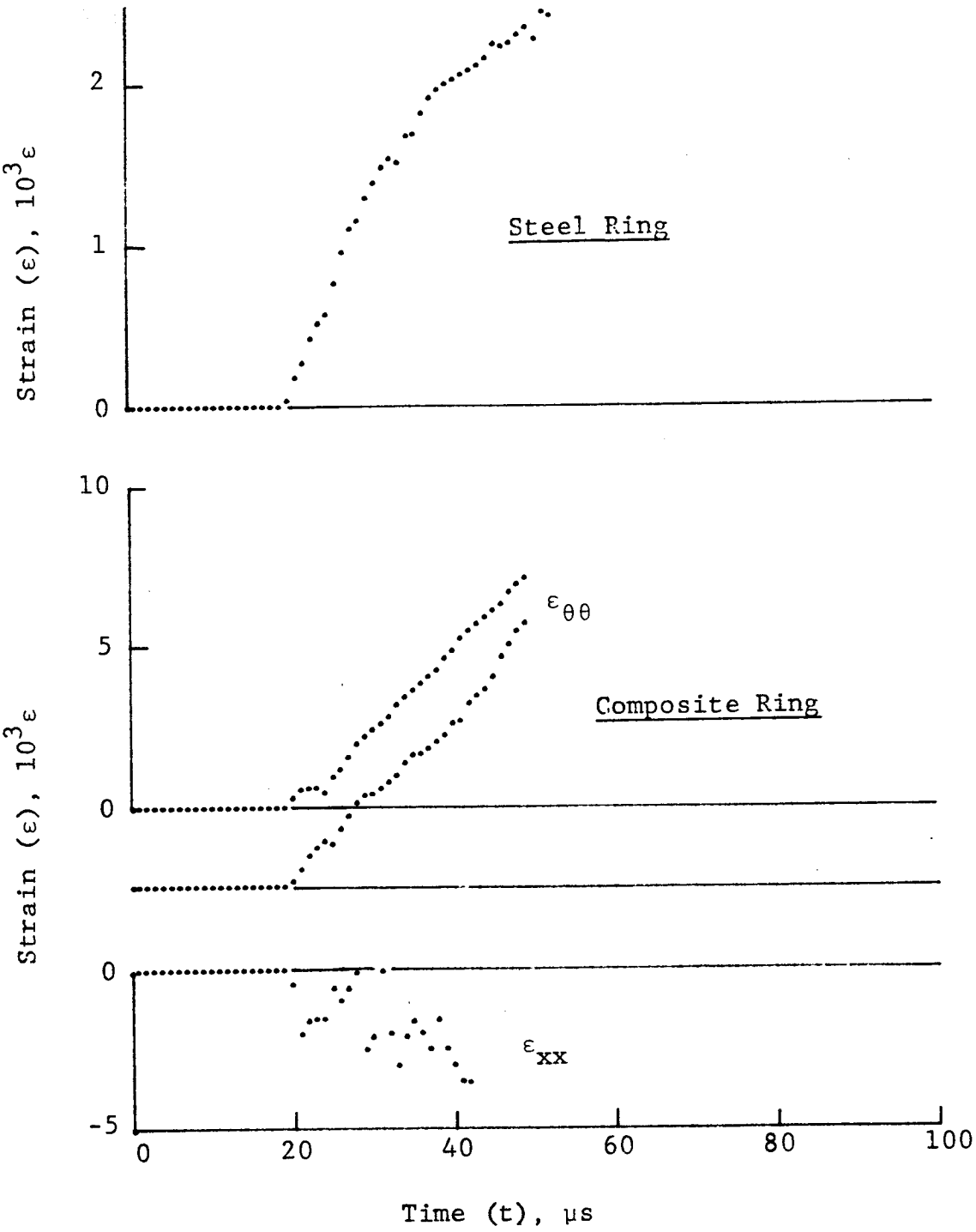

Figure 4-143. Strain records in steel ring and SP288/AS $[\pm 75]_{2S}$ graphite/epoxy ring under dynamic loading for Specimen No. 20-4 (1.56 g pistol powder, $KC\ell O_4$, and aluminum dust).

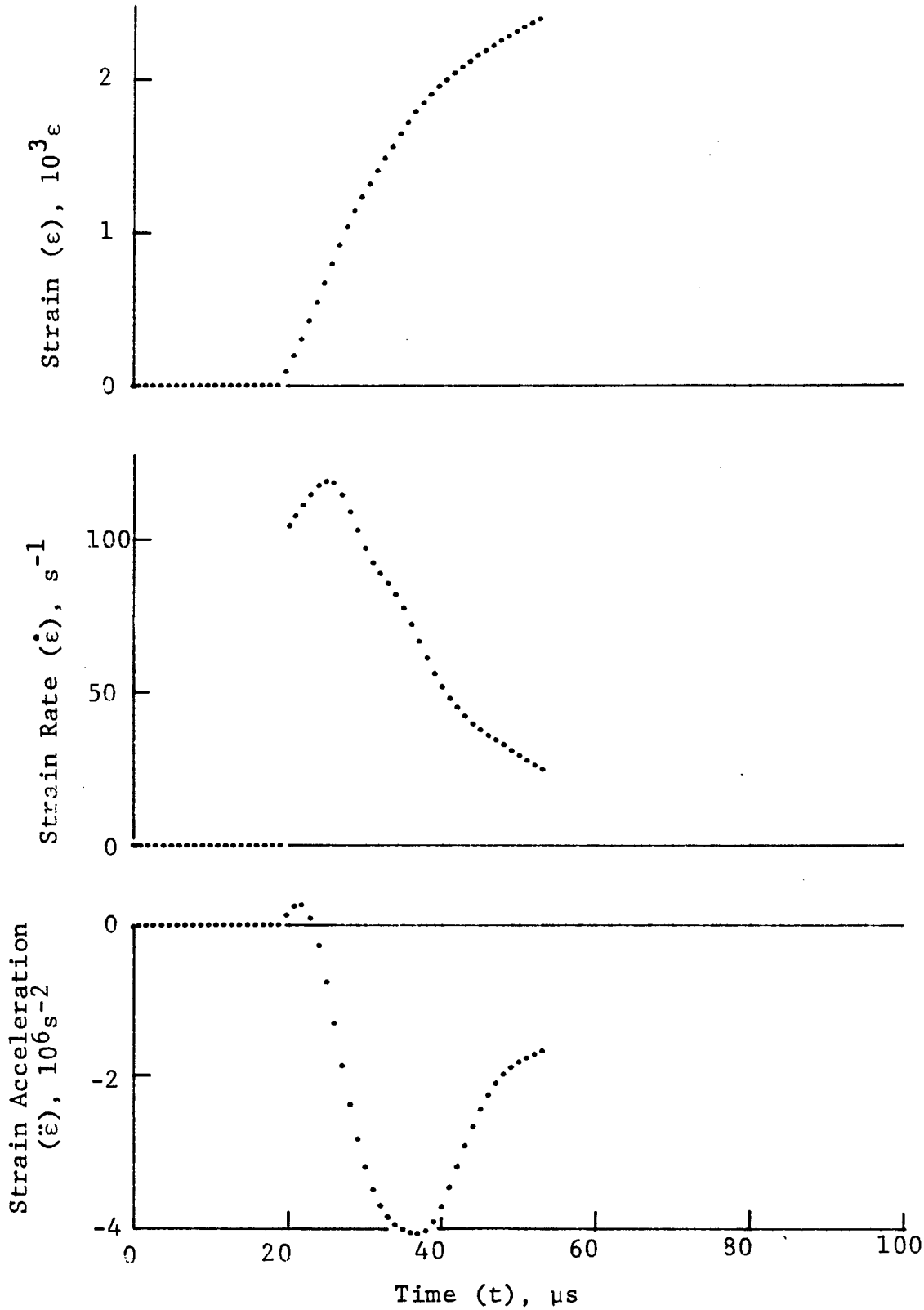

Figure 4-144. Strain and its derivatives in steel ring for Specimen No. 20-4.

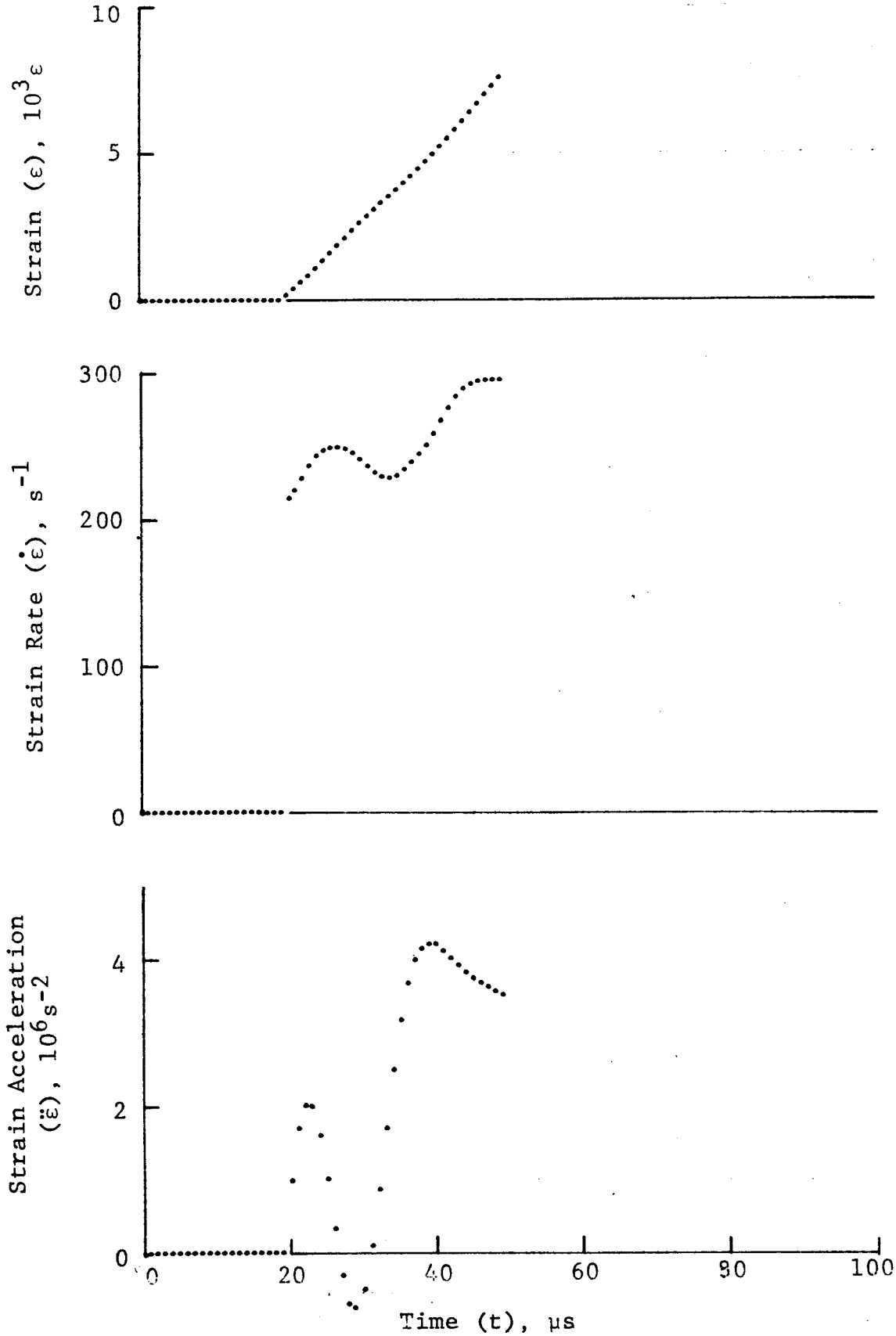

Figure 4-145. Circumferential strain and its derivatives in SP288/AS $[\pm 75]_{2S}$ graphite/epoxy ring under dynamic loading for Specimen No. 20-4 (1.56 g pistol powder, $KC\ell O_4$, and aluminum dust).

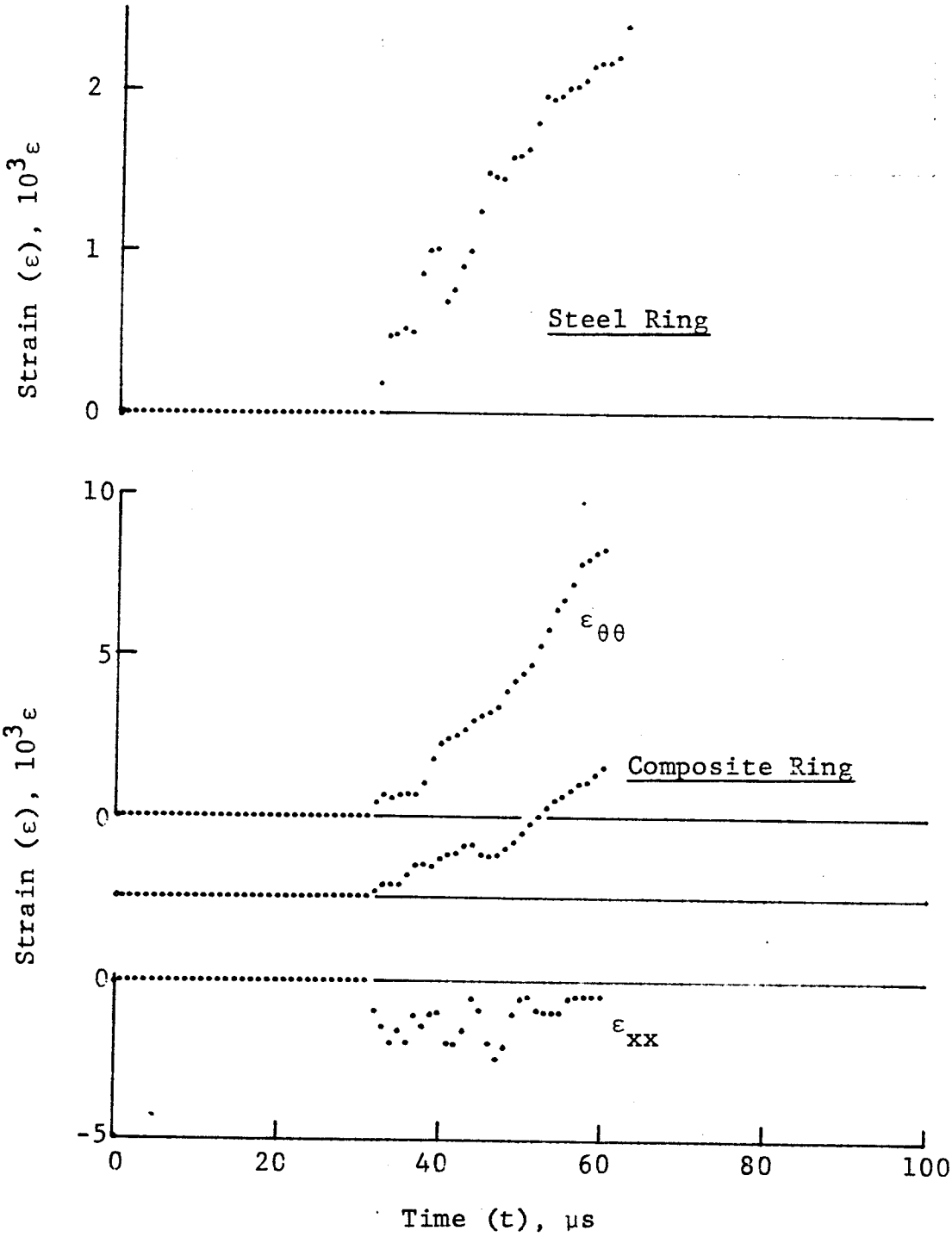

Figure 4-146. Strain records in steel ring and SP288/AS $[\pm 75]_{2S}$ graphite/epoxy ring under dynamic loading for Specimen No. 20-7 (1.56 g pistol powder, $KC\ell O_4$, and aluminum dust).

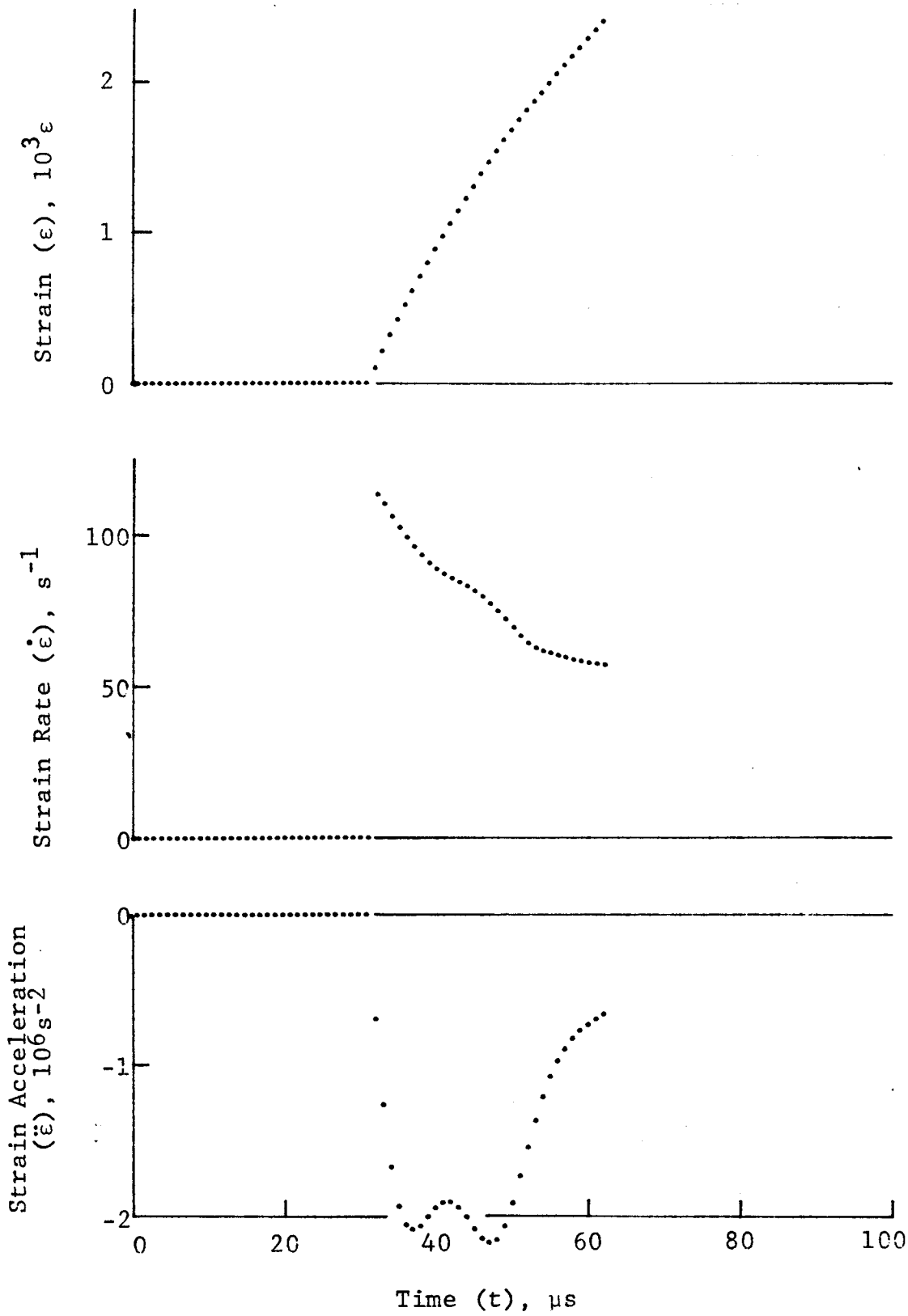

Figure 4-147. Strain and its derivatives in steel ring for Specimen No. 20-7.

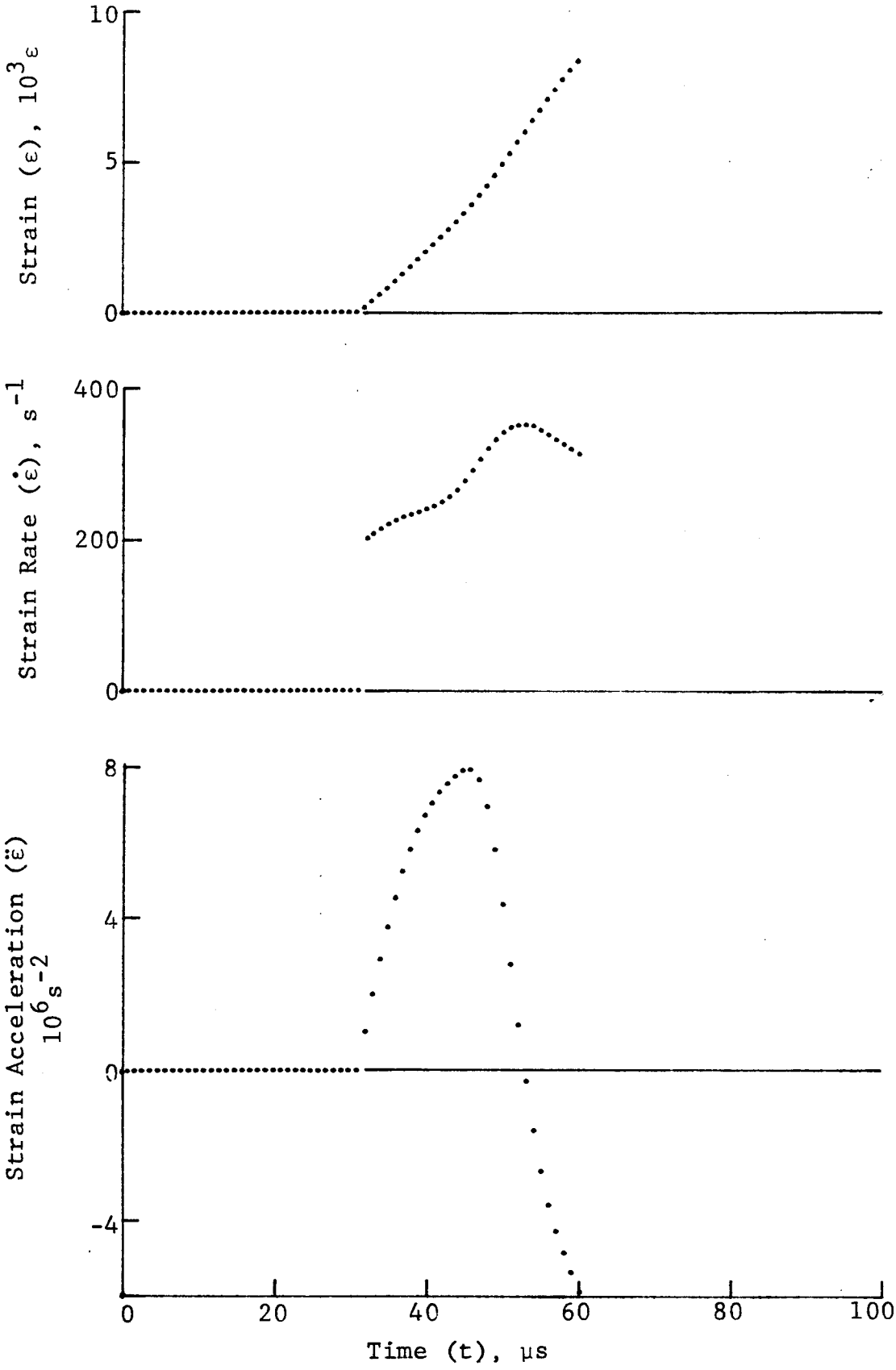

Figure 4-148. Circumferential strain and its derivatives in SP288/AS $[\pm 75]_{2s}$ graphite/epoxy ring under dynamic loading for Specimen No. 20-7 (1.56 g pistol powder, $KC\ell O_4$, and aluminum dust).

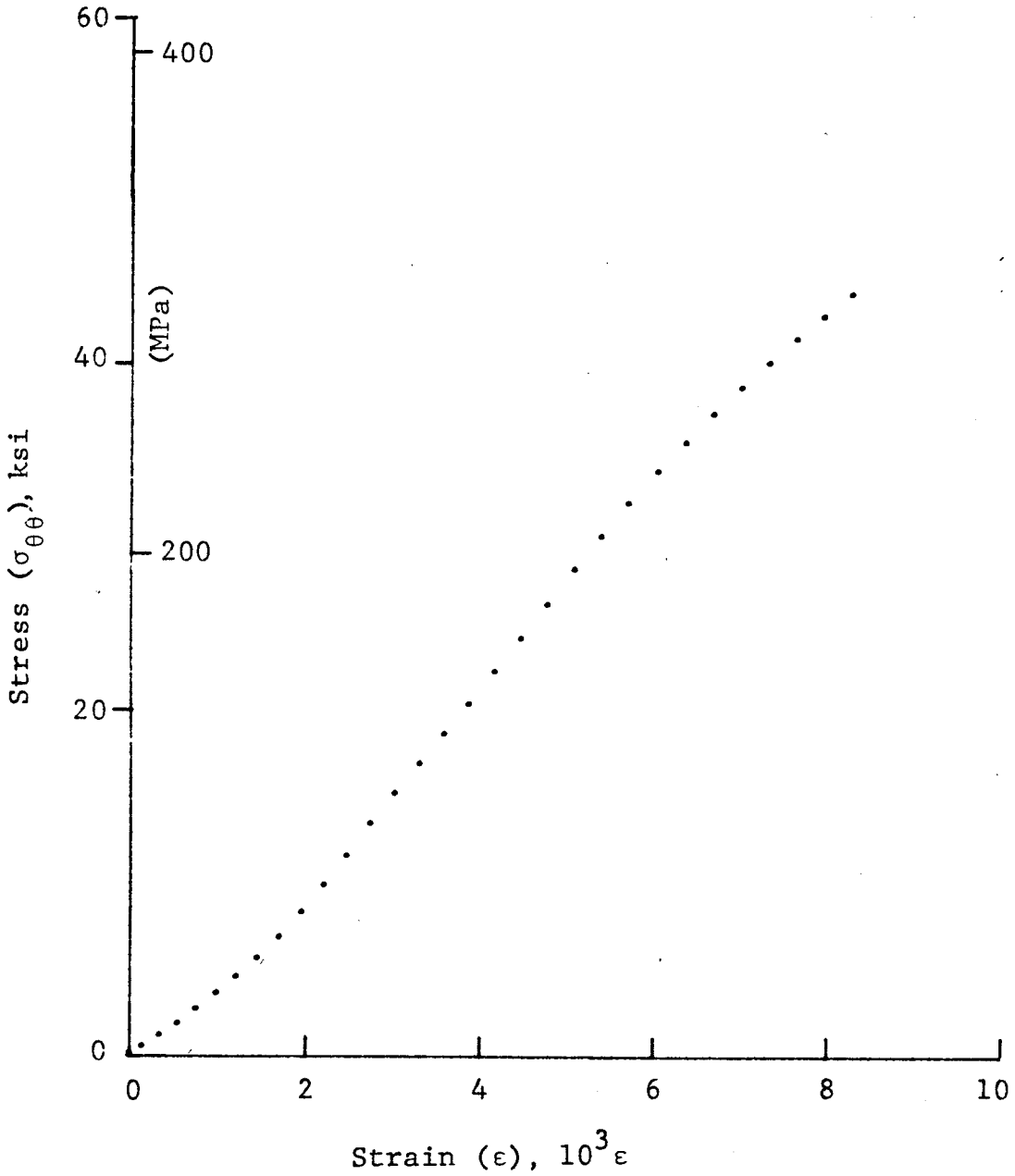

Figure 4-149. Stress-strain curve for dynamically loaded SP288/AS $[\pm 75]_{2s}$ graphite/epoxy ring, Specimen No. 20-2 (1.56 pistol powder, $KC\ell O_4$, and aluminum dust).

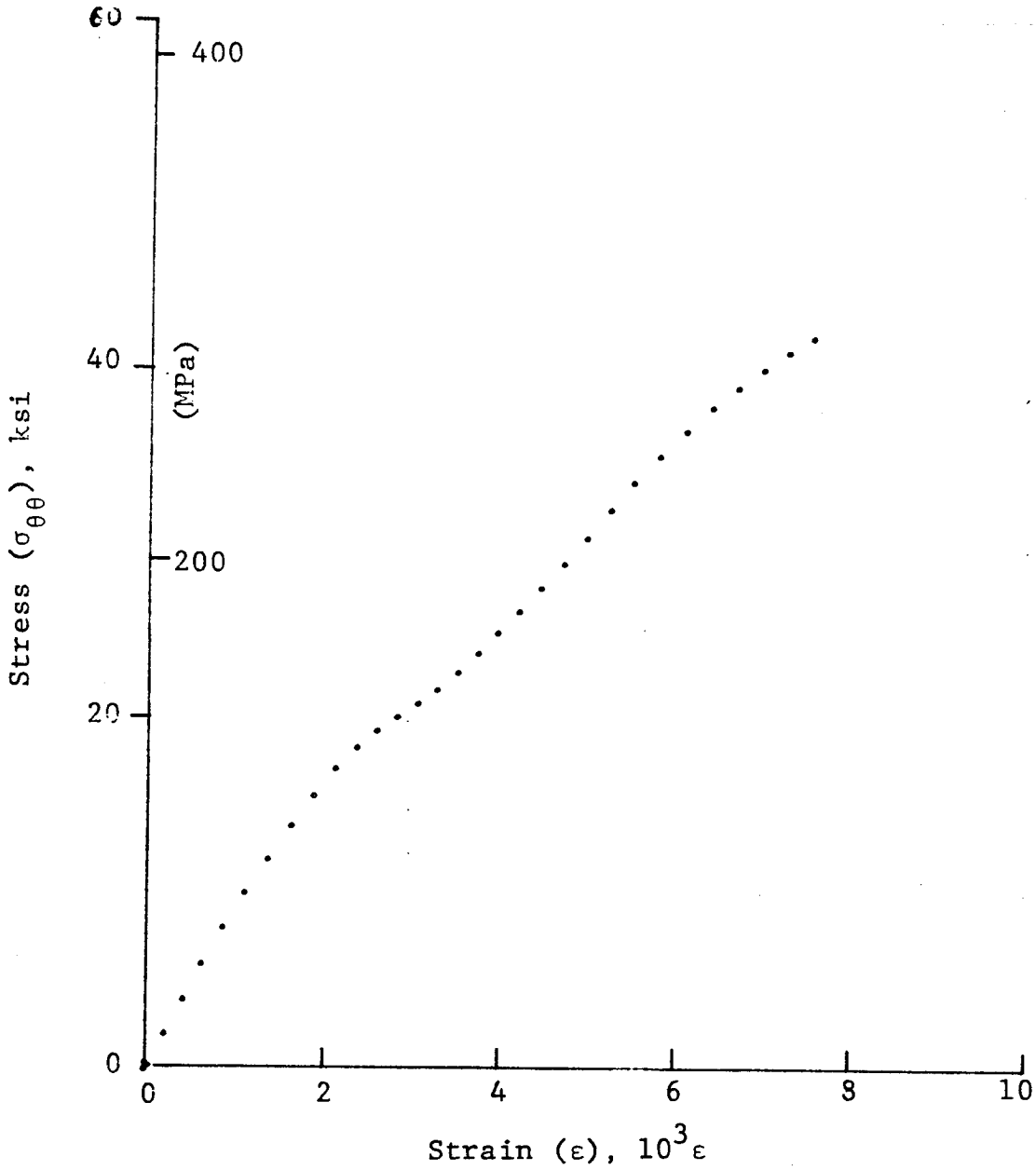

Figure 4-150. Stress-strain curve for dynamically loaded SP288/AS $[\pm 75]_{2s}$ graphite/epoxy ring, Specimen No. 20-4 (1.56 g pistol powder, $KC\ell O_4$, and aluminum dust).

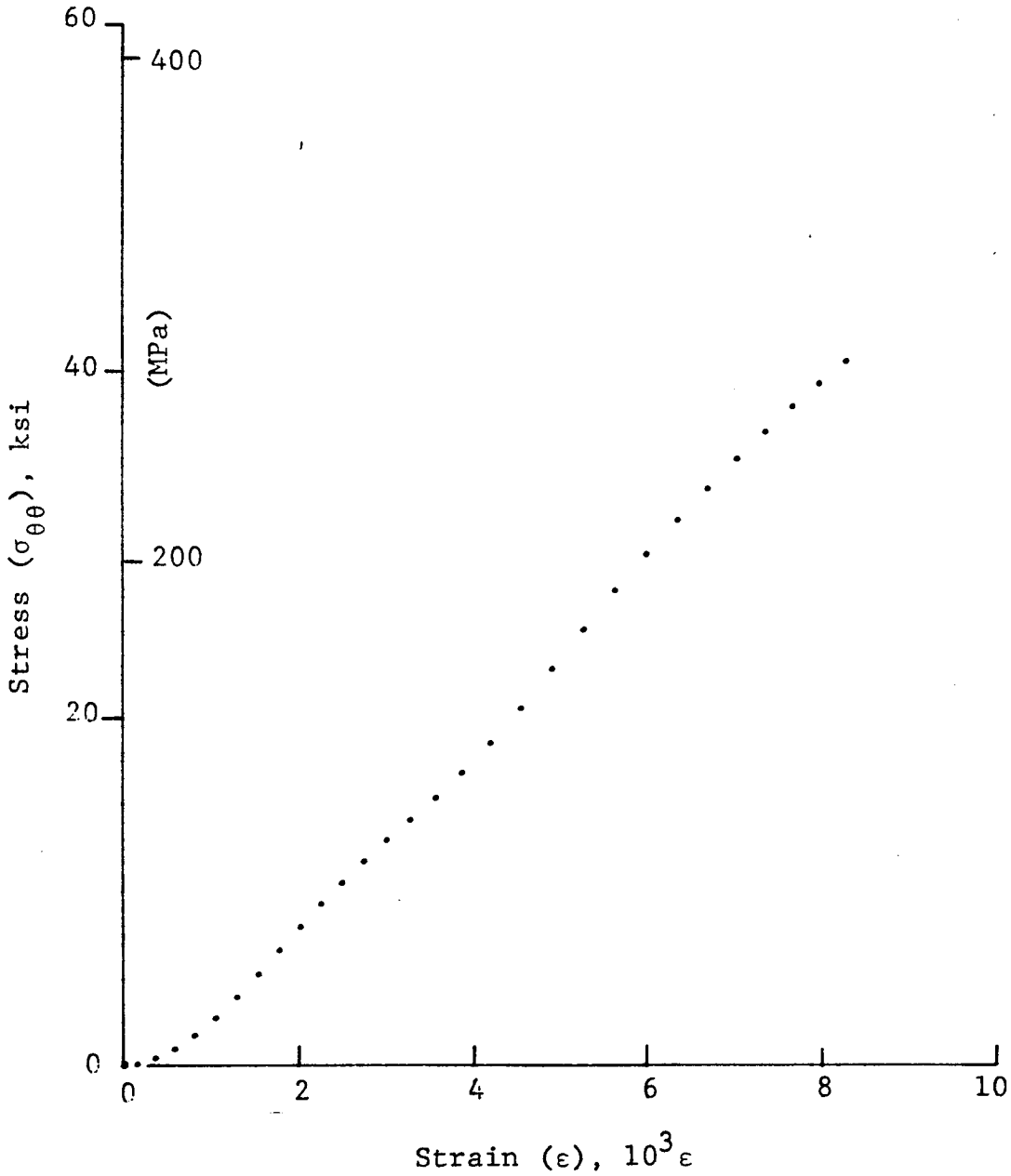

Figure 4-151. Stress-strain curve for dynamically loaded SP288/AS $[\pm 75]_{2s}$ graphite/epoxy ring, Specimen No. 20-7 (1.56 g pistol powder, $KC\ell O_4$, and aluminum dust).

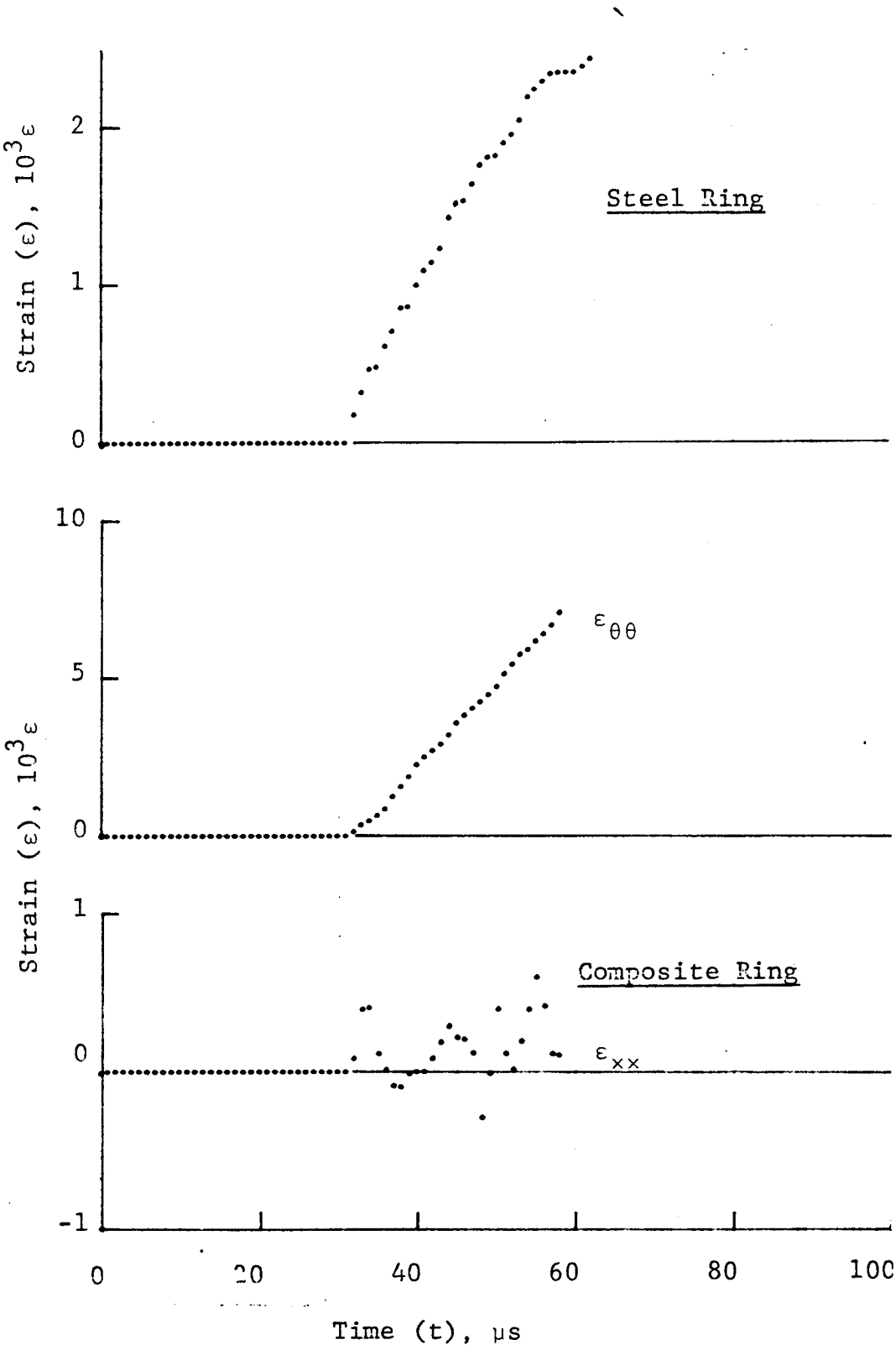

Figure 4-152. Strain records in steel ring and 80AS/20S/PR288 $[\pm 75]_{2S}$ graphite/S-glass/epoxy ring under dynamic loading for Specimen No. 21-2 (1.56 g pistol powder, $KC\ell O_4$, and aluminum dust).

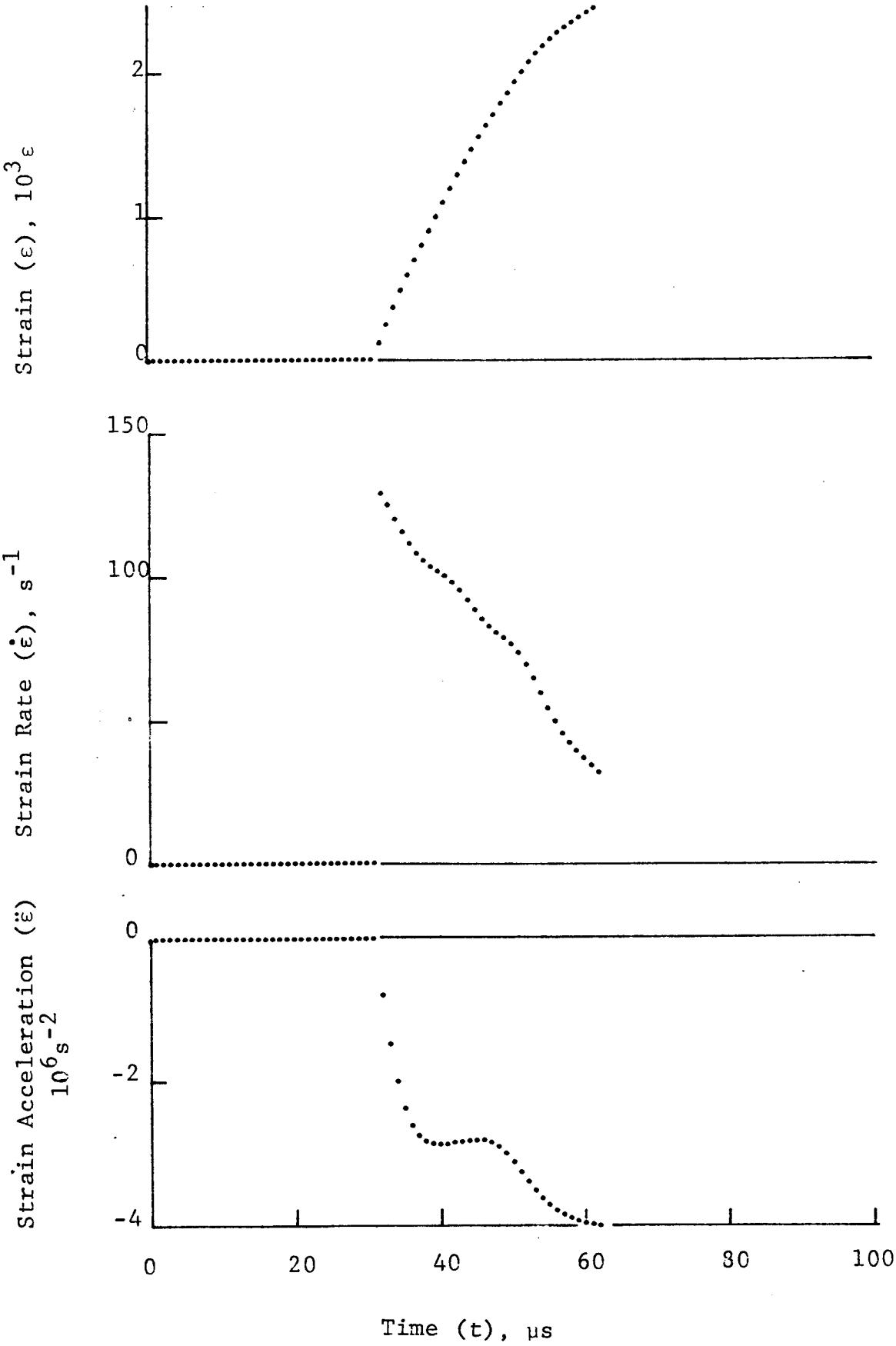

Figure 4-153. Strain and its derivatives in steel ring for Specimen No. 21-2.

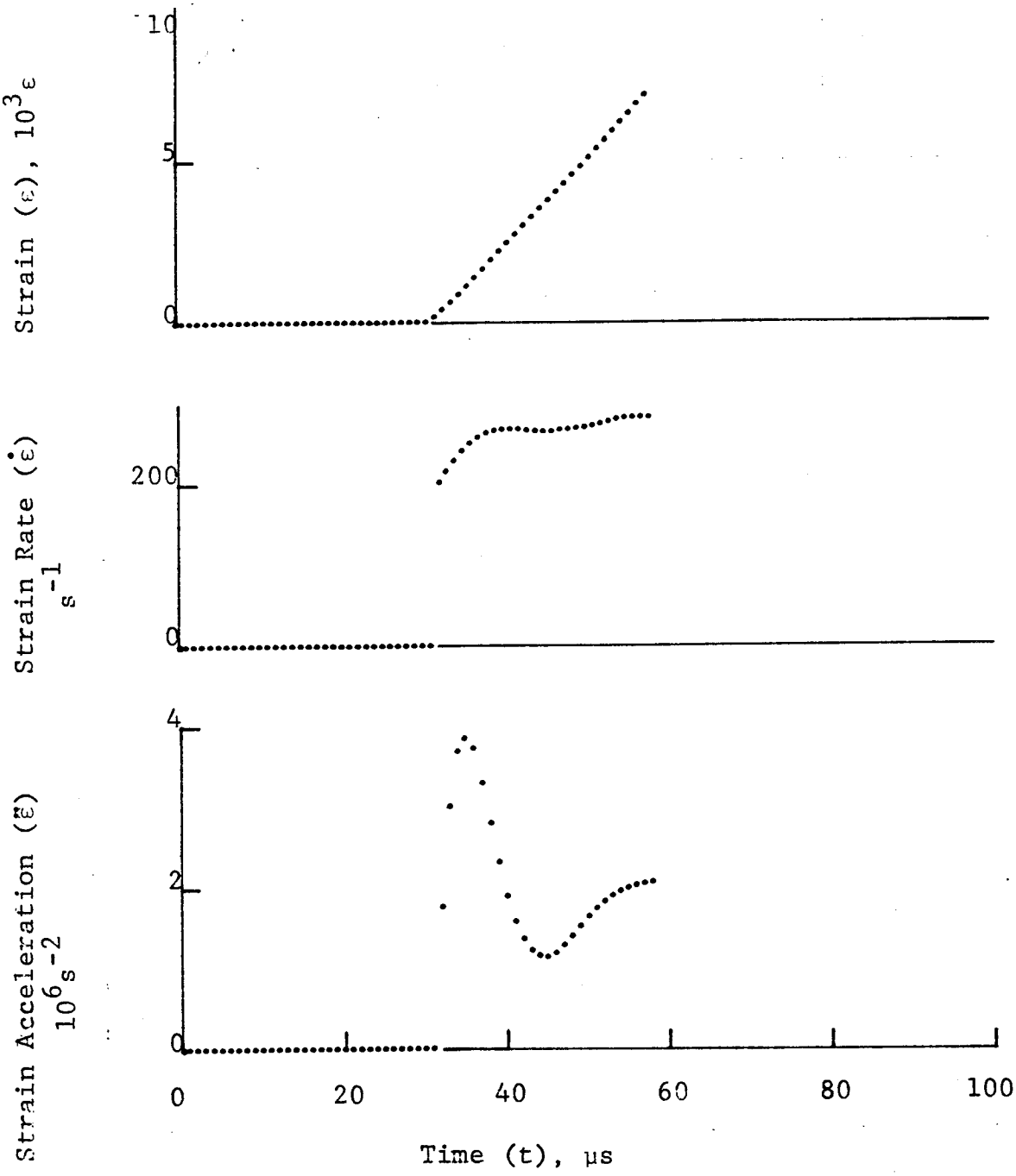

Figure 4-154. Circumferential strain and its derivatives in $[\pm 75]_{2s}$ 80AS/20S/PR288 graphite/S-glass/epoxy ring under dynamic loading for Specimen No. 21-2.

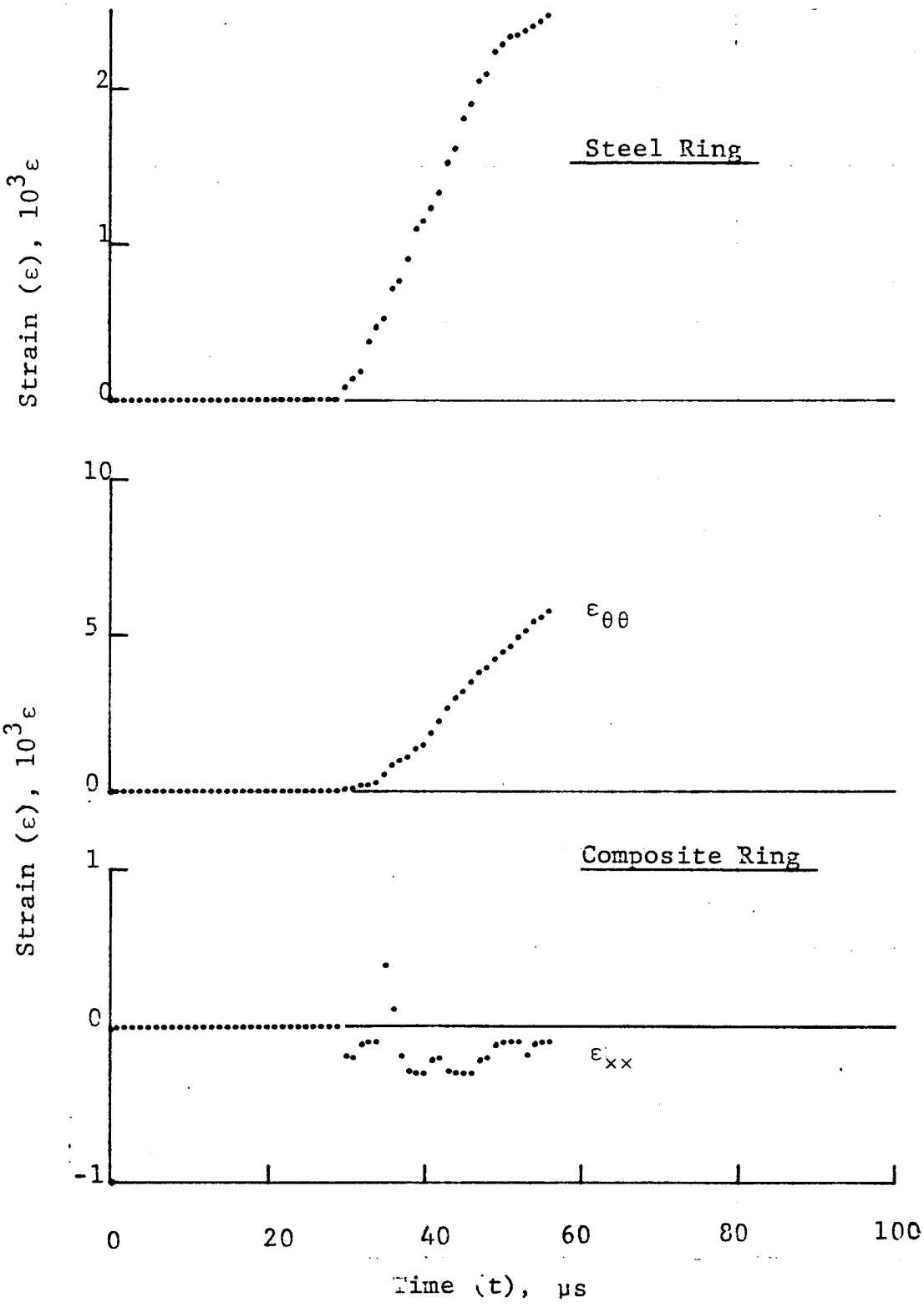

Figure 4-155. Strain records in steel ring and 80AS/20S/PR288 $[\pm 75]_{2S}$ graphite/S-glass/epoxy ring under dynamic loading for Specimen No. 21-4 (1.56 g pistol powder, $KC\ell O_4$, and aluminum dust).

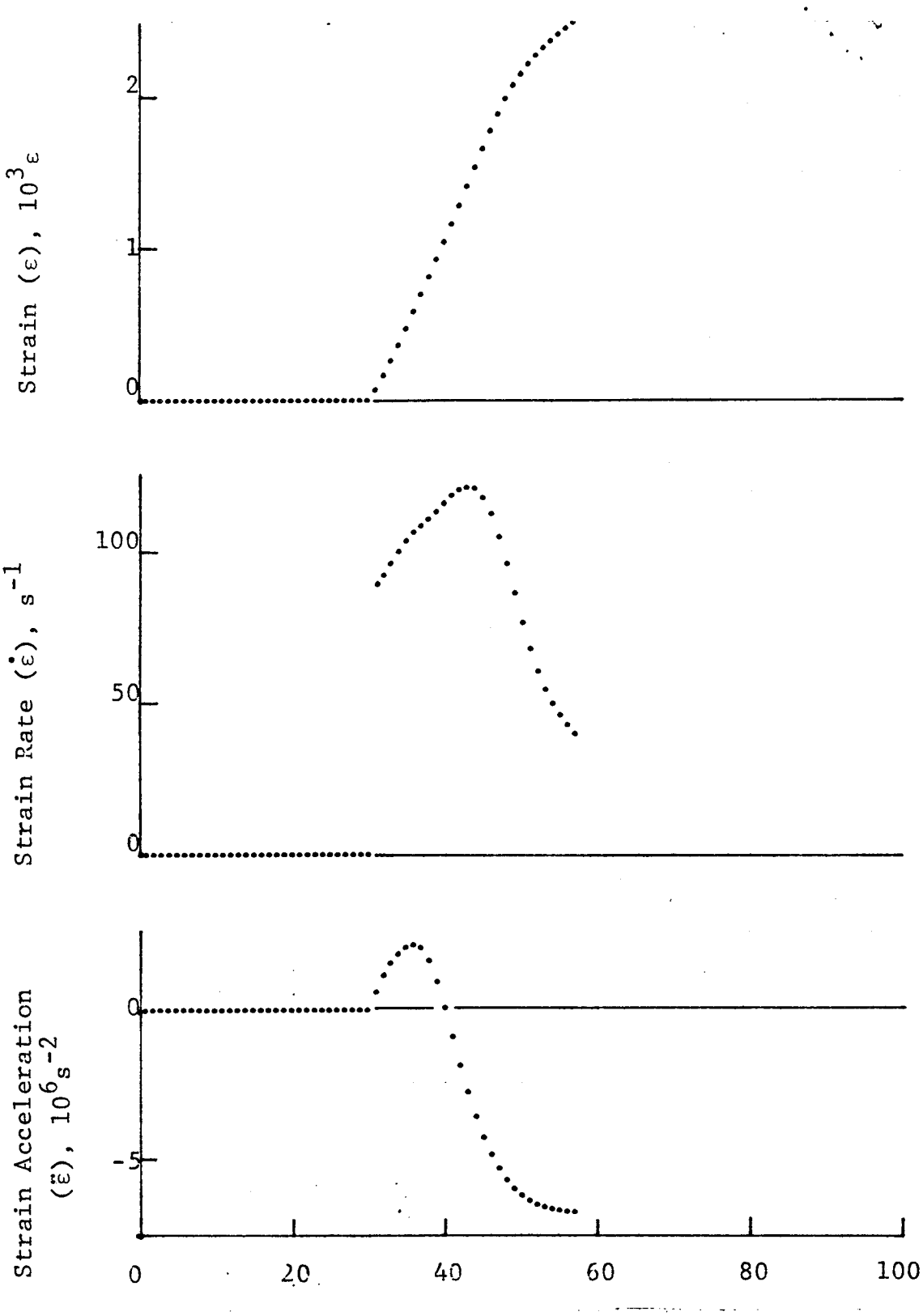

Figure 4-156. Strain and its derivatives in steel ring for Specimen No. 21-4.

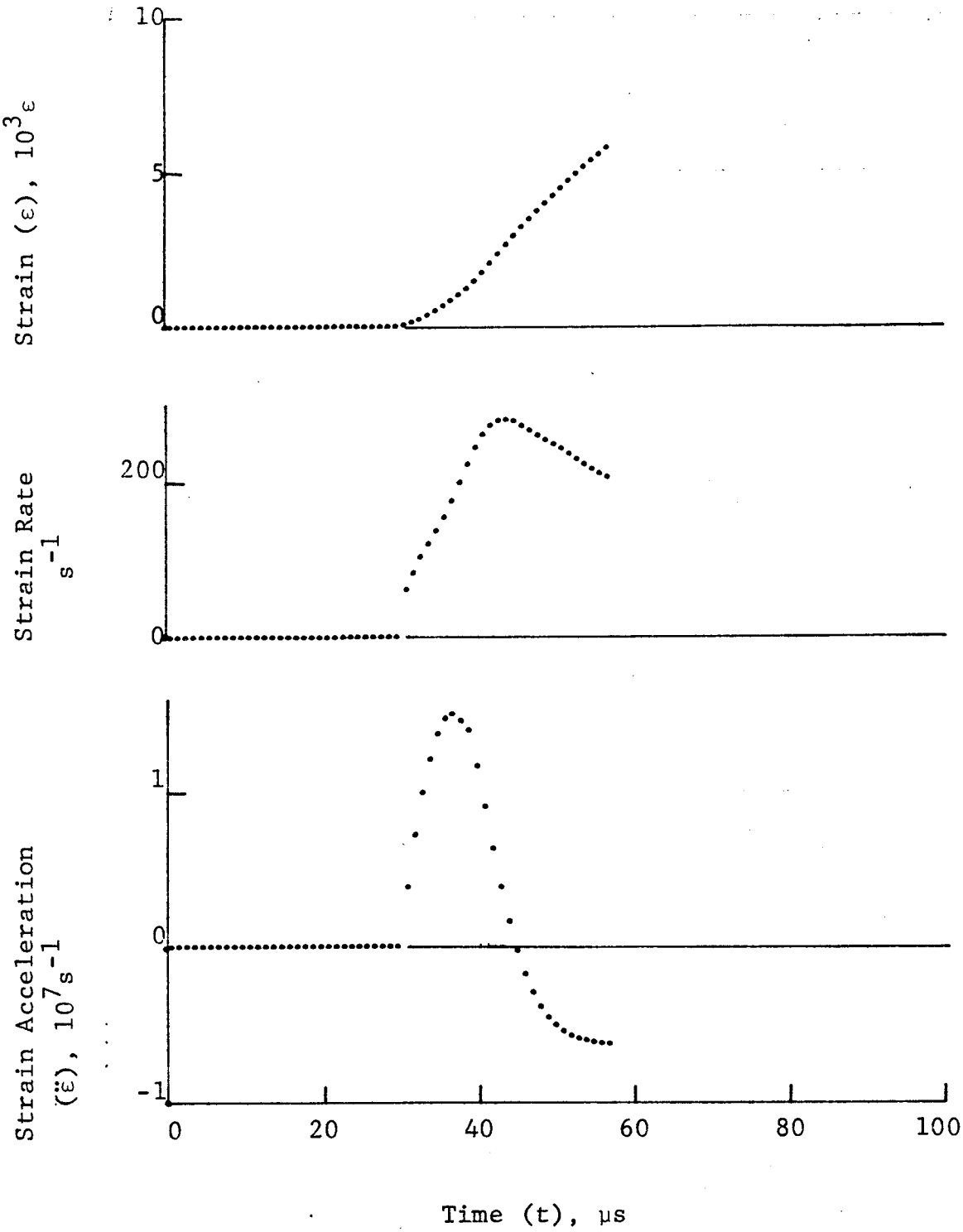

Figure 4-157. Circumferential strain and its derivatives in $[\pm 75]_{2s}$ 80AS/20S/PR288 graphite/S-glass/epoxy ring under dynamic loading for Specimen No. 21-4.

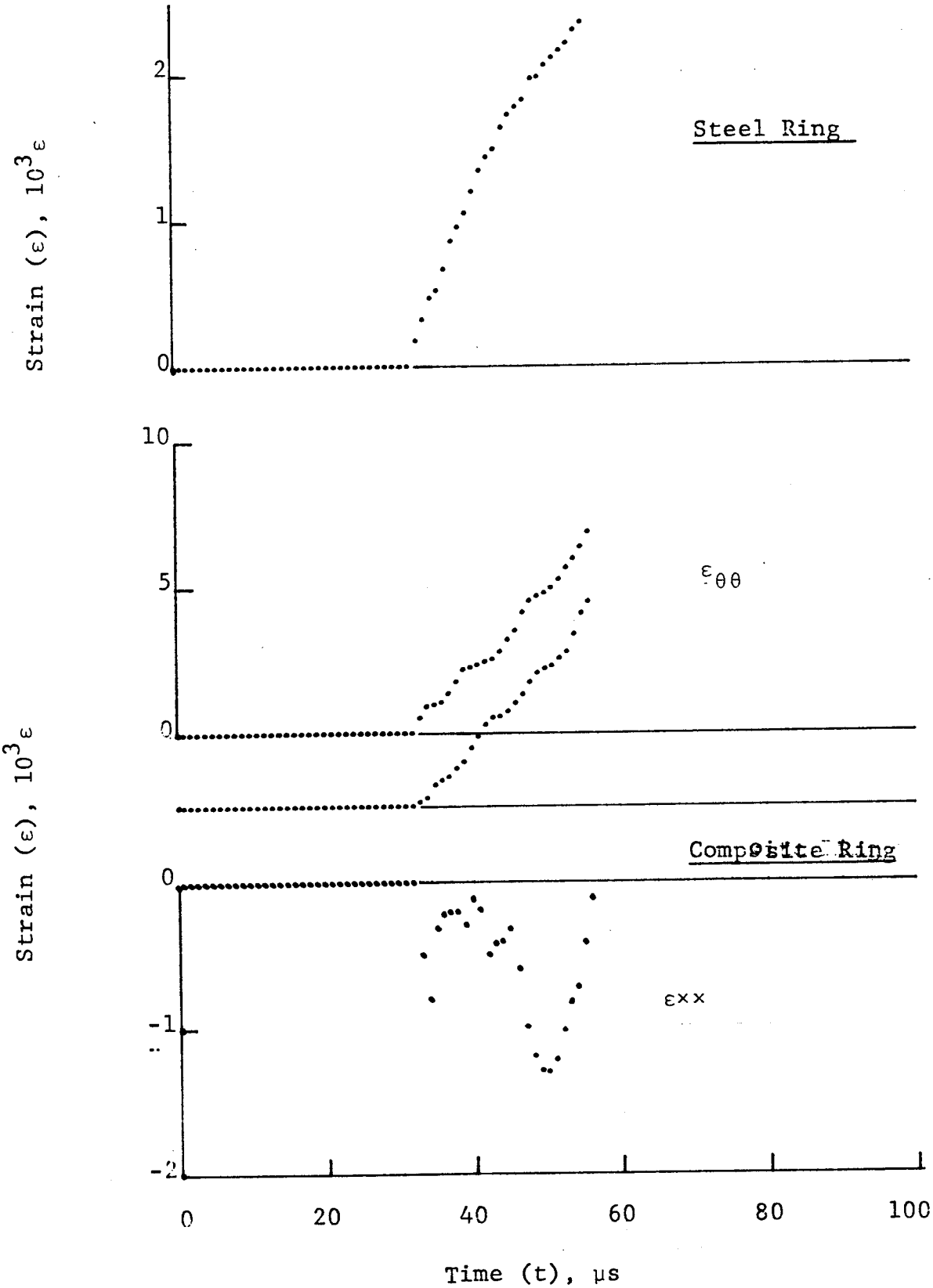

Figure 4-158. Strain records in steel ring and 80AS/20S/PR288 $[\pm 75]_{2s}$ graphite/S-glass/epoxy ring under dynamic loading for Specimen No. 21-6 (1.56 g pistol powder, $KC\ell O_4$, and aluminum dust.

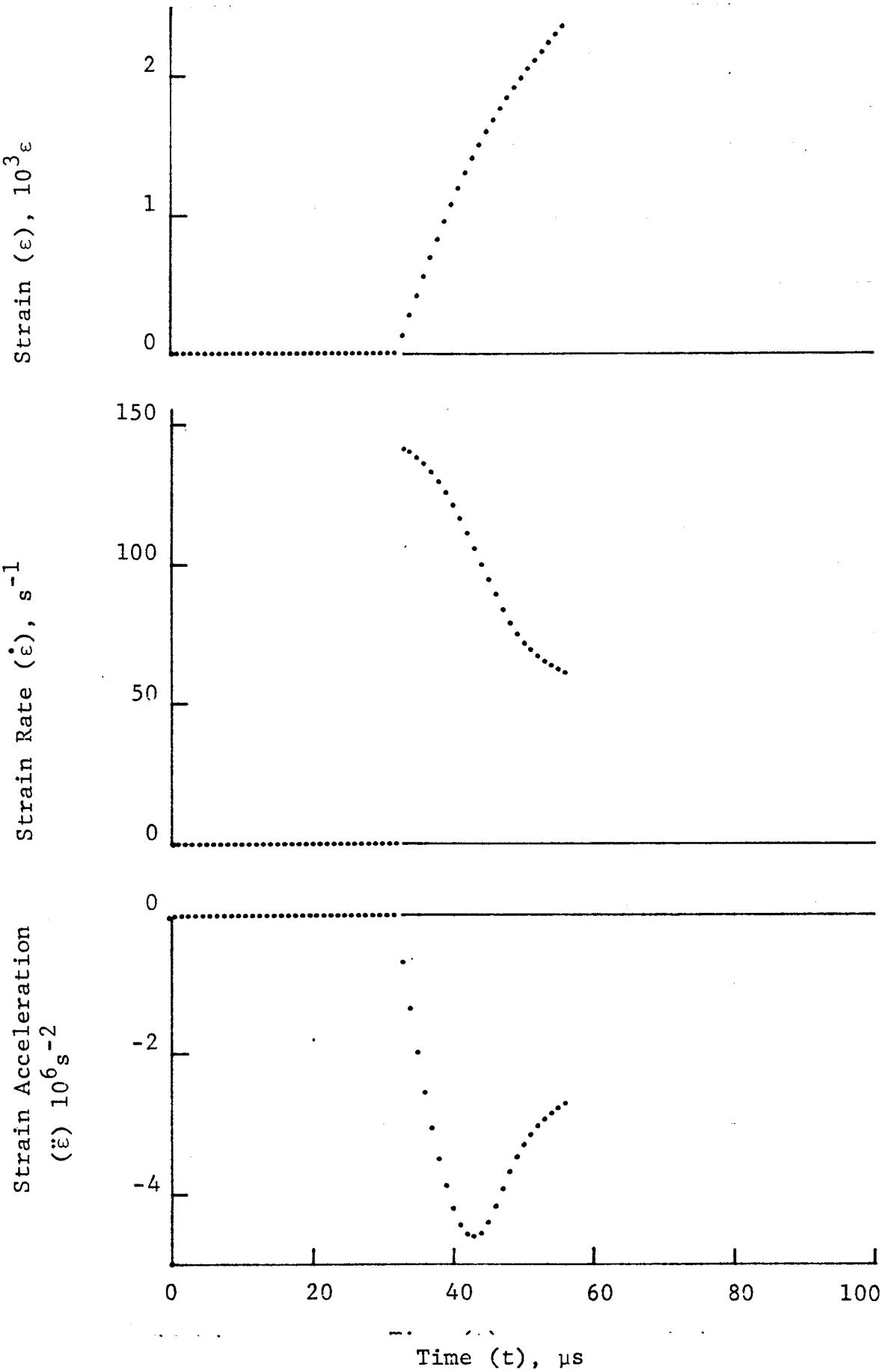

Figure 4-159. Strain and its derivatives in steel ring for Specimen No. 21-6.

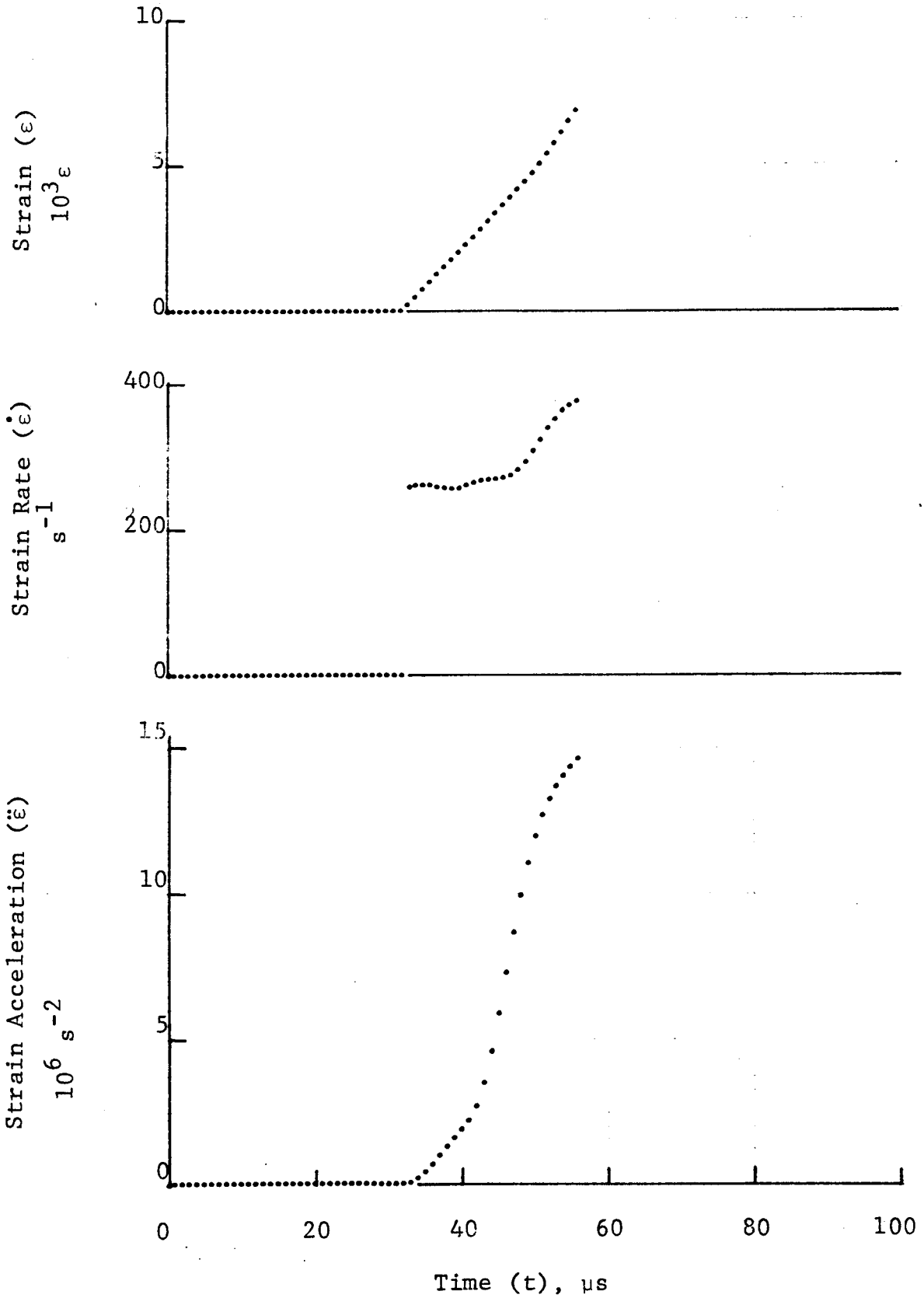

Figure 4-160. Circumferential strain and its derivatives in $[\pm 75]_{2s}$ 80AS/20S/PR288 graphite/S-glass/epoxy ring under dynamic loading for Specimen No. 21-6.

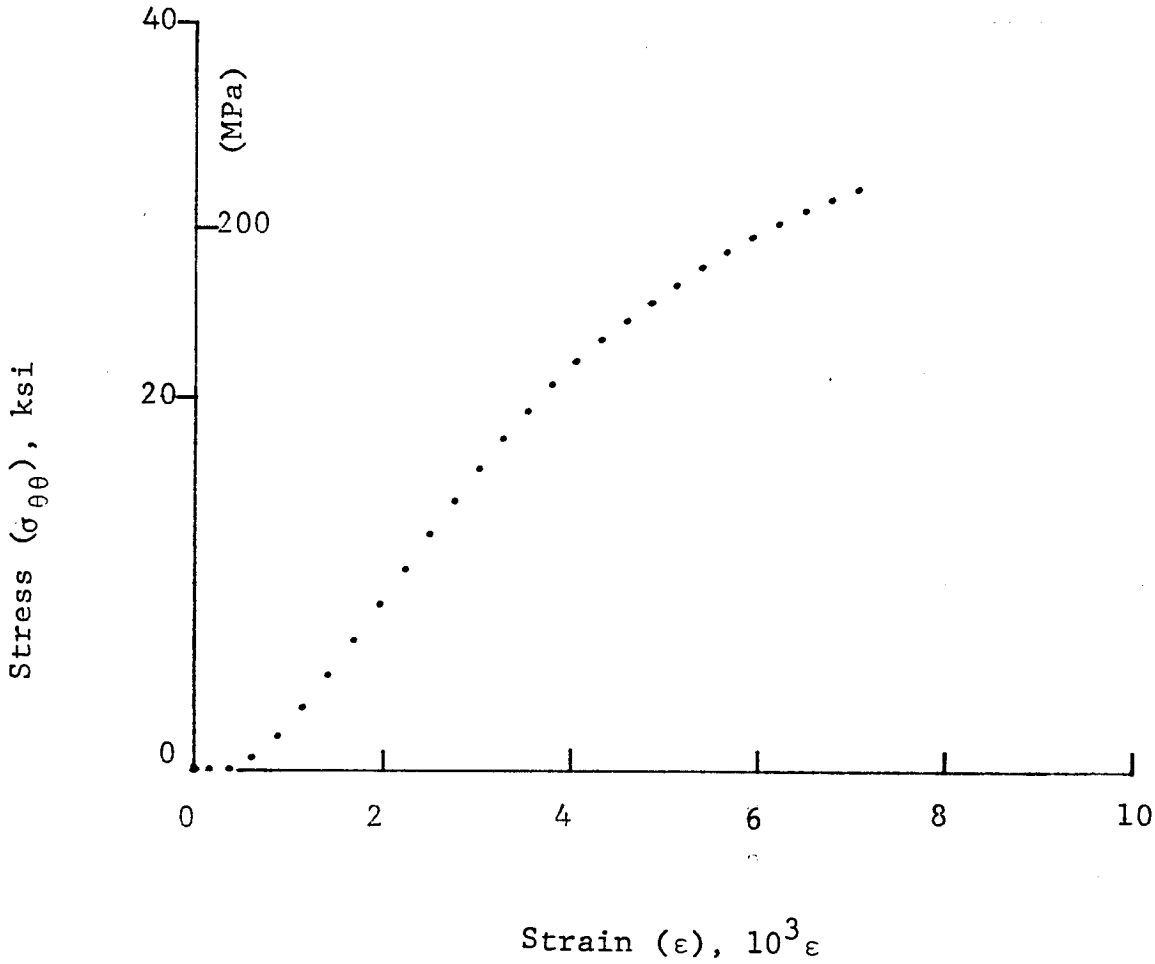

Figure 4-161. Stress-strain curve for dynamically loaded 80AS/20S/PR288 $[\pm 75]_{2s}$ graphite/S-glass/epoxy ring, Specimen No. 21-2 (1.56 g pistol powder, $KC\ell O_4$, and aluminum dust).

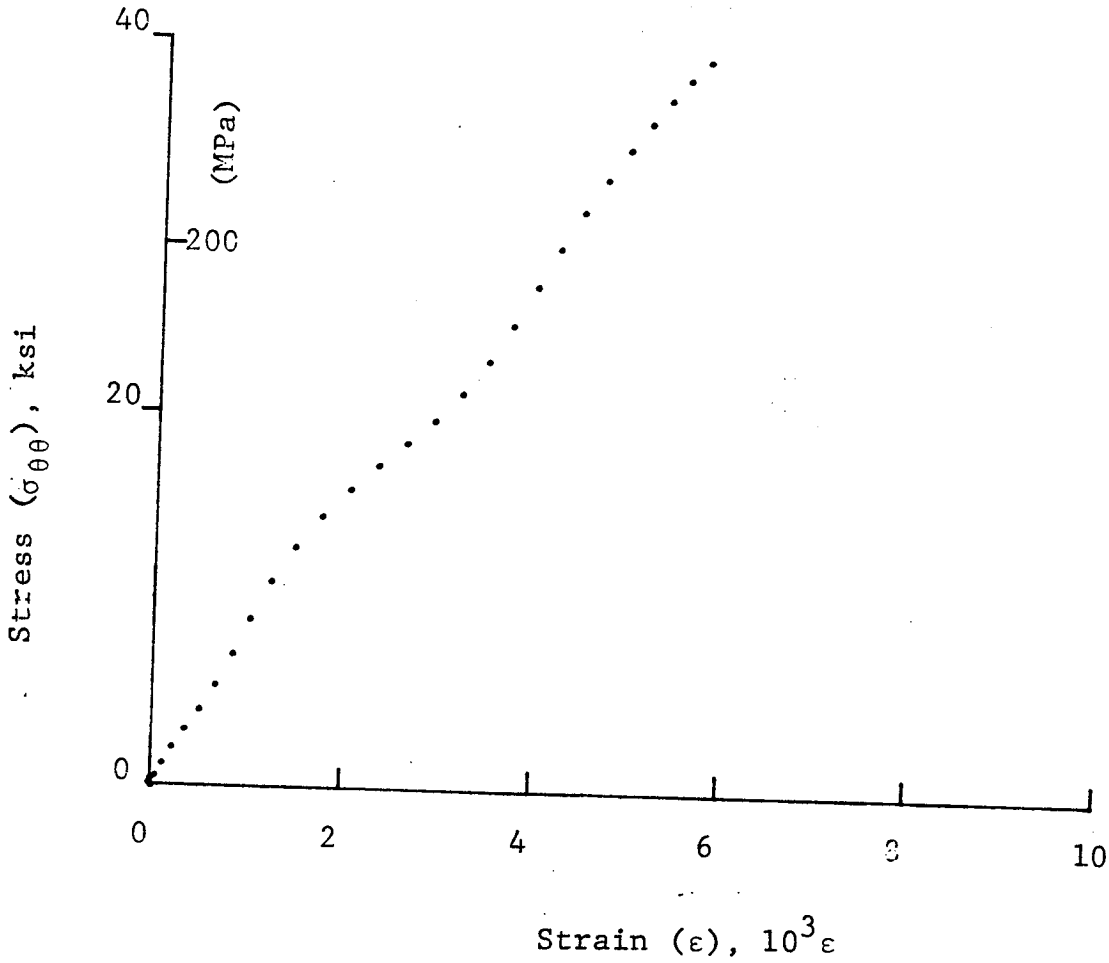

Figure 4-162. Stress-strain curve for dynamically loaded 80AS/20S/PR288 $[\pm 75]_{2s}$ graphite/S-glass/epoxy ring, Specimen No. 21-4 (1.56 g pistol powder, $KC\ell O_4$, and aluminum dust).

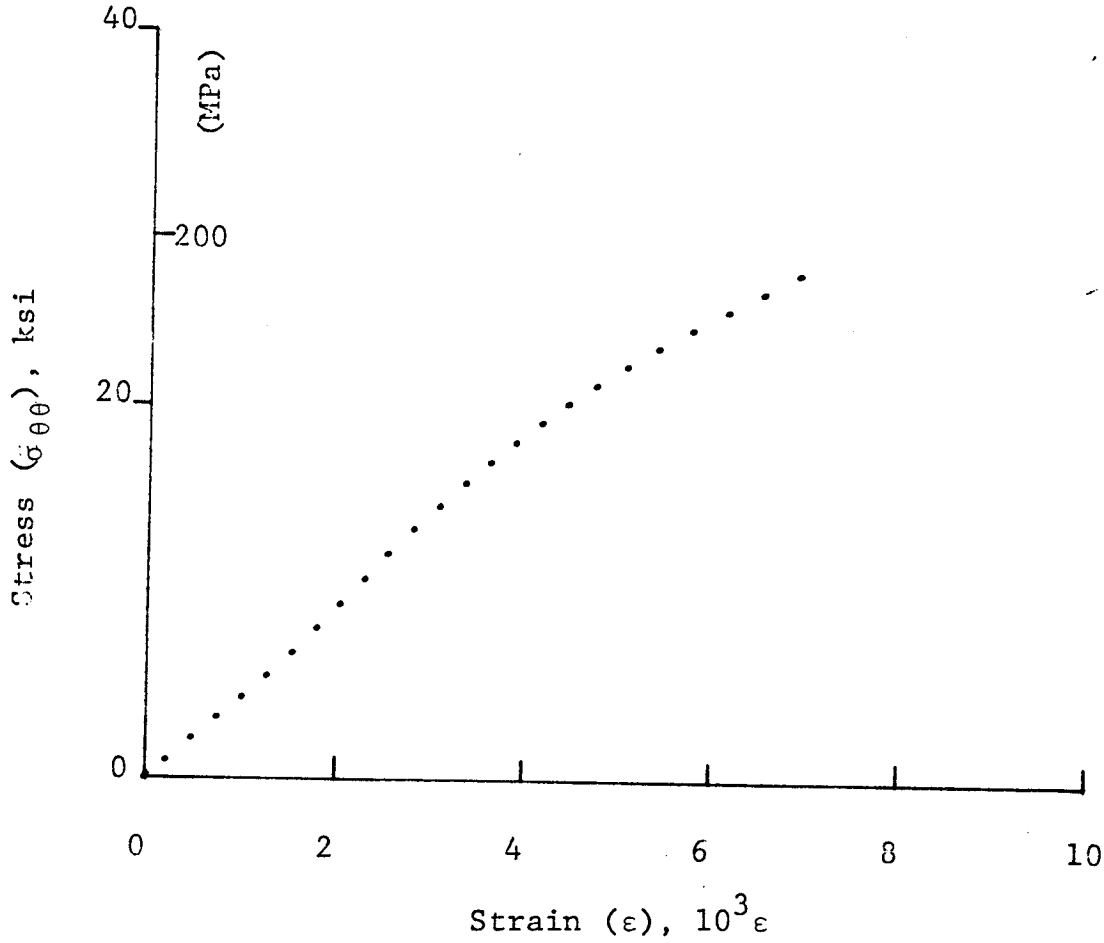

Figure 4-163. Stress-strain curve for dynamically loaded 80AS/20S/PR288 $[\pm 75]_{2s}$ graphite/S-glass/epoxy ring, Specimen No. 21-6 (1.56 g pistol powder, $KC\ell O_4$, and aluminum dust).

5. SUMMARY AND CONCLUSIONS

Methods developed and described in Part I of this report were applied to the characterization of angle-ply laminates. Two material systems, SP288/AS graphite/epoxy and 80AS/20S/PR288 graphite/S-glass/epoxy, were characterized in uniaxial tension at three strain rates, ranging from quasi-static to over $500s^{-1}$. Laminate ring specimens of $[\pm 15]_{2s}$, $[\pm 22.5]_{2s}$, $[\pm 30]_{2s}$, $[\pm 45]_{2s}$, $[\pm 60]_{2s}$, $[\pm 67.5]_{2s}$, and $[\pm 75]_{2s}$ layups were loaded under internal pressure. Results were obtained and presented in the form of stress-strain curves to failure. Properties determined included moduli, Poisson's ratios, strength, and ultimate strain.

Average results for all specimens tested are tabulated in Tables 5-1 through 5-14. The effect of strain rate varies with layup, being lowest for the fiber dominated $[\pm 15]_{2s}$ laminates and highest for the matrix dominated $[\pm 75]_{2s}$ laminates. The initial and secant moduli show small increases with strain rate for the $[\pm 15]_{2s}$ layup. The average increase with strain rate for the secant modulus increases from 10% for the $[\pm 15]_{2s}$ layup to over 200% for the $[\pm 75]_{2s}$ layup. For the same range of laminates the initial modulus increases with strain rate from 25% for the $[\pm 15]_{2s}$ laminate to over 230% for the $[\pm 75]_{2s}$ laminates. The highest strength increments over the static values vary from approximately 14% for the $[\pm 15]_{2s}$ layup to 275% for the $[\pm 75]_{2s}$ layup. The ultimate strains in general do not show any significant trends with strain rate for all layups. In six of the fourteen types of specimens tested the ultimate strains at the various strain rates were within ±10% of the mean value. In five other groups of specimens the ultimate strain variations were within ±20% of the mean. In the case of the two $[\pm 45]_{2s}$ groups the results were not conclusive because only lower values were obtained for the static ultimate strain.

TABLE 5-1. HIGH STRAIN RATE TENSILE PROPERTIES OF $[\pm 15]_{2s}$ SP288/AS GRAPHITE/EPOXY

Specimen Numbers	Strain Rate ($\dot{\varepsilon}_{\theta\theta}$), s^{-1}	Modulus ($E_{\theta\theta}$), GPa (10^6 psi)	Poisson's Ratio ($\nu_{\theta x}$)
		Initial Properties	
35-1,3,5	1×10^{-4}	105 (15.2)	0.86
35-7,10,11	16	121 (17.5)	0.80
35-2,4,6	190	113 (16.4)	0.76
		Secant Properties	
35-1,3,5	1×10^{-4}	105 (15.3)	1.00
35-7,10,11	44	122 (17.8)	0.81
35-2,4,6	224	118 (17.1)	0.84
		Terminal Properties	
35-1,3,5	1×10^{-4}	106 (15.4)	1.22
35-7,10,11	101	147 (21.3)	0.67
35-2,4,6	273	112 (16.2)	0.71
		Ultimate Properties	
	Time to Failure (t_f), μs	Strength ($S_{\theta\theta T}$), MPa (ksi)	Strain ($\varepsilon^u_{\theta\theta T}$)
35-1,3,5	1×10^8	823 (119)	0.0078
35-7,10,11	199	1049 (152)	0.0086
35-2,4,6	40	1029 (149)	0.0088

TABLE 5-2. HIGH STRAIN RATE TENSILE PROPERTIES OF $[\pm 15]_{2s}$ 80AS/20S/PR288 GRAPHITE/S-GLASS/EPOXY

Specimen Numbers	Strain Rate ($\dot{\varepsilon}_{\theta\theta}$), s^{-1}	Modulus ($E_{\theta\theta}$), GPa (10^6 psi)	Poisson's Ratio ($\nu_{\theta x}$)
	Initial Properties		
36-1,3,5	1×10^{-4}	95 (13.7)	0.68
36-6,10,11	17	104 (15.1)	0.44
36-2,4,7	140	133 (19.3)	0.88
	Secant Properties		
36-1,3,5	1×10^{-4}	95 (13.8)	0.75
36-6,10,11	43	95 (13.7)	0.50
36-2,4,7	194	101 (14.7)	0.92
	Terminal Properties		
36-1,3,5	1×10^{-4}	95 (13.7)	0.86
36-6,10,11	212	91 (13.2)	0.51
36-2,4,7	245	50 (7.2)	1.08
	Ultimate Properties		
	Time to Failure (t_f), μs	Strength ($S_{\theta\theta T}$), MPa (ksi)	Strain ($\varepsilon^u_{\theta\theta T}$)
36-1,3,5	1×10^8	806 (117)	0.0085
36-6,10,11	240	967 (140)	0.0103
36-2,4,7	43	837 (121)	0.0083

TABLE 5-3. HIGH STRAIN RATE TENSILE PROPERTIES OF $[\pm 22.5]_{2s}$ SP288/AS GRAPHITE/EPOXY

Specimen Number	Strain Rate ($\dot{\varepsilon}_{\theta\theta}$), s^{-1}	Modulus ($E_{\theta\theta}$), GPa (10^6 psi)	Poisson's Ratio ($\nu_{\theta x}$)
	Initial Properties		
33-1,3,5	1×10^{-4}	81.4 (11.8)	1.18
33-10,11,13	17	78.4 (11.4)	1.21
33-4,6,7	138	131.7 (19.1)	1.57
	Secant Properties		
33-1,3,5	1×10^{-4}	75.2 (10.9)	1.25
33-10,11,13	45	84.0 (12.2)	1.22
33-4,6,7	197	93.4 (13.5)	1.22
	Terminal Properties		
33-1,3,5	1×10^{-4}	70.7 (10.2)	1.44
33-10,11,13	137	67.6 (9.8)	1.23
33-4,6,7	287	62.4 (9.0)	1.35
	Ultimate Properties		
	Time to Failure (t_f), μs	Strength ($S_{\theta\theta T}$), MPa (ksi)	Strain ($\varepsilon^u_{\theta\theta T}$)
33-1,3,5	1×10^8	773 (112)	0.0103
33-10,11,13	208	771 (112)	0.0093
33-4,6,7	43	790 (115)	0.0084

TABLE 5-4. HIGH STRAIN RATE TENSILE PROPERTIES OF $[\pm 22.5]_{2s}$ 80AS/20S/PR288 GRAPHITE/S-GLASS/EPOXY

Specimen Numbers	Strain Rate ($\dot{\varepsilon}_{\theta\theta}$), s^{-1}	Modulus ($E_{\theta\theta}$), GPa (10^6 psi)	Poisson's Ratio ($\nu_{\theta x}$)
		Initial Properties	
34-1,3,5	1×10^{-4}	68.5 (9.9)	0.83
34-2,10,11	17	75.7 (11.0)	1.11
34-4,6,7	133	126.1 (18.3)	0.98
		Secant Properties	
34-1,3,5	1×10^{-4}	63.0 (9.1)	0.98
34-2,10,11	47	72.3 (10.5)	1.02
34-4,6,7	217	76.5 (11.1)	0.97
		Terminal Properties	
34-1,3,5	1×10^{-4}	57.4 (8.3)	1.12
34-2,10,11	206	70.2 (10.2)	1.28
34-4,6,7	296	35.4 (5.1)	1.02
		Ultimate Properties	
	Time to Failure (t_f), μs	Strength ($S_{\theta\theta T}$), MPa (ksi)	Strain ($\varepsilon^u_{\theta\theta T}$)
34-1,3,5	1×10^8	653 (95)	0.0104
34-2,10,11	227	753 (109)	0.0104
34-4,6,7	45	731 (106)	0.0095

TABLE 5-5. HIGH STRAIN RATE TENSILE PROPERTIES OF $[\pm 30]_{2s}$ SP288/AS GRAPHITE/EPOXY

Specimen Numbers	Strain Rate ($\dot{\varepsilon}_{\theta\theta}$), s^{-1}	Modulus ($E_{\theta\theta}$), GPa (10^6 psi)	Poisson's Ratio ($\nu_{\theta x}$)
	Initial Properties		
28-1,3,5	1×10^{-4}	58.6 (8.50)	1.25
28-2,12,13	8	48.4 (7.02)	1.01
28-9,10,11	220	85.7 (12.4)	1.22
	Secant Properties		
28-1,3,5	1×10^{-4}	43.3 (6.28)	1.50
28-2,12,13	58	44.7 (6.48)	1.17
28-9,10,11	297	49.8 (7.2)	1.20
	Terminal Properties		
28-1,3,5	1×10^{-4}	34.1 (4.94)	1.75
28-2,12,13	179	38.0 (5.50)	1.33
28-9,10,11	428	35.2 (5.1)	1.16
	Ultimate Properties		
	Time to Failure (t_f), μs	Strength ($S_{\theta\theta T}$), MPa (ksi)	Strain ($\varepsilon^u_{\theta\theta T}$)
28-1,3,5	1×10^8	566 (82)	0.0132
28-2,12,13	223	571 (83)	0.0128
28-9,10,11	45	660 (96)	0.0133

TABLE 5-6. HIGH STRAIN RATE TENSILE PROPERTIES OF $[\pm 30]_{2s}$ 80AS/20S/PR288 GRAPHITE/S-GLASS/EPOXY

Specimen Numbers	Strain Rate ($\dot{\varepsilon}_{\theta\theta}$), s^{-1}	Modulus ($E_{\theta\theta}$), GPa (10^6 psi)	Poisson's Ratio ($\nu_{\theta x}$)
		Initial Properties	
29-1,3,5	1×10^{-4}	44.9 (6.51)	1.26
54-2,3,5	17	43.5 (6.31)	1.11
29-10,11,12	207	93.5 (13.60)	1.12
		Secant Properties	
29-1,3,5	1×10^{-4}	36.2 (5.25)	1.33
54-2,3,5	72	41.9 (6.07)	1.23
29-10,11,12	324	51.5 (7.50)	1.06
		Terminal Properties	
29-1,3,5	1×10^{-4}	29.9 (4.33)	1.55
54-2,3,5	292	41.7 (6.04)	1.43
29-10,11,12	440	43.0 (6.30)	1.51
		Ultimate Properties	
	Time to Failure (t_f), μs	Strength ($S_{\theta\theta T}$), MPa (ksi)	Strain ($\varepsilon^u_{\theta\theta T}$)
29-1,3,5	2×10^8	503 (73)	0.0141
54-2,3,5	201	611 (89)	0.0144
29-10,11,12	42	690 (100)	0.0135

TABLE 5-7. HIGH STRAIN RATE TENSILE PROPERTIES OF $[\pm 45]_{2s}$ SP288/AS GRAPHITE/EPOXY

Specimen Number	Strain Rate ($\dot{\varepsilon}_{\theta\theta}$), s^{-1}	Modulus ($E_{\theta\theta}$), GPa (10^6 psi)	Poisson's Ratio ($\nu_{\theta x}$)
	Initial Properties		
24-1,3,5	1×10^{-4}	20.4 (2.95)	0.69
24-10, 52-2,3,4	14	19.1 (2.77)	0.90
24-11,12,13	168	111.4 (16.15)	0.78
	Secant Properties		
24-10, 52-2,3,4	85	17.6 (2.55)	0.80
24-11,12,13	330	40.3 (5.83)	0.88
	Terminal Properties		
24-10, 52-2,3,4	359	11.5 (1.66)	0.85
24-11,12,13	415	20.4 (2.97)	0.88
	Ultimate Properties		
	Time to Failure (t_f), μs	Strength ($S_{\theta\theta T}$), MPa (ksi)	Strain ($\varepsilon^u_{\theta\theta T}$)
24-1,3,5	3×10^8	>224 (32.5)	>0.0305
24-10, 52-2,3,4	329	494 (72)	0.0279
24-11,12,13	>76	927 (134)	0.0245

TABLE 5-8. HIGH STRAIN RATE TENSILE PROPERTIES OF $[\pm 45]_{2s}$ 80AS/20S/PR288 GRAPHITE/S-GLASS/EPOXY

Specimen Numbers	Strain Rate ($\dot{\varepsilon}_{\theta\theta}$), s^{-1}	Modulus ($E_{\theta\theta}$), GPa (10^6 psi)	Poisson's Ratio ($\nu_{\theta x}$)
		Initial Properties	
25-1,3,5	1×10^{-4}	21.5 (3.12)	0.74
25-9, 53-1,4,5	17	21.1 (3.06)	0.77
25-11,12,13	277	50.8 (7.37)	0.76
		Secant Properties	
25-9, 53-1,4,5	111	13.7 (1.99)	0.68
25-11,12,13	555	20.3 (2.95)	0.77
		Terminal Properties	
25-9, 53-1,4,5	388	11.2 (1.62)	0.67
25-11,12,13	853	4.8 (0.69)	0.60
		Ultimate Properties	
	Time to Failure (t_f), μs	Strength ($S_{\theta\theta T}$), MPa (ksi)	Strain ($\varepsilon^u_{\theta\theta T}$)
25-1,3,5	3×10^8	>191 (27.7)	>0.0265
25-9, 53-1,4,5	255	371 (54)	0.0270
25-11,12,13	64	711 (103)	0.0353

TABLE 5-9. HIGH STRAIN RATE TENSILE PROPERTIES OF $[\pm 60]_{2s}$ SP288/AS GRAPHITE/EPOXY

Specimen Numbers	Strain Rate ($\dot{\varepsilon}_{\theta\theta}$), s^{-1}	Modulus ($E_{\theta\theta}$), GPa (10^6 psi)	Poisson's Ratio ($\nu_{\theta x}$)
		Initial Properties	
22-1,3,5	1×10^{-4}	14.0 (2.03)	0.32
22-9,10,11	22	23.0 (3.34)	0.25
22-6,7,8	250	45.5 (6.59)	0.48
		Secant Properties	
22-1,3,5	1×10^{-4}	9.1 (1.32)	0.34
22-9,10,11	60	13.9 (2.01)	0.39
22-6,7,8	342	34.6 (5.02)	0.34
		Terminal Properties	
22-1,3,5	1×10^{-4}	5.6 (0.82)	0.33
22-9,10,11	166	12.1 (1.75)	0.37
22-6,7,8	547	25.7 (3.75)	0.34
		Ultimate Properties	
	Time to Failure (t_f), μs	Strength ($S_{\theta\theta T}$), MPa (ksi)	Strain ($\varepsilon^u_{\theta\theta T}$)
22-1,3,5	1×10^8	105 (15.2)	0.0116
22-9,10,11	226	182 (26.4)	0.0134
22-6,7,8	43	511 (74)	0.0145

TABLE 5-10. HIGH STRAIN RATE TENSILE PROPERTIES OF $[\pm 60]_{2s}$ 80AS/20S/PR288 GRAPHITE/S-GLASS/EPOXY

Specimen Numbers	Strain Rate ($\dot{\varepsilon}_{\theta\theta}$), s^{-1}	Modulus ($E_{\theta\theta}$), GPa (10^6 psi)	Poisson's Ratio ($\nu_{\theta x}$)
	Initial Properties		
23-1,3,5	1×10^{-4}	18.2 (2.64)	0.30
23-7,10,11	26	24.7 (3.58)	0.24
23-2,4,6	220	48.0 (6.96)	0.34
	Secant Properties		
23-1,3,5	1×10^{-4}	11.2 (1.62)	0.33
23-7,10,11	59	13.9 (2.01)	0.38
23-2,4,6	280	47.4 (6.86)	0.29
	Terminal Properties		
23-1,3,5	1×10^{-4}	7.2 (1.05)	0.36
23-7,10,11	165	9.9 (1.44)	0.35
23-2,4,6	440	42.5 (6.16)	0.24
	Ultimate Properties		
	Time to Failure (t_f), μs	Strength ($S_{\theta\theta T}$), MPa (ksi)	Strain ($\varepsilon^u_{\theta\theta T}$)
23-1,3,5	1×10^8	94.8 (13.7)	0.0085
23-7,10,11	195	155.5 (22.5)	0.0112
23-2,4,6	44	566 (82)	0.0122

TABLE 5-11. HIGH STRAIN RATE TENSILE PROPERTIES OF $[\pm 67.5]_{2s}$ SP288/AS GRAPHITE/EPOXY

Specimen Numbers	Strain Rate ($\dot{\varepsilon}_{\theta\theta}$), s^{-1}	Modulus ($E_{\theta\theta}$), GPa (10^6 psi)	Poisson's Ratio ($\nu_{\theta x}$)
		Initial Properties	
26-1,3,5	1×10^{-4}	12.0 (1.74)	0.17
26-10,11,13	26	17.3 (2.51)	0.15
26-2,4,6	243	48.8 (7.07)	0.17
		Secant Properties	
26-1,3,5	1×10^{-4}	10.5 (1.52)	0.17
26-10,11,13	73	12.8 (1.86)	0.18
26-2,4,6	270	36.2 (5.24)	0.19
		Terminal Properties	
26-1,3,5	1×10^{-4}	8.7 (1.26)	0.17
26-10,11,13	167	8.5 (1.23)	0.20
26-2,4,6	347	22.9 (3.32)	0.20
		Ultimate Properties	
	Time to Failure (t_f), μs	Strength ($S_{\theta\theta T}$), MPa (ksi)	Strain ($\varepsilon^u_{\theta\theta T}$)
26-1,3,5	1×10^8	85.1 (12.3)	0.0081
26-10,11,13	142	132.2 (19.2)	0.0103
26-2,4,6	36	339 (49)	0.0096

TABLE 5-12. HIGH STRAIN RATE TENSILE PROPERTIES OF $[\pm 67.5]_{2s}$ 80AS/20S/PR288 GRAPHITE/S GLASS/EPOXY

Specimen Numbers	Strain Rate ($\dot{\varepsilon}_{\theta\theta}$), s^{-1}	Modulus ($E_{\theta\theta}$), GPa (10^6 psi)	Poisson's Ratio ($\nu_{\theta x}$)
		Initial Properties	
27-1,3,5	1×10^{-4}	14.4 (2.08)	0.16
27-10,11,13	32	20.3 (2.94)	0.13
27-2,4,6	261	45.0 (6.52)	0.23
		Secant Properties	
27-1,3,5	1×10^{-4}	12.4 (1.79)	0.17
27-10,11,13	61	15.7 (2.28)	0.14
27-2,4,6	236	42.7 (6.18)	0.20
		Terminal Properties	
27-1,3,5	1×10^{-4}	9.9 (1.43)	0.17
27-10,11,13	134	13.9 (2.02)	0.20
27-2,4,6	253	41.7 (6.05)	0.17
		Ultimate Properties	
	Time to Failure (t_f), μs	Strength ($S_{\theta\theta T}$), MPa (ksi)	Strain ($\varepsilon^u_{\theta\theta T}$)
27-1,3,5	1×10^8	76.1 (11.0)	0.0062
27-10,11,13	144	136.6 (19.8)	0.0087
27-2,4,6	36	356 (52)	0.0083

TABLE 5-13. HIGH STRAIN RATE TENSILE PROPERTIES OF $[\pm 75)_{2s}$ SP288/AS GRAPHITE/EPOXY

Specimen Numbers	Strain Rate ($\dot{\varepsilon}_{\theta\theta}$), s^{-1}	Modulus ($E_{\theta\theta}$), GPa (10^6 psi)	Poisson's Ratio ($\nu_{\theta x}$)
		Initial Properties	
20-1,3,5	1×10^{-4}	12.1 (1.75)	0.09
20-12	19	19.7 (2.86)	-
20-2,4,7	230	45.2 (6.55)	-
		Secant Properties	
20-1,3,5	1×10^{-4}	10.0 (1.46)	0.08
20-12	45	10.9 (1.58)	0.04
20-2,4,7	272	36.1 (5.24)	0.15
		Terminal Properties	
20-1,3,5	1×10^{-4}	7.9 (1.14)	0.06
20-12	132	6.0 (0.87)	0.08
20-2,4,7	315	29.7 (4.31)	-
		Ultimate Properties	
	Time to Failure (t_f), μs	Strength ($S_{\theta\theta T}$), MPa (ksi)	Strain ($\varepsilon^u_{\theta\theta T}$)
20-1,3,5	1×10^8	74.8 (10.8)	0.0075
20-12	201	98.3 (14.2)	0.0090
20-2,4,7	30	290 (42)	0.0081

TABLE 5-14. HIGH STRAIN RATE TENSILE PROPERTIES OF $[\pm 75]_{2s}$ 80AS/20S/PR288 GRAPHITE/S-GLASS/EPOXY

Specimen Numbers	Strain Rate ($\dot{\varepsilon}_{\theta\theta}$), s^{-1}	Modulus ($E_{\theta\theta}$), GPa (10^6 psi)	Poisson's Ratio ($\nu_{\theta x}$)
	Initial Properties		
21-1,5	1×10^{-4}	15.5 (2.25)	0.10
21-10,11,12	34	16.9 (2.45)	-
21-2,4,6	217	45.1 (6.53)	0.03
	Secant Properties		
21-1,5	1×10^{-4}	14.0 (2.03)	0.06
21-10,11,12	64	13.4 (1.94)	0.04
21-2,4,6	223	35.1 (5.09)	0.02
	Terminal Properties		
21-1,5	1×10^{-4}	11.0 (1.59)	0.11
21-10,11,12	116	11.7 (1.69)	0.11
21-2,4,6	295	25.7 (3.72)	-
	Ultimate Properties		
	Time to Failure (t_f), μs	Strength ($S_{\theta\theta T}$), MPa (ksi)	Strain ($\varepsilon^u_{\theta\theta T}$)
21-1,5	1×10^8	61.4 (8.9)	0.0047
21-10,11,12	110	94.9 (13.8)	0.0070
21-2,4,6	26	223 (32)	0.0066

REPORT DOCUMENTATION PAGE

Form Approved
OMB No. 0704-0188

1. AGENCY USE ONLY (*Leave blank*)	2. REPORT DATE	3. REPORT TYPE AND DATES COVERED
	December 1991	Final Contractor Report

4. TITLE AND SUBTITLE

High Strain Rate Properties of Angle-Ply Composite Laminates
Part III—Final Report

5. FUNDING NUMBERS

WU-505-63-5B
C-NAS3-21016

6. AUTHOR(S)

I.M. Daniel

7. PERFORMING ORGANIZATION NAME(S) AND ADDRESS(ES)

IIT Research Institute
10 West 35th Street
Chicago, Illinois 60616

8. PERFORMING ORGANIZATION REPORT NUMBER

None

9. SPONSORING/MONITORING AGENCY NAMES(S) AND ADDRESS(ES)

National Aeronautics and Space Administration
Lewis Research Center
Cleveland, Ohio 44135-3191

10. SPONSORING/MONITORING AGENCY REPORT NUMBER

NASA CR-189085

11. SUPPLEMENTARY NOTES

Project Manager, C.C. Chamis, Structures Division, NASA Lewis Research Center, (216) 433-3252.

12a. DISTRIBUTION/AVAILABILITY STATEMENT

Unclassified - Unlimited
Subject Category 24

12b. DISTRIBUTION CODE

13. ABSTRACT ***(Maximum 200 words)***

Angle-ply graphite/epoxy and graphite/S-glass/epoxy laminates were characterized in uniaxial tension at strain rates ranging from quasi-static to over $500s^{-1}$. Laminate ring specimens of $[\pm 15]_{2s}$, $[\pm 22.5]_{2s}$, $[\pm 30]_{2s}$, $[\pm 45]_{2s}$, $[\pm 60]_{2s}$, $[\pm 67.5]_{2s}$, and $[\pm 75]_{2s}$ layups were loaded under internal pressure. Results were presented in the form of stress-strain curves to failure. Properties determined included moduli, Poisson's ratios, strength, and ultimate strain. In all seven laminates for the two materials tested the modulus and strength increase with strain rate. The effect of strain rate varies with layup, being lowest for the fiber dominated $[\pm 15]_{2s}$ laminates and highest for the matrix dominated $[\pm 75]_{2s}$ laminates. The highest increments over the static values are 10% to 25% for the $[\pm 15]_{2s}$ layup and 200% to 275% for the $[\pm 75]_{2s}$ layup. Ultimate strains do not show any significant trends with strain rate. In almost all cases the ultimate strain values are within ±20% of the mean value and in half of the cases the deviations from the mean are less than 10%.

14. SUBJECT TERMS

Angle-ply laminates; Graphite/epoxy; S-glass/epoxy; Ring specimens; Stress-strain; Strengths; Properties; Initial; Terminal; Ultimate; Data; Graphs; Tables

15. NUMBER OF PAGES
382

16. PRICE CODE
A17

17. SECURITY CLASSIFICATION OF REPORT	18. SECURITY CLASSIFICATION OF THIS PAGE	19. SECURITY CLASSIFICATION OF ABSTRACT	20. LIMITATION OF ABSTRACT
Unclassified	Unclassified	Unclassified	